

UNCLASSIFIED

AD NUMBER

AD250229

LIMITATION CHANGES

TO:

Approved for public release; distribution is unlimited. Document partially illegible.

FROM:

Distribution authorized to U.S. Gov't. agencies and their contractors;  
Administrative/Operational Use; 1958. Other requests shall be referred to Office of Naval Research, 875 North Randolph Street, Arlington, VA 22203-1995.

AUTHORITY

ONR ltr, 1 Sep 1977

THIS PAGE IS UNCLASSIFIED

**Best  
Available  
Copy**



THIS REPORT HAS BEEN DELIMITED  
AND CLEARED FOR PUBLIC RELEASE  
UNDER DOD DIRECTIVE 5200.20 AND  
NO RESTRICTIONS ARE IMPOSED UPON  
ITS USE AND DISCLOSURE.

DISTRIBUTION STATEMENT A

APPROVED FOR PUBLIC RELEASE;  
DISTRIBUTION UNLIMITED.

UNCLASSIFIED

---

AD 250 22

---

*Reproduced  
by the*

ARMED SERVICES TECHNICAL INFORMATION  
ARLINGTON HALL STATION  
ARLINGTON, VIRGINIA



---

UNCLASSIFIED

**UNCLASSIFIED**

---

**AD 250 229**

---

*Reproduced  
by the*

**ARMED SERVICES TECHNICAL INFORMATION AGENCY  
ARLINGTON HALL STATION  
ARLINGTON, VIRGINIA**



---

**UNCLASSIFIED**

NOTICE: When government or other drawings, specifications or other data are used for any purpose other than in connection with a definitely related government procurement operation, the U. S. Government thereby incurs no responsibility, nor any obligation whatsoever; and the fact that the Government may have formulated, furnished, or in any way supplied the said drawings, specifications, or other data is not to be regarded by implication or otherwise as in any manner licensing the holder or any other person or corporation, or conveying any rights or permission to manufacture, use or sell any patented invention that may in any way be related thereto.

2505

Second Symposium on  
**NAVAL HYDRODYNAMICS**

**HYDRODYNAMIC NOISE  
CAVITY FLOW**

*Sponsored by the*  
**OFFICE OF NAVAL RESEARCH**  
*and the*  
**NATIONAL ACADEMY OF SCIENCES—  
NATIONAL RESEARCH COUNCIL**

**NOX**  
61-2-1

**August 25-29, 1952**  
Washington, D.C.

**ACR-38**  
**OFFICE OF NAVAL RESEARCH—DEPARTMENT OF THE NAVY**  
Washington, D.C.

## FOREWORD

In September of 1956, the first Symposium on Naval Hydrodynamics, sponsored by the Office of Naval Research and the National Academy of Sciences - National Research Council, was held for the specific purpose of presenting authoritative, critical surveys of those areas of Hydrodynamics that are of significance in naval science.<sup>1</sup> In keeping with the original plans set down for this series, subsequent meetings were to be devoted to one or more themes selected on the basis of importance and need for research stimulation, on the one hand, or of achievement of important "breakthroughs" and hence of interest for wide dissemination, on the other. Thus, the present symposium achieved an example of each criterion: hydro- and aerodynamic noise (of great importance in both warfare and commercial usage of ships and aircraft), and supercavitating and ventilated flows (which promise, for example, possibilities of high-speed marine propulsion at efficiencies hitherto not thought attainable).

Recent declassification of many research results in both subjects made possible the wealth and excellence of contributions presented at the meetings in August of 1958 and now reproduced in this volume. Unlike the first symposium which defined the framework of the field of interest, this meeting was devoted in largest part to original contributions. Again, as for the earlier meeting, each paper was invited from the active research centers without regard to geographic location.

Aside from the military importance of the two theme topics, they are rather remarkable from other standpoints. In each case, the important scientific contributions that stimulated further research occurred within the last seven or eight years. Furthermore, they clearly illustrate a characteristic of the field of Hydrodynamics that the most important practical problems require for their solution research of a nature that is "basic" in the classical sense. In the case of hydrodynamic noise problems, only an understanding of the physical mechanisms of cavitation, turbulence, etc., could lead to the progress that has been made. Of particular interest in recent years has been the question of turbulence noise in both aerodynamic and hydrodynamic application; the clues to the direction of research were provided by Lighthill's treatment of jet noise only eight years ago. In the case of cavitating flows, the difficulties of the nonlinear free stream line theory and of experimental observations made progress very difficult and seemed to lead inevitably to the conclusion that cavitation and cavitating flows were to be avoided at all costs. It was only following the development of a linearized theory of such flows by Tulin in 1953 and his subsequent discoveries of low-drag supercavitating strut and hydrofoil profiles that realization grew of the significant benefits that can be achieved with supercavitating flows and, in fact, that for certain applications, operation under supercavitating conditions is to be sought rather than avoided. In another context, Tulin's accomplishments are an outstanding triumph of theory in providing results that can be used without modification and with confidence in engineering design. The basic achievement itself will certainly rank with linearized airfoil theory and thin ship theory in importance and practical consequence.

---

<sup>1</sup> Symposium on Naval Hydrodynamics, National Academy of Sciences - National Research Council, Publication 515, 1957, Washington, D. C.

While papers were included on noise in multiphase and multicomponent flows in that part of the program devoted to noise, the major emphasis was given to shear flow noise, and in particular, turbulence noise, in recognition of the growing importance of this source in both aerodynamic and hydrodynamic applications. Because of their close relationship, both scientifically and technologically, both supercavitating and ventilated flows were included in the second part of the program. In addition, to bring out the relationships between cavity flows of these types and separated flows, at least insofar as the usefulness and applicability of modern methods of analysis are concerned, a paper was also included on "aerodynamic cavities." In this way, it was hoped to illustrate and bring about a unification of the various viewpoints of research in the diverse disciplines of fluid dynamics.

It is my privilege to extend our thanks to the authors for their willingness to participate in the program. The responsibility for the organization of the technical sessions was assumed by the Mechanics Branch of the Office of Naval Research. It is indeed a pleasure to acknowledge the assistance of the following, who individually or collectively made a number of suggestions of papers and authors from which the final program was selected:

J. S. Coleman, Executive Secretary, Physical Sciences  
Division, National Academy of Sciences

S. Corrsin, The Johns Hopkins University (Representing the  
National Research Council Committee on Undersea Warfare)

J. B. Parkinson, Chief, Hydrodynamics Division, National  
Aeronautics and Space Administration

M. Strasberg, David Taylor Model Basin

A. J. Tachmindji, David Taylor Model Basin

M. P. Tulin, Office of Naval Research Branch Office, London

The administrative arrangements were very kindly undertaken by the National Research Council and special thanks are due Messrs. George Wood, John Cooper, and Mrs. Helen Ray of that organization. Yeoman work in connection with the technical details of the meeting was performed by CRD H. B. Keller, USN, of ONR's Mechanics Branch, and A. G. Fabula and R. J. Mindak of the Office of Naval Research Branch Offices in Pasadena and Chicago, respectively. Though it is never possible adequately to thank the Editor of symposium proceedings such as these, particular recognition is due Mr. Ralph D. Cooper for his courage in accepting this assignment and for the professionally excellent way in which he accomplished his task. Not only must he live with the meeting long after it is over, but he must, unfairly to be sure, bear the brunt of the clamor that invariably arises when delays in publication occur.

Finally, I should like to express our gratitude to the Commanding Officers of the David Taylor Model Basin and the Naval Ordnance Laboratory, and to their scientific staffs, for their kindness and efforts in providing the technically stimulating tours through these laboratories on the third day of the meeting.

PHILLIP EISENBERG  
Head, Mechanics Branch  
Office of Naval Research  
Chairman



## CONTENTS

Foreword . . . . .	iii
THEORY AND EXPERIMENT IN AERODYNAMIC NOISE, WITH A CRITIQUE OF RESEARCH ON JET FLOWS IN THEIR RELATIONSHIP TO SOUND. . . . .	1
Alan Powell	
A THEORY OF TURBULENCE DYNAMICS. . . . .	29
Robert H. Kraichnan	
SOME EXPERIMENTAL AND THEORETICAL RESULTS RELATING TO PRODUCTION OF NOISE BY TURBULENCE AND THE SCATTERING OF SOUND BY TURBULENCE OR SINGLE VORTICES . . . . .	45
Ernst-August Muller	
SIMILARITY RELATIONS IN AERODYNAMIC NOISE MEASUREMENTS . . . .	65
E. Mollo-Christensen and N. W. Liepmann	
NOISE PRODUCTION IN A TURBULENT BOUNDARY LAYER BY SMOOTH AND ROUGH SURFACES . . . . .	75
Eugen Skudrzyk and Gillian Haddle	
PRESSURE FLUCTUATIONS ON THE WALL ADJACENT TO A TURBULENT BOUNDARY LAYER . . . . .	107
Mark Harrison	
THE FLUCTUATING SURFACE PRESSURE CREATED BY TURBULENT BOUNDARY LAYERS ON HYPERSONIC VEHICLES . . . . .	127
Edmund E. Callaghan	
EXCITATION OF ACOUSTIC RESONATORS BY FLOW . . . . .	137
Uno Ingard and Lee W. Dean, III	
SOUND RADIATION INTO A CLOSED SPACE FROM BOUNDARY LAYER TURBULENCE . . . . .	151
Ira Dyer	
RECENT INVESTIGATIONS ON SONIC AND ULTRASONIC CAVITATION IN GÖTTINGEN . . . . .	179
Erwin Meyer	
CAVITATION NOISE. . . . .	201
Hugh M. Fitzpatrick	
PRESSURE WAVES FROM COLLAPSING CAVITIES. . . . .	207
T. Brooke Benjamin	
NEW DEVELOPMENTS IN THE THEORY OF SUPERCAVITATING FLOWS. . .	235
Marshall P. Tulin	
JETS, WAKES, AND CAVITIES . . . . .	261
Garrett Birkhoff	

CAVITY FLOWS OF VISCOUS LIQUIDS IN NARROW SPACES . . . . .	277
Sir Geoffrey Taylor and P. G. Saffman	
UNSTEADY SUPERCAVITATING FLOWS. . . . .	293
T. Y. Wu	
THE INFLUENCE OF DEPTH OF SUBMERSION, ASPECT RATIO, AND THICKNESS ON SUPERCAVITATING HYDROFOILS OPERATING AT ZERO CAVITATION NUMBER . . . . .	317
Virgil E. Johnson, Jr.	
WALL EFFECTS IN CAVITATING FLOWS. . . . .	367
Hirsh Cohen and R. C. DiPrima	
SOME AERODYNAMIC CAVITY FLOWS IN FLIGHT PROPULSION SYSTEMS . . . . .	391
William G. Corneli	
MECHANICS OF VENTILATION INCEPTION . . . . .	425
Kenneth L. Wadlin	
VENTILATION OF BODIES PIERCING A FREE SURFACE . . . . .	447
J. M. Wetzel	
AIR ENTRAINMENT BEHIND ARTIFICIALLY INFLATED CAVITIES . . . . .	467
I. J. Campbell and D. V. Hulse	
ON SUPERCAVITATING PROPELLERS . . . . .	483
H. W. Lerbs	
THE DESIGN AND ESTIMATED PERFORMANCE OF A SERIES OF SUPERCAVITATING PROPELLERS . . . . .	489
A. J. Tachmindji and W. E. Morgan	
AN EXPERIMENTAL STUDY OF CAVITATING INDUCERS . . . . .	533
A. J. Acosta	
A GENERAL LINEARIZED THEORY FOR CAVITATING HYDROFOILS IN NONSTEADY FLOW . . . . .	559
R. Timman	
AUTHOR INDEX . . . . .	583

# THEORY AND EXPERIMENT IN AERODYNAMIC NOISE, WITH A CRITIQUE OF RESEARCH ON JET FLOWS IN THEIR RELATIONSHIP TO SOUND

Alan Powell  
*University of California*

## INTRODUCTION

When I accepted the invitation to add to existing surveys (1-6) of the interesting study of aerodynamic noise, I had in mind a more generous coverage than I am offering you today. However it soon became apparent that it would have grown beyond reasonable bounds. So, apart from the generalities of Part I below, I shall discuss only various jet flows and their relationships with sound and concentrate on the debatable or rather vaguely-understood aspects, endeavoring to indicate many research problems that remain, both theoretical and experimental, large and small, and how these fit into the general picture. Consequently there is no attempt to present an encyclopedia on the subject, the references serving only the purpose of providing foundation for my comments. These aspects illustrate well the vagueness of the boundary between "ordinary" fluid motion and acoustics, a boundary not recognized by Lord Rayleigh and Sir Horace Lamb. The general situation was summed up nicely by John Leconte, in that we can "look upon all jets as musically inclined," and although he was alluding mainly to the "sensitive" jets of low Reynolds number, it might be applied to all jets—at least if one's ideas of modern music are liberal enough!

## Part I GENERAL THEORETICAL ASPECTS

There are several types of flow, all sound-producing, that can be distinguished. These are characterized by the absence or presence of a solid surface and if present, whether such surfaces are rigid or not. All these have in common the equations of motion, and the solution as a radiation problem shows how the various types are related. If there is no introduction of matter and no externally applied body forces, the equations of continuity and momentum are

$$\frac{\partial \rho}{\partial t} + \nabla \cdot (\rho \mathbf{V}) = 0$$

$$\rho \frac{d\mathbf{V}}{dt} = -\nabla p$$

These can be manipulated (7) just as if the ordinary wave equation were being obtained, except that no terms are discarded and  $a_0^2$  is introduced on both sides,  $a_0$  being the speed of sound in regions of still fluid far removed from the primary disturbances whose sound-producing properties we are to investigate. This yields the inhomogeneous wave equation

$$\frac{\partial^2}{\partial t^2} - \nabla_0^2 = \frac{\partial^2}{\partial x_i \partial x_j} \left[ \left( v_i v_j + p_{ij} - a_0^2 \delta_{ij} \right) \right]$$

Strictly speaking this is an integral equation. But if the sound-generating flow is assumed given (and therefore unaffected by the sound produced) then sound perturbations can be found well away from it. Then the "right-hand side"—in other words the source distribution—is given and the solution is well known, from electromagnetic theory, for example. It can be expressed in a useful form for our purpose by using Gauss' theorem (8) twice over on the complementary function, the result being

$$4 \left( \frac{\partial^2}{\partial t^2} - \nabla_0^2 \right) \phi(x, t) = a_0^2 \int_{x_i} \frac{\partial^2}{\partial x_i \partial x_j} \left[ \left( v_i v_j + p_{ij} - a_0^2 \delta_{ij} \right) \right] \frac{\partial \phi}{\partial x_j} \quad (a)$$

$$+ \int_{x_i} \frac{\partial}{\partial x_i} \left[ \left( v_i v_j + p_{ij} - a_0^2 \delta_{ij} \right) \right] \frac{\partial \phi}{\partial x_j} \quad (b)$$

$$\int \left( \frac{\partial^2}{\partial t^2} - \nabla_0^2 \right) \phi \quad (c)$$

Here  $r$  is the distance from a point  $x$  in the sound-generating flow to the point  $y$  at which the perturbations are estimated, and the asterisk indicates a time retardation corresponding to the transit time over that distance.

The first group (a) alone survives in the absence of solid boundaries and has provided the basis of our understanding of sound production by turbulence. While little has been done for shear flow turbulence, as such, isotropic turbulence has been considered (9) and the results are very encouraging when applied to turbulent jet flow (10). An important effect for a high-order source is the susceptibility of the directional characteristics to motion through the medium—the introduction of moving axes (rather than the resolution into higher-order stationary sources) permits a very simple point of view to explain the gross directionality of the sound field so characteristic of turbulent subsonic jets (7). The question of the noise generated by isotropic turbulence has been the subject of more recent attention (11,12), and shows well the need for some careful experimental work measuring the rather low acoustic output of a stationary mass of isotropic turbulence. Turbulent wakes have not yet been considered theoretically or experimentally, except in connection with the vortex noise of propellers.

The same approach may be used to study the scattering of sound waves by turbulence or more relevant here, the scattering of acoustic energy from the interaction of turbulence with shockwaves (13,14). An interesting result of this is that most of the acoustic energy tends to catch up with the shockwave, and so be absorbed by it. This rather general approach is compatible with the result of studies of the interaction between a single vortex and a shockwave (15,16), obtained by superimposing shear waves, the effects of which had been considered earlier (17). Although these studies are very approximate, they do account for the characteristic directional effects observed experimentally (18) (Fig. 1). Of course shear waves are just one of the three modes of elementary motion perturbing a uniform flow, the others being sound

itself and temperature (entropy) (19,20,21). It is interesting that the shockwave acts as an amplifier for colliding sound waves, but practically absorbs those catching up with it.

There are several important applications of the principles just mentioned. The noise in supersonic wind tunnels is one aspect. Another is the interaction of eddies with the shockwaves of supersonic jet flow, being particularly important for cold jets, when the interaction appears to account for almost the whole of the sound output. The situation when the eddy is centered on the edge of a jet—or the related situation when the jet acquires a sinusoid—has not been studied in detail; the overall picture is shown in Fig. 6, in which, however, the details of this particular aspect are obscured.

The second group (b) concerns surface effects, suggesting that surface stresses act like dipole generators, supporting an earlier and more intuitive approach (22). This certainly seems to be the case for the fluctuating forces on circular cylinders (23), and is presumably the case in the edge-tone type of phenomena. It is important to notice that the dipole as found is an artifact, for there is no physical dipole supplying energy; this can only come from the volume of the fluid about the obstacle.

But for plane surfaces, the contribution from fluctuating pressures is thought to vanish (24,25) and, with fairly loose restrictions, that from shear stresses also (25). This then suggests that quadrupole generation from the volume of turbulence in a boundary layer may be the most important source of noise when the surface is rigid (26).

When the surface is not rigid, the boundary layer stresses—particularly pressure—set the surface into motion (27-30) and in several practical systems this may be the predominating effect. Although the general principles are now clear, more information concerning the pressure fluctuations at the wall is required. So far spectra and a few space (31) and space-time (32) correlations at subsonic speeds have been made. The patterns of pressure convected across the "fixed" surfaces do not appear to be as "frozen" as might be necessary for some simple theoretical concepts to apply. A convection effect is certainly present, the convection velocity being a rather large fraction (0.8 or so) of the free stream velocity. This tends to draw attention to the region of irregular vorticity fronts of the boundary layer. The surface becomes a sounding board, and radiates into the space away from the flow according to expression (c). On the other side the presence of the flow itself may influence the radiation; and if the flow is at anything but a very low Mach number, the directionality effects will be influenced by the moving source effects. In addition the first term of expression (b)



Fig. 1. Vortex-shock wave interaction. The vortex is the starting vortex, shed from an aerobell; the picture to the left and a shockwave traversed it from left to right. The whorls to the right are entrainment fronts associated with this. The shockwave was then reflected from the plane, right-hand end of the shocktube interacting with that starting vortex. The impulsive radiation is in the form of an arc centered in the vortex and intersecting the now distorted shockwave close to its vicinity, being the most powerful. From M. J. Hollingworth and B. J. Richards (18).

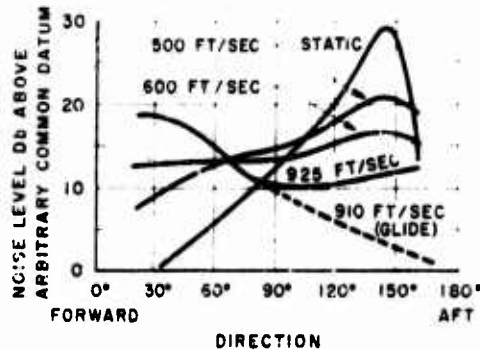


Fig. 2. Noise of a jet aircraft in flight. As the forward speed of the aircraft increases, the jet noise, mainly radiated rearwards, decreases, and the noise due to the motion of the airplane through the air increases and is radiated in the forward direction. (Constructed from unpublished data kindly supplied by Dr. H. H. G. George.)

suggests that the motion of the surface results in a dipole radiation because of the effective introduction of momentum across the fixed surface of the integral—this aspect seems to have been overlooked.

The noise sources due to the passage of an airplane through the air are complex in character—all of the above types being present to some degree. Its motion through the ambient atmosphere results in the generated noise having a marked preference for forward radiation, increasing with flight speed; while the jet noise displays a lessening of its downstream preference, its level naturally decreasing because of the reduced relative jet velocity. These effects are shown very well in Fig. 2.

The distributions of simple sources represented by expression (c), already mentioned, can be used

in connection with fluctuating flow from an orifice, such as for pulse jets or organ pipes. On the other hand, the continuity equation could be supplemented by a source of matter term, and the result could be used in the same cases by employing suitable boundaries for the integrals; and it should be supplemented by a dipole term if the surrounding fluid is in motion, corresponding to its deficit of momentum.

Although the general theory of the relationships between vorticity, pressure and entropy (21.33) cannot come within the scope of this survey, it seems to me that the development of such aspects is likely to be very revealing and should lead to a better understanding of many scattered facets that so far have not been too closely knitted together.

## Part II JET FLOWS DISPLAYING DISCRETE FREQUENCIES

### THE SENSITIVE JET AND FLAME

The sensitivity to external disturbances of a jet, operating somewhat below its critical Reynolds number for early turbulent development, seems to be a key to more than one phenomenon. Thus it is useful to mention the well-known sensitive jet or flame, although in itself it has little to do with the generation of sound.

The visible dipping of the flame, say of coal gas, is an indicator that increased jet mixing has taken place prior to the original flame front, tripped by certain disturbances of the jet. These disturbances are traditionally acoustic—thus indicating that the jet is really sensitive!—and ordinarily arise from distortion of the jet as it leaves the nozzle (34,35). This is confirmed by the fact that sound waves propagating along the jet axis are usually ineffective, as are the pressure antinodes of a standing-wave system and laterally propagating waves shielded from the orifice. Contrary to earlier reports (34), it appears that vibration of the orifice itself results in effects



Fig. 3 - The "sensitive" jet. A laminar flow jet emerges from the slit exit and is disturbed by sound waves whose particle velocity is in a horizontal direction across the picture. The disturbance amplitude presumably grows exponentially until it is large enough to result in vortex development ultimately disintegrating into turbulence. (This photograph was taken by G. B. Brown (35).)



Fig. 4 - Low-speed edge tones. The disturbed jet flow is very similar to that of Fig. 3, the action of the edge replacing the externally applied acoustic disturbances. (G. B. Brown took this photograph using a stroboscopic method (36).)

quite similar to those caused acoustically (35). This is a necessary requirement if ideas based upon the classical dynamics of jet instability are valid. Provided that a small sinusoid of the jet, caused by distortion as it leaves the orifice, lies in the unstable regime, it will develop to produce the beautiful (nonlinear!) vortex forms shown in Fig. 3, which sooner or later degenerate into a mass of turbulence. The phenomenon takes place at relatively small Reynolds numbers when, lacking externally applied disturbances, a substantial portion, if not all, of the jet flow would be of a laminar character. Thus small periodic disturbances in the pertinent range of Strouhal number can completely alter the appearance of the jet flow; the disturbed jet produces sound, but it is of quite negligible proportions. However, an undisturbed laminar jet can produce no sound: it is steady flow.

It is worth mentioning that such jets have a very unstable regime. For example, assuming a square velocity profile and neglecting viscosity, "for a frequency of 1.26 cps and a slit width of 1 mm, stream velocities of 380, 150, and 100 cm/sec result in disturbance amplifications over a distance of 5 mm of 30.8, 8400, and 54,000 respectively" (Ref. 8).

Microphone surveys reveal directional properties which are characteristic of dipoles (42). This is just what one would expect from theoretical reasoning, (indicated by the pressure part of  $\phi_{1111}$  in group (b) of Part I). However, the directional pattern sometimes displays an apparently more complex form than the dipole's figure of eight, in the classical low-speed case (42); in the high-speed case the radiation is much more suggestive of simple source radiation, the high-velocity stream apparently offering sufficient impedance to the lateral motion to prevent a dipole forming from the generation of the sources arising from differential flow on either side of the edge. Sometimes the sound wave radiated away is far from sinusoidal (38,42) (see Fig. 5, for example). It would be particularly interesting therefore to study the details of the flow about the edge and to measure the forces acting upon it. It is interesting to note in passing that the edge may be relatively large or quite small, from the point of view of the circulation about it, since it can be replaced by a wire (39). In the latter case the connection between the new eddies springing from the wire and the force upon it is evident: there is clearly some analogy to aeolian tones, for which the effective dipole concept is now quite well established (23). It is relevant—indeed, it seems essential—that the vortex system shedding from a cylinder can have its frequency forced to be in step with that of externally applied disturbances (43), if they are large enough.

The foregoing type of mechanism of edge tones has been subject to doubt in the past because of a few "crucial" tests. For example, a jet having no edge was placed near one having an edge (41). The failure of the edgeless one to show vortex development was taken as evidence that the feedback from edge to orifice was not propagated as a wave; but, the disturbing signal at the edgeless one would be reduced, because of the increased distance from the assumed effective dipole at the edge, to not more than about 1/125 of its proper value (judging from the published data). The test is therefore not so crucial as it would seem at first sight. Again, concerning the intensity required of a loudspeaker to produce similar vortex formation in an edgeless jet (26), "the loudspeaker had to be easily audible, whereas no audible edge tone occurred." This would have been a very impressive argument had the velocity fluctuations at the orifice been directly compared, an experiment worthy of attention.

It is interesting that a yet much simplified model of the jet-tone flow yields disturbances having an encouraging likeness to some of those photographed (44). Here the jet is considered as a continuous stream of particles of mass subjected to transverse pressure gradients proportional to the displacement of the "stream" at the edge (45). The apparent success of the method lies partly in the suitable choice of a necessary arbitrary function, and also in that the instability of the jet photographed was relatively very small as such jets go.

I hope that this attempt at bringing together the "rival camps" is of some avail, and that most of the numerous theories ("acoustic," "hydrodynamic," "impulse," "vortex street," etc.) will be recognized as being different emphases upon the same essential theme. There seem to me to be no surviving conflicts of any import, some of the very earliest theories containing the essence of the matter, despite the considerable experimental difficulties of those times. However, while I think the overall picture is taking shape, we are still far from fully understanding the details of it. In particular, the sound intensity cannot yet be calculated,<sup>2</sup> ab initio. Since this is

<sup>2</sup>However, definite progress along the lines indicated is being made and there is hope of an early approximate solution. A development of the "gain criterion" (36) reveals the particular importance of a certain nondimensional parameter  $h^2/V$ . Here  $h$  is the effective orifice-edge distance,  $\omega$  the angular frequency, and  $V$  is the jet velocity, from the orifice of width  $2a$  and length  $l$ . The significance of the slit length  $l$  is interesting, since it probably is a critical one, had been it varied to it.



supposed to be a result of a feedback mechanism, it would seem necessary for non-linear effects to play an essential part in determining the amplitude. This role may be played by the stream disturbances becoming "large" (developing into vortices), perhaps by the flow about the edge becoming less effective: in any event the "gain round the cycle" must exceed unity during establishment of the motion, but clearly must equal unity when established (38).

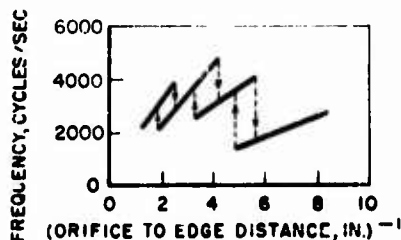


Fig. 6 - Edge-tone frequencies. The wavelength of the disturbances of the jet stream increases steadily as the edge is moved away from the orifice, but after a certain point a jump occurs when another disturbance wavelength fits itself in between the orifice and the edge, restoring the wavelength to that corresponding to the most unstable regime. Note the prominent hysteresis effect. (Data from G. B. Brown (36).)

Most edge-tone studies have been concerned with the flow itself, and especially with the frequency characteristics, a distinguishing feature being the jumps in frequency (Fig. 6). These occur when either the height of the edge or velocity is varied, in such a manner that the disturbance wavelength is never far removed from that of maximum instability. What few sound intensity measurements are available (42) indicate that the acoustic power is of the order of a hundredth of the jet kinetic power: a surprisingly high figure in view of the extremely low speeds involved, although the presence of a baffle may have increased the acoustic efficiency above its normal value.

The proximity of reflectors or resonators greatly influences the edge-tone characteristics (38,42,46). The overall picture is now much more complex; the salient feature is that the pressure fluctuations at the edge may disturb the stream at the orifice more effectively via the action

of the reflector or resonator, and so impress upon it their characteristic frequencies. This situation is clearly related to the steady tone of an organ pipe, although its establishment is another matter (47).

In some unreported tests using a 4:1 elliptic nozzle at a Reynolds number of about half a million, the author found it easy to produce edge-tone phenomena, and also to demonstrate the effects of reflectors. The acoustic power generated was uncomfortably high, since the jet exit had a minimum dimension of one inch, and the exit velocity was near sonic! The acoustic power was an appreciable fraction of the jet power, perhaps a tenth.

#### OTHER DISCRETE VORTEX PHENOMENA IN SUBSONIC JETS

There is another class of jet phenomena in which the development of discrete vortices is a characteristic; however, the situation differs from the foregoing in that while appreciable sound is generated, the effect of the sound\* so generated on the jet itself is not of recognized importance.

"Jet tones" are intimately connected with the vortex shedding of jets issuing from orifices. These orifices must have a sharp entrance (48), so that flow separation occurs within the orifice. The vortices are thought to be conceived in this region of separated flow and escape periodically in the embryo stage, resulting in the toroidal vortex structure of the jet (49), as shown in Fig. 7. The nature of the sound-generating

\* This word is used loosely!

mechanism has yet to be investigated; it seems probable that the flow rate fluctuates in sympathy with the eddy shedding, so giving rise to a "simple source" type of sound generation. When a circular orifice is this, the characteristic frequency is roughly proportional to the exit velocity and inversely proportional to the axial thickness of the orifice (51,52). When it is comparatively thick the frequency is more dependent on the diameter instead of the thickness. But now a very interesting facet emerges; the frequency for a given geometry is not unique, since there is a choice of several frequencies for a given velocity. There are such that if the thickness is altered by one or two times the diametral dimension then the choice of frequencies remains substantially the same. This naturally leads one to contemplate on the eddy structure, in the stagnant region within the orifice, and what controls it. These phenomena range over Reynolds numbers from some hundreds to about 10,000 for various configurations. When the orifice is preceded by a pipe, the situation is analogous in some ways to the edge-tone system supplemented by a resonator. The pipe has its set of resonant frequencies depending upon the geometry, and the formerly continuously varying jet-tone is greatly reinforced at these frequencies, sounding "pipe tones" (53,51). No data appear to be available concerning the efficiency by which jet tones or pipe tones give rise to acoustic energy.

An interesting variation on this scheme is to replace the sharp entrance to the orifice by a carefully designed throat to eliminate flow separation there, but opening out the nozzle exit to cause flow separation from the curved surface. At a Reynolds number of the order of 800,000, regular though turbulent vortex formations were disclosed by Schlieren photographs (54) (one of which is shown in Fig. 8) accompanied by an increase in sound output of up to nearly a hundredfold (55), thus raising it to nearly a hundredth of the jet power. The turbulent jet noise was quite swamped by the latter, which had a discrete frequency of roughly  $0.4 V / l$ . The directional property of this radiation is much more uniform than for turbulent jet noise, and so is suggestive of the vortex formations being associated with a fluctuation of the mass flow, constituting a simple acoustic source. (The simple source effect almost certainly overpowers the dipole effect arising from the momentum fluctuations.) To account for the acoustic power on this basis the mass flow would have to fluctuate by roughly  $1/20$  of the mean value, which seems reasonable. The interesting question is: do the disturbances of the vortex formations control the point of flow separation from the nozzle wall so giving rise to embryo eddies, or can it be that a nozzle



Fig. 7 - The flow of jet-tones. Flow separation occurs within the orifice and the periodic shedding of the vortices with the associated fluctuation in flow results in the characteristic toroidal vortex formations. (From a photograph by W. H. Darlington (50).)



Fig. 8 - Vortex formations at high speed. In this case the separation occurs at the diverging nozzle exit, and the Reynolds number is sufficiently high (800,000) for the flow to be in the turbulent regime except for a narrow "laminar collar." The regular vortices do not have the clear definition of the jet tone flow at low Reynolds numbers. (From A. Powell (54).)

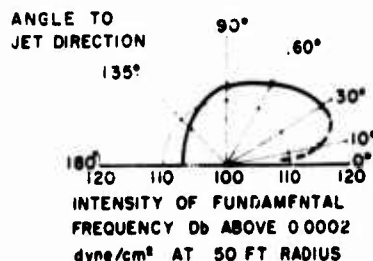


Fig. 9 - Directional distribution of pulse-jet noise. The diagram refers to the radiation at the fundamental frequency. The average value can be calculated by assuming the action to be that of a classical simple source, but the deviations from that average are not easily accounted for. Refraction of the sound seems to occur very close to the jet direction. (Reconstructed from data by A. Powell (54).)

contraction results in convected pressure waves being reflected to a sufficient extent,\* and so yield "resonant" frequencies?

The last variation to be discussed in this section concerns the pulse jet. The periodicity superimposed upon the mean flow is in this case controlled by resonance properties of the combustion chamber and exhaust nozzle; it is maintained by the periodic combustion of fuel, again controlled by the resonance properties. Thus, while the heat supply is variable, and the flow through the engine likewise, the whole process is self-governed and so bears a strong resemblance to "pipe tones." Presumably the fluctuating velocity results in toroidal vortex formations. It is logical therefore to include the pulse jet under the present grouping. The pulsating flow can be looked upon as constituting a simple source (either expression (c) taken over the jet exit, or a source of matter distribution enclosed in the volume in the neighborhood of the exit) and this leads to a good approximation to the acoustic power produced (56,57). While the energy of the fundamental is apparently easily dealt with, the same is not true for the harmonics—and sometimes the acoustic power is very rich in harmonic structure (58,59), presumably because any harmonics of the flow rate would be amplified, relatively, as a consequence of the higher radiative efficiency of higher frequencies. In practice the directional properties are nowhere near as uniform as for the simple source, the levels close to the jet direction exceeding those in the opposite direction by a noticeable amount, as indicated in Fig. 9. In the particular case considered (56), this asymmetry could not be accounted for either by taking into account the pulsations of the intake or the fluctuating thrust (expression (b) in one form or another). This is really not remarkable, since the acoustic approximations, requiring small amplitude fluctuations, can hardly be expected to be very good when the velocity pulsations actually exceed the ambient speed of sound. Perhaps the real question rather concerns why the simple acoustic theory should yield such good results! Two other features are worth noting. Firstly, the levels close to the jet fall very sharply, presumably because of refraction effects; and secondly, it appears that turbulent

\* Sound waves entering a nozzle with the flow certainly undergo a large reflection according to the author's non-dimensional approach. Calculations for the present case are not complete at the time of writing.

mixing may account for an appreciable contribution to the high-frequency end of the noise spectrum. Thus while the dominating feature can be readily accounted for, many details remain for further investigation.

It is interesting that the classical jet tones and edge tones, with or without resonators, being essentially laminar flow phenomena, all appear again in one form or another in turbulent flow regimes. Further, a close analogy with edge tones exists with certain highly supersonic jets, as will be discussed next.

Finally, before turning to high-speed phenomena proper, I would like to pose the following question. Wakes and jets have a great similarity, one often being considered the inverse of the other. Does this similarity extend, in some way or another, to the details of the flow mechanisms governing the vortex production behind bluff bodies and in jets? Again, would the placing of an edge in the vortex street behind a cylinder result in a flow having any similarity to edge tones? This seems a very worthwhile experiment, which I do not think has been done. Finally, is it at all possible that the eddy formations in turbulent jets exert any influence on the creation of embryo disturbances in "ordinary" circumstances? Such questions are very fundamental and their joint study may well yield a more complete understanding than would result from their being treated separately.

#### THE CHOKED JET

When a jet is operated at a sufficiently high pressure ratio, shockwaves exist in the jet stream (unless the nozzle happens to have just the correct amount of divergence). These shockwaves form at more or less regular intervals along the jet in connection with the "cellular" structure of the flow. The phenomenon with which we are now concerned happened to be discovered by optical means (55) for choked (nondivergent) slit-type jets. For these the frequency of the characteristic motion is very steady (60,61), setting in quite suddenly at a pressure somewhat higher than the critical and remaining until pressure ratios of about seven are reached (62).

The direction of the flow leaving the edge of the orifice is governed by the external atmospheric pressure there, and hence by fluctuations of that pressure. Thus eddies in the flow are born, and these grow and their motion along the jet results in sound being generated as they pass through the shockwaves, since the boundary of the jet at these positions moves so as to accommodate the varying flow conditions. If a train of eddies is present, then their spacing can be such that the sound waves arriving at the orifice from the various shockwaves reinforce each other, sometimes having the appearance shown in Fig. 10. Careful measurements of eddy spacing and velocity show that this is in fact the case (60-62). It is interesting



Fig. 10 - Choked-jet noise. The flow is very similar to that for high-speed edge tones; but here the interaction of the eddy formations with the regularly spaced standing shockwaves produces the sound. The jet pressure is considerably higher than the edge-tone case of Fig. 5. (This photograph is by M. G. Davies (62).)

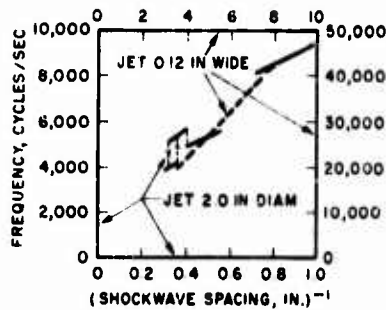


Fig. 11 - Choked jet frequencies. The jumps in frequency arise from a rearrangement of the eddy pattern so that the disturbances propagated from each shock reinforce each other at the orifice. The two-dimensional (slit) jet displays no such discontinuities. (Data reconstructed from A. Powell (61).)

that while most of the fundamental radiation is thus in the upstream direction, the same conditions resulted in the prediction that sound of twice that frequency would have a sharp preference for radiation at approximately right angles to the jet stream and this, happily, was found to be the case (60). The efficiency by which the kinetic energy of the jet stream is converted to acoustic energy is high, being of the order of from a hundredth (61) to a tenth (62)—a very high figure.

For jets having circular orifices, the phenomenon bears a closer analogy to edge tones in that jumps of frequency take place (61) (Fig. 11). While the eddy formation for the slit jet is always of an alternate structure, it appears that just the first stage for the round jet has toroidal vortices (63). It appears to be a fortuitous circumstance that the increase of spacing of the shockwaves with pressure ratio happens to be such that no jumps are present in the case of the slit jet.

There are several reasons why this "screech" may not make an appearance in a supersonic jet. Clearly the absence of shockwaves will guarantee this: a properly designed convergent-divergent nozzle thus will exhibit a limited range over which "screech" is absent (64), while the equalization of pressure at the nozzle by a perforated sleeve achieves the same result over a wider range of pressures (55,65). Like the jet tones of a completely different flow regime, any roughness of the edges of the orifice tends to inhibit the mechanism (55), presumably by thickening the boundary layer and so decreasing the instability of the eddy formation. This of course is suggestive from the point of view of noise-reduction devices (66). Not only does the mechanism display features in common with edge tones, but also the status of research is similar: the essentials of the mechanism are understood, and certain isolated aspects of it are amenable to analysis under simplifying conditions. The frequencies can be found; but the calculation of sound intensity, *ab initio*, is quite beyond our present means.

This characteristic motion appears to be confined to "cold" jets. There are probably two reasons for this. A hot choked jet has a much higher velocity, and this results both in increased stability of the jet boundaries and greatly increased noise due to the inevitable turbulent mixing process, which would also tend to mask any discrete frequency phenomena. Certainly indications so far are that it is not of importance for jet engines (67) or rockets (68). Here the noise from turbulent mixing is all important, and in the next section the question of how much of the experimental data can be explained by theory is dealt with.

### Part III JET FLOWS DISPLAYING NO DISCRETE FREQUENCIES

#### THE TURBULENT JET

In recent years the turbulent jet has received much attention, and this section will be devoted to aspects concerning noise generation in the absence of the discrete

frequency phenomena associated with the periodic vortex formations discussed in the preceding section.

The overall picture of the spread of a turbulent subsonic jet is now well established (69,70). Initially the turbulence springs from the shear layer adjacent to the exit, spreading outwards and inwards at a steady rate. After about four-and-a-half-diameters distance the turbulence reaches the axis, so annihilating the cone of "potential" flow, after which the axial velocity commences to fall in a roughly hyperbolic manner with the distance from the exit. The profiles of mean velocity soon become similar, suggesting profitable techniques of analysis; but unfortunately the turbulence levels do not fall in line until much further downstream, due to the persistence of the high-turbulence levels at positions corresponding to the original high-shear layers. This basic structure of course suggests that intense high-frequency radiation emanates from the region of high turbulence and shear near the exit, the frequency falling in the downstream direction. The intensity would be expected to commence to fall sharply in sympathy with the axial velocity in downstream locations. Indeed, early exploratory experiments (71) indicated just this. The success of similarity ideas on the mixing problem probably encouraged the application to noise generation (72,73); but it is apparent that the proper form of the similarity rules is not yet known to us, despite the theoretical concepts at our disposal, and that existing efforts should be regarded as first attempts.

Perhaps the principal difficulty lies in the fact that it is far from easy to design an experiment to yield the distribution of sound sources (of varying frequency bands) within the volume of the jet. Space, or space-time, correlations can indicate effective regions associated with the areas where the noise leaves the jet boundaries (74). Measurements very close to the jet flow itself (75) mainly concern the very local turbulent fluctuations, so that the connection with the noise sources distributed throughout the volume of turbulence must be regarded as being rather vague, at least until proved otherwise. A method of some promise (in principle at least) seems to be the correlation between points in the turbulent field itself with a point(s) in the acoustic field. (The difficulty, of course, is with Doppler effects, but I imagine this might not be insuperable.) But then one might just as easily (?) measure the correlations required by the general quadrupole theory (7).

The quadrupole theory certainly yields acoustic powers of the right order of magnitude, and it accounts for the gross radiation characteristic of marked asymmetry (10). There are, however, many aspects that are not yet fully understood, and it is upon these I wish to dwell.

The directional properties of the radiation from turbulent jets appear to follow no simple law, although the principal characteristics can be easily stated and accounted for in a general manner. Most of the radiation from jets of low or moderate speed occurs at angles noticeably less than 45 degrees to the jet axis (71,76,55,77), the lower frequency being found closest to the axis, as illustrated in Fig. 12. Theoretical ideas are in accord with this, since both convected lateral quadrupoles associated with the shear layer and convected assemblies of longitudinal quadrupoles associated with regions of weak shear further downstream will display this property. However, additional sources, especially longitudinal quadrupoles normal to the axis, have to be postulated to obtain a satisfactory agreement at all angles (65,76). The possible influence of convection and refraction effects upon the directional properties have not been very seriously considered (2) although there is almost certainly some effect in view of the very noticeable decrease in noise levels as one approaches the jet in positions where the energy of the jet is almost spent.

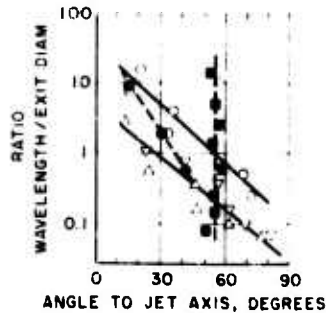


Fig. 12 - Angles for most intense radiation. The radiation of any frequency band (here represented by the ratio of wavelength to jet exit diameter) reaches its maximum intensity at a definite angle from the jet axis. The pair of parallel lines refers to jet engine noise, the dotted one between them to cold air jets. Here, the higher the frequency, the greater will be the angle from the jet axis at which the maximum occurs. Rocket noise, represented by the vertical line, displays its maximum for all frequencies at about the same angle. (Data respectively collected from F. B. Greatrex (57), H. E. von Gierke et al. (77), L. W. Lassiter and H. H. Hubbard (78), and J. N. Cole et al. (68).)

As the eddy convection velocities increase for faster jets, the eddy structure will more and more tend to generate its own system of shockfronts (65,60,10) and this may account for fast jets (i.e., those probably having eddy convection at supersonic speeds) displaying maxima at increasing angles from the axis. A helium jet exhausting at 2600 ft/sec displays the maximum intensity at very nearly 45 degrees to the axis (78), while rockets, having exhaust velocities of upwards of 5000 ft/sec, have maxima, apparently for all frequency bands, at angles between 50 and 60 degrees (68). The main directional properties of these three types of jet are shown in Figs. 12 and 13. If the radiation in these cases is essentially associated with the eddy shocks, then it is implied that the eddies accounting for the major noise contribution have a convection velocity of rather less than half the exit velocity. That does not seem unreasonable.

Another outstanding characteristic of turbulent jet noise is its rapid variation with jet velocity. The quadrupole theory yields the well known similarity form  $\propto V^8$  when the field of quadrupoles is not convected. By some fortuitous circumstance, experimental data produce not only the  $V^8$  but also the  $V^6$ , to a good approximation. However it should really be looked upon as an empirical result, since in accounting for the characteristic directionality the convection effects (10) necessarily supplement the above form by a not at all negligible positive power of Mach number  $V/c$ . Of course any such form should also be supplemented by an unknown function of Reynolds, Mach number, temperature ratio, density ratio, and any other parameter that may have a bearing upon the noise production.

One naturally tends to think of characteristic frequencies of the radiated sound in terms of Strouhal numbers (79,80). One might choose the peak of the spectrum (on an "energy-per-cycle-per-sec" basis) as the characteristic frequency. Although the spectra are rather flat, there is a definite tendency for this peak frequency of the total acoustic power to increase less quickly than the velocity (resulting in a decreasing Strouhal number), as shown in Fig. 14. Most of the energy however is contained by frequencies higher than the true spectral peak, the peak of an octave analysis being more representative of the overall noise produced, since it corresponds roughly to the median of the energy-frequency distribution. On this basis the departure from proportionality is marked, both at individual points (55) (Fig. 15) and for the total sound power (76). The more pronounced effect in the latter cases arises because of the dependency of the spectral shape on the velocity, it being much flatter at low speeds. This is in itself a noteworthy fact and is clearly shown in Figs. 14 and 15. It also raises the question of what is the most significant choice for a "characteristic frequency": the peak of the energy-per-cycle-per-sec spectrum, the peak of the energy-per-octave (or similarly proportional) spectrum, or the frequency corresponding to the median of the energy? A departure from Strouhal concepts also arises in

connection with the directionality of various frequency bands of the noise. The angle of the peak seems to be more dependent upon the ratio of wavelength to exit diameter (2,76), rather than upon Strouhal number.

It has been suggested that there is some possibility that the turbulence is "damped" at high Mach numbers (10), and since presumably the smallest eddies would be most affected, it may affect the shape of the spectrum and so be contributory to the failure of proportionality with Strouhal number. There is some experimental evidence that this may be so (70,81) (at least for rms turbulence levels) although there will remain some doubt until suitable Mach number corrections have been applied (82).

Density and temperature effects of the jet flow itself are still somewhat uncertain. Experiments using different gases (air, helium, and Freon) at essentially the same

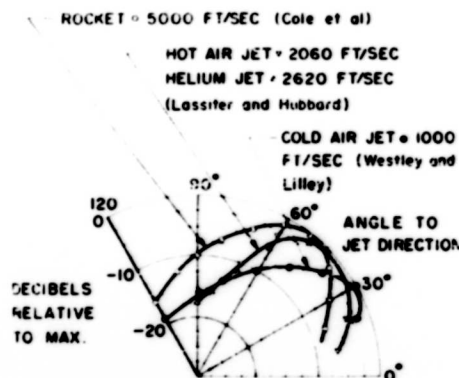


Fig. 13 - Directional characteristics for overall radiation. This plot concerns the directional distribution of the total noise output. As the jet velocity increases, the maximum moves outward from the jet axis. The cold helium jet and the hot air jet have very similar distributions. (Data obtained from the following sources: cold air jet from R. Westley and G. M. Lilley (71), hot jet from L. W. Lassiter and H. Hubbard (84), helium jet from L. W. Lassiter and H. H. Hubbard (78), rocket from J. N. Cole et al. (68).)

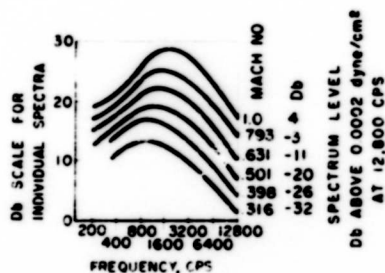


Fig. 14 - Spectrum of jet noise power. Note the change in the shape of the spectrum as the velocity increases. The peak does not shift in frequency proportionally to velocity, so the Strouhal number falls. The spectrum is on an energy-per-cycle basis (constructed from data concerning jet flow from a pipe of appreciable length, published by J. H. Gerrard (74)).

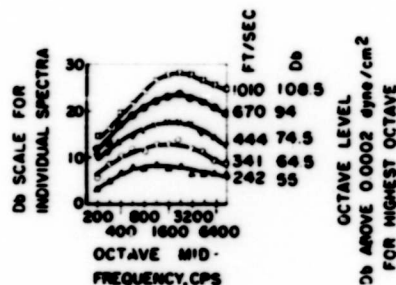


Fig. 15 - Octave spectra at given position. The peak frequency of an octave spectra corresponds roughly to the median of the energy-frequency distribution when the octave spectra display fairly symmetrical peaks. Thus the peak is fairly representative of the overall noise. Its frequency varies only slowly with velocity. The change in spectral shape is marked in this case at 30° to the jet axis and 24 diameters distance from the jet exit. (Constructed from data by A. Powell (85)).



temperature certainly tend to confirm the density factor (of  $\rho^2$ ) arising from the similarity argument, although the only reported measurement (78) concerns positions at right angles to the jet axis (where convection effects would be expected to be least).

Temperature effects have yet to be fully investigated. Early indications that the effect was small (2) seem to be confirmed by recent experiments (78,83). The acoustic power seems to be hardly affected, implying that care should be taken in the interpretation of the  $\rho^2$  factor, for which there is some verification for different gases. Thus the introduction of the molecular weight (to replace jet density) might be expected to yield a useful empirical rule. So far as frequency is concerned it seems to me that the statement of decreasing characteristic Strouhal number with temperature (80) (at a given pressure ratio) is less significant than the fact that the "median-energy" frequency did not change much with velocity. This means that it seems to make little difference whether the velocity increase is due to increasing temperature at a constant pressure ratio, or vice versa. Apparently the effects of reduced gas density are just about offset by increased noise-generating capacity (10). Directional effects, however, have yet to be thoroughly investigated, but again it looks as though jet velocity is more important than temperature, per se, since a helium jet and a hot air jet display similar directional properties at the same speed (84) (Fig. 13).

So far there is hardly any data throwing light on the validity of the  $\rho_0 c_0^5$  of the ambient fluid in the denominator of the similarity form. Ambient temperature and density effects are normally rather small but may have a measurable influence—at least some full-scale measurements suggest that possibility. It would therefore be most interesting to perform an experiment in the atmosphere of another gas, for example helium, (remembering that most microphone techniques give a measure of  $p^2$ , while the acoustic power is connected with  $p^2 \rho_0 c_0$ ).

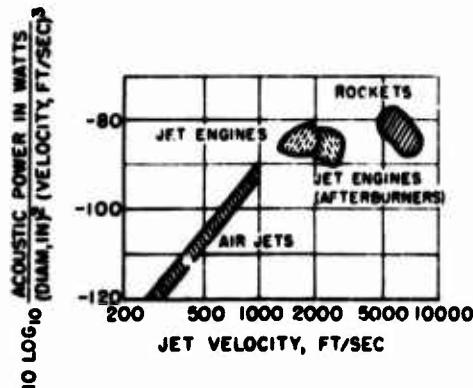


Fig. 16 - Power output and velocity. The rapid increase in noise-producing efficiency for low-speed air jets cannot prevail for very high speeds, otherwise the noise power would become ridiculously high. For cold air jets the efficiency is about  $10^{-4} M^5$  ( $M$  being the exit Mach number) while for rockets it appears to be about one hundredth, far below the extrapolation of the low-speed efficiency. No allowance has been made for the gas density whose effects are yet uncertain. (Data collected from many sources, especially J. N. Cole et al. (68).)

The noise of rocket effluxes is particularly interesting. The low-speed dependency on velocity must be superseded by another form, otherwise the acoustic power would become impossibly large. Presumably the acoustic power is likely to be asymptotic to some fraction of the total power, in contrast to the low-speed case where the conversion to acoustic power depends on about the fifth power of the Mach number. It turns out that this fraction appears to be about a hundredth of the total power (68,86). This is shown in Fig. 16, where a comparison is made with cold air jets, jet engines, and jet engines with afterburners. In view of the foregoing comments concerning temperature effects, no allowance has been made for density variations. The essential characteristic of the rocket efflux is its high absolute velocity. It seems to me that model tests using supersonic cold air jets may be very misleading in relation to rocket-noise because of

the limited velocity, whatever the pressure ratio. For example, the turbulence noise level of an unheated air jet still appears to follow the velocity to about the power of eight, provided the "expanded" velocity is used if the jet is choked (55), up to pressure ratios of thirty (85). There is an indication (86) that the bulk of the noise energy generated by rocket jets emanates from relatively far downstream, possibly where the jet velocity falls from supersonic to subsonic speed (but this is not in accord with the idea that supersonic eddies may be responsible, as discussed earlier). Another interesting feature of rocket noise is that radiations from all the frequency ranges so far measured display the maxima between  $50^\circ$  and  $60^\circ$  to the jet axis.\* (Low-speed jets display a much wider variation (Fig. 12).) Does this imply that the major part of the noise production is by supersonic eddies lying within a comparatively small speed range? What is the nature of the mechanism which limits the fraction of available energy convertible to acoustic energy? (I cannot appreciate the argument that because there is only about 1 percent of the jet power resident in turbulent kinetic form, then this must be a limit to the acoustic power (87). By the same token would it not also be a limit to dissipation?) Close to such jets the pressure amplitudes are great enough to invalidate linear acoustic theory—is this responsible for any gross effect, e.g., by increased dissipation? Another (and possibly associated) feature of interest is that while the spectrum of turbojet engine noise is quite broad, the pressure maxima do not possess a Rayleigh distribution; the highest peaks reach at least four times the rms level (88). This aspect is very important in respect to fatigue troubles; corresponding data for rocket noise is not yet available, but will be of interest from more than one point of view. Knowledge concerning these aspects no doubt will cast light on a curious fact that has been observed (88). While the jet flow, delayed combustion effects, and near-by pressures are greatly affected by upsetting the stream at the nozzle, the noise radiated away is not appreciably altered.

It is interesting to reflect upon the changes that the immersion of a turbulent jet in a moving fluid would effect. Again, similarity arguments (73) come to mind, but, to judge by the limited experimental data available, yield results less satisfactory even than for the static case. There is some evidence that the reductions in the peak and low frequencies are much greater than such arguments suggest (89), although all measurements do not show this (90).

#### THOUGHTS ON JET NOISE REDUCTION

As the biggest financial expenditure on jet noise has been directly aimed at methods for its reduction, it is perhaps appropriate to mention a few major features. Study of some of the results of this work soon convinces one that our understanding of the overall problem is still very sketchy (although partial explanations are invariably forthcoming after any particular experiment!).

Perhaps the most simple variation on the jet having a circular orifice is that having an elliptical orifice. Experiments (91) with a 4:1 exit showed the increase in high-frequency noise in positions along the minor axis. This would be expected, yet the anticipated corresponding reductions along the major axis were absent; low-frequency changes were small but unexpected. Another simple variation concerns a change of the velocity profile at the exit, most easily obtained by using a long pipe prior to the exit (92,93). Here the high frequencies suffer reduction, but the overall reduction is not great. In particular if the jet velocity is increased to restore the thrust to its original value, there is a net increase in noise. There is now a little

\*A recent report (89) casts some doubt on this, reporting maxima between  $30^\circ$  and  $45^\circ$  to the jet axis, but details are not available at the time of writing.

better understanding why this should be so (73,74) (for example, because the most intense part of the spectrum apparently emanates from the region at the end of the potential cone which would be little effected by the reduction of velocity gradients at the exit).

Those faced with the practical problem, not lacking in urgency, have tried numerous ad hoc devices. One might illustrate their diversity by reference just to nozzles having axially corrugated walls (67), a multiplicity of separate jets (94,95), combinations of several rectangular orifices (95), or the combination of the corrugated type with ejectors (97). Of course, for devices to be used in flight the question of net propulsive efficiency (98,99) is very important, and this is an essential factor in their design.

Our understanding of the mechanism by which the noise suppression is obtained is sketchy to say the least, although it has been the subject of much conjecture. The views that follow are by no means entirely original and are quite tentative, but seem (to me at least!) to be the most satisfying and, I hope, do not invite counter arguments of comparable strength. I shall conclude my lecture on this controversial (and challenging?) note.

First, confine attention to those variations of nozzle shape which eject all parts of the jet in a direction essentially parallel to the axis, for example that of Fig. 17.



Fig. 17 - Jet noise-reduction device. There is a wide variety of nozzle designs which are known to give less noise than a simple circular one. They all eject the initial axial momentum in a distributed manner so as to minimize the transverse turbulent diffusion process and encourage induced flow between the high-velocity regions so as to reduce the turbulence levels. This particular nozzle evolved from a logical engineering development (67) and is used for the flight trials of the Douglas DC-8 airliner. (Photograph by courtesy of Douglas Aircraft Co.)

There will be a considerable amount of induced flow between the jet flows from the various segments, greater than in the absence of neighboring segments. The result of this is to reduce the rate of mixing, i.e., the individual potential cores persist longer than they would individually (100); the observed reduction in turbulent velocity fluctuations, and in the frequency (100,101) more than offset the greater volume of turbulence so far as the noise production is concerned, at least according to existing similarity arguments (73). The greatest reduction will occur at frequencies corresponding to the regions where the induced velocity is the most effective: this view is consistent with the selectivity associated with nozzles having various numbers and depths of corrugations around the periphery (67).

This also sheds some light on the noise-reducing action of ejectors. The flow leaving an ejector forms a new, larger, but slower jet of lower noise-producing capacity. The answer to the question of why less noise is made in the ejector than in the corresponding section of a free jet seems to lie at least partly in the fact that the action of the ejector directs the induced flow so as to reduce the total shear of the mixing region, and this is the most important single parameter so far as noise production is concerned.

Another point of view—which does not seem to have attracted previous attention—hinges on the fact that the predominant effect of turbulent mixing is the diffusion of momentum in transverse planes. Is it not reasonable to argue that the noise produced is connected with the amount of diffusion that has to take place? (There is some theoretical backing in this direction, in that the transverse velocity fluctuations are presumably connected with the amount of diffusion, and fluctuations across shear layers serve to amplify the noise output (7).) And all the fancy exit shapes considered do reduce the amount of diffusion, because some momentum is ejected from the exit at greater distances from the axis. While it may be useful to think of these as separate effects, of course they are inseparable in practice. Perhaps the optimum configuration is a nice balance between these two points of view, namely to spread out the initial momentum, yet taking care to lessen the total shear by induced flow.

The addition of a slower moving sheath of air has not proved very effective (102), less effective than some measurements (73) suggest for the flight case of jet engines, even for very moderate aircraft speeds. The reason seems to be that the part of the jet responsible for the peak of the noise spectrum—the most important single region—probably lies rather far from the exit (at the end of the potential cone, or a little farther downstream (73)) and that the outside sheath has already been annihilated. In other words, to be really effective one would expect that the sheath should certainly exceed the jet diameter in thickness—an arrangement the airplane designer is unlikely to welcome, compared, say, to an ejector arrangement.

There is another class of nozzle in which the efflux does not all leave the nozzle parallel to the axis, and which is known to result in diminished noise output. Typical of these is the one in which a parallel pipe has axial slots at the ends, some of the resultant "teeth" or "fingers" being bent inwards, some outwards. The situation here is less easy to see. The jet spreads at a faster rate (103), thus reducing the volume of noise-producing turbulence, but why is it not offset by the presumably higher turbulence levels? Firstly, some efflux is ejected outwards from the axis, and would not this reduce the "work" the turbulence would have to do in achieving the necessary diffusion? Also, may not secondary flows be set up, like vortices with their axes lying along the mean velocity surface of the jet, this rotation being a direct help to the diffusion process, since it would provide a mean flow between regions of high and low velocity and vice-versa? Finally, the effect of the teeth is to corrugate the jet leaving the nozzle: then is not the induced flow argument just as effective in these circumstances? The conjectural nature of the foregoing suggestions is all

apparent—the practical reduction of jet-engine noise is clearly still more an engineering art than science!

I appreciate very much having been invited to undertake the task of preparing the survey I have just presented to you, a task which proved to be both pleasant and revealing (at least to myself!), and I regret only that time did not permit me to include phenomena involving solid boundaries and heat. This also seems an opportune time to express my appreciation to all the many who have helped me in many ways at one time or another and have given me so much encouragement. Of these, Professor E. J. Richards is directly responsible for my interest in the field and he gave me limitless help and encouragement while I worked at the University of Southampton. Since my association with the Douglas Aircraft Company, Mr. M. M. Miller has given me encouragement that I am glad to place on record. A third name is that of Mr. H. B. Irving, lately of the Ministry of Supply who, in his quiet gentlemanly manner, I am sure has achieved much by way of encouraging those, including myself, pursuing noise research in England.

#### REFERENCES

1. Richards, E.J., "Research on Aerodynamic Noise from Jets and Associated Problems," J. Roy. Aero. Soc., 57:319-342 (1953)
2. Powell, Alan, "Survey of Experiments on Jet-Noise," Aircraft Engineering, 26:2 (1954)
3. Fowell, L.R., and Korbacher, G.K., "Review of Aerodynamic Noise," U. of Toronto, Inst. of Aerophysics. U.T.I.A. Review No. 8. 1955
4. Richardson, E.G., "Acoustics in Relation to Aerodynamics," J. Aero. Sci., 22:775-780 (1955)
5. Richards, E.J., "Noise Research in the United Kingdom," Canadian Aero. J., pp. 341-357 (1957)
6. Nyborg, W.L., "Self-maintained Transverse Oscillations of a Jet," Paper delivered at Acoustical Society Meeting, Washington, D. C., May 1958
7. Lighthill, M.J., "On Sound Generated Aerodynamically, Part I-General Theory," Proc. Roy. Soc. A211:564-587 (1952)
8. Curle, N., "The Influence of Solid Boundaries upon Aerodynamic Noise," Proc. Roy. Soc. A231:505-514 (1955)
9. Proudman, I., "Generation of Noise by Isotropic Turbulence," Proc. Roy. Soc. A214:119 (1952)
10. Lighthill, M.J., "On Sound Generated Aerodynamically, Part II-Turbulence as a Source of Sound," Proc. Roy. Soc. A222:1-32 (1954)
11. Meecham, W.C., and Ford, G.W., "Acoustic Radiation from Isotropic Turbulence," J. Acoust. Soc. Am. 30:318-322 (1958)
12. Kraichnan, R.H., "Sound Radiation from High Reynolds Number Turbulence," (abstract) J. Acoust. Soc. Am. 30(No. 7):675-678 (1958)

Theory and Experiment in Aerodynamic Noise

13. Lighthill, M.J., "The Energy Scattered from the Interaction of Turbulence with Sound or Shockwaves," *Proc. Camb. Phil. Soc.* 49:531 (1953)
14. Kovassnay, L.S.G., "Interaction of a Shockwave and Turbulence," 1955 Heat Transfer and Fluid Mechanics Institute, Univ. of Calif., 1955
15. Hollingsworth, M.A., and Richards, E.J., "On the Sound Generated by the Interaction of a Vortex and a Shockwave," *Aero. Research Council Paper* 18257, 1956
16. Ram, G.S., and Ribner, H.S., "The Sound Generated by Interaction of a Single Vortex with a Shockwave," U. of Toronto, Inst. of Aerophysics, U.T.I.A. Report (to be published)
17. Ribner, H.S., "Convection of a Pattern of Vorticity through a Shockwave," *N.A.C.A. Report* 1164, 1954 (formerly T.N. 2864, 1953)
18. Hollingsworth, M.A., and Richards, E.J., "A Schlieren Study of the Interaction between a Vortex and a Shockwave in a Shocktube," *Aero. Research Council Paper* 17985, 1955
19. Burgers, J.M., "On the Transmission of Sound through a Shockwave," *K. Nederland, Akad. v. Wetenschappen*, Vol. 44, 1946
20. Powell, Alan, "A Note on the Sound from Weak Disturbances of a Normal Shockwave," *Aero. Research Council, Current Paper No.* 194, 1955 (to be revised)
21. Kovassnay, L.S.G., "Sound, Vorticity and Entropy," (abstract) *J. Acoust. Soc. Am.* 30(No. 7):689 (1958)
22. Yudin, E.Y., "On the Vortex Sound from Rotating Rods," *N.A.C.A. TM* 1136, 1947
23. Phillips, O.M., "The Intensity of Aeolian Tones," *J. Fluid Mech.* 1:607-624 (1956)
24. Powell, Alan, "Thoughts on Boundary Layer Noise," *Aero. Research Council Paper No.* 16727, 1954
25. Phillips, O.M., "On the Aerodynamic Surface Sound from a Plane Turbulent Boundary Layer," *Proc. Roy. Soc.* A234:327-335 (1956)
26. Phillips, O.M., "Aerodynamic Sound Radiated from a Turbulent Boundary Layer," (abstract) *J. Acoust. Soc. Am.* 30(No. 7):680 (1958)
27. Ribner, H.S., "Boundary Layer-Induced Noise in the Interior of Aircraft," U. of Toronto, Inst. of Aerophysics, U.T.I.A. Report 37, 1956
28. Kraichnan, R.H., "Noise Transmission from Boundary Layer Fluctuations," *J. Acoust. Soc. Am.* 29:65-80 (1957)
29. Corcos, G.M., and Liepmann, H.W., "On the Contribution of Turbulent Boundary Layers to the Noise inside a Fuselage," *N.A.C.A. TM* 1420, 1958
30. Powell, Alan, "On Structural Vibrations Excited by Random Pressures, with Reference to Structural Fatigue and Boundary Layer Noise," *Douglas Aircraft Company Report SM* 22795, 1957

31. Harrison, M., "Correlations and Spectra of Pressure Fluctuations on the Wall Adjacent to a Turbulent Boundary Layer," (abstract only) *J. Acoust. Soc. Am.* 29:1252 (1957)
32. Willmarth, W.W., "Space-time Correlations of the Fluctuating Wall Pressure in a Turbulent Boundary Layer," *J. Aero. Sci.* 25:335-336 (1958)
33. Trilling, L., "On Thermally Induced Sound Fields," Office of Scientific Research Tech. Note 55-47, 1954
34. Andrade, E.N. da C., "The Sensitive Flame," *Proc. Phys. Soc.* 53:329 (1941)
35. Brown, G.B., "On Vortex Motion in Gaseous Jets and the Origin of their Sensitivity to Sound," *Proc. Phys. Soc.* 47:703 (1935)
36. Brown, G.B., "The Mechanism of Edge-tone Production," *Proc. Phys. Soc.* 49:508 (1937)
37. Curie, N., "The Mechanics of Edge-tones," *Proc. Phys. Soc.* A216:412-424 (1953)
38. Powell, Alan, "On Edge-tones and Associated Phenomena," *Acustica*, 3:233 (1953)
39. Lenihan, J.M.A., and Richardson, E.G., "Observations on Edge-tones," *Phil. Mag.* 29:400-406 (1940)
40. Brown, G.B., "On the Vortex Motion Causing Edge-tones," *Proc. Phys. Soc.* 49:493 (1937)
41. Richardson, E.G., "Edge Tones," *Proc. Phys. Soc.* 43:394-404 (1931)
42. Nyborg, W.L., Burkhard, M.D., and Schilling, H.K., "Acoustical Characteristics of Jet-Edge and Jet-Edge-Resonator Systems," *J. Acoust. Soc. Am.* 24:293-304 (1952)
43. Garber, D.L., "The Effect of External Sound on the Vortex Shedding from Cylinders," *J. Aero. Sci.* 25(No. 4):275-276 (1958)
44. Bouyoucos, J.V., and Nyborg, W.L., "Oscillations of the Jet in a Jet-Edge System, II," *J. Acoust. Soc. Am.* 26(No. 4):511-514 (1954)
45. Nyborg, W.L., "Self-Maintained Oscillations of the Jet in a Jet-Edge System," *J. Acoust. Soc. Am.* 26(No. 2):174-182 (1954)
46. Nyborg, W.L., Woodbridge, C.L., and Schilling, H.K., "Characteristics of Jet-Edge-Resonator Whistles," *J. Acoust. Soc. Am.* 25:138-146 (1953)
47. Mercer, D.M.A., "The Voicing of Organ Flue Pipes," *J. Acoust. Soc. Am.* 23:45-54 (1951)
48. Anderson, A.B.C., "Metastable Jet-Tone States of Jets from Sharp-Edged Circular, Pipe-Like Orifices," *J. Acoust. Soc. Am.* 27(No. 1):13-21 (1955)
49. Anderson, A.B.C., "Vortex-Ring Structure-Transition in a Jet Emitting Discrete Acoustic Frequencies," *J. Acoust. Soc. Am.* 28(No. 5):914-921 (1956)

50. Darlington, W.H., "Air Jets for Use in Gas Turbine Combustion Chambers," University of London, Ph.D. Thesis, 1949
51. Anderson, A.B.C., "A Circular -Orifice Number Describing Dependency of Primary Pfeifenton Frequency on Differential Pressure, Gas Density and Orifice Geometry," J. Acoust. Soc. Am. 25(No. 4):626-631 (1953)
52. Anderson, A.B.C., "A Jet Tone Orifice Number for Orifices of Small Thickness-Diameter Ratio," J. Acoust. Soc. Am. 26(No. 1):21-25 (1954)
53. Anderson, A.B.C., "Dependence of Pfeifenton (Pipe Tone) Frequencies on Pipe Length, Orifice Diameter and Gas Discharge Pressure," J. Acoust. Soc. Am. 24(No. 6):675-681 (1952)
54. Powell, Alan, "Noise of Jets," University of Southampton, Ph.D. Thesis, 1953
55. Powell, Alan, "A Schlieren Study of Small Scale Air Jets, and Some Noise Measurements on Two-inch Diameter Jets," Aero. Research Council Paper 14726, 1951
56. Powell, Alan, "The Noise of a Pulse Jet," J. Helicopter Ass'n of Great Britain, 7:32 (1953)
57. Lassiter, L.W., "Noise from Intermittent Jet Engines, and Steady Flow Engines with Rough Burning," N.A.C.A. TN 2756, 1952
58. Veneklasen, P.S., "Noise Characteristics of Pulsejet Engines," J. Acoust. Soc. Am. 25:380-383 (1953)
59. Oleson, S.K., and Ingard, V., "Acoustical Characteristics of Model Pulsed Jets," J. Acoust. Soc. Am. 20(No. 10):1145-1146 (1957)
60. Powell, Alan, "On the Noise Emanating from a Two-dimensional Jet above the Critical Pressure," Aero. Quarterly, 4:103 (1953)
61. Powell, Alan, "On the Mechanism of Choked Jet Noise," Proc. Phys. Soc. B66:1039 (1953)
62. Davies, M.G., "Acoustic Radiation of Discrete Frequency from a Choked Rectangular Jet," Aero. Research Council Paper 19016, 1957
63. Lassiter, L.W., and Hubbard, H.H., "The Near Noise Field of Static Jets and Some Model Studies of Devices for Noise Reduction," N.A.C.A. TN 3187, 1954
64. Franklin, R.E., "Noise Measurements of Cold Jets using Convergent-Divergent Nozzles," Aero. Quart., 8:346-359 (1957)
65. Lilley, G.M., "Aerodynamic Noise Work at the College of Aeronautics," Proc. International Congress on Theoretical and Applied Mechanics, Istanbul, 1952
66. Powell, Alan, "The Reduction of Choked Jet Noise," Proc. Phys. Soc. B67:313 (1954)
67. Greatrex, F.B., "Jet Noise," Fifth International Aero. Conference, I.A.S. Preprint 559, 1955



68. Cole, J.N., von Gierke, H.E., Kyrakis, D.T., Eldred, K.M., and Humphrey, A.J., "Noise Radiation from Fourteen Types of Rockets in the 1000 to 130,000 Pounds Thrust-Range," W.A.D.C. Tech. Report 57-354, 1957
69. Corrsin, S., "Investigation of Flow in an Axially Symmetrical Heated Jet of Air," N.A.C.A. ACR 3L23 (also Wartime Report W-94), 1943
70. Laurence, J.C., "Intensity, Scale and Spectra of Turbulence in Mixing Region of Free Subsonic Jet," N.A.C.A. Report 1292, 1956 (supersedes TN3561 and TN3576)
71. Westley, R., and Lilley, G.M., "Investigations of the Noise Field from a Small Jet, and Methods for its Reduction," College of Aeronautics, Cranfield, Report 53, 1952
72. Ribner, H.S., "On the Strength Distribution of Sources along a Jet," U. of Toronto, Inst. of Aerophysics, U.T.I.A. Report 61, 1958
73. Powell, Alan, "Similarity Considerations of Noise Production from Turbulent Jets, both Static and Moving," Douglas Aircraft Co. Report SM 23246, 1958
74. Richards, E.J., Private communication concerning work in progress at the University of Southampton
75. Dyer, Ira, "Distribution of Sound Sources in a Jet Stream," (abstract) J. Acoust. Soc. Am. 30(No. 7):676 (1958)
76. Gerrard, J.H., "An Investigation of the Noise Produced by a Subsonic Air Jet," J. Aero. Sci., 23(No. 9):855-866 (1956)
77. von Gierke, H.E., Parrack, H.O., Gannon, W.J., and Hanson, R.G., "Noise Field of a Turbojet Engine," J. Acoust. Soc. Am. 24:169 (1952) (correction 25:369 (1953))
78. Lassiter, L.W., and Hubbard, H.H., "Experimental Studies from Subsonic Jets in Still Air," N.A.C.A. TN 2757, 1952
79. Coles, W.D., and Callaghan, E.E., "Investigation of Far Noise Field of Jets: II Comparison of Air Jets and Jet Engines," N.A.C.A. TN 3591, 1956
80. Rollin, V.G., "Effect of Temperature on Jet Noise Generation," N.A.C.A. TN4217, 1958
81. Lassiter, L.W., "Turbulence in Small Air Jets at Exit Velocities up to 705 feet per Second," J. Appl. Mech. 24:349-354 (1957)
82. Morkovin, M.V., Comments upon the above paper by L.W. Lassiter, J. Appl. Mech., Vol. 25, pp. 314-315, 1958
83. Tyler, J.M., and Perry, E.C., "Jet Noise," Pratt & Whitney Aircraft Report, PWA Inst. 451, 1954
84. Lassiter, L.W., and Hubbard, H.H., "Some Results of Experiments Relating to the Generation of Noise in Jets," J. Acoust. Soc. Am. 27:431-437 (1955)
85. Mull, H.R., and Erickson, J.C., "Survey of the Acoustic Near Field of Three Nozzles at a Pressure Ratio of 30," N.A.C.A. TN 3978, 1957

Theory and Experiment in Aerodynamic Noise

86. Mayes, W.H., "Some Near- and Far-Field Noise Measurements for Rocket-Engine Operating at Different Nozzle Pressure Ratios," (abstract) J. Acoust. Soc. Am. 30(No. 7):694 (1958)
87. Westervelt, P.J., Dyer, I., and Franken, P.A., "Changes in Jet Noise by Mixing, and an Upper Limit on Jet Noise Production," (abstract) J. Acoust. Soc. Am. 29(No. 6):778 (1957)
88. Kamps, E.C., "Statistical Evaluation of Near Field Sound Pressures Generated by Exhaust of a High Performance Jet Engine," (abstract) J. Acoust. Soc. Am. 30(No. 7):692 (1958)
89. Douglas Aircraft Company, Unpublished data
90. von Gierke, H.E., Private communication concerning work in progress at Wright Air Development Center
91. Powell, Alan, "A Comparison between the Noise from Jets having 4:1 Elliptic and Circular Orifices," J. Acoust. Soc. Am. 30(No. 7):642-643 (1958) (formerly Aero. Research Council Paper 18123, 1956)
92. Powell, Alan, "The Influence of the Exit Velocity Profile on the Noise of a Jet," Aero. Quarterly, 4:341 (1954)
93. Waterhouse, R.V., and Berendt, R.D., "Reverberation Chamber Study of the Sound Output of Subsonic Air Jets," J. Acoust. Soc. Am. 30:114-121 (1958)
94. Howell, H.H., "Summary Progress Report on Jet Noise Suppression," Boeing Airplane Co. Report, February 1957
95. Tyler, J.M., and Towle, G.B., "A Jet Exhaust Silencer," Pratt and Whitney Aircraft Report, PWA Inst. 469
96. Coles, W.D., and Callaghan, E.E., "Full Scale Investigation of Several Jet Engine Noise Reduction Nozzles," N.A.C.A. TN 3974, 1957
97. Douglas Aircraft Company, Unpublished data
98. Ciepluch, C.C., North, W.J., Coles, W.D., and Antl, R.J., "Acoustic, Thrust and Drag Characteristics of Several Full Scale Noise Suppressors for Turbojet Engines," N.A.C.A. 4261, 1958
99. North, W.J., "Transonic Drag of Several Jet-noise Suppressors," N.A.C.A. TN 4269, 1958
100. Laurence, J.C., and Benninghoff, J.M., "Turbulence Measurements in Multiple Interfering Air Jets," N.A.C.A. TN 4029, 1957
101. Coreos, A.M., "Some Measurements Bearing on the Principles of Jet Silencing Devices," Douglas Aircraft Co. Report SM-23114, 1958
102. Lees, R., and Smith, E.B., "Experimental Investigation of Noise Radiated by Concentric Jets," General Electric Co., Report R 57 AGT 381, 1957
103. Dryburgh, W.W., "Noise Tests on an Avon R.A.7 Engine on the Open Air Test Bed - 1st Report," Rolls Royce Report Gtx/WWD:1 JB., Jan. 1, 1954

A. Powell

## DISCUSSION

R. H. Kraichnan (New York University)

I'd like to say a few words about why the maximum frequency doesn't seem to go up with Mach number as fast as one might expect. I have done some work recently on predicting quantitatively the amount of noise from isotropic turbulence, which is a very idealized approach to the jet problem but it does seem to indicate some qualitative features. One of the results is that at high Reynolds numbers the radiation is principally at high frequencies coming from small eddies and, in fact, the spectrum at high frequencies falls off inversely with frequency.

The radiated power is proportional to the rate of dissipation of power in the jet itself, and to the fifth power of the Mach number. For Mach numbers of the order of unity the acoustic damping of the turbulence becomes very strong. This indicates a strong coupling between the acoustical and vortical modes at high frequencies. In the region of appreciable Mach numbers, because of the strong damping at the relatively high frequencies, one would expect that these frequencies could no longer increase in power and, therefore, that the maximum in the acoustic radiation curve would not go up as fast.

This doesn't solve Lighthill's paradox in a neat form because it doesn't answer why one begins and ends with the eighth power law. Aside from any specific investigation for nonlinear phenomena, one would certainly expect things not to increase as fast, so certainly the power law is going to drop off.

There is a slight increase in efficiency if the Reynolds number is separated from Mach number dependence. This increase would give a decrease in the power law. The turbulence itself is damped.

We will accept the experimental evidence. I have no competence to do otherwise, and I would like to point out what seems to be the great danger in all of this. The theoretical explanations are very simple and it is not too difficult to find a theoretical effect which agrees with any given experimental effect. Whether you are happy in doing this depends on how strongly you want to support a particular theory.

A. Regier (National Advisory Committee for Aeronautics)

In our earlier experiments we soon became aware of the fact that the frequency in the far field did not increase as rapidly as the velocity. However, in the near field we found that both the turbulence in the jet and the pressures close to the jet did agree nicely with the velocity increase. I wondered if Dr. Kraichnan or Dr. Powell would accept this as an experimental fact and explain it, or is there anything further to be said on that, whether the near field does follow the velocity but the far field does not?

E. Mollo-Christensen (California Institute of Technology)

From the dimensional analysis in the near field I think there is no doubt that things should scale with velocity, but in the far field one has radiation and there feels something quite different. In the far field, as I show in my paper, we find that certain

frequency ranges scale with velocity very precisely. We also find in other parts of the far field that we do have scaling with the velocity of sound, suggesting an acoustic mechanism of sound radiation. There are apparently two mechanisms involved. This is speculation now, but it agrees with our experimental results.

I think that one can get more out of narrow band measurements. The measurements to which Mr. Regier refers are octave-band measurements on the decibel scale.

J. H. Gerrard (University of Manchester)

I should like to comment on Dr. Powell's question, "would the placing of an edge in the vortex street behind a cylinder result in a flow analogous to edge tones?"

Edge tones have been produced by placing a circular cylinder in a jet. One might expect the similarity suggested by Powell to be detected, therefore, when two cylinders were placed one behind the other in an air flow. I have made some exploratory observations of the pressure fluctuations on the surface of a one-inch-diameter cylinder when a second cylinder was placed parallel to it a short distance, 2 in. to 6 in., upstream and downstream (also to port and starboard). Increased amplitude of pressure fluctuation at the surface corresponds to increased Aeolian tone intensity radiated from that cylinder. If the flow assumed the character of an edge tone one would expect: (a) the surface pressure fluctuation would increase when a second cylinder was placed upstream or downstream, and (b) the character of the fluctuation would change from that characteristic of Aeolian tones to the pure-tone form associated with edge tones. No change in intensity was detected when the second cylinder was interposed in the fore or aft position. When, however, the cylinders were separated across the stream the signal intensity increased about twofold. In neither case did the appearance of the signal change from that of a narrow band of noise. The Reynolds number of this experiment was about  $5 \times 10^4$ .

\* \* \* \* \*

# A THEORY OF TURBULENCE DYNAMICS

Robert H. Kraichnan

*Institute of Mathematical Sciences  
New York University*

## 1. INTRODUCTION

A fundamental difficulty in the development of the theory of noise produced by turbulence has been the absence of a satisfactory quantitative theory of turbulence itself. This lack is the more serious because the prediction of acoustic phenomena associated with turbulent flows requires a considerably more intimate knowledge of the structure of the velocity fluctuations than is contained in the energy spectrum function, or two-point velocity correlation, whose determination has been the principal concern of pure turbulence theory.

The purpose of the present paper is to survey the foundations of an approach to turbulence dynamics which holds some promise of yielding useful approximations to the pressure field associated with certain classes of flows - those which display substantial homogeneity in at least one direction in space. Parts of this theory have been published recently (1-3), and other aspects, including the extension to acoustic phenomena, will be treated in future papers. The discussion here necessarily will be largely qualitative. The intention is only to describe the basic dynamical concepts which characterize the theory, particularly those which have elements of novelty. Consequently, the treatment will be confined entirely to the simplest case, isotropic turbulence of a completely incompressible fluid, and acoustic phenomena will not be considered.

## 2. THE STATISTICAL EQUATIONS OF MOTION

Let us consider an incompressible fluid in a state of isotropic turbulence within a large domain of side  $L$ . If we analyze the velocity field  $u_i(\mathbf{x}, t)$  within the domain by a Fourier series expansion

$$u_i(\mathbf{x}, t) = \sum_{\mathbf{k}} u_i(\mathbf{k}, t) e^{i\mathbf{k} \cdot \mathbf{x}}, \quad (2.1)$$

where the summation is over all wave vectors allowed by the boundary conditions, equations of motion for the Fourier coefficients can be deduced from the Navier-Stokes equation. In this way we find (4)

$$\left( \frac{\partial}{\partial t} + \nu k^2 \right) u_i(\mathbf{k}, t) = -i \sum_{\mathbf{k}' + \mathbf{k} = \mathbf{k}} u_j(\mathbf{k}', t) u_j(\mathbf{k}, t). \quad (2.2)$$

NOTE: This work has received support from the Office of Naval Research under Contract N(0001)-285(53).

where  $\nu$  is the kinematic viscosity and

$$P_{ij}(\mathbf{k}) = -\nu k_i k_j P_{ij}(\mathbf{k}). \quad (2.3)$$

The first term of  $P_{ij}(\mathbf{k})$  serves to include the Reynolds stresses, and the second term, the pressure. We shall regard the  $u_i(\mathbf{k}, t)$  as the fundamental dynamic variables of the flow system.\*

In discussing turbulence we do not seek an exact description of the exceedingly complicated velocity field but rather the average values of physically interesting functions of the field. The averages can be defined in several ways. We shall adopt here the most customary procedure, in which the averages, to be denoted by  $\langle \dots \rangle$ , are taken over a suitable representative ensemble of individual flows (4). The statistical quantity of greatest interest is the second-order covariance tensor  $\langle u_i(\mathbf{k}, t) u_j^*(\mathbf{k}, t') \rangle$ . It can be shown as a consequence of isotropy that this tensor must have the form

$$(L/2\pi)^3 \langle u_i(\mathbf{k}, t) u_j^*(\mathbf{k}, t') \rangle = \frac{1}{2} P_{ij}(\mathbf{k}) U(k; t, t'), \quad (2.4)$$

where the scalar  $U$  is real, does not depend on the direction of  $\mathbf{k}$ , and is a symmetric function of  $t$  and  $t'$  (Refs. 4,5). The normalization by  $(L/2\pi)^3$  is done so that, in the limit  $L \rightarrow \infty$ , when the spacing of the allowed  $\mathbf{k}$  vectors becomes infinitely close, the mean energy per unit mass is given by

$$\frac{1}{2} \sum_{\mathbf{k}} \langle u_i(\mathbf{k}, t) u_i^*(\mathbf{k}, t) \rangle \rightarrow \int_0^\infty E(k, t) dk, \quad (2.5)$$

where

$$E(k, t) = 2\pi k^2 U(k; t, t). \quad (2.6)$$

is the energy spectrum function, as usually defined.†

We shall also define the function

$$r(k; t, t') = \frac{2\pi k^2 U(k; t, t')}{[E(k, t) E(k, t')]^{1/2}}, \quad (2.7)$$

which satisfies  $r(k; t, t) = 1$  and measures the phase correlation between the amplitudes of a Fourier mode at times  $t$  and  $t'$ .

From Eq. (2.2) we may obtain the statistical equation of motion

$$\left( \frac{\partial}{\partial t} + \nu k^2 \right) U(k; t, t') = S(k; t, t'), \quad (2.8)$$

\*In the following, we frequently shall write  $u_i(\mathbf{k})$  instead of  $u_i(\mathbf{k}, t)$  when it is not desired to specify a particular value of the time argument. The same procedure will be followed with other time-dependent quantities also.

†The particular normalization chosen is appropriate to cyclic boundary conditions on the domain. Other usual boundary conditions require minor changes in the definitions.

where

$$S(k, t, t') = (1/2) \sum_{\mathbf{k} + \mathbf{k}' = \mathbf{k}} u_i(\mathbf{k}, t) u_{ij}(\mathbf{k}', t) u_j^*(\mathbf{k}, t') \quad (2.9)$$

Because of the symmetry of  $u_{ij}(k, t)$  in  $i$  and  $j$ , the similar equation of motion involving  $U(k, t, t')$  is redundant with Eq. (2.8). For  $t = t'$ , we find that Eq. (2.8) reduces to

$$\left( \frac{1}{t} + 2\nu k^2 \right) T(k, t) = F(k, t), \quad (2.10)$$

where

$$T(k, t) = 4^{-1} S(k, t, t) \quad (2.11)$$

is the energy transfer function as usually defined (4). Equation (2.10) expresses the conservation of energy. It exhibits the opposing contributions of viscous dissipation  $2\nu k^2 T(k, t)$  and net energy input from interaction with other modes.

Equation (2.10), or Eq. (2.8), cannot be solved directly for  $T(k, t)$ , or  $U(k, t, t')$ , because of the presence of the third-order moments on the right sides. Equations of motion for the third-order moments can be obtained by multiplying Eq. (2.2) with suitable bilinear expressions and averaging, but as a consequence of the nonlinearity these equations contain fourth-order moments. One does not obtain a closed set of equations for moments of any given orders simply by multiplying Eq. (2.2) with various functions and averaging.

Several theories of turbulence have been based on making Eq. (2.10) determinate by assuming an expression for the triple moment  $T(k, t)$  in terms of  $F(k, t)$ , obtained usually from some simple analogy for the energy-transfer process together with dimensional considerations. The best-studied example is the eddy-viscosity theory of Heisenberg (6). Other theories have been based on the assumption that fourth-order moments have the same expression in terms of second-order moments as they would have if the velocity field were normally distributed. In this way a closed set of equations can be obtained which involve only the second- and third-order moments. Examples of this type include the second theory of Heisenberg (6) and the theory of Proudman and Reid (7).

The approach to be outlined in the present paper is not based on direct surmises about the relations of various moments. Instead, it involves a well-defined approximation on the dynamical processes by which statistical interdependence of the Fourier modes is produced. The closed equations thus obtained turn out to represent the exact behavior of a model system whose dynamical structure is related to that of the actual system. Thereby it can be inferred that the theory obeys important consistency conditions. In formulating this approach it is necessary to consider not only the moments describing the actual statistical state of the system, such as  $U(k, t, t')$  and  $S(k, t, t')$ , but also functions which give the average response of the system to small perturbations. The latter functions embody essential additional aspects of the dynamical behavior.

Let us suppose that at time  $t = 0$  the amplitude of mode  $\mathbf{k}$ , but of no other mode, is suddenly increased an arbitrary infinitesimal amount  $u_i(\mathbf{k}, 0)$  by some impulsive force. The subsequent history of this perturbation in amplitude - the infinitesimal impulse response - will be very complicated, in general, because of the interaction

of mode  $\mathbf{k}$  with all the other modes. However, if the response is averaged over the isotropic statistical distribution of the unperturbed amplitudes, we may expect it to become a much simpler function. Therefore we introduce the average impulse-response function  $\phi(\mathbf{k}, \mathbf{t}, \mathbf{t}')$  defined for  $\mathbf{t} > \mathbf{t}'$  by

$$u_i(\mathbf{k}, \mathbf{t}) = u_i(\mathbf{k}, \mathbf{t}') + \phi(\mathbf{k}, \mathbf{t}, \mathbf{t}'). \quad (2.12)$$

Note that the averaging implied is only over the unperturbed state, not over the prescribed initial perturbation  $u_i(\mathbf{k}, \mathbf{t}')$ . The response indicated by Eq. (2.12) is proportional to the initial amplitude jump, despite the nonlinearity of the system, because we are considering only infinitesimal perturbations. In the following, we shall usually call  $\phi(\mathbf{k}, \mathbf{t}, \mathbf{t}')$  simply the response function.

By using Eq. (2.2), an equation of motion for  $\phi(\mathbf{k}, \mathbf{t}, \mathbf{t}')$  analogous to Eq. (2.8) may be obtained. As in Eq. (2.8), the right side of this equation contains higher-order averages than the left, thereby giving rise to similar difficulties. In the present case, the higher averages involve the cross-response of other modes  $\mathbf{k}'$  to the initial applied jump in the amplitude of mode  $\mathbf{k}$ ; they are connected with the contribution to the decay of this jump due to spreading of its energy to the other modes. An additional contribution arises, of course, from the viscous dissipation in mode  $\mathbf{k}$ .

### 3. THE STRUCTURE OF THE INTERACTION

The nonlinear interaction described by Eq. (2.2) is quite complex: each mode interacts with every other mode. However, the total interaction may be considered the resultant of very many elementary interactions of simple structure, each of which involves just three Fourier modes. When  $\mathbf{k} = \mathbf{p} + \mathbf{q}$ , we shall define the elementary interaction of three modes  $\mathbf{k}$ ,  $\mathbf{p}$ , and  $\mathbf{q}$  by the terms

$$\begin{aligned} & i(k_p p_{ij}(\mathbf{k}) u_j(\mathbf{p}) u_m(\mathbf{q}) + u_j(\mathbf{q}) u_m(\mathbf{p})) \\ & - i(p_m p_{ij}(\mathbf{p}) u_j(\mathbf{q}) u_m(\mathbf{k}) + u_j(\mathbf{k}) u_m(\mathbf{q})) \\ & - i(q_m p_{ij}(\mathbf{q}) u_j(\mathbf{k}) u_m(\mathbf{p}) + u_j(\mathbf{p}) u_m(\mathbf{k})) \end{aligned} \quad (3.1)$$

in the equations of motion of the form (Eq. (2.2)) for  $u_i(\mathbf{k})$ ,  $u_i(\mathbf{p})$ , and  $u_i(\mathbf{q})$  respectively. We may represent this elementary interaction by the diagram of Fig. 1.

Fig. 1 - Diagram of the elementary interaction among modes  $\mathbf{k}$ ,  $\mathbf{p}$ , and  $\mathbf{q}$

It follows from the reality of the velocity field that  $u_i(-\mathbf{k}) = u_i^*(\mathbf{k})$ . Therefore we shall consider the mode  $\mathbf{k}$  to be represented by the amplitude  $u_i(-\mathbf{k})$  as well as  $u_i(\mathbf{k})$ , and we shall include in the definition of elementary interaction the conjugate terms to (3.1) which appear in the equations of motion for  $u_i(-\mathbf{k})$ ,  $u_i(-\mathbf{p})$ , and  $u_i(-\mathbf{q})$ . It is clear in general that elementary interactions exist only for mode triads whose wave vectors can form a triangle.

The Reynolds stresses and pressure are conservative, so that the nonlinear interaction serves only to distribute the energy among the modes without overall gain or loss. The aptness of the concept of elementary interactions is enhanced by the fact, verifiable from Eq. (2.2), that each elementary interaction is individually conservative: the sum of the energy transfers to modes  $\mathbf{k}$ ,  $\mathbf{p}$ , and  $\mathbf{q}$  arising from the terms (3.1) is zero. Thus the whole process of energy transport may be considered the sum of elemental transfers associated with the individual interactions.



The total process is very complicated. Transfer from modes  $k$  and  $p$  to mode  $q$  may take place not only through the elementary interaction which directly links these modes (Fig. 1) but also through networks of elementary interactions, involving intermediate modes, which can branch out to extreme complexity (Fig. 2). The branching is a graphical expression of the nonlinearity of the equations of motion.

Fortunately, the complexity associated with the multiplicity of transfer paths is compensated by a related feature: each elementary interaction actually represents a very weak dynamical coupling among the modes involved - provided the domain containing the turbulence is very large. Let us consider what happens as the limit  $l \rightarrow \infty$  is approached. The number-density in wave vector space of the modes allowed by the boundary conditions increases as  $l^3$ . Consequently, the number of terms contributing to the right side of Eq. (2.2) in any wave vector range increases as  $l^3$ . In the limit, each individual term, representing a

single elementary interaction, makes only an infinitesimal contribution to the motion of the mode  $k$ . This implies that in the limit the effective dynamical coupling among any three individual modes  $k$ ,  $p$ , and  $q$  due to the elementary interaction which directly links them (Fig. 1) becomes infinitesimal in strength. The same conclusion is suggested if one takes the terms in the first line of (3.1), which contribute to the motion of  $u(k)$ , and regard them as giving a coupling between the pair of modes  $k$  and  $p$  with the amplitude  $u(q)$  acting as a modulating factor. As  $l \rightarrow \infty$ , the energy-per-unit-mass is spread over an infinitely increasing number of individual modes. Thus the rms value of the amplitude  $u(q)$  becomes infinitesimal, and so does the strength of the pair coupling.

It is not difficult to verify, by keeping account of the orders-of-magnitude of relevant quantities as  $l \rightarrow \infty$ , that the weakness of dynamical coupling among any triad of modes is still valid when all the possible paths of coupling involving many elementary interactions and intermediate modes (Fig. 2) are taken into account. In fact, the weakness of the total coupling of any three modes is actually a dynamical requirement for the consistency of our underlying assumption of statistical homogeneity. As  $l \rightarrow \infty$ , homogeneity implies that the phase relations among individual Fourier amplitudes become increasingly random,\* and this would not be possible if strong dynamic couplings persisted among individual modes. It is extremely important to keep in mind here that these weak couplings do not become negligible as the limit is approached. As they become weaker, there become more of them because there are more allowed modes. Similarly, as the statistical dependencies which they induce among individual modes become weaker, there are more individual cross-moments to be added up in the Fourier sums which represent measurable averages. Indeed, the essential problem of turbulence theory may be considered the evaluation of these cross-moments.

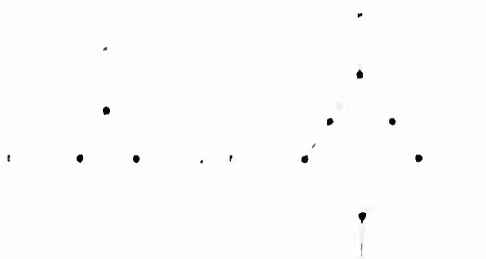


Fig. 2 - Examples of complex interaction networks linking modes  $k$ ,  $p$ , and  $q$ . The unlabelled lines denote modes other than  $k$ ,  $p$ , and  $q$ .

\*See Batchelor (Ref. 4, Section 2.5)

## 4. THE DIRECT-INTERACTION APPROXIMATION

Let us consider the case where at an initial time  $t_0$  the Fourier amplitudes are all statistically independent and the state of the system is specified by the initial spectrum  $F(k, t_0)$ . This represents a very considerable idealization of any actual flow, as does our previous assumption of isotropy. However, this initial condition is an especially simple and useful one for studying how the nonlinear interaction induces statistical interdependence of the modes at later times.

We are particularly interested in finding the triple moment

$$u_i(\mathbf{p}, t) u_m(\mathbf{q}, t) u_i^*(\mathbf{k}, t) \quad (\mathbf{k} = \mathbf{p} + \mathbf{q}), \quad (4.1)$$

which contributes to  $S(k, t, t')$ . The most obvious way in which the nonlinear interaction can induce a nonvanishing value for this moment is through the elementary interaction which directly links the three modes involved (Fig. 1). We would also expect the value of the moment to be affected by the more complicated paths of dynamical coupling involving networks of other elementary interactions, and intermediate modes. The distinction just made suggests breaking up the moment into the sum of direct and indirect contributions defined below.

Let us remove from the equations of motion of the system the terms (3.1) representing the single elementary interaction directly linking modes  $\mathbf{k}$ ,  $\mathbf{p}$ , and  $\mathbf{q}$ ; but let us leave unaltered all the other nonlinear terms, which express the elementary interactions among the rest of the modes and those between  $\mathbf{k}$ ,  $\mathbf{p}$ ,  $\mathbf{q}$  and the rest of the modes. We shall call the value of the moment (4.1) induced by these altered equations of motion the indirect contribution. The direct contribution will be defined as the difference between the true value of the moment (with all elementary interactions retained) and the indirect contribution. Thus the direct contribution represents the part of the moment which is induced by the direct elementary interaction acting against the background of all the other elementary interactions.

The approximation fundamental to the present theory is to neglect the indirect contribution to the triple moment. We shall call this the direct-interaction approximation. The dynamical picture underlying it is the following. The elementary interaction directly linking modes  $\mathbf{k}$ ,  $\mathbf{p}$ , and  $\mathbf{q}$  induces an increment in the amplitude of each of these three modes which bears a phase relation to the product of the amplitudes of the other two modes. Thus it yields a contribution to the triple moment. However, this interaction does not take place in isolation. Each of the three modes is coupled to the rest of the system. As a result of this coupling, the induced increments do not simply continue to build up. A relaxation process takes place whereby the energy of the increments is distributed, or mixed, by the overall interaction into many other modes. At the same time, an additional relaxation is caused by the action of viscosity. Thus we have the picture of phase relations among  $u(\mathbf{k})$ ,  $u(\mathbf{p})$ ,  $u(\mathbf{q})$  being continually induced by the direct coupling of the three modes and continually broken down by relaxation effects associated with the dynamical interaction as a whole.

Now neglecting the indirect contribution to (4.1) amounts to assuming that the effect of the overall interaction - without the direct interaction - consists entirely of the relaxation process just described. Thus we are ignoring any induction of phase correlation by networks of elementary interactions which can couple modes  $\mathbf{k}$ ,  $\mathbf{p}$ , and  $\mathbf{q}$  only through the agency of intermediate modes. Examples of such networks are shown in Fig. 3. It will be noticed that in the diagrams shown each intermediate mode (represented by a line without a free end) is involved in two elementary

interactions. This has the effect of eliminating from the associated contribution to (4.1) any dependence on the (random) phases of the amplitudes of the intermediate modes.\*

The only justification for the direct-interaction approximation which we can cite at the present point is the wholly intuitive argument that in view of the complexity of the dynamical system the round-about paths of interaction among three modes should be much less effective in inducing definite mutual phase relations than the direct coupling. Later, we shall see that the approximation exhibits important self-consistency properties which strongly indicate its dynamic naturalness and that it actually represents the exact dynamics of a certain model system.

Approximations similar to that described for (4.1) can be defined for moments of fourth and higher orders. We shall not deal with them in the present paper.

It is not very difficult to obtain an exact analytical expression for the direct contribution to (4.1). According to definition, this contribution may be constructed by introducing the elementary interaction of Fig. 1 as a perturbation on the equations of motion. Although this single interaction is expected to induce the principal contribution to the triple moment, it is clear from the discussion in the previous Section that actually it can represent only an infinitesimal perturbation of the motion of each of the three modes involved, in the limit  $L \rightarrow \infty$ .<sup>†</sup> Thus we can express its effects in terms of the response of the modes  $k$ ,  $p$ , and  $q$  to arbitrary infinitesimal disturbances. Then we may average the result over the statistical distribution, taking account of the weakness of the total dynamic coupling and consequent statistical interdependence among the three modes in the limit. After summing the results over  $p$  and  $q$ , we arrive at the following exact expression (3) for the direct contribution to  $S(k, t, t')$ :

$$S(k, t, t') = -ik \iint_{\Lambda} p q d p d q \left\{ \int_{t_0}^{t'} a(k, p, q) g(k, t', s) U(p, t, s) U(q, t, s) ds + \int_{t_0}^t b(k, p, q) a(p, t, s) U(k, t', s) U(q, t, s) ds \right\} \quad (4.2)$$

In this equation the summation over  $p$  and  $q$  has been replaced in the limit by an equivalent integration. The symbols  $k$ ,  $p$ , and  $q$  denote wave numbers, and the

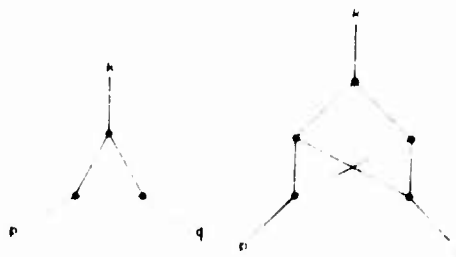


Fig. 3 - Examples of contributing classes of interaction networks which are neglected in the direct-interaction approximation for the triple moment Eq. (4.1)

\*The diagrams in Fig. 2 depict examples of more general networks in which some intermediate modes enter only once. Because of the random phases of the intermediate modes, it can be shown, without approximation, that such networks give a vanishing contribution to (4.1) when they are summed over all possible choices of intermediate modes in the limit  $L \rightarrow \infty$ .

<sup>†</sup>These two properties are consistent since the moment (4.1) represents in toto only an infinitesimal phase correlation among the three modes when  $L \rightarrow \infty$ .

integration is over the entire domain (denoted by  $\Delta$ ) such that  $l, p$ , and  $q$  can form the legs of a triangle. The quantities  $a(l, p, q)$  and  $b(l, p, q)$  are geometrical factors which depend on the shape, but not the size, of this triangle. They are given by

$$a(l, p, q) = \frac{1}{2} (1 + \cos \alpha + 2\cos^2 \alpha/2) \quad (4.3)$$

$$b(l, p, q) = \frac{1}{2} (1 + \cos \alpha + \cos^2 \alpha/2)$$

where  $\cos \alpha, \cos \beta, \cos \gamma$  are the cosines of the interior angles opposite the legs  $l, p, q$  respectively. They obey the identities

$$\begin{aligned} a(l, p, q) &= a(p, q, l) \\ a(l, p, q) &= a(l, q, p) \end{aligned} \quad (4.4)$$

$$l^2 b(l, p, q) = p^2 b(p, l, q)$$

$$b(l, p, q) + b(l, q, p) = 2a(l, p, q)$$

which, as we shall indicate a little later, express important dynamical properties.

In order to facilitate the physical interpretation of Eq. (4.2), let us specialize to  $\tau = \tau_1$ . Then we find for the transfer function defined by Eq. (2.11),

$$T(k, s) = 4^{-2/3} \iint_{\Delta} \rho(k, p, q) \int_0^\infty a(l, p, q) u(k, t, s) U(p, t, s) U(q, t, s) \quad (4.5)$$

$$b(l, p, q) u(p, t, s) U(l, t, s) U(q, t, s) dt.$$

The structure exhibited by Eq. (4.5) may be interpreted rather directly. The  $u$  functions on the right express the decay of infinitesimal perturbations (here associated with the direct interaction) under the influence of viscosity and the overall nonlinear coupling. Let us write each  $U$  factor in Eq. (4.5) in the form

$$U(k, t, s) = (2^{-2/3})^{1/2} \tilde{u}(k, t, s) \tilde{v}(k, t) \tilde{v}(k, s)^{1/2}. \quad (4.6)$$

Now the  $\tilde{v}$  functions express the loss of phase autocorrelation in the mode amplitudes under the overall interaction. Thus the appearance of these  $\tilde{v}$  and  $\tilde{u}$  functions embodies the dynamical relaxation effects discussed above.

It will be noted that the right side of Eq. (4.5) is the integral of the difference between two terms. The term containing  $a(k, p, q)$  involves the response function for the mode  $k$ . As this would suggest, it arises from the induction by the direct interaction of an increment in  $u(k)$  having a phase relation with the product of the amplitudes of modes  $p$  and  $q$ . Similarly, the term containing  $b(k, p, q)$  involves  $u(p, t, s)$  and arises from the induction of an increment in  $u(p)$  phased with the product of the amplitudes of modes  $k$  and  $q$ . (Note that we may exchange the roles of  $p$  and  $q$  simply by a change of integration variables.)

Since both the  $\tilde{v}$  and  $\tilde{u}$  functions express the relaxation effects associated with the overall interaction, we may anticipate that they are either non-negative or have only unimportant negative regions. Now from the first of identities (4.4) we see that  $a(l, p, q)$  is non-negative, and the last of these relations suggests (correctly, it

turns out) that  $\beta(k, p, q)$  is typically positive. Thus, the term in Eq. (4.5) containing  $\beta(k, p, q)$  plays the role of an absorption term, which always represents a positive flow of energy to mode  $k$ , while the term containing  $\beta(q, p, k)$  acts as an emission term. Using Eq. (4.6) we find that the absorption term contains the factors

$$F(k, t) F(p, s)^{-1/2} F(q, t) F(q, s)^{-1/2}$$

but does not contain  $F(k, s)$ . In contrast, the emission term contains the factors

$$F(k, t) F(k, s)^{-1/2} F(p, t) F(p, s)^{-1/2}$$

and thus is linearly proportional to  $F(k, s)$ . Consequently, the stronger the excitation in mode  $k$ , the more the relative flow out of this mode into modes  $p$  and  $q$ . Conversely, the stronger the excitation in modes  $p$  and  $q$ , the more the relative flow from them to mode  $k$ . It appears that the transfer function (4.5) describes a plausible tendency for the kinetic energy in the various wavenumbers to seek some equilibrium through the agency of the nonlinear interaction.

By inserting Eq. (4.2) in Eq. (2.8) we obtain an equation of motion for  $V(k; t, t')$  which involves only the functions  $g$  and  $V$ . In order to have a complete system we should obtain a similar equation of motion for  $g(k; t, t')$  by a consistent extension of the direct-interaction approximation. This can be done (3) without great difficulty, and the result is

$$\left(\frac{\partial}{\partial t} + \nu k^2\right) g(k; t, t') = -\frac{1}{2} \iint p dp q \beta(k, p, q) \int_0^t g(p; t, s) g(q; s, t') V(q; t, s) ds. \quad (4.7)$$

It will be noticed that in contrast to Eq. (4.2) the right side here is bilinear in the response functions and linear in the covariance scalars. It is possible to give a simple dynamical interpretation of Eq. (4.7) which parallels closely the actual derivation.

We can break up the relaxation process described by  $g(k; t, t')$  into two parts, conceptually. First, an initial perturbation in mode  $k$  will induce increments in the amplitudes of other modes  $p$ . For each mode  $p$  the magnitude of this increment will be proportional to the amplitude of a third mode  $q$  which acts as a modulating factor. Second, there will be a reaction on mode  $k$ . The increment induced in the amplitude of mode  $p$  will in turn induce a counter-increment in mode  $k$ , again proportional to the amplitude of the third mode  $q$ . The counter-increment will on the average be out of phase with the original perturbation in mode  $k$  and thus represent a drain of the perturbation energy out of mode  $k$ . This process is represented diagrammatically in Fig. 4. The arrows indicate the "signal path" from mode  $k$  to mode  $p$  and back to mode  $k$ .

Turning to Eq. (4.7) and writing out  $V(q; t, s)$  as an explicit covariance according to Eq. (2.4), we may interpret the factors in the time-integral as follows. If the amplitude of mode  $k$  is perturbed an infinitesimal amount at time  $t'$  then  $g(k; s, t')$  represents the average fraction of this perturbation which remains at time  $s$ . Together with the amplitude factor in  $V(q; t, s)$  which has argument  $s$ , it represents the perturbing force applied to mode  $p$  at time  $s$ .

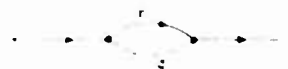


Fig. 4 - Diagram for the direct-interaction contribution to the response function  $g(k; t, t')$

\*We use  $F(k)$  to denote the spectrum function when it is not desired to specify the value of the time argument.

through the elementary interaction directly linking modes  $k$ ,  $p$ , and  $q$ . This force integrated with the response function  $\chi(p; t, s)$  gives the increment induced in mode  $p$  at time  $t$ . This increment, together with the remaining amplitude factor in  $\chi(q; t, s)$  (argument  $t$ ), represents the perturbing force reacting at time  $t$  to produce a counter-increment in mode  $k$ .

The approximation made in obtaining Eq. (4.7) is the neglect of classes of longer paths of action and reaction on mode  $k$  which involve successive transfers of excitation along chains of modes instead of to single modes  $p$ . Typical neglected contributions are shown in Fig. 5. Here again,

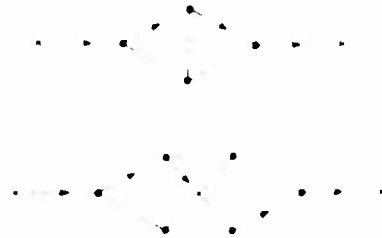


Fig. 5 - Examples of contributing processes neglected in the direct-interaction approximation for  $\chi(k; t, t_0)$ .

the arrows trace the "signal path" from mode  $k$  back to mode  $k$ . It should be noted that even in Eq. (4.7) the interaction of modes  $k$ ,  $p$ , and  $q$  with all the rest of the modes is implicitly taken into account to the extent of the relaxation effects included in the  $\chi$  and  $\chi'$  functions on the right. As in Eq. (4.2), we treat the effects of the direct interaction not in isolation but against the background of the rest of the interaction.

If we append to Eqs. (2.8), (4.2), and (4.7) the boundary condition

$$\chi(k; t, t_0) = 1, \quad (4.8)$$

which according to the definition of  $\chi(k; t, t_0)$  must hold for all  $t$ , we have a complete set

of equations which should determine the response and correlation functions once the initial values  $\chi(k; t_0, t_0) = 2 \cdot k^2 U(k; t_0, t_0)$  are prescribed.

## 5. REPRESENTATION BY A MODEL SYSTEM

Before asking how accurate a picture of turbulence the direct-interaction approximation represents, we have to inquire whether our approximate integro-differential equations lead to any physically meaningful solution at all. This is by no means an academic question. If an arbitrary approximate expression is assumed for  $S(k; t, t_0)$ , it is not to be expected that the solution of Eq. (2.8) will be the covariance scalar of a possible random process or that it will go to zero in a physically sensible fashion as  $|t - t_0| \rightarrow \infty$ . Furthermore, an arbitrary approximation will not preserve the conservation properties of the interaction discussed in Section 3. These observations reflect the general fact that usually we cannot make approximations within a differential or integro-differential equation and obtain a solution which displays the same asymptotic and integral properties as the solution of the exact equation.

It can be seen in a rather simple fashion that the direct-interaction approximation does actually satisfy the consistency requirements we have mentioned. This can be shown by demonstrating that Eqs. (4.2) and (4.7) are obeyed exactly by a model system in which the coupling of the Fourier modes is altered from that in the real system but the conservation properties of the interaction are preserved. The comparison of this model system with the actual system gives an insight into the real meaning and the domain of validity of our approximation.

For example,  $\chi(k; t, t_0)$  might turn out to have a frequency spectrum which is negative for some frequencies, thereby implying a negative power spectrum for  $u_1(k, t)$ .

Let us consider instead of Eq. (2.2) the more general equation of motion for  $u_i(\mathbf{k}, t)$

$$\left(\frac{d}{dt} + k^2\right) u_i(\mathbf{k}, t) = -ik_n E_{ij}(\mathbf{k}) \sum_{\mathbf{k}' + \mathbf{k} = \mathbf{k}} C(\mathbf{k}, \mathbf{k}', \mathbf{k}) u_j(\mathbf{k}', t) u_n(\mathbf{k}, t), \quad (5.1)$$

where the coefficient  $C(\mathbf{k}, \mathbf{k}', \mathbf{k})$  is real, symmetric in  $\mathbf{k}$ ,  $\mathbf{k}'$ , and  $\mathbf{k}$ , and invariant under replacement of any of these three vector arguments by its negative. With this change, Eq. (2.8) requires that Eq. (2.9) be replaced by the new definition

$$S(k, t, t') = (1/2) k_n \sum_{\mathbf{k}', \mathbf{k} = \mathbf{k}} C(\mathbf{k}, \mathbf{k}', \mathbf{k}) u_j(\mathbf{k}', t) u_n(\mathbf{k}, t) u_i^*(\mathbf{k}, t'). \quad (5.2)$$

It is clear from the symmetry properties of the  $C$ 's that all the terms (2.1), representing the elementary interaction linking modes  $\mathbf{k}$ ,  $\mathbf{p}$ , and  $\mathbf{q}$ , are multiplied by the same factor  $C(\mathbf{k}, \mathbf{p}, \mathbf{q})$ . From this it follows that the individual conservation property of the elementary interaction is unaltered by the generalization.

Our actual fluid system is represented, of course, by  $C(\mathbf{k}, \mathbf{p}, \mathbf{q}) = 1$  for all  $\mathbf{k}$ ,  $\mathbf{p}$ , and  $\mathbf{q}$ . Let us consider instead the new system obtained by letting  $C(\mathbf{k}, \mathbf{p}, \mathbf{q})$  take the value  $+1$  or  $-1$  entirely at random (subject to the symmetry conditions above) when  $\mathbf{k}$ ,  $\mathbf{p}$ , and  $\mathbf{q}$  range over the various values allowed by the boundary conditions on our large volume of side  $L$ . For this system all the elementary interactions have the same strength as in the original system, but the relative sign of the coefficients of any two (or more) elementary interactions is entirely random.

If one now goes through the direct-interaction approximation for the new system, it is not hard to verify that as a result of the multiplication of (3.1) by  $C(\mathbf{k}, \mathbf{p}, \mathbf{q})$ , the expression (in the limit  $L \rightarrow \infty$ ) for the triple moment (4.1) in terms of  $\phi$  and  $\psi$  functions is multiplied by this same factor. Since  $C(\mathbf{k}, \mathbf{p}, \mathbf{q})^2 = 1$ , it follows that  $S(k, t, t')$ , as defined by Eq. (5.2), is still given by the expression (4.2). Consequently, the equation of motion for  $\psi(k, t, t')$  is identical for the original and the new systems in the direct-interaction approximation. Similarly, it can be verified that the equation of motion for  $\phi(k, t, t')$  is given by Eq. (4.7) for both new and old systems. (This can be inferred from the double appearance of the direct elementary interaction in Fig. 4.) Thus, the direct-interaction approximation yields identical  $\phi(k, t, t')$  and  $\psi(k, t, t')$  for the new system and the old.

Now let us consider the indirect contributions, neglected by our approximation. Referring to Figs. 3 and 5 we note that the indirect contributions necessarily involve several distinct elementary interactions. For the new system the coefficients associated with these interactions are quite randomly related in sign. It is not very hard to see that when one sums over all possible sets of participating interactions the consequence is a random cancellation of the contributions from different sets. In the limit  $L \rightarrow \infty$ , it can be shown that this results in complete suppression of the indirect contributions to  $\psi(k, t, t')$  and the equation of motion for  $\psi(k, t, t')$ . This means that for the new system, Eqs. (2.8), (4.2), and (4.7) actually constitute exact equations of motion for  $\phi(k, t, t')$  and  $\psi(k, t, t')$ . We may infer from this the consistency of the direct-interaction approximation in the respects mentioned previously.

1. The representation of the coefficient  $C(\mathbf{k}, \mathbf{p}, \mathbf{q})$  as a sum of two terms as in the new representation in Eq. (4.1) is not essential to the argument.

The direct-interaction approximation appears to be the simplest dynamical approximation which embodies the consistency properties in question - that is, realizability of  $\langle U(t), U(t) \rangle$  as a covariance scalar, proper asymptotic behavior, and detailed energy conservation. Higher approximations with these properties can be constructed also (3). The next such approximation involves obtaining an approximate expression for fourth-order moments in terms of third-order moments, second-order moments, and higher response functions and using it to close off the set of moment equations. Like the direct-interaction approximation, this leads to integro-differential equations which are exact for a modified system. Now, however, the modified system bears a closer resemblance to the actual system in that the proper sign relations between different elementary interactions are taken approximately into account. There appear to be a well-defined sequence of successively higher approximations which exactly describe model systems embodying more and more accurately the dynamical structure of the actual system. The higher approximations provide, in principle, a means of estimating the errors associated with the direct-interaction approximation, but they promise severe mathematical difficulties.

The fact that the direct-interaction approximation gives an exact description of our model system suggests the nature of the inaccuracies it generates. As we have noted before, the model system preserves the strengths of all the elementary interactions of mode triads but loses completely the correlation in sign between the coefficients of different elementary interactions. It seems plausible that the mean energy transfer among the modes should depend principally on the relative excitation of the various modes and on the strengths of the interactions which link them. Thus we might expect that it should be fairly well described by the direct-interaction approximation. This surmise is supported by the reasonableness of the dynamical interpretation we have been able to give for the transfer function Eq. (4.5). Some further support is given by the application of the theory discussed in the next Section.

Now, however, let us turn to the question of the detailed structure of the turbulence in coordinate space. The evolution of the flow can be partially described as due to the convection, stretching, and twisting of the velocity field by itself. These phenomena seem fairly simple intuitively, but they involve, in essential fashion, the algebraic summation of contributions from all the elementary interactions linking the Fourier components of any given "eddy structure." In the model system, consequently, they become scrambled beyond recognition with regard to appearance in coordinate space. This suggests that the direct-interaction approximation should give increasingly poor results when extended to the evaluation of successively higher-order moments, sensitive to the precise spatial form of the velocity structures.

## 6. THE INERTIAL-AND DISSIPATION RANGES AT HIGH REYNOLDS NUMBERS

Some characteristics and limitations of the direct-interaction approximation may be illustrated by consideration of the inertial and dissipation ranges at very high Reynolds numbers. Let the rms turbulent velocity in any direction be  $v_0$ , and let the rate of dissipation by viscosity per unit mass be  $\epsilon$ . Then, a wavenumber characterizing the energy-containing range of the turbulence is given (3,4) by

$$k_0 \sim v_0 / \epsilon^{1/3} \quad (6.1a)$$

and a Reynolds number for this range by

$$R_0 \sim v_0 k_0^{-1} \epsilon^{-1/3} \quad (6.1b)$$



When  $v_0^{1/3} \gg 1$ , the integro-differential equations of the direct-interaction approximation simplify greatly for high wavenumbers. Using them, it is found (3) that the inertial range and the range of principal energy dissipation involve wavenumbers  $k$  satisfying the inequalities

$$v_0^{1/3} \ll k \ll v_0^{2/3}. \quad (6.2)$$

Also, it is found that the transfer of energy is local in wavenumber space, there being no appreciable direct transfer from the energy-containing range to the wavenumbers satisfying Eq. (6.2).

The characteristic times for modes satisfying Eq. (6.2) are very short compared to the decay time of the turbulence. This has the consequence that  $\phi(k; t, t')$  and  $r(k; t, t')$  may be considered explicit functions of only the difference time  $t - t'$ . The solution of the system Eqs. (2.8), (4.2), and (4.7) in this range then gives the result (3)

$$\phi(k; t, t') = r(k; t, t') = \frac{J_1(2v_0 k(t - t'))}{v_0 k(t - t')}. \quad (6.3)$$

(It must be remembered here that  $\phi(k; t, t')$  is defined only for  $t \geq t'$ .) Thus the characteristic time for mode  $k$  is the order of  $1/v_0 k$ , the time associated with the convection of a structure of this wavenumber by an rms velocity component. The transfer function in the range (6.2) reduces to the form (3)

$$T(k) = k \iint d\mathbf{p} d\mathbf{q} k^2 \phi(k, \mathbf{p}, \mathbf{q}) F(\mathbf{p}) + \mathbf{p}^2 \phi(k, \mathbf{p}, \mathbf{q}) F(\mathbf{q}) = F(q) = (k, \mathbf{p}, \mathbf{q}) \frac{d\mathbf{p} d\mathbf{q}}{p^3}. \quad (6.4)$$

where

$$(k, \mathbf{p}, \mathbf{q}) = \int_0^\infty \frac{J_1(2v_0 ks)}{v_0 ks} - \frac{J_1(2v_0 ps)}{v_0 ps} - \frac{J_1(2v_0 qs)}{v_0 qs} ds = \frac{(1 - 2)^{1/2}}{v_0(k^2 + p^2 + q^2)^{1/2}}. \quad (6.5)$$

We have suppressed the time-dependence of  $T$  and  $F$  in Eq. (6.4), since this variation is slow compared to the characteristic times of the modes involved.

The quantity  $(k, \mathbf{p}, \mathbf{q})$  has the dimensions of a time. In view of our previous discussion of the direct-interaction approximation, we may interpret  $(k, \mathbf{p}, \mathbf{q})$  as the effective time during which the direct elementary interaction of modes  $k$ ,  $p$ , and  $q$  can build up phase relations before they are wiped out by the relaxation due to the overall nonlinear interaction, to put it very crudely. In the present case the relaxation evidently is dominated by the action of the energy-containing range, as demonstrated by the factor  $v_0$  in Eq. (6.5). Thus, in the direct-interaction approximation the energy-containing region exerts an influence on the rate at which energy is transferred within the high-wavenumber region, even though there is negligible direct transfer from the energy-containing region to the high wavenumbers.

The inertial-range spectrum law in the direct-interaction approximation is easily found from the form of Eq. (6.4) and the fact that the energy-transfer turns out to be local in wavenumber space. It is apparent from Eq. (6.4) that the rate at which energy is transferred by each elementary interaction involves the spectrum function bilinearly and the velocity  $v_0$  inversely. Since the transfer is local, the rate

at which energy passes from below to above the wavenumber  $k$  can depend only on the spectrum function in the neighborhood of  $k$ . Thus,

$$\epsilon = \frac{k^3}{v_0} [F(k)]^2, \quad (6.6)$$

where the factor  $k^3$  makes the dimensions of both sides the same, and may be deduced from Eq. (6.4). Inverting Eq. (6.6) we have the spectrum law

$$F(k) = \text{const. } (\epsilon v_0)^{1/2} k^{-3/2}. \quad (6.7)$$

This law is corroborated and a value obtained for the constant of proportionality by a detailed treatment of Eq. (6.4) in Ref. (3).

It is well-known (4) that according to the Kolmogorov theory the spectrum in the inertial range is given not by Eq. (6.7) but by

$$v_i(k) = \epsilon^{1/3} k^{-5/3}. \quad (6.8)$$

The origin of the discrepancy lies in the different roles played by the energy-containing modes in the two cases. Under the direct-interaction approximation, the action of these modes on the high wavenumbers may be described as follows. They induce a rapid (characteristic time  $\sim 1/v_0 k$ ) exchange of energy among very many modes in the neighborhood of a given high  $k$  whose wave vectors differ by the order of  $k_0$ . Although these high-lying modes have nearly the same wave vectors, their phases are effectively almost randomly related (see Section 3). Therefore the energy-mixing results in a relaxing of the phase relations, essential for mean energy-transfer, among individual triads consisting of one of the modes in the neighborhood and modes  $p, q$  in other neighborhoods.

In the Kolmogorov theory, on the other hand, the energy-containing modes have only a trivial convective effect on high  $k$  modes and do not directly influence the dynamics in the high  $k$  range. On this basis, the energy-containing range should not contribute to the relaxation of energy-transferring phase relations among modes  $k, p$ , and  $q$ . In fact, if in the expression (6.5) for  $\langle k, p, q \rangle$  we replace  $v_0$  by, say,  $\langle v^2 \rangle^{1/2} \sim \epsilon^{1/3} k^{-5/3}$ , which may be considered the rms velocity associated with wavenumbers the order of  $k$  only, it may be seen that the modified Eq. (6.4) thereby obtained leads to the Kolmogorov law Eq. (6.8).

It does not seem very easy to decide which of the two inertial range laws is asymptotically correct for infinite  $Re$ , or, for that matter, whether either of them is. The argument basic to the Kolmogorov theory - that the energy-range has only a trivial convective effect on high wavenumbers - is open to some doubt. This is because high Reynolds number turbulence tends to display sharp shear fronts (4) which contribute significantly to the high  $k$  spectrum, and across which the jump in velocity can be an appreciable fraction of  $v_0$ . It does not clear how to separate the low and high wavenumbers in such regions in a physically satisfying fashion. On the other hand, if the Kolmogorov theory is correct, it is not a surprise that the direct-interaction approximation fails to reproduce it. The convection, with only small distortion, of a small-scale velocity structure by a large-scale structure is not a very elementary process in 3-space. It involves in essential fashion the fact that the coefficients of many elementary interactions linking low wavenumbers with pairs of high wavenumbers are nearly the same. Consequently, as indicated by the discussion in Section 5, the convection process is badly reproduced in the model system which the direct-interaction approximation describes.

The really surprising fact, perhaps, is that the very different dynamical pictures called for by the Kolmogorov theory and the direct-interaction approximation lead to asymptotic laws which are nearly the same. This appears to support the surmise made in the last Section that so far as energy equilibrium is concerned it does not make much difference how the elementary interactions are phased. One might expect, moreover, that the accuracy of the direct-interaction approximation very likely improves at wavenumbers below the inertial range, where convection-without-appreciable-distortion clearly does not occur in any event.

The experimental evidence is not much help in choosing between the two inertial range laws. An analysis (3) of one of the most careful high-Reynolds-number laboratory experiments (8) seems slightly to favor the  $k^{-5/3}$  law, but not much can be made of this. The Reynolds number ( $Re = 4000$ ) is not really high enough to be sure that asymptotic behavior was observed, and there are large deviations from isotropy and homogeneity. What seems a better way to check the direct-interaction approximation is to compare measured and calculated values of the absolute spectrum level in the inertial range. This may provide a meaningful test of the usefulness of the approximation even at Reynolds numbers still too low to discriminate the difference in the power law.

#### REFERENCES

1. Kraichnan, R.H., Phys. Rev. 109:1407 (1958); errata: 111:1747 (1958)
2. Kraichnan, R.H., Phys. Fluids 1:358 (1958)
3. Kraichnan, R.H., J. Fluid Mech. 5:497 (1959)
4. Batchelor, G.K., "The Theory of Homogeneous Turbulence," Cambridge University Press, 1953
5. Meecham, W.C., Phys. Fluids 1:408 (1958)
6. Heisenberg, W., Z. Physik 124:628 (1948)
7. Proudman, I., and Reid, W.H., Phil. Trans. Roy. Soc. (London) A, 247:163 (1954)
8. Laufer, J., N.A.C.A. Report 1174, 1954

. . . . .

#### DISCUSSION

L. S. G. Kovasznay (Johns Hopkins University)

I make my comment here as an experimentalist in turbulence research. I want to reassure those who are startled by the difference between an exponent of  $-5/3$  and  $-3/2$  that, percentage-wise, this is not very great (most of you are familiar with turbulence spectra—drawing on Vu-Graph). In a logarithmic plot of power spectrum versus wave number one always obtains a gently "drooping" curve. Any power law

R. H. Kraichnan

is given by a straight line, whose slope is the exponent, while a measured spectrum always looks slightly curved. One may, therefore, always draw a tangent representing a particular power law. So, I believe, for a long time to come the dispute will not be decided by experimental evidence alone.

\* \* \* \* \*

# SOME EXPERIMENTAL AND THEORETICAL RESULTS RELATING TO THE PRODUCTION OF NOISE BY TURBULENCE AND THE SCATTERING OF SOUND BY TURBULENCE OR SINGLE VORTICES

Ernst-August Müller

*Max-Planck-Institut für Strömungsforschung,  
Göttingen*

## EXPERIMENTS WITH REDUCING VALVES

In the piping system of steam power plants, reducing valves (see Fig. 1) are often installed to control the flow rate of the steam and to reduce the steam from a high pressure to a lower pressure under certain operating conditions of the plant. In many cases the flow rate of the steam and the pressure difference are large; for example, a maximum flow rate of 200 tons per hour may have to be reduced from 150 atm at the high pressure side of the valve (left) to 20 or 30 atm at the low pressure side (right). The physical process of pressure reduction consists in the conversion of kinetic energy, which is produced by the valve in its smallest cross section, to heat by turbulent mixing in the region R, a process in which the enthalpies (per unit of mass) before and after the valve are approximately equal because the losses by heat-conduction and heat- and sound-radiation are small. In the above example, the energy being converted per second is of an order of magnitude of 10 MW (megawatts), but sometimes it is even higher (up to 100 MW). Of course, turbulent mixing at such a high power produces noise in the vicinity of the valve of a strength which often lies beyond the threshold of pain. In addition, strong vibrations of the valve and the piping system are caused which lead to vibration breakages of screws, welds, etc. (1) and thereby threaten the safety of operation. In Fig. 2 one sees a typical broad noise spectrum with some dangerous high peaks which obviously are due to resonance phenomena.

Because of these difficulties, an association of power plant operators asked the Max-Planck-Institut für Strömungsforschung to design valves which would work reliably even if the flow rates, the pressures and the temperatures increase more and more, as seems to be the general trend today. At first, model experiments were



Fig. 1 - Schematic diagram of a typical reducing valve. S seat, C cone, s.C. smallest cross section, R mixing region.

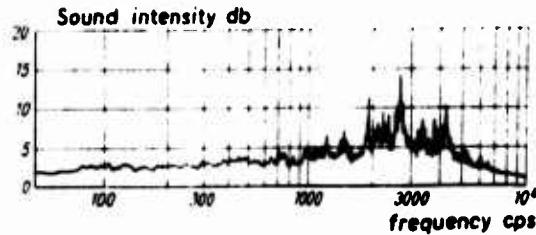


Fig. 2 - Sound intensity in the vicinity of a reducing valve (with arbitrary reference intensity)

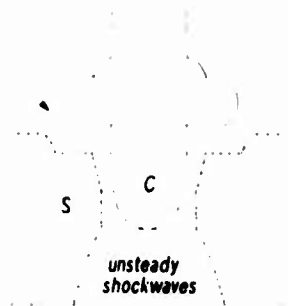


Fig. 3 - Unsteady shock waves at cone and seat of the valve

made with air with a pressure reduction from 4 to 1 atm. Attention was focused on two regions of the valve:

1. The surroundings of the valve cone and the valve seat (Fig. 3). Here the flow is supersonic; unsteady shock waves occur and cause vibrations, especially of the valve cone, and, thus, of the whole reducing valve.
2. The mixing region R (see Fig. 1) and its shape.

The vibrations were measured in the following way (Fig. 4): Different valve cones C (Fig. 4b) and different bottoms B (Fig. 4c) were fixed on thin iron plates. The plate with the bottom could be mounted at a variable distance from the seat. Opposite the outer sides of the plates electromagnetic microphones were set up in which voltage oscillations were induced by the vibrations of the cone and the bottom. (The characteristic frequencies of the fixing plates did not play a role as was checked by earlier experiments.) The experiments gave the following results (details in Ref. 2):

1. The surroundings of cone and seat are not of great importance for the vibrations of the valve. The vibrations are of minimum strength if the nozzle contour formed by the seat and the cone has a ratio of throat cross section to exit cross section (into the region R) which is equal to the well-known ratio one has to use for the design of supersonic nozzles at a given pressure ratio. This result corresponds to results found by other authors (see Ref. 3, for instance) using convergent-divergent nozzles.
2. The main source of the vibrations and the noise is the mixing region R. Here, a change in the shape of R by use of a smooth contour a certain distance from the valve seat gave a reduction in the strength of the vibrations of 12 db. However, if the mixing region was changed so as to completely eliminate the bend after the valve, the performance was almost as bad as in the original case.

The reduction of 12 db was not yet large enough for practical purposes. Therefore, two other possibilities were considered:

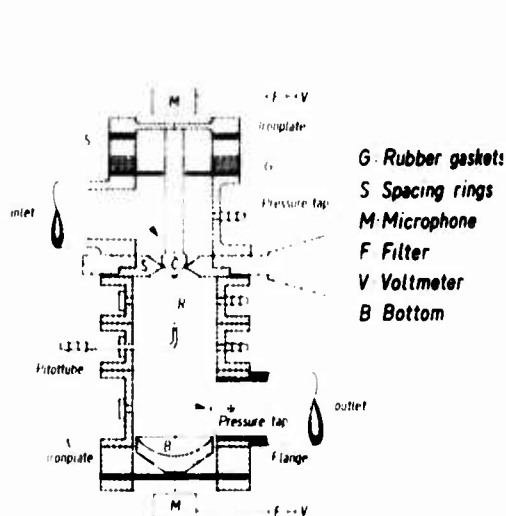


Fig. 4a - Schematic diagram of the model valve

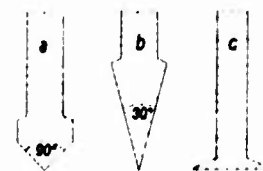


Fig. 4b - Shapes of the cones and seats



Fig. 4c - Bottom shapes

1. A reduction of the flow velocity from supersonic to subsonic values. Such a reduction would result in the disappearance of the unsteady shock waves. Further, the noise level would decrease according to the  $v^6$  law (or a similar power-law of a characteristic velocity  $v$ ) which governs the production of noise by turbulent mixing. Of course, this decrease of velocity is limited by the demand for a small cross section of the valve.
2. A great decrease in the size of the turbulent eddies. The physical argument for this device is not only the shifting of the dominant frequencies toward the ultrasonic domain, but also the influence on the turbulent mixing process itself. This can be understood if one recognizes that the conversion of kinetic energy into heat is performed by a kind of cascade-type mixing process in which the energy is transferred from the energy containing wave numbers (eddies in the size of the mechanism producing the turbulence) through a region of mean wave numbers (mean-size eddies) up to the dissipative domain of wave numbers (small eddies). Qualitatively, one may say that during this transfer, the turbulent eddies strike one another and thereby produce noise. If the process of energy transfer from large eddies (small wave numbers) to small eddies (large wave numbers) is cut off in such a way that the initial size of the eddies is smaller than before, a part of the transfer process does not take place, and the noise production decreases. (This process will be discussed in more detail in the next section.)

In order to test the possibilities mentioned above, a "labyrinth system" (Fig. 5) was designed which was set directly below the valve seat. It consisted of a set of plates with many small holes (1 to 4 mm in diameter) which were placed so that each hole of one plate lay opposite a closed part of the next plate. The spacing between subsequent plates was also very small. The flow velocity through the system could be controlled by varying the number and the size of the holes and the spacing of the



Fig. 5a - Schematic diagram of labyrinth set

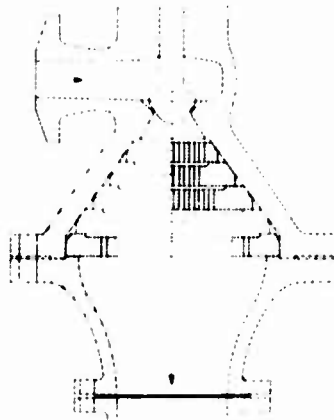


Fig. 5b - Valve with labyrinth set

plates. The degree of turbulence was increased by sharp edges. In this way a drag was produced which was large enough to reduce the pressure at subsonic velocity, at least at maximum flow rate. This type of reducing valve worked very well and gave an improvement of 24 db in the model experiments (measured again by the vibrations of a bottom mounted below the labyrinth system).

On the basis of these experiments, several full-scale valves (Fig. 6) with labyrinth sets were designed and installed in some heating and electric power plants. They worked very satisfactorily. At one plant, for instance, the inhabitants of the surrounding apartment houses had filed suit, charging that the company was disturbing the peace with the noise caused by the old-type valve. After the new valve was installed the noise outside the engine house was very low and no longer disturbed the inhabitants. Inside the engine room the noise production of the other machines placed there was larger than that of the valve. Measurements gave a noise level of 91 phons in this room, whereas the noise level produced by the valve alone was about 85 phons. The acceleration of the material, which is important for the vibration breaking strength, was determined at different points of the valve surface. The measured values ranged from 10 to 20 m/sec<sup>2</sup>, which was several orders of magnitude below the critical acceleration for vibration breakage.

In another application, a valve was also used for pressure reduction at extreme pressure ratios. A flow rate of 64 tons per hour had to be reduced from 116 to 3 atm. Even at this supercritical ratio the valve performed very satisfactorily, both from the standpoint of noise and from that of vibrations.

#### CALCULATION OF THE INFLUENCE OF THE EDDY SIZE ON NOISE PRODUCTION

In the last section the supposition was made that noise generation is influenced by the eddy size of the turbulent motion. In the language of statistical analysis this means a dependence on the spectral distribution of the turbulent properties. In order to check this supposition, the noise output was calculated for several different distributions of turbulent energy in wave number space for the case of decaying, homogeneous, isotropic turbulence with zero mean velocity. This flow may be considered as representing the flow in a jet, in which the turbulence of the different fluid volume elements (in the moving system) also decays.

The following assumptions were made: At the time  $t = t_0$  a homogeneous, isotropic turbulent motion exists in the volume  $V$ . The mean velocity is zero. The spectral energy distribution at  $t = t_0$  is given by the function  $F$  so that

$$e_{ij} = \int_0^\infty F(k, t_0) \delta_{ij} dk \quad (1)$$



where  $e_0$  is the kinetic energy per unit mass at  $t = t_0$  and  $k$  is the wave number. The shape of  $F(k, t_0)$  is rectangular (see Fig. 7):

$$\begin{aligned} F &= 0 & \text{for } 0 < k < k_0 \\ F &= F_0 \frac{e_0}{k_0(a-1)} & \text{for } k_0 < k < ak_0 \\ F &= 0 & \text{for } ak_0 < k \end{aligned} \quad (2)$$

( $a > 1$ ). At  $t = t_0$  the turbulence begins to decay. The total sound energy  $E$  radiated from the volume  $V$  during the decay process is to be calculated, especially its dependence on the initial condition Eq. (2).

The initial condition, Eq. (2) contains three parameters  $e_0$ ,  $a$  and  $k_0$ . For the purposes of this calculation, only  $k_0$  is of interest, because  $1/k_0$  is proportional to the longitudinal scale

$$L_0 = \int_0^\infty r(r, t_0) dr$$

which is a measure of the eddy size ( $r$  is the longitudinal correlation function,  $r$  the distance). Therefore, constant values of  $e_0$  and  $a$  were assumed and the noise output for different values of  $k_0$  was calculated. The parameter  $a$  was taken equal to 2. This value of  $a$  means that the energy is contained in an octave of wave numbers at the beginning of the decay.

With a derivation similar to that in I. Proudman's paper (5) the energy  $E$  was found to be (for details see Ref. 6)

$$E = \frac{c_0 V}{c_0^5} \int_{t_0}^{\infty} \left( \int_0^\infty \frac{[v^2]}{L(t)} t dt \right) dt \quad (3)$$

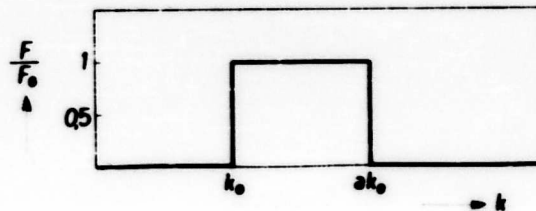


Fig. 7 - Spectral energy distribution  $F$  at  $t = t_0$  vs wave number  $k$

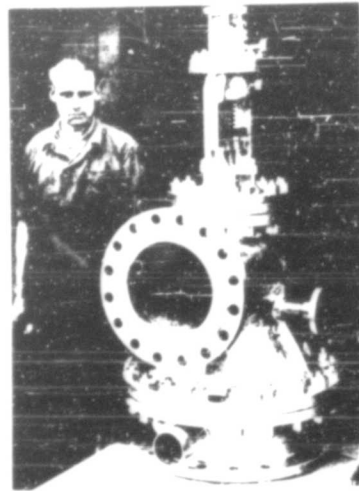


Fig. 6 - Full-scale valve with labyrinth set (after Pontow (4))

where  $\rho_\infty$  and  $c_\infty$  are the density and the speed of sound at infinity, respectively,  $v^2$  is the instantaneous mean square value of any velocity component (arbitrary because of isotropy),

$$L = \int_0^\infty f(r, t) dr$$

is the longitudinal scale, and  $f(r, t)$  is a function dependent on the shape of  $r$  only. The dependence of the integrand on  $r$  was calculated by Heisenberg's integro-differential equation for the decay of homogeneous, isotropic turbulence, which was solved as an initial value problem. The results are given in Fig. 8, in which the energy  $E$ , divided by  $M_0^5$  and by the total initial turbulent energy  $\rho_\infty c_\infty^5 V$  contained in  $V$ , is plotted against  $Re_L$ , the initial Reynolds number of the turbulence. The following definitions apply:

$$M_0 = \frac{(v_0^2)^{1/2}}{c_\infty}$$

and

$$Re_L = \frac{(v_0^2)^{1/2} L_0}{\nu}$$

$v_0^2$  is the mean square of one velocity component at  $t = t_0$  and  $\nu$  is the kinematic viscosity.

Figure 8 shows that the expected general trend indeed exists. At low Reynolds numbers (small eddies) less noise is produced than at high Reynolds numbers (large eddies), the other parameters remaining unchanged. For example, a decrease in  $Re_L$  from  $3 \times 10^4$  to  $3 \times 10^1$  gives a decrease in the noise output of about 7 db. Quantitatively, the dependence of the noise output on  $Re_L$  is small at high Reynolds numbers (in agreement with Proudman's considerations (5)) and larger at lower Reynolds numbers.

The result can easily be understood by means of a dimensional analysis. For this purpose, the integration in Eq. (3) is replaced by multiplying the initial sound power, which is proportional to

$$\frac{\rho_\infty V}{c_\infty^5} \cdot \frac{[v_0^2]^4}{L_0}$$

with the time of decay of the turbulence. For large Reynolds numbers, this time is proportional to

$$\frac{L_0}{(v_0^2)^{1/2}}$$

Hence,  $E$  is independent of  $L_0$ . For smaller Reynolds numbers, a part of the initial

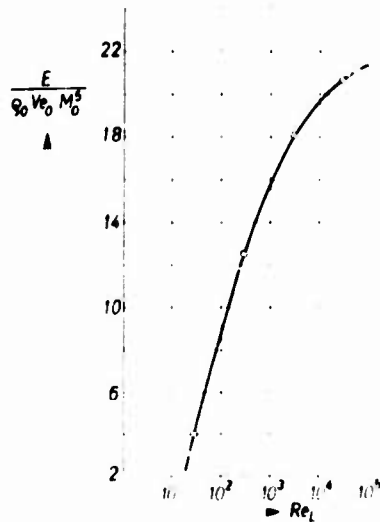


FIGURE 8. Dimensionless total sound energy  $E / (\rho_\infty v_0^5 M_0^5)$  versus Reynolds number  $Re_L$ . (—) calculated points; (---)  $n = 2$ .

energy  $\epsilon_0$  is contained in the dissipative domain of wave numbers, and another characteristic time becomes important which involves the viscosity, namely the time  $l_v^2$  (this also follows from Heisenberg's equation). Therefore, if this time becomes significant, the energy  $E$  becomes proportional to  $l_v$  and decreases with decreasing  $l_v$ . The curve shown in Fig. 8 covers the upper part of the transition region between the two laws.

What practical conclusions can be drawn from these results? The calculations were only concerned with homogeneous, isotropic turbulence, but one can assume that the results are also qualitatively correct for inhomogeneous, non-isotropic turbulence. Hence, one can say that the reduction in the size of the turbulent eddies is an effective means of noise suppression if the size of the eddies can be made very small. In the case of a reducing valve this is easily possible. In the investigations of the last chapter, for instance, the Reynolds number  $Re_L$  lay between  $10^2$  and  $10^4$ , but even smaller values could have been attained. For jet engines, the overall benefit incurred in reducing the eddy size is problematic, because the reduction may lead to a too large increase of weight and drag and also to thrust losses.

Some remarks concerning some devices for the reduction of jet noise are perhaps in order. The above calculations show the effect of changing eddy size on sound output and thereby offer a possible explanation for the reduction of overall sound power effected by some jet noise suppressors. For instance, the reduction of about 7 db achieved by the slit-type nozzle proposed by E. J. Richards (7) can be due - at least partially - to the decreased eddy size. Further, one can expect that certain other changes in the distribution of turbulent properties also reduce the rate of noise production. For example, the avoidance of strong inhomogeneities or nonisotropies may result in a reduction of the sound level by eliminating the eddy exchange processes needed to smooth out a region of strong gradients. This seems to be the situation with some suppressors for jet planes (at the jet edge of the corrugated nozzles, for example). These proposed explanations ought to provide a basis for further experimental investigations in which particular care should be taken regarding measurements in the higher frequency bands.

## SCATTERING OF SOUND BY A SINGLE VORTEX AND BY TURBULENCE

Another subject of the investigations of the Max-Planck-Institut für Strömungsforschung concerning the interaction of sound and turbulence is the scattering of external sound by a turbulent medium. This research is still going on and, hence, only preliminary results can be given here. Both theoretical and experimental investigations have been made. First the theoretical considerations will be described.

### Scattering by a Single Vortex

General studies of the scattering of light or sound have already been made by various authors who have considered wave propagation in a medium with fluctuating refraction coefficient (see the references listed in (8), also (9,10) and others). Special theories for the scattering of sound by turbulence have been developed by Lighthill (11), Kraichnan (12), and Batchelor (13). These theories, while having general validity, have been applied specifically to homogeneous, isotropic turbulence. In addition the noise generated by the interaction of shock waves and turbulence has been considered (14,14).

<sup>1</sup>These calculations are due to the author and to the late Dr. A. F. C. Collins (11). The theory of scattering of sound by turbulence is given in (12) and (13).

The starting point for the investigations of the Max-Planck-Institut was the problem of the scattering of a sound wave as it passes through a single vortex. This single-vortex scattering may be considered as a kind of elementary model for the process of scattering by turbulent eddies. As will be shown, the knowledge gained from a study of this elementary model provides an understanding of the scattering caused by both extreme non-isotropic and by isotropic turbulence.\* Of course, scattering by a single vortex is also in itself a problem of mathematical and physical interest.

The problem was formulated as follows: Consider a steady potential vortex of circulation  $\Gamma$ . The axis of the vortex coincides with the  $z$ -axis of a cylindrical coordinate system  $(r, \theta, z)$  and extends from  $-\infty$  to  $+\infty$ . In the  $r, \theta$  plane the vortex extends from  $r = r_i$  to  $r = r_o$ . In the domains  $r < r_i$  and  $r > r_o$  the fluid is at rest. This vortex interacts with a plane sound wave of wave length  $\lambda$ . The projection of the normal of wave propagation into the  $r, \theta$  plane is taken as the line  $\theta = 0$ . The direction of wave propagation includes an angle  $\theta$  with the axis of the vortex (see Fig. 9). The polar diagram of scattering intensity and the scattering power are required as functions of the five parameters of the problem  $\Gamma, \lambda, r_i, r_o, \theta$ .

The problem was solved by applying the method of small perturbations to the frictionless equations of motion, the equation of continuity and the equation for the conservation of entropy of a mass element. This means that terms involving the square of the amplitude of the sound wave were neglected.

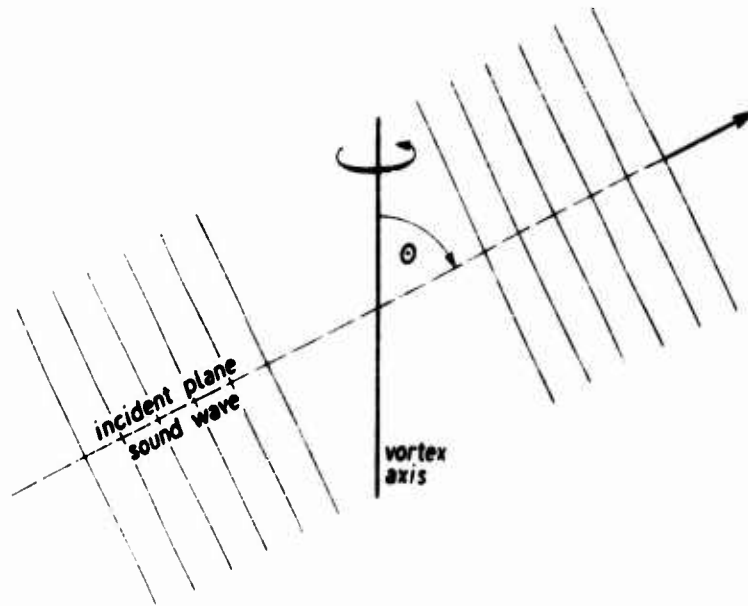


Fig. 9 - Schematic drawing of obliquely incident sound wave

It may be mentioned that a related problem - the interaction of a shock wave and a single vortex - has been treated in several papers (16,17). A kinematical consideration of the sound wave-vortex interaction is given in (18).

# Results Relating to the Production of Noise by Turbulence

The five parameters of the problem can be reduced to four by defining new dimensionless parameters  $c_0 = R_0 / (t_0 + R_1)$ ,  $R_1 / (t_0 + R_1)$  ( $c_0$  is the speed of sound),  $\epsilon$  is assumed to be small compared with 1. Therefore, if all variables are expanded in power series in  $\epsilon$ , terms of order  $\epsilon^2$  and smaller may be neglected. With these approximations, the potential of the sound reads  $\phi = \phi_0 + \phi_1$ .  $\phi_0$  is the potential of the original plane sound wave,

$$\phi_0 = R_0^2 \exp(-R) \sin(\cos \theta + Z \cos \theta) \quad (4)$$

where  $R$  is a constant,  $R = r / c_0$ ,  $Z = z / c_0$ ,  $r, z$  are the dimensionless independent variables and  $t$  is the time.  $\phi_1$  is the potential of the scattered sound. For  $\phi_1$  one obtains the inhomogeneous wave equation

$$\Delta \phi_1 = -\Delta \phi_0 \quad (5a)$$

in the region  $R_1 < R < R_0$ , and the homogeneous wave equation

$$\Delta \phi_1 = 0 \quad (5b)$$

in the regions  $0 < R < R_1$  and  $R > R_0$ .  $\Delta$  is the Laplacian operator

$$\Delta = \frac{1}{R} \frac{\partial}{\partial R} \left( R \frac{\partial}{\partial R} \right) + \frac{1}{R^2} \frac{\partial^2}{\partial \theta^2} + \frac{\partial^2}{\partial Z^2}$$

Equation (5) can be solved by the well-known method of retarded potentials.

Special care has to be taken regarding the discontinuities in the potential  $\phi_1$  and its derivatives at  $R = R_1$  and  $R = R_0$ . From dynamical considerations it follows that the sound pressure for  $R \rightarrow R_0 - 0$  and  $R \rightarrow R_0 + 0$  has to be continuous. This requirement leads to the jump condition

$$\left[ \frac{\partial \phi_1}{\partial R} \right]_{R_0+0} - \left[ \frac{\partial \phi_1}{\partial R} \right]_{R_0-0} = \frac{1}{2} \frac{1}{R_0^2} \left[ \frac{\partial \phi_0}{\partial R} \right]_{R_0} \quad (6a)$$

for all  $\theta, Z$ . Further, from the requirement that the flow velocities normal to the interface between the vortex and the outer flow be continuous, a second jump condition results:

$$\left[ \frac{\partial \phi_1}{\partial R} \right]_{R_1+0} - \left[ \frac{\partial \phi_1}{\partial R} \right]_{R_1-0} = \frac{1}{2} \frac{1}{R_1^2} \left[ \frac{\partial \phi_0}{\partial R} \right]_{R_1} \quad (6b)$$

for all  $\theta, Z$ . With this condition, the ripples at the interface due to the original sound wave are taken into account.<sup>\*</sup> At  $R = R_1$  corresponding conditions apply. Conditions (6a) and (6b) require doublet layers and source layers respectively at both  $R = R_0$  and  $R = R_1$ .

The solution of Eqs. (5) and (6) gives the following formula for the total scattering potential in the far zone ( $R \sin \theta \rightarrow R_0$ ) for the case  $R_1 > 0$ :

<sup>\*</sup>Compare the papers (19,20) that treat other but similar problems in which these ripples are of great importance.

$$1 - \frac{R}{R_0 \sin \theta} \left( 1 - 4 \frac{R^2}{R_0^2} + 2 \frac{R^4}{R_0^4} \right) - F \sin^2 \theta \cos^2 \theta \left[ J_0 \left( 4 \frac{R}{R_0} \sin \theta - \sin^2 \theta \right) + 1 \right] \cdot \left[ 1 - 2 \sin^2 \theta - \sin^2 \theta \cos^2 \theta \right] \quad (7)$$

where  $J_0$  is the zero-order Bessel function of the first kind. For  $\theta = 90^\circ$  (sound wave falling perpendicularly on the vortex) this is a cylindrical wave, while for  $\theta \neq 90^\circ$  (sound wave falling obliquely on the vortex) it is a conical wave. This means that the surfaces of constant phase are cones moving outward as indicated in Fig. 10.

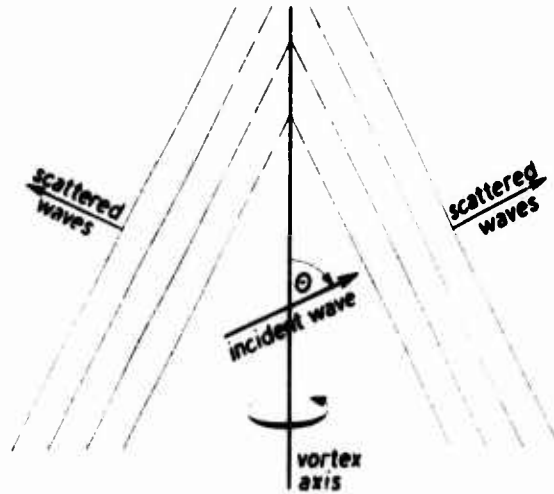


Fig. 10 - Cross-sectional view of the phase surfaces of the scattered sound waves

With the help of Eq. (7) polar diagrams of the scattering intensity

$$I_{sc} = \overline{p v_n} = \frac{2}{R \sin \theta} F \left( \frac{R}{R_0} \right)^2 + I_0 \quad (8)$$

can be drawn. Here,  $p$  is the sound pressure,  $v_n$  is the particle velocity normal to the phase surfaces of the scattered sound, and  $I_0$  is the sound intensity of the incident wave. The bar indicates mean value and  $F$  is equal to

$$F = J_0 \left( 4 \frac{R}{R_0} \sin \theta - \sin^2 \theta \right) + 1 \cdot \left[ 1 - 2 \sin^2 \theta - \sin^2 \theta \cos^2 \theta \right] \quad (8a)$$

Such polar diagrams were constructed for four different values of  $\theta$  ( $90^\circ$ ,  $60^\circ$ ,  $45^\circ$ ,  $15^\circ$ ) and three different values of  $R_0$  (10, 1, 0.1) and are shown in Fig. 11.  $I_{sc}$  is referred to  $(I_{sc})_{max}$ , the value of maximum intensity. The waviness of the curves for  $R_0 = 10$  is due to the oscillations of the Bessel function or, physically, to interference effects.

# Results Relating to the Production of Noise by Turbulence

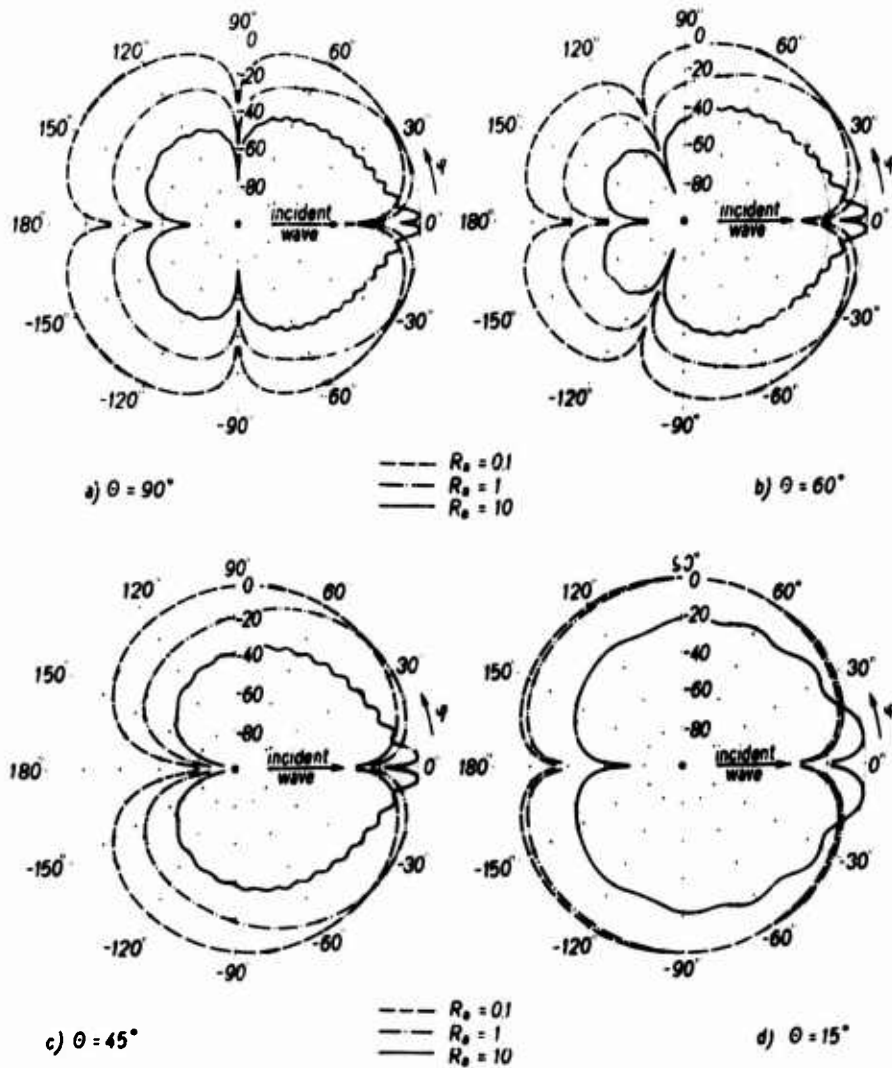


Fig. 11 - Polar diagrams of scattering intensity for different values of  $R_s$  and  $\theta$ . Plotted is

$$10 \log_{10} \frac{I_{sc}}{(I_{sc})_{\theta=0}}$$

For  $\alpha = 90^\circ$  the intensity is zero in four directions ( $\beta = 0^\circ, \pm 90^\circ, 180^\circ$ ), but only for  $R_n \rightarrow 0$  do the four leaves of the characteristic appear symmetrical and have the same maximum intensity (at  $\beta = \pm 45^\circ, \pm 135^\circ$ ). For  $R_n \gg 1$  the intensity of the two leaves in the half circle  $-90^\circ \leq \beta \leq 90^\circ$  is much greater than that of the other two leaves. Therefore, scattering by vortices with diameters of the order of magnitude of the wave length or larger is a forward scattering. Further, for  $R_n \gg 1$ , the intensity is contained in a very sharp angle interval (see  $R_n = 10$  in Fig. 11) and the angle  $\beta_{\max}$  of maximum intensity is proportional to  $1/R_n$ . It should be mentioned here that for  $R_n = 1$  the angular distribution  $F$  (Eq. (8a)) agrees exactly with Lighthill's distribution for the case of homogeneous, isotropic turbulence (see Ref. 11, Eq. (25) with  $F(k) = k^4$  for  $k \gg 1$ ).

For  $\alpha = 90^\circ$  (see Fig. 11b, c, d) the zeros at  $\beta = 0$  and  $180^\circ$  remain, while the zeros at  $\pm 90^\circ$  are shifted toward  $\beta = 180^\circ$ , as one can also see from Eq. (8a). For  $\alpha = 45^\circ$  only two leaves can exist, because the second term in the second bracket of Eq. (8a) can no longer attain the value 1. For fixed  $R_n$  and  $\alpha \rightarrow 0^\circ$  the angle  $\beta_{\max}$  approaches the value  $90^\circ$ .

By use of Eq. (8) one can easily calculate the total scattering power  $L_{sc}$  emitted per unit length of the vortex. One obtains

$$\frac{L_{sc}}{L_n} = \frac{1}{2} R_n^2 \sin^2 \alpha \int_0^{2\pi} F d\beta \quad (9)$$

$L_n = 2\pi r_n \sin \alpha \cdot I_n$  is the sound power falling on the vortex per unit length. Because the most interesting question is the dependence on the frequency of the incident sound wave - the other parameters remaining unchanged - this ratio is plotted in Fig. 12 against  $R_n$ , which is proportional to  $\omega$ . (For this purpose  $\omega$  is written

$$\frac{\omega}{2c_n} R_n = \frac{1}{2} M R_n \quad (10)$$

where

$$M = \frac{1}{2\pi} \int_0^{2\pi} \int_0^{2\pi} v d\beta d\alpha$$

is the mean value of the azimuthal velocity  $v$  of the vortex and  $M$  is the mean Mach number.) For  $R_n \ll 1$ ,  $L_{sc}/L_n$  varies with the 5<sup>th</sup> power of  $R_n$ , for  $R_n \gg 1$  with the 2<sup>nd</sup> power. In the vicinity of  $R_n = 1$  the  $R_n^5$  law changes to the  $R_n^2$  law.

The scattering power per unit volume is  $L_{sc}/\pi r_n^2$  which has the limiting values

$$\frac{L_{sc}}{\pi r_n^2} \sin^2 \alpha \left( \sin^4 \alpha + 4 \cos^4 \alpha \right) \frac{I_n}{I_0} \quad R_n \ll 1 \quad (11a)$$

and

$$\frac{32}{3} \frac{\omega^2}{c_n^2} \left( 1 + \frac{2}{3} \right) \sin^2 \alpha \frac{I_n}{I_0} \quad R_n \gg 1 \quad (11b)$$

The last formula can also be written (by use of Eq. (10)) as

$$\frac{L_{sc}}{\pi r_n^2} \frac{\omega^2}{c_n^2} \left( 1 + \frac{2}{3} \right) \sin^2 \alpha \frac{I_n}{I_0} \quad (11'b)$$



# Results Relating to the Production of Noise by Turbulence

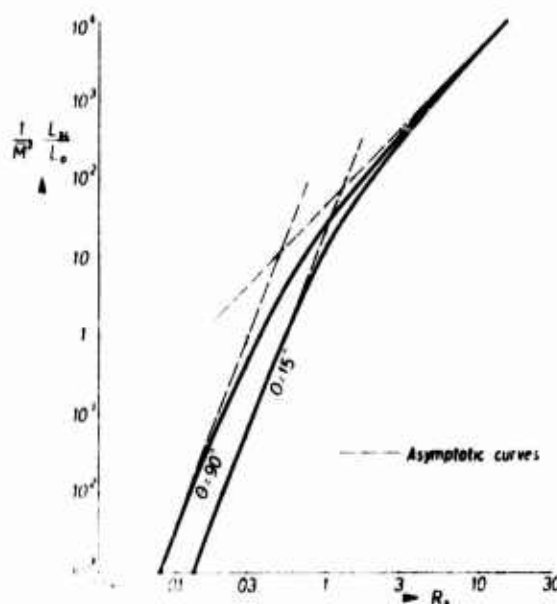


Fig. 12 -  $I/I_0$  vs  $R_0$  for  $\theta = 90^\circ$  and  $15^\circ$

which has exactly the same structure as Lighthill's formula (20) in Ref. 11 for the same limiting case. This again shows, as expected, that scattering by a single vortex contains the essential features of the scattering process in a turbulent medium and may be considered as a kind of elementary process.

## Scattering by Turbulence

In order to apply the above results to turbulence it is assumed that the turbulence can be described by a statistical superposition of vortices of different radii  $r_0$ , circulations  $\Gamma$ , and inclinations  $\theta$  with respect to the incident sound wave. Because the different vortices (eddies) are statistically independent of one another, the intensities of the scattered sound produced by them can be simply added. Further, it is assumed that the time required for the external sound wave to pass through one vortex is small as compared with the time in which the vortex undergoes any sensible change. This assumption is equivalent to the requirement that  $R_0 \gg 1$  (or  $M \gg 1$ ). One may then proceed as follows:

Let  $W(R_0, \theta, \Gamma) = W(x, y, z) \delta(R_0 - 1)$  be the probability that the volume element  $dV = dx dy dz$  ( $x, y, z$  are the coordinates of a cartesian system) belongs to a vortex having a radius between  $R_0$  and  $R_0 + dR_0$ , a dimensionless circulation between  $\Gamma$  and  $\Gamma + d\Gamma$ , and an angle  $\theta$  (see Fig. 9) between  $\Gamma$  and  $\Gamma + d\Gamma$ .  $W$  has to satisfy the condition

$$\int_0^\infty \int_0^\infty \int_0^\pi W(R_0, \theta, \Gamma) dR_0 d\theta d\Gamma = 1$$

With this probability function, the total sound radiation  $L$  from the turbulent volume  $V$  is

$$L = \int_V \int_0^{2\pi} \int_0^\pi \int_0^\infty W(R_n, \dots, x, y, z) \cdot (R_n, \dots) dR_n d\Omega dV. \quad (12)$$

This general expression was evaluated for two different cases, namely extreme non-isotropy (applicable for boundary layers or jet edges, for instance) and isotropy. (Non-isotropy is a case treated only with difficulty by the method given in Ref. 11.) For simplicity, it was assumed that all vortices had the same radius  $R_n$  and the same absolute value of circulation  $\Gamma$ , and that the field was homogeneous ( $W$  independent of  $x, y, z$ ). Then, non-isotropy means that all vortices have parallel axes making an angle  $\theta$  with the direction of external wave propagation and can turn clockwise or counterclockwise. In the isotropic case  $W$  was taken proportional to the differential element of solid angle. The results are plotted in Fig. 13. This figure shows that the greatest scattering power occurs for  $\theta = 90^\circ$  (normal incidence) and that it decreases as  $\theta \rightarrow 0$  (where it becomes zero). The scattering power in the isotropic case is approximately equal to that in the non-isotropic case with  $45^\circ \leq \theta \leq 60^\circ$ . Hence, one can say that there is no significant difference between isotropic and non-isotropic scattering.

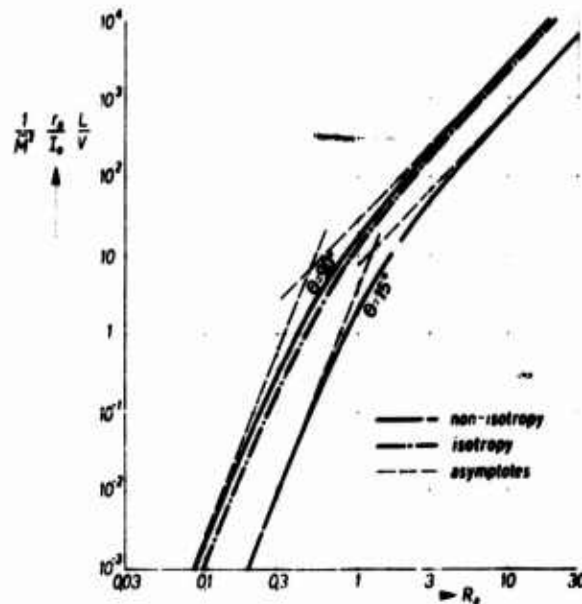


Fig. 13 - Dimensionless total scattering power radiated from the volume  $V$ , for two cases of non-isotropy ( $\theta = 90^\circ$  and  $15^\circ$ ) and for the case of isotropy

#### Experimental Investigations

Figure 14 shows the apparatus which is being used for the experimental investigations. The laminar air flow within the entrance region of a circular duct 300 mm in diameter is made turbulent by a grid consisting of parallel circular rods, 5 mm in

### Results Relating to the Production of Noise by Turbulence

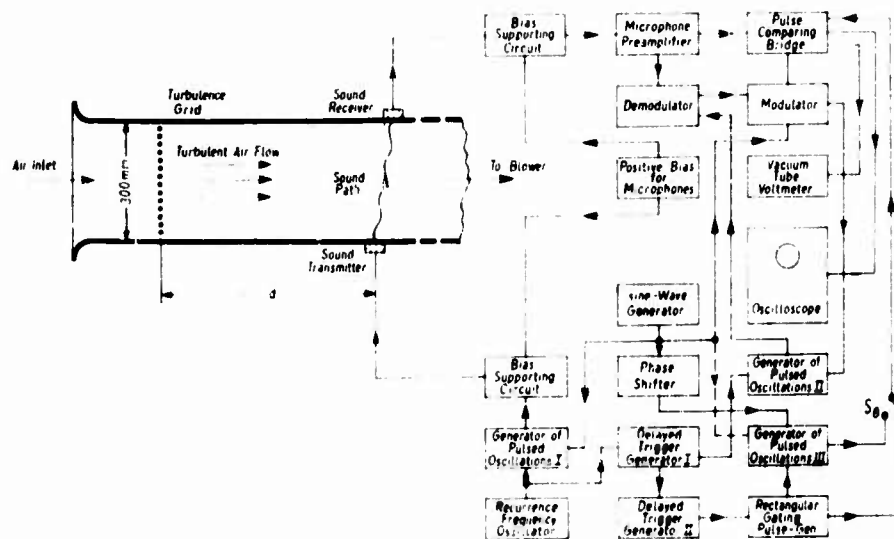


Fig. 14 - Block diagram of equipment used for tests of scattering of sound in a turbulent medium

diameter and 12.8 mm distant from one another. The flow velocity is 25 m/s. Short sound pulses are transmitted perpendicular to the flow direction from one side of the duct and are received at the opposite side. The degree of turbulence of the flow traversed by the sound waves can be changed by varying the distance of the turbulence grid from the test section. For the exact measurement of the intensity of the received sound pulses, electronic equipment is used which is shown in the right part of the figure. The main element, a "pulse comparing bridge," contains a bridge consisting of two condensers and two electron tubes controlling the charge of the condensers. In this bridge the effect caused by the received sound pulses on one arm is compensated by the effect of electrically produced pulses of the same shape on the other arm. The height of these electrically produced pulses can be measured easily and, if the bridge is balanced, is equal to the height of the sound pulses. The other parts of the electronic system shown in the figure are needed to compensate for the delay time incurred in the transmission of the acoustical pulses through the flow and to compensate for the amplitude modulation imposed on these pulses by disturbing noise and other influences.

Some experimental results concerning the dependence of scattering intensity on the frequency of sound are given in Fig. 15. The measurements were made in the following manner: At first, by shifting the receiving microphone, the position of the maximum intensity of the sound at the wall opposite to the transmitter was determined without scattering (that is to say, with the grid far removed from the test section or with laminar flow in the duct). The microphone was then left in this position and the grid was brought closer to the test section. In this way one obtains the intensity  $I_{\text{max}}$

\*The sound transmitter and the receiver are identical condenser type microphones with solid dielectric, which have been developed by W. Kuhl, G. R. Schodder and E.-K. Schröder in the III. Physikalisches Institut of the University of Göttingen (21).

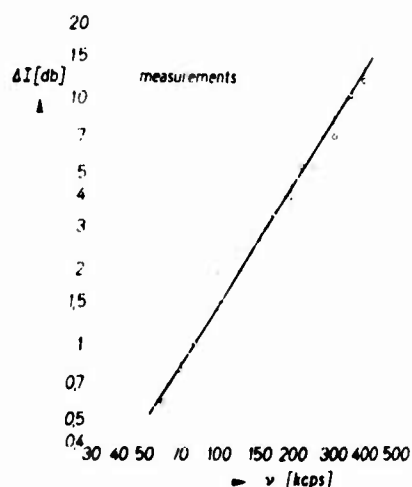


Fig. 15 -  $10 \log_{10} \frac{I_{\text{scat}}}{I_{\text{amb}}}$  vs frequency of sound. Distance 1120 mm.

(without scattering) and the intensity  $I_{\text{scat}}$  (with scattering) for each frequency  $\nu$  of the sound. The quantity  $10 \log_{10} \frac{I_{\text{scat}}}{I_{\text{amb}}}$  is plotted against  $\nu$  in Fig. 15. It must be proportional to  $\frac{1}{\nu^2}$  given by Eq. (9), since it represents the attenuation of the intensity due to scattering (see Ref. 15).

The calculations gave asymptotic power laws  $\frac{1}{\nu^2}$  with  $n = 5$  for the lower frequency range and  $n = 2$  for high frequencies. The measuring values obtained until now seem to obey the  $\frac{1}{\nu^2}$ -law. Further measurements are being made and will be published later.

#### ACKNOWLEDGMENTS

The author wishes to express his thanks to Prof. Dr. W. Tollmien for his steady encouragement, to his colleagues in these investigations, Dr. E. Koppe, Dr. K. Matschat, and Dipl. Phys. D. Schmidt, for their constant enthusiasm, to Mr. W. G. Nelson for his valuable help with the problems of English technical composition. Further, the author is grateful to the sponsors of this symposium for giving him the opportunity to present this paper.

#### REFERENCES

1. Buhr, W., "Erfahrungen mit Hochdruck-Reduzieranlagen bei den Hamburgischen Electricitäts-Werken," Mitteilungen der Vereinigung der Grosskesselbesitzer 41:93-99, April 1956
2. Koppe, E., and Müller, E.-A., "Modellversuche zur Klärung von Geräusch- und Vibrationstragen an Reduzierventilen," Mitteilungen der Vereinigung der Grosskesselbesitzer 41:65-83, April 1956
3. Callaghan, E.E., Sanders, N.D., and North, W.J., "Recent NACA Investigations of Noise-Reduction Devices for Full Scale Engines," Aeron. Engin. Review 14(6) 66-71 (1955)
4. Pontow, W., "Wege zur Beherrschung von Geräuschen und Vibrationen bei der Dampfdruckminderung durch Reduzierventile," Mitteilungen der Vereinigung der Grosskesselbesitzer 41:83-93, April 1956
5. Proudman, I., "The Generation of Noise by Isotropic Turbulence," Proc. Roy. Soc. A214:119-132 (1952)
6. Müller, E.-A., and Matschat, K., "Zur Lärmerzeugung durch abklingende inhomogene isotrope Turbulenz," Zeitschrift für Flugwissenschaften 6:161-170 (1956)
7. Richards, E.J., "New Type of Tip Jet to Reduce Noise," J. Helicopter Assoc. Great Britain 9:404-413 (1956)

Results Relating to the Production of Noise by Turbulence

8. Müller, E., und Müller, E.-A., "Strahlärm, ein wissenschaftliches und technisches Problem der Luftfahrtforschung," Jahrbuch der Wissenschaftlichen Gesellschaft für Luftfahrt, pp. 155-164 (1956)
9. Onuchow, M.A., "On the Influence of Weak Inhomogeneities of the Atmosphere on the Propagation of Sound and Light," Izvestiya Akademii Nauk 2:155-165 (1953) (in Russian)
10. Potter, D.S., and Murphy, S.R., "On Wave Propagation in a Random Inhomogeneous Medium," J. Acoust. Soc. Am. 29:197-198 (1957)
11. Lighthill, M.J., "On the Energy Scattered from the Interaction of Turbulence with Sound or Shock Waves," Proc. Cambridge Phil. Soc. 49:531-551 (1953)
12. Kraichnan, R.H., "The Scattering of Sound in a Turbulent Medium," J. Acoust. Soc. Am. 25:1096-1104 (1953); errata: J. Acoust. Soc. Am. 28:314 (1956)
13. Batchelor, G.K., "Wave Scattering due to Turbulence," Proceedings 1st Symposium on Naval Hydrodynamics, Nat'l Academy of Sciences - National Research Council, Publication 515, Washington, pp. 409-430 (1956)
14. Ribner, H.S., "Shock-Turbulence Interaction and the Generation of Noise," NACA Report 1233 (1955)
15. Müller, E.-A., and Matschat, K.R., "The Scattering of Sound by a Single Vortex and by Turbulence," Tech. Rpt., Max-Planck-Institut für Strömungsforschung, Göttingen, Jan. 1959
16. Ram, G.S., and Ribner, H.S., "The Sound Generated by Interaction of a Single Vortex with a Shock Wave," (preprint)
17. Hollingsworth, M.A., and Richards, E.J., "On the Sound Generated by the Interaction of a Vortex and a Shock Wave," ARC 18:257, F.M. 2371 (1956)
18. Lindsay, R.B., "Compressional Wave Front Propagation through a Simple Vortex," J. Acoust. Soc. Am. 20:89-94 (1948)
19. Miles, J.W., "On the Reflection of Sound at an Interface of Relative Motion," J. Acoust. Soc. Am. 29:226-228 (1957)
20. Ribner, H.S., "Reflection, Transmission and Amplification of Sound by a Moving Medium," J. Acoust. Soc. Am. 29:435-441 (1957)
21. Kuhl, W., Schodder, G.R., and Schröder, F.-K., "Condenser Transmitters and Microphones with Solid Dielectric for Airborne Ultrasonics," Acustica 4:519-532 (1954)

\* \* \* \* \*

## DISCUSSION

W. Willmarth (University of Michigan)

I wish to compliment the author on his excellent experimental and theoretical work. The experiments on sound scattering are very well done. In particular, the use of sound pulses produced and detected by identical transducers eliminates difficulties with sound reflection and transducer calibration. It is gratifying to see that the simple, or relatively simple, results of scattering from a single vortex can be superimposed to give a description of the sound scattering from turbulence.

With regard to the noise produced by a high-pressure steam valve: by the use of a set of small passageways the turbulence and shock waves within the valve were reduced in scale. The small scale motion which is produced probably does not vibrate the pipe as much because the mechanical impedance of the walls for the high-frequency, small-scale fluctuations is greater.

A related problem of valve noise is being studied at the Stanford University Medical Center. They are working on the valve noise produced by a heart valve, and would like to know what types of obstructions in the heart valve produce what types of noise. Of course, the sound intensity for the heart valve is very much lower than that for the steam valve discussed by Professor Müller.

R. H. Kraichnan (New York University)

The comment I wish to make concerns the dependence of sound-radiation-efficiency upon the turbulence parameters. Work which we have done recently on the radiation from isotropic turbulence at high Reynolds numbers has yielded the formula

$$W = (v^3/c^5) \ln R,$$

where  $W$  is the radiated power per unit mass,  $\epsilon$  is the power dissipated by shear viscosity per unit mass,  $v$  is the r.m.s. fluctuation velocity,  $c$  is the velocity of sound, and  $R$  is the Reynolds number defined by  $R = vL/\nu$ , where  $L$  is the length scale of the energy-containing range of the turbulence and  $\nu$  is the kinematic viscosity. This formula differs from the earlier result of Proudman only in the presence of the  $\ln R$  factor, which arises from a slowly-decreasing, high-frequency component to the radiation spectrum suggested by our work.

It is well-known empirically that

$$\epsilon \sim v^3 L^{-1}$$

Thus,  $W$  depends on the basic parameters according to

$$W \sim (v^8 L) \ln v L / \nu$$

and varies, approximately, inversely with  $L$ . However, the efficiency of the conversion of turbulent energy into sound is given by

$$\eta = W/\epsilon \sim \ln v L / \nu$$

and, apart from the very-slowly-varying logarithmic factor, is unaffected by a change of length scale, provided  $v$  is fixed.

A. Regier (National Advisory Committee for Aeronautics)

I am rather interested in relating the scattering from a large vortex to the valve-noise problem. At Langley we have a test facility for producing turbulent noise for testing aircraft and missile components, and we are interested in making as much noise as possible from a jet. We found that by turning the air supply pipe through a 90-degree turn we can raise the jet noise levels about 5 decibels, possibly because of the large vortices generated in the turns. Actually, we can shape our spectrum and increase the lower frequencies by these large pipe bends. In our test set-up we are using a 12-inch pipe which has four 90-degree turns near the jet exit, and have succeeded in increasing our noise considerably and in bringing our frequencies down.

I. Dyer (Bolt, Beranek, and Newman, Massachusetts)

Several years ago I made an analysis of scattering from a single vortex. The flow field I used started at the origin with zero velocity, increased linearly, and then, at a given value, decreased as the inverse distance law. I, too, obtained good agreement with Lighthill's theory. This seems to be a very different flow model compared to that of Müller's, in the sense that the velocity was not divergent at the origin and contained a central core as a true single vortex might. Thus the model doesn't appear to be too critical in the computation of the scattering.

H. S. Ribner (University of Toronto)

Dr. Müller attributes the noise reduction in the large steam valves to the great reduction in scale; he supports the idea by a theoretical analysis of the noise radiation of homogeneous, isotropic turbulence during its decay as a function of the initial scale. This reviewer believes, on the other hand, that the dominant factor is the reduction of the turbulent velocities in the labyrinth: note that  $v$  enters as the eighth power in Eq. (3), scale  $l$  as the minus first power. A similar argument applies to jet-muffler silencing. It is to be noted that, according to Fig. 8, a factor of  $10^3$  in  $l$ —a wholly implausible amount—is required to explain the 7-db noise reduction attributed to Richards' slit-type nozzle.

\* \* \* \* \*

# SIMILARITY RELATIONS IN AERODYNAMIC NOISE MEASUREMENTS

E. Mollo-Christensen and H. W. Liepmann  
*California Institute of Technology*

## INTRODUCTION

Turbulence still remains the least understood and most interesting field of fluid mechanics. The interaction of sound and turbulent flow thus presents a problem for which one cannot hope at the present time to obtain a complete analytical solution, since besides our ignorance about the structure of turbulent flow in general the added feature of a non-linear interaction between the two fields enters. Consequently the need for analytical experiments in the field is obvious. Experimentation in aerodynamic acoustics is anything but easy, not because of any insurmountable difficulties with the measuring technique but rather because it is quite difficult to set up a clean and simple problem, free of parasitic effects, and in addition to decide what the really important quantities to be measured are. Experimental studies of turbulence, even in the absence of interaction with sound, have given ample evidence of these difficulties.

In the following we will illustrate some very simple similarity considerations with experimental results obtained at GALCIT in the course of a study of aerodynamic noise sponsored by the NACA.

The experimental results which will be used for illustration have been obtained by Willmarth (1), Weyers (2), and Narasimha and Mollo-Christensen. Willmarth (1) measured power spectral densities and space-time correlations of pressure fluctuations on the wall under a turbulent boundary layer. Weyers (2) measured the pressure fluctuations on the wall and in the emitted sound field of a pipe with extremely thin walls with turbulent flow inside. Narasimha and Mollo-Christensen measured noise from subsonic jets.

In all these experiments, great care was taken to avoid parasitic effects, such as noise from unknown sources, diffraction, and scattering.

## PARAMETERS OF THE PROBLEM

In the study of turbulence-produced sound, the fluctuating pressure  $p(\vec{R}, t)$  is measured. Its statistical properties determine the structure of the sound field and its relation to the original turbulence. The simplest and most important quantities to be measured are the mean-square pressure  $\overline{p^2(\vec{R}, t)}$  and the power spectral density  $\overline{p^2(\vec{R}, t)}_f$ . These are related by

$$\overline{p^2(\vec{R}, t)} = \int_0^\infty \overline{p^2(\vec{R}, t)}_f df$$



The fluid properties and the sound-producing turbulent field are specified by a set of parameters which involve at least the following: density  $\rho$ , viscosity  $\mu$ , and velocity of sound  $a$ ; a characteristic flow velocity  $U$  and a characteristic length  $b$ . One can of course think up many other, parasitic, parameters, such as: the dimension of the pressure transducer, the turbulence level and the sound level of the stream used, the cutoff frequencies of the recording equipment, the length of time averaging, the dimension of the receiving volume.

Indeed, a very important and in some cases decisive part of an experimental study of aerodynamic noises lies with the identification and elimination of as many parasitic parameters as possible. This is obvious for any experiment; it is emphasized here for the case of aerodynamic noise since the nature of the problem, namely the study of a random wavefield of small intensity without a priori knowledge of what to expect, often makes it very difficult to know whether one has succeeded in measuring what was intended or not.

It is therefore especially important to check the similarity properties of the experimental data before any detailed conclusions can be drawn.

#### DIMENSIONAL ANALYSIS

If it is assumed that the problem is defined in the minimum number of parameters listed, dimensional analysis yields for the form of  $p^2$  and  $f(f)$ :

$$p^2 = U^3 b^2 f(R, D, Re, Ma)$$

where  $Re = U b / \nu$  and  $Ma = U / a$  are Reynolds number and Mach number. For the power spectral density it follows:

$$f(f) = U^3 b^2 f(f, R, D, Re, Ma)$$

Any measurement which cannot be represented in this form must be influenced by at least one additional parameter, and the above relations can then be used to eliminate such a parameter by a limiting procedure.

As examples, measurements by Weyers (2) and Willmarth (1) will be cited. Figures 1 and 2 taken from Weyers' paper demonstrate the similarity relations in intensity and spectrum. Figure 3 shows a plot of spectra of wall-pressure fluctuations under a turbulent boundary layer obtained by Willmarth (1), in which the ratio of the diameter of the pressure transducer  $d$  to the boundary layer thickness  $\delta^*$  is the parameter which is different for the different spectra. The effect of a finite transducer size can thus be estimated, and eliminated by an extrapolation to  $d/\delta^* \rightarrow 0$ .

In both sets of measurements the influence of Reynolds number and Mach number were found to be small; this agrees with the expectation that the turbulence at not too high Mach numbers is unaffected by compressibility and that at sufficiently high Reynolds number no viscous effects remain.

We have not investigated the near field of a jet or wake, for which similar relations are bound to hold. However, in measurements of the far field it becomes quite obvious that microphone size and orientation can cause very large deviations from the proper similarity laws due to diffraction effects.

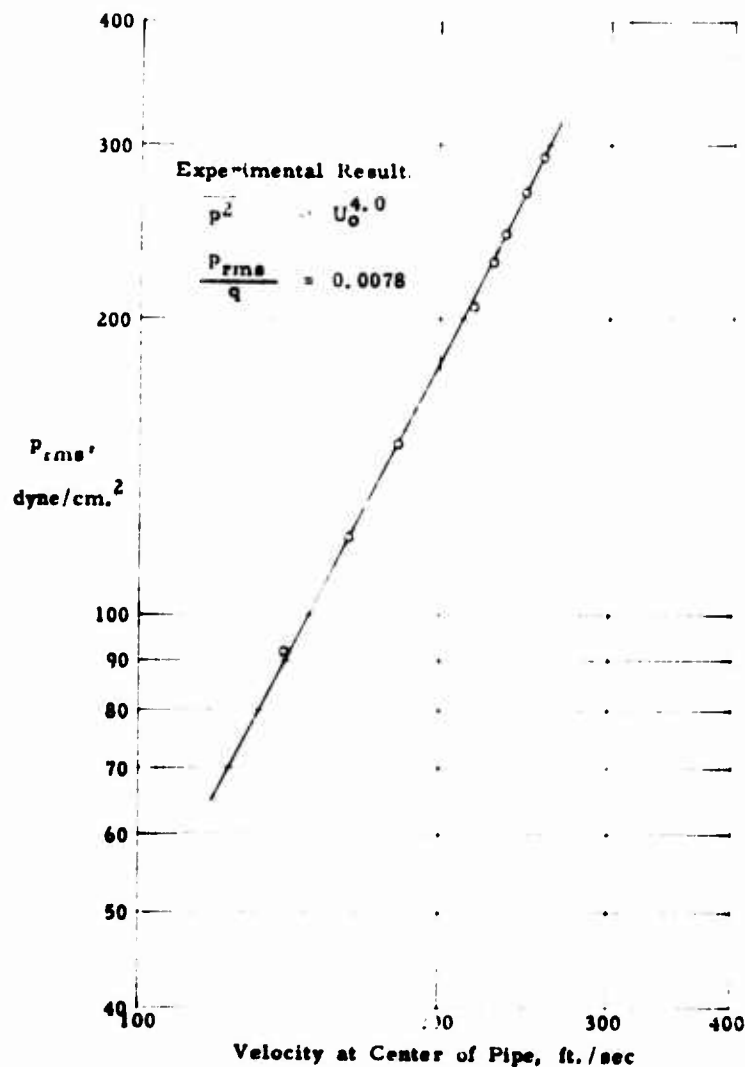


Fig. 1 - Variation of  $p_{rms}$  with velocity.  $t = 0.0005$  inch,  $d = 1$  inch,  $r/d = 1/2$

### SIMILARITY

If we supplement the bookkeeping of dimensional analysis with some insight into the physics of the problem, such as can be obtained from general conservation laws or the differential equations of the problem, one can attempt to reduce the number of variables further specifying the forms of  $p^2$  and  $\lambda$  more closely. One may also turn the process around and discuss the physical mechanism which must be involved to give a certain experimentally obtained similarity law.

# Similarity Relations in Aerodynamic Noise Measurements

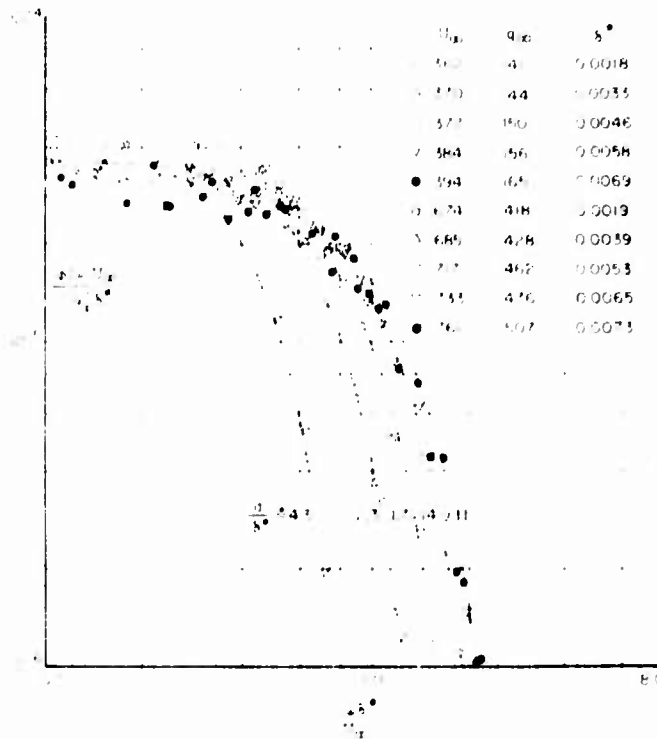


Fig. 3 - Power spectra of the fluctuating wall pressure in a turbulent boundary layer

and

$$2\pi \frac{D^3}{x^2} \left( \frac{D}{x} \right) = Ma, Re$$

where the vector  $\vec{r}$  has been replaced by its magnitude  $r$  and its inclination  $\theta$  to the jet axis.

To go beyond this stage, more and more detailed physical models must be adopted, or else the emphasis is thrown entirely on the measurements per se. For example, if the emitter contains travelling sources, the combination  $Ma \cos \theta$  will be characteristic, rather than  $Ma$  and  $\theta$  by themselves.

## INTERPRETATION OF JET NOISE

While the measurements of wall-pressure fluctuations under a turbulent boundary layer and turbulent pipe flow are measurements of noise from a practically homogenous surface emitter, jet noise is emitted from highly nonhomogenous turbulence which occupies a small region.

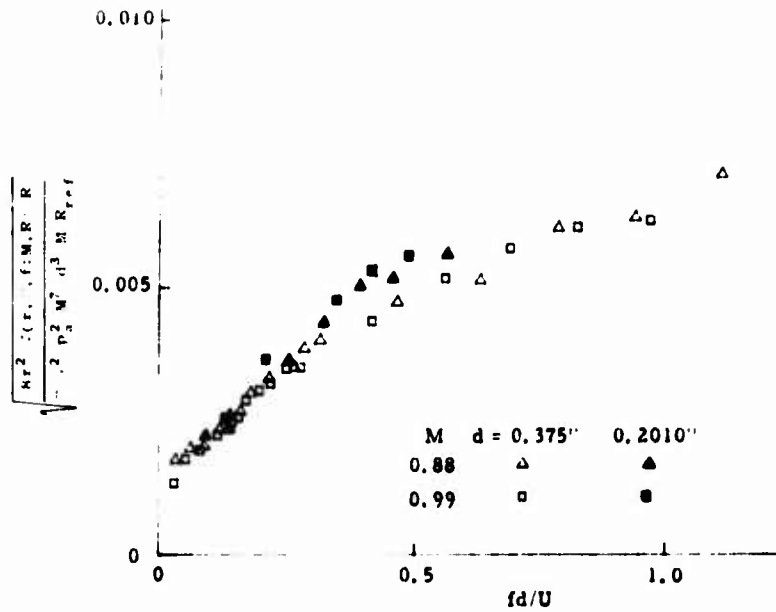


Fig. 4 - Power spectra of jet noise at  $90^\circ$

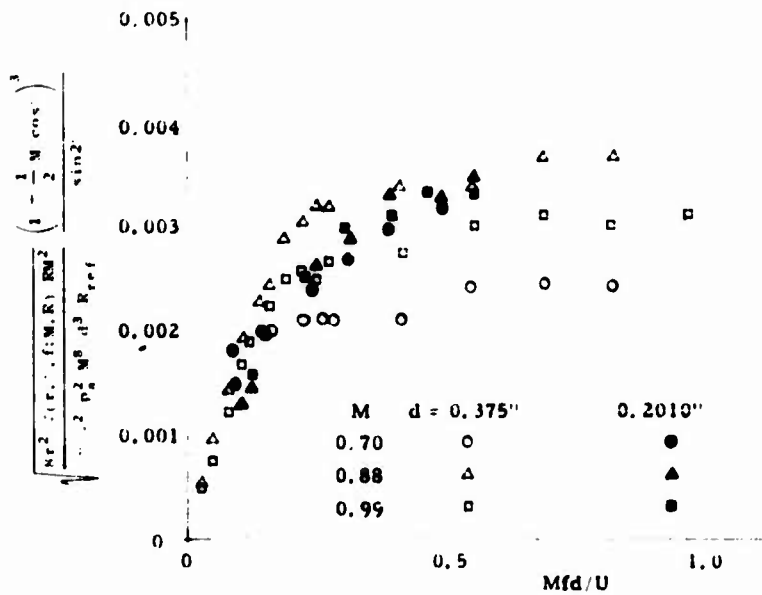


Fig. 5 - Power spectra of jet noise at  $40^\circ$

It is usually attempted to interpret measurements of jet noise in terms of the concepts introduced by Lighthill (3) in his now famous paper. It may still be true that this is still too ambitious an undertaking, since a true comparison with Lighthill's theory demands a detailed knowledge of the flow field far beyond what has so far been obtained. Lighthill's theory attempts to determine the overall sound field of a turbulent flow in terms of elementary, characteristic sound sources, the quadrupole field of turbulence. Between such an approach and the still comparatively crude measurements, one may well interpose a more naive and restricted interpretation, in which for example the jet is considered as an axially symmetric line emitter, as far as the far field is concerned. The gross features of this emitter can be determined from experiment. An application of this intermediate approach will be given in the forthcoming paper by Mollo-Christensen and Narasimha; a few features will be illustrated here.

The most surprising result of our measurements of jet noise was the marked Reynolds number influence both on intensity and spectrum. This we believe can only be explained in terms of transition to turbulence in the free shear layer. Since a turbulent flow induces more influx than a laminar shear layer, one may interpret the corresponding sound field as produced by a source on the axis if the transition is axially symmetric. If the transition is antisymmetric about the jet axis, the jet is whipping around, one can describe the sound emission as that due to dipoles perpendicular to the axis. If the whipping of the jet is strongly anticorrelated along the jet axis for one-half wavelength, the field will be that of a lateral quadrupole.

In part, emitted sound may have wavelengths comparable to the size of the emitter, and to determine the spectra one then has to consider the antenna problem involved. In any case the gross motion of transition and its influence upon the sound field is a feature which is relatively easily tractable.

An example of the effect of Reynolds number on the sound field is shown in Fig. 4, where spectra from two jets from geometrically similar nozzles of two diameters are shown, with a Reynolds number factor included in the spectra. In Fig. 5, similarly, we show spectra measured at  $M = 40$ , at three Mach numbers, and two nozzle diameters. In addition to a Reynolds number correction, we have attempted to include a factor to account for the possibility of source convection. The same spectra, without the Reynolds number correction, are shown in Fig. 6. As can be seen, there appears to be a strong Reynolds number dependence. Finally, in Fig. 7, some spectra obtained at  $M = 25$  are shown.

## CONCLUSIONS

It seems to be imperative to utilize dimensional analysis and similarity relations to the extent possible in experiments on aerodynamic noise. Only by this approach can one identify and eliminate spurious effects; also, it appears to be the only possible framework for analysis of experimental results and synthesis of possible mechanisms of emission, in short, for understanding.

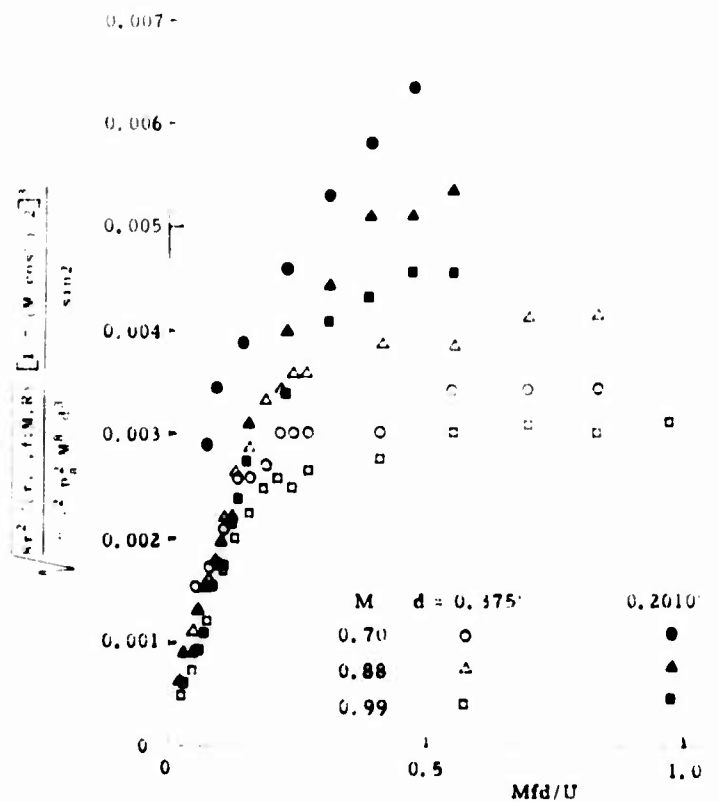


Fig. 6 - Power spectra of jet noise at ...

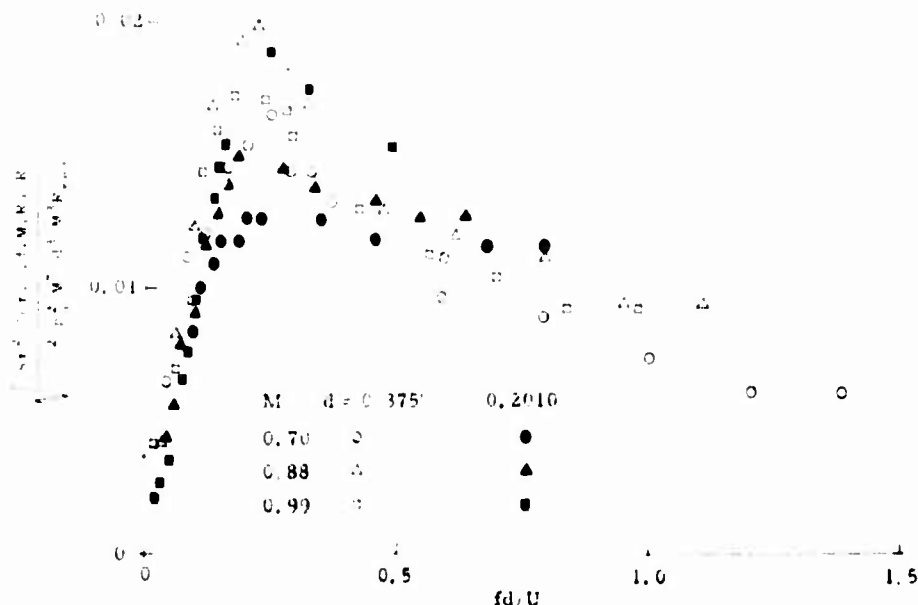


Fig. 1. Power Spectra of the Wall Pressure

## REFERENCES

1. Willmarth, W.W., "Space-Time Correlations and Spectra of the Wall Pressure in a Turbulent Boundary Layer," NACA Technical Note in print.
2. Weyers, Paul F.R., "The Vibration and Acoustic Radiation of Thin-Walled Cylinders Caused by Internal Turbulent Flow," submitted to NACA, Aug. 1957.
3. Lighthill, M.J., "On Sound Generated Aerodynamically - I. General Theory," Proc. Roy. Soc. A211:564-577 (1952).

• • • • •

## DISCUSSION

M. Strasberg (David Taylor Model Basin)

At the David Taylor Model Basin we have performed measurements of pressure fluctuations. For those measurements involving essentially incompressible flow, that is, pressure fluctuations in the near field (at distances from the source that are

less than a quarter wavelength of whatever frequency is of interest), we have found that similarity is maintained. These include the near field of a turbulent jet at low Mach numbers and the pressure fluctuations in the wake of a cylinder. In those cases, similarity was maintained, that is, when we plotted a non-dimensional, spectral density versus a Strouhal number, we would get a spectral curve that applied at all velocities. We were not surprised by this. We would have been more surprised if this hadn't been the case.

I would like to mention a convenient way for expressing spectral distributions. It has been common to express the spectrum in terms of spectral density, which is the mean square pressure in a narrow band divided by the bandwidth, but for non-dimensional parameters one might consider expressing the spectrum in a slightly different way as the mean square pressure itself, which remains proportional to the frequency. This is just a matter of convenience, the advantage being that when going from one scale to another it is not necessary to correct for the bandwidth. The bandwidth automatically changes in the right way. For example, one can give the mean square pressure in a half octave band. The reason I am suggesting this is that I have seen many cases where people scale from one dimension to another, and forget to change the bandwidth proportionally.

E. Mollo-Christensen

In response to Dr. Strasberg's remark that similarity should be expected in individual measurements, I would like to point out that if only one parameter is varied it may be easy to obtain apparent similarity, but no evidence has been obtained that the phenomenon is independent of the variables which were not changed during the experiment.

One has not demonstrated similarity, for example, when measuring the pressure fluctuations in a turbulent boundary layer if a part of the observed fluctuations could be due to turbulent flow in the tunnel. Such pressure fluctuations would probably scale with velocity the same way as the pressure fluctuations due to boundary layer turbulence. Thus, parasitic effects may follow the same similarity law as does the process one intended to observe. To avoid this, one must either eliminate or change the wind tunnel turbulence. I believe the disagreement between the results obtained by Dr. Willmarth and those obtained by Dr. Strasberg may be due to the fact that Willmarth's measurements were performed with virtually zero free-stream turbulence, while Strasberg's were obtained in an existing wind tunnel where there apparently was some free-stream turbulence, judging from the difference in spectra and space-time covariance observed in the two investigations.

About the suggestion that one plot constant-Q spectra: I feel it may take some time to become accustomed to the relation (for example, between such spectra and the correlation function).

. . . . .



# NOISE PRODUCTION IN A TURBULENT BOUNDARY LAYER BY SMOOTH AND ROUGH SURFACES

Eugen Skudrzyk and Gillian Hamble

*Department of Physics, University of*

*California, San Diego, California 92161*

The flow noise pressure produced in a turbulent boundary layer is proportional to the square of the fluctuations in turbulent velocity; consequently, it is also proportional to the coefficient of the drag, and to the square of the free-stream velocity of the fluid. For a turbulent boundary layer, the coefficient of drag is practically independent of the Reynolds number, and of the shape of the body. This property makes possible a general investigation of the boundary layer noise, without consideration of the shape of the body.

The flow noise turns out to consist of two components: one being due to the ordinary turbulence in the boundary layer, the other due to the small-scale turbulence generated by the surface roughnesses. At higher frequencies, the regular boundary layer noise seems to increase at a rate of 18 db, the roughness noise at a rate of 18 to 35 db per speed surface and unit area density of the roughnesses. For plainly machined surfaces, roughness noise and boundary layer noise are equal at a frequency of 20 kc, at about a speed of 20 knots. At higher speeds the roughness noise predominates over the boundary layer noise. If the diameter of the receiving hydrophone is halved, its flow noise sensitivity increases by approximately 12 db. A hydrophone mounted in the stagnation region of a streamlined body emits less flow noise at higher frequencies, but more flow noise at lower frequencies than one mounted flush with the side walls of a streamlined body.

## INTRODUCTION

Acoustic communication through the water medium is greatly handicapped by the noise produced by the moving vehicle and its machinery. At low speeds, the machinery noise seems to predominate over all other disturbances. But as the speed increases, the flow noise becomes greater until finally, at very high speeds, it seems to mask all other components of noise. The flow noise seems to be generated mainly in the boundary layer and in a turbulent boundary sublayer of the moving vehicle. The paper represents a first attempt to investigate theoretically and experimentally the component of flow noise produced by the surface roughnesses and the turbulence in the boundary layer of a body moving in water.

## EXPERIMENTAL EQUIPMENT

To ensure well-defined experimental conditions, a boundary layer of constant thickness had to be generated. This regularity could be obtained with a rotating cylinder. There were reasons to believe that the finite length of the cylinder had little effect on the inner part of the boundary layer, which is known to be responsible for most of the flow noise, and that the results could be generalized later for any other curved surfaces.

The first experiments were made in the Ordnance Research Laboratory. It was certain that the properties of the cylinder walls would play an active part in the experiments. The fluctuating pressure could be expected to excite resonant modes; and the resonating modes would, in turn, excite the sound receiver, whether it was attached to the shell or placed far away from it. This complex behavior to be expected in any practical situation was the reason for leaving purely theoretical ground, for using the same hydrophones as are used with some in-service torpedoes, and for making up a cylinder of 1 8-inch steel, 17.9 inches outer diameter, and 24 inches long, with aluminum domes fastened on each end. The overall length was 42-3 4 inches (Fig. 1). It was driven by an 11.5-hp motor utilizing V-belts. Figure 2 shows the cylinder mounted in the acoustic water tank wherein all the measurements were taken. The sound receivers were two magnetostrictive hydrophones, one 2.5 inches in diameter, the other 5 inches in diameter. The hydrophones were mounted 180 degrees apart at the midpoint on the inside wall. Figure 3 shows the frequency responses of these hydrophones. The external-noise measurements were made with a similar receiver, a 24.5-ke hydrophone located one yard from the surface of the cylinder and at the same depth as the center of the cylinder.

The machinery noise is very small at high frequencies (as can be deduced from the curves for a smooth metal surface) - to be discussed later. The background noise may therefore be attributed to the structure-borne noise transmitted into the water tank, and to the thermal-noise level of the transducers. For small speeds the noise level equals the background noise level (-30 db below 1 dyne).

Other equipment was used in additional measurements performed in the Garfield Thomas Water Tunnel. The test section has a diameter of 48 inches. Each hydrophone was made up of two barium titanate discs, one inch in diameter, each 0.27 inches thick. One disc was fitted with a small hole in the middle of its face, that served to take up the lead to the hot electrode, which was at the interface between the two crystals. The unit was enclosed in a rigid brass box with a 1 16-inch thick membrane in front. Great care was taken to ensure perfect contact with the casing and between the crystals by using castor oil as a coupling agent. The unit was calibrated at the Black Moshannon Calibration Station. On the average its sensitivity was the same as the theoretical value of -100 db per bar re 1 volt. A second set of hydrophones of similar construction had a diameter of 1 2 inch, a thickness of 0.1 inch. Hydrophones were also mounted at the nose and at the side of a streamlined body having a maximum diameter of 4 1 8 inches and a length of 20 inches. This body was held in position in the middle of the test section of the channel by a strut. The frequency analysis was performed over the bands 250 to 500 cps, 500 cps to 1 ke, 1 ke to 2 ke, 2 ke to 4 ke, 4 ke to 8 ke, 8 ke to 10 ke, 10 ke to 15 ke, 20 ke to 25 ke, 30 ke to 40 ke, 60 ke to 80 ke, 80 ke to 100 ke, except for the results plotted in Fig. 16, which were obtained by a 5-cycle-band analysis.

## THE VELOCITY DISTRIBUTION NEAR THE ROTATING CYLINDER AND IN THE TEST SECTION OF THE GARFIELD THOMAS WATER TUNNEL

The pressure distribution in the boundary layer of the rotating cylinder was measured with a multiple-rake manometer from a distance of 1 4 inch to about 6



Fig. 1. Rotating cylinder and drive shaft assembly.

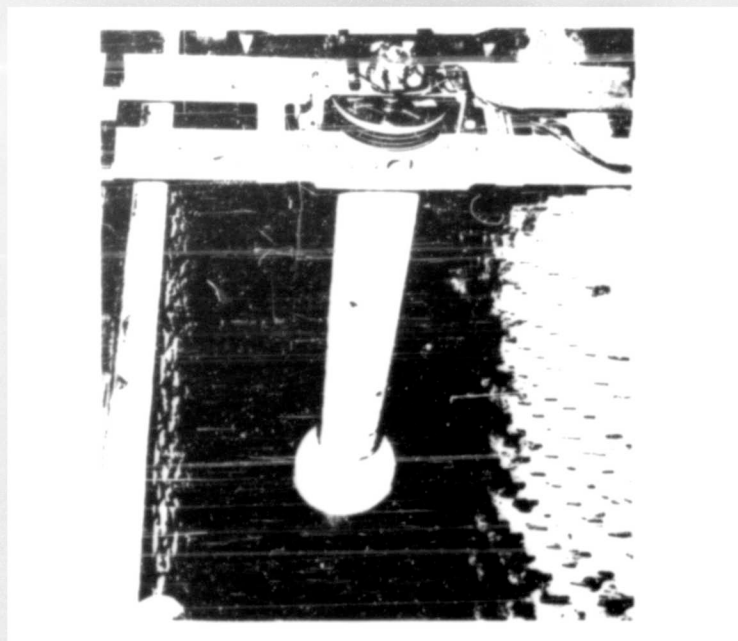


Fig. 2 - Rotating cylinder and tank

inches. The velocity distribution could then be computed. The measurements were in good agreement with the Prandtl-von Kármán logarithmic-velocity formula (1) as shown in Fig. 4. For the plane of symmetry of the cylinder the following result was obtained:

$$\frac{u}{u_0} = 5.75 \log_{10} \frac{y}{\delta} \quad (2)$$

This unexpected result seems to be due to the fact that the shear velocity was very nearly constant over the whole boundary layer. It varied only by a factor of two from the innermost part of the boundary layer to the regions a few inches distant from the surface of the cylinder. This could be deduced from the drag measurements published by Theordorsen (2) and the value determined from the results represented in Fig. 4. A graph of the time variation of the pressure distribution (Fig. 5) proved that there was practically no time lapse between the surface speed of the cylinder and the building up of the inner regions of the boundary layer.

The velocity distribution over the major part of the cross section of the tunnel was uniform. Figure 6 shows the variation of the velocity over the boundary layer at sections 10 feet from the front end of the test section.

#### DERIVATION OF THE THEORY ON THE BASIS OF THE EXPERIMENTAL RESULTS

Whenever the Reynolds number of flow exceeds a limiting value, the flow becomes unstable and turbulent. This instability is caused by a predominance of the kinetic

# Noise Production in a Turbulent Boundary Layer

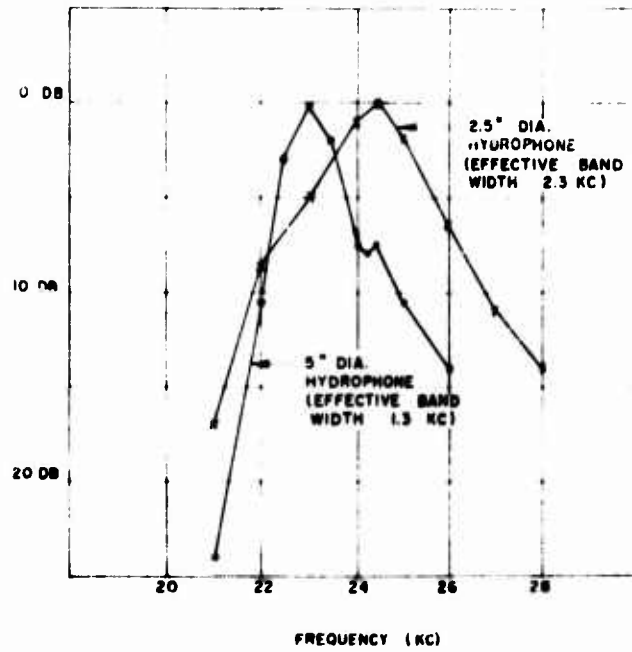


Fig. 3 - Hydrophone frequency responses

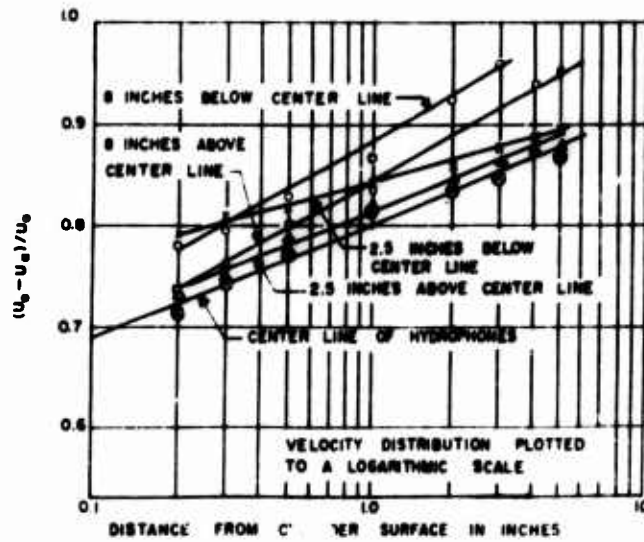


Fig. 4 - Mean velocity vs distance from surface of rotating cylinder

forces over the viscous forces. The kinetic forces such as the Kutta-Joukowski lift and the Coriolis force are all proportional to the square of the velocity, whereas the frictional forces increase with only the first power of the velocity. At small Reynolds numbers, the velocity  $v$  is large in comparison to  $v^2$  and friction governs the motion. Any disturbance in the velocity field therefore decreases rapidly to zero. At high

speeds,  $v^2$  is greater than  $v$ , and the kinetic forces determine the flow. Friction then becomes almost entirely negligible and the fluid behaves similar to an ideal gas or to a collection of ideal elastic balls. A disturbance introduced into the flow no longer decreases but persists or even increases with time, because of the production of mechanical energy by the surface drag.

The Reynolds number for which the kinetic forces become larger than the viscous forces can be crudely estimated. If we identify the disturbances with a cylindrical or, better, a spherical particle, a value of 50 to 100 is obtained, which agrees well with the experimental value 60 observed for the generation

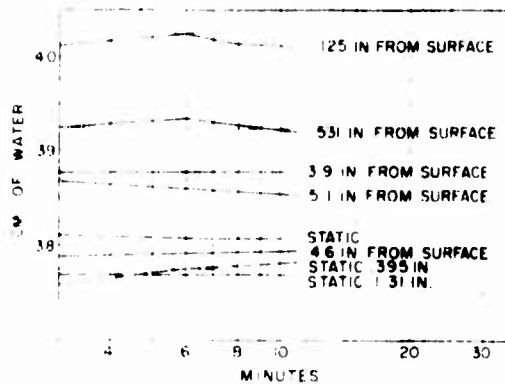


Fig. 1. — Relationship between the velocity of water and time after setting free cylinder in motion.

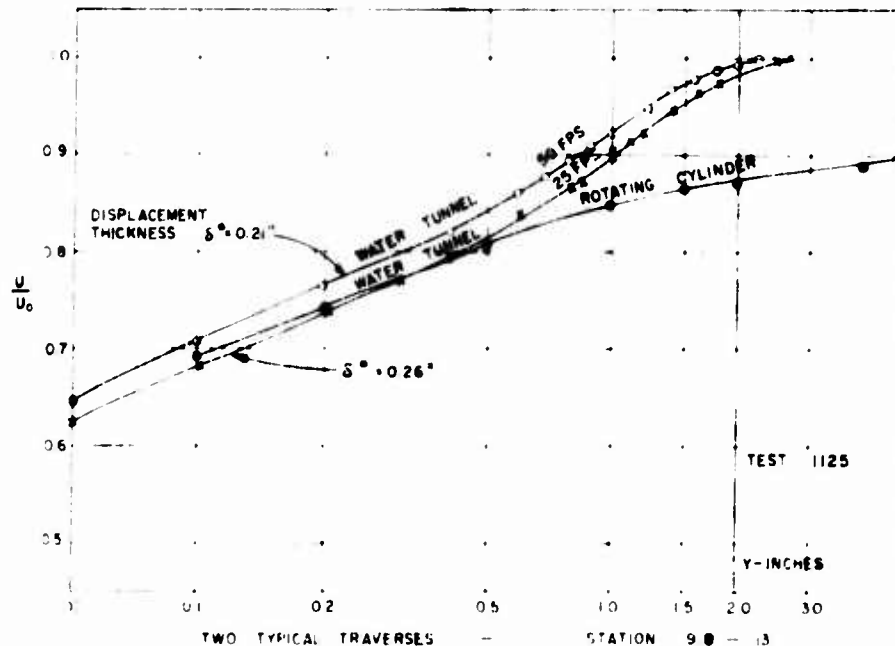


Fig. 2. — Velocity of water over the boundary layer of the rotating cylinder. The displacement thickness is indicated by the dashed line.

of turbulence in a wake. The corresponding Reynolds number for the onset of turbulence in the boundary layer of the rigid body is at least 40 times as large. This signifies that the turbulence in the boundary layer of a rigid body is completely different in nature from the turbulence in a wake. This fact may be interpreted as follows: Because of the attractive forces exerted by the wall and the increased internal friction owing to the proximity of the wall, turbulence is much harder to start. Recent research (3) shows that turbulence is initiated by a phenomenon that is similar to a series of internal explosions of the fluid. But the moment turbulent patches or vortices have been formed, they possess so much kinetic energy that they may split up into smaller and smaller ones of less than 1/50th of the original diameter, and all these patches or vortices will still possess sufficient energy to have an appreciable lifetime ahead of them. The diameters of the vortices in the boundary layer of a rigid body therefore vary between a diameter equal to the thickness of the boundary layer and a diameter at least 40 times smaller; and the space-wave-number spectrum of this turbulence is continuously distributed over a fairly large volume in wave-number space. Under this condition, equilibrium laws such as the Kolmogorov laws (see Appendix A) for homogeneous turbulence may be expected to apply. In fact, it is possible to estimate the root-mean-square velocity fluctuation of the turbulence on the basis of this law, the result having at least the same order of magnitude as the measured values. Kraichnan (4a) has recently improved the Kolmogorov theory on the basis of statistical mechanics and has derived a slightly different wave-number dependency.

The velocity fluctuations caused by the turbulent patches increase the transportation of momentum and generate the drag. Our first task is to compute the magnitude of the velocity fluctuations, assuming the drag to be known. This computation can be performed in two different ways. We may start with the Stokes-Navier equations. If the mean values of the components of the velocity are denoted by  $u, v, w$ , and the fluctuating velocity components are denoted by  $u', v', w'$ , this equation becomes

$$\rho \frac{d\mathbf{u}}{dt} = \mu \nabla^2 \mathbf{u} + \mathbf{F}$$

The expression in the parentheses on the right-hand side represents the drag. Outside the laminar sublayer, the first term  $\mu \nabla^2 \mathbf{u}$  is negligible; and the drag becomes

$$\mathbf{F} = \mathbf{F}_d$$

The second method is based on the gas-kinetic considerations. Since friction is negligible at high Reynolds numbers, computing the drag in a similar manner is permissible, as the viscous force is gas-kinetic. The above expression is then re-obtained. If the flow is homogeneous,  $u'$  and  $v'$  are the same; but the turbulence in the boundary layer is not homogeneous. We may, however, define an effective velocity by the equation

$$u'^2 = v'^2$$

This velocity  $u'$  represents the geometric average of the fluctuating velocities, in the direction of the flow and perpendicular to the wall in the innermost part of the turbulent boundary layer at a distance from the wall, where the viscous forces just become negligible. According to the classical Prandtl theory of turbulence,  $u'$  should be practically constant according to the von Kármán theory,  $u'^2$  should decrease proportionally to the distance from the laminar sublayer to zero at the outer limit of the boundary layer, an assumption that agrees well with Lauter's (7) measurements. The magnitude of  $u'$  determines the shear force near the wall, the so-called surface drag; it is known as the shear velocity.

The surface drag has been thoroughly studied for pipes (1,5) and channels (1,6) as well as for flat plates (1,6) and rotating cylinders (2). The experimental results show that the surface drag is approximately proportional to the square of the free-stream velocity  $u_\infty$ . The surface drag can therefore be expressed as the product of the coefficient of drag  $c_D$  and the square of the free-stream velocity:

$$C_D = \frac{1}{\rho} v^{*2}$$

denoting the density of the fluid.

This coefficient of drag proves to be practically a constant and to be equal to  $3 \times 10^{-4}$  whenever the flow is turbulent. It changes by only a factor of 3 when the velocity is changed by as much as a factor of 5000 (Ref. 1). Since this surface drag is generated in the inner part of the boundary layer, we may expect that it will not greatly depend on the curvature of the surface nor on the size of the body that generated it. This conclusion has been verified by Theodorsen (2) for a series of rotating cylinders. The ratio of the height to the diameter has been varied by as much as a factor of 20. Nevertheless, all the measured points seem to lie on the same curve (Fig. 7). We may therefore assume that the coefficient of drag is independent of the curvature and of the size and shape of the body. This approach means a considerable simplification in the study of flow noise.

The fluctuating velocity  $v^*$  can be computed by equating the theoretical and experimental results.

$$v^{*2} = \frac{1}{2} C_D u_\infty^2 = 15 \cdot 10^{-4} u_\infty^2 \text{ or } v^* = 0.04 u_\infty$$

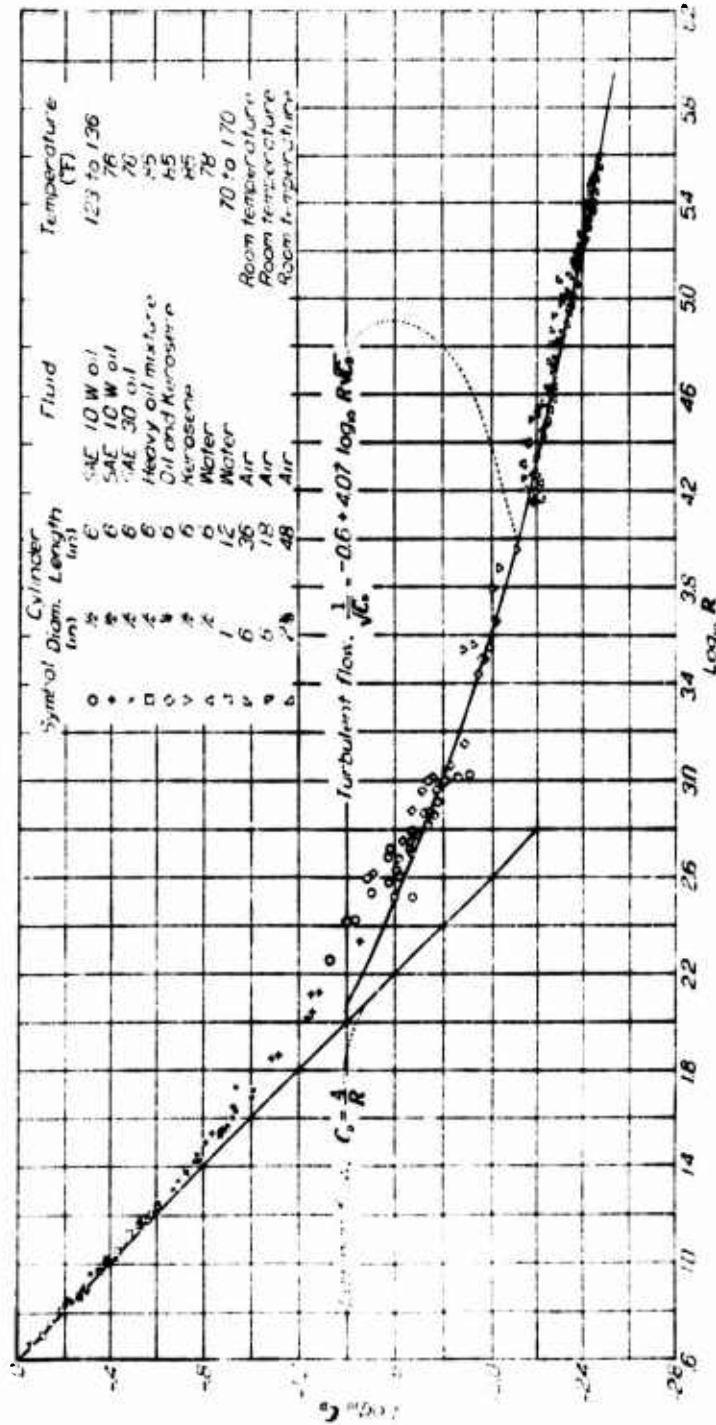
The effective velocity then turns out to be very nearly equal to 4 percent of the free-stream velocity.

This result is in good agreement with Laufer's channel measurements (7). The shear velocity reaches 4 percent at the outside of the laminar sublayer, and then decreases linearly with the distance until it becomes zero at the outer side of the boundary layer. Laufer's measurements also show that  $u'$  is about 8 percent of  $u_\infty$ , and  $v$  slightly less than 4 percent of  $u_\infty$ ; because of the imperfect correlation between these two,  $uv$  is only 4 percent of  $u_\infty^2$ .

The next task is to derive the connection between the fluctuating velocity  $v^*$  and the pressure at a point in the boundary layer. The boundary layer is usually thin and the scale of the turbulence we are interested in small in comparison to the acoustic wavelength. Because of this fact the pressure fluctuations in the boundary layer will be primarily kinetic. They are generated by the centrifugal and similar forces of the rotating vortices; they represent the near field of the dipole, quadrupole, and octupole sources that mathematically describe the turbulence. To distinguish these pressure fluctuations from a true sound field, they are usually summarized under the name quasi sound. In addition to this quasi sound, true sound that is radiated off to greater distance is produced because of the unsteadiness of the flow. But this true sound seems to be negligible in the boundary layer in comparison to the internal near field generated by the rotating vortices. This fact makes it possible to establish the connection between the fluctuating velocity and the sound pressure by an equation of the type of the Bernoulli equation (Appendix B) with a slightly modified constant

$$p = \rho v^{*2}$$



Fig. 7 - Drag coefficient  $C_D$  for rotating cylinders as function of Reynolds number

where  $C$  is a constant of the order of magnitude one. This quasi sound pressure would be actually measured, if the sound receiver were infinitely small.

A receiver of finite size measures the average value of the pressure over its sensitive area. This average value is the smaller, the larger the area, since the pressure maxima and minima compensate one another. If the hydrophone area is very large in comparison to the scale of the turbulence, the average quasi sound pressure will be very small, and the hydrophone reading will be mainly determined by the true radiation field generated in the whole space that surrounds the hydrophone. The above formula will then no longer apply.

Let us consider a practical case, such as a vehicle traveling with a velocity of 20 knots or 10 meters per second. The effective fluctuating velocity would be 40 centimeters, and the noise pressure as given by the above equation would be 1600 dynes/cm<sup>2</sup>. This result is very interesting, but it does not yet give any information about the flow noise actually produced by the moving body. The frequency spectrum is still unknown. The flow noise spectrum may be centered at extremely low frequencies and be inaudible, or may be in the audible or supersonic range.

First of all, we have to find the connection between the frequency spectrum of the noise pressure and the scale of the turbulence. We may identify the patches with the maxima and minima in a progressive wave that moves with the local mean speed  $u$  of the flow along the surface of the receiving hydrophone. This local speed  $u$  varies according to how far away from the laminar sublayer the patches are between  $u_0$  and  $u'$ . The pressure fluctuations as recorded by the hydrophone will then have a frequency

$$f = u/\lambda$$

where  $\lambda$  is the distance between successive vortices or is the scale (the effective diameter) of the turbulent patches. For low-frequency noise, this local velocity  $u$  will have to be assumed to be roughly equal to the free-stream velocity of the fluid.

There are two possible ways to compute the frequency spectrum of the flow noise. Kraichnan (4c) assumed a Gaussian correlation function for the velocity correlation, his supposition being equivalent to assuming a Gaussian energy spectrum of the turbulence. The pressure spectrum is then derived by a series of integrations. The result still resembles a Gaussian spectral distribution in its sharp cutoff at frequencies above a limiting frequency represented by

$$f = u/\delta$$

where  $\delta$  is the thickness of the boundary layer. If we substitute numerical values and assume a speed of 20 knots or 10 meters per second and a thickness of 1 centimeter for the boundary layer, this frequency will be 1 kc.

The second procedure is as follows: We may divide the spectrum into a low-frequency spectrum and a high-frequency spectrum. For the derivation of the low-frequency spectrum, the patch of turbulence may be considered as equivalent to a pulse of a width equal to the diameter of this patch. If we assume this diameter to be roughly equal to the thickness of the boundary layer, the spectrum then turns out to be constant up to a space wave-length equal to the diameter of the patch or to the thickness of the boundary layer. From there on it decreases as  $(\lambda/\delta)^{-5/3}$ . For the derivation of the high-frequency part of the spectrum, the details are furnished at least approximately by the equilibrium laws of turbulence. The Kolmogorov law, for instance, predicts that at high frequencies the energy spectrum decreases inversely as the  $3/2$  power of

the space wavelength. The spectral density of the turbulence noise may thus be expected to be approximately constant at lower frequencies up to the frequency  $\omega_m$  determined by the ratio of the free-stream velocity to the thickness of the boundary layer. From there on, it may be expected to decrease approximately inversely as the  $3/2$  power of the scale of the turbulence or the space-wave number.<sup>2</sup>

Figure 8 shows some measurements performed in the Garfield Thomas Water Tunnel at State College. The method used in making these measurements will be described later. The noise level is shown as a function of frequency for several flow speeds. Up to a certain frequency, which in this particular case should be about 400 cycles per second, the noise level should be constant; and from there on should approximately decrease inversely as the  $5/3$  power of the frequency.

The experimental results show that we must distinguish between two types of flow noise. The first type is the one we just discussed: it is the flow noise produced by the velocity fluctuation in the turbulent boundary layer that has been studied thoroughly, in great detail, and very ingeniously by R. H. Kraichnan (4b). M. Harrison (8) verified the predictions of the Kraichnan theory experimentally in air-channel flow and proved that the assumptions in Kraichnan's work are indeed very reasonable.

The second component of flow noise is produced by the surface roughness. With an increasing speed of flow, the laminar boundary layer becomes continuously thinner. When the velocity reaches a certain value, the roughnesses become greater than the thickness of the laminar boundary sublayer and penetrate the laminar boundary sublayer. They then become capable of shedding vortices or of producing a von Kármán vortex street (9). The vortices generated this way increase the surface drag and create a turbulent sublayer on top of the laminar boundary sublayer. Because of its small scale and its great energy content, this turbulence may be expected to create a high noise level with an essentially high-frequency spectrum. Before going more into detail, let us prove that this "roughness noise" does indeed exist. Figure 9 shows measurements that have been performed with the aid of a rotating cylinder 42 inches high and about 23 inches in diameter, and with a microphone mounted flush with the wall of the cylinder. The abscissa in this figure represents the surface velocity of the cylinder; the ordinate represents the noise level. Let us first concentrate on the measurements performed with a smooth painted cylinder surface, a surface as smooth as possible. Until the speed exceeds a certain value, the noise level is that of the ambient noise; from there on, it increases at a rate of roughly 13 db per speed octave, as for true boundary layer noise. Now let us consider a second measurement that has been performed under the same conditions except that the surface of the cylinder has been roughened (grit 180). The noise level now exceeds that of the ambient noise at a much slower speed than in the previous case. For the same velocities the flow noise produced by the rough surface is 20 to 50 db greater than that produced by the smooth painted surface. Since nothing else has been changed, the greater noise must be attributed to the effect of the surface roughnesses. There is no doubt that roughnesses generate flow noise.

The effect of surface roughnesses on the drag has been thoroughly studied in the literature for flat plates (1), pipes (1,5,6), and a rotating cylinder (2). The results are always the same. Whenever the surface roughnesses penetrate the laminar boundary sublayer, they increase the surface drag. The theory shows that the roughnesses

<sup>2</sup> It is to be noted that the mean frequency content of the velocity fluctuations comes from the random velocity fluctuations of the mean motion of the fluid, and that the frequency content of the latter is a function of the statistical properties of the mean motion, and is not a function of the statistical properties of the mean motion of the fluid. The mean motion of the fluid is a function of the statistical properties of the mean motion of the fluid.

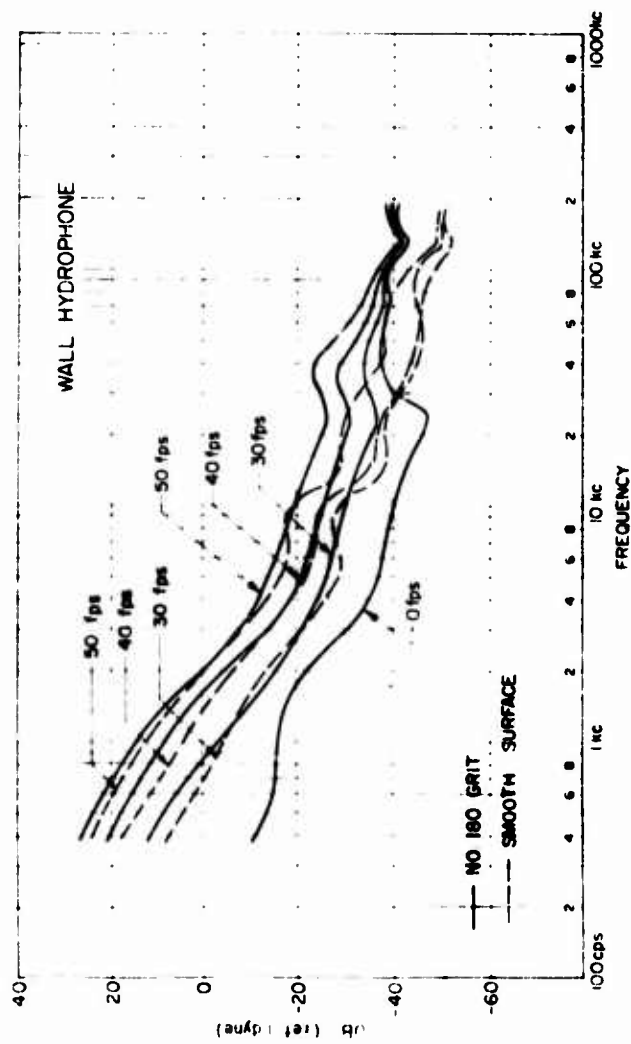


Fig. 8 - Spectrum (half-octave measurements) of the boundary layer noise in the test section of the Garfield Thomas Water Tunnel for various water speeds

# Noise Production in a Turbulent Boundary Layer

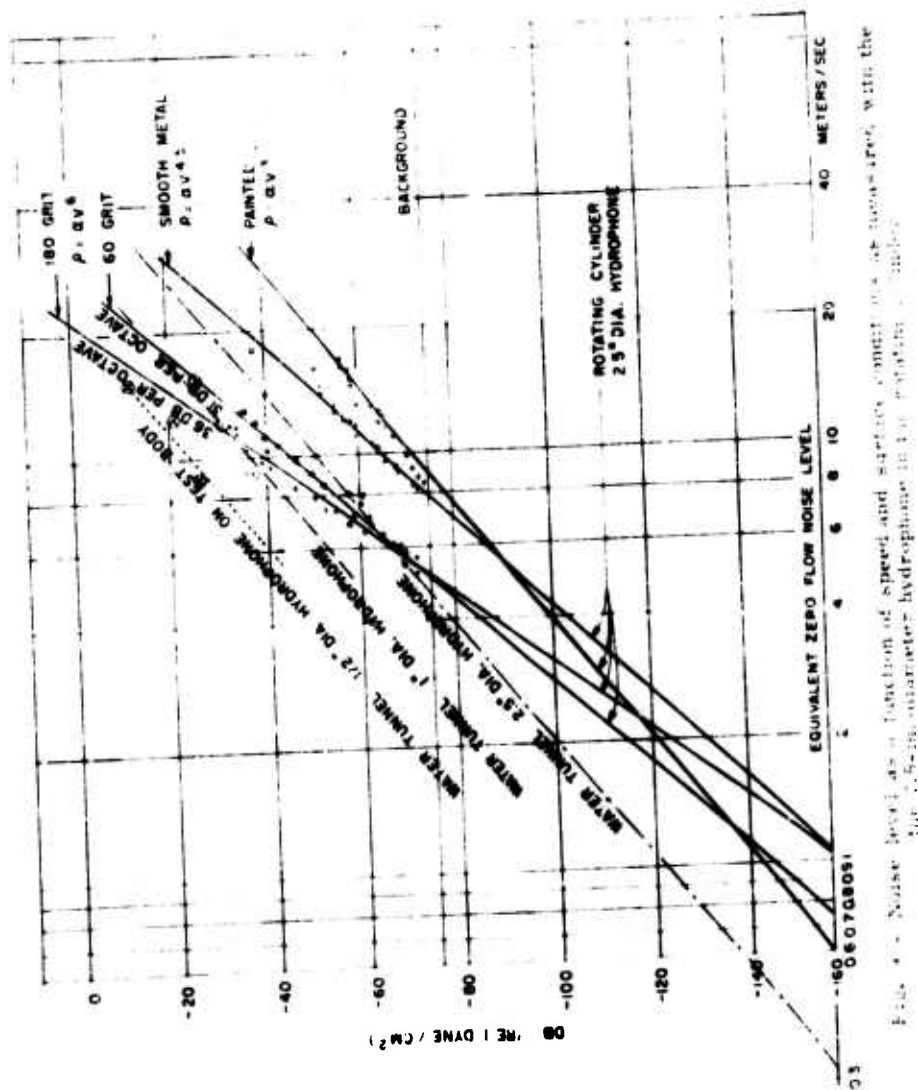


Fig. 1 - Noise level as a function of speed and surface condition as measured with the 2.5" dia. rotating cylinder hydrophone in the rotating cylinder.

become larger than the thickness of the boundary sublayer if their Reynolds number becomes greater than 5:

$$S = 1/5.$$

The velocity in the immediate vicinity of the laminar sublayer is approximately equal to the shear velocity. The above Reynolds number had therefore to be formed with the height of the roughnesses and the shear velocity.

With the aid of the previous results, the above Reynolds number of 5 can be expressed as a function of the free-stream velocity. The roughnesses are then found to become effective when the speed is greater than the critical value given by

$$V_{crit} = 10^{-2} / \epsilon \text{ knots/sec.}$$

where  $\epsilon$  is the height of the roughnesses in inches. An analogous condition can be derived for the shedding of vortices by roughnesses in a nonturbulent boundary layer: the Reynolds number then has to be formed with the height of the roughnesses and the laminar velocity at a distance  $\epsilon$  from the walls. This Reynolds number increases toward the stagnation point, as would be expected because of the greater velocity gradients. For roughnesses of  $10^{-2}$  inch and a distance from the edge of the body greater than a few centimeters numerically, very nearly the same results are derived for the roughness noise; and it should make little difference whether the bulk of the boundary layer is turbulent or laminar. However, the regular boundary layer noise will not be generated in the stagnation region because of its predominant laminar nature. It is hard to predict the reduction of flow noise that could be expected in such a case because flow noise will also be radiated back from the other parts of the moving surface into the stagnated area.

Figure 10 illustrates the above results for rotating cylinders covered with roughness of various grain sizes. Whenever the Reynolds number of the roughnesses exceeds 5, the drag becomes greater than that for a smooth surface. The speed at which these increases are observed is thus a function of the height of the roughnesses only, but the magnitude of the increase of the drag is a function of the density of the roughnesses. This is illustrated in Fig. 11, which represents measurements where the density of the roughnesses has been varied.

The noise pressure has been shown to be proportional to the drag. The increase in drag because of the small-scale surface roughnesses may therefore be expected to show up in a corresponding increase of high-frequency flow noise. That this assumption is essentially correct is illustrated in Fig. 9. No flow noise can be observed at lesser speeds. At the critical Reynolds number, flow noise may be expected to be generated, but the intensity of this noise is still so small that it is completely masked by the ambient noise. From a certain speed onwards, a speed that depends on the size and density distribution of the surface roughnesses, the level of the flow noise exceeds that of the ambient noise; it increases at a rate of 15 to 35 db per speed octave, according to whether the surface is rough or smooth.

For unit 10, 90 percent of the particles have a height of about  $5 \cdot 10^{-3}$  inch. The critical speed is therefore 2 knots or 1.94 m/sec. If we extrapolate the curve for this kind of unit down to a speed of 2 knots, from whence the roughnesses would be expected to become acoustically effective, the noise level turns out to be -15 db. This minimum is considered to be the equivalent of 0 m flow noise level for the comparison of the experiment. The other curves should then intersect with the speed-flow

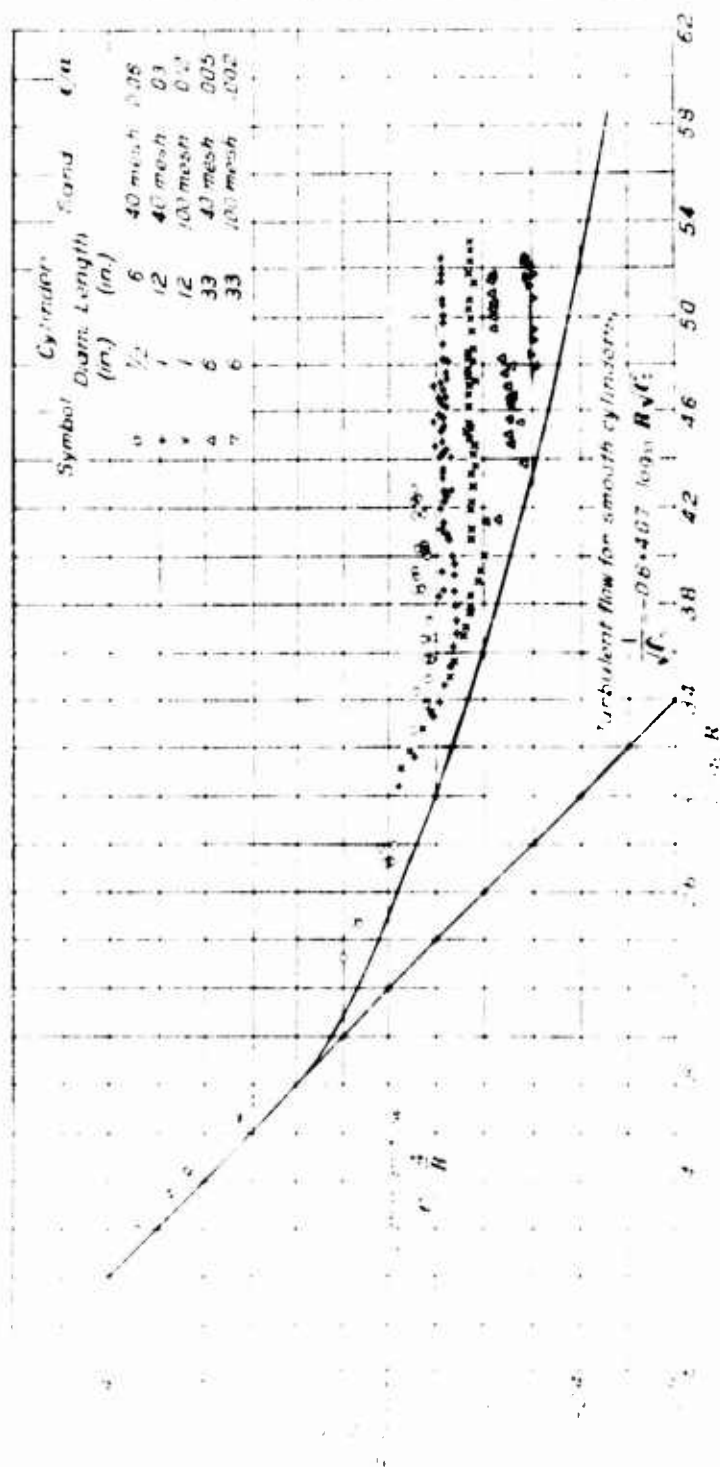


Fig. 1. Relationship between  $\sqrt{h}$  and  $R$  for turbulent flow over smooth cylinders. The case of saturated steam at 100 psia is shown in parentheses.

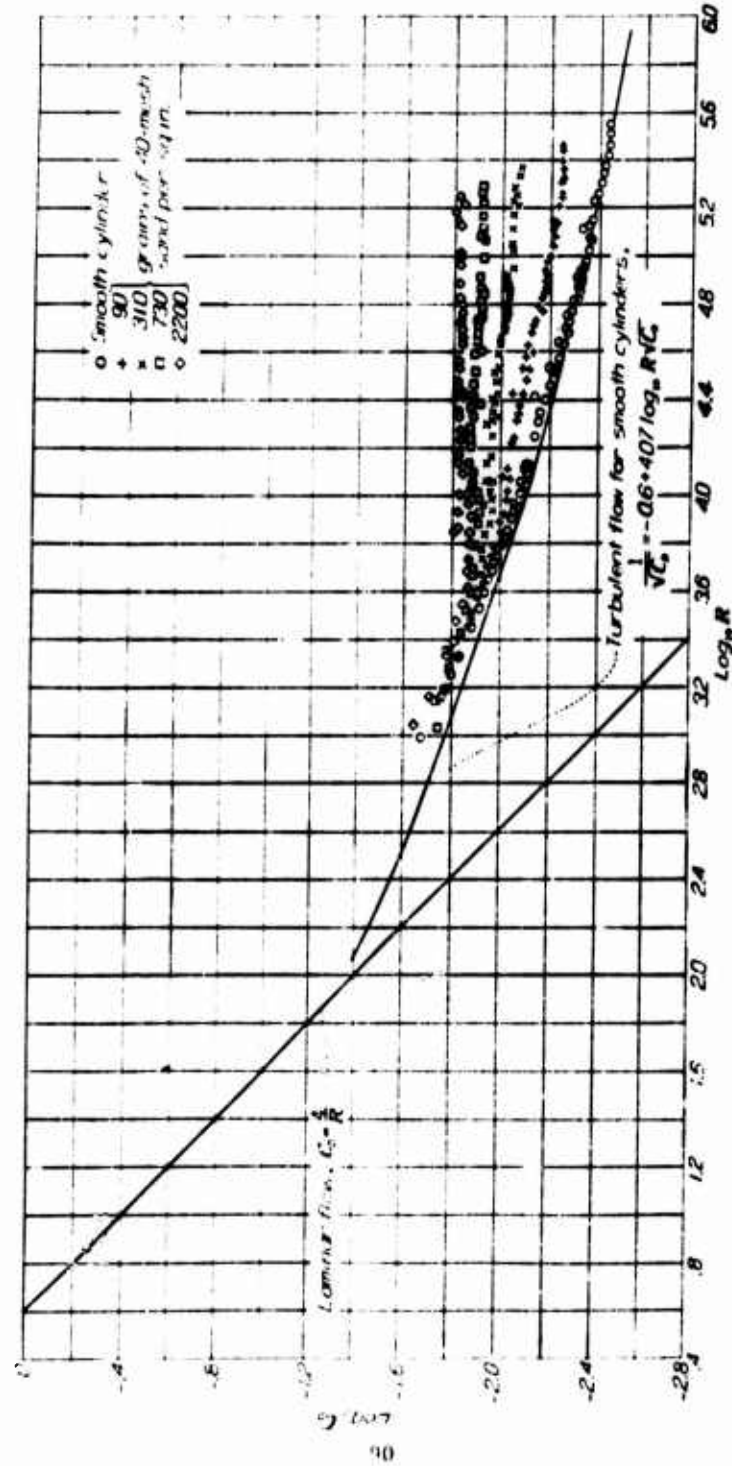


Fig. 11 - Effect of varying density of surface roughness on the drag coefficient (From Ref. 2)



noise" level - 158 db at speeds equal to the corresponding critical values; and this indeed seems to be what happens if we allow for a small experimental error and for the fact that the energy of the background and that of the flow noise add up to the resultant noise level and change the shape of the curves at lower noise levels. Grit 60 exhibits maximum dimensions of  $10^{-2}$  inch ( $v_{crit} = 1$  knot). The corresponding critical speed is therefore 0.54 m/sec. The measured line intersects very nearly at the point  $v = v_{crit} = 0.70$  m/sec with the equivalent zero flow-noise level at -159 db. For a smooth machine-polished metal surface,  $v_{crit} = 0.75$  m/sec (1.5 knots). Paint seems to cover the smaller roughnesses and appears to increase the larger-size roughnesses with paint streaks so that the corresponding  $v_{crit}$  is 0.5 m/sec (1 knot). The extrapolation of the measurements to levels considerably below the ambient noise level is, of course, thoroughly hypothetical; and the assumption of a zero effective or equivalent flow noise level is likewise tenuous. But this assumption seems to represent a working assumption that is borne out by the experimental results, at least as long as no detailed theory is available.

Like the slope of the curves for the drag, the slope of the noise curves is also a function of the density distribution of the roughnesses. The noise level increases linearly with the logarithm of the speed by 18 db per octave of increase in speed if the surface is very smooth and by up to 35 db per octave increase in speed if the surface is rough. The flow noise generated by a surface with small but densely distributed roughnesses may thus exceed the ambient noise level at much slower speeds than that generated by a surface with large roughnesses if the density of the large roughness is sufficiently small. The noise levels have been measured simultaneously with two hydrophones, one 2.5 inches in diameter, the other 5 inches. The results are identical except for a constant difference in level, the smaller hydrophone being more sensitive by 10 - 13 db (Fig. 12). These results show the average pressure over the hydrophone area that determines the hydrophone reading and the compensation of the pressure maxima and minima over the area of the hydrophone. This average pressure is greater, the smaller the diameter of the hydrophone.

One of the most puzzling results of these investigations was the fact that the noise level measured with a similar hydrophone outside the boundary layer at a distance of one yard proved to be approximately the same as that measured in the boundary layer (Fig. 13). This result can be explained again as a consequence of the compensation of the pressure maxima and minima. The hydrophone used did not indicate the true pressure fluctuations in the boundary layer, but the average value over an area of a diameter of about the magnitude of the acoustical wavelength. On the basis of diffraction theory, it can be shown that the pressure at a certain distance from the source distribution can be computed as a function of the pressure at the boundary surface. In this computation the average value of the pressure for an area roughly equal to the square of the wavelengths determines the result, and this is exactly the quantity that was responsible for the hydrophone reading inside the boundary layer. This result shows that in the presence of flow noise a small hydrophone will always be a poorer sound receiver than a large one.

Damping the shell by coating it internally with a damping varnish had only a small effect on the measured levels (Fig. 12). This result might be expected. At high frequencies, the resonances of the shell overlap to a continuous background, and individual resonances do not greatly contribute to the result.

It is hardly worthwhile to try to improve the quality of the extrapolation by assuming the noise level to be proportional to a power of the velocity difference ( $v - v_{crit}$ ) since  $v_{crit}$  usually is small in comparison to  $v$ .

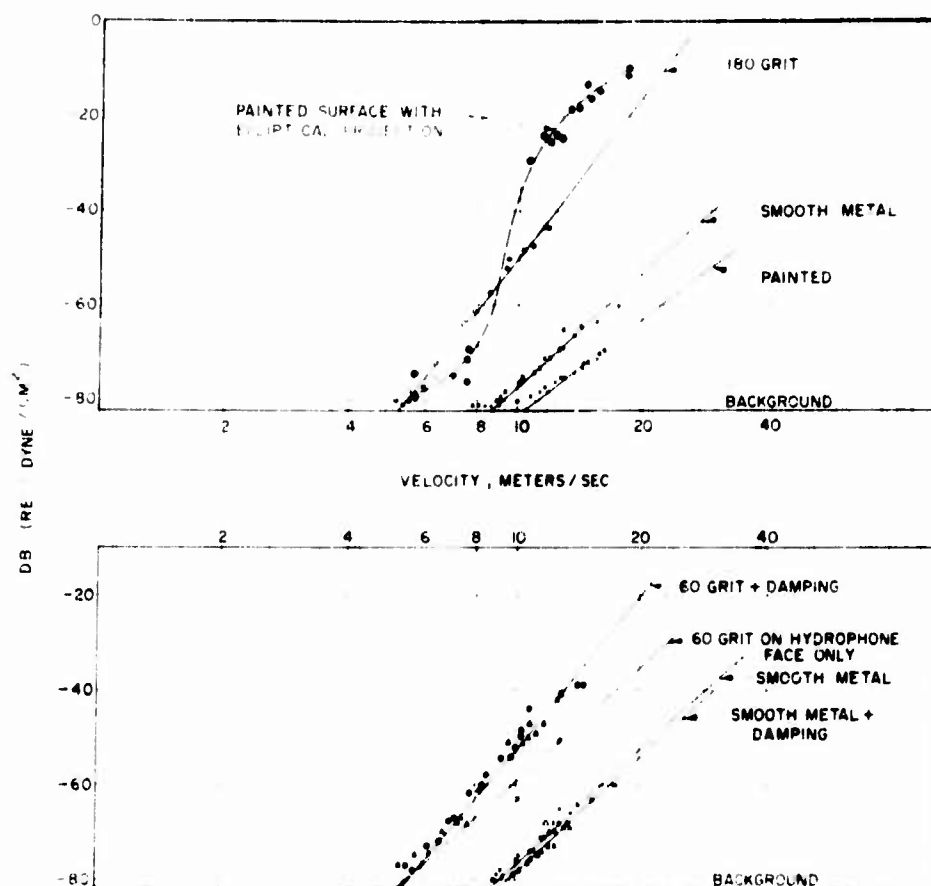


FIGURE 12. Internal noise level as measured with the five-inch-diameter hydrophone with correct damping and of a large elliptical projection on the internal noise level.

Figure 14 shows some measurements performed in the Garfield Thomas Water Tunnel\* with a microphone mounted on a very smooth laminar-flow-noise head. The roughnesses are relatively large, but not numerous. The slope is 18 db per octave speed change, as would be expected for true boundary layer noise.

A number of flow noise measurements on ships have been reported for which the slopes are 18 to 22 db per speed octave, but the absolute levels are larger by 10 to 20 db than those found in the measurements obtained by using the cylinder. This means that in practical cases the roughnesses generating the flow noise are usually relatively large, but few in number.

The cylinder measurements lead to a rough estimate of the noise level as a function of the speed, the size, and the density of the roughnesses. The experimental results can be expressed as

\*The Garfield Thomas Water Tunnel is at the University of Maryland.

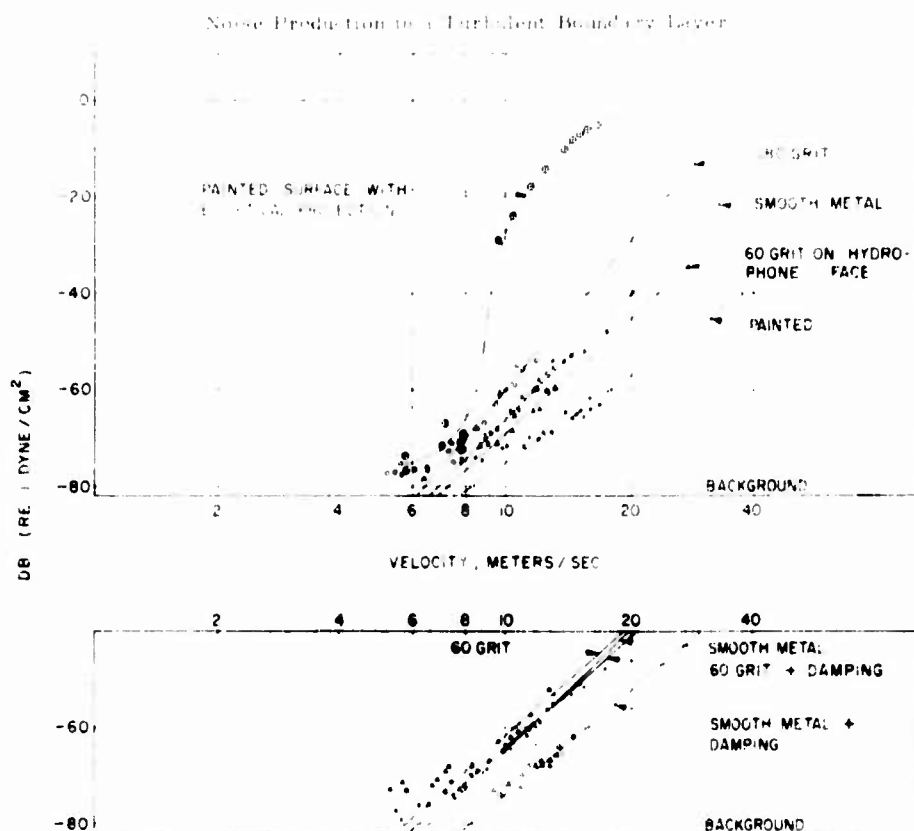


Fig. 15 - External noise at one meter from the cylinder surface for different treated surfaces.

$$p = 158 \times 10^{-6} \text{ dynes/cm}^2$$

for the 2.5-inch-diameter hydrophone as receiver, where  $n$  is a factor varying between 20 and 25 db per octave of speed change, according to whether the surface is smooth and painted and the roughnesses scarce, or completely rough as when treated with grit. Since  $n$  represents the number of octaves above the critical speed,

$$p = 158 \times 10^{-6} \left( \frac{v}{v_c} \right)^n$$

The experimental results can then be summarized. The flow noise level at 25 kc measured with a hydrophone of a diameter of 2.5 inches and a bandwidth of 2 kc attains -20 db below 1 dyne per centimeter square (spectral level, per cycle), when the speed is 20 times the critical speed if the surface is smooth (carefully painted) or 5 times the critical speed if the surface roughnesses are densely distributed (as for instance in the case of a grit-covered surface). The noise level then increases at a rate of 20 db per octave of increase in speed if the surface is smooth (roughnesses widely distributed) or at 25 db per octave of increase in speed if the surface is completely covered with roughnesses. This means that for a concrete traveling at a speed of 50 ft/min, the critical speed may be at least 125 ft/min. The roughnesses then have

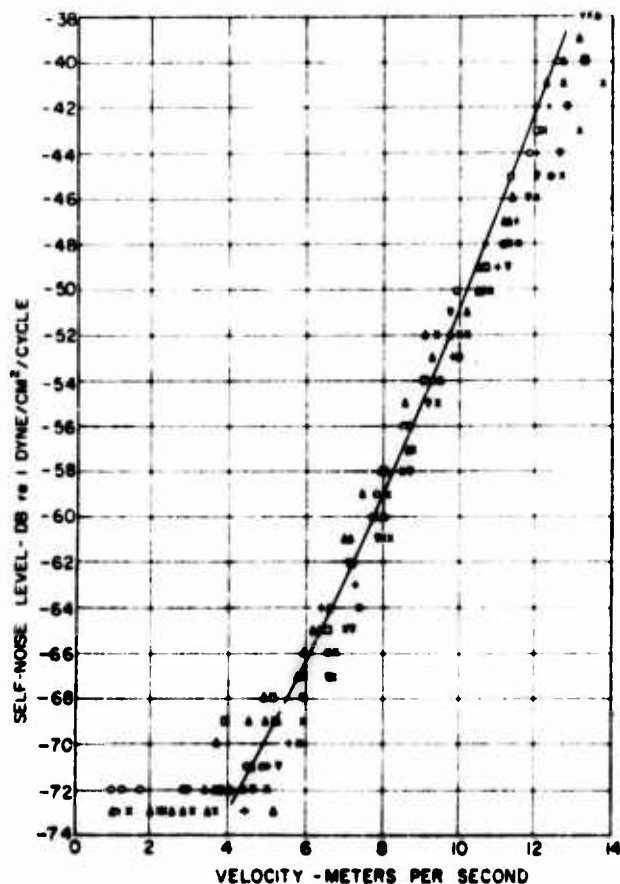


Fig. 14 - Flow noise level in the Garfield Thomas Water Tunnel

to be smaller than  $1.25 \cdot 10^{-3}$  inch. Such a vehicle will then generate no audible roughness noise.

To gain additional information about flow noise, measurements were performed in the boundary layer at the Garfield Thomas Water Tunnel. Four hydrophones were mounted flush with the walls of the Tunnel and two hydrophones were mounted in the streamlined body in the middle of the tunnel, one hydrophone at its nose and the other at its side. Figure 8 which shows the results measured with the hydrophone flush with the wall of the Tunnel has already been discussed in connection with the speed frequency spectrum of flow noise. Figure 15 shows the measurements with the hydrophones mounted on the streamlined body. The noise level received by the nose hydrophone at frequencies between 500 cps and 20 kc is 5 to 20 db smaller than that recorded by the side hydrophone. But at low frequencies the picture reverses. The nose hydrophone receives considerably more flow noise than the side hydrophone. This is very apparent when listening to tape recordings. The noise received with the stagnating hydrophone sounds bubbly and seems to be very rich in low frequencies;

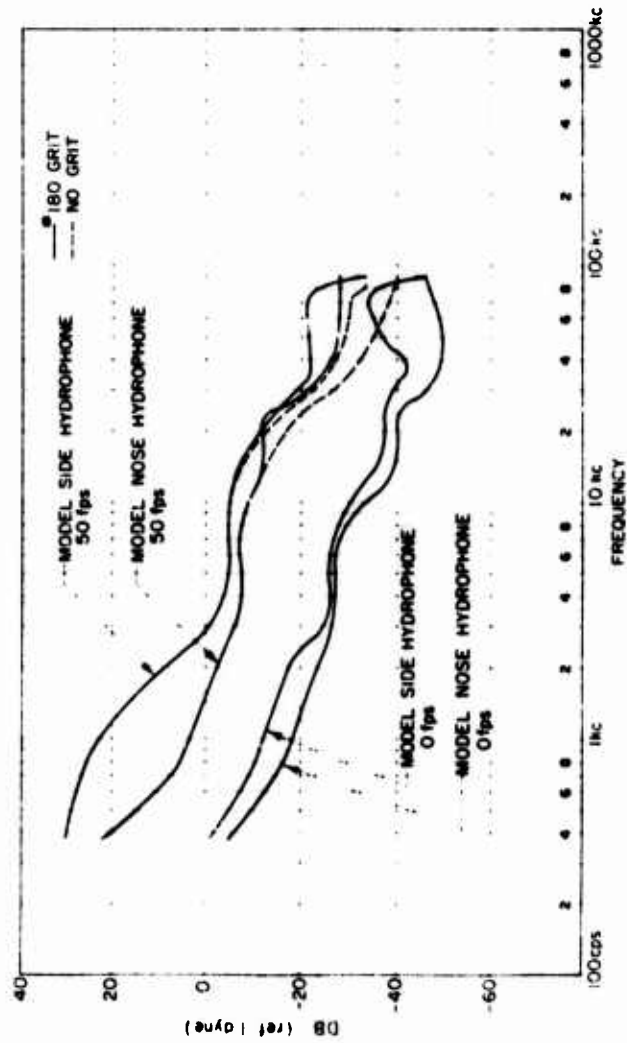
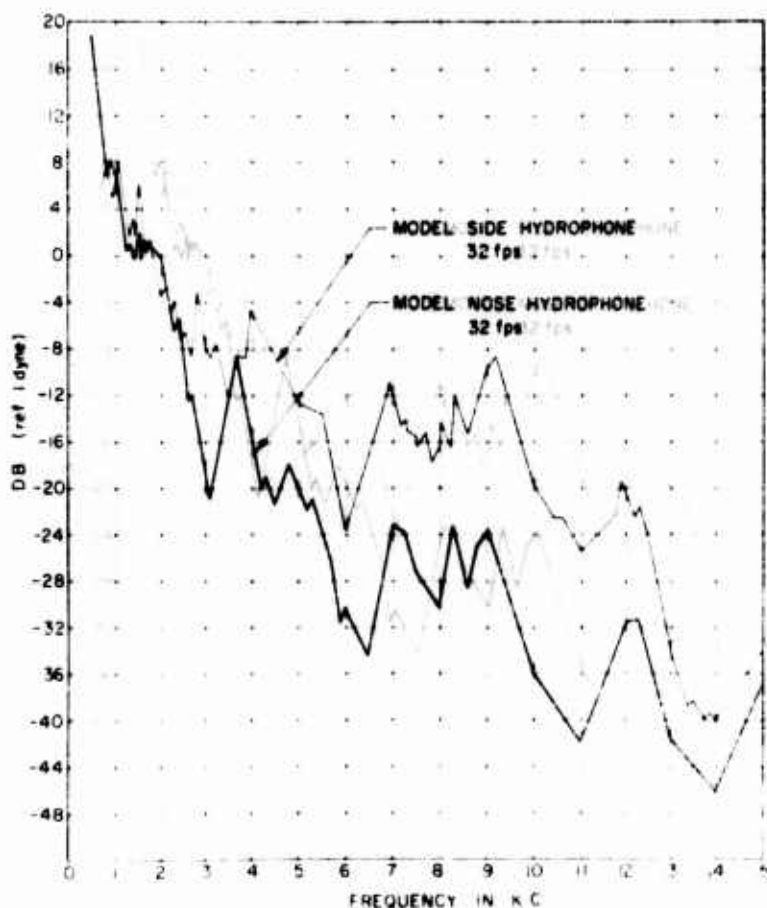


Fig. 15 - Measurements with two hydrophones mounted flush with nose and side wall of a streamlined body

the higher frequencies are almost completely masked. The noise received by the side hydrophone resembles more a hissing sound with very small low-frequency contents. This phenomenon can be traced through all recordings. This low-frequency sound received by the stagnating hydrophone seems to be due to the stagnation pressure generated by the larger-scale turbulence that hits its sensitive area. The smaller-scale turbulence does not seem to produce a similar effect; it is very likely that this turbulence is damped out entirely by the stagnation of the flow. Figure 16 shows a narrowband analysis of a second series of such measurements.

The boundary layer noise in the Garfield Thomas Water Tunnel is relatively large. But the effect of different shapes of test vehicles and of the position of the hydrophones could still be investigated if these objects were densely covered with coarse grit and if the speed of the flow were sufficiently high. Preliminary measurements performed on grit-covered surfaces (grit 180) and surfaces covered with a resilient coating did not yet lead to new results (Fig. 17), since the grain size of the



grit and the speed of the flow (50 ft/sec) still were too low. But there seems to be little doubt that proper treatment of the surfaces and the use of greater flow velocities will make possible detailed flow-noise studies in such a channel.

## RELIABILITY OF THE MEASUREMENTS

To test the reliability of the results, all the measurements were repeated five months later. Identical results were obtained. Special tests have been made to ensure that cavitation did not interfere with the measurements.

Cavitation usually starts at a certain speed, increases the noise almost abruptly to a high value, and then for a time remains almost constant; later, it even decreases again. The dashed curve in Fig. 13 is an example of a case where cavitation was produced intentionally by welding a projection shaped as a semi-ellipse (6 inches long, 4 inches high, and 1.4 inch thick) to the cylinder surface at the height of the hydrophone. The moment cavitation starts, the noise intensity jumps quite suddenly by almost 60 db. In spite of the relatively large size of the projection, cavitation is seen to take place only at speeds above 7 meters per second. Typical for the measurement was a continuous fluctuation of the noise level around a mean value.

Another proof that cavitation did not interfere with the measurements is given by a curve in Fig. 12 for which the area of the larger hydrophone was covered with grit. The noise level is much greater than that of the painted surface, being almost exactly the same at the untreated hydrophone area, if its 10-db greater sensitivity to incoherent flow noise is taken into account. Cavitation would have affected the response of the first hydrophone to a much greater extent than that of the second, 17 inches distant from the first and in the sound shadow.

During the measurements performed in the water tunnel, cavitation could be easily identified by increasing the pressure. The unsteadiness of the noise (like a series of explosions) makes recognition of this phenomenon very easy.

The noise level owing to extraneous noise would be expected to increase continuously with a relatively low power of the speed; and it would be independent of the conditions of the surface of the cylinder. Extraneous noise could not have affected the rough-surface measurements of the cylinder, but very likely it also had no effect on the results for the smooth and the painted surfaces.

## SUPPLEMENTARY WORK

The study described above represents an attempt to derive a general understanding of the features of flow noise. The measurements in the Water Tunnel will be repeated in the near future with more sensitive hydrophones and with hydrophones of variable area. Work with buoyant units has been taken up, and the field program has just started at Key West to supplement and to verify the previous conclusions. A paper submitted to the Journal of the Acoustical Society contains the experimental data described above and theoretical derivations performed since the Flow Noise Symposium. This paper contains a quantitative analysis of the near-field component and of the flow-noise component radiated to greater distances. The high-frequency boundary-layer noise pressure turns out to be directly proportional to the thickness of the boundary layer, a relation which is in agreement with the derivations published in the literature and the experimental results of M. Harrison (3). Because of the large thickness of the boundary layer of the cylinder, even at the boundary-layer component of flow noise, the radiated flow noise is not too far from noise whose spectral distribution

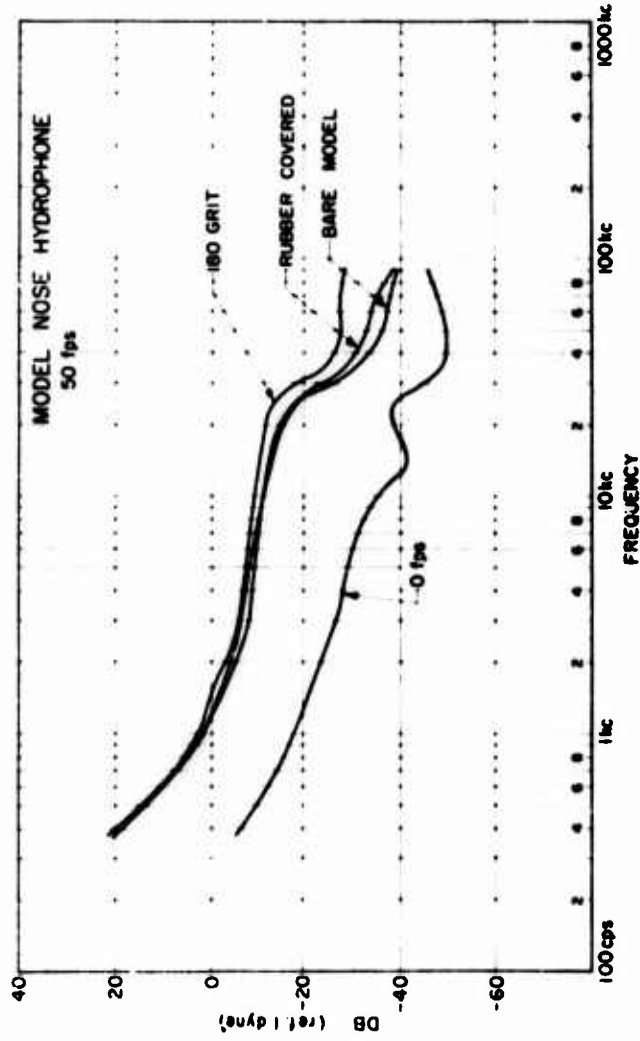


Fig. 17 - The effect of grit and a pressure resilient coating on flow noise. The velocity of the flow and the size of the roughnesses are not yet sufficiently large to mask the tunnel boundary layer noise.



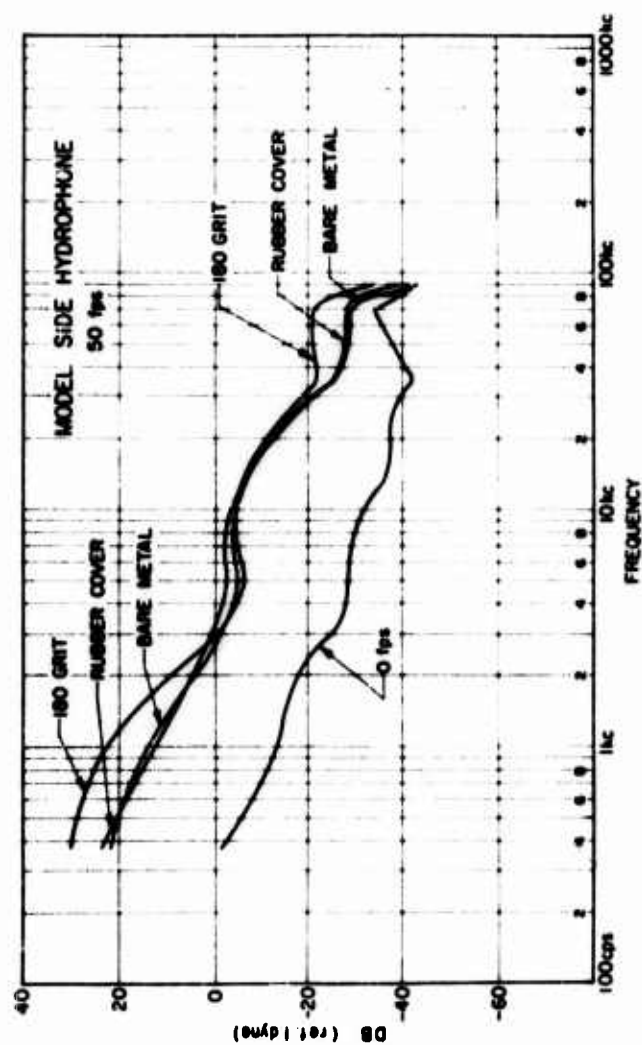


Fig. 17 (Continued) - The effect of grit and a pressure resilient coating on flow noise. The velocity of the flow and the size of the roughnesses are not yet sufficiently large to mask the tunnel boundary layer noise.



where  $\epsilon = \nu \nabla^2 u$  is the rate of dissipation of kinetic energy.

If  $\epsilon \ll 1$ ,  $\epsilon$  may be neglected in the term

$$-\frac{1}{2} \frac{d}{dt} \int_V u^2 dV,$$

it follows from equation (3) that results

$$E = D = \frac{\epsilon}{4\pi^2 \lambda^2} \quad (4)$$

Comparison of the components left and right yields  $\lambda = 2\pi$ ,  $\lambda^2 = 5.2 \times 10^{-6}$  is therefore necessarily of the form

$$E = D = D_0 \lambda^{-5.2} = \lambda^{-5.2} \times \text{constant}.$$

Since the energy flow  $E$  is independent of the properties of the system and in particular of the space-wave lengths in this system, the spectral intensity decreases as  $\lambda^{-5.2}$  with increasing wave-number (decreasing patch size). For the case of homogeneous turbulence, this law was derived by Kolmogorov in 1941 and by von Weizsäcker independently in 1943. The derivation shows that the nature of this law is very general and that it applies to many other phenomena that have no relation to turbulence.

Kraichnan (4) has shown that this classical derivation of the Kolmogorov equilibrium law is not rigorous; and he has derived an improved distribution law on the grounds of statistical mechanics. His result is

$$E = D = D_0 \lambda^{-5.15} = \lambda^{-5.15} \times \text{const.}$$

In practical cases, the difference between the two laws is very small, and which of the two is best makes very little difference.

## Appendix B

### THE BERNOLLI EQUATION FOR SMALL-SCALE MOTION

The Euler equation

$$\frac{1}{\rho} \frac{d}{dt} (\rho \mathbf{v}) = -\frac{1}{\rho} \nabla p + \nu \nabla^2 \mathbf{v}$$

can be integrated along a streamline as follows:

$$\frac{d}{dt} \left( \frac{1}{2} \rho v^2 \right) + \rho \frac{d}{dt} \left( \frac{1}{2} v^2 \right) = \rho \frac{d}{dt} \left( \frac{1}{2} v^2 \right) + \rho \frac{d}{dt} \left( \frac{1}{2} v^2 \right)$$

We now introduce the following assumptions that the decay time of the turbulence is large in comparison to the period of the frequency of interest and that the building-up time of the turbulence is small in comparison to the decay time. The flow may then be considered to be steady ( $\frac{d}{dt} = 0$ ) when viewed from a coordinate system carried along by the mean flow  $\mathbf{v}_0$ . Since  $\mathbf{v}_0 = \mathbf{v}$ , and the above equation simplifies to

$$\rho \frac{d}{dt} \left( \frac{1}{2} v^2 \right) = \rho \frac{d}{dt} \left( \frac{1}{2} v^2 \right)$$

Curl  $v$  can be expressed by the angular velocity  $\text{curl } v = 2\omega$ ; and, since we are interested only in patches of turbulence,

$$v = \omega a,$$

where  $a$  is the patch radius (or the correlation distance of the velocity fluctuation). To find the acoustic effect of the noise of the pressure fluctuations, we are interested only in small-scale turbulence distributed over a very small region. For a small region the flow may be considered always to be two-dimensional. For a two-dimensional flow,  $v$  is perpendicular to  $\text{curl } v$  and

$$p + \frac{v'^2}{2} = \text{const} - 2\omega \int_0^a r^2 dr.$$

The maximum value of the integral will result when  $dr$  is equal to the patch radius  $a$ ; this maximum is therefore of the same order of magnitude as

$$= 2a^2 = 2v'^2 = 2v^*{}^2,$$

where  $v' = v^*$  is the fluctuating velocity because of the turbulence. On the average, therefore,

$$p = -2v^*{}^2 + v^*{}^2 = -v^*{}^2,$$

and the result reduces to the standardized Bernoulli equation except that the numerical factor is slightly different

$$p = -2v^*{}^2 + \text{const}.$$

The above estimate gives an indication of the order of magnitude of the maximum pressure fluctuation. The average pressure fluctuations will probably be about ten times smaller. In this estimate the effect of the velocity gradient in the boundary layer has been neglected. Because of this gradient, the patches are continuously deformed and the motion is no longer stationary. Additional forces are set up that produce considerable fluctuations in pressure. Kraichnan (4b,c) derived the theory for this case on the assumption of a Gaussian velocity correlation. He obtained a similar equation; but the numerical constant now is of the order of magnitude 7:

$$p = -7v^*{}^2.$$

#### REFERENCES

1. Schlichting, H., "Boundary Layer Theory," New York: McGraw-Hill Book Co., 1955
2. Theodorsen, T. and Regier, A., "Experiments on Drag of Revolving Disks, Cylinders, and Streamline Rods at High Speeds," NACA, Report No. 793, 1945
3. Lindgreen, E., "The Transition Process and Other Phenomena in Viscous Flow," Arkov for Fysik, Stockholm, 12:1-169 (1957)
4. (a) Kraichnan, R.H., "Statistical Mechanics of Stationary Homogeneous Hydrodynamic Turbulence," New York University, Research Report No. MH-7, Contract N. AF 19(604)2138, April 1957
- (b) "Pressure Field Within Homogeneous Anisotropic Turbulence," J. Acoust. Soc. Am. 28(No. 1):64-72 (January 1956)

- (c) "Pressure Fluctuations in Turbulent Flow Over a Flat Plate," J. Acoust. Soc. Am. 28(No. 3):378-390 (May 1956)
- (d) "Noise Transmission from the Turbulent Boundary Layer," J. Acoust. Soc. Am. 29:65 (1957)
- 5. Nikuradse, J., "Untersuchung ueber die Geschwindigkeitsverteilung in turbulenten Stroemungen," VDI Forschungsheft, No. 281, Berlin, 1926
- 6. (a) Wieselsberger, C., "Reports on the Aerod," Versuchsanstalt Göttingen, I, series, 120-126, 1921
- (b) Gebers, F., Schiffbau, 9:435, 475 (1908); also Schiffbau, 22 (1919)
- (c) Schoenherr, K.E., "Resistance of Flat Surfaces Moving Through a Fluid," Trans. Soc. Nav. Arch. and Mar. Engrs. 40:279 (1932)
- (d) Kempf, G., "Neue Ergebnisse der Widerstandsforschung," Werft, Reederei, Hafen, 10:234, 247 (1929)
- (e) Nikuradse, J., "Turbulente Reibungsschichten an der Platte," Munich:R. Oldenbourg, 1942
- (f) Kempf, G., "Über den Einfluss der Rauigkeit auf den Widerstand von Schiffen," Jahrb. d. Schiffbautechn. Gesellschaft, 38:159, 233 (1937); and "The Effect of Roughness on the Resistance of Ships," Engineering, London, 143:417 (1937), see also Trans. Inst. Nav. Architects, 79, 109, and 137, 1937.
- 7. Laufer, J., "Investigation of Turbulent Flow in a Two-Dimensional Channel," NACA. Report V. 1053, 1951
- 8. Harrison, Mark, "Correlation and Spectra of Pressure Fluctuations on the Wall Adjacent to a Turbulent Boundary Layer," J. Acoust. Soc. Am. 29:1252A, 1957
- 9. Goldstein, M., "A Note on Roughness, A.R.U., Report and Memo No. 1763, 1936
- 10. Kolmogorov, A.N., "The Local Structure of Turbulence in Incompressible Viscous Fluid for very Large Reynolds' Numbers," C. R. Acad. Sci. U.R.S.S. 30:301 (1941)
- 11. Kolmogorov, A.N., "Dissipation of Energy in the Locally Isotropic Turbulence," C. R. Acad. Sci. U.R.S.S. 32:16 (1941)

. . . . .

## DISCUSSION

R. H. Kraichnan (New York University)

I should like to ask if when you go through the transition in which the roughnesses push up through the laminar sublayer you observe the same proportionality between drag and noise. Also, I should like to express a doubt that the  $1/5$  behavior which

you observe has much relevance to inertial range phenomena. Actually, the inertial range law for pressure which might reasonably be expected on the basis of the Kolmogorov theory is approximately  $\omega^{-2}$ , or steeper. My guess would be that the pressure fluctuations which you observe at high frequencies arise not from the fine structure of the outer part of the boundary-layer (where an inertial range might perhaps be expected) but from the intensely-sheared dissipation layer just above the laminar sublayer.

F. Meyer (Physikalisches Institut der Universität Göttingen)

In connection with the very interesting statements of Dr. Skudrzyk I would like to report on some experiments dealing with "noise of streaming water" which were carried out in our institute in Göttingen by Mr. Dinkelacker.

The characteristic feature of the experiments is the simplicity of the apparatus (Fig. 1). Water from the water mains streams through the test tube with an adjustable velocity. The walls of the test tube may consist of different materials (in Fig. D1 a glass tube is shown). The inner surface of the tubes can be treated to give different degrees of roughness. Having passed the test tubes, the water is collected in a storage tank. The test tube is connected to the water mains by means of a long rubber tube. This rubber tube works as an acoustic wave guide below its cut-off frequency, thus separating the test tube from the mains with respect to structure-borne sound. The measurements are carried out with a structure-borne sound microphone attached to the outside of the test tube. The frequency response of the set-up including the test tube can be determined.

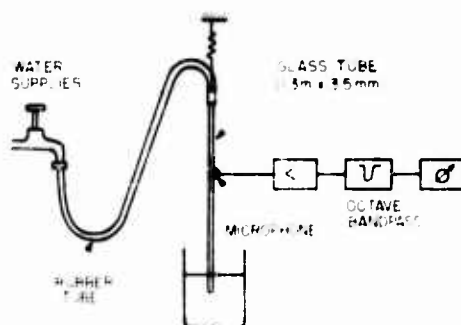


Fig. D1 - Noise of streaming water in a tube (arrangement)

In Fig. D2 the sound level of octave bands is plotted against the frequency with the stream velocity as a parameter. It is obvious from the diagram that the maximum of the sound intensity shifts to higher frequencies with rising stream velocity.

These relations are more clearly visible in Fig. D3, where the same results are plotted, but with the stream velocity as abscissa and the octave ranges as parameter. The onset of the noise is given when, with rising streaming velocity the Reynolds number is approximately reached. In the beginning, most of the noise is concentrated on the lowest octave band. For the higher octave bands the point of onset shifts to higher stream velocities.

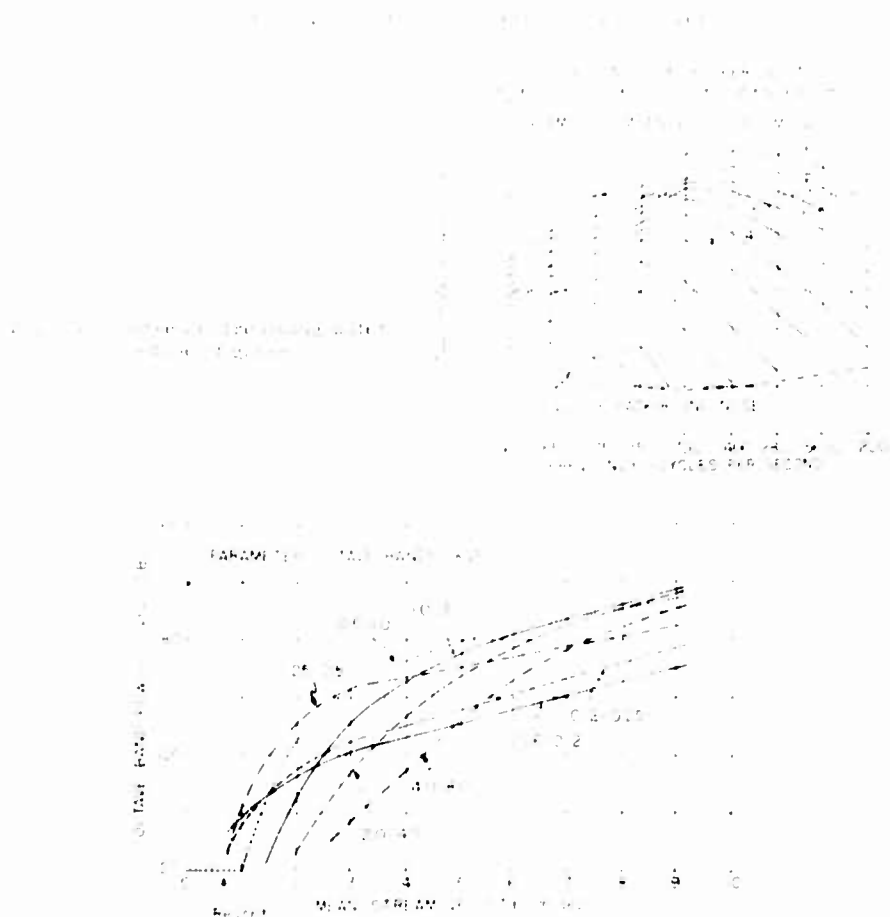


Fig. D3 - Noise of streaming water in a tube of glass.

These preliminary results seem to indicate that the turbulence patches have smaller dimensions at higher velocity.

#### E. Skadrzyk

With regard to the drag-noise ratio: the extrapolation is very hypothetical but is somewhat in agreement with experimental results. As long as nothing better is available we feel we should stick to that.

Of course the spectrum interpolation is again highly hypothetical and the only thing I am really allowed to admit is that the experimental results do not contradict our theoretical concept at the moment.

# PRESSURE FLUCTUATIONS ON THE WALL ADJACENT TO A TURBULENT BOUNDARY LAYER

Mark Harrison  
*David Taylor Model Basin*

A fully developed turbulent boundary layer with a zero pressure gradient has been studied in a subsonic windtunnel. The pressure fluctuations on the wall of the wind tunnel were measured by small flush-mounted microphones. Data for the dimensionless spectral density of the pressure fluctuations,  $P(f) / \rho^2 U_\infty^3 \delta$ , as a function of the frequency parameter  $f \delta / U_\infty$  are presented;  $P(f)$ ,  $\rho$ ,  $U_\infty$ , and  $\delta$  are respectively the spectral density, fluid density, free stream velocity, boundary layer displacement thickness, and frequency. Data for the coefficient

$$\rho^{2/3} \delta^{1/3} / 1.2 U_\infty^2$$

are also presented. The transverse cross correlation for the pressure fluctuations was studied by using two flush-mounted microphones. Rather than the longitudinal cross correlation, the longitudinal cross-spectral density was studied, yielding a measure of the coherence of the pressure fluctuations at two points as a function of  $x / U_\infty$ , where  $x$  is the longitudinal spacing of the two points and  $U_\infty$  is the effective convection velocity of the spatial pattern.

## INTRODUCTION

Pressure fluctuations necessarily coexist with velocity fluctuations in a turbulent flow. For incompressible flow, the pressure and velocity are related by the equation

$$\nabla^2 p = -\rho \nabla \cdot \mathbf{u} \quad (1)$$

which can be obtained by combining the continuity and the Navier-Stokes equations. The solution to this equation is given in terms of an integration over all space and shows that for the case of boundary-layer flow, the vanishing of the velocity fluctuation at the wall does not imply the vanishing of the pressure fluctuations at the wall.

It is these pressure fluctuations on the wall adjacent to the turbulent boundary layer that are the focus of interest in this study. Some measurements of the characteristics of these pressure fluctuations are reported and the meaning of the measurements are interpreted.



There are several reasons for being interested in the characteristics of the pressure fluctuations. A direct and immediate need exists for data in the field of noise due to unsteady flow. When a turbulent boundary layer develops on a flexible wall, the motion of the wall which results from the pressure fluctuations penetrates a sound field. Some of the noise in aircraft has been attributed to this mechanism. Kramann (1,2) has given a theoretical discussion of the problem which he links with the interpretation of Eq. (1) for the case of boundary-layer flow.

There are also fundamental reasons for being interested in the pressure fluctuations associated with a turbulent boundary layer. There is considerable uncertainty as to how energy is produced, convected, diffused, and dissipated in the turbulent boundary layer. In particular, the role of pressure fluctuations is but vaguely understood. Although this work does not measure the pressure fluctuations inside the boundary layer, it does constitute a start on this very challenging problem and it is believed that a further extension of this work will prove valuable.

To obtain the data for this report, the boundary layer on the wall of a subsonic wind tunnel was studied. Pressure transducers with a very small active area were mounted flush with the wall. Using conventional sound analysis equipment consisting of a narrow tunable filter and an rms meter, it was possible to obtain the spectral density of the pressure fluctuations at a point on the wall.

By measuring the pressure fluctuations in the total frequency range, it was possible to obtain the mean-square value for the pressure fluctuations. This value was also checked by integrating over the spectral density.

By using two pressure transducers and studying the correlation and the cross-spectral density between the pressure fluctuations at the two points, it was possible to study the spatial pattern of the pressure fluctuations and how rapidly it evolves as it is convected downstream. By measuring the time delay necessary to maximize the correlation between the two points, it was possible to measure the velocity at which the pattern was convected.

## EXPERIMENTAL APPARATUS

### The Wind Tunnel

The wind tunnel was a closed-circuit subsonic tunnel. The velocity range of the tunnel was from 50 to 200 ft/sec. The transverse dimensions of the working section were 20 by 15 inches. The measurements were performed on the wall of the working section, 5 feet downstream from the entrance nozzle. At this point the displacement thickness of the boundary layer was 0.105 inch at a velocity of 100 ft/sec. By comparing the mean velocity profiles with those given by Klebanoff and Diehl (3) it was judged that the boundary layer was nearly well enough developed to show similarity. Unfortunately, the working section was not long enough to permit working further downstream so as to prove that the boundary layer was exhibiting similarity.

### The Pressure Transducer

The pressure transducer was an adaptation of the Altec 21-BR-180 open-faced microphone (4). This microphone was modified as shown in Fig. 1 to produce the transducer used for the spectral density measurements. A different modification was

\*The term  $\bar{p}^2$  will be defined in the next section. The results of the measurements.

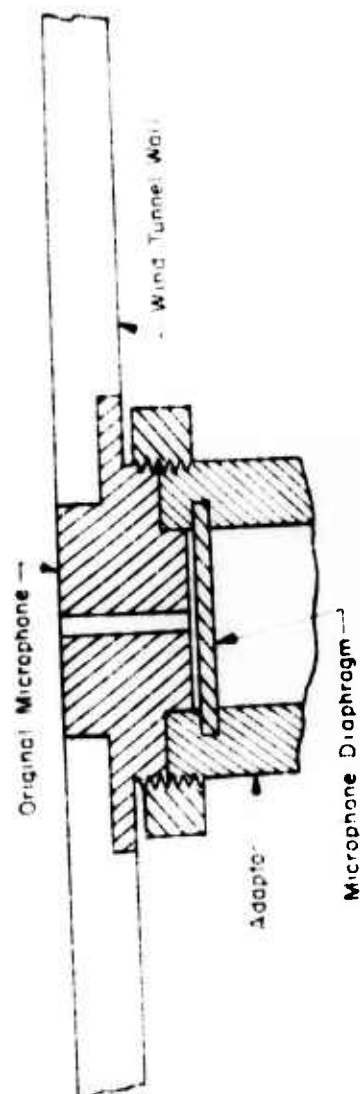


FIG. 1. Schematic representation of the ATEX microphone mounted on a wind tunnel wall for density measurements.

required for the correlation measurements. In both cases the upper frequency limit is determined by a resonance between the mass of the air in the orifice and the stiffness of the air in the chamber adjacent to the diaphragm. Well above this resonance frequency the sensitivity is inversely proportional to the frequency range. The resonant response was damped by a cotton plug in the orifice so that some of this frequency range was salvaged.

For the correlation measurements it was necessary to measure at two points separated by a small distance. This necessitated the use of the transducer in the form shown in Fig. 2. Unfortunately, this arrangement resulted in a much lower resonant frequency due to increased mass in the tube. Using this transducer, arrangements were made to have a series of holes spaced at 0.125 inch apart in the transverse and longitudinal directions which permitted correlation measurements to be made up to 1.5 inches in 0.125-inch steps.

The sensitivity of the transducer was -61 db below 1 volt for 1 dyne/cm<sup>2</sup>. For the spectral density measurements the usable frequency range was up to 8500 cps and for the correlation measurements the usable frequency range was up to 2000 cps. The lower limit on the frequency range was imposed by wind-tunnel noise and not the transducer.

In order to prove that the active area of the transducer was sufficiently small to insure that the pressure was coherent over its entire face, various size orifices were used. It was found that orifices up to 0.125 inch in diameter were satisfactory for obtaining the data on spectral densities. Smaller orifices were used for the correlation measurements in order to improve the accuracy in the measurement of the separation distance between the transducers.

#### Electrical Equipment

The spectral density of the pressure fluctuations was obtained by the use of the Muirhead-Pametrada wave analyzer. A frequency band of a nominal 10 percent was used in the analysis. The levels were read on the Ballantine True-rms voltmeter. In the section giving the results of the measurements, the details of how to obtain the spectral density from the observed data are given.

The correlation between the pressure fluctuations at two points was measured using rather simple apparatus. The basis for the method used is contained in the algebraic identity

$$\overline{p_1 p_2} = \frac{1}{2} (\overline{p_1 + p_2}^2 - \overline{p_1 - p_2}^2)$$

where the term on the left is the correlation between  $p_1$  and  $p_2$ . The bars indicate time averages.  $p_1$  and  $p_2$  are here regarded as voltages that are proportioned to the fluctuating pressures  $p_1(t)$  and  $p_2(t)$ , respectively, where the subscripts denote the two points at which the measurements are performed. With reference to Fig. 3, the addition and subtraction of the voltages were accomplished by the transformer. The time averages were accomplished by the Ballantine True-rms voltmeter, whose time constant had been increased to 2 seconds. This produced satisfactory smoothing of the fluctuations. Measuring the correlations is then a matter of making four meter readings,  $\overline{p_1 + p_2}^2$ ,  $\overline{p_1 - p_2}^2$ ,  $\overline{p_1}^2$ , and  $\overline{p_2}^2$ , and doing the computations indicated by the above algebraic identity.

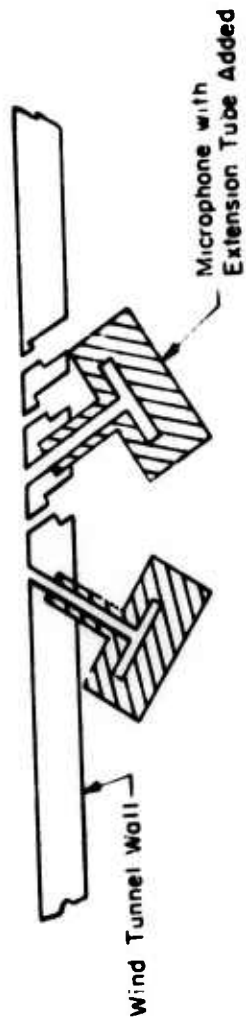


Fig. 2 - Schematic of microphone adapted for cross-spectral and correlation measurements

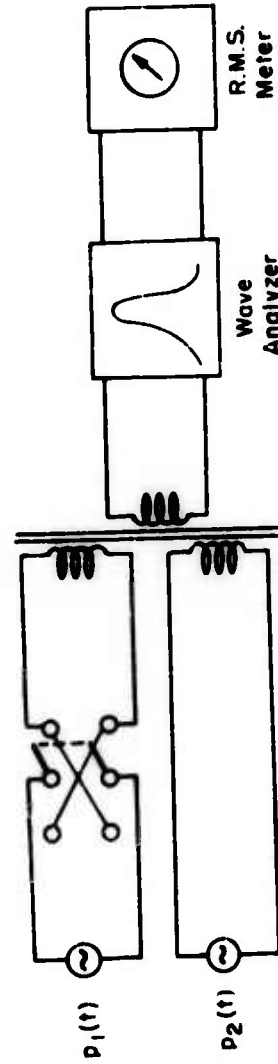


Fig. 3 - Schematic diagram of the equipment used in the measurement of the cross-spectral density



TABLE 1. The values of  $\beta$  obtained from the analysis of the data of Figure 3, and the values of  $\beta$  obtained from the analysis of the data of Figure 4. The values of  $\beta$  obtained from the analysis of the data of Figure 3 are shown in parentheses, and the values of  $\beta$  obtained from the analysis of the data of Figure 4 are shown in brackets. The values of  $\beta$  obtained from the analysis of the data of Figure 3 are shown in parentheses, and the values of  $\beta$  obtained from the analysis of the data of Figure 4 are shown in brackets.

Figure 3 shows the values of  $\beta$  obtained from the analysis of the data of Figure 3. The data exhibit a clear trend, increasing over the whole range of  $\omega$ . As mentioned earlier, the values of  $\beta$  obtained from the analysis of the data of Figure 4 are shown in brackets. It is seen that the trend of  $\beta$  is also exhibiting similarity.

TABLE 2. The values of  $\beta$  obtained from the analysis of the data of Figure 3.

$\omega$	$\beta$
0.0	0.0
0.1	0.1
0.2	0.2
0.3	0.3
0.4	0.4
0.5	0.5
0.6	0.6
0.7	0.7
0.8	0.8
0.9	0.9
1.0	1.0

where  $\beta$  is the value of the spectral density, or by direct measurement of  $\beta$ . However, at the lack of similarity exhibited in Fig. 4, a definite value cannot be obtained. The values obtained for  $\beta$  have an average value of about  $9.5 \times 10^{-4}$  sec<sup>2</sup>/cm<sup>2</sup>, which is close to the value obtained by Wallin et al. (1961).

A significant feature of the spectral density is that it does not increase appreciably with the frequency of the current. For these frequencies, which correspond to the values of  $\omega$  smaller than the frequency of the characteristic lengths of the turbulent flow, it is assumed that the spectral density should be proportional to the square of the frequency. There is some evidence that intermolecular forces have a strong influence on the pressure fluctuations at the lower frequencies. The pressure observations at the lower frequencies revealed an increase in the value of  $\beta$  of the spectral density when it did not have a definite value.

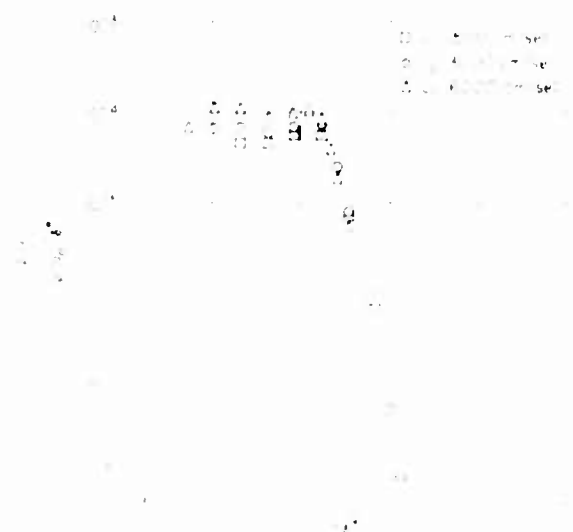


FIGURE 3. The values of  $\beta$  obtained from the analysis of the data of Figure 3. The values of  $\beta$  obtained from the analysis of the data of Figure 4 are shown in brackets.

randomness of the process. This intermittency gave pressure versus time records not unlike those observed by Klebanoff (7) for the velocity fluctuations in the boundary layer. This type of behavior diminished with increasing frequency and was not noticeable for values of  $u^+ U_\infty$  exceeding  $4 \times 10^{-2}$ . Further support for the possibility that intermittency plays a role at the lower frequencies can be found in the fact that at these frequencies, the measurements of the convection velocity yielded a value of about  $0.8 U_\infty$ . That part of the boundary layer that moves with a mean velocity of  $0.8 U_\infty$  is strongly intermittent.

The validity of the above conjectures could be established by repeating this study using fully developed pipe flow.

In view of the preceding, it would have been desirable to have procured data at lower frequencies. Unfortunately, this was not possible due to the tunnel noise which limited the lowest usable frequencies to between 100 and 200 cps. The signal-to-noise ratio above this range was always in excess of 20 db. This figure was obtained by placing the pressure pickup in the middle of the working section of the tunnel where the flow was essentially laminar. Actually, some noise was undoubtedly induced by the flow around the microphone, so that a better signal-to-noise ratio might actually have existed at the wall.

Vibration pickup by the transducer was not a problem. By simply plugging up the hole in the transducer, the vibration excitation could be measured, which in this case was too low to even consider.

#### Longitudinal Cross-Spectral Density

In this work it was decided to study the longitudinal cross-spectral density rather than the longitudinal correlation. Since this is a novel approach, a few words of explanation are needed in order to explain the measurement procedure.

The cross-spectral density of the pressure fluctuations is defined as

$$P_{12}(\omega) = \frac{1}{T} \int_0^T A_1^*(t) B_1(t) dt$$

where the asterisk denotes the complex conjugate, and where

$$A_1(t) = \int_0^T p_1(t) e^{-i\omega t} dt$$

$$B_1(t) = \int_0^T p_2(t) e^{-i\omega t} dt$$

with the subscripts 1 and 2 denoting the two observation points.

Using the arguments of Ref. 5 which show that the spectral density and the autocorrelation are Fourier transforms, it can be shown that the cross correlation and the cross-spectral density are also Fourier transforms:

$$R_{12}(\tau) = p_1(t) p_2(t + \tau) = \frac{1}{2\pi} \int_{-\infty}^{\infty} P_{12}(\omega) e^{i\omega\tau} d\omega$$

Since  $P_{12}(t)$  is complex, we can write

$$P_{12}(t) = U_{12}(t) + iV_{12}(t)$$

where it follows from the definition of  $P_{12}(t)$  that the real functions  $U_{12}(t)$  and  $V_{12}(t)$  are even and odd, respectively. Accordingly, we can write

$$R_{12}(t) = \int_0^\infty U_{12}(t) \cos \omega t \, d\omega - \int_0^\infty V_{12}(t) \sin \omega t \, d\omega.$$

This last equation provides the basis for an experimental method of measuring the real and imaginary parts of the cross-spectral density. If the cross correlation is measured with zero time delay, then

$$R_{12}(0) = \int_0^\infty U_{12}(t) \, d\omega.$$

If the cross correlation is measured in a narrow band of frequencies  $\omega$  as shown in Fig. 3, then

$$U_{12}(\omega) = \frac{R_{12}(\omega)}{\Delta\omega}$$

where  $R_{12}(\omega)$  denotes the cross correlation measured in the narrow frequency band. The real part of the normalized cross-spectral density  $u_{12}(\omega)$  is then

$$u_{12}(\omega) = \frac{U_{12}(\omega)}{[P_1(\omega)P_2(\omega)]^{1/2}}.$$

Similarly,  $v_{12}(\omega)$  is obtained by using a time delay

$$\tau = \frac{1}{4\omega_n}$$

where  $\omega_n$  is here the midband frequency of the narrow filter. The imaginary part of the normalized cross-spectral density  $v_{12}(\omega)$  is

$$v_{12}(\omega) = \frac{V_{12}(\omega)}{[P_1(\omega)P_2(\omega)]^{1/2}}.$$

It is noted that the measurement of  $u_{12}(\omega)$  and  $v_{12}(\omega)$  yields more information than the more commonly measured normalized cross correlation since the normalized cross correlation may be obtained by integration.

For this work  $P_1(t) = P_2(t)$ , since the two measurement points are sufficiently close together that the boundary layer has not changed in character.

The real and imaginary parts of the cross-spectral density as a function of  $t_n \times 0.8U_n$  are shown in Fig. 5. The distance between the two measurement points has been designated as  $x$ , and the midband frequency of the narrow filter has been designated as  $\omega_n$ . The factor of 0.8 will now be accounted for.

By measuring the cross correlation in a narrow band of frequencies, and by determining the time delay  $\tau$  that maximized this correlation, an effective convection



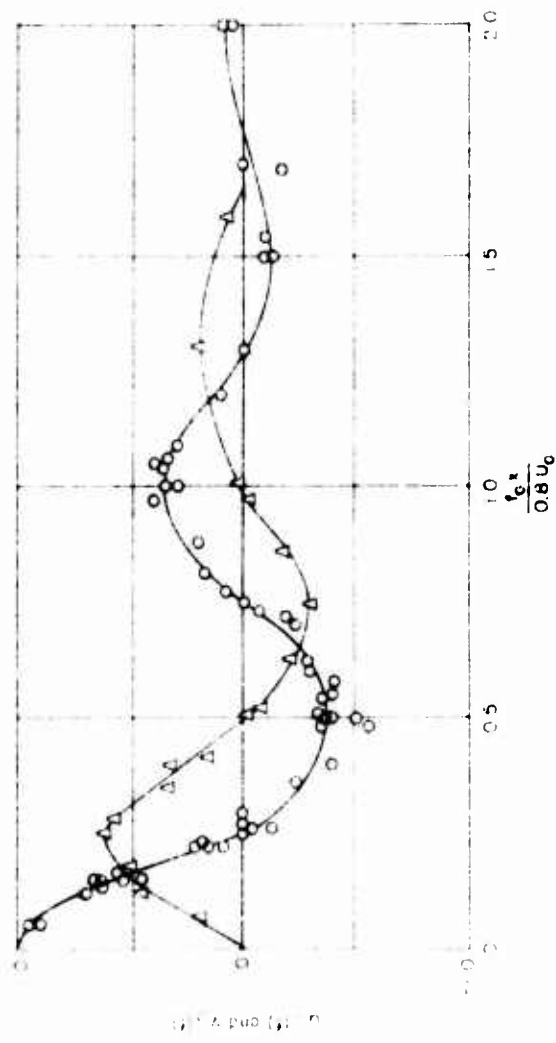


Fig. 1. Variation of the ratio of the maximum velocity to the average velocity,  $\frac{V_{max}}{V_{avg}}$ , versus the ratio of the maximum velocity to the average velocity,  $\frac{V_{max}}{V_{avg}}$ .

velocity  $U = 8.1$  of the spectral pattern was determined. For all frequencies up to 2000 cps (the upper limit of the transducer for this circumstance), it was found that the convection velocity was about  $0.8 U$ . It was expected that the convection velocity would decrease with increasing values of frequency as a consequence of the quadrupole nature of the right-hand term in Eq. (1). The measurement procedure was not sufficiently precise to reveal such a relationship even though there is reasonable certainty of its existence.

It can be seen that the spatial pattern of the pressure fluctuations is not convected downstream as though it is frozen. If this were so, the real part of the normalized cross-spectral density can be shown by a simple computation, for the case of a filter with a rectangular frequency response, to be

$$\frac{P_{12}}{P_1 P_2} = \frac{1}{\left(\frac{2 - 1.8}{0.8 U}\right)} \frac{1}{\left(\frac{2 - 1.8}{0.8 U}\right)} \cos \left(\frac{2 - 1.8}{0.8 U}\right)$$

where the first factor on the right is an effect due to the finite bandwidth  $\Delta f$ . Since, in these measurements, a constant 10 percent bandwidth was used, this factor is negligibly different from unity.

The departure, for the real part of the data of Fig. 5, from  $\cos(2 - 1.8)/0.8 U$  is a measure of the development of an uncorrelated component in the pressure fluctuations during its travel from the upstream to the downstream measurement point.

A measure for the uncorrelated component can be formulated mathematically. The downstream pressure fluctuation  $p_2(t)$  can be resolved into three components whose cross-spectral densities with the upstream pressure fluctuation  $p_1(t)$  respectively, real, imaginary, and zero. That is,

$$p_2(t) = p_1(t) + p_3(t) + p_4(t)$$

where  $P_3 = P_{12}$ ,  $P_4 = iV_{12}$ ,  $P_1 = 0$ . The vanishing of the spectral density is equivalent to saying that the correlation for  $p_1(t)$  and  $p_4(t)$  is zero. This resolution can be effected using the definition for cross-spectral density. The spectral densities for  $p_1(t)$ ,  $p_3(t)$ , and  $p_4(t)$  are

$$\begin{aligned} P_1 &= U_{12}^2 P_1 \\ P_3 &= V_{12}^2 P_1 \\ P_4 &= P_2 - P_{12}^2 P_1 \end{aligned}$$

so that

$$P_2 = \frac{1}{P_1} (P_1 + P_4)$$

and can be computed in terms of the measured data  $P_1(t)$ ,  $P_2(t)$ , and  $P_{12}^2 = U_{12}^2 + V_{12}^2$ . Perhaps of greater interest is the quantity

$$\frac{P_{12}^2}{P_1 P_2} = 1 - \frac{P_4}{P_2}$$

which can be taken as a measure of the coherence of  $p_2(t)$  with  $p_1(t)$ . This quantity is plotted in Fig. 6.

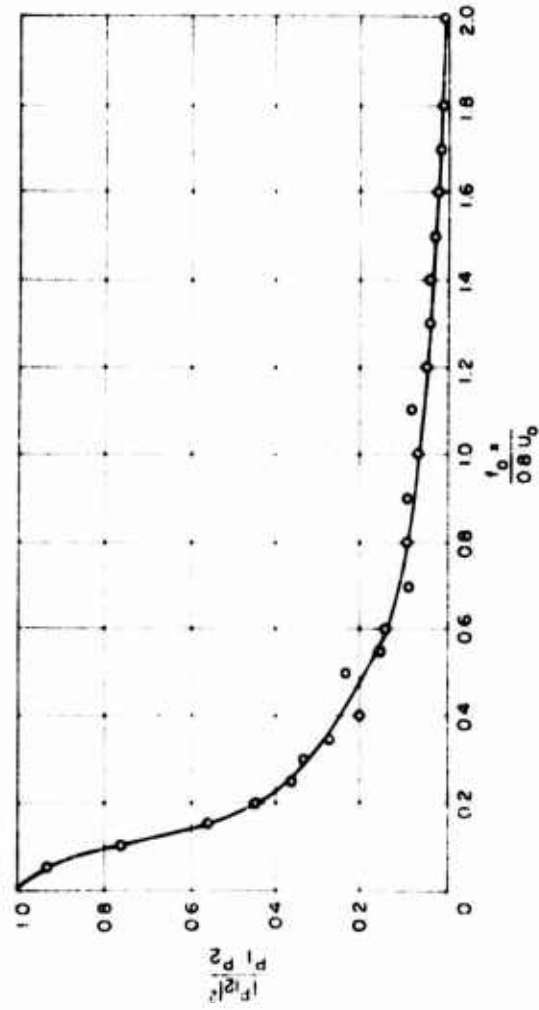


Fig. 6 - Longitudinal coherence of the pressure fluctuations

There are several important limitations in the data presented in Fig. 5. One trend in the data that is desirable to investigate is the effect of the parameter  $x^+ U_{\infty}$ . Unfortunately, the transducer used for the cross-spectral density measurements had a usable frequency range up to only 2000 cps. Consequently, only the flat part of the spectral density, as shown in Fig. 4, could be investigated. The upper limit of 2000 cps set an upper limit on  $x^+ U_{\infty}$  between 0.083 and 0.33. As can be seen in Fig. 4, this does not permit investigation of the cross-spectral density of the pressure fluctuations in the range where the spectral density is rapidly decreasing with frequency. With reference to the velocity fluctuations in the boundary layer, the region investigated corresponded to the region where the velocity spectral density is described by the  $-5/3$  law where inertia forces dominate. It would be interesting to procure data for the cross-spectral density in the range where viscous forces dominate.

### THE TRANSVERSE CORRELATION

The transverse correlation was measured using the equipment of Fig. 3 with the wave analyzer omitted. The data are presented in Fig. 7. Unfortunately, these data

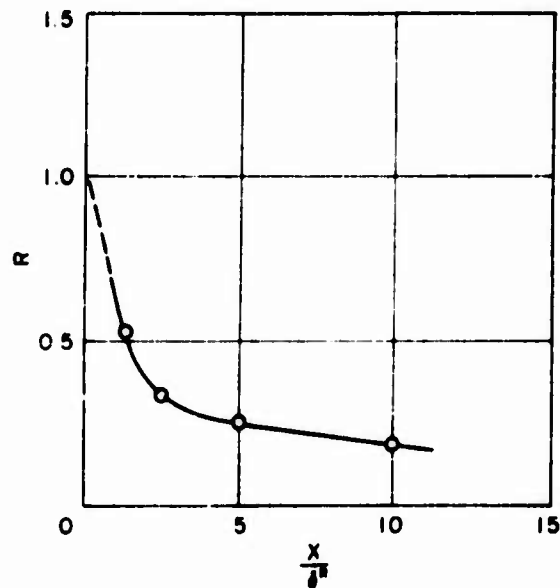


Fig. 7 - Transverse correlation function

have not been checked carefully since they were taken on the last day the wind tunnel was available for this work. Since we are not concerned here with the convection of a nearly frozen pattern, the cross-spectral densities were not investigated. For the purpose of a cross check, however, it would have been valuable to have obtained these data. Another limitation of the data is that their variation of speed was not checked because of limitations on experimental time.

# REFERENCES

1. Kraichnan, R.H., J. Acoust. Soc. Am. 28:378 (1956)
2. Kraichnan, R.H., J. Acoust. Soc. Am. 29:65 (1957)
3. Klebanoff, P.S., and Diehl, Z.W., NACA Report 1110, 1952
4. Hilliard, J.K., and Finia, W.T., J. Acoust. Soc. Am. 29:254 (1957)
5. James, Nichols, and Phillips, "Theory of Servomechanisms," Chapter 6 New York:McGraw-Hill, 1947
6. Willmarth, W.W., J. Acoust. Soc. Am. 28:1048 (1956)
7. Klebanoff, P.S., NACA Report 1247, 1955

• • • • •

# DISCUSSION

W. Willmarth (University of Michigan)

I think Dr. Harrison's work is a valuable contribution to the existing measurements of the wall pressure fluctuations in a turbulent boundary layer. I would like to state that, in general, his experiments agree with those that I did at the California Institute of Technology which will soon be available as an NACA technical note.

However, I would like to point out that Dr. Harrison's value for the root mean square pressure

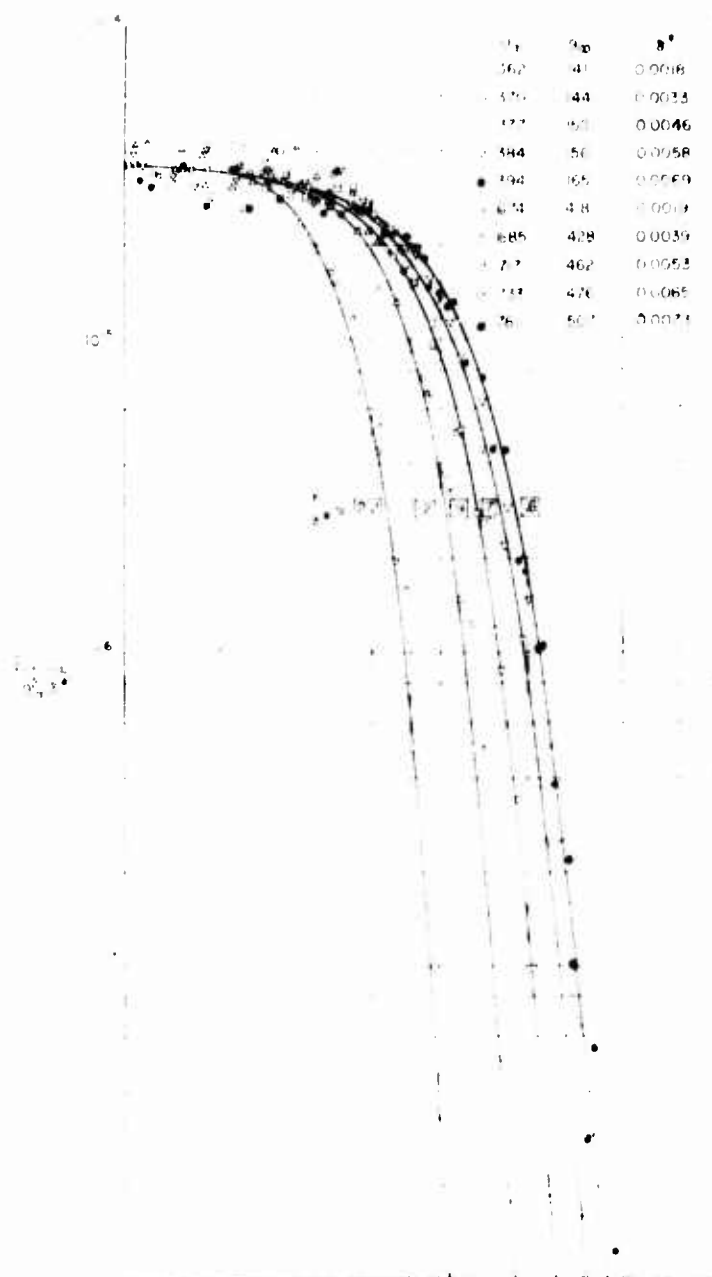
$$p'^2_{rms}$$

is considerably higher ( $9.5 \times 10^{-5}$ ) than the value I found ( $6 \times 10^{-5}$ ) and higher than the value found by others ( $\approx 4.5 \times 10^{-5}$ ) in unpublished NACA technical notes. I don't know why this discrepancy exists.

My measurements of the nondimensional spectra are, of course, lower than Dr. Harrison's, but show qualitatively the same behavior at low values of the Strouhal number ( $\approx 0.1$ ). I was able to measure the spectra at various stream velocities and boundary layer thicknesses. The data are shown in Fig. D1. It can be seen that the high-frequency response is affected by the size of the transducer. I have attempted to correct these spectra using the method of Uberoi and Kovasznay<sup>1</sup> with the assumptions that the entire pressure pattern is "frozen" and passes by the transducer at  $0.83 \times$ , and that the statistical properties of the pressure have radial symmetry in the coordinate system moving at  $0.83 \times$ . The results are shown in Fig. D2.

<sup>1</sup>Uberoi, M. S., and Kovasznay, L. S. G., "The Effect of Transducer Size on the Measured Spectrum of Wall Pressure Fluctuations in a Turbulent Boundary Layer," NACA Technical Note 1247, 1955.

Figure 1. Pressure Fluctuations in Turbulent Boundary Layer



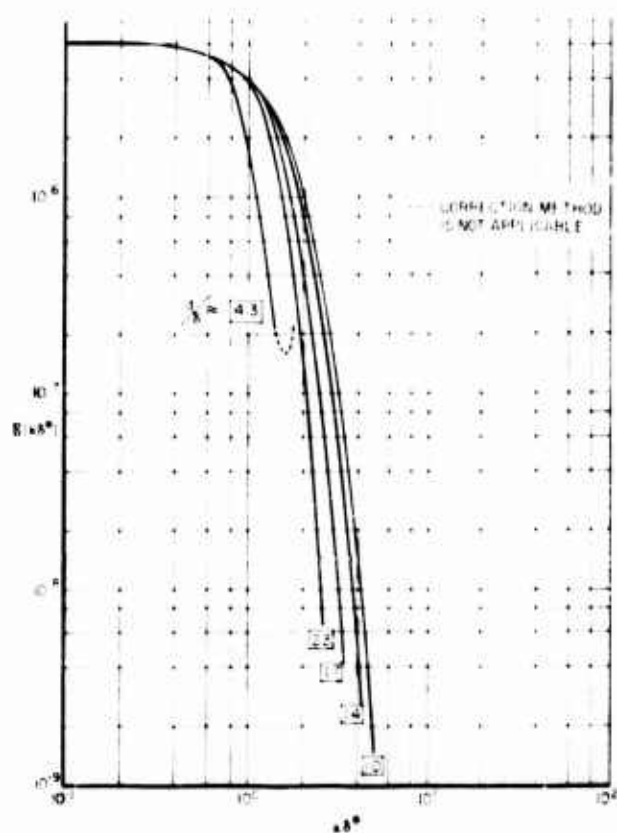


Fig. D2 - Corrected nondimensional spectrum of the wall pressure

The nondimensional spectra and spatial correlation in Fig. 2 are defined by the relations

$$\begin{aligned}
 \phi(k) &= \frac{k^2}{q^2 + 2} = \frac{1}{2(q^2 + 2)} \int_0^\infty R(r) e^{-\frac{1}{2} k^2 (N_1^2 + N_2^2)} dN_1 dN_2, \\
 R(r) &= \frac{R(r, 0)}{q^2 + 2} = \frac{1}{(q^2 + 2)^2} \int_0^\infty \int_0^\infty e^{-\frac{1}{2} k^2 (N_1^2 + N_2^2)} R_{k_1, k_2} dN_1 dN_2.
 \end{aligned} \quad (1)$$

Here  $\phi$  is the two dimensional spectrum in wave-number space and  $R$  is the pressure correlation with respect to distance along the wall. It can be seen in Fig. 2 that the "corrected" spectra are not in agreement for the various ratios of transducer radius to displacement thickness,  $r_0/\delta^+$ .

I believe this is caused by the lower convection velocity of the small-scale pressure fluctuations. The reasoning is as follows: if everything is moving at  $0.83 U$

then the wave number is given by  $k = 0.83/2 U_0$ . The correction factor for the spectra, which takes into account the transducer size, turned out to be quite small even for the highest frequencies or wave numbers. The corrected data, however, obviously still depend on the transducer size. Thus, the wave number at high frequency must be much smaller and that means that the convection velocity must be considerably lower than  $0.83 U_0$  for the high frequencies.

Finally, I think that we have found out something about the turbulent boundary layer when we see that the cross-spectral density of the pressure is a function of the parameter  $x/U_0$ . Both Dr. Harrison and I are in agreement on this point. My measurements of the cross correlation of the pressure,<sup>†</sup> see Fig. D3, taken at

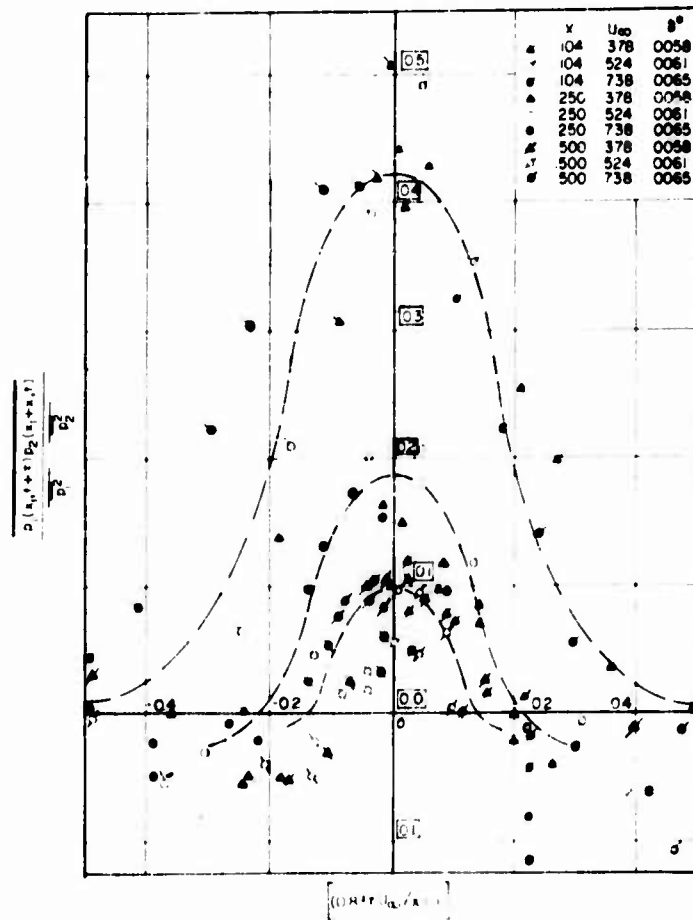


Fig. D3 - Cross correlation of the pressure

<sup>†</sup>W. W. Willmarth, "Space-Time Correlations of the Fluctuating Wall Pressure in a Turbulent Boundary Layer," J. Aeronaut. Sci., Vol. 25, No. 5, May, 1958.



velocities between three and seven times that of Dr. Harrison's stream velocity, can be written as the function  $R(x) = 0.83 U_0 + x$ , which means, in my case, that the cross-spectral density (i.e., the transform of the cross correlation) can be expressed as the function  $(x - 0.83 U_0) \rho_{12}(x - x - 0.83 U_0)$ . I do not understand why Dr. Harrison's results do not show this additional dependence on  $x$ . I believe this is an important result. It means that the low frequency or larger scale motion dies out much more slowly than the small scale motion, and that the rate of decay of a disturbance of any given scale is related to the distance it travels downstream.

M. Harrison

As Dr. Willmarth pointed out, in the flat part of the spectrum you might expect the convection velocity to travel because of the scale over which the velocity is fluctuating. The very high frequency components on the part of the curve that is falling might be related to a region approaching the inner part of the boundary layer, but not really there, so you might expect the convection velocity for the spatial pattern, which is made up of higher frequency components, to travel at a higher velocity. I tried to measure that but, unfortunately, from the way my pressure components were constructed when I used them for making the wind tunnel measurement, I had a much lower frequency range to work in. So, I may add, all my measurements on the cross-spectral densities were really over the flat part of the spectrum. Consequently I wasn't able to measure the convection velocity very far down, where the spectrum is falling and I got essentially a constant convection velocity with a slight tendency to fall for the higher frequencies, or higher wave numbers. This was rather marginal so I didn't report it because I wasn't sure whether it was real or just an experimental error.

H. S. Ribner (University of Toronto)

Given two microphones at a specified separation, Willmarth measures the product signal as a function of time delay. Harrison, on the other hand, puts the product signal through a tuned filter and measures a spectral density, with and without selected time delays. Harrison is to be commended for developing this cross-spectral density technique. He has given a very nice demonstration that his cross-spectral density and Willmarth's space-time correlation must be Fourier transforms of each other.

Harrison's experimental cross-spectral density functions, as plotted, look like damped cosine and sine functions. The paired curves exhibit a damping factor that varies as the product  $t_0 x$ . The Fourier transform of a function that simulates Willmarth's measurements, on the other hand, shows a damping depending on  $t_0$  and  $x$  separately. Moreover, the inverse Fourier transform of Harrison's curves appears to become infinite at the origin, which is inadmissible. One wonders if Harrison's two curves should not really be two families, with damping depending separately on  $t_0$  and  $x$  in each family. More combinations of  $t_0$  and  $x$  in the data points are needed.

O. M. Phillips (Johns Hopkins University)

This paper provides a clear verification of the concept of convection velocity of the surface turbulent pressure fluctuations. This is central in Lighthill's theory of

aerodynamic sound and in recent attacks on the problem of wave generation by turbulent wind blowing over a water surface.

There are two remarks that I should like to offer. The first concerns the theoretical prediction of the instantaneous pressure covariance on a fixed surface when one point is held fixed and the other is integrated over the entire plane. This prediction has been made, under conditions of increasing generality, by Phillips,<sup>†</sup> Kraichnan<sup>‡</sup> and Phillips, and expresses the fact, required by the incompressibility and boundary conditions, that the mean-square-linear momentum, per unit area of the boundary layer, normal to the surface vanishes. It requires that the surface pressure covariance should be somewhere negative to balance the positive contributions to the integral. Figure 7 of this paper gives little indication that the transverse correlation will be negative; it is still about 0.2 for  $x/x^* = 10$ . Perhaps the longitudinal instantaneous correlation has negative regions. Unfortunately, Dr. Harrison's data do not appear to bear on this question. The theoretical result appears to be sound, but we would be happier with experimental confirmation (or denial!) of it.

The second remark concerns the spectral densities shown in Fig. 4. The pressure fluctuations are associated with the turbulent velocity fluctuations, whose mean-square-magnitude is proportional to the square of the friction velocity  $U^*$ . One would expect, therefore, that this, rather than  $U_\infty$ , would be the relevant velocity scale to be used in making  $f(f)$  dimensionless. If this minor modification is made, it is found that the points for  $U_\infty = 1500$  cm/sec are raised by about 30 percent relative to those for  $U_\infty = 6000$  cm/sec, and those for  $U_\infty = 3000$  cm/sec by about 15 percent, bringing the three sets of results into very close coincidence over the flat, low frequency range and removing the apparent Reynolds number effect indicated by Fig. 4.

<sup>†</sup>O. M. Phillips, Proc. Roy. Soc., A, 234:327-335 (1956).

<sup>‡</sup>R. H. Kraichnan, J. Acoust. Soc. Amer., 28:378-390 (1956).

O. M. Phillips, Talk to Acoustical Society Meeting, Washington, D. C., May, 1958.

\* \* \* \* \*

# THE FLUCTUATING SURFACE PRESSURE CREATED BY TURBULENT BOUNDARY LAYERS ON HYPERSONIC VEHICLES

Edmund E. Callaghan

*National Advisory Committee for Aeronautics*

There are a great number of specialized problems which result from flight at extremely high speeds. Some of these problems are new, others are merely magnified by the higher speeds. The fluctuating surface pressures generated by subsonic turbulent boundary layers has received considerable attention in recent years. These fluctuating surface pressures are transmitted through the vehicle skin and result in high internal noise levels. The current crop of jet transports has required considerable insulation to minimize this effect and achieve reasonable passenger comfort. The question arises then as to what levels might be expected by flight at hypersonic speeds. It is the purpose of this paper to make some estimates of the order of magnitude of the levels which might be expected for several cases of current interest.

The fluctuating surface pressures created by a turbulent boundary layer are, of course, dependent upon the physical characteristics of the boundary layer. A considerable body of data now exists, which relates these surface pressures to the local flow conditions for the case of subsonic turbulent flow over a flat plate. In general, these results show that the root mean square of the fluctuating pressures on the surface are directly proportional to the local dynamic pressure of the flow and are largely independent of both Reynolds and Mach numbers. This general result stems from the fact that turbulent boundary characteristics over flat plates change only slowly with both Reynolds and Mach numbers. If, for example, we take the skin friction coefficient as a measure of boundary-layer characteristics we can see that only small changes occur over wide ranges of Reynolds and Mach numbers. Indeed, if we look at dimensionless velocity profiles, either mean or turbulent, we see that such relationships are quite general in nature. Hence, the fact that the dimensionless ratio of root-mean-square fluctuating surface pressure to stream dynamic pressure is essentially constant for the case of subsonic turbulent boundary layers on flat plates or slightly curved surfaces is not surprising and, in fact, provides a clue that subsonic results may be extrapolated to hypersonic speeds for cases where the boundary-layer characteristics are not greatly altered by effects of cooling, pressure gradient, or gas dissociation.

The data to date are summarized in Table 1. The agreement is excellent even though the tests were made in widely varying environments. The data of Willmarth was obtained in a small 4-inch-diameter pipe. The data of Serafini was obtained in a specially designed rectangular acoustic channel, 8 x 18 inches. In these tests the pressure gradient was controllable. The flight data of Mull was obtained on the wing and fuselage of a jet aircraft.

Table 1

Ratio of Root-Mean-Square Fluctuating Surface Pressure  $p$  to  
Stream Dynamic Pressure  $q$  from Various Sources

$p/q$	Mach number	Reynolds number	Pressure Gradient	Type of Test	Author
$3.5 \cdot 10^{-3}$	0.3 to 0.8	$1 \text{ to } 20 \cdot 10^6$	Favorable	Channel	Willmarth - NACA TN 4139
$5.0 \cdot 10^{-3}$	0.65	$10 \text{ to } 100 \cdot 10^6$	None	Channel	Serafini - NACA unpublished
$5.0 \cdot 10^{-3}$	0.3 to 0.8	$2 \text{ to } 20 \cdot 10^6$	Favorable or none	Flight	Mull - NACA unpublished
$6.0 \cdot 10^{-3}$	0.3 to 0.7	$2 \text{ to } 20 \cdot 10^6$	Favorable	Channel	Willmarth - NACA unpublished

It would appear that a mean value of about  $4.5 \cdot 10^{-3}$  could be chosen to represent all these data; especially when it is remembered that all these data were measured using microphones and the results measured in decibels.

If we choose the ratio of  $p/q = 4.5 \cdot 10^{-3}$  and assume that this ratio holds even at hypersonic speeds, then it is obvious that the highest values of  $p$  will be obtained when  $q$  is a maximum. With this in mind, let us consider what cases might currently be of most interest. Two immediately come to mind; the high-speed nose-cone reentry and the take-off of a powered rocket. At the present time we can probably ignore the problems which might arise from sustained flights at hypersonic speeds. In this instance a great number of other problems must be solved before continuous flight at Mach numbers greater than 5 will be achieved.

We will, therefore, limit the discussion to the reentry of manned or unmanned vehicles and to the take-off and climb-out phase in powered flight. First let us consider the unmanned vehicle, i.e., the ballistic missile, since this represents a somewhat different problem than the manned vehicle. The principal difference is in the deceleration rates which are permissible. This aspect is not too important for the unmanned vehicle; but it is extremely important in the case of a manned vehicle, particularly if we expect the occupant to perform a useful function. Even if the occupant is a passenger only, he would probably object strenuously to being both squashed and fried.

Let us therefore look at the nose-cone reentry problem and see what is involved and whether it appears likely that we can make such a calculation with some hope that the results are correct. Considerations other than noise have determined nose-cone shape, that is, heat transfer. In order to keep the heat transfer rates to the vehicle surfaces to acceptable values, current considerations dictate a blunt-nosed, high-drag body such as shown in Fig. 1. Such a shape has a very strong shock wave ahead of it and even though the stream Mach number is of the order of 20, the flow field between the body and the shock wave is subsonic or slightly supersonic. As a result, it should be possible to use the results presented in Table 1 with an excellent expectation of obtaining the correct result. Furthermore, the pressure gradient around the body is favorable and it would be expected that the boundary-layer characteristics would not be greatly different from subsonic results. Considering then the case of such a body reentering the earth's atmosphere, we will use the following notation to describe the quantities of interest.

# Fluctuating Surface Pressures

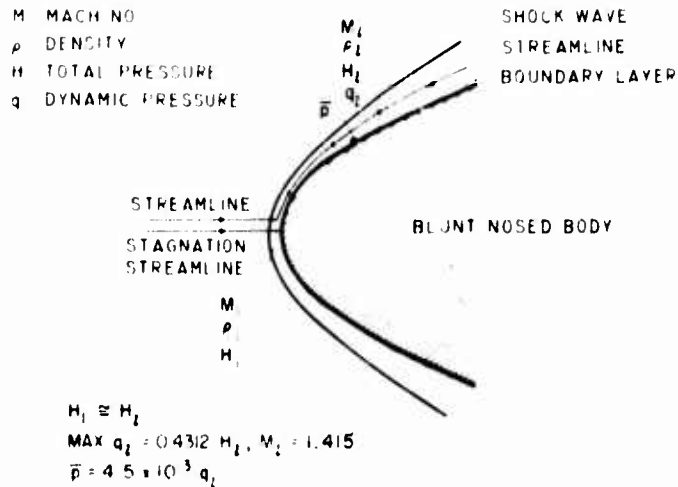


Fig. 1 - Blunt-nosed body at hypersonic speeds

The subscript 1 refers to conditions immediately behind the shock at the nose. The subscript 2 relates to local conditions between the shock wave and the boundary layer, aft of the nose. Since the root-mean-square pressure  $p$  is linearly related to  $q$ , the point on the body of most interest is where the value  $q_1$  is a maximum.

At high Mach numbers an extremely strong bow wave precedes the body and the value of  $M_1$  is about 0.4 for a range of stream Mach numbers from 4 to 20.

If we follow the path of a streamline through the shock and around the body, we get the following picture: Streamlines which go through the shock wave near the nose are bent and flow around the body between the shock wave and the boundary layer. As a streamline moves around the body, the flow speeds up but the total pressure along the streamline is essentially constant. If we take a streamline which lies close to the boundary layer, we see that such a streamline crosses the shock wave very near the stagnation streamline and hence we can assume that the total pressure  $H_1$  along this streamline behind the shock is essentially equal to the total pressure of the stagnation streamline behind the shock  $H_1$ . With this assumption, the total pressure of this streamline behind the shock can be calculated quite simply from the normal shock relations. The compressible flow relations tell us that the maximum value of  $q_1$  for a given total pressure  $H_1$  or  $H_2$  in this case, occurs at a Mach number of 1.415. This then determines our point of interest and is independent of the geometry, i.e., we don't need to know the exact shape of the nose; we will pick the particular point where maximum  $q_1$  is obtained. This value is uniquely related to  $H_1$  at a value of  $M_1 = 1.415$  and the ratio  $q_1/H_1 = 0.4312$ . It should be noted that the calculation procedures used here do not account for any effects associated with extremely high temperatures, such as dissociation or variable ratio of specific heats. It is felt that all such effects would be small in terms of the final answer, which is required only to perhaps the nearest  $\pm 3$  db.

If we concern ourselves only with the maximum value of  $q_1$  and, hence, the maximum root-mean-square pressure at the surface  $p$  it is possible to calculate  $p$  during reentry using the normal shock relationships and the reentry calculation procedure described by Allen and Eggers in NACA TN 4047.

Allen and Eggers derived an equation which yields the velocity at any point along the trajectory from reentry into the atmosphere until impact. The velocity at any point was found to be dependent on the initial velocity at reentrance  $V_E$  and a parameter herein designated as  $\beta$ . The parameter  $\beta$  describes the characteristics of the vehicle, i.e., its drag coefficient  $C_D$ , its mass  $m$ , its area  $A$ , and its reentrance angle into the atmosphere  $\theta_E$ . It can be assumed that over the trajectory range of interest, i.e., where the Mach numbers and  $q$  values are high, that  $\beta$  is essentially constant. That is, for a given missile does not vary along the trajectory. Knowing the relationship between vehicle velocity and altitude, an equation relating local dynamic pressure and altitude can be derived in terms of parameter  $\beta$  and reentrance velocity  $V_E$ .

Figure 2 shows the variation of  $q$  with altitude for a reentrance velocity of 20,000 feet per second and for several values of parameter  $\beta$ . The vehicle reenters the atmosphere at approximately 200,000 feet and plummets toward the earth. The values of  $q$  increase to a maximum and then decrease. The peak or maximum value of  $q$  along the trajectory is dependent on  $\beta$ . High  $\beta$  values give low maximum values which occur at relatively high altitudes, whereas low  $\beta$  values give large maximum values of  $q$  which occur at relatively low altitudes. High  $\beta$  values give rapid vehicle decelerations at high altitudes where heat can be radiated rapidly away from the body, which is desirable from heat transfer considerations. The high vehicle deceleration at high altitude results in low velocities at low altitude, which may not be desirable.

In any case, the maximum values of  $q$  shown here are much higher than anything heretofore experienced. Even with a  $\beta$  value of 7000, the peak of  $q$  is over 4000 pounds per square foot, which is five to ten times the values to which we are normally accustomed. The sound pressure levels associated with values of  $q$ , using  $p = 4.5 \cdot 10^{-3} q$ , are shown on Fig. 3 where sound pressure level is plotted as a function of altitude. The reentrant velocity for these curves is 20,000 feet per second. Curves are shown for  $\beta$  values of 7000, 4000, and 1000.

It can be seen from this figure that one result of achieving low  $\beta$  values will be increasing values of surface sound pressure level. For example, if a  $\beta$  value of 1000

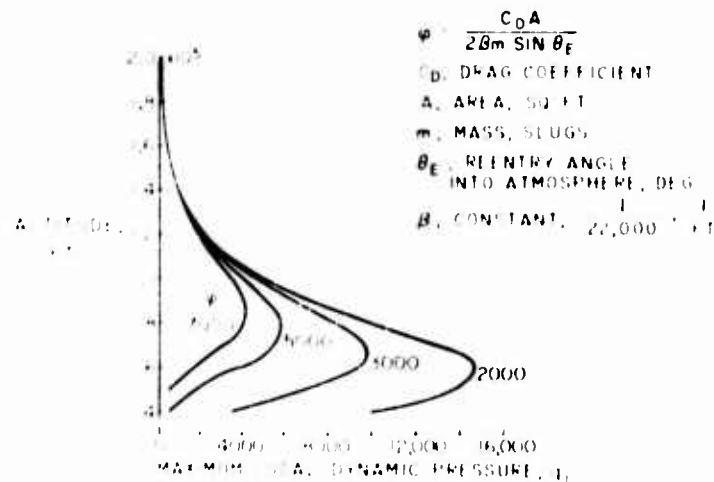


Fig. 2 - Variation of maximum local dynamic pressure during reentry

# Fluctuating Surface Pressures

is achieved, the maximum sound pressure level will be 170 db. This is extremely high and might well result in structural deterioration of the vehicle. This is particularly true since other forces and temperatures are also at near maximum values at this same stage.

One important factor which must be considered is the exposure time. For a value of  $\phi$  of 7000 the time for the vehicle to fall from say 140,000 feet to 50,000 feet is perhaps 30 seconds. For a value of 1000, the time for the vehicle to travel from 140,000 to 40,000 feet is of the order of 15 seconds.

Figure 4 shows the variation of the maximum sound pressure level encountered during reentry; i.e., this corresponds to the peak or maximum of the curves shown on Fig. 3. The sound pressure levels corresponding to this condition have been plotted as a function of the parameter  $\phi$  for various reentrance velocities. It is evident from this figure that quite high values of sound pressure level will be encountered for nearly all unmanned missiles under current consideration.

It is obvious that the high external levels may well create a structures problem or result in high internal levels which could affect the operation of the vehicle.

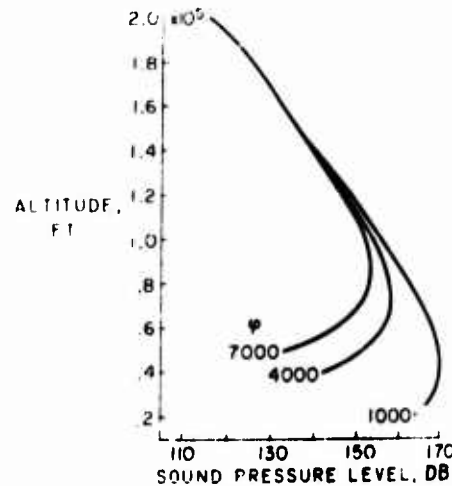


Fig. 3 - Maximum local sound pressure level during reentry

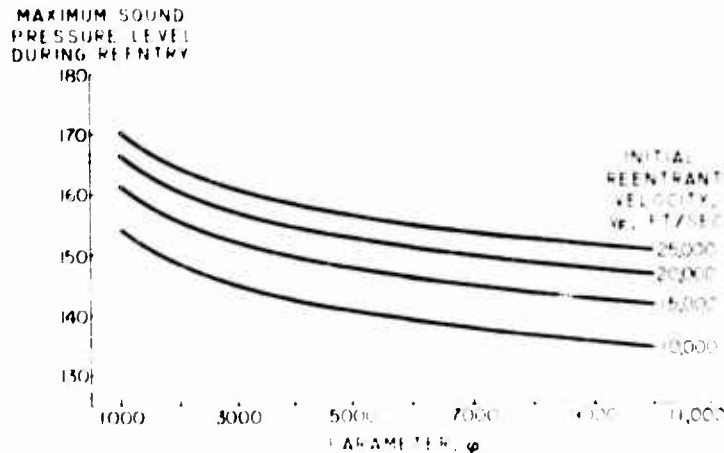


Fig. 4 - Maximum sound pressure level as a function of parameter

Let us now consider briefly the flight of a manned space vehicle. First let us look at the powered or take-off phase and then the reentry phase. Again, as in the previous example, we will consider only what is happening on the nose cone, which in this case contains the occupant and related equipment. Figure 5a gives the velocity, acceleration, and altitude as a function of time from take-off to first-stage burnout. The weight of the payload chosen is 3000 pounds and the orbital altitude approximately 200 miles. As can be seen from the figure, the maximum acceleration is about  $130 \text{ ft/sec}^2$  or  $4 \text{ g's}$ . The velocity at the end of burnout is  $8600 \text{ ft/sec}$  and the altitude, about 164,000 feet. The sound pressure levels which would be expected on the nose-cone region using these results are shown in Fig. 5b. The shape of the nose cone has been assumed to be similar to that for the unmanned vehicle except that it will probably be even more blunt in shape. The results shown represent the maximum value achieved at a single point on the nose-cone surface. The solid curve is the noise which results from boundary-layer turbulence. The dotted curve shows the levels

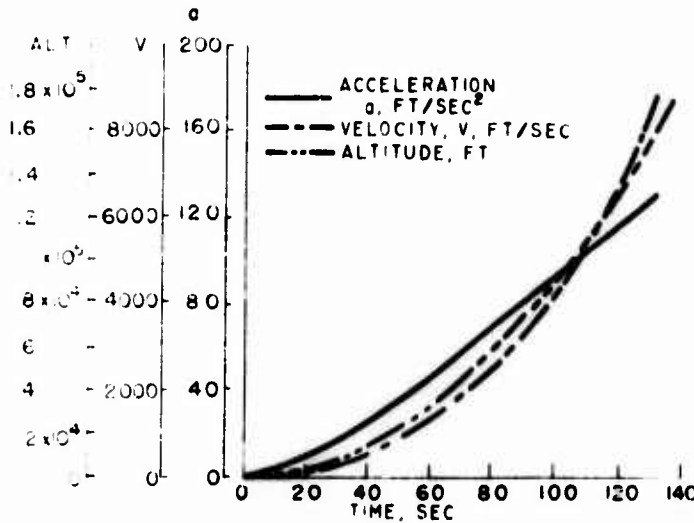


Fig. 5a - Powered phase manned vehicle

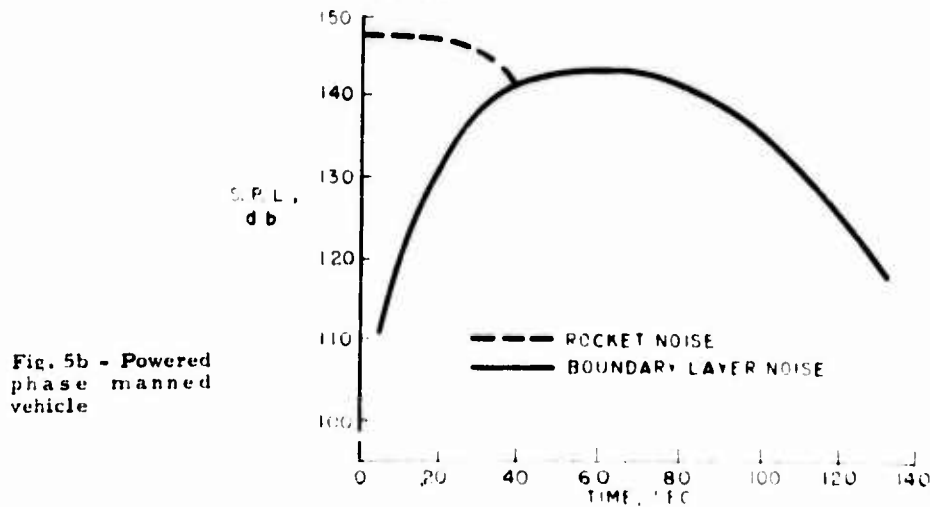


Fig. 5b - Powered phase manned vehicle

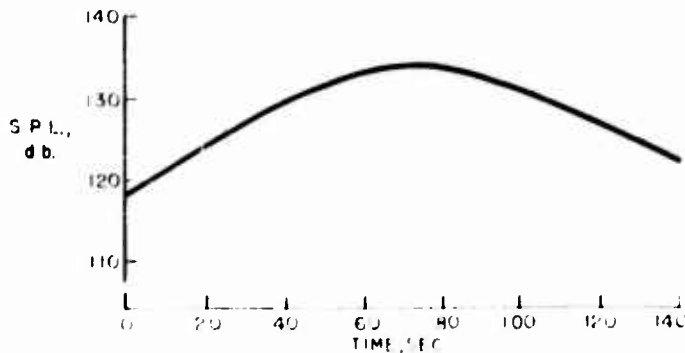
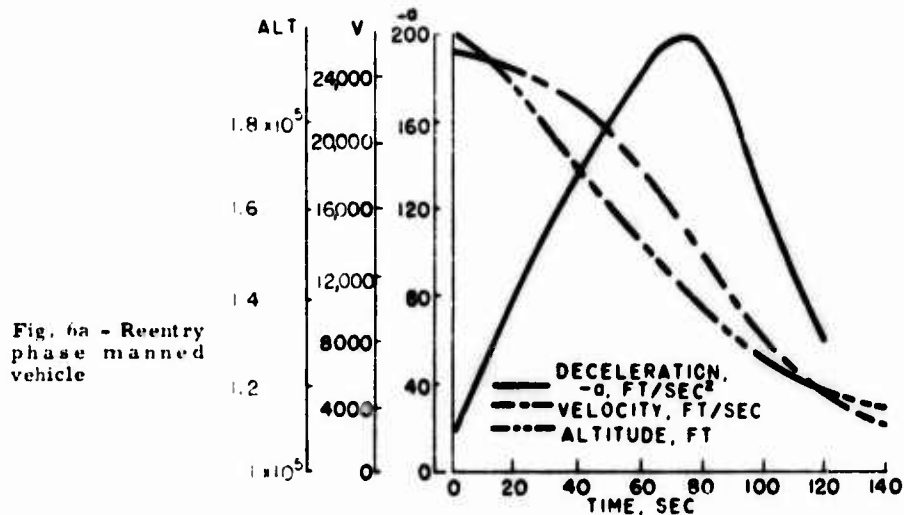


### Fluctuating Surface Pressures

which might be expected from the rocket itself. Rocket noise predominates for the first 40 seconds and then the boundary-layer noise takes over. The principal reason for the decrease in rocket noise is that after a flight Mach number of 1 is achieved, the rocket noise is directed predominantly rearward and only a very small amount can be propagated forward. It is apparent from the figure that the levels are low and in fact no higher than we currently experience subsonically. This results from the fact that high dynamic pressures are never achieved since the high velocities only occur at high altitudes.

It would appear that no serious noise problem should occur around the nose region of such a rocket during the initial powered phase of the flight.

Let us now look at the reentry portion of the flight. The velocities, deceleration, and altitudes as a function of time for the assumed vehicle are shown in Fig. 6a. The deceleration is a maximum of approximately 200 feet/second<sup>2</sup> or a little over 6 g's. Notice that high deceleration rates, over 5 g's, exist for about 20 seconds. It might be possible that higher deceleration rates (10 g's) can be used but it would seriously impair the occupant's ability to perform useful functions. If it is noted that the velocity decreases from 26,500 feet/second to 4000 feet/second between 200,000- and



E. E. Callaghan

about 120,000-foot altitude, then the low values of sound pressure level experienced during reentry (Fig. 6b) are not surprising. Figure 6b shows a maximum value of sound pressure level of about 135 db, which is quite low and should not create any serious problems.

In conclusion it can be said that the noise levels in the nose-cone region for manned vehicles will probably be low, largely as a result of human limitations to g forces.

The unmanned vehicle, i.e., the ballistic missile, may well have extremely severe noise problems which could result in structural failures or instrument malfunctions. The absolute levels are quite high, perhaps 155 db, for cases of current interest and will probably increase as heat transfer problems are solved.

\* \* \* \* \*

## DISCUSSION

L. S. G. Kovasznay (Johns Hopkins University)

All the data which shows this rather spectacular constancy of sound pressure level compared to dynamic pressure is based solely on data available up to Mach number 0.8, yet we know that the general nature of supersonic boundary layers is somewhat different. This disturbs me, because Mr. Callaghan has shown that the maximum dynamic pressure "q" will be experienced at a Mach number of 1.415, and we do not yet have boundary-layer noise data for this Mach number.

Now, when looking at, say, shadow pictures of shells, one sees another kind of interesting sound wave pattern and we know from the little information we have obtained, mostly by hot-wire measurements in supersonic tunnels just outside the boundary layer, that the boundary layers don't seem to emit anything spectacular as long as the wall is smooth, uninterrupted and there is only a little sound. But if there is any edge of roughness, then the amount of sound increases tremendously. This may be especially true for ablation cooling, or any kind of pitting on the nose cone, and I expect strong effects of this nature.

There is another question, and it might be possible to treat it theoretically. If one has a hypersonic, blunt body, where the shock wave is hugging the contour, there is an interesting space of subsonic flow between the shock wave and the boundary layer; any disturbance present there will affect the location of the shock wave causing the shock wave to move or "jiggle." There will be an interactive zone which might give reinforcement of fluctuations.

My only caution is that even these aspects of the problem have to be considered in great detail before we accept this type of treatment as even approximate.

I. Dyer (Bolt, Beranek, and Newman, Massachusetts)

Here is a short list of the sources of pressure fluctuations that may also be of importance in missile flights.

## Fluctuating Surface Pressures

We can certainly have rocket engine noise, as Mr. Callaghan has mentioned; rocket engine vibration, which is directly transmitted from the rocket engine to the missile itself; boundary-layer pressure fluctuations, as Mr. Callaghan has also mentioned; and another phenomenon that hasn't been mentioned which we call wake noise. Wake noise is associated with the field downstream of the missile or re-entering body. Also, we have what we might call base-pressure fluctuations for supersonic conditions, and these fluctuations are going to be particularly important for re-entry; oscillating shocks, mentioned by Mollo-Christensen, which depend on the particular design of the missile or re-entry body; the possibility of transmission or convection of vorticity through shocks, a problem which was discussed by Ribner not too long ago. Finally we have the convection of a missile through a turbulent atmosphere.

While many of these sources of pressure fluctuations are probably not too important, I think in re-entry we are probably going to have to worry about base-pressure fluctuations probably to the same extent that we might worry about the boundary-layer pressure fluctuations. This is what preliminary measurements and calculations seem to indicate.

One final comment is this: that the base-pressure fluctuations would likely maximize at the maximum dynamic pressure of the missile, just as in the case of boundary-layer fluctuations.

It may be difficult, on an experimental basis, to look at pressure fluctuations as a function of time and decide whether it is one or another mechanism. An important feature is the scale of the pressure fluctuations. The base-pressure fluctuations are apt to be of a much larger scale and hence more important in exciting vibrations of the missile, even though they may only be the same order of magnitude in pressure as the boundary-layer field.

G. M. Corcos (University of California, Berkeley)

There is very little reason to expect that the pressure fluctuation level at the wall of the boundary layer ought to be independent of pressure gradient. This is a general comment, not restricted to this paper, since other participants have pointed out possibly more serious other sources of noise. Since shear force at the wall and turbulence level depend on the pressure gradient, I think it's a fairly safe guess that the pressure fluctuation would also depend on the pressure gradient and generally increase in positive pressure gradients.

H. S. Ribner (University of Toronto)

Mr. Callaghan makes frequent reference to the fluctuating pressures in terms of "sound pressure levels"; these "hydrodynamic" or incompressibly generated pressures are not sound in the strict sense, and I would prefer Blokhintsev's term "pseudo-sound."

F. E. Callaghan

In reply to Professor Kovasznay, the effect of Mach number on the rates of root-mean-square surface pressure to dynamic pressure  $\frac{p_{rms}}{q}$  would appear to be small

in extrapolating subsonic results to low supersonic speeds. A recently declassified paper<sup>†</sup> shows no Mach number effect on  $P/q$  for a range of flight Mach numbers from 0.8 to 1.4.

It is certainly agreed that the type of calculations performed in this paper can merely predict order of magnitude. It would be expected that strong favorable pressure gradients would lower the ratio of  $P/q$  whereas adverse gradients would raise it.

In regard to jiggling the bow wave, it would be expected that as long as the stream Mach numbers are 3 or larger the bow wave is exceedingly stable. It would only be at the lower Mach numbers, say 2 or less, that shock wave instability would give rise to large surface pressure fluctuations.

It is impossible to assess what effect ablation type nose cones will have on internal noise. Undoubtedly, the rough surface resulting from ablation will greatly increase the surface pressure fluctuations. On the other hand, the ablating material would be expected to have a very high transmission loss, so that one effect may balance the other.

I agree completely with Dr. Corcos. The case discussed here assumes that the pressure gradient is favorable but not strong. Strong gradients should greatly alter the results. We do have some unpublished flight data which show that strong favorable gradients reduce the ratio of  $P/q$  considerably. We also have data in the presence of a strong adverse gradient, and for such a case the levels are very high. In one case, separated flow on a wing resulted in a sudden increase of 25 decibels.

For the most part, I must agree with the comments by Dr. Dyer. We have looked at the possibility of noise generation of the type discussed by Ribner<sup>‡</sup> and even if we assume very severe atmospheric turbulence the noise levels generated are very low. Mostly because severe atmospheric turbulence is not really very turbulent at all in comparison to boundary layers or jet mixing, etc.

The question of fluctuating base pressures may well be a very severe problem. It looks very much like the kind of a problem which must be studied in either wind tunnels or rocket-powered models.

<sup>†</sup>Norman J. McLeod and Gareth Jordan, "Preliminary Flight Survey of Fuselage and Boundary Layer Sound Pressure Levels," NACA RM H58B11, 1958.

<sup>‡</sup>H. S. Ribner, "Shock-Turbulence Interaction and the Generation of Noise," NACA TR 1223, 1955.

\* \* \* \* \*

# EXCITATION OF ACOUSTIC RESONATORS BY FLOW

Uno Ingard and Lee W. Dean, III  
*Physics Department*  
*Massachusetts Institute of Technology*

## INTRODUCTION

The study of excitation of cavities by wind or jets of air has a long history. All wind instruments and their antecedents consist of cavities excited by a jet or a larger flow of air which is blown through them or across their openings. The effects on the frequency and quality of the tone, which are produced by varying the dimensions of the cavity or the strength of the air stream, have been studied for centuries.

Helmholtz (1) in 1868 published what appears to be the first significant paper on the actual mechanism of excitation. He describes the boundary between two layers of fluid moving with different velocities as being composed of parallel vortex threads. If these threads initially lie in one plane — so that the boundary between the two regions of fluid is flat — they will remain so in unstable equilibrium. However, if one is disturbed from its position, it will continue to move out of line so as to cause the dividing surface of hump and eventually curl over. Helmholtz concludes that the "vis viva" of the oscillations which is lost by radiation is replaced by energy from the blast of air blowing across or through the mouth. This blast is directed slightly into or out of the pipe in proper phase for reinforcement by movement of the vortex threads at the boundaries.

The understanding of the mechanism of excitation has advanced only slightly since this early paper by Helmholtz. P. M. Morse (2) in 1948 indicates that there is a nonlinear coupling between the driver, or air jet, and the pipe. He also points out that the presence of a pressure node at the opening of the pipe identifies the excitation as a pressure fluctuation because the system aligns itself so as to extract a maximum of energy from the jet. His concluding remark — "A great deal of experimental and theoretical work is needed before we can say we understand thoroughly the behavior of any of the wind instruments" — points not only to the lack of a good theoretical model for the mechanism of excitation, but also to the general lack of experimental evidence. This report describes some studies of the excitation of a pipe by flow past the open end of the pipe. These studies are restricted to one particular pipe geometry, but most other parameters are considered, including the internal damping of the pipe resonator.

Note. This work was done at the Acoustics Laboratory at Massachusetts Institute of Technology under Contract AF 33(616)-3397, Task No. 71705, with the Wright Air Development Center, Wright-Patterson Air Force Base, Ohio.

It appears that one can distinguish two different regions or mechanisms of oscillation of the pipe, a linear and a nonlinear region. The linear region corresponds to low flow speeds in which the acoustic oscillations in the resonator do not affect the flow about it. The pressure fluctuations about the resonator are then determined solely by the geometry of the pipe at the mouth and the nature of the incident stream, and they are independent of, for example, the length of the pipe. The acoustic oscillations in the pipe are then linearly related to the pressure fluctuations in the flow which are already present in the incident stream or which are caused by the turbulence generated when the stream strikes the pipe. As the flow speed increases, there is a transition to more violent nonlinear oscillations in which the sound field in the pipe indeed reacts back on the flow.

The sound generated in the linear region is generally very weak and can be considered as background noise for the purposes of this report, which is concerned mainly with the nonlinear oscillations.

Blokhintzev (3) has investigated the behavior of a pipe resonator in the linear region and finds on the basis of dimensional arguments that the sound pressure in the resonator is proportional to the square of the flow speed. His theory does not explain any of the features of the nonlinear oscillations. There are several discrete modes of nonlinear oscillations, of which only the fundamental is considered in this report.

This study starts with an investigation of the flow about the mouth of the resonator involving both schlieren photography and hot-wire measurements. The acoustic response of the resonator is then studied as a function of flow speed and the angle of attack of the flow. Finally, a study is made of the effect of internal damping of the resonator on its acoustic output, with particular emphasis on a determination of the critical damping beyond which the nonlinear oscillations no longer can be sustained.

## STUDIES OF THE FLOW PATTERN ABOUT THE RESONATOR AND THE MECHANISM OF OSCILLATION

### Schlieren Studies

The pipe, 2 cm in diameter and 30 cm long, was placed in an air flow the speed of which could be varied from 0 to about 4000 cm/sec. The air stream was uniform over an area of about  $3 \times 3$  cm. The mouth of the resonator was introduced into this region.

To obtain some over-all ideas concerning this oscillation mechanism of the flow, exploratory experiments were made which were designed to study the flow pattern about the opening of the resonator. After several attempts involving hot-wire measurements, a schlieren system was arranged which made possible direct visual observation of the flow field (Fig. 1). It utilizes two optical systems. One, consisting of the light source, condenser, flat mirror, concave mirror, and knife edge, is arranged so that the light source is imaged in the plane of the knife edge. The other, consisting of the camera, is arranged so that the field of view, located directly in front of the mirror, is focused onto a screen or photographic plate. Each point in the field receives light from every point of the source. Therefore, the field, as seen from the camera, darkens uniformly when the knife edge cuts off part of the image of the source. Local density gradients in the field bend the light rays, causing a larger or smaller number of them to be intercepted by the knife edge with the result that the field appears locally lighter or darker. In practice, the knife edge is moved back and forth until the field is uniformly illuminated.

This system using a concave mirror has three main advantages over one in which the mirror is replaced by a lens and the light source is placed to the right of the lens as in (2) with the camera. First, this system is more sensitive because light passes

# Excitation of Acoustic Resonators by Flow

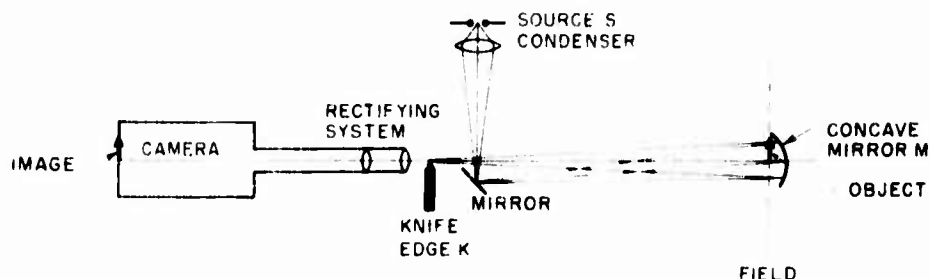


Fig. 1 - The schlieren system

through the field twice. Second, the size of the field is limited to the size of the lens or mirror; large mirrors are easier to make. Third, schlieren systems are extremely sensitive to chromatic dispersion, which is avoided by use of a mirror.

In order to increase the contrast, the air flow was heated by loops of a heated wire placed in the air stream. In the direct visual observations, stroboscopic illumination was used — obtained by means of a steady light source followed by a rotating disc chopper. The photograph of the flow pattern shown in Fig. 2 was obtained using a high-intensity flash source. This picture does not show the field as clearly as direct observation under stroboscopic illumination. However, it does indicate the general features of the flow field.

## Mechanism of Oscillation

The flow field about the mouth of the resonator appears to be similar to the flow about a knife-edge oscillator. When the flow strikes the downstream edge of the

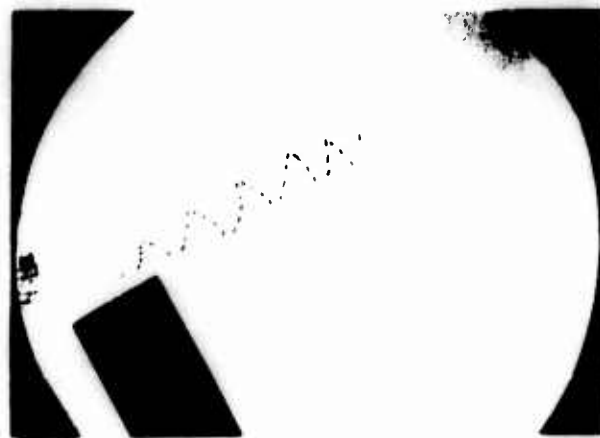


Fig. 2 - Flow field about the mouth of the resonator, showing the oscillatory pattern.

resonator, eddies are shed at a rate corresponding to the resonance frequency of the resonator. There is a class of hydrodynamic oscillations in which a disturbance produced at an edge travels downstream. On meeting a second edge, a sound signal is sent back which triggers a second disturbance. This causes reinforcement at a particular frequency, the period of which is approximately  $d(U + c)/c$ , where  $U$  is the velocity of the flow,  $c$  the speed of sound, and  $d$  the distance between the edges. Ordinarily,  $dU$  is much greater than  $d c$  so that the frequency of oscillation is of the order of  $U/d$ . The jet-edge oscillator is a striking example of such a system (4,5). In addition to this hydrodynamic "feedback," there may also be an acoustic coupling resulting from a reflection of the sound wave from a boundary in the neighborhood of the edge system. If the reflector is a distance  $l$  away, the sound signal will return after a time  $2l/c$ .

In general, one might expect that both of the feedback mechanisms described above might be of importance in hydrodynamic nonlinear oscillators. Furthermore, it is expected that in the case of such a dual feedback the oscillations should be particularly strong if  $dU$  and  $2l/c$  are the same.

In the present pipe-resonator oscillator, the major feedback mechanism seems to be acoustic, as indicated by the acoustic characteristics discussed in the next section. The two edges referred to above are represented by the edges of the pipe opening. The acoustic reflector is the rigid termination at the end of the pipe. The frequency of oscillations is found to be approximately equal to  $c/2l$  for a relatively large range of flow velocities, where  $l$  is the length of the pipe. The characteristic time  $dU$  corresponding to the hydrodynamic coupling between the two edges seems to be of less importance in the pipe-resonator. Similar acousto-hydrodynamic oscillators have been discussed by Anderson (6) and von Gierke (7).

#### Hot-Wire Measurements of the Flow Gradient in the Mouth of the Resonator

In addition to the schlieren studies mentioned above, some measurements were made of the flow in the opening of the resonator by means of a hot wire. The variation in the flow speed as one goes from the outside into the pipe is shown in Fig. 3. The velocity profile has a strong gradient, which can be shown to promote transfer of energy from steady to oscillatory flow (8). This is further evidence to support the picture of a nonlinear mechanism producing oscillations at the mouth of the resonator.

#### ACOUSTIC MEASUREMENTS

The sound field generated by the flow as it passes the pipe was measured at a distance of 15 cm from the mouth of the resonator. Some measurements were also made when the microphone was inserted at the bottom of the resonator. However, the sound-pressure levels inside the pipe often exceeded 140 db, the upper limit of the dynamic range of the microphone without special acoustic attenuating devices. Therefore, most of the measurements were taken outside the resonator, as indicated in Fig. 4. Both the sound-pressure amplitude and the frequency were measured on a General Radio Wave Analyzer with a 4-cps bandwidth.

The air supply consisted of a compressor and regulator set to deliver air at a constant pressure of 30 psi gauge. The volume flow was measured on a Flowrater. The air then passed through a settling tank, and issued from the tank into the room through a pipe 3 cm in diameter and about 10 cm long. The air velocity was measured by a hot-wire anemometer and was found to be uniform over an area of about  $3 \times 3$  cm in front of the pipe. It was in this region that the mouth of the resonator was placed.



# Excitation of Acoustic Resonators by Flow

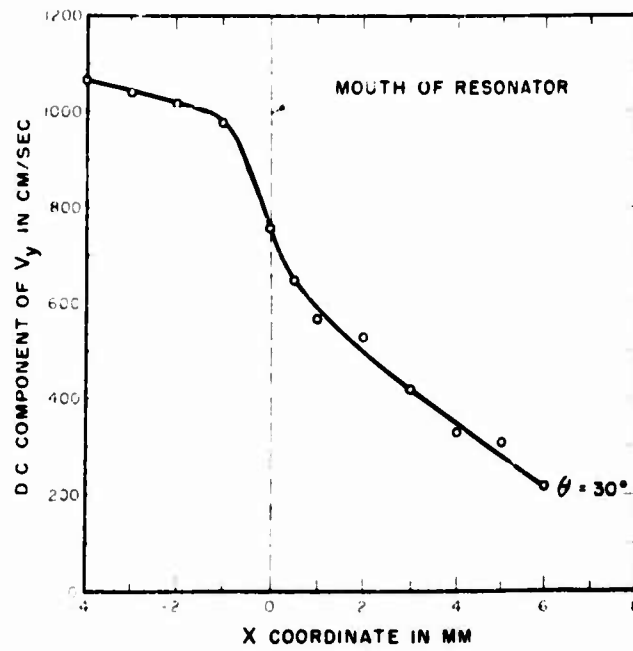


Fig. 3 - The variation of flow speed along the axis of the resonator

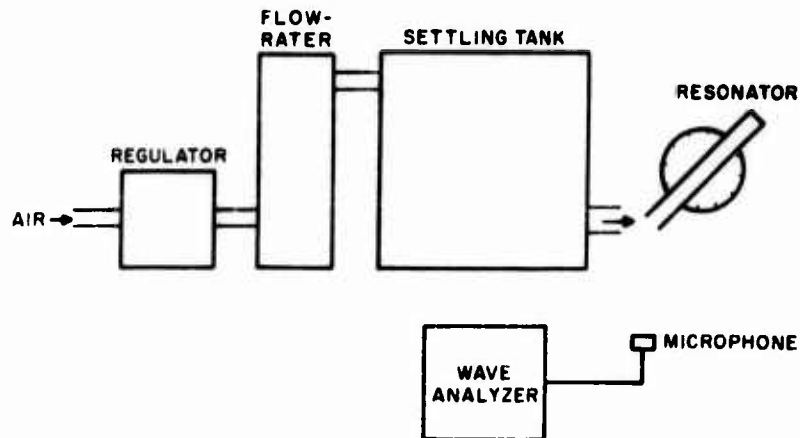


Fig. 4 - The experimental setup for acoustic measurements

### Sound Pressure as a Function of Flow Speed and the Angle of Attack

Measurements of the sound pressure were made for flow speeds up to about 3500 cm/sec and angles of attack from 0 to 50 degrees, as defined in Fig. 5.

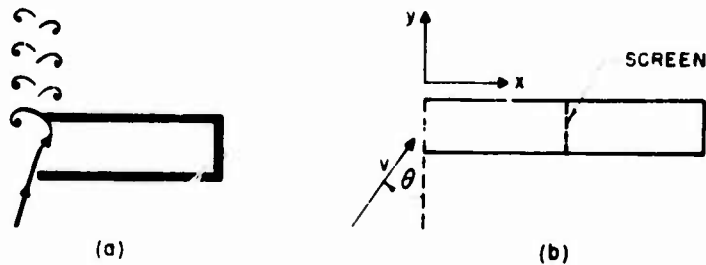


Fig. 5 - Resonator pipe (with damping screen)

In Fig. 6 are shown results of such measurements. There is a critical angle of about 15 degrees and a critical air speed of about 1000 cm/sec below which no oscillations are observed. Not only is there a lower limit of the flow speed but also an upper one at which oscillations cease. This upper limit increases with the angle of attack. With the flow equipment available in the present experiment, the highest flow speed was about 3500 cm/sec. The largest angle of attack at which oscillations could be sustained at this speed was about 50 degrees.

The envelope of the pressure versus flow-speed curves for the various angles of attack indicates a sound pressure which is approximately a linear function of the flow speed. At the lowest measured sound pressures shown in Fig. 6, it is difficult to decide whether the oscillations are nonlinear with an oscillating flow pattern described above or if they result from the turbulence already present in the incident air stream.

One interesting aspect of the problem is that the air flow must be directed into the resonator for oscillations to occur. In fact, the more the air stream is directed into the resonator, the stronger the oscillations become. It may be that the disturbances produced at the mouth of the resonator by the sound field direct the main flow into and out of the tube. The oscillations would then be driven by a switching of the air flow rather than by vortices which would be generated regardless of the angle of attack. This aspect of the problem could be clarified by more detailed observations of the flow field in the vicinity of the mouth of the resonator.

### Frequency of Oscillation vs Flow Speed

As already mentioned, the frequency of oscillation of the tube stays almost constant, independent of the flow speed. Some measurements of the slight frequency variation that does occur are shown in Fig. 7. This result is for an angle of attack of the flow of 30 degrees. It is seen how closely the oscillations are held to a single frequency for a wide range of the flow speeds. This result supports the observation that in most of the flow range the coupling between the flow and the sound wave seems

# Excitation of Acoustic Resonators by Flow

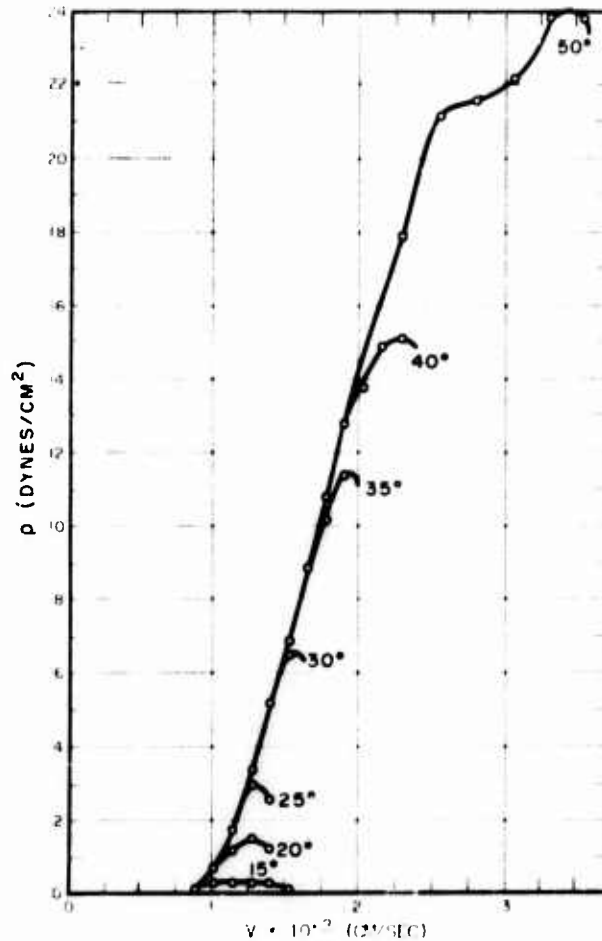


Fig. 6 - Measured sound pressure at a distance 15 cm from the mouth

to be dominant in the mechanism of oscillation. On the other hand, in a purely hydrodynamic self-oscillator, such as the jet-edge system, the hydrodynamic boundary conditions determine the characteristic frequencies of oscillations which are of the order of  $U/D$ , where  $U$  is the flow speed and  $D$  is a characteristic length of the system.

## The Effect of Damping in the Resonator

A factor which affects the oscillations of the resonator to a considerable degree is damping. The damping in the pipe system consists of radiation damping and the viscous and heat conduction losses at the walls of the resonator. The damping in a system is often described in terms of the  $Q$  value which for  $Q = 1$  equals  $\frac{1}{2}$ , where  $f_0$  is the resonance frequency and  $\Delta f$  is the half-power bandwidth of the resonator.

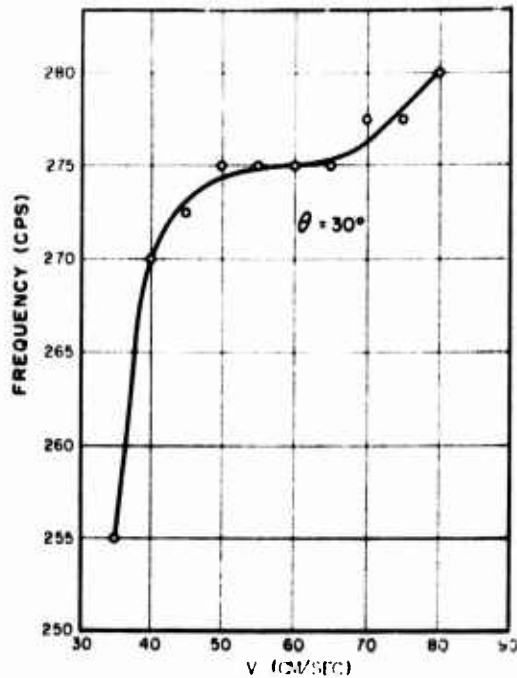


Fig. 7 - Variation of the frequency of oscillation with flow speed

The largest value which ordinarily can be obtained with acoustic resonators in air under standard conditions is of the order of 50. The resonator tube used in the experiments described above was about 42.

**Variation of the  $Q$  of the Resonator** - It is of considerable practical importance to investigate the effect of the damping on the flow-excited oscillations. In order to vary the damping in the resonator, a damping element in the form of a fine screen was introduced into the tube, as indicated in Fig. 5. The particle velocity is zero at the rigid termination of the tube. If the screen is placed close to the wall, the damping effect of the screen is clearly negligible. The damping effect increases as it is moved toward the mouth of the tube. In fact, if the screen does not change the original flow distribution  $\cos(\pi x / 2L)$  appreciably, it follows that the  $Q$  value will vary with the position of the screen as

$$Q = \frac{Q_0}{1 + (R_s + R) \left( \cos \frac{\pi x}{2L} \right)^2} \quad (1)$$

where  $x$  is measured from the open end of the tube,  $R_s$  is the screen resistance, and  $R$  is the resistance caused by the radiation, viscous, and heat-conduction losses.

Using a fine-mesh screen (open area 29 percent, 306 holes  $\text{cm}^2$ , diameter of strands 0.101 mm), the  $Q$  value of the resonator may be varied from the maximum

value of 42 down to a value of about 19 by moving the screen from the bottom to the mouth of the tube. This is shown by the top curve in Fig. 8. The second curve in the figure shows the measured  $Q$  value in the case when three screens are introduced into the tube. In that case, the  $Q$  value was brought down to a value of about 8. The curves obtained in this way are in quite good agreement with Eq. (1).

It is interesting to note in passing that this method of introducing damping into the tube may readily be used for the measurement of small flow resistances.

In the measurements of the  $Q$  value as given in Fig. 8, the microphone itself formed the rigid termination of the tube. The frequency response of the pipe to an incident sound wave was determined and the  $Q$  value was evaluated as the ratio  $\frac{P_{max}}{P_{6db}}$ . Here  $P_{6db}$  is the "width" of the pressure-frequency curve at the points where the pressure is 6 db below the maximum pressure.

**The Effect of  $Q$  on the Flow-Excited Oscillations -** Varying the  $Q$  value of the resonator as described above, a series of measurements was made of the strength of the flow-excited oscillations of the resonator pipe as a function of the  $Q$  value. The angle of attack of the flow was kept constant at 35 degrees. The sound pressure was measured at the bottom of the resonator, but the experimental setup was otherwise

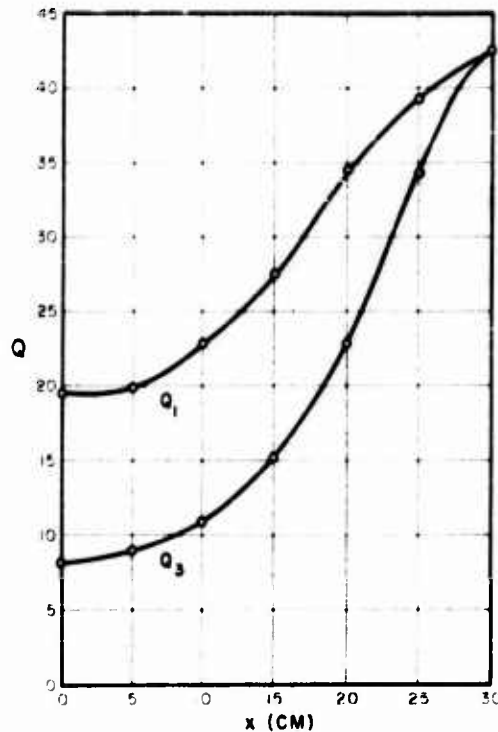


Fig. 8 - Variation of the  $Q$  of the resonator with the position of the screen (see Fig. 5).  $Q_1$  corresponds to one screen.  $Q_3$  to a combination of three screens.

identical to that described above. The flow speed was varied as before. The results of these measurements are shown in Fig. 9. In this figure, the value 100 on the velocity scale corresponds to a speed of 1150 cm/sec. At the lower wind speeds, the sound pressure increases quite rapidly at first and then levels off so that it is approximately proportional to  $Q$  for large values of  $Q$ . At the higher wind speeds, oscillations were obtained only for large values of  $Q$ . For example, with a wind speed corresponding to 120 in the figure, a decrease of the  $Q$  to about 34 stopped the oscillations completely. At lower wind speeds the limiting  $Q$  value, below which no oscillations can be sustained, is not defined as sharply.

As indicated already in Fig. 6, the resonator can be kept in oscillation only in a certain flow speed range. This range depends on the  $Q$  value of the resonator as illustrated in Fig. 10, where the upper and lower flow speeds, which define the oscillation range, are plotted as a function of  $Q$ . The curve refers to an angle of attack of about 35 degrees, and the sound pressure was measured with the microphone forming the termination of the resonator.

As far as the lower speed limit is concerned, it is often difficult to decide when the oscillations are of the nonlinear type and when they are excited (linearly) by

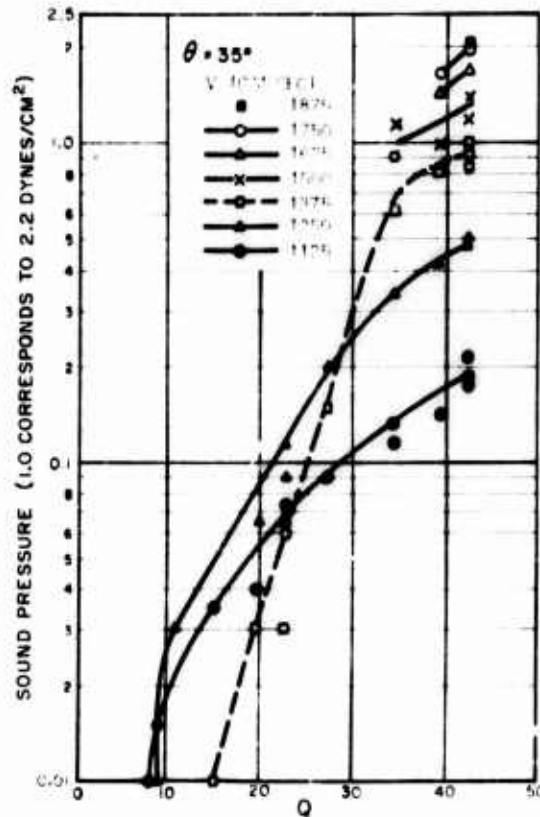


Fig. 9 - Variation of the sound pressure with the  $Q$  of the resonator

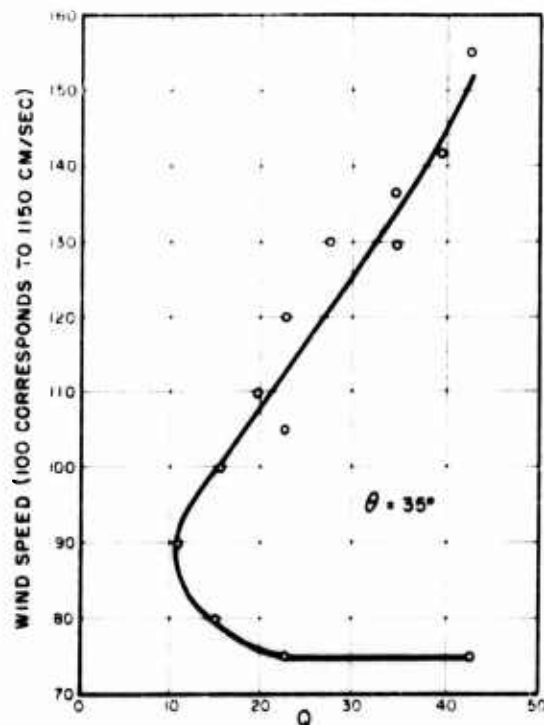


Fig. 10 - The upper and lower limits of the flow speed between which the nonlinear oscillations of the resonator can be sustained

turbulence in the incident flow. Although presumably there is a smooth transition between these two kinds of oscillations, it seems reasonable in the present case to use a sound pressure of  $0.02 \text{ dynes cm}^2$  as representing the dividing line between the two regions. Above this pressure the oscillations were definitely of the nonlinear type.

As the  $\theta$  decreases, the range of oscillations clearly decreases until it narrows to a point at a  $Q$  value of about 11. Below this  $Q$  value, only the weak "background" oscillations will remain, but the self-sustained nonlinear oscillations can be considered to be completely stopped at the particular angle of incidence of 35 degrees. The existence of a limiting  $\theta$  value, below which the resonator cannot be brought into oscillations by flow, should be of particular interest in connection with noise control in cases where some of the noise is produced by air rushing past cavities of various kinds.

The shape of the curve in Fig. 10 is also interesting inasmuch as it indicates a rapid increase of the range of oscillation in the region of high  $Q$  values. A small increase of  $\theta$  in this region would produce a relatively large increase in the oscillation range. This same characteristic feature is probably typical for all acousto-hydrodynamic oscillators.

# REFERENCES

1. Helmholtz, H.L.F., "Sensations of Tone," New York:Dover, 2nd English edition, translated by A. J. Ellis, 1954, pp. 394-397
2. Morse, P.M., "Vibration and Sound," New York:McGraw-Hill, 1948, pp. 244-254
3. Blokhintzev, D.I., "Acoustics of a Nonhomogeneous Moving Medium," NACA TM 1399, translated by S. Reiss, 1956
4. Curle, N., "The Mechanics of Edge Tones," Proc. Roy. Soc. A216:412 (1953)
5. Nyborg, W.L., et al., "Acoustical Characteristics of Jet-Edge and Jet-Edge-Resonator Systems," J. Acoust. Soc. Amer., 24 (No. 3):293-304 (1952)
6. Anderson, A.B.C., "Vortex-Ring Structure-Transition in a Jet Emitting Discrete Acoustic Frequencies," J. Acoust. Soc. Amer. 28 (No. 5):914-921 (1956)
7. Von Gierke, H., "Über Schnidentöne an kreisrunden Gasstrahlen und ebenen Lamellen," Z. angew. Phys. 2:97 (1950)
8. Lin, C.C., "Theory of Hydrodynamic Stability," New York:Cambridge University Press, 1955, pp. 52-60

\* \* \* \* \*

# DISCUSSION

M. Strasberg (David Taylor Model Basin)

It might be worth describing a possible phenomenological explanation for the excitation. It is based on certain observed facts, namely, the sound only occurs when the speed is in certain ranges; there are jumps in these ranges of speed; and, another fact which was not mentioned, but which I believe Prof. Ingard has observed, that the radiator impedance seen by the mouth of a resonator is a function of the air velocity past the mouth. This means that the flow past the mouth of the resonator provides a possible mechanism for varying the acoustic impedance seen by the resonator.

Now one can assume that there is some instability in the flow, causing a variation in velocity of flow past the mouth. This instability is inherent in the flow and has nothing to do with the resonator; it would occur even for a hole without a resonator. The flow instability results in a periodic fluctuation in the mass reactance seen by the resonator. Now, for a mechanical or acoustic system which is linear, if there is a periodic variation in one of the parameters of the system, and if the variation occurs at the right frequency and amplitude, it is known that an instability of the system can cause self-maintained oscillations.

More specifically, suppose one has a simple mechanical system, whose differential equation can be represented by:

$$m \frac{d^2x}{dt^2} + kx = F \cos \omega_0 t$$



This is called a Mathieu linear differential equation and is discussed by T. Brooke Benjamin in his comment on Prof. Meyer's paper in this Proceedings.

In the present situation it may be possible that these fluctuations of the flow past the mouth of the resonator, which occur even if the resonator were not there, cause such a periodic variation in the frequency, and if the amplitude  $a$  of this fluctuation is large enough, instability can occur and the system will oscillate naturally.

If the instability inherent in the flow past the neck is at twice the frequency of the resonator, i.e., if  $\omega_1 = 2\omega_0$ , oscillations will occur at small amplitude  $a$ . If there were no damping, zero amplitude would do it, but with damping a certain finite amplitude is needed if instability occurs at twice the frequency of the resonator. If it occurs at a frequency that is equal to that of the resonator, oscillations will also occur at relatively small amplitude; in fact, oscillations will occur at small values of the amplitude whenever  $\omega_0$  is an integral or half-integral number of times  $\omega_1$ .

This doesn't explain the details, but it is a possible way of looking at what happens. There is one way that we could ascertain whether this is a reasonable explanation, and that is to actually observe the flow past the hole in a plate in the absence of the resonator and see if it is essentially the same as with the resonator.

M. C. Harrington (David Taylor Model Basin)

Some experiments which have been done in the David Taylor Model Basin are related to those mentioned above.\* In this case, the flow passed over a plate in which the aperture was located. The resonant cavity was situated behind this plate. It has been mentioned in some of the previous papers that the increase in the frequency of resonance with increase in the speed of air flow was relatively small. In our experiments, however, we found that the frequency increased considerably, in some cases by 30 or 40 percent of the initial frequency with which the resonator started to oscillate. The frequency approached a final value asymptotically and as the air speed was further increased the oscillation died out abruptly. This increase in frequency of resonance may be explained by a decrease in the equivalent acoustic mass reactance of the air in the opening with increasing turbulence as the air speed increases. This interpretation is consistent with the results reported by McAuliffe† and Ingard‡ in which the resonators were driven by an independent source of sound of known frequency and intensity. There it was found that the resonant frequency increased (within limits) with increasing air flow through or past the opening.

In the Model Basin experiments when the air speed was doubled, provided that this was within the range of speeds available, the oscillator began again to resonate at the same frequency and the regime was repeated. If the actuation of resonance can be explained in terms of vortices, there would appear to be a double set of vortices in the second case. Occasionally resonance was actuated again at triple the initial speed.

\*M.C. Harrington, "Excitation of Cavity Resonance by Air Flow, Abstract J4, Jour. Acoust. Soc. Am., 29:187 (1957).

†G.E. McAuliffe, "The Influence of High Speed Air Flow on the Behavior of Acoustic Elements," M.S. Thesis, M.I.T., 1950.

‡K.U. Ingard, "On the Theory and Design of Acoustic Resonators," Jour. Acoust. Soc. Am., 25:1037-1061 (1953).

E. E. Covert (Massachusetts Institute of Technology)

At MIT, we have been conducting a series of tests on cavities that are similar in nature to those that Dr. Harrington just reported on. They are essentially holes in the bottom of a wind tunnel with a solid wall. There are several shapes: triangular, circular and rectangular, and we have been running them from Mach number of 1.5 up to 3. These cavities seem to vibrate at the Helmholtz room frequencies. If they are deep and long they seem to vibrate in the up and down mode. If they are shallow they seem to slosh back and forth, much in the same manner as reported by Krishnamurty of the California Institute of Technology.

We have observed that for the most part, for the rectangular boxes, the behavior is independent of the cross-wise characteristic length. In other words, the behavior is two-dimensional, as you would expect. However, at the higher Mach numbers a narrow box seems always to sing out fairly loud and clear at about 165 decibels. The wider boxes are not easy to excite and we don't know why at the moment.

Another point of interest is that these can be correlated in terms of a Strouhal number if one uses the correct velocity of sound within the box and the Mach number of the free stream. They exhibit also the same edge-tone type behavior that everyone else has remarked on, where it will take off at a certain frequency and at some speed will jump to a higher frequency. We have taken some observations with rectangular boxes that had glass walls, and it seems that the sound is radiated from the upstream edge of the box. We get nice circular waves moving down into the box. Of course, this gives us a shock wave at the leading edge and we get nice waves going out.

\* \* \* \* \*

# SOUND RADIATION INTO A CLOSED SPACE FROM BOUNDARY LAYER TURBULENCE

Ira Dyer

*Bolt Beranek and Newman, Inc.*

\* \* \* \* \*

A theory of noise generation by the action of boundary layer turbulence on an elastic system has been developed, with particular reference to underwater application. The elastic system considered is a rectangular plate closed off by a rectangular liquid-filled volume. A simple yet physically meaningful form is assumed for the boundary layer pressure correlation. The resulting plate vibration and sound radiation are derived, taking into account coupling between the plate motion and the sound field in the liquid. In the theory, coupling is manifested by radiation-induced masses and viscous damping which, in effect, may be added to the mass and damping of the plate considered to be vibrating in vacuo. It is shown that the noise in the closed space decreases with decreasing free-stream speed and boundary layer thickness. Also the noise decreases with increasing mass and damping of the plate, and with increasing distance from the plate. The use of plate damping as a means of noise reduction is predicted to be limited on the one hand by radiation damping, and on the other hand by correlation decay in the assumed turbulence pressure field.

\* \* \* \* \*

## INTRODUCTION

Noise caused by boundary layer turbulence is important in several fields of application. Boundary layer turbulence is believed to be an important factor in the generation of noise by underwater devices, and is the prime motivation for the present study. In addition, the noise in aircraft cabins at high speeds and at high frequencies is determined mainly by boundary layer turbulence. Also the vibration caused by boundary layer turbulence may have an important bearing on problems of equipment damage and structural fatigue in missiles and aircraft.

There are two mechanisms of noise generation by boundary layer turbulence. First, the turbulence pressure field may excite the plate adjacent to it; the plate vibrations then radiate noise to the surrounding medium. Second, the boundary layer turbulence may radiate noise directly by virtue of the fluctuations in the fluid properties. For nonrigid plates such as met in practice the first mechanism is more important, and consequently we exclude consideration of the second mechanism in the present investigation.

We wish to study the mechanics of excitation of plates exposed to boundary layer turbulence and the consequent transmission and radiation of the vibrations. In particular, we wish to treat the case in which the excited plate forms one of the surfaces of a closed space. Figure 1 shows the idealized geometry we have chosen for study. The boundary layer is assumed to be in contact with a large flat plate, the other side of which is in part a closed volume.

The problem may be thought to consist of three elements: determination of the boundary layer pressure field, calculation of the vibration in the plate adjacent to the boundary layer, and calculation of the sound field radiated by the plate vibrations. It is tempting to assume that these elements can be investigated independently, but only in the case of a plate immersed in a gas is this assumption likely to be acceptable. For a plate in contact with a liquid, it is well known that the sound radiation will greatly influence the vibrations. On the other hand, it is probably acceptable to assume that the boundary layer pressure field can be investigated independently of the plate vibrations, provided that the resulting plate displacement is small compared with the boundary layer displacement thickness. In what follows we shall assume that the boundary layer pressure field can be specified independently, while the plate vibrations and consequent radiation are coupled phenomena.

In the present investigation we are not primarily concerned with the basic properties of the boundary layer pressure field but rather with the mechanics of excitation and consequent transmission and radiation. We are primarily concerned with the understanding of the structural and acoustical elements of the problem, with the ultimate objective of devising geometries and treatments that may lead to boundary layer noise control.

Several recent works have direct bearing on the present investigation. Kraichnan (1), Ribner (2), and Corcos and Liepmann (3) computed the noise radiated from plates excited by boundary layer turbulence. Because their work concerned plates immersed in air, no account was made of possible plate vibration and sound radiation coupling, such as may be important in liquids. Kraichnan considered the radiation from finite square plates while Ribner and Corcos and Liepmann considered radiation from large plates.

Lyon (4) made theoretical and experimental studies on the excitation of strings by a random pressure field resembling that of boundary layer turbulence. Eringen (5) studied the excitation of beams and plates to a purely random pressure field, without particular reference to boundary layer excitation. Strasberg (6) used boundary layer pressure measurements by Harrison (7) to compute the excitation of both finite membranes and finite plates.

In addition to Harrison, Willmarth (8) has made spectral and correlation measurements on boundary layers in wind tunnels. Kraichnan (9) studied the boundary layer pressure field theoretically as a preliminary to his later work on plate excitation (1). Kraichnan's (10) most recent work on turbulence holds promise of providing additional information on boundary layer turbulence. In addition to the foregoing, there is a very rich literature on turbulent boundary layers and their more general aspects.

Boundary layer pressure fields have also been measured on airplane wings by Mull and Algranti (11). Their results are subject to some uncertainty, however, because the microphone used was not small compared with the boundary layer displacement thickness. Earlier, Rogers and Cook (12) made measurements relevant to the boundary layer noise problem in aircraft spaces. Also Dyer (13) has reported boundary layer pressures as determined indirectly from noise measurements within aircraft cabins. These latter two studies are largely heuristic in nature.

## GENERAL EQUATIONS FOR PLATE EXCITATION

The vibration on a plate exposed to an external pressure field  $p(x, y, t)$  is assumed to obey the classical thin-plate equation:

$$B \nabla^4 w + M \frac{\partial^2 w}{\partial t^2} + \gamma \frac{\partial w}{\partial t} = (p_1 - p_2) / L_z = F(x, y, t) \quad (1)$$

where  $w(x, y, t)$  is the displacement of the neutral plane of the plate,  $B$  the bending stiffness,  $M$  the mass per unit area of the plate,  $\gamma$  the damping coefficient, and  $p_i$  the sound pressures on either side of the plate (at  $z = \pm L_z$ ). Figure 1 shows the geometry relevant to the problem. The bending stiffness is given by

$$B = \frac{E h^3}{12(1 - \nu^2)} \quad (2)$$

where  $E$  is Young's modulus,  $h$  the plate thickness, and  $\nu$  Poisson's ratio. The damping coefficient is assumed to include both viscous and hysteretic damping, a step that is possible only if we make a special assumption on the time dependence in Eq. (1), as we shall do later.

Boundary conditions (assumed time-independent) and initial conditions for Eq. (1) are specified in a later section.

The sound field on either side of the plate is assumed to obey the non-dissipative linear wave equation of acoustics

$$\nabla^2 p_i - \frac{1}{c^2} \frac{\partial^2 p_i}{\partial t^2} = 0 \quad (3)$$

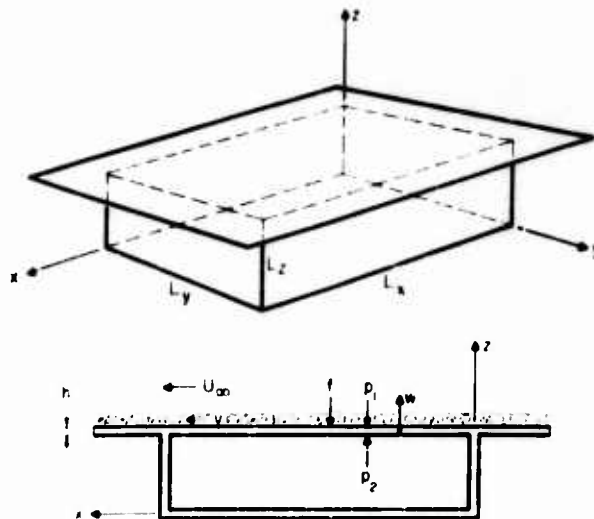


Fig. 1 - Geometry and coordinate system for boundary layer excitation

where  $\phi$  is the velocity potential and  $c$  the sound speed. We have assumed that the fluid is the same on both sides of the plate, but it will prove simple to consider the more general case should the need arise. The velocity potential is related to the sound pressure and sound particle velocity  $v$  by

$$\begin{aligned} p_j &= -\rho \frac{\partial \phi}{\partial t} \\ v &= -\frac{\partial \phi}{\partial x} \end{aligned} \quad (4)$$

where  $\rho$  is the fluid density. The space  $j = 1$  is taken to be free from boundaries, except at  $z = L$ . The space  $j = 2$  is a closed space with reflective boundaries. More precise boundary and initial conditions must also be specified with Eq. (3) but we shall leave this also to a later section.

Equation (3) is coupled to Eq. (1) by virtue of the continuity condition on velocity:

$$\frac{\partial w}{\partial t} = \frac{\partial \phi}{\partial z} \Big|_{z=L_1} = -\frac{\partial \phi}{\partial z} \Big|_{z=L_2} \quad (5)$$

We may associate with Eq. (1) the corresponding equation for the impulse response  $w(x, y, t; x_0, y_0, t_0)$  of the plate:

$$B \nabla^2 w + M \frac{\partial^2 w}{\partial t^2} + \frac{\partial w}{\partial t} = \delta(x - x_0) \delta(y - y_0) \delta(t - t_0) \quad (6)$$

where  $\delta$  is the Dirac delta function. Then an integral equation for  $w$  may be written (14):

$$w(r, t) = \int_{-\infty}^t dt_0 \int_A dS_0 g(r, t; r_0, t_0) F(r_0, t_0) \quad (7)$$

where we have abbreviated  $r$  for  $x, y$  and  $dS_0$  for  $dx_0 dy_0$ . We note that Eq. (7) is a sum of all responses of the plate for every time  $t_0$  before time  $t$ . For the uncoupled case in which  $F$  is independent of  $w$ , Eq. (7) is a solution for  $w$ . For both the coupled and uncoupled cases, however, we require a representation of the impulse response  $g$ .

We may obtain a formal representation of the impulse response in terms of the eigenfunction or normal modes of oscillation of the plate. The normal mode  $w_{mn}$  for a mode designated by the two order numbers  $m$  and  $n$  is of the form

$$w_{mn}(x, y, t) = \psi_{mn}(x, y) \exp[-\alpha_{mn}t - i\omega_{mn}t] \quad (8)$$

where  $\alpha_{mn}$  is the modal damping and  $\omega_{mn}$  the damped resonance frequency. Both  $\alpha_{mn}$  and  $\omega_{mn}$  are positive and real. The normal mode satisfies the equation

$$B(1 - i\alpha_{mn}) \nabla^2 w_{mn} + M \frac{\partial^2 w_{mn}}{\partial t^2} + \frac{\partial w_{mn}}{\partial t} = 0 \quad (9)$$

where we have made explicit division of the damping into hysteretic damping (determined by the loss factor  $\eta$ ) and viscous damping (determined by the resistance coefficient  $\gamma_0$ ).

Substitution of Eq. (8) into Eq. (9) gives the equation for the eigenfunctions

$$\frac{d^4 \phi_{mn}}{dx^4} + \omega_{mn}^2 \phi_{mn} = 0 \quad (10)$$

where the eigenvalues  $\omega_{mn}$  are taken to be real. It is convenient to have the eigenfunctions normalized such that

$$\int_0^1 \phi_{mn} \phi_{pq} dx = \delta_{mp} \delta_{nq} \quad (11)$$

where  $\delta$  is the Kronecker delta. Solutions of Eq. (10) are to obey the same boundary conditions as those of Eq. (1). The eigenvalues  $\omega_{mn}$  are then determined by the particular boundary conditions of interest.

The modal damping and damped resonance frequency are determined by the damping coefficients and eigenvalues as follows: We assume that the damping meets the inequalities

$$\gamma_{mn} < \frac{1}{3} \quad \text{and} \quad 2 \gamma_{mn} M_{mn} < \frac{1}{3} \quad (12)$$

These restrictions insure that the damping is not too large, but they do not exclude cases of practical interest. Then the modal damping is given by

$$\alpha_{mn} = \frac{\gamma_{mn}}{2M_{mn}} + \frac{4}{2M_{mn}} \frac{B_{mn}}{M_{mn}} \left[ \left( 1 + \frac{\gamma_{mn}^2}{M_{mn}^2} + 2 \right)^{1/2} - 1 \right] \quad (13)$$

which follows as a consequence of Eqs. (8), (9), and (10). Important limiting values of  $\alpha_{mn}$  are

$$\alpha_{mn} \approx \frac{\gamma_{mn}}{2} \quad \text{if} \quad \frac{B_{mn}}{M_{mn}} \rightarrow 0 \quad (14)$$

$$\alpha_{mn} \approx \frac{\gamma_{mn}}{2M_{mn}} \quad \text{if} \quad \frac{B_{mn}}{M_{mn}} \rightarrow \infty \quad (15)$$

$$\alpha_{mn} \approx \frac{\gamma_{mn}}{2} + \frac{2}{2M_{mn}} \quad \text{if} \quad \frac{B_{mn}}{M_{mn}} \rightarrow \infty \quad (16)$$

The damped resonance frequency is also determined from Eqs. (8), (9), and (10).

$$\omega_{mn}^2 = \frac{B_{mn}}{M_{mn}} + \frac{4}{M_{mn}} - \alpha_{mn}^2 \quad (17)$$

and requires simultaneous solution with Eq. (13). However, for most cases of practical interest  $\alpha_{mn}$  may be closely approximated by

$$\alpha_{mn} \approx \left( \frac{B_{mn}}{M_{mn}} \right)^{1/2} \quad (18)$$

and is independent of damping.

We now turn to the representation for the impulse response. We introduce the Green's function  $G$ , which is the Fourier transform of  $g$ ,

$$g(\mathbf{r}, t | \mathbf{r}_0, t_0) = \frac{1}{2\pi} \int_{-\infty}^{\infty} G(\mathbf{r}, \mathbf{r}_0, \omega) \exp[-i\omega(t - t_0)] d\omega, \quad (19)$$

substitute into Eq. (6), and obtain

$$\Delta_i = -\Delta_i + \frac{1}{2}(\mathbf{x} - \mathbf{x}_0) \cdot \nabla(\mathbf{y} - \mathbf{y}_0) \quad (20)$$

where

$$\Delta_i = \frac{2M + i}{B(1 - i)} \quad (21)$$

The Green's function  $G$  can be expanded in terms of the eigenfunctions  $\psi_{mn}$ :

$$G(\mathbf{r}, \mathbf{r}_0, \omega) = \sum_{m,n} A_{mn}(\mathbf{r}_0, \omega) \psi_{mn}(\mathbf{r}), \quad (22)$$

We evaluate the coefficients  $A_{mn}$  by placing Eq. (22) in Eq. (20), using Eq. (10), multiplying by  $\psi_{mn}$ , and integrating over  $S$ . The result is

$$G(\mathbf{r}, \mathbf{r}_0, \omega) = \sum_{m,n} \frac{\psi_{mn}(\mathbf{r}) \psi_{mn}(\mathbf{r}_0)}{4 - \Delta_{mn}^2} \quad (23)$$

We then use Eq. (19), which is evaluated by the calculus of residues at the poles  $\omega_{mn} = \pm \omega_{mn}$ , to obtain (14)

$$g(\mathbf{r}, t | \mathbf{r}_0, t_0) = \sum_{m,n} \frac{\psi_{mn}(\mathbf{r}) \psi_{mn}(\mathbf{r}_0)}{\omega_{mn}} \left[ \exp(-i\omega_{mn}(t - t_0)) + \sin \omega_{mn}(t - t_0) U(t - t_0) \right] \quad (24)$$

where  $U(t - t_0)$  is the unit step function.

Equations (7) and (24) complete the formal representation for the plate displacement  $w$ .

## THE BOUNDARY LAYER PRESSURE FIELD

Although it is not our purpose to investigate the basic structure of a turbulent boundary layer, we must obtain an appropriate description of the field to understand satisfactorily the mechanics of excitation and the possibilities for noise control. We assume that the boundary layer pressure field has the following characteristics:

1. The pressure field is a stationary random process.
2. The pressure correlation decays with time.
3. The pressure correlation has a spatial extent small compared with the plate size of interest.
4. The pressure correlation is convected along the surface of the plate, in the direction of the free-stream velocity.



5. The spatial correlation is homogeneous, depending upon the difference in the spatial coordinates in a frame of reference moving with the mean convection speed.

Accordingly, we adopt the form given in Eq. (25) as a possible phenomenological description of the boundary layer pressure field:

$$\overline{f(x, y, t) f^*(x', y', t')} = \overline{f^2} \exp \left[ -\frac{\sqrt{(x-x')^2 + (y-y')^2}}{R} - \frac{|t-t'|}{\tau} \right] \quad (25)$$

where

$\overline{\quad}$  symbolizes the time average operation

$*$  denotes the complex conjugate

$R$  is the normalized pressure correlation

$\overline{f^2}$  is the mean-square boundary layer pressure

$x = x - x'$

$y = y - y'$

$t = t - t'$

$v$  is the mean convection speed, taken to be in the positive  $x$  direction

$R$  is a measure of the inverse radius of the turbulence "eddy"

$\tau$  is the mean statistical lifetime of the turbulent state.

The correlation area  $A$  is obtained by integration of Eq. (25) over  $x$  and  $y$ :

$$A = \frac{2\pi}{R} \quad (26)$$

Recent measurements by Willmarth (8) show that the root-mean-square boundary layer pressure is given by

$$p_{rms} = 0.16 \sqrt{\frac{1}{2} \rho U^2} \quad (27)$$

where  $U$  is the free-stream velocity. Harrison (7) obtained a numerical coefficient somewhat greater than that given in Eq. (27), namely  $9.5 \times 10^{-4}$ . (Earlier results by Dyer (13) from aircraft cabin noise measurements yielded a value very close to that of Eq. (27).) We shall use the value given in Eq. (27) in examples later in the report.

The normalized pressure correlation of Eq. (25) is shown in Fig. 2 for an arbitrary value of the product  $\sqrt{R\tau}$ . We see that the correlation decreases as the time delay increases, and that the correlation peaks for particular values of  $\sqrt{R\tau}$ . Measurements on pressure correlation generally exhibit these characteristics (as do measurements on velocity correlation (15)). However, the measurements also show that the correlation is somewhat less peaky than that shown, and tends to become slightly

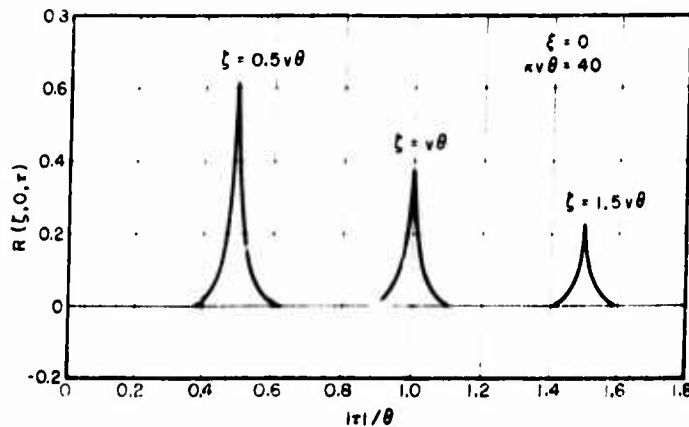


Fig. 2 - Normalized boundary layer pressure correlation for an arbitrary value of  $-v$

negative and oscillatory beyond the major peak. Thus, Eq. (25) is an idealization of the pressure field, although it contains all the elements assumed to be of importance. The added complexity required to obtain a more exact fit with measurements does not appear to be warranted for the present investigation.

The spectral density  $S(\omega)$  may be determined from the pressure correlation by the Fourier inversion

$$S(\omega) = 2 \int_0^\infty R(\xi, 0, \tau) \exp[i\omega\tau] d\tau \quad (28)$$

With the use of Eq. (25), the spectral density is found to be

$$S(\omega) = \left( \frac{4f^2}{\pi\omega} \right) \frac{1}{1 + \left( \frac{\omega}{\omega_0} \right)^2} \quad (29)$$

where

$$\omega_0 = -v + \frac{1}{\tau_0} \quad (30)$$

$\omega_0$  is a characteristic frequency determined by the sum of the "eddy" convection frequency and the inverse time constant of the decay.  $S(\omega)$  is plotted in Fig. 3 as a function of  $\omega/\omega_0$ . Measurements by Harrison (7) and Willmarth (8) are in general accord with Fig. 3, except that the data fall off more rapidly with frequency above  $\omega_0$  equal to about 3.

Comparison of Eqs. (25) and (28) with measurements (7,8) lead to the following self-consistent estimates for the parameters describing the boundary layer pressure field:

# Sound from Boundary Layer Turbulence

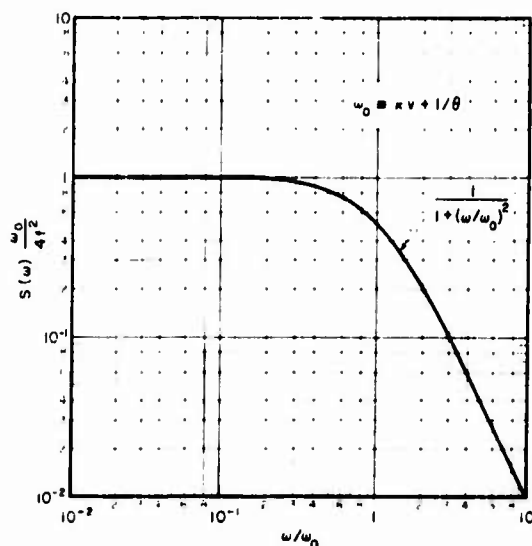


Fig. 3 - Spectrum of the boundary layer pressure field corresponding to the assumed pressure correlation

$$\begin{aligned} d &= 2 \\ &= 30 \frac{d}{U_r} \\ v &= 0.8 U_r \\ \omega_0 &= v \end{aligned} \quad (31)$$

where  $d$  is the displacement boundary layer thickness. We see that the characteristic frequency  $\omega_0$  appears to be determined mainly by the eddy passage frequency, a result obtained theoretically by Kraichnan (1). Thus, the spectrum  $S(\omega)$  for boundary layer turbulence is nearly independent of the lifetime  $\tau$ , although the correlation  $R(\tau, \tau, \tau)$  is strongly  $\tau$  dependent.

The correlation area  $A$  is of the order of  $d^2$ , as may be seen from Eqs. (26) and (31). If we make the relatively unrestrictive assumption that  $A$  is much smaller than the plate area  $L_x L_y$ , we may simplify Eq. (25) to the form

$$\langle p(r, t) p^*(r', t') \rangle = A \tau^2 (1 - \nu^2) S(\tau) \exp \left[ -\frac{r^2 + r'^2}{2L^2} \right] \quad (32)$$

In essence, Eq. (32) is a valid simplification of Eq. (25) for  $L \gg 1$ , where  $L$  is the smaller plate dimension. Equation (32) gives analytical simplicity to the boundary layer pressure field, while at the same time retaining the essential properties of a

decaying and convecting field of small scale. Lyon (4) used a correlation of the form of Eq. (32) to compute the response of strings in a convecting turbulent field.

It is of interest to note that, in the limit of very short lifetime, Eq. (32) approaches

$$\langle f(r, t) f(r', t') \rangle \rightarrow 2A \delta^2(r - r') \delta(t - t') \quad (33)$$

Also, for  $v$  small compared with  $c$ , the correlation approaches that of a purely random field, sometimes described as "rain on the roof," for which Eringen (5) has computed the excitation of finite plates. On the other hand, in the limit of very long lifetime, the exponential factor in Eq. (32) is unity for nearly all  $r$ , corresponding to the case of convection of a frozen pattern in the turbulent field.

In what follows we shall use the form of Eq. (32) and the estimates of the field parameters given by Eq. (31) as a description of the boundary layer pressure field. It is important to emphasize that this description is not precise, but is intended to display in a simple way the essential features of boundary layer excitation.

#### RESPONSE OF A FINITE UNLOADED DAMPED PLATE

We consider here the case of a plate immersed in a low-density fluid\* such that the radiation reaction on the plate may be neglected (i.e.,  $p_1 = p_2 = p$ ). Then the sound field external to the plate and the vibration field on the plate can be considered independently. Actually we shall find that the effect of fluid coupling does not change the form of the results, so that much of what is done here can be carried over with appropriate modification to the more general case. Thus, we proceed to the limit of zero fluid load, and the plate displacement becomes

$$w(r, t) = \int_{-\infty}^t dt_0 \int_S dS_0 g(r, t_0 - r_0, t_0) f(r_0, t_0). \quad (34)$$

Also, Lyon (16) has shown that the correlation may be obtained from an ensemble average, and may be written as

$$\begin{aligned} \langle w(r, t) w^*(r', t') \rangle &= \int_{-\infty}^t dt_0 \int_{-\infty}^{t'} dt'_0 \int_S dS_0 \int_{S'} dS'_0 g(r, t - r_0, t_0) \\ &\quad \cdot g^*(r', t' - r'_0, t'_0) = f(r_0, t_0) f^*(r'_0, t'_0). \end{aligned} \quad (35)$$

The source correlation required in Eq. (35) is given by Eq. (32); we now proceed to the explicit form for the eigenfunctions required in the impulse response  $g$ .

For simplicity, let us assume simply supported boundaries at the plate edges:

$$w = \frac{\partial w}{\partial x} = 0 \quad \text{at } x = 0, L_x; \quad w = \frac{\partial w}{\partial y} = 0 \quad \text{at } y = 0, L_y. \quad (36)$$

These boundary conditions are not apt to be met precisely in practice, but they lead to relatively simple eigenfunctions. Furthermore, the use of Eq. (36) is likely

\*The quantitative requirement on the density will be evident from the results of the next section.

to lead to error only for the very lowest modes; the eigenfunctions and eigenvalues are not too sensitive to the boundary conditions for higher modes. Normalized solutions of Eq. (10) that obey Eq. (36) are

$$\psi_{mn}(r) = \frac{2}{(L_x L_y)^{1/2}} \sin \frac{m\pi x}{L_x} \sin \frac{n\pi y}{L_y} \quad (37)$$

with

$$\lambda_{mn}^2 = \left( \frac{m\pi}{L_x} \right)^2 + \left( \frac{n\pi}{L_y} \right)^2. \quad (38)$$

Equation (35) involves the product of two doubly infinite sums, a typical term of which is the cross-product of two modes  $(m,n)$  and  $(p,q)$ :

$$\begin{aligned} \lambda(r,t)\lambda^*(r',t') = \sum_{m,n} \sum_{p,q} & A t^2 \frac{\psi_{mn}(r) \psi_{pq}(r')}{\lambda_{mn}^2 \lambda_{pq}^2} \int_0^t dt_1 \int_0^{t'} dt'_1 \\ & \times \left[ \int_S dS_0 \int_S dS'_0 \psi_{mn}(r_0) \psi_{pq}(r'_0) \exp \left\{ -i\lambda_{mn}(t-t_1) - i\lambda_{pq}(t'-t'_1) \right. \right. \\ & \left. \left. + i\sin \lambda_{mn}(t-t_1) \sin \lambda_{pq}(t'-t'_1) (v-v') \right\} \right] \quad (39) \end{aligned}$$

The  $y$  integration is simple because of the delta function  $\delta(y-y')$ . Thus the  $y'$  integration follows readily and yields  $\lambda_{pq} L_y/2$ . The  $x$  integration is equally simple if we assume

$$v = L_x. \quad (40)$$

The quantity  $v$  is essentially the greatest distance over which the source is correlated. From Eq. (31) we estimate  $v$  to be about  $24\delta$ . Consequently we require the plate length to be much greater than about 24 displacement thicknesses, or about 3 boundary layer thicknesses,\* a condition that includes all but the very thick boundary layers or very small plates.

With the use of Eq. (40) the  $x$  and  $x'$  integrations yield

$$\frac{L_x}{2} \sum_{m,p} \cos \lambda_{mp} x_0$$

where

$$\lambda_{mp} = \frac{m\pi v}{L_x}. \quad (41)$$

$\lambda_{mp}$  may be termed the convection frequency, and is interpreted as the frequency at which the turbulent field is convected past a length of plate equal to the  $m$ -modal wavelength. We see that by virtue of the Kronecker deltas,  $\delta_{mn}$  and  $\delta_{pq}$ , the plate modes are statistically independent. Physically this result is due in essence to the largeness of the plate compared with the correlation size of the source.

\*Inches as the boundary layer thickness is about 10 times the displacement thickness.

We now turn to the time integrals of Eq. (39). To facilitate integration we introduce the variables

$$\begin{aligned} t' - t_0' &= (t - t_0) - t_0 = \tau \\ t' - t_0' &= (t - t_0) + \tau \end{aligned} \quad (42)$$

The new coordinate system  $\tau, \tau'$  is shown in Fig. 4 in relation to the coordinates  $t_0, t_0'$ . By use of the Jacobian, the differentials become

$$dt_0 dt_0' = \frac{1}{2} d\tau d\tau' \quad (43)$$

and the limits are, as can be seen from Fig. 4,

$$\begin{aligned} \tau &\text{ to } \infty, \text{ for } \tau' > 0 \\ 0 &\text{ to } \tau', \text{ for } \tau' < 0 \end{aligned}$$

Then Eq. (39) becomes

$$w(r, t) w^*(r', t') = \frac{A t^2}{4 \sqrt{2} \sqrt{r}} \int_{-\infty}^{\infty} \int_{-\infty}^{\infty} d\tau d\tau' \exp \left[ -i \omega \tau - i \omega' \tau' \right] I_{mn}(\tau) I_{mn}(\tau') \quad (44)$$

where the time correlation integral  $I_{mn}(\tau)$  is given by

$$I_{mn}(\tau) = \int_{-\infty}^{\infty} d\tau' \int_{-\infty}^{\infty} d\tau \exp \left[ -i \omega \tau - i \omega' \tau' \right] \cos \left( \frac{\pi}{2} \left( \frac{\tau}{\tau'} \right)^2 \right) \cos \left( \frac{\pi}{2} \left( \frac{\tau'}{\tau} \right)^2 \right) \quad (45)$$

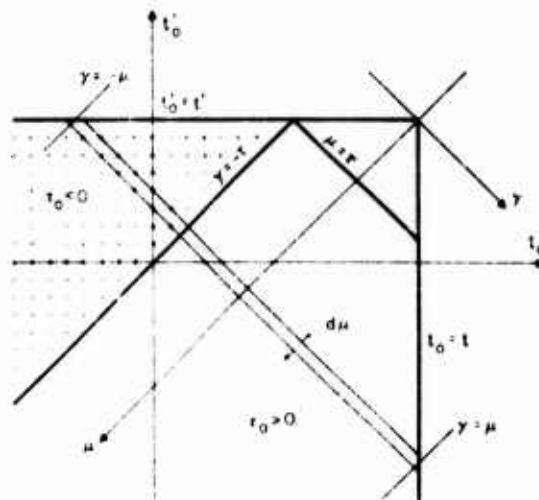


Fig. 4 - Region of integration and coordinate systems in the time domain.

Equation (45) is similar to an integral used by Lyon (4) in the string response problem, except that he specialized to the case  $\beta = 0$ . Because of the absolute value sign in the integrand we must integrate Eq. (45) in separate regions, depending in part upon whether  $\beta$  is greater than or less than  $\beta_{mn}$  (i.e.,  $\beta > 0$  or  $\beta < 0$ ). Figure 4 shows the regions within which the integral must be evaluated. Thus, Eq. (45) becomes

$$I_{mn}(\beta) = \left\{ \int_{-\beta}^{\beta} d\alpha \int_{-\alpha}^{\alpha} d\gamma \exp \left[ \frac{i(\alpha - \gamma)}{2} \right] + \int_{\beta}^{\infty} d\alpha \int_{\beta}^{\alpha} d\gamma \exp \left[ \frac{i(\alpha - \gamma)}{2} \right] \right. \\ \left. + \int_{-\infty}^{-\beta} d\alpha \int_{-\alpha}^{-\beta} d\gamma \exp \left[ \frac{i(\alpha - \gamma)}{2} \right] \right\} \exp -i\beta_{mn} \\ \times \cos \left( \frac{\beta + \beta_{mn}}{2} \right) \cos \left( \frac{\beta - \beta_{mn}}{2} \right) = \cos \frac{\beta}{2} \cos \frac{\beta_{mn}}{2} \quad (46)$$

The integral for  $\beta < 0$  is identical to Eq. (46) except that  $\beta$  is replaced by  $-\beta$  throughout. Although the integrals of Eq. (46) involve elementary functions, they are exceedingly laborious to evaluate in generality. Rather it is more convenient to give the results for special cases, in order to avoid horrendously long expressions and to maintain physical clarity.

It is of interest to note that the results expressed by Eqs. (44) and (46) can be obtained in a somewhat different but equivalent way, using the formalism of Powell (17).

#### Mean-Square Response at Coincidence

We consider first the case of great importance in aircraft and missile applications, where the mean convection speed  $v$  of the boundary layer pressure field can be the same order as the free flexural phase velocity  $c_B$  in the plate.\*

Integration of Eq. (46) shows that for  $\beta > 1$  maximum response occurs when the convection frequency equals the resonance frequency (i.e.,  $\beta = \beta_{mn}$ ). The foregoing condition  $\beta = 1$  (or  $c_{mn} = 1$ ) corresponds to the requirement that the boundary layer pressure field be correlated over a distance greater than the  $m$ -modal wavelength. Inasmuch as the correlation distance is also taken to be smaller than the plate length see Eq. (40), we find that for maximum response at  $\beta = \beta_{mn}$  the mode number  $m$  is restricted by

$$m \leq \frac{L_x}{\lambda} \approx 1. \quad (47)$$

With the use of Eqs. (18), (38), and (41), we can see that  $\beta$  is equal to  $\beta_{mn}$  for a particular speed  $v_c$  given by

$$\frac{v_c}{c_B} = \left[ 1 + \frac{m^2 L_x^2}{m^2 L_y^2} \right]^{1/2} \quad (48)$$

The speed  $v_c$  is termed the hydrodynamic coincidence speed. We see that for modes  $m \gg n$ ,  $v_c$  is approximately equal to  $c_B$ , corresponding to the situation expected in one dimension (2,13). For  $n$  the same order or greater than  $m$ , the coincidence speed

\*The free flexural phase velocity for thin plates is given by  $c_B^4 = \frac{1}{12} \frac{E}{\rho} h^3$  (B.M.).

is increased by the requirement that matching occur with the component of  $v$  projected on the direction of the standing wave. This result is similar to the result of Ribner (2) for infinite plate excitation.

The time correlation integral  $I_{mn}(\tau)$  is now specialized to  $\tau = 0$  as well as  $\omega = \omega_m$  (i.e.,  $v = v_m$ ). We find

$$I_{mn}(0) = \frac{a_{mn}(a_{mn} + 1)}{(a_{mn} + 1)^2 + 4} \left[ \frac{2 - a_{mn}}{4} \right], \quad a_{mn} \gg 1. \quad (49)$$

Equation (49) plus Eq. (44) gives us the mean-square displacement  $w^2$  at hydrodynamic coincidence ( $v = v_m$ ).

We may specialize Eq. (49) further. Consider the case of low damping. Then

$$I_{mn}(0) = \frac{1}{a_{mn}} \approx a_{mn} \gg 1. \quad (50)$$

As expected, the mean-square response in this case increases with increasing lifetime and decreasing damping.

Next consider the case of very high frequencies. Then we get

$$I_{mn}(0) = \frac{1}{a_{mn}} \approx a_{mn} \gg 1. \quad (51)$$

Note that the mean-square response may be proportional to  $a_{mn}^{-2}$  if  $a_{mn}$  is much greater than unity, corresponding to the situation in which damping decreases the displacement at resonance without appreciably broadening the bandwidth of the resonance.

#### Mean-Square Response Below Coincidence

In underwater applications the mean convection speed is much smaller than the coincidence speed (i.e.,  $v \ll v_m$ ). Consequently, we investigate Eq. (46) for  $\omega \ll \omega_m$ . Also we specialize to the case  $\tau = 0$  in order to obtain the mean-square response. The result is

$$I_{mn}(0) = \frac{2}{1 + \frac{2}{a_{mn}}} \left[ \frac{\frac{2}{a_{mn}} - (a_{mn} + 1)}{2 + \frac{2}{a_{mn}} + (a_{mn} + 1)^2} + \frac{1}{a_{mn}} \right] \quad (52)$$

$$= \frac{2}{1 + \frac{2}{a_{mn}}} \left[ \frac{a_{mn} + 1}{2 + \frac{2}{a_{mn}} + (a_{mn} + 1)^2} - \frac{a_{mn}}{2} \right].$$

For ease in interpretation, we consider two special cases of Eq. (52), for low damping and for high frequencies, respectively:

$$I_{mn}(0) = \frac{2}{a_{mn} + 1} \approx \frac{1}{a_{mn}} \approx a_{mn} \gg 1. \quad (53)$$



and

$$I_{mn}(0) = \frac{2}{\pi} \left[ 1 + \frac{1}{\alpha_{mn}} + \frac{1}{1 + \alpha_{mn}^2} \right], \quad \alpha_{mn} \gg 1. \quad (54)$$

Note that for underwater problems we cannot apply these results directly because we have assumed the plate to be immersed in a low-density fluid. However, we may anticipate a result of the next section that shows the correct result to be of the same form. Consequently, we may proceed with a discussion in the frame of underwater application.

For definiteness, let us make  $\alpha_{mn}$  small, so that  $\alpha_{mn} \ll 1$ . The resulting value of  $I_{mn}(0)$  is plotted in Fig. 5 for various values of  $\alpha_{mn}$ . Several important conclusions and comments may be made from Fig. 5 and the foregoing:

1. For usual underwater conditions the plot is estimated to cover the frequency range from about 10 to 10,000 cps, with some extension below 10 and 10,000 cps possible, depending on  $\alpha_{mn}$ .

2.  $I_{mn}(0)$  is proportional to the mean-square modal velocity. This quantity has a varying slope as a function of  $\alpha_{mn}$ . At low frequencies the slope is about -3 db octave, at intermediate frequencies about -10 db octave, and at high frequencies about -6 db octave.

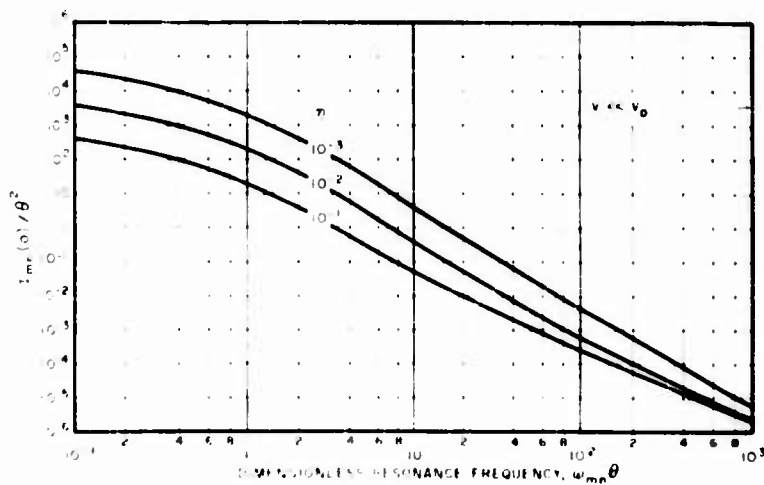


Fig. 5 - Time correlation integral below coincidence for zero time delay

3. With the use of information presented previously in the Section on Boundary Layer Pressure Field it is found that  $\Gamma_{\text{min}}^{(0)}$  varies with about the 3rd power of  $U$ , at low frequencies and about the 5th power of  $U$ , at high frequencies. Also the dependence on boundary layer thickness is the 3rd power at low frequencies and the 1st power at high frequencies.

4. Hysteretic damping is an important means of noise reduction. Above a certain frequency, however, damping is seen to have a decreasing influence on the response.

We wish to expand upon the last comment. Damping appears to be an important mechanism for boundary layer noise reduction. Recent researches on the mechanisms of damping by applied treatments (18-21) are therefore of major interest in the present problem. As implied above, however, there is a transition frequency  $\nu_t$ , above which increased hysteretic damping brings diminishing returns. This frequency is given by the condition  $\alpha_{\text{min}} = 1$  from Eq. (54), and is

$$\nu_t = \frac{1}{\theta} \quad (55)$$

Equation (55) is charted in Fig. 6. A typical small value of  $\theta$  for underwater applications is estimated to be about  $3 \cdot 10^{-3}$  sec (corresponding to  $U = 20$  fps  $\cdot 12$

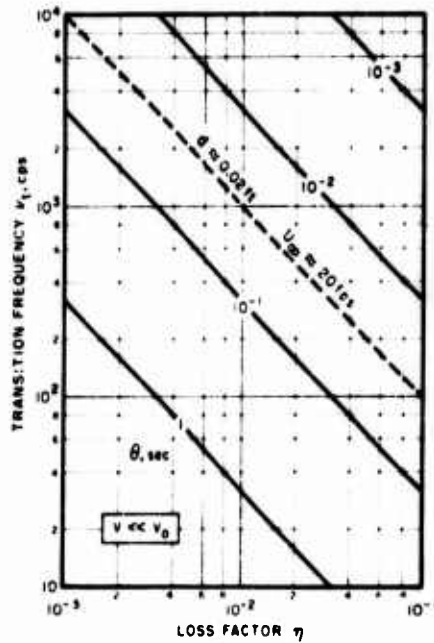


Fig. 6 - Transition frequency for hysteretic damping below coincidence

knots and  $\pm 0.02$  ft). We see, for example, that if  $\gamma$  is  $10^{-2}$  (a quality factor  $Q$  of  $10^2$ ) there would be diminishing returns in increasing  $\gamma$  above 1000 cps, although great benefit would be derived below 1000 cps. Qualitatively, we may conclude that damping of a plate and decay of turbulence play analogous roles in the plate response below coincidence, and that usually, but not always, damping is the dominant factor.

We may understand the foregoing result on damping effectiveness by appeal to the following physical arguments. In general, the response of a plate to an arbitrary spatially extended driving force is a combination of the "forced motion" (which would result if the plate were unbounded) and the "free motion" (which takes into account boundary conditions and is manifested by resonances). For short lifetimes ( $\gamma$  small) the plate response is largely that of the "free motion" of the plate, and is therefore damping controlled. For longer lifetimes ( $\gamma$  larger) the plate response contains more of the "forced motion," and is therefore controlled less by damping. Thus, for frequencies less than the transition frequency, the plate response is largely that of "free motion," and the plate vibration is controlled by hysteretic damping. Above the transition frequency, the reverse situation is obtained.

#### Displacement Correlation Below Coincidence

With reference again to underwater applications, we consider  $\gamma$  for  $\gamma$  different from zero. For the case of low damping, integration of Eq. (46) yields

$$1 - \gamma^2 = \frac{2}{\alpha_{mn}} \frac{\exp - \alpha_{mn}^2}{1 + \frac{2}{\alpha_{mn}^2} \frac{\cos \alpha_{mn}}{\alpha_{mn}}} \quad \alpha_{mn} \rightarrow 1 \quad (56)$$

from which, of course, we could have obtained Eq. (53). Then from Eq. (44) we get

$$\begin{aligned} \langle \mathbf{u}(\mathbf{r}, t) \mathbf{u}(\mathbf{r}', t') \rangle_{mn} &= \frac{A}{2} \frac{r^2}{\alpha_{mn}^2} \frac{\exp - \alpha_{mn}^2}{1 + \frac{2}{\alpha_{mn}^2} \frac{\cos \alpha_{mn}}{\alpha_{mn}}} \langle \mathbf{r} \rangle \cdot \langle \mathbf{r}' \rangle \\ &= \frac{A}{2} \frac{r^2}{\alpha_{mn}^2} \frac{\exp - \alpha_{mn}^2}{1 + \frac{2}{\alpha_{mn}^2} \frac{\cos \alpha_{mn}}{\alpha_{mn}}} \langle \mathbf{r} \rangle \cdot \langle \mathbf{r}' \rangle \quad (57) \end{aligned}$$

In general, the plate correlation is required for the computation of the radiated sound field. Eq. (57) reduces to the result obtained by Eringen (5) for the case of zero lifetime.

#### SOUND RADIATION INTO A CLOSED SPACE

We shall investigate the radiation of boundary layer noise into a closed space with reference to the geometry of Fig. 1, and in particular to the underwater case. Our major concern is the sound within the closed space. But we shall see that the radiation into free space influences the resulting sound field in the closed space as well, and hence must be considered.

##### Influence of the Closed Space on Plate Vibrations

Consider first the closed space ( $\gamma = 2$ ). The Fourier transform  $\Psi_2$  of the velocity potential  $\phi_2$  satisfies the Helmholtz equation

$$\nabla^2 \Psi_2 + k^2 \Psi_2 = 0 \quad (58)$$

where  $k = 0$ . Assume all the interior surfaces with the exception of the exposed plate are pressure release surfaces, i.e.,

$$\Psi_2 = 0, \quad \begin{cases} x = 0, L_x \\ y = 0, L_y \\ z = 0 \end{cases} \quad (59)$$

These boundary conditions correspond approximately to an interior lining of, say, air-filled rubber, or adjacent air-filled compartments, when the closed space is liquid filled.

A general solution of Eq. (53) that obeys Eq. (59) is

$$\Psi_2(x, y, z) = \sum_{p,q} D_{pq} \phi_{pq}(r) \sin k_{pq} z \quad (60)$$

where

$$k_{pq}^2 = k^2 - k_{pq}^2 \quad (61)$$

and where  $\phi_{pq}$  and  $k_{pq}$  are the eigenfunctions and eigenvalues given by Eqs. (37) and (38). Because of the coupling condition given in Eq. (5),

$$\sum_{p,q} k_{pq} D_{pq} \phi_{pq}(r) \cos k_{pq} L_z = - \sum_m H_{mn} \phi_{mn}(r) \quad (62)$$

where  $H_{mn}$  is the modal plate velocity. Consequently, the modal coefficients are related by

$$D_{mn} = - \frac{H_{mn}}{k_{mn} \cos k_{mn} L_z} \quad (63)$$

The pressure transform is equal to  $-i \Psi_2$ . We form the ratio of the coefficients of the modal pressure to the negative of the modal velocity; at  $z = L_z$  this ratio is the impedance  $Z_{mn}$  felt by the plate as a result of radiation into the closed space. Thus

$$Z_{mn} = \frac{-i}{k_{mn}} \tan k_{mn} L_z = -i M_2 \quad (64)$$

where  $M_2$  is the effective mass per unit area associated with coupling to sound waves in the closed space. We see that  $M_2$  may be positive or negative, corresponding to the situation where the radiation load is truly a mass, or a stiffness, respectively.

Equation (64) tells us that we can include the influence of the closed space on the plate response by adding  $M_2$  to the mass  $M$  appearing in Eq. (44). It is important to note that for liquids,  $M_2$  may be the order of or appreciably greater than  $M$ .

Let us define a sound coincidence frequency,  $\omega_c$ , such that  $\omega_c = c_{\text{pl}}/L_z$ . Then from Eq. (61),  $k_{mn}$  is imaginary for  $\omega_{mn} < \omega_c$ , and real for  $\omega_{mn} > \omega_c$ . Thus

$$M_2 = \begin{cases} \frac{1}{k_{mn}^2} \tanh k_{mn} L_z & \omega_{mn} < \omega_c \\ \frac{1}{k_{mn}^2} \tan k_{mn} L_z & \omega_{mn} > \omega_c \end{cases} \quad (65)$$

A 1-inch steel plate in water, for example, will have a coincidence frequency  $f_c \approx 2 \cdot 10,000$  cps. For thinner plates the coincidence frequency will be correspondingly higher inasmuch as  $f_c$  is proportional to  $h^{-1}$ . For the frequency range of interest in most practical applications,  $\omega$  will be less than  $\omega_c$ , corresponding to  $M_1$  positive (i.e., massive).<sup>17</sup>

It is of interest to add that Berry and Reissner (22) have computed the analogous case of radiation into a cylindrical enclosure by vibration of the cylinder surface. Dyer (23) has applied this work to the case of missile vibration.

#### Influence of the Free Space on Plate Vibration

The situation for radiation into free space is not as clear cut. A rigorous treatment of radiation from two-dimensional standing waves on a plate is not yet available. However, Morse (24), Goesele (25), and Westphal (26) have studied the case of one-dimensional standing waves. Their results show that for frequencies higher than  $f_c$ , the radiation reaction on the plate is purely resistive, corresponding to the propagation of energy away from the plate. On physical grounds we may take this to be the case for two-dimensional standing waves also.

For frequencies less than  $f_c$  it was found that the resistive reaction became small, corresponding to very little radiation of energy away from the plate. Also, Morse found that the reaction was primarily massive such that a fraction of the plate length

$$1 - \frac{\omega}{\omega_c}$$

behaved as if it were an infinite plate having a mass impedance determined (in present notation) by

$$M_1 = \frac{\rho h}{k_{\omega}} \quad (66)$$

Inasmuch as we are primarily concerned with frequencies below the sound coincidence frequency, Eq. (66) may be used as an approximation to the present case, provided that the mode number is not too low.

Correspondingly, when the mode number is low, we must expect that radiation of energy away from the plate is the important phenomenon, giving rise to a resistive impedance (viscous damping):

$$1 - \frac{\omega}{\omega_c} \quad (67)$$

where  $s$  is the radiation efficiency. For  $\omega \ll \omega_c$  and for infinite plates,  $s$  is zero because of complete destructive wave interference in the fluid. For finite plates,  $s$  may be greater than zero because of incomplete destructive wave interference. The higher the mode number for a given plate size, the lower  $s$  becomes because of increased destructive interference.

<sup>17</sup>For curved plates this simplification may not always be possible.

For  $\omega \gg \omega_c$ ,  $s$  approaches the radiation efficiency of a piston radiator.

# I. Dyer

As a rough approximation formula for the radiation efficiency we may take

$$\eta = \left[ \frac{2}{\pi} + \frac{2}{\pi} \right] \frac{\left( \frac{\rho_{mn} L}{c} \right)^2}{1 + \left( \frac{\rho_{mn} L}{c} \right)^2} \quad (68)$$

where

$$L = \frac{1}{2} (L_x L_y)^{1/2}$$

The first term in Eq. (68) is suggested by the aforementioned work on one-dimensional standing waves; the second term, by the classical radiation efficiency of a piston in a flat plane.

For frequencies less than  $c$ , the influence of radiation to free space is thus that of viscous damping ( $\gamma_1$ ) at low mode numbers and mass reaction ( $M_1$ ) at high mode numbers. Unfortunately, these quantities have not as yet been determined rigorously, but the rough approximations presented above will be of use in estimating boundary layer excitation.

## Plate Excitation

Equation (44) gives the modal displacement correlation for a plate in a low-density medium. We have seen that the effect of radiation into a medium of arbitrary density is to add to the mass per unit area and to the viscous damping. Thus, Eq. (44) may be applied directly to the case of liquid coupling with the use of a new mass  $M'$  and damping  $\gamma'_{mn}$  such that

$$M' = M + M_1 + M_2 \quad (69)$$

and

$$\gamma'_{mn} = \frac{\gamma_{mn}}{2M'} + \frac{4}{2M'} \frac{B^2}{\rho_{mn}} + \frac{1}{2M'} \quad (70)$$

Liquid coupling below sound coincidence thus influences the modal plate response in three ways: It tends to increase the effective mass of the plate, thus reducing the motion. Because of the increased mass, coupling tends to reduce the resonance frequencies, as may be seen from Eq. (17). And it changes the damping; coupling adds the term in  $\gamma_1$ , but reduces the original terms because of the increased mass. On the other hand, the forms of the plate response solutions discussed previously are unchanged.

For most cases we can set the plate viscous damping coefficient  $\gamma_0$  equal to zero. Then we see from Eqs. (16) and (70) that hysteretic damping is an important noise-reduction mechanism if

$$\frac{1}{\rho_{mn} M'} \quad (71)$$

The equality sign in Eq. (71) defines a set of conditions on either  $\rho_{mn}$  or  $M'$  for which noise reduction by hysteretic damping is not efficient. These conditions can

be estimated for a particular case with the use of Eq. (68). However, noise reduction by hysteretic damping can be achieved efficiently for high enough mode numbers, inasmuch as  $\gamma$  tends to zero in this range. Hence we see that there are two factors limiting the use of hysteretic damping for noise reduction; one the limit of energy radiation given by Eq. (71), and the other the limit of turbulence decay given by Eq. (55).

#### Sound in the Closed Space

In general, we desire the sound pressure correlation to describe the sound field within the closed space. The pressure correlation is determined by the plate displacement correlation, as in Eq. (57), plus the velocity potential field, as in Eq. (60). Dyer (27) has recently worked out an analogous problem, that of noise propagation in a circular space, the methods of which apply to the present case. We shall therefore pass onto a simpler problem, that of determining the mean-square pressure adjacent to the excited plate.

The modal mean-square pressure  $p_{mn}^2$  at the plate is simply determined by Eqs. (44) and (64):

$$p_{mn}^2 = \alpha_{mn}^2 \frac{4}{\pi} W_2^2 \left( \frac{A}{L_x L_y} \right)^2 \sin^2 \frac{m\pi x}{L_x} \sin^2 \frac{n\pi y}{L_y} \frac{2}{\pi} I_{mn}(0), \quad (72)$$

and the spatial average of  $p_{mn}^2$  is simply

$$p_{mn}^2 = \frac{A}{4L_x L_y} \left( \frac{W_2}{W_1} \right)^2 \frac{2}{\pi} I_{mn}(0). \quad (73)$$

As an example, consider the following case of a steel structure in water:

$$h = 1.2 \text{ in.}$$

$$L_x = L_y = 5 \text{ ft}$$

$$L_z = 1 \text{ ft}$$

$$U_1 = 20 \text{ fps} \approx 12 \text{ knots}$$

$$d = 0.02 \text{ ft}$$

$$\tau = 3 \cdot 10^{-2} \text{ sec}$$

$$\gamma = 10^{-2} (Q = 100)^{-1}$$

In this case the sound coincidence frequency is about 20,000 cps. Let us restrict attention to the case  $m, n \ll 1$ . Then for frequencies less than 10,000 cps we may approximate  $k_{mn}$  by  $k_{mn}$ . Furthermore, for simplicity, let us restrict attention also to frequencies greater than about 200 cps, in which case  $W_1 \approx W_2 \approx 2 \cdot 10^{-3} \text{ m}$ , and  $\gamma \approx 0$ , as can be calculated from Eqs. (69) and (67). Under these conditions,

$$\left( \frac{W_2}{W_1} \right)^2 = \frac{1}{12} \frac{L_x L_y}{\pi h} \quad (74)$$

and  $\omega_{mn}$  is the uncoupled resonance frequency given approximately by Eq. (18).<sup>\*</sup>  $c_L$  is the longitudinal bar velocity in steel ( $\approx 17,000$  fps).

Equation (73) can be evaluated with the use of Eq. (52) (or Fig. 5) and the information given above. It is customary, however, to measure noise in frequency bands of width  $\Delta f$ . The average number of modes  $N$  in a band  $\Delta f$  may be determined from Eq. (18), and is approximately

$$N \approx \frac{3}{c_L h} L_x L_y \Delta f \quad (75)$$

Thus, the mean-square pressure as measured by frequency analysis in bands of width  $\Delta f$  will be on the average

$$\overline{p^2} = f^2 \frac{A}{8h^2} \left( \frac{c_L}{\omega_{mn}} \right)^2 \rho_{mn} I_{mn}(0) \quad (76)$$

where we now consider  $\omega_{mn}$  to be a continuous frequency variable, and where  $\rho_{mn}$  is the density of the plate. Note that the plate area does not appear in the expression for  $\overline{p^2}$ . Equation (76) is plotted in Fig. 7 for the conditions given above, in terms of the Spectrum Level (SL) defined by

$$SL = 10 \log_{10} \frac{(\overline{p^2})}{(p_0^2)} \text{, db.} \quad \text{for } \Delta f = 1 \text{ cps.} \quad (77)$$

where the reference pressure  $p_0$  is 1 microbar (1 dyne/cm<sup>2</sup>).

Of course, measured spectra would tend to appear less regular than that shown in Fig. 7, particularly at the lower frequencies where the measurement bandwidth may be small compared with the frequency spacing of the resonances. Also a hydrophone spaced out somewhat from the excited plate would be expected to record considerably less than that predicted in Eq. (76). From Eq. (60) we see that the mean-square pressure for a location away from the excited plate would be reduced by the factor

$$\left[ \frac{\sinh \gamma_{mn} z}{\sinh \gamma_{mn} L_z} \right]^2 \quad (78)$$

As an example, if  $z = 0.9 L_z$ , the above factor is about -2 db at 100 cps and -17 db at 1000 cps. Even larger reductions are predicted at frequencies larger than 1000 cps, but these are not likely to be realized in practice because of the presence of non-ideal boundaries, dissipation in the water, and other noise sources.

On the basis of Eqs. (76) and (78) we may reach the following tentative conclusions on possibilities for the reduction of boundary layer noise associated with underwater devices:

1. The slower the speed and the thinner the boundary layer, the less the noise.
2. The greater the mass per unit area of the excited plate, the less the noise.

\*The fundamental resonance of the plate considered to be vibrating in vacuo is at about 25 cps.



# Sound from Boundary Layer Turbulence

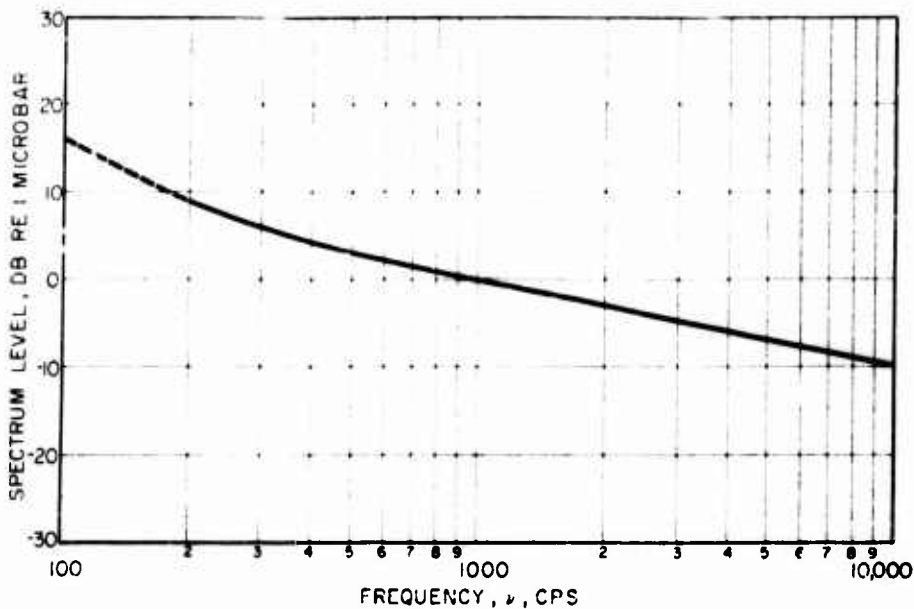


Fig. 7 - Calculated average mean-square pressure at the excited plate. Levels are reduced considerably at locations removed from the plate (see text for conditions).

3. The greater the plate damping, the less the noise (within the limits noted in the foregoing).
4. The greater the distance from the excited plate, the less the noise.

## REFERENCES

1. Kraichnan, R.H., J. Acoust. Soc. Am. 29:65-80 (1957)
2. Ribner, H.S., University of Toronto, UTIA Report No. 37, April 1956
3. Corcos and Liepmann, NACA TM 1420, December 1956
4. Lyon, R.H., J. Acoust. Soc. Am. 28:391-398 (1956)
5. Eringen, A.C., J. App. Mech. 24:46-52 (1957)
6. Strasberg, M., J. Acoust. Soc. Am. 30:680 (Abstract) (1958)
7. Harrison, M., J. Acoust. Soc. Am. 29:1252 (Abstract) (1957)
8. Willmarth, W.W., NASA Memo 3-17-59W, 1959
9. Kraichnan, R.H., J. Acoust. Soc. Am. 28:378-390 (1956)
10. Kraichnan, R.H., Phys. Rev. 109:1407-1422 (1958)

I. Dyer

11. Mull and Algranti, NACA RM E55K07, March 1956
12. Rogers and Cook, WADC TR 52-341, December 1952
13. Dyer, I., J. Acoust. Soc. Am. 28:782 (Abstract) (1956)
14. Morse and Feshbach, "Methods of Theoretical Physics, Part II," Chap. 11, New York:McGraw-Hill
15. Favre, Gaviglio, and Dumas, J. Fluid Mech. 2:313-344 (1957)
16. Lyon, R.H., J. Acoust. Soc. Am. 28:76-79 (1956)
17. Powell, A., Chapter 8 in "Random Vibration," edited by S.H. Crandall, Cambridge:Technology Press
18. Oberst, H., Acustica 6: (Akust. Bieh. 1) 144-153 (1956)
19. Lienard, P., Anal. d. Tele. 12-10:359-366 (1957)
20. Kerwin, E.M., J. Acoust. Soc. Am. 30:698 (Abstract) (1958) (also to be published)
21. Ross, Kerwin, and Dyer, Bolt Beranek and Newman Inc., Report No. 564, ONR Contract Nonr-2321(00), Task NR 062-205, June 1958
22. Berry and Reissner, Ramo-Wooldridge Report No. EM 7-5, May 1957
23. Dyer, I., Chapter 9 in "Random Vibration," edited by S.H. Crandall, Cambridge: Technology Press
24. Morse, P.M., Bolt Beranek and Newman Inc., Informal Report, December 1952
25. Goesele, K., Acustica 3:243-248 (1953)
26. Westphal, W., Acustica 4:603-610 (1954)
27. Dyer, I., J. Acoust. Soc. Am. 30:833-841 (1958)

\* \* \* \* \*

## DISCUSSION

H. S. Ribner (University of Toronto)

Dyer's formulation in his Eq. 25 is, I think, a plausible space-time correlation function for the turbulence pressures. With his numbers, it is almost a frozen, convected pattern: convection contributes about 50 times as much as fluctuation to the observed microphone frequencies. A different view is that an eddy is convected about 50 times its length before it has been destroyed by fluctuation. The ratio of 50, for convection-to-fluctuation, can be approximated as infinity in two ways: the time scale can be made infinite (frozen pattern, treated by Ribner and by Kraichnan), or

the length scale can be set equal to zero. Dyer does the latter—he effectively reduces the eddy size to zero—by inserting delta-functions in his correlation. The entire later analysis utilizes this modified correlation, Eq. 32.

The assumption of zero eddy size appears to be related to Dyer's finding that the plate modes are statistically independent. It seems unlikely that such an independence can hold in reality for modes of wavelength less than the eddy size (the high frequency modes).

Further, zero eddy size implies that the cutoff frequency ( $f_0$ ) goes to infinity: the analysis implies excitation of the plate by "white" noise. For a given mean-square pressure, the "white" noise spectrum robs from the low frequencies to add to the high frequencies. The analysis, therefore, presumably leads to underexcitation of the low modes and overexcitation (failure to show a cutoff) of the high modes. In this matter of the correlation function I cannot resist the conclusion that the frozen convected pattern would give more realistic results, since it preserves the eddy size and exhibits a realistic frequency spectrum.

Dyer discusses the role of "coincidence" of moving pressure waves with possible free-running, sinusoidal, flexural waves in the plate. The speed of these free waves is a function of the wavelength. Thus only certain Fourier components of a moving, fluctuating pressure pattern will have the correct wave length and speed for coincidence. The assumption of what amounts to zero "eddy" size in the pattern will grossly change the Fourier components and therefore the degree of coincidence.

#### I. Dyer

In comment to Dr. Ribner's statement I wish to note that the eddy size, in my estimation, has not been taken out of the problem. While the delta function appears, the eddy size is still retained in the quantity  $\alpha$ . Of course the delta function was used as a matter of analytical simplicity. The consequence of this is that the modes one obtains are statistically independent. I think that in practice this is probably a very good approximation. While there are probably some modes that would be poorly approximated, they would have to be fairly close together in frequency space in order for any kind of correlation.

#### G. M. Corcos (University of California, Berkeley)

I wish to compliment Dr. Dyer for the clarity of his presentation. I would like him to comment on three points.

First, I fail to see the origin of the "viscous damping" term in the differential equation. It was assumed that the boundary layer was undisturbed by the plate, and I don't see how a plate oscillating normally to itself will dissipate energy if it doesn't modify the boundary layer.

Second, there have been at least two detailed attempts at solution of essentially the same problem by normal mode methods, one by Dr. Kraichnan and the other by Dr. Powell, and there have been other attempts using slightly different methods. Since the analysis is on the heavy side, it would be informative to indicate what new information, beyond that already available, has arisen out of the work presented here.

I. Dyer

My third point is in regard to the use of normal modes. Is it possible to offer a simpler solution of the differential equation by using a fundamental solution which, in effect, ignores the effect of the boundaries? An answer is provided, in my opinion, by some work, to be published soon, by Dr. Paul Weyers of the California Institute of Technology, who has studied the generation of sound on the outside of a very thin plastic tube, inside of which is a fully developed turbulent flow. The point is that in the problem you consider, the scale of the turbulent phenomenon is small compared to the size of the plate. In Weyers' case, even though they are of the same order, the transmitted sound spectrum exhibits no peaks for frequencies higher than the very lowest range. Most of the energy is contained in the continuous portion, and I wonder why the use of a fundamental solution, ignoring all the details of effective boundaries, has not been considered.

I. Dyer

Dr. Kurtze will answer the question about how one can get viscous damping without modifying the external field.

As far as what new results are obtained, I think the primary result of this work is that it shows in a clear way the influence of the decay of the turbulence on the design of damping treatments for the reduction of boundary layer noise. I would say that this is the prime result and that the solutions at high frequencies ought to merge together and be independent of the particular details of the modes. In effect the formula is a manifestation of this.

Skudrzyk has also made some calculations along these lines and you might be interested in seeing what he has done on that basis. The use of that theory is not unique; it's just a matter of taste and convenience on my part.

K. U. Ingard (Massachusetts Institute of Technology)

It might be of interest to mention work by Dr. Lyon on the problem of excitation of a membrane caused by a flowing turbulence. It is interesting in the sense that in Dr. Dyer's treatment it was assumed that the convective velocity of the turbulence was small compared to the flexural wave speed and hence the resonance effects obtained in that manner were completely ignored. On the other hand, if one uses the membrane, the tension of which can be varied as you please, he can very easily adjust the flexural wave speed of the membrane to be coincident with the convective speed of the turbulent flow and, in that way, both theoretically and experimentally, show the resonance caused by this coincidence. Such experiments have been performed and have been shown to be in agreement with the calculations.

E. Mollo-Christensen (California Institute of Technology)

Figure D1 shows the results obtained by Weyers for the sound radiation from his pipe at the high frequencies only. This is the high-frequency part of his result. One finds this spectrum is practically continuous, in agreement with Corcos' comment. At the low frequency Weyers finds that he gets a spectrum with peaks in it, which then descends into a continuous spectrum for higher frequencies.

One may ask why the author did not find the stream directionality of the radiated flow field to free space. Listening to the bend of a garden hose lying on the lawn, one is impressed by the strong directionality of the emitted sound field.

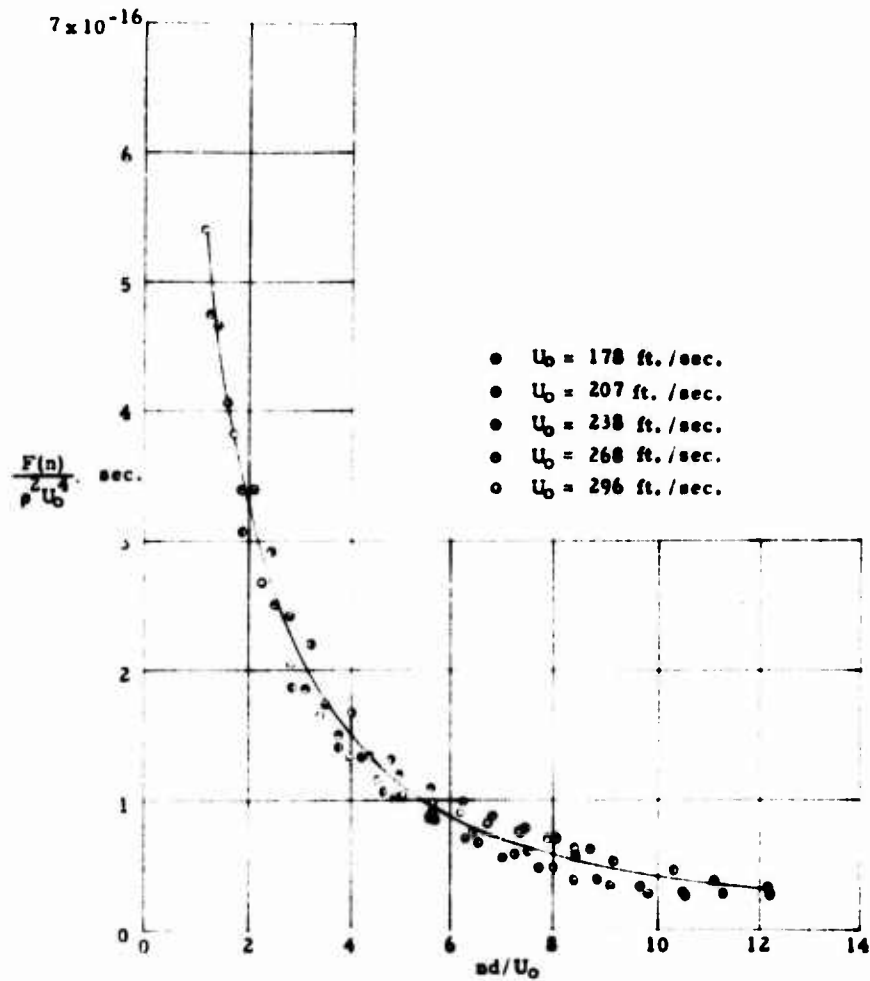


Fig. D1 - Similarity of power spectra of  $p(t)$   
 $r = 0.0615 \text{ in.}, d = 1 \text{ in.}, r/d = 3/4 \text{ in.}$

I. Dyer

The spectrum, of course, that would be predicted on the basis of the theory would also exhibit these peaks corresponding to the modes, I think, and what I plotted in the last slide was essentially this portion of it. There should be no directionality to the emitted sound field as long as essentially the flexural wave speed on the plate is less than the wave speed in the water. It is only above that so-called coincidence frequency that such directionality should occur.

\* \* \* \* \*

# RECENT INVESTIGATIONS ON SONIC AND ULTRASONIC CAVITATION IN GÖTTINGEN

Erwin Meyer

*Physikalisches Institut der Universität Göttingen*

## INTRODUCTION

The investigations to be discussed here are divided into the following subjects:

1. The noise spectrum of cavitation with steady sinusoidal excitation and its relation to the oscillation of the bubbles.
2. The cavitation caused by a single underpressure pulse.
  - a. excited with a barium titanate calotte
  - b. excited by the sudden retardation of a moving water column.
3. The relations between sound pressure and luminescence.
4. The measurement of the surface tension and surface viscosity from the excitation of capillary waves at frequencies up to 1.5 Mc/s.

It is generally known that the onset of streaming or ultrasonic cavitation is accompanied by noise; the noise has a very broad frequency spectrum and in many cases the audible part of it is so noticeable that it is often used as a criterion for the onset of cavitation. It was, for example, during the war very easy to determine the upper limit for the creeping speed of a submarine as function of the diving depth by simply listening to the onset of cavitation or the onset of formation of air bubbles caused by a sufficient number of revolutions of the screw with a kind of a stethoscope attached to the screw shaft; already with the first experiment the increase of the critical number of revolutions of the screw with the square root of the diving depth (static pressure) was stated.

As was shown in an older paper by Th. Lange (1) also for ultrasonic cavitation the onset of noise is so sharp that it is preferred to the formation of visible bubbles as a criterion for cavitation. It is to a far extent without significance which part of the noise spectrum is used for detecting the onset of cavitation. From the work of Th. Lange only one figure (Fig. 1) will be given to confirm the above statements. Vibration cavitation was excited with a quartz crystal at 575 kc/s. The driving voltage of the quartz is plotted on the abscissa against the noise level in the frequency interval from 520 to 540 kc/s on the ordinate. Here the onset of cavitation is much easier recognized than by using e.g. the nonlinearity of the sound pressure increase of the exciting frequency (575 kc/s) as a criterion.

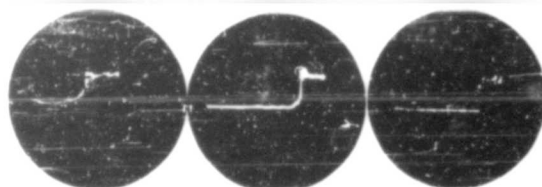


Fig. 1 - Noise voltage (520 to 540 kc/s) vs. transmitter voltage (575 kc/s) for different stages of degassing

#### NOISE SPECTRUM AND SOUND PRESSURE OSCILLOGRAM FOR THE ONSET OF CAVITATION AND THEIR RELATION TO THE OSCILLATIONS OF THE BUBBLES

In a thorough investigation R. Esche (2) has studied the spectrum of sonic or ultrasonic cavitation for a great number of frequencies ranging from 100 c/s up to 3 Mc/s. He found out, that there is always a line and a continuous spectrum simultaneously. In the line spectrum the exciting frequency appears, of course, with high intensity and also the harmonics are observed. This seems to be obvious. But Esche could, perhaps for the first time, ascertain that also a number of subharmonic frequencies occur. In his investigation he came to the conclusion that the occurrence of a continuous spectrum might be a proper method to distinguish true cavitation (formation of bubbles containing only water vapor) from that type of cavitation where air bubbles are formed.

The occurrence of subharmonic frequencies (Fig. 2) is of special interest, as subharmonics one-half, one-third, and one-fourth the exciting frequency are observed. Also the overtones of the subharmonics are present. In a more recent investigation on the detailed structure of the spectra L. Bohn (3) found not only subharmonics within the range of the fundamental frequency but also - mostly as overtones of half-order subharmonics - up to the 30th or 40th order, their level sometimes being 10 db under the level of the integer harmonics.

The occurrence of subharmonics is not difficult to understand. In a high-intensity sound field the oscillating air bubbles change their volume to a great extent during one period. That means that the compliance of air and the mass of water taking part in the oscillation are functions of time. In this case we have a rheolinear oscillation, the differential equation of which admits also subharmonics as solutions. W. Güth (4) starts from the principle that the oscillation is nonlinear, since the compliance of the air cushion is a function of the oscillation amplitude. The compliance increases with increasing amplitude. The resonance curve of such a system is, as is well known, not symmetrical. The maximum of the curve moves towards lower frequencies with increasing amplitude. At the same time the occurrence of subharmonics is possible. It is, however, surprising that especially one-half the exciting frequency and the corresponding overtones are so clearly observable. This means that in the oscillation of the bubble a periodic amplitude or phase modulation with one-half the exciting frequency is very prominent.

Varying the conditions for ultrasonic cavitation such as air content or exciting amplitude, more astonishing results with respect to the sound pressure oscillogram or to the sound spectrum may be obtained. Such investigations were carried out by



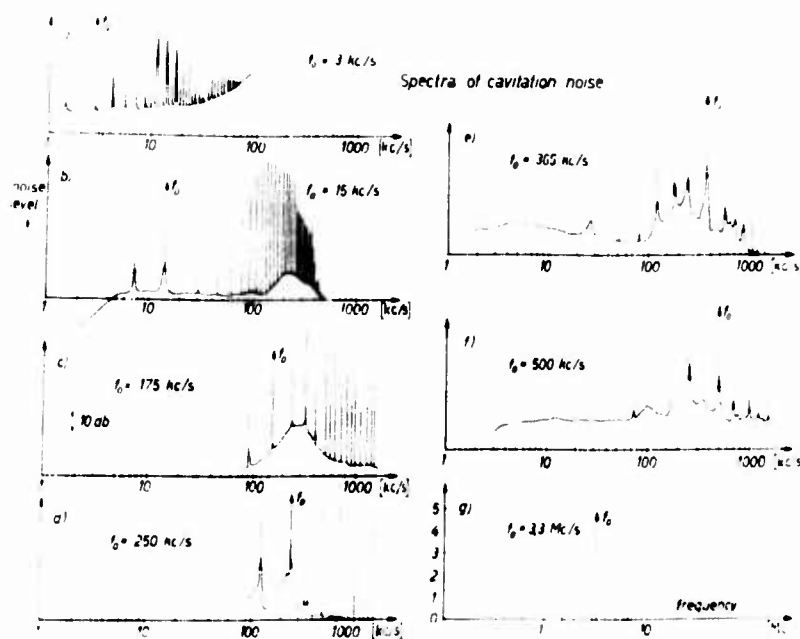


Fig. 2 - Spectra of cavitation noise

L. Bohn (3). His apparatus was very simple in principle (Fig. 3). Twenty-one magnetostrictive systems with a resonance frequency of 14.6 kc/s connected in parallel were arranged in such a way that the sound was focused on a small area. In the focus a microphone was placed, consisting of a thin nickel wire of about 0.5-mm diameter (5). Only the tip of the nickel wire was sensitive to sound since the rest of the wire immersed in the water was covered with a thin plastic tube. The part of the wire outside the water had considerable length and its end was covered with a wedge-shaped layer of wax so that only progressive waves are excited at the tip of the wire. These extensional waves generate an ac voltage in a solenoid around the nickel wire. The microphone responded to frequencies up to 1 Mc/s and it is of minor importance whether the frequency response curve rises with frequency, as corresponds to the principle of the magnetostrictive transducer, or is leveled out by an electrical network.

The cavitation bubbles have to be formed at the tip of the microphone to excite directly the microphone with their vibrations. In order to really accomplish

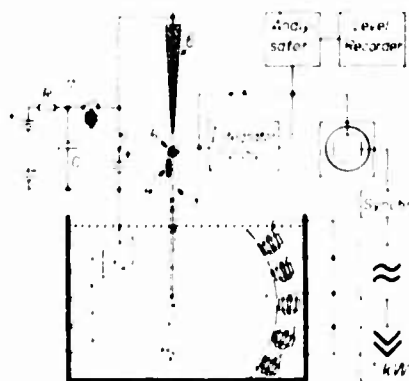


Fig. 3 - Measuring arrangement. 1. Magnetostrictive emitter system, tuned at 14.6 kc/s. 2. probe microphone. 3. nickel wire. 4. permanent magnet. 5. pickup coil. 6. absorbing material. 7. electrical circuit. 8. recorder. 9. cable.

the onset of cavitation at the very tip of the microphone, especially with degassed water, a current pulse (shortened condenser discharge) was led through the wire into the water; so by either increasing the temperature of the water over a very small area or by a weak, transient electrolysis gas bubble nuclei were injected at the tip of the wire.

Of special interest is the cavitation noise for weak excitation in saturated or moderately undersaturated water. Then the cavitation bubbles are excited (by pulses) in their natural pulsation oscillation and reverberate with this frequency. The bubbles are preferably stabilized at certain sizes. Sometimes clouds of very tiny bubbles are then intermittently pushed away from an oscillating bubble. This is probably caused by strong oscillations of the bubble surface excited by the high acceleration related to the pulsation. It therefore suggests itself to assume that in this case the natural pulsation coincides with a natural surface oscillation of the bubble. For weak excitation the surface vibrates on a subharmonic overtone based upon one-half the natural frequency of the pulsation oscillation. For strong excitation a higher order of the surface oscillation coincides directly with the natural frequency of the pulsation oscillation.

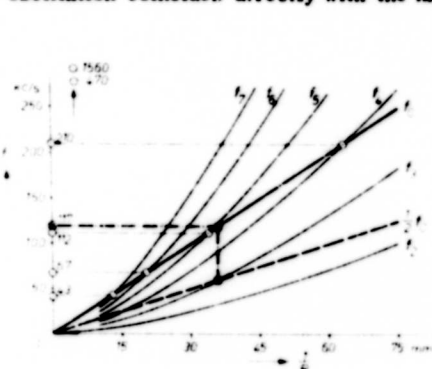


Fig. 4 - Frequencies of the natural radial oscillations and of some modes of surface oscillations for air bubbles in water as a function of the reciprocal radius.

In Fig. 4 the eigenfrequency  $f_0$  of the pulsation oscillation and, the half-order subharmonic  $f_{0.2}$  as well as the different overtones ( $f_1$  to  $f_n$ ) from the second to the seventh order are plotted against the reciprocal bubble radius according to the formula given by Minnaert. It is evident from the graphs that for 43, 67, 112, and 210 kc/s the eigenfrequency of the pulsation oscillation for the corresponding bubble size coincides with the seventh, sixth, fifth, and fourth order respectively of the surface oscillation. The third order can also coincide with one-half the fundamental frequency of the pulsation oscillation, resulting in a "stable" oscillation at 117 kc/s.

A quantitative confirmation of statements is given in Figs. 5 and 6.

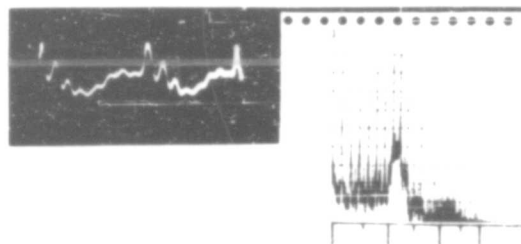


Figure 5 - Bubble oscillation during cavitation process. Exciting frequency: 117 kc/s. Amplitude (calculated): Natural frequency of bubble: 110 - 120 kc/s. Saturation of system: 70 - 80%.

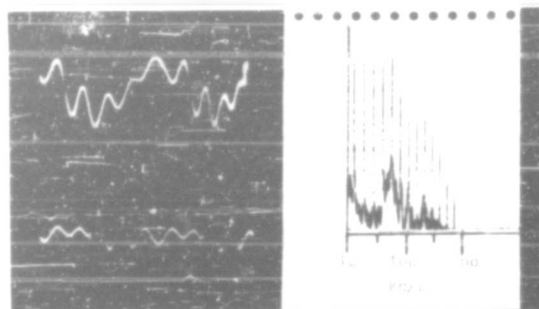


Fig. 6 - Bubble oscillations during cavitation process. Exciting frequency: 14.6 kc/s. Amplitude ca. 1 atm. Natural frequency of bubble: 65 - 70 kc/s. Saturation of water: 80 - 90%.

Here we have weak cavitation; the sound pressure is 0.7 atm and the saturation with air about 70 to 80 percent (Fig. 5). The corresponding values for Fig. 6 are 1 atm and 80 to 90 percent saturation. In the oscillogram as well as in the spectrum the preference of a certain frequency range - using a term from physiological and musical acoustics one might say "formant frequency" - is obvious. In Fig. 5 this is 110 to 120 kc/s, in Fig. 6 it is 65 to 70 kc/s. Also lower "formant" frequencies might occur, as for example the frequencies 15.8 and 16.6 kc/s respectively and 22 kc/s in Fig. 7 for a sound pressure of 1 atm and air-saturated water. On the other hand also higher formant ranges are possible (see Fig. 8); the saturation corresponding to Fig. 8 is 60 to 70 percent and the sound pressure is relatively high (2 atm).

For very strong sound excitation things become rather complex. There occur reverberating oscillations of the bubbles at certain frequencies. Also stabilization in the above described sense is observed. As is expected, the energy of the spectrum in all cases increases with frequency. There are sharp maxima in the oscillograms with a pulse width of only some microseconds. The width of these pulses can be calculated from the minima in the respective frequency ranges of the spectrum. In Fig. 9 a spectrum of this type is given. There is a marked minimum at about 200 kc/s.

Another example illustrating how the noise spectrum extends to higher frequencies when the exciting sound pressure is raised from 1 to 4 atm is given in Fig. 10.

On the other hand in saturated or, better, oversaturated water larger bubbles are formed which are in resonance with the exciting frequency of 14.6 kc/s. Then there are no sharp sound pulses and the oscillogram resembles more or less a sine curve.

Very sharp pulses are naturally observed in extremely undersaturated water at higher exciting sound pressure amplitudes. The spectrum is then exclusively given by the

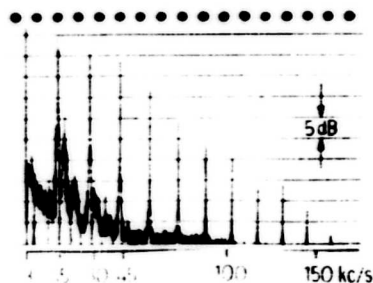


Fig. 7 - Noise spectrum of oscillating bubbles in air-saturated water. Sound pressure about 1 atm.

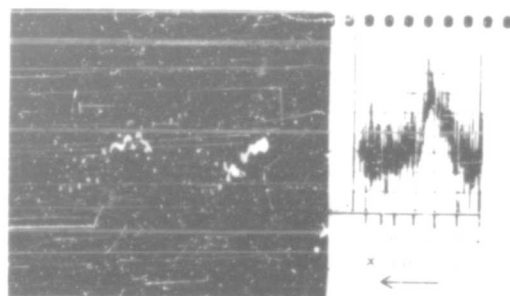


Fig. 8 - Bubble oscillation during cavitation process. Exciting frequency: 14.6 kc/s. Amplitude ca. 2 atm. Saturation of water: 60 - 70%.

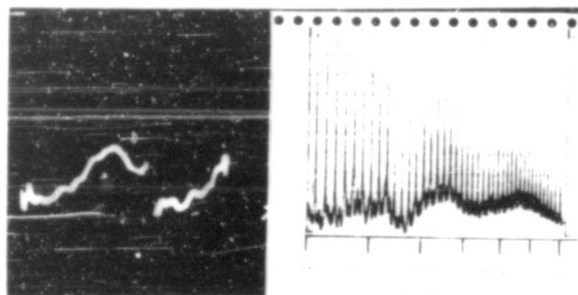


Fig. 9 - Pressure shock caused by bubble collapse. Exciting frequency: 14.6 kc/s. Amplitude about 4 atm. Saturation of water: 70%.

form of the pulses (Fig. 11). The envelope of the spectrum can easily be explained with the assumption of a cosine pulse of 6 to 7  $\mu$ sec duration.

The occurrence of a continuous spectrum has often been the subject of detailed discussion. For some time it was believed that the continuous spectrum was a criterion for real cavitation, that is, cavitation of vapor bubbles. A more simple reason for the existence of a continuous spectrum is that the amplitude or the phase of the gas bubble oscillation is subjected to statistical fluctuations, which consequently render a continuous spectrum. The vapor bubble cavitation, if it at all has to be distinguished from the formation of gas bubbles, is supposed to be the stronger the higher the frequencies in the spectrum are.

Simultaneously with the above mentioned investigations E. Mundry and W. Güth (6) filmed the gas bubble oscillation itself. In these experiments the oscillating cavitation bubble is generated at the tip of a magnetostrictive nickel rod (2.5 kc/s). The bubble is lighted up with an intermittent electric spark and then recorded on a stationary film with the help of a revolving mirror; the maximal number of exposures is about 105,000 frames/sec. As soon as the bubble has been registered the sound is

cut off at once and the size of the bubble at rest is measured. The film is then evaluated by planimetry of the bubble. Thus an "average" bubble radius is found. This radius is plotted as a function of time for a number of bubbles of different sizes in Fig. 12. The average radius of the bubbles in this figure ranges from 1.42 mm down to 0.3 mm. These sizes are indicated with the dash-dot lines in the detailed pictures in Fig. 12. The dashed lines give the corresponding decay curves according to the theory of Rayleigh. Two conclusions may be drawn from the results. Firstly, the time interval during which the bubble is larger than in the equilibrium position (under-pressure phase) is longer than the time interval during which the bubble is smaller. This means that if gas diffusion occurs the direction of the diffusion from the liquid into the bubble is preferred to the opposite direction, so that the bubble is growing. Even more interesting than this phenomenon is the reverberation of the bubble excited by the implosion. Especially for the smaller bubbles this is clearly visible. The reverberation frequency is practically given by the natural frequency of the pulsation oscillation calculated according to the linear theory of the bubble oscillation. In Fig. 13 a number of examples of such measurements are collected. Plotted against the measured length of the period of the natural oscillation of the bubble is the measured radius of the bubble in equilibrium position. The line corresponds to the calculations of Minnaert. The results are obviously in good agreement with the above mentioned investigations on the cavitation spectrum.

It is also possible to make the shock waves, caused by the implosion of the bubble in the water, visible with a schlieren method (Fig. 14). Thereby a number of shock waves are observed in temporal succession, all of them having their center on the surface of the transmitter but at different points. This is no wonder. It only indicates

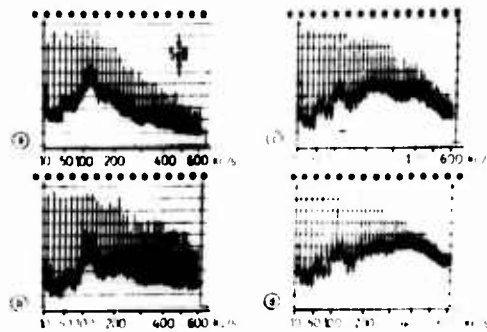


Fig. 10 - Noise spectra for increasing exciting sound pressure

	Exciting sound pressure (atm)	Air saturation (%)
a.	1.0	80
b.	2.0	80
c.	3 to 4	60 to 70
d.	3 to 4	60 to 70

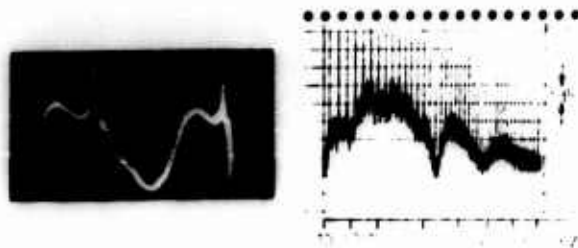


Fig. 11 - Implosion of a bubble in water. Noise spectrum for the implosion of a bubble in water. Air saturation: 60 to 70%.

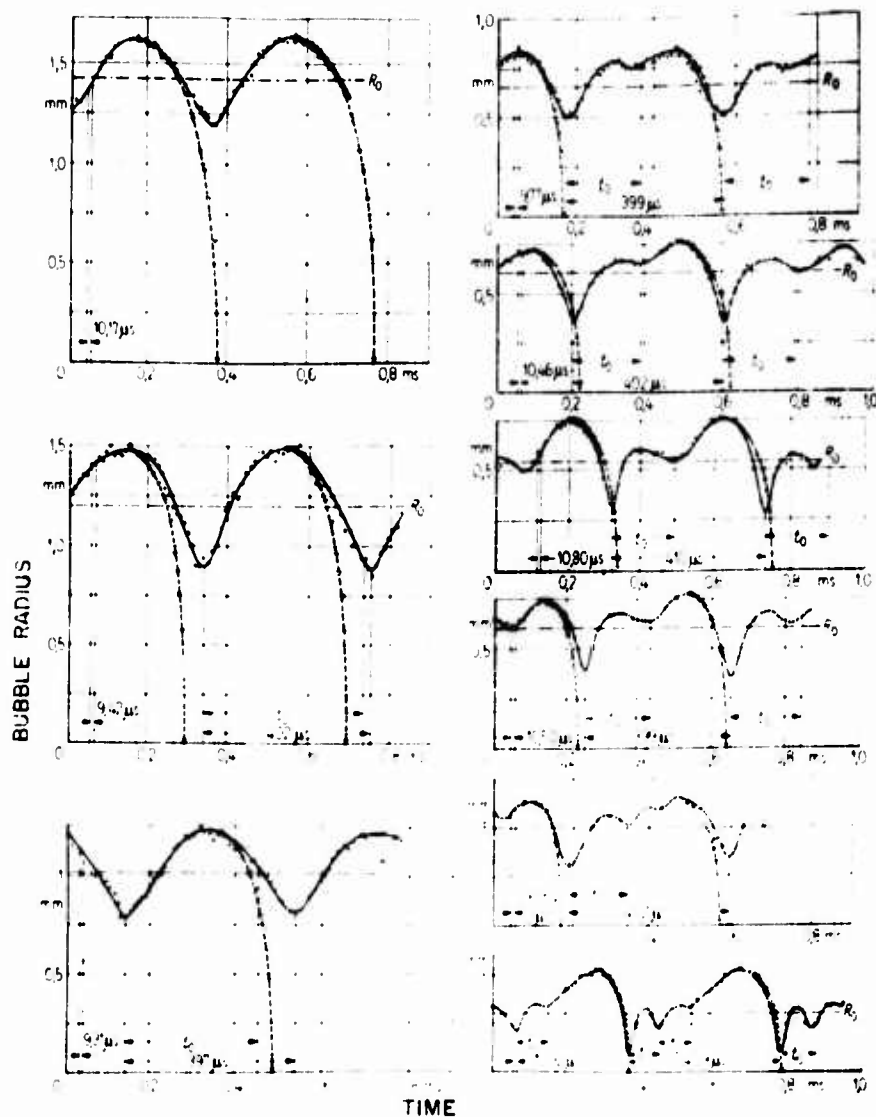


Fig. 12 - Radius of oscillating gas bubbles as a function of time for bubbles with different diameters

that there are different centers of implosion. That again may be taken as an optical argument or proof for the occurrence of a continuous spectrum in the cavitation noise; the shock waves illustrated in Fig. 14 for example are generated within a time interval of at least 80  $\mu$ sec.

A more detailed study of the shock waves shows a slow pressure increase at the front of the shock waves whereas on the backside there is a steep decrease. According

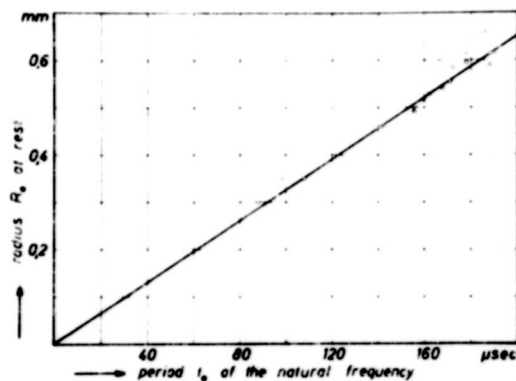


Fig. 13 - Periods of the (linear) natural oscillations of gas bubbles as a function of their radius at rest.

to W. Güth (7) this can be explained by looking at the acceleration of the water as a function of time; we have an increase of the acceleration to the center and then a sudden retardation.

At this point some short remarks will be put in on cleaning of surfaces with ultrasonics, which in the past years became an often-used practice. J. Olaf has worked on this problem in our institute. By making measurements in a larger frequency range he has found out that for the speedy cleaning of a dirty surface (in his case glass plates with polishing rouge ( $\text{Fe}_2\text{O}_3$ ) contamination) cavitation is absolutely necessary. If - without changing the sound pressure - the cavitation is prevented by a high static overpressure the cleaning effect is practically gone. The differences in the cleaning effect at different frequencies are of secondary nature. They are for example caused by the directivity of the transmitter a.o. It has also to be kept in mind that at higher frequencies cavitation is generated at higher expense.

#### CAVITATION BY A SINGLE UNDERPRESSURE PULSE

For the elucidation of the formation and growth of cavitation bubbles it is of advantage not to use periodic underpressure intervals but to apply only one single underpressure pulse. This problem was tackled by G. Kurtze (9). His experimental setup is given schematically in Fig. 15. A barium titanate calotte of 10-cm diameter and 6-mm thickness is terminated at its backside by a long



Fig. 14 - Schlieren optical pictures of shock waves

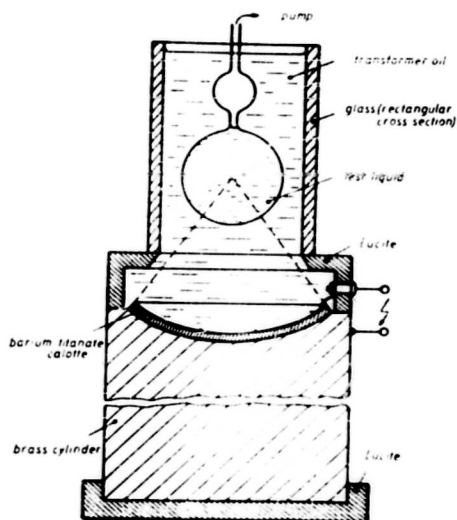


Fig. 15 - Experimental setup for the excitation of cavitation by a single underpressure pulse

brass cylinder. The front surface is adjoining to a liquid. The sound is focused into this liquid. The liquid under test is contained in a thin-walled glass sphere in the focal point. The static pressure inside this glass sphere can be reduced to the vapor pressure of the test liquid. The sound is generated by slowly charging the barium titanate calotte to 12 kv and discharging it with a time constant of 2.5 sec. The time constant is slightly higher than half the period of the natural vibration of the barium titanate calotte. Thus during the reverberation of the barium titanate the underpressure amplitude is dominating. The brass cylinder on the backside of the barium titanate calotte is long enough to delay the sound reflected at its other end until the process in the test liquid is finished. The oscillogram of the sound pressure in the focal point as a function of time was measured with the help of a tiny barium titanate cube of  $1\text{-mm}^3$  volume. There is practically only an underpressure pulse (Fig. 16).

With this apparatus it is possible to measure the sound pressure necessary to initiate cavitation and to observe the growth of the cavitation bubble. Of course, for that purpose it is indispensable to make a large visible bubble. This could only be achieved by subjecting the test liquid to a static underpressure. On the other hand the growth of the bubble could be calculated under certain assumptions as for example a disappearing hydrostatic pressure and an underpressure pulse of 1-sec duration and 20-atm amplitude. The results are plotted as a dotted line in Fig. 17. The two experimental curves show that the assumptions made for the calculation can be realized to a certain extent.

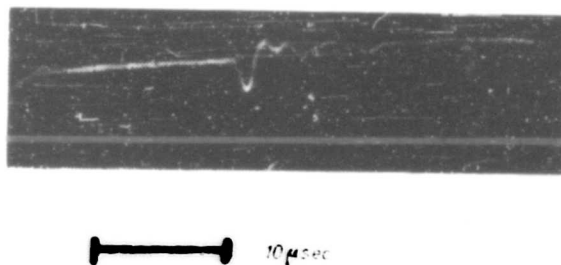


Fig. 16 - Pressure in the focal point of the barium titanate calotte as a function of time. Sound pressure: 10 atm.



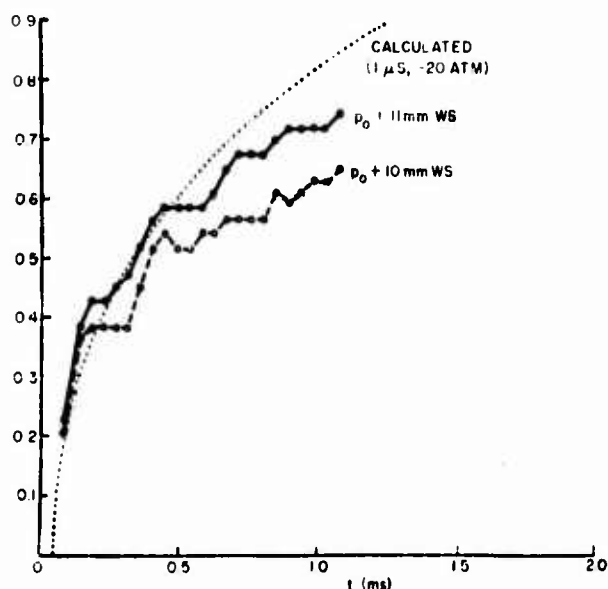


Fig. 17 - Bubble radius as a function of time with a single pulse of 2- $\mu$ sec pulse width and 20-atm pressure amplitude ( $P_0 = 0$ )

In the apparatus described here the cavitation threshold reaches 20 atm for all liquids under test such as water, transformer oil, carbon tetrachloride, and others after exposing them for a longer or shorter time to air and is independent of the dissolved air content.

Also another method to obtain a single cavitation process was studied in Göttingen (J. Schmid (10)). A water column contained in a glass tube is given a high translatory velocity which is then suddenly retarded. Thus high retardation forces are set free and the water is torn apart. To let this happen at a given point a bubble nucleus is injected by a short-time electrolysis. The process is filmed with a high-speed camera. Two examples of such registration are given in Figs. 18a and 18b. The maximal diameter of the bubbles is 1.5 and 1.2 cm respectively. The camera operates at the rate of 5000 and 63,000 frames/sec. The growth of the bubble takes about 2.5 ms, the decay about 0.9 ms. Naturally also in this case an oscillation is observed during the decay of the bubble. The growth of the bubble during the second period is diffuse and irregular in relation to space. This is generally known and was already observed by W. Güth (7) for the collapse of hot water vapor bubbles. It is worth mentioning that the implosion at the first as well as at the second collapse of the bubble is so violent that the radiated shock waves can directly be photographed without any schlieren optics (Fig. 18c). Figure 18c shows that there is a number of implosion centers which are located close together but act in temporal succession.

#### RELATION BETWEEN PRESSURE AND LUMINESCENCE FOR VIBRATION CAVITATION

Closely related to sonic or ultrasonic cavitation is sonoluminescence, this being the phenomenon that small oscillating gas bubbles contained in the liquid emit light.

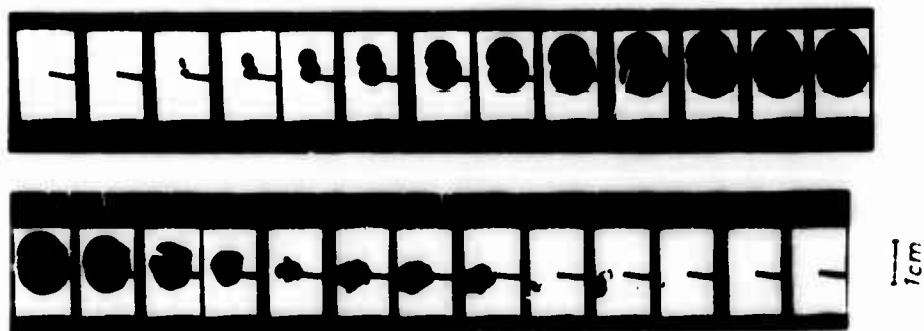


Fig. 18a - Cavitation excited by the sudden retardation of a fast moving water column. Repetition frequency, 4800 frames/sec. Maximum diameter of the bubble about 1.5 cm. Time of growth about 2.5 ms. Time of decay about 0.9 ms (without rebound).

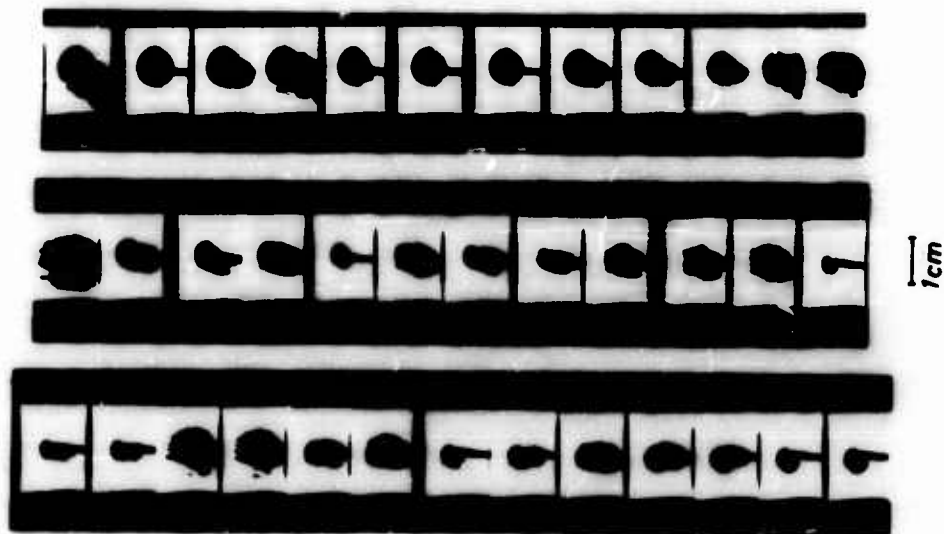


Fig. 18b - Decay and rebound of a bubble. Repetition frequency, 65,000 frames/sec. Maximum diameter of the bubble about 1.2 cm.

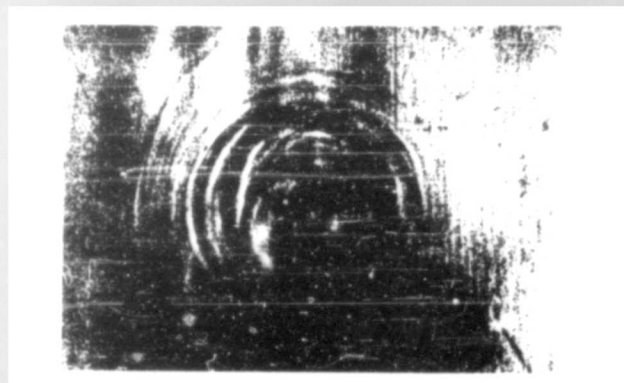


Fig. 18c - Shock waves radiated by collapsing bubbles without Schlieren optics

The sonoluminescence has often been the subject of investigations, and there are a number of theories trying to explain it. One of them is the "hot-spot theory." According to this theory the gas in a collapsing bubble is exposed to an extremely high compression and is consequently heated up, thus emitting light. Another theory starts with the separation of electric charges at the surface of a bubble when this is torn apart; the gas discharge inside the bubble is the decisive effect. Also the chemoluminescence and the triboluminescence are discussed in this connection. Now very recently W. U. Wagner has in our institute completed a series of experiments.

His experimental setup is in principle arranged as in Fig. 19. A quartz crystal with a resonance frequency of 260 kc/s generates standing ultrasonic waves in front of a  $\frac{1}{4}$  metal reflector. With a very small barium titanate microphone (M) with a volume of 1 mm<sup>3</sup>, carefully isolated acoustically from the leads and its mounting, the alternating sound pressure is measured. The microphone can be moved in the field of standing waves. The tiny gas bubbles oscillating probably below their resonance frequency are collected in the pressure maxima of the standing wave. This effect is, of course, generally known and it can again clearly be seen in Fig. 20 showing the emission of light. One might, in this case, speak of a radiating grating made up of a great number of separate light sources, namely, the light-emitting bubbles. Because of the alternating phase only every second row of radiating bubbles in the standing wave is focused (L) on a photomultiplier (PM) by means of a suitable grating (G). The microphone, sensitive to sound pressure, is situated in one of those pressure maxima, which are used "optically." Pressure and underpressure indication of the microphone have been carefully determined with several calibration methods. On the screen of an oscilloscope the alternating sound pressure as well as the emission of light are registered simultaneously.

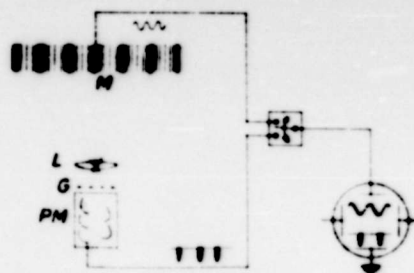


Fig. 19 - Schematic of the experimental setup for the investigation of sonoluminescence: M, microphone; G, grating; PM, photomultiplier; L, lens

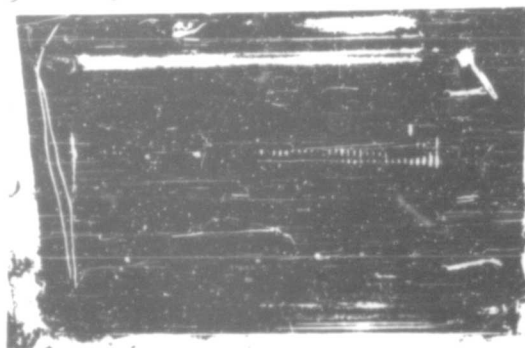


Fig. 20 - Sonoluminescence in a standing wave

Wagner found out that the emission of light is certainly not constant with time, as is the case when, for example, Luminol is added to the water, but that it is emitted in pulses. The most important result, however, is that the emission of light coincides rather accurately with respect to time with the underpressure phase of the alternating sound pressure (Fig. 21). These measurements were carried out in water saturated with air or with krypton. In the case of krypton the luminescence is considerably stronger. In Fig. 21 the upper oscillogram gives the course of the sound pressure and the lower one the corresponding output voltage of the photomultiplier. In the sound-pressure diagram, overpressure is always plotted upwards.

In Fig. 21 the temporal duration of the emission of light is relatively long, which is probably due to statistical fluctuations of the cavitation as well as the emission of light. The sound pressure curves are often distorted because of the cavitation, and without cavitation there is no luminescence. But also in the case of a more sinusoidal course of the sound pressure light pulses are observed. With proper exciting conditions the light pulses can be short and high.

It must be mentioned that the measuring curvette allows for variation of static pressure and temperature of the liquid under test. Most of the figures given here were made with an overpressure of 0.5 atm. At very high overpressures cavitation is prevented and also luminescence is not to be observed anymore.

This is just a short summary of the results of the investigation. They show that the hot-spot theory probably does not hold true in this case, since the luminescence

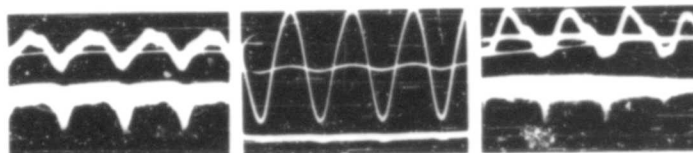


Fig. 21 - Sound pressure and luminescence. Upper oscillogram: sound pressure (overpressure upwards). Lower oscillogram: output voltage of the photomultiplier.

does not coincide with the overpressure phase. But there is the preassumption that the bubbles are smaller than the resonance size, i.e., that they are vibrating in phase with the sound pressure, which is not known with certainty.\*

## SURFACE TENSION AND SURFACE VISCOSITY

Surface tension and an eventual surface viscosity may play an essential part for the nucleation in the liquid, and I will go into the particulars of a new work by W. Eisenmenger (12) dealing with the dynamic surface tension and a potential surface viscosity in liquids. During the recent years we have made several approaches to this problem at Göttingen. In the beginning the problem was studied with gas bubbles in liquids, especially very small bubbles, where the surface tension has a decisive influence on the resonance frequency. The logarithmic decrement of the natural vibration of the bubble was measured. Unfortunately these measurements, which were made with all sizes of bubbles down to very small ones with a resonance frequency of about 300 kc/s, show that the high thermal damping in the gas contained in the bubble makes any statement about the surface viscosity impossible. One thing was learned from these experiments: one has to make a really free surface and to use capillary waves at the boundary surface between liquid and air. This has been tried formerly, but without much success. In our case the trick is to excite rheolinear oscillations of the surface with the help of a parametric excitation: a small volume of water is set vibrating vertically and the exciting amplitude is increased until at a critical amplitude capillary waves occur at the surface. The frequency of these capillary waves is one half of the exciting frequency.

The plane capillary wave is described by

$$y = a \cdot \sin(\omega t) \cos kx$$

where  $a$  is the amplitude. The onset of the capillary waves is given by the solution of a Mathieu differential equation in the first ranges of instability:

$$\frac{d^2 y}{dx^2} + 2 \left( 1 - \frac{1}{2} \cos 2x \right) \frac{dy}{dx} + \left( \frac{1}{2} - \frac{1}{2} \cos 2x \right) y = 0.$$

Here  $\frac{1}{2} \cos 2x$  is the capillary wave frequency, in which  $\tau$  is the surface tension and  $\rho$  is the density,  $h \cos \frac{1}{2} x$  is the exciting oscillation of the water volume, and  $\eta$  is the viscosity damping. For small capillary wave amplitudes,  $\eta = 2 \cdot k^2$ , where  $\eta$  is the viscosity and  $k$  is the wave number. The solution of the above equation renders for the onset amplitude of the rheolinear oscillation the expression

$$h_{\text{onset}} = 2 \sqrt{\frac{\tau}{k}}$$

This onset amplitude  $h_{\text{onset}}$  of the exciting frequency is given by the surface tension  $\tau$  and the viscosity  $\eta$ .

\*Since the preparation of this manuscript some other observations have been made. For very low frequencies (2 kc/s) a relatively strong luminescence has been found too, in water, in glycol and in glycerine. In this case the phase of luminescence did not coincide with the underpressure phase. Therefore, it was necessary to coordinate the phase of the bubble motion and the phase of luminescence. The result is that the luminescence pulses coincide with the collapsing bubbles, more precisely with the last collapsing bubble out of a larger number of bubbles (cf. Meyer and H. Rottkuhl (11)).

When the amplitude  $h$  of the exciting vibration is increased over the critical point of onset  $h_0$ , the capillary wave amplitude  $a$  follows this law:

$$\frac{h-h_0}{h_0} = C \frac{a^2}{2}$$

where  $C$  is a constant. In other words, the damping of the capillary waves has an amplitude- and frequency-dependent additional expression of the form

$$\left(1 + C \frac{a^2}{2}\right)$$

where  $C$  is, according to the theory of Klemm, given by

$$C = \frac{2}{s} \frac{\nu^2}{k}$$

where  $\nu$  is introduced by Klemm as a surface viscosity. Unfortunately in the expression for  $a = h - h_0$ , that is, in the constant  $C$ , a further additional expression has to be added, given by the second power of the normal viscosity damping. This term is, however, independent of frequency.

The experimental setup is very simple in principle. For frequencies up to about 200 kc/s hollow barium titanate cylinders with Mason horns attached to them were

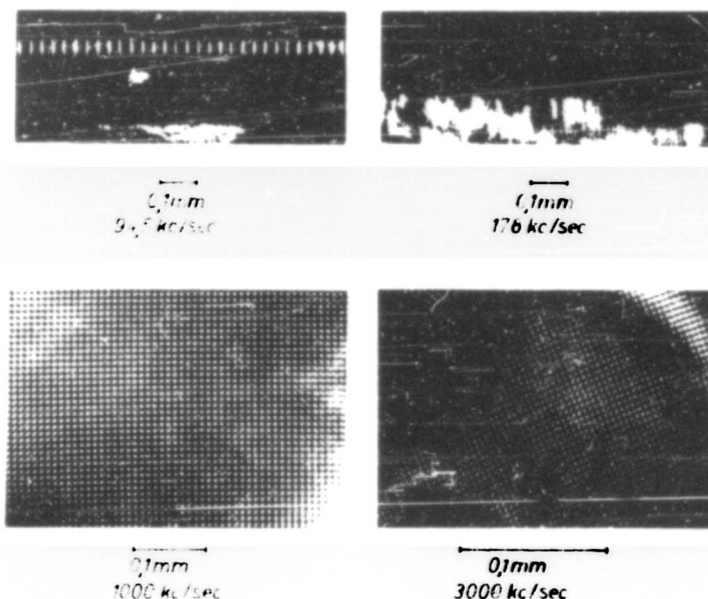


Fig. 22. Capillary waves generated by parametric excitation.

used. There are small grooves at the tops of the Mason horns filled with water. Thus plane capillary waves are forcibly excited. The absolute amplitude ( $h$ ) of the exciting Mason horn is measured electrostatically with a second Mason horn. The amplitude ( $a$ ) of the capillary waves is determined optically from the reflection of a light beam at the steepest parts of the sinusoidal capillary wave.

In the frequency range from 400 kc/s to 3 Mc/s concave barium titanate shells filled with water are used. A very thin, platinized copper foil is placed in the focal plane of the shell so that a water droplet on its surface is at the focal point. In the first case plane capillary waves are excited in the grooves; in the second case the capillary waves generated have the form of crossed gratings. Examples for both cases are found in Fig. 22 for exciting frequencies of 94.5 kc/s, 178 kc/s, 1 Mc/s, and 3 Mc/s. Photographs of this kind allow for an easy measurement of the capillary wavelength and for the determination of the surface tension therefrom. In Fig. 23 this was done for a larger frequency range (up to  $\lambda = 1.5$  Mc/s) in pure water for the onset amplitude of the oscillation, i.e., for a capillary wave amplitude  $a = 0.01$ . In another case the same measurements were made with a higher amplitude  $a = 0.12$  and there it became obvious, as a first result, that the surface tension is amplitude dependent, but this only at higher frequencies. This effect is obviously caused by the fact that the filling-in of the extended surface with water molecules from inside the liquid needs a certain time.

It is also not without interest that the measured onset amplitude  $h_0$  of the capillary waves, substantially given by the viscosity of the medium, satisfies the equation

$$h_0 = \sqrt{\frac{4\eta}{\rho \lambda}}$$

very well. In Fig. 24 the measured values are compared with the theoretical curves for  $\tau = 75$  dyne-cm<sup>-1</sup>,  $\eta = 20$  cP, and  $\rho = 10^{-2}$  dyne-cm<sup>-2</sup>-sec for the given frequency range.

The relation between exciting amplitude  $h$  and capillary wave amplitude  $a$  for values up to  $a = 0.12$  is treated very thoroughly for 41 kc/s. The curve is displayed in Fig. 25. Given as abscissa is the exciting amplitude  $h$  or  $ch = h_0 + h_1$ . The curve

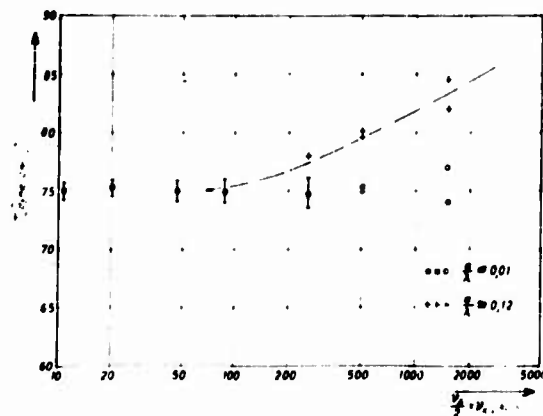


Fig. 23 - Surface tension on impure water as a function of frequency and amplitude

E. Meyer

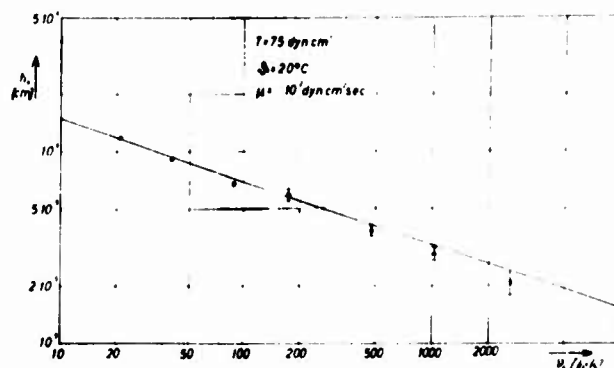


Fig. 24 - Onset amplitude of the exciting oscillation as a function of the exciting frequency for pure water

is in very good agreement with the theoretical relation. For the constant  $C$ , introduced above, one finds  $C = 16.7$ . The respective values for other liquids with different surface tensions are of the same order of magnitude.

It is only necessary to determine the constant  $C$  for water for a number of frequencies in order to find out about a potential surface viscosity. It is thereby stated that for water the frequency dependence is very small and that a potential surface viscosity is certainly smaller than  $10^{-5}$  dyne-cm $^{-1}$ -sec.

Realizing that a higher surface viscosity, as it was supposed by other authors, was not found in water, the question arises whether the admixture of surface active substances would render a higher frequency dependence of  $C$ , thereby also indicating a higher surface viscosity. Therefore different concentrations ( $10^{-4}$  and  $10^{-1}$  weight percent) of an emulgator (Renex 688) and two wetting agents (Hostapal and Tween 80) were examined. In this case the whole range of amplitudes of the capillary waves as

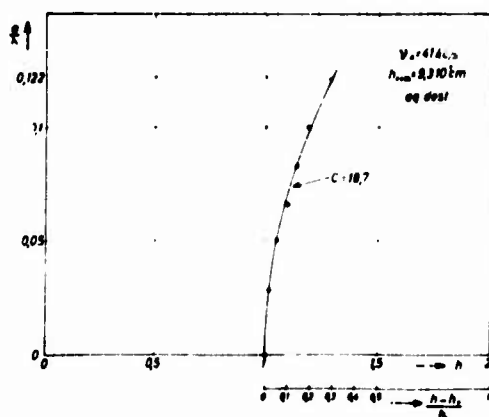


Fig. 25 - Capillary wave amplitude as a function of the exciting amplitude



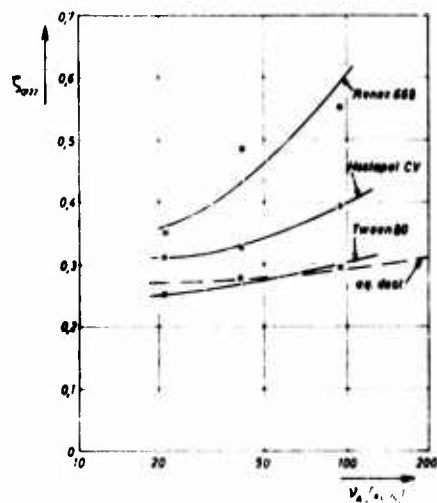


Fig. 26 - Relative difference of the exciting amplitude  $(h-h_0)/h_0$ ,  $a = 0.122$  as a function of the frequency for different surface-active substances. Capillary wave amplitude  $a = 0.122$ .

a function of the excitation was not measured. Only the onset amplitude  $h_0$  and the exciting amplitude  $h$  for a given ratio  $a = 0.122$  was examined. The corresponding value  $(h-h_0)/h_0$ ,  $a = 0.122$  is plotted in Fig. 26 versus frequency. The considerable frequency dependence of Renex 688 is evident. Here we find a surface viscosity of about  $1 \cdot 10^{-4}$  dyne-cm<sup>-1</sup>-sec, being much higher than for "pure" water.

The above paper contains a short survey of some investigations specializing on sonic and ultrasonic cavitation carried out in Göttingen. I do hope, that some of the results might be of general interest.

#### REFERENCES

1. Lange, Th., "Methoden zur Untersuchung der Schwingungskavitation in Flüssigkeiten mit Ultraschall," *Acustica* 2:AB75 (1952)
2. Esche, R., "Untersuchung der Schwingungskavitation in Flüssigkeiten," *Acustica* 2:AB208 (1952)
3. Bohn, L., "Schalldruckverlauf und Spektrum bei der Schwingungskavitation," *Acustica* 7:201 (1957)
4. Güth, W., "Nichtlineare Schwingungen von Luftblasen in Wasser," *Acustica* 6:532 (1956)
5. Koppelman, J., "Beiträge zur Ultraschallmesstechnik in Flüssigkeiten," *Acustica* 2:92 (1952)

E. Meyer

6. Mundry, E. and Guth, W., "Kinematographische Untersuchungen der Schwingungskavitation," *Acustica* 7:241 (1957)
7. Guth, W., "Kinematographische Aufnahmen von Wasserdampfblasen," *Acustica* 4:445 (1954)  
Guth, W., "Zur Entstehung der Stosswellen bei der Kavitation," *Acustica* 6:526 (1956)
8. Olaf, J., "Oberflächenreinigung mit Ultraschall," *Acustica* 7:253 (1957)
9. Kurtze, G., "Über die Bedingungen für das Auftreten von Kavitation," *Nachrichten Akademie der Wissenschaften in Göttingen, Math. Nat. Klasse, No. 1*, 1958
10. Schmid, J., "Kinematographische Untersuchung der Einzelblasen-Kavitation," *Acustica* 9:321 (1959)
11. Meyer, Erwin, and Kuttruff, H., "Zur Phasenbeziehung zwischen Sololumineszenz und Kavitationsvorgang bei periodischer Anregung," *Z. f. angew. Phys.* 11:325 (1959)
12. Eisenmenger, W., "Dynamic Properties of the Surface Tension of Water and Aqueous Solutions of Surface Active Agents with Standing Capillary Waves in the Frequency Range from 10 kc/s to 1.5 Mc/s," *Acustica* 9:327 (1959)

. . . . .

## DISCUSSION

T. Brooke Benjamin (University of Cambridge)

I wish to comment upon the formation of capillary waves on the surface of a mass of liquid which is contained in a vessel undergoing vertical vibrations. This was the subject of a paper by Ursell and myself and the problem has continued to interest me since it appears to exemplify very nicely a general class of phenomena, many instances of which arise in practical acoustics. For example, Murray Strasberg and I have shown that the waves in question have counterparts in the behavior of small bubbles undergoing radial pulsations in response to a sound field: such bubbles may develop large nonspherical oscillations when the amplitude and frequency of the radial motion take certain values, and the explanation which we suggested is the same, exactly, in principle as that for the waves on a plane free surface.

I think it may be of interest to remark that the mechanism of these waves was the subject of a historic controversy extending well over a century. They were first studied by Michael Faraday about 130 years ago. He observed that a pattern of standing waves sometimes appeared on a layer of liquid covering a vertically vibrating plate, and he noticed that the frequency of the waves was only one-half that of the plate. About 50 years after, the famous German physicist Matthiessen re-investigated the problems and found in his experiments that the waves were synchronous with the

vibrations of the vessel. The discrepancy between this and Faraday's result led Lord Rayleigh to make a further series of experiments, which supported Faraday's observation. You may recall, incidentally, that Rayleigh gave to the waves the appealing term "crispations": this term will perhaps be remembered by anyone familiar with Rayleigh's textbook "Theory of Sound."

The theory set out in the paper by Ursell and myself appeared, happily, to reconcile the observations of Faraday and Rayleigh and those of Matthiessen; for it was shown that both half-frequency and synchronous waves can be generated in suitable circumstances. The essential explanation of these waves, and also of the many similar phenomena which I wish to keep in view here, can be summarized without need for much mathematics.

I think that to emphasize the general character of the explanation we should consider any mechanical system in which free vibrations are possible in certain normal modes. Now, suppose that one of the physical parameters of the system is made to vary in simple-harmonic fashion with time through the action of some external agency. (We may consider, to fix our ideas, that the parameter varied is one that would enter the equation for the frequency of the normal modes: e.g., it is a stiffness or inertial coefficient.) Now, with this modification, small displacements in the system will be determined by an equation of motion having at least one periodic coefficient. This equation will be linear, of course, provided the displacements are small enough and, in the absence of dissipation, it will nearly always be reducible to Mathieu's equation, whose standard form may be written

$$\frac{d^2 x}{dt^2} + (p - 2q \cos 2t) x = 0.$$

In general,  $x_0$  is the amplitude of, say, the  $n$ th mode of disturbance, and  $T = 2\pi/\omega$  is the frequency of the applied oscillation. Also, the parameter  $q$  is proportional to the amplitude of this oscillation, and  $p = 2\pi^2 \nu_n^2 T^2$  where  $\nu_n$  is the frequency of free vibrations in the  $n$ th mode.

Now, the general solution of Mathieu's equation is known to be unstable for certain values of  $p$  and  $q$ , i.e., it becomes unbounded as  $T \rightarrow \infty$ , and this provides the explanation of why the mechanical system in question may spontaneously develop large oscillations. The stability chart is sketched in Fig. D1: the diagram is symmetrical about the  $p$ -axis, and the third and fourth quadrants do not concern us here. (Note that when  $p = 1$ , i.e., when  $\nu_n = 2\nu$ , instability is possible for small values of  $q$ .)

When  $p = 4$ , instability may again occur for small values of  $q$ , and the developed frequency is then  $\nu$ , i.e., the applied and developed oscillations are synchronous.

In the capillary wave problem, the disturbed motion of the free surface is the same as if the

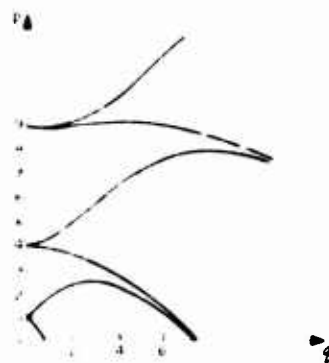


Fig. D1. Stability chart for Mathieu's equation. The shaded regions are stable, the unshaded regions are unstable.

E. Meyer

vessel were at rest, and the gravitational acceleration were given a periodic component in addition to the constant  $g$ . We now see that the plane, free surface becomes unstable when the amplitude and frequency of this component have the appropriate values. The waves are not, of course, forced vibrations in the usual sense; they develop quite suddenly as  $p$  or  $q$  is varied so as to bring the point  $(p, q)$  into an unstable region of the stability chart, and they grow in amplitude until eventually they are restrained by non-linear effects, not so far considered, or until the free surface disintegrates.

The effects of friction tend, of course, to inhibit the growth of waves. For instability to occur in practice, the point  $(p, q)$  must lie somewhere inside an unstable region of the chart, so that the rate of growth of the frictionless solution exceeds the rate of frictional damping. Thus, as Professor Meyer has pointed out in his paper, an estimate of the damping can be obtained from a careful experimental observation of the onset of instability. In my own experiments on these waves, the frequency of the vessel was about 30 cycles per second, which is considerably less than in the experiments at Göttingen. In mine, most of the damping was evidently due to the boundary layer at the sides of the vessel and was quite small. I was unable to get a good agreement between experimental and theoretical estimates of the rate of damping, and I concluded that the discrepancy was mainly due to extra dissipation in the vicinity of the meniscus at the edge of the free surface. However, I am very pleased to learn that at Göttingen this method has given satisfactory measurements of the damping at high frequencies.

E. Meyer

The point here is that this is not only the damping of this surface, but also the damping given by the normal damping, i.e., by the viscosity of the liquid itself. Then there is an additional term, the damping by the surface, and this is very difficult to separate. There is also a quadratic term for the normal damping and you have to distinguish this from the surface damping. The distinguishing term is the frequency.

\* \* \* \* \*

# CAVITATION NOISE

Hugh M. Fitzpatrick

*David Taylor Model Basin*

\*      \*      \*      \*      \*

Many of the features of cavitation noise may be illustrated by consideration of the pressure field surrounding an idealized spherical cavity growing and collapsing in an incompressible fluid. The pertinent hydrodynamic relations are reviewed and extended to the computation of the frequency spectrum of the sound. Some criteria for the limits of applicability of the incompressible theory are given.

\*      \*      \*      \*      \*

## INTRODUCTION

This paper is concerned with the sound pressure generated by a growing and collapsing cavity in a liquid, for example, a cavity which, in the flow of the liquid past a curved rigid boundary, grows in a region of low pressure and subsequently collapses in a region of higher pressure downstream. The existence, circumstances, and typical behavior of such cavities have been so fully discussed in the literature (1,2,3) as to require no further elaboration here. The discussion will be restricted to those aspects of the sound which may be elucidated by consideration of spherical cavities. In the earliest history of the study of the dynamics of cavitation, the concept of a spherical cavity was recognized as a useful idealization. Thus, Rayleigh's famous solution (4) gives the motion of an empty spherical cavity in an incompressible liquid of infinite extent with constant external pressure. More recently, Rayleigh's concept has been extended to allow for time-varying external pressure and the bubble motions so computed have been shown to correspond reasonably well with actual behavior of cavities which grow and collapse in fluid flow (5). The present work, without adding anything new in principle, extends the description to include the pressure radiated by the growing and collapsing cavity.

## HYDRODYNAMIC RELATIONS

The relation between the radial motion of a growing and collapsing cavity and the pressure in the surrounding liquid have been treated extensively in the literature relating to cavitation and to underwater explosions—at least for the case of incompressible flow of the liquid (6, 7). It will be useful to take the relation valid for incompressible flow as our focal point since during the whole of the period of growth and the greater part of the collapse of the cavity the incompressible theory adequately describes not only the motion of the cavity but also the sound pressure which

H. M. Fitzpatrick

appears (after an interval of time) at a distance. Accordingly, we note the relation for incompressible flow (6):

$$p(r, t) = p(r, t) + \frac{R^2 \ddot{R}}{r} + 2 \frac{R \dot{R}^2}{r} + \frac{R^4 \dot{R}^2}{2r^4} \quad (1)$$

Here,  $p(r, t)$  is the pressure in the liquid at radial coordinate  $r$  and time  $t$ ;  $\rho$  is the density of the liquid;  $R$  (equal to  $R(t)$ ) is the radius of the cavity at time  $t$ ; and  $\dot{R}$  and  $\ddot{R}$  are the first and second time derivatives, respectively, of  $R$ .

In the special case,  $r = R$ , Eq. (1) gives the differential equation relating the growth and collapse of the cavity to the "driving pressure"  $P - p_0$ :

$$R\ddot{R} = \frac{3}{2} \dot{R}^2 \quad P = p_0. \quad (2)$$

Here,  $p$  has been written for  $p(R, t)$  and  $p_0$  for  $p(-, t)$ .

At a sufficiently great distance from the cavity, the second term on the right side of Eq. (1) is negligible. The remaining pressure will be called the sound pressure,  $p$ :

$$P_s = \frac{R}{2} \ddot{R} + 2\dot{R}^2 \quad (3)$$

or, identically,

$$p_{\alpha} = 3r \frac{d^2 R^3}{dt^2} \quad (4)$$

Thus, the sound pressure associated with the growth and collapse may be computed from the motion of the cavity or, indirectly, from the environmental pressure which the cavity encounters.

## THE CAVITY MOTION

In general, if the pressure difference  $P - p_0$  is given as a function of  $R$  and  $r$ , Eq. (2) can be integrated (to find  $R(r)$ ) only by nonanalytic methods (5,9). Exceptions are two special cases discussed by Rayleigh (4,6).

In the case of an "empty" cavity collapsing or rebounding under the influence of a time-varying external pressure, positive and equal to  $P$  at the instant of complete collapse, a series solution useful in describing the motion in the region of collapse and rebound may be obtained in the form

$$\frac{R}{R_1} = \sum_{i=1}^N A_i \left( \frac{1}{R_1} + \frac{1}{P_i} \right)^{-1} \quad (5)$$

$P_0$  is the initial pressure in the liquid before the pressure in the liquid at the end of the initial stage is transferred to the vapor. During the collapse of vapor cavities in the liquid the pressure in the liquid is contained in the cavity, since the velocity of the collapse is much greater than the velocity of the sound in the liquid. The pressure in the cavity is equal to the initial pressure  $P_0$  in the liquid.

### Cavitation Noise

Here,  $R_1$  is a radius characteristic of the motion at collapse and defined so that the limiting value approached by the kinetic energy

$$E = R_1^3 \dot{R}^2$$

at collapse is equal to  $4/3 R_1^3 P$ . The time  $t_c$  is the instant of collapse.

The coefficients  $A_n$  may be evaluated by substituting Eq. (5) in Eq. (2) and equating the coefficients of like powers of  $(t - t_c)$ . Thus, if the time-varying pressure difference is expressed as a power series:

$$p_c = P - P' = 1 + \sum_{n=1}^{\infty} A_n \frac{(t - t_c)^n}{R_1^3 P} \quad (6)$$

The coefficients are given below

$n$	$A_n$	$n$	$A_n$	$n$	$A_n$
2	1.330325	18	-0.05593 $\frac{1}{2}$	24	-0.0139 $\frac{1}{2}$
8	-0.284733	19	-0.02689 $\frac{1}{2}$		-0.00516 $\frac{1}{2}$
13	-0.106775 $\frac{1}{2}$	20	-0.009007 $\frac{1}{2}$	25	-0.010133 $\frac{1}{2}$
14	-0.035848	23	-0.034418 $\frac{1}{2}$	26	-0.002810

For other values of  $n$ , ( $n > 26$ ),  $A_n = 0$ .

The series converges rapidly enough to provide a useful solution of Eq. (2) for the period of collapse and the period of growth after rebound. For the purpose of describing the later stages of collapse, one or two terms of the series suffice.

### THE SPECTRUM OF THE SOUND PRESSURE

Typical behavior patterns for the growth, collapse, and multiple rebound of a cavity and for the pulse of sound pressure have been shown in a previous survey (8). The spectral distribution of the energy radiated as sound may be determined by means of the Fourier transformation applied to the sound pulse. Let  $p_s(r, t)$  be the sound pressure\* which appears at radial coordinate  $r$  at time  $t$ . Then a Fourier transform  $S(\omega, r)$  corresponding to the sound pressure is defined by

$$S(\omega, r) = \int_{-\infty}^{\infty} p_s(r, t) e^{-i\omega t} dt \quad (7)$$

A spectral density  $s(\omega, r)$  describes the distribution of the sound "energy" with respect to frequency,

$$s(\omega, r) = 2\pi |S(\omega, r)|^2 \quad (8)$$

\*For the purposes of this paper, the limiting value of the kinetic energy of a cavity, characterized by the total energy  $E = 4/3 R_1^3 P$ .

The dependence of the sound pressure on the radial coordinate  $r$  is of course, largely immaterial to the present study. The only point of interest is that the sound pressure is a function of  $r$  and  $t$ .

H. M. Fitzpatrick

In order to consider the actual energy radiated acoustically, it is necessary to depart from the assumption of incompressibility of the liquid to the extent necessary to include the process of acoustic propagation. According to the usual laws of acoustics, the energy radiated in a band of frequencies  $\omega$  will be

$$\frac{4}{c} \int_{\omega}^{\omega + \Delta\omega} S_{\text{rad}}(\omega) d\omega$$

and the total radiated energy

$$\frac{4}{c} \int_0^{\infty} S_{\text{rad}}(\omega) d\omega$$

equals

$$\frac{4}{c} \int_0^{\infty} \dot{r}^2 \omega^2 d\omega$$

Here,  $c$  is the velocity of propagation of sound in the liquid.

#### THE LIMITATION OF INCOMPRESSIVE THEORY

The use of incompressive flow theory (to determine the gross flow and the pressures) and the laws of acoustics (to account for the radiation) represents the slightest possible departure from strictly incompressive theory. A crude criterion for applicability of this procedure in estimating the sound pressure radiated by a collapsing empty cavity is that the wall velocity not exceed about one tenth of sonic velocity. Substitution of this condition ( $\dot{r}/c = 0.1$ ) in Eq. (5) results in values of the radius and "time before collapse" as given by

$$\frac{R}{R_1} = \frac{1}{4} \left[ \frac{P_{\infty}}{c^2} \right]^{1/3} \quad (9)$$

and

$$\frac{t - t_0}{R_1 / P_{\infty}^{1/2}} = 16 \left[ \frac{P_{\infty}}{c^2} \right]^{5/6} \quad (10)$$

The value of  $c^2$  for water is approximately 21,000 atmospheres. Equation (9) shows that the collapse of a cavity under an external pressure of one atmosphere or more begins to be influenced by the compressibility of the water while the radius of the cavity is still as large as one-sixth of its maximum value. At that stage, the effect of the vapor and the minute amount of gas ordinarily contained in the cavity is quite negligible. Thus, whatever mechanisms are involved in the collapse and rebound, the compressibility of the liquid plays a primary role.

Equation (10) gives a rough criterion for the range of frequency for which the sound-pressure spectrum, computed according to the incompressive theory, is valid. It may be assumed that the details of the pulse of sound pressure associated with the



# Cavitation Noise

part of the motion where compressive effects are present do not greatly affect the spectrum for frequencies several times smaller than the reciprocal of the time interval appearing in the numerator in Eq. (10). If the numerical factor is taken, conservatively, to be 4, it follows that the required upper limit on the frequency is

$$0.005 \frac{P_0}{R_1} \approx \left[ \frac{c^2}{P_0} \right]^{\frac{5}{6}}$$

A number of investigators have presented theories which take into account, in some degree, the effects of compressibility and which show remarkable agreement with experiment in certain respects (9,10). A full explanation of the generation of cavitation noise awaits a solution of the flow problem involved not only during the later part of the collapse but also during the early part of the rebound.

## REFERENCES

1. Mueller, H., "Über den gegenwertigen Stand der Kavitationsforschung," Die Naturwissenschaften, 16:No. 22 (1928)
2. Knapp, R.T., and Hollander, A., "Laboratory Investigations of the Mechanism of Cavitation," Trans. A.S.M.E. 70:419 (1948)
3. Parkin, B., "Scale Effects in Cavitating Flow," Calif. Inst. Tech. HL-CIT Report 21-7, December 1951
4. Lord Rayleigh, "On the Pressure Developed in a Liquid During the Collapse of a Spherical Cavity," Phil. Mag. 34:94 (1917)
5. Plessett, M.S., "Dynamics of Cavitation Bubbles," App. Mech. 16:277 (1949)
6. Lamb, H., "Hydrodynamics," New York:Dover Publications (1945)
7. Kennard, E.H., "Radial Motion of Water Surrounding a Sphere of Gas in Relation to Pressure Waves," Taylor Model Basin Report 517, September 1943
8. Fitzpatrick, H., and Strasberg, M., "Hydrodynamic Sources of Sound," Naval Hydrodynamics, Publication 515, National Academy of Sciences, National Research Council, 1957
9. Keller, J.B., and Kolodner, I., "Damping of Underwater Explosion Bubble Oscillations," J. App. Phy. 27:1152 (1956)
10. Gilmore, F.R., "The Growth and Collapse of a Spherical Bubble in a Viscous Compressible Liquid," Hydro. Lab. Calif. Inst. Tech. Report 26-4, April 1952

\* \* \* \* \*

# PRESSURE WAVES FROM COLLAPSING CAVITIES

L. Brooke Benjamin  
*University of Cambridge*

The topic of this paper relates to the practical problem of noise generated in the collapse phase of cavitation. The account is mainly theoretical; but a brief reference is made to some recent experiments on isolated vapour bubbles. The compressibility of water is pointed out to be an essential consideration in this aspect of cavitation, and a certain property of observed cavitation noise spectra is interpreted as evidence of the presence of shock waves. A method is demonstrated whereby a theory of the collapse of cavities in compressible liquids can in principle be developed to an arbitrary degree of accuracy; and the second-order approximation is presented as illustration. This approximation is definite in the sense that all second order effects are correctly represented, and it reveals an error in the Kirkwood-Bethe hypothesis on which much previous work on this problem has been based. The second-order theory is shown to admit the possibility that, as a consequence of compressibility of the liquid, the collapse of an empty cavity may be concluded at a finite radial velocity. However, even though this possibility remains when higher approximations are worked out, the author now considers it to be unlikely. Some very recent ideas on this matter, which have been developed since the first draft of this paper was written, are summarized in an appendix.

A feature of the present theory is that it accounts in a straightforward manner for nonlinear distortion of the transmitted pressure wave. The conditions under which the wave radiated from a pulsating gas-filled cavity will develop a shock front are examined; and a simple practical criterion for shock formation is derived.

## 1. INTRODUCTION

Notwithstanding the variety of means by which transient cavitation may be generated in liquids, one can in general identify three distinct phases in the history of any individual cavity. The sequence begins with its initiation from a microscopic nucleus and a brief period during which the influence of the nucleus contents remains significant. The cavity then grows to observable size, and behaves almost exactly as if it were completely empty and in an incompressible inviscid liquid. Finally, as the formative agency is removed, it collapses back to microscopic size and may then

disappear or perhaps "rebound." It is in this third phase that the more remarkable effects of cavitation arise. If the cavity contains only vapour or a very small quantity of gas, the collapse even under a very moderate hydrostatic pressure takes place with great violence: in the concluding stages enormous velocities and accelerations are attained by the intruding wall, and a large transient pressure is transmitted to distant parts of the liquid. The abruptness of such pressure pulses accounts for the sharp crackling sound which is often audible from severe cavitation, as may for instance occur in the draught-tube of a hydraulic turbine; and also much of the noise energy is contained in the ultrasonic range of the frequency spectrum. The practical importance of cavitation noise in the context of Naval Hydrodynamics need scarcely be pointed out here: it is sufficient to recall that the spectral properties of noise from severe propeller cavitation make it quite distinct from other forms of underwater noise. We may also note that the cavitation erosion is a consequence of the large pressures developed in the collapse phase.

These remarks merely rephrase some familiar ideas. To anyone interested in cavitation, the violent action of a contracting cavity is likely to form a vivid intuitive concept; and it is easy to appreciate in a qualitative way how cavitation noise pulses arise. However, this third phase of the cavitation process is by far the least amenable to precise experimental or theoretical study. On the experimental side, the extreme rapidity of the vital events makes adequate observation difficult, and a further source of difficulty is the minute size of cavitation bubbles at the stage having most interest. The theoretical side of the problem is even more formidable. Towards the end of the collapse many factors become important which can safely be assumed to be insignificant when the cavity is fully grown; and to account for them comprehensively would seem a hopeless task. Nevertheless, as in many other physical problems, a lot may be learned from even severely simplified theoretical models. The effect of compressibility of the liquid is the factor probably worth closest study, and the theoretical model of an empty spherical cavity contracting under constant pressure in a compressible liquid appears to be a primary key towards physical understanding of cavitation collapse. Other factors arising in the final stages include viscosity, in stability of the spherical form, and compression of the enclosed vapour due to delayed heat exchange with the liquid.

This paper reports some current researches on the collapse of cavities and the resulting pressure waves. The main topic considered is the effect of compressibility on the radial flow, and some new results will be summarized concerning the motion of an empty cavity and the formation of shock waves. No attempt is made to survey all that is known about this phase of cavitation; several excellent reviews of the literature are available (for instance that by Fitzpatrick and Strasberg (1)), and we may turn to these for background. Rather, the aim of this paper is to explain the objects of work still in progress and to offer some ideas about aspects of the problem which remain debatable.

Although a passing reference will be made later to some recent results from the author's experiments on isolated cavities (2), the material of this paper is mainly theoretical. This choice of subject matter reflects a belief that in the present state of the subject the greatest need is for further clarification on the theoretical side. The general physical characteristics of cavitation noise appear now to be fairly well established: for instance, there is plentiful experimental evidence that shock waves are always present when the cavitation is reasonably severe, and many measurements of cavitation noise spectra appear to comply with a well-defined general picture. This state of affairs owes notably to the careful experimental work of Mellen (3,4). On the other hand, a good deal of existing theoretical work seems open to doubt. It is not of course disputed that perfectly sound qualitative descriptions have been given of such effects as shock-wave formation (e.g., see (1)). Further, a certain measure of

success has undoubtedly been achieved in predicting the motion of a cavity over certain ranges of the radial velocity. But it remains that the theory of collapsing cavities, taking account of the compressibility of the liquid, has yet to be put on a secure foundation, so that results of a definite character can be calculated.

The valuable theoretical work of Gilmore (5), Mellen (4), and Flynn (6) has in the past gone furthest towards the solution of the present problem. All three of these authors developed their theories from the assumption, which recalls the Kirkwood-Bethe hypothesis in the theory of blast waves, that in radial flow the quantity  $r \cdot \dot{\phi}$  (where  $r$  is the radius and  $\dot{\phi}$  the velocity potential) is propagated approximately unchanged along a characteristic. The Kirkwood-Bethe hypothesis is accurate for spherical disturbances whose wavelength is small compared with radius (e.g., a blast wave in its initial stages), owing mainly to the fact that the motion is then approximately the same as in a plane wave. Again, it is accurate for weak spherical disturbances far from the centre. These facts provide some justification for the use of this assumption in the cavitation problem, when even the fluid velocities are comparable with the velocity of sound; and some further justification may be found by comparing results calculated on this basis with numerical solutions of the equations of motion (5). However, a more cautious assessment shows the assumption to be far from as well founded as one might wish. It would seem in general to represent merely a correction to acoustic theory and does not appear even to be an accurate second-order approximation (in the sense that incompressible-fluid theory comprises a zeroth-order and acoustic theory a first-order approximation). Nevertheless, although errors in the Kirkwood-Bethe hypothesis are easily detected, it is a quite different matter to assess the accuracy of complicated calculations based on it. The principal aim here is only to emphasize the need for further study, and to suggest alternative ways of dealing with the problem.

In this paper a method is given by means of which the theory of collapsing cavities in a compressible liquid can be worked out without recourse to any special hypothesis. The method is one of successive approximations, and can in principle be carried through to an indefinitely high degree of accuracy—although of course the work becomes more laborious in successive stages. The second-order approximation will be given explicitly: this is a formally correct approximation in that all possible second-order effects are properly included; and there appears to be a discrepancy between this and the theory based on the Kirkwood-Bethe hypothesis. The method is an example of Lighthill's celebrated "technique for rendering approximate solutions to physical problems uniformly valid" (7), and has previously been applied by Whitham (8,9,10) to several problems of spherically symmetric flow. Readers will recall that Lighthill's technique obviates a type of difficulty which often arises when the solution of a physical problem is attempted by a conventional perturbation method, whereby successive approximations are obtained in powers of a suitable small parameter. If the zeroth-order solution has a singularity within the domain of interest, progressively worse singularities appear in the higher-order solutions. The principle of the technique is to expand the independent variables as well as the dependent variable in terms of the small parameter, the expansion of the independent variables being evaluated term by term in the process of determining the dependent variable.

In the present application, successive approximations are made to the "characteristic" variable for outgoing spherical waves. This closely follows the work of Whitham cited above. Although the method provides a uniformly valid approximation over the whole flow field, this particular advantage may not be specially worth while in certain cases. Dr. Ian Proudman at Cambridge has recently investigated the collapse of an empty cavity by using a Lighthill-Whitham type of approximation for the "outfield," that is the region far from the cavity, yet using a more conventional

perturbation method for the "infield" adjoining the cavity wall. This course apparently leads to a considerable simplification of the work in getting higher approximations. Dr. Proudman has carried his calculations to terms involving the fourth power of the Mach number at the cavity wall, and has accordingly found fairly strong evidence that the method of approximation is convergent even when a substantial part of the flow is supersonic (although the condition of unit Mach number does not appear to have any particular physical significance in this problem).

Now, the first object of most theoretical work on the present problem is the derivation of an ordinary differential equation for the radius  $R$  of a spherical cavity as a function of time. The equation will of course be only approximate, and if the cavity is taken to be empty so that the collapse proceeds to completion, there is necessarily some uncertainty in deciding from the equation how the velocity  $|R|$  behaves in the limit as  $R \rightarrow 0$ . This uncertainty derives from the fact that although the behaviour  $|R| \rightarrow \infty$  is always indicated as a possibility, the method of approximation leading to the equation for  $R$  breaks down for very large velocities. (We recall that the terminal velocity is definitely infinite according to Rayleigh's theory (11) which neglected the compressibility of the liquid.) However, on the basis of the second-order theory presented below, it will be shown that another possibility, which is perfectly consistent with the overall approximation, is that  $|R|$  has a finite value as  $R \rightarrow 0$ , a result which apparently has not been noted before. This remains a consistent interpretation on the basis of the more accurate calculations worked out by Dr. Proudman—which seem to give by far the most complete analytical results yet available; and since the apparent terminal velocity is not especially large, being not much greater than the velocity of sound in the undisturbed liquid, there would appear to be reasonably strong evidence in favour of this conclusion. (It may be noted that previously obtained approximations to the equation for  $R$ , such as Gilmore's (5), also admit this conclusion when the solution is appropriately interpreted.) At the time of writing the first draft of this paper, the author was strongly inclined to the view that an empty cavity does have a finite velocity of collapse; but upon further reflection this conclusion now appears doubtful. The main reason for this change of mind was a numerical calculation performed with the EDSAC II computer. The results indicate that the velocity of collapse of an empty cavity increases indefinitely; and although this indication is not yet conclusive, since there is still some slight uncertainty about the control of errors during the computation, the need has obviously arisen for thinking again. Some recent considerations concerning the asymptotic behaviour of a collapsing empty cavity are summarized in the Appendix to this paper; work now in progress along these lines seems to be leading to a final clarification of the interesting theoretical question of how the collapse is concluded.

Nevertheless, though this question may at first sight seem crucial and the idea of a finite terminal velocity may now seem a possible serious misinterpretation from the point of view of the physical application of the theory, the matter is after all not particularly important physically. The more important conclusion is that in any case the energy of the motion near the centre towards the end of the collapse becomes vanishingly small; the greater part of the overall energy has already been stored in a compressive wave well before the collapse is terminated, and so what happens in practice very close to the centre may well have an insignificant effect on the wave as observed from a distance. This conclusion is important since it implies that there is often justification for neglecting the additional physical factors arising near the end of a collapse, such as viscosity and vapour compression.

An advantage of the theory to be presented is that it provides a very simple description of shock-wave formation by rebounding gas-filled cavitation bubbles, and leads easily to an estimate of how severe a collapse need be for a shock wave to develop (mild "gassy" cavitation may of course still give rise to brief noise pulses;

but a typical pressure wave will not have a shock front). The generation of shock waves is a feature of cavitation which has practical importance in several ways, notably in relation to cavitation damage. In the next section of the paper we digress slightly from the main discussion to comment on another effect attributable to this cause.

## 2. THE EFFECT OF THE PRESENCE OF SHOCK WAVES ON CAVITATION NOISE SPECTRA

Discounting experiments where isolated cavities are generated by special means (4,12,13), cavitation is in most circumstances an erratic process during which a large number of transient cavities appear in scattered positions throughout the region under reduced pressure. The behaviour of individual cavities with an irregular assembly can sometimes be observed, as was done by Knapp and Hollander (14); but in measurements of the radiated noise, the contribution from any particular cavity is generally impossible to identify. Determination of the frequency spectrum is then the most useful object of noise measurements, and reasons can be found for supposing that the spectrum of the aggregate of the received pressure waves is not widely discrepant from the spectrum of a typical component pulse (we note that the spectrum of a random sequence of similar pulses has the same form as the spectrum of a single pulse). Thus, theoretical spectra calculated on the basis of single-cavity models may be relevant to observed cavitation noise (3); and indeed a fair measure of agreement has established (1).

A usual feature of measured energy spectra is a slope of approximately -6 db octave at high frequencies, i.e., the spectral density varies as  $\omega^{-2}$ , where  $\omega$  is frequency. It has often been pointed out that this feature can be explained by the presence of shock waves in the received pressure signals. A shock front in water would appear an abrupt discontinuity in pressure unless it could be observed on a time scale much less than the order of 1 microsecond; and this apparent discontinuity would therefore exert a dominant influence on the high-frequency end of the spectrum well into the megacycle range. The discontinuity need not have the familiar form of a fully developed shock (e.g., the blast wave from an explosion) for it to affect the spectrum in the required way: the only essential property is that there should be a finite discontinuity in some part of the wave form.

Although this explanation of the asymptotic form of the spectrum appears to be fairly widely known, a mathematical demonstration of it seems worth giving here since this has apparently not been done before. It is instructive to consider the special case of  $\omega^{-2}$  dependence as part of a general classification, and indeed this is the only way of showing that the presence of shocks is necessary, not merely sufficient, to account for this case in practice. We restrict the argument to a single noise pulse possessing only one singularity: the extension of the argument to a random sequence of identical pulses is quite straightforward; and although an extension to a more general type of random noise would be difficult to make with complete rigour, it seems clear intuitively that the spectral properties due to an isolated singularity, as considered below, are common to any noise in which singularities of the sort in question occur at random.

Suppose that  $p(t)$  is a typical noise pulse with finite duration, as for instance detected by a hydrophone. Its energy spectrum may be defined as

$$S(\omega) = \int_{-\infty}^{\infty} p(t)^2 e^{-i\omega t} dt$$

where

$$p(t) = \int_{-\infty}^{\infty} p(\tau) \delta(t - \tau) d\tau \quad (2.1)$$

If desired, some convenient normalization factor can be introduced into the definition; but this is unnecessary for the purpose of the present argument.

We suppose  $p(t)$  to be always finite, although there is a singularity of its derivatives at, say,  $t = 0$ . A large class of such singularities is characterized by the behaviour  $p(t) \sim O(t^{-\alpha})$  as  $t \rightarrow 0$ , where  $\alpha > 0$  but is not an integer; thus, if  $(n-1) < \alpha < n$  where  $n = 1, 2, 3, \dots$ , then the  $n$ th and higher derivatives of  $p(t)$  tend to infinity as  $t \rightarrow 0$ . (For complete generality we would need also to consider cases where  $p(t)$  is an odd function in the neighbourhood of  $t = 0$ , and where the singularity is logarithmic, but this would be a pointless digression here.) To find the asymptotic form of  $S(f)$  in this case, the most satisfactory course is to make use of a theorem given by Bromwich (15). It is sufficient here to quote the final result: we find that  $S(f) \sim O(f^{-2(n+1)})$  as  $f \rightarrow \infty$ . Thus, all possible asymptotic slopes of the spectrum (on a logarithmic plot) are covered except the cases where the dependence of  $p(t)$  is  $t^{-1}, t^{-2}, t^{-3}, \dots$ .

The latter cases are more interesting to us than the intermediate ones. They are given by functions of  $t$  which undergo abrupt discontinuities or whose derivatives do. To deal with singularities of this type, the following method is quite lucid though to an extent only intuitive. For further detail we may refer to various treatises dealing with asymptotic expansions.

The case which directly concerns us, as it represents a shock front, is where  $p(t)$  changes abruptly at  $t = 0$  from a value  $p(0^-)$  to another value  $p(0^+)$ ; here  $0^-$  and  $0^+$  indicate arbitrarily small negative and positive value of  $t$ , respectively. All the derivatives of  $p(t)$  are infinite—or rather, meaningless—at  $t = 0$ ; but it can be assumed that the derivatives are integrable over the whole range  $(-\infty, \infty)$ . Hence, integration of Eq. (2.1) by parts gives directly

$$g(f) = \frac{p(0^+) - p(0^-)}{2\pi if} + \frac{1}{2\pi if} \int_{-\infty}^{\infty} \frac{dp}{dt} e^{-2\pi ift} dt. \quad (2.2)$$

According to the Riemann-Lebesgue theorem, the integral in Eq. (2.2) tends to zero as  $f \rightarrow \infty$ . Therefore, if the step in  $p(t)$  is of finite height (i.e.,  $p(0^+) - p(0^-)$ ), we have that

$$g(f) \sim O(f^{-1}) \text{ as } f \rightarrow \infty. \quad (2.3)$$

Hence,  $S(f)$  decreases asymptotically at the rate of  $10 \log_{10}(2\pi^2) = -6.02$  db/octave. It is now perhaps obvious that no function other than one with a finite discontinuity like a shock wave has a spectrum with this asymptotic property.

Incidentally, an extension of the above line of argument, wherein the integral on the right-hand side of Eq. (2.2) is reduced by successive integrations by parts, leads to the following rule: if  $p, p', p'', \dots, p^{(n-1)}$  are all finite and continuous, and if  $p^{(n)}$  is finite yet discontinuous, then  $g(f) \sim O(f^{-(n+1)})$  as  $f \rightarrow \infty$ . It follows from this that if  $p(t)$  and all its derivatives are continuous,  $S(f)$  must decrease asymptotically more rapidly than any negative power of  $f$ , i.e., it must decrease at least in exponential fashion. Thus, even when shocks are present in cavitation noise, the spectrum must ultimately decrease exponentially when the frequency is so high that its reciprocal is comparable with the time of passage of a shock front, so that on such a time scale the shock no longer appears discontinuous.

We also note that if the signal  $p(t)$  is passed through a recording system which is resonant at  $t = t_0$ , the "apparent" spectral response (i.e., the spectrum of the

forced vibration) is of the form  $g_n(f) = g(f) f / 2\pi(f^2 - f_n^2)^{1/2}$ . Therefore, at frequencies much above  $f_n$ , the "apparent" energy spectrum for a discontinuous signal has the property

$$S_n(f) = g(f)^2 \propto O(f^{-2}) \propto O(f^{-4}). \quad (2.4)$$

That is, the spectrum is sustained at a slope of -12 db/octave. The author has remarked in the past (16) that this may be a useful consideration regarding the response to cavitation noise of practical hydrophones, which are always subject to self-resonances at a number of frequencies.

### 3. SOME POINTS FROM THE THEORY OF CAVITATION IN INCOMPRESSIBLE LIQUIDS

Although the main interest at present is in effects due to the compressibility of water, it will be helpful to fix our ideas by recalling some simple results according to incompressible-flow theory. In awareness of the severe difficulties arising when compressibility is taken into account, problems of radial bubble motion in an incompressible liquid appear on the whole refreshingly straightforward; of course they are not always easy, particularly as the equations of bubble motion are non-linear; but, generally speaking, treatments of these problems are clear-cut and unequivocal. The subject is well-covered by the contributions of Rayleigh (11), Lamb (17,18), Cole (19), Plessett (20), Noltingk and Neppiras (21), Robinson and Buchanan (22) and numerous others.

Consider first an empty spherical cavity of radius  $R(t)$  collapsing to zero volume in a large expanse of incompressible fluid. In the later stages of the collapse, the motion becomes insensitive both to the way it was started and to the (hydrostatic) pressure  $P$  at a large distance from the centre. The only crucial parameter is the total energy  $E$  of the motion, which may be assumed to be approximately constant. Note that if the cavity starts contracting with a radius  $R_0$  and if  $P$  is a constant  $P_0$ , then obviously  $E = 4/3 \pi P_0 (R_0^3 - R^3)$  which tends to a constant value as  $R \rightarrow 0$ . If  $P$  varies during the initial stages of the motion,  $E$  will vary in a rather more complicated fashion, but the final stages occur so rapidly that  $E$  will again be practically constant towards the end. Putting the kinetic energy of the fluid equal to  $E$ , we have

$$2\pi R^3 \dot{R}^2 = E, \quad (3.1)$$

where  $\dot{R}$  denotes  $dR/dt$  and  $\rho$  the density. This equation has the integral

$$R = \left( \frac{25 E}{\pi \rho} \right)^{1/5} (-t)^{2/5} \quad (3.2)$$

on the assumption that the collapse is completed at  $t = 0$ . This gives the well-known result that  $-R \rightarrow 0 (-t)^{-3/5}$  as  $R \rightarrow 0$ . The velocity of the cavity wall thus becomes infinite in the limit. Further, the pressure throughout the fluid becomes momentarily infinite, but the velocity at a fixed point is zero at the instant of collapse, being proportional to  $R^2 \dot{R}$ . Thus, in the limit as  $R \rightarrow 0$ , the energy of the motion becomes concentrated wholly at the centre.

It can easily be shown that the pressure  $p$  at a radius  $r$  from the centre is given by

$$p = P \left[ 1 - \frac{R}{r} \right] + \frac{1}{2} \rho \dot{R}^2 \left[ \frac{R}{r} - \frac{R^4}{r^4} \right]. \quad (3.3)$$



This expression demonstrates some features of the pressure distribution which have particular interest in the present context. Note first that  $p = 0$  at  $r = 0$ , which is consistent with the assumption of an empty cavity. Next note that in the later stages of the collapse,  $\dot{R}$  is negligibly small compared with  $R^2$ ; and so the term in  $\dot{R}$  on the right-hand side of Eq. (3.3) can be neglected in any region not too far from the cavity. Thus, the pressure is seen to rise from zero at the cavity wall to a maximum value  $\frac{3}{4} \frac{1}{4} \frac{1}{R^2} \dot{R}^2$  at  $r = \frac{1}{4} R$ , and to decrease steadily for greater  $r$ . Figure 1 illustrates changes in the pressure distribution as  $R$  decreases. The vertical and horizontal scales are arbitrary, but the figure is easily interpreted. The three curves represent the pressures when, respectively, the cavity radius is 1, 1.5, and 2 in arbitrary units. Since  $\dot{R}^2$  is proportional to  $R^{-3}$ , the maximum pressure in the last case is eight times that in the first. The figure shows clearly how towards the end of the collapse the pressure increases very rapidly in magnitude and its distribution becomes less dispersed.

Now, if we allow that behaviour at least qualitatively similar to this may occur in a compressible liquid, an interesting possibility is suggested. Positive pressure distributions of the kind illustrated in Fig. 1 suffer a tendency to steepen in the direction away from the centre, and so develop into shock waves. Admittedly, the wave-form is being carried rapidly towards the centre of collapse, and the process of shock formation necessarily occupies a certain time. But it seems at least conceivable that a compressible liquid moving inward to close an empty cavity could develop a shock at some moment before the instant of final collapse, the shock being convected inwards by a supersonic flow. This point will be taken up again in a later part of the discussion.

It scarcely needs to be said that the present simple model of cavitation collapse ceases to be valid well before the cavity disappears. When the velocities and pressures near the cavity become large, the effects of compressibility are no longer

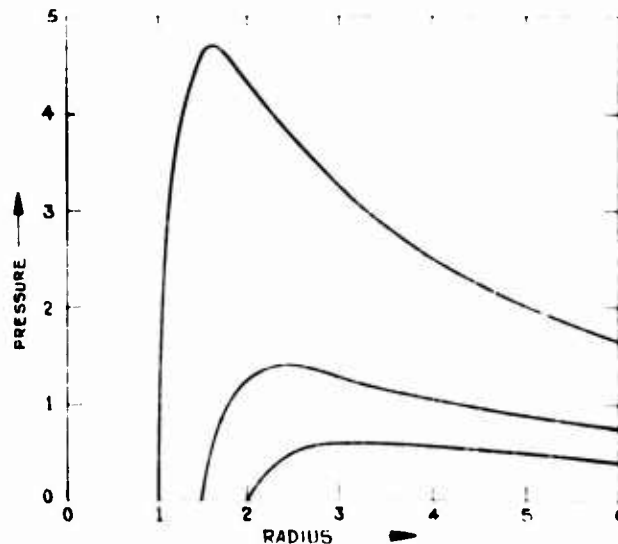


Fig. 1. Pressure distribution near the end of the collapse of an empty cavity, for three different values of  $R$ .

negligible, and also the assumption of an empty cavity may become unrealistic. However, as Rayleigh (11) was first to point out, the singularity in the incompressible-fluid solution is avoided if the cavity is assumed to enclose a quantity of insoluble gas. The compression of the gas eventually arrests the inward motion, and a "rebound" takes place. It may be shown that as the gas pressure rises, the peak in the pressure distribution illustrated by Fig. 1 is displaced inwards; and ultimately, at the instant when the collapse is halted, the maximum pressure occurs right at the cavity wall.

While serving to remove a mathematical difficulty, the chief merit of this modification is that it represents a definite feature of cavitation in practice (and, incidentally, leads to a very useful account of the pulsations of underwater explosion bubbles (19)). There is plentiful evidence that rebounds often occur (e.g., (13,14)), and presumably they are due to the action of the cavity contents. Of course, the model of a gas-filled cavity surrounded by incompressible liquid still falls far short of reality; for instance, no mechanism for energy dissipation is included, whereas rebounding cavitation bubbles appear always to be considerably smaller than their maximum size before the first collapse. Nevertheless, this model is definitely relevant to cases of fairly "mild" collapse, and gives a useful first approximation to such quantities as the peak noise pressure.

Some numerical results calculated on this basis will be useful for reference later. We consider a cavity initially at rest with  $R = R_0$  and containing gas at pressure  $Q$ . The hydrostatic pressure  $P$  is constant and greater than 0, so that the initial motion is inward. The gas is assumed to be compressed according to the law  $pV^\gamma = \text{const} = 1$ , i.e., its pressure is given by  $p = Q(R_0/R)^\gamma$ , and its inertia is neglected. The equation of motion of the cavity is expressible in the form

$$\dot{R}^2 = \frac{2P}{3} \cdot \left( \frac{R_0}{R} \right)^3 - 1 + \frac{Q}{1+P} \left[ \left( \frac{R_0}{R} \right)^3 - \left( \frac{R_0}{R} \right)^{\gamma+1} \right]. \quad (3.4)$$

From this the minimum radius  $R_m$  is easily deduced, since it is a root of  $\dot{R} = 0$ . Assuming that  $(R_0/R_m)^\gamma$  is fairly large, we find that, very approximately,

$$R_m/R_0 = (1+K)^{-1/(\gamma+1)} \quad (3.5)$$

where  $K = Q/(1+P)$ . The maximum gas pressure is therefore

$$P_m = Q(R_0/R_m)^\gamma = Q(1+K)^{\gamma/(\gamma+1)} \quad (3.6)$$

Also, the peak pressure rise (i.e., above  $P$ ) at a radius  $r = R_m$  is  $P_m R_m / r$ . The maximum velocity of the cavity wall is found by differentiation of Eq. (3.4). This occurs when  $R = R'$ , this radius being given by

$$R/R_m = (1+K)^{1/(\gamma+1)} \quad (3.7)$$

and is very approximately

$$R/R_m = 2P/3 \quad (3.8)$$

Equations similar to (3.5) and (3.6), although rather less accurate, were given by Noltingk and Neppiras (21). Lamb (17) obtained Eq. (3.6) in a related problem concerning underwater explosions, but gave the formula incorrectly; the mistake was reproduced in his well known book (18).

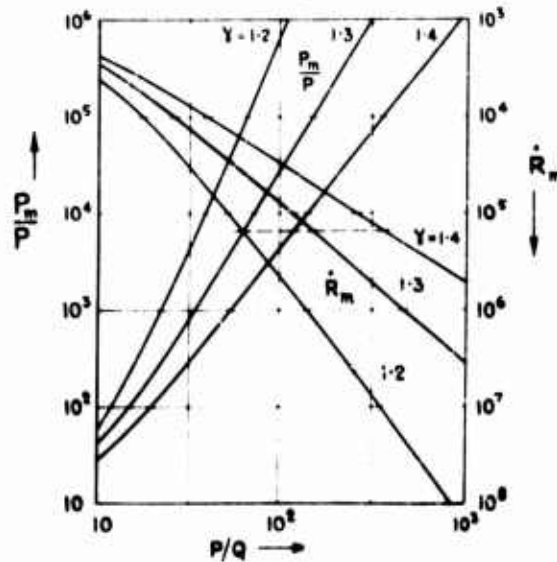


Fig. 2 - Values of the maximum gas pressure and maximum radial velocity occurring during the collapse of a gas-filled cavity in an incompressible liquid.

Figure 2 shows graphs of  $P_m/P$  vs  $P/Q$  for three values of  $\gamma$ . Graphs of the value in cm/sec of  $\dot{R}_m$  corresponding to  $P = 1$  bar and  $\rho = 1 \text{ g/cm}^3$  are also shown; for other values of  $P$  or  $\rho$ ,  $\dot{R}_m$  can be scaled proportionately to  $(P/\rho)^{1/2}$ . On the graph of  $\dot{R}_m$ , the dashed line denotes the speed of sound in water at a pressure of 1 bar. Figure 2 illustrates clearly how the maximum pressures generated during a collapse may greatly exceed the hydrostatic pressure. For example, if a cavity contains air at an initial pressure of one one-hundredth the hydrostatic pressure and the air is compressed adiabatically ( $\gamma = 1.4$ ), the air pressure at the end of the collapse is 4420 times the hydrostatic pressure. When we consider that  $P$  is of the order of 1 bar in many instances of cavitation, the extent of the magnification of pressure is most impressive. The feature of Fig. 2 which has particular interest later in the discussion is that for  $P_m/P \approx (10^3)$ , the magnitude of  $\dot{R}_m$  is still a reasonably small fraction of the speed of sound, so that the error due to neglect of the compressibility of water is probably still fairly small.

#### 4. THE NATURE OF THE PROBLEM FOR COMPRESSIBLE LIQUIDS

To develop a theory on a secure basis, the attempt must be made to solve the exact equations of radial motion in a compressible fluid. We shall now derive a second-order approximation to the effects of compressibility; but, as remarked in Section 1, this is done primarily as an illustration of method and to show how the way is clear to higher approximations.

For spherically symmetric isentropic flow, the velocity potential satisfies

$$c^2 \left( \frac{\partial^2 \phi}{\partial r^2} + \frac{2}{r} \frac{\partial \phi}{\partial r} \right) = \frac{\partial^2 \phi}{\partial t^2} + \frac{2}{r} \frac{\partial \phi}{\partial t} \frac{\partial c^2}{\partial t} + \frac{1}{r} \frac{\partial^2 \phi}{\partial t^2} \frac{\partial c^2}{\partial t} + \frac{1}{r} \frac{\partial^2 \phi}{\partial t^2} \frac{\partial c^2}{\partial t} \quad (4.1)$$

where  $c$  is the local velocity of sound which in general varies with pressure. (It is worth noting that Lamb (18, 285) presents this equation in its correct form, but under the unnecessary restriction that  $c$  is constant.) As a reasonable first step towards a solution, one may use a linearized (acoustic) theory in which the terms on the right-hand side of Eq. (4.1) are neglected and  $c$  is taken to be a constant  $c_0$ , the sound velocity in the undisturbed fluid. According to this theory, the characteristic curves in the  $(r, t)$ -plane are straight lines, given by  $t - r/c_0 = \text{const}$  for outgoing waves. But there are two respects in which a linearized theory is inadequate. The first, the obvious one, is that for the very rapid flow near a cavity in the later stages of collapse, the non-linear terms in Eq. (4.1) may have an effect which is by no means negligible. Second, the linearized solution is well known to become progressively less valid at large distances from the origin. Even though the magnitude of  $\dot{r}$  decreases steadily (like  $r^{-1}$ ), the effect of the non-linear terms accumulates and eventually predominates over that of the linear terms. For instance, the characteristics at the head of a positive pressure wave diverge, tending to form a shock wave if one is not already present. The linearized theory is therefore not even a valid first approximation at large distances.

A great deal has previously been written on this matter (7,8,25), and there is no need to go into any general detail here. To obtain an approximate solution of Eq. (4.1) which is uniformly valid over the whole flow, the Lighthill-Whitham method is used; the solution is expressed in terms of an implicit exact characteristic, to which successive approximations are made. This approach seems the only way to proceed without ambiguity to high-order approximations to the equation of the cavity motion. It appears that the method would remain tractable even when a fully developed shock wave is present, but we shall not deal explicitly with this case here, being content to examine the circumstances of the initial formation of a shock.

If  $p$  denotes the pressure relative to the constant pressure  $P$  far from the centre of the motion (so that  $p \rightarrow 0$  for large  $r$  and  $p = -P$  at the wall of an empty cavity), the Bernoulli integral of the equations of motion can be written

$$\frac{1}{2} \dot{r}^2 + \int_0^p \frac{1}{\rho} dp = 0 \quad (4.2)$$

where  $\dot{r} = \dot{r}$  is the velocity. Now, the density  $\rho$  is a function of  $p$  only; and so, if  $\rho^{-1}$  is expanded as a Taylor series and integrated term by term, the right-hand side of Eq. (4.2) becomes

$$= -\rho_0 + \frac{1}{2} p^2 \rho_0^{-2} c_0^{-2} + \dots$$

Here  $\rho_0$  is the density where  $p = 0$  and  $c_0^2 = (dp/d\rho)_p=0$ . Only these first two terms of the expansion are required at present; the third term is  $O(c_0^{-4})$ , and we are going to develop the theory only as far as  $O(c_0^{-2})$ . Thus, a sufficient approximation to Eq. (4.2) is

$$\frac{1}{2} \dot{r}^2 - \frac{P}{\rho_0} + \frac{1}{2} \frac{P^2}{\rho_0 c_0^2} = 0 \quad (4.3)$$

The sound velocity is next expanded as

$$c = c_0 + \left( \frac{1}{\rho} \right)_p p + \dots \quad (4.4)$$

Again, terms after the second can be neglected, being of fourth order. Hence, using Eq. (4.3), we may write

$$c_1 = 1 - \frac{1}{2} \left( \frac{1}{2} \frac{a^2}{r^2} \right) \quad (4.5)$$

Here  $\gamma$  is a dimensionless coefficient of the order of unity; for water it is about 2.7. (Experimental data on the properties of water under high pressures (see (6) for a review) show that a linear relation between sound velocity and pressure, as assumed here, holds approximately up to pressures of the order of 2000 bars. To deal adequately with the case of pressures much higher than this, the expansion Eq. (4.4) would have to be taken further than the first two terms; but this is not justified in a second-order theory. In fact, it will appear that the variation of  $\gamma$  does not affect the cavity motion to the second order, although this has an important effect on the surrounding pressure field.)

We next suppose the characteristic curves in the  $(t, r)$ -plane to have the form  $r = r_0(t) \exp \theta$ . The equation determining  $\theta$  is then

$$\frac{d\theta}{dt} = \left( \frac{r_0}{r} \right) \frac{dr_0}{dt} - 1 = -\frac{1}{2} \frac{a^2}{r^2} \quad (4.6)$$

We may also arbitrarily introduce the condition

$$\theta = 0 \quad \text{at} \quad r = R_0 \quad (4.7)$$

which lends to  $\theta$  the useful interpretation of a "retarded time" measured with respect to the cavity wall.

To complete the basic details of the mathematical problem, the boundary conditions at the cavity wall will now be written down. First, there is the kinematical condition

$$\left( \frac{r}{R_0} \right) \frac{dR_0}{dt} = \frac{dR}{dt} \quad (4.8)$$

Second, there is the condition that the (relative) pressure of the cavity contents, say  $p_{\text{rel}}$ , is the same as the pressure just inside the liquid (surface tension being neglected in this account). According to Eq. (4.3), this implies that

$$\left( \frac{r}{R_0} \right) \frac{dR_0}{dt} = \frac{1}{2} \frac{a^2}{R_0^2} \quad \text{or} \quad \left( 1 - \frac{1}{2} \frac{a^2}{R_0^2} \right) \quad (4.9)$$

We also have, of course, that  $\theta = 0$  for  $r = R_0$ .

## 5. THE LINEARIZED THEORY

This has been used by several authors (23,24) to derive an equation of cavity motion with a first-order correction for the effects of compressibility. The right-hand side of Eq. (4.1) is neglected, and one puts  $\gamma = \gamma_0$ . The solution then is

$$\frac{R}{R_0} = 1 + \frac{1}{2} \frac{a^2}{R_0^2} \quad (5.1)$$

together with

$$t = \frac{r}{c_0} + \frac{\dot{R}}{c_0} \quad (5.2)$$

(Note that Eq. (5.2) is the first-order solution of Eq. (4.6) subject to the boundary condition Eq. (4.7)).

From Eq. (5.1) it follows that

$$u = \frac{f(r)}{r^2} + \frac{f'(r)}{c_0 r} \quad (5.3)$$

When this is substituted in Eq. (4.8),  $f(r)$  can easily be calculated as far as terms in  $c_0^{-1}$ . A first estimate gives  $f(r) = R^2(r) \dot{R}(r)$ ; and a second gives

$$f = R^2 \ddot{R} - \frac{1}{c_0} (R \ddot{R} + 2R^2 \dot{R}^2) \quad (5.4)$$

From Eqs. (5.1) and (5.4), we get

$$\begin{aligned} \left( \frac{\partial \phi}{\partial t} \right)_{r=R} &= \left[ -f(r) \left\{ \frac{1}{r} + \frac{\dot{R}}{c_0} \right\} \right]_{r=R} \\ &= -R \ddot{R} - 2\dot{R}^2 - \frac{1}{c_0} (R^2 \ddot{R} + 6R \dot{R} \ddot{R} + 2\dot{R}^3), \end{aligned} \quad (5.5)$$

which, when substituted in Eq. (4.9), leads immediately to

$$R \ddot{R} + \frac{3}{2} \dot{R}^2 - \frac{1}{c_0} (R^2 \ddot{R} + 6R \dot{R} \ddot{R} + 2\dot{R}^3) = S \quad (5.6)$$

This is exact to  $O(c_0^{-1})$ . To the same order, the equation may be arranged in several other ways, for instance in the form

$$R \ddot{R} \left( 1 - \frac{\dot{R}}{c_0} \right) + \frac{3}{2} \dot{R}^2 \left( 1 - \frac{\dot{R}}{3c_0} \right) = S + \frac{1}{c_0} \left( R \frac{S}{t} + \dot{R} S \right) \quad (5.7)$$

## 6. HIGHER-ORDER SOLUTIONS

To proceed to higher approximations, one may write

$$\phi = \phi_1(r, t) + \frac{1}{c_0} \phi_2(r, t) + \frac{1}{c_0^2} \phi_3(r, t) + \dots \quad (6.1)$$

where  $\phi_1(r, t)$  is the linearized solution given above, and then solve Eq. (4.1) to successively higher powers of  $c_0^{-1}$  (i.e.,  $\phi_2$  is first determined, then  $\phi_3$ , etc.). At the same time, successive approximations are made to the characteristic determined by Eq. (4.6). The solution of the latter equation is most suitably expressed in the form

$$t = F(r, c_0) \quad (6.2)$$

which, of course, in the linearized theory reduces to

$$t = \frac{r}{c_0} + \frac{R(t)}{c_0} \quad (6.3)$$

Thus, the present method is clearly seen to be an instance of Lighthill's general technique of "coordinate perturbation" (7,25). In applying the method, it is helpful to rewrite the equation for  $\psi$  in terms of partial derivatives with respect to  $r$  (i.e., with  $t$  constant) and  $t$  (with  $r$  constant). Thus, Eq. (4.1) is replaced by

$$\frac{1}{r} \frac{\partial^2 \psi}{\partial r^2} + \frac{2}{r} \frac{\partial \psi}{\partial r} + \frac{1}{r^2} \frac{\partial^2 \psi}{\partial t^2} = \frac{1}{r^2} \left( \frac{\partial^2 \psi}{\partial r^2} + \frac{\partial^2 \psi}{\partial t^2} \right) + \text{non-linear terms.} \quad (6.4)$$

the terms on the right-hand side being equivalent to  $\epsilon^2$  times the non-linear terms on the right-hand side of Eq. (4.1).

Let us now work out the solution as far as terms in  $\epsilon_0^2$ . We first observe, on substituting Eq. (4.5) in Eqs. (4.1) or (6.4), that the variation of  $\epsilon$  does not affect the equation for  $\psi$  to this order. Next, the linearized solution is used to obtain the second-order approximation to the right-hand side of Eq. (6.4): this is

$$\frac{1}{\epsilon_0^2} \left( \frac{2\psi}{r^4} - \frac{2\psi}{r^2} \right) \quad (6.5)$$

with  $\psi = R^2 \ddot{R} + \dot{R}^2$ .

An approximation to the explicit form of Eq. (6.2) is now found. When Eqs. (5.1) and (4.5) are substituted in Eq. (4.6), the integral of the equation to  $O(\epsilon_0^3)$  is

$$\frac{r}{\epsilon_0} + \frac{t^2}{10\epsilon_0^2} = \frac{1}{\epsilon_0^3} (1 + \psi) + \frac{1}{10\epsilon_0^3} r + \frac{(2\psi + t^2)}{2r^4\epsilon_0^3} + A(r),$$

where  $\psi$  is given by Eq. (5.4) and  $A(r)$  is an arbitrary function arising in the integration. If  $A$  is chosen so as to satisfy the boundary condition Eq. (4.7), we have

$$\frac{r}{\epsilon_0} + \frac{t^2}{10\epsilon_0^2} = \frac{1}{\epsilon_0^3} \left( \frac{1}{r} + \psi \right) + \frac{(1 + \psi)}{10\epsilon_0^3} + \frac{r}{10\epsilon_0^3} + \frac{(2\psi + t^2)}{6\epsilon_0^3} + \left( \frac{1}{R^3} - \frac{1}{r^3} \right) \quad (6.6)$$

This expansion is far more accurate than we need at present, but it will be useful later.

When Eqs. (6.1), (6.5), and (6.6) are substituted in Eq. (6.4), the first term on the right-hand side (i.e., the first term in Eq. (6.5)) is cancelled, and collection of the second-order terms gives

$$\frac{1}{r^2} \frac{\partial^2 \psi}{\partial r^2} + \frac{2}{r} \frac{\partial \psi}{\partial r} + \frac{1}{r^2} \frac{\partial^2 \psi}{\partial t^2} = \frac{2R^6 \ddot{R}^3}{r^7} \quad (6.7)$$

which has the solution

$$\frac{1}{2} \frac{F(r)}{r^2} = \frac{R^6 \ddot{R}^3}{10 r^5} \quad (6.8)$$

The arbitrary function  $F(r)$  is determined from Eq. (4.8). Hence, the complete second-order solution is found to be

$$\frac{1}{r} \frac{\partial^2 \psi}{\partial r^2} + \frac{1}{\epsilon_0} \left( R^4 \ddot{R} + 2R^2 \dot{R}^2 \right) + \frac{1}{10\epsilon_0^2} (R^4 \ddot{R} + R^4 \ddot{R} \ddot{R} + \frac{7}{2} R^2 \dot{R}^3) + \frac{R^6 \ddot{R}^3}{10\epsilon_0^2 r^5} \quad (6.9)$$

This result is exact to the second-order. The last term on the right-hand side is negligible far from the cavity, but near the cavity it has the same importance as the other second-order terms. The appearance of a term in  $r^{-5}$  in this solution does not imply that powers between  $r^{-1}$  and  $r^{-5}$  are absent from higher-order solutions: in fact terms in  $r^{-2}$  arise in the next approximation (compare the solution of the blast wave problem given by Whitham (8, see also 25)). Note that the present result discloses an error in the Kirkwood-Bethe hypothesis, which states  $r_{11}$  to depend only on  $r_0$ .

An equation for  $R(t)$  corresponding to Eq. (5.6) can now be obtained by putting Eq. (6.9) in Eq. (4.9). However, at this point it is convenient to introduce a simplification which has been suggested by Dr. Proudman (it was in fact used in his work referred to in the introduction). We have remarked earlier that the motion of a cavity towards the end of a collapse depends very little on the hydrostatic pressure, but is controlled essentially by the total energy  $E$ . Therefore, for the concluding stages of the collapse of an empty cavity, it is permissible to put  $S = 0$  in Eq. (4.9). The vital parameter  $E$  then enters as a constant of integration in a first integral of the differential equation for  $R$ . (The case of a gas-filled bubble near the end of its collapse may be simplified in a similar way by putting  $S$  equal to the absolute (instead of relative) pressure of the gas contents, which is justified when this pressure becomes very large compared with the pressure  $P$  far from the centre; however, to illustrate the theory we shall consider here only the case of an empty cavity.) The step of putting  $S = 0$  can also be justified by considering that the motion in the final stages would be the same approximately as for a cavity which collapses from infinite size under zero pressure, but which is initially given a finite kinetic energy. Hence, after a certain amount of straightforward calculation, we arrive at the equation

$$R\ddot{R} + \frac{3}{2}\dot{R}^2 + \frac{\dot{R}^3}{c_0} + \frac{13}{20}\frac{\dot{R}^4}{c_0^2} = 0. \quad (6.10)$$

Consider now the expression

$$\frac{k}{R^3} + \dot{R}^2 \left( 1 + A\frac{\dot{R}}{c_0} + B\frac{\dot{R}^2}{c_0^2} \right),$$

where  $k$ ,  $A$ , and  $B$  are constants. On differentiation this is found to satisfy Eq. (6.10) to  $O(c_0^{-2})$  if  $A = -4/3$  and  $B = 9/10$ . Also,  $k$  can be identified with  $E/2\pi\rho_0$ ; for we must have  $2\pi\rho_0 R^3 \dot{R}^2 = E$  when the cavity is still large enough for the velocity to be small and the effect of compressibility negligible (see Eq. (3.1)). Thus we have

$$E/2\pi\rho_0 R^3 \dot{R}^2 \left( 1 - \frac{4}{3}\frac{\dot{R}}{c_0} + \frac{9}{10}\frac{\dot{R}^2}{c_0^2} \right). \quad (6.11)$$

This result shows clearly that compressibility of the liquid slows down the cavity motion: i.e., at a given radius  $R$ , the magnitude of the (negative) velocity  $\dot{R}$  is less than if the terms in  $\dot{R}/c_0$  were zero.

Now, there are various ways one might interpret this equation. If it were supposed to remain a valid approximation right up to the instant of total collapse, one would conclude that  $-\dot{R} = O(R^{-3/4})$  as  $R \rightarrow 0$ , so that the velocity ultimately becomes infinite. However, this argument is obviously unsound. Equation (6.11) is only a second-order approximation in terms of  $\dot{R}/c_0$ ; and clearly in successive higher approximations the series in powers of  $\dot{R}/c_0$  would be carried on indefinitely. Thus, if  $-\dot{R}$  is in fact infinite in the limit, the truncated series would be incapable of determining



the exact nature of the singularity. On the other hand, there is an approximate solution of Eq. (6.11), satisfying the equation to the second order in  $R/c_0$ , which gives a finite velocity in the limit as  $R \rightarrow 0$ . At first sight it seems possible that this solution is a uniformly valid approximation right to the end of the collapse, so that the finite terminal velocity is a realistic result; for we note that in order to keep the right-hand side of Eq. (6.11) constant as  $R \rightarrow 0$ , it may be sufficient for the series in  $R/c_0$ —of which only the first three terms are given in the present approximation—to diverge in a certain way for some finite value of  $R$ .

To obtain the result in question, we introduce the dimensionless variables  $x = R/2 \cdot 2^{-1/2} E^{1/2}$  and  $\tau = 5t/2 \cdot 2^{-3/5} E^{1/2} c_0^{5/2} E^{1/2}$ . In terms of these, a solution accurate to the second-order is found to be

$$x = 2^{-1/2} \left( 1 - \frac{2}{3} \tau + \frac{2\tau^2}{45} \right) \quad (6.12)$$

$$\frac{\dot{R}}{c_0} = \left( 1 - \frac{1}{3} \tau + \frac{2\tau^2}{45} \right) \quad (6.13)$$

According to Eq. (6.12), the collapse ends at  $\tau = 1.500$ . When this value is put in Eq. (6.13), the velocity at the end is given as  $\dot{R}/c_0 = 2/3 = 0.667$ .

It was noted in the Introduction that this speculation about the terminal velocity of collapse is probably wrong. The author became convinced of this only very recently. Previously the available analytical evidence seemed substantially in favour of a finite collapse velocity—for instance, this interpretation was consistent with a fourth-order approximation obtained by Dr. Proudman (which at first sight would appear more reliable than a theory based on the Kirkwood-Bethe hypothesis). However, sufficient evidence for rejecting this interpretation was provided by a numerical solution of the problem which Mr. C. Hunter at Cambridge has found by use of the EDSAC II digital computer. The numerical results indicate that the velocity  $\dot{R}$  increases without bound as  $R \rightarrow 0$ , which is as Gilmore (5) suggested a number of years ago. This temporary mistake might nevertheless be said to fit naturally into the story of recent work on this problem; and even though a finite collapse velocity may not after all be a true theoretical result, it is not inconsistent with the physical picture of events at the centre of a cavity collapse. The chief physical implication of a theoretically finite velocity (in fact the only really significant aspect of such a result) would be that there is no concentration of energy at the centre, as we noted in Section 3 occurs in the case of an incompressible liquid. This apparently is a valid conclusion. Some recent work, to be summarized in the Appendix, has demonstrated that the flow field surrounding a collapsing empty cavity possesses an inner core which holds a vanishingly small share of the total energy of the motion. It therefore appears that the pressure wave radiated from a practically empty cavity would be scarcely affected by events near the centre immediately preceding the final closure of the cavity; the properties of the wave are mainly determined by the flow outside the central core, for which part of the flow the above theory provides a valid second approximation.

It remains to reconsider the possibility that a shock is formed before the end of the collapse, as suggested earlier in the paper. If this occurred, calculations of the present sort would subsequently become invalid. Analytical work on this question has so far been inconclusive, but the machine calculations carried out by Mr. Hunter have indicated that no shock is in fact formed up to the instant when  $R = 0$ .

## 7. THE PRESSURE WAVE

An advantage of the preceding method of analysis is that it provides a uniformly valid approximation for the pressure pulse transmitted away from the cavity, even when there is distortion of the wave-form due to non-linear effects. To illustrate the theory, we shall now focus attention on the question whether a rebounding gas-filled cavity may generate a shock wave.

At a large distance from the cavity, the pressure due to the radial motion is

$$p = \frac{\rho_0 \dot{r}}{r} \quad (7.1)$$

where  $\dot{r}$  is prescribed on the cavity wall and is  $R^2 \ddot{R}$  to a first approximation; also, according to Eq. (6.6),  $\dot{r}$  is given by

$$\dot{r} = \frac{r}{c_0} \left( 1 + \frac{1}{3} \frac{r}{c_0} \log \frac{r}{R} \right) \quad (7.2)$$

The last term in this expression has the effect that in a positive pressure wave ( $\ddot{R} > 0$ ), the characteristics progressively diverge from the approximate characteristic  $r = r_0$  given by the acoustic theory. Thus, as we have remarked earlier, the acoustic approximation always breaks down when the wave has travelled far enough.

The result of the diverging of characteristics is that a positive wave is made skew in the outward direction and may eventually develop a shock as its slope becomes infinite. Now, since  $\dot{r}$  is continuous, we can only have  $p \rightarrow \infty$  if  $\dot{r} \rightarrow \infty$ ; i.e., if  $\ddot{R} \rightarrow \infty$ . Therefore, from Eq. (7.2), the condition for the initial formation of a shock is approximately (taking  $\log r/R$  to be large)

$$\ddot{R} > 1 + \frac{1}{3} \frac{\dot{r}}{c_0} \log \frac{r}{R} \quad (7.3)$$

This gives the radius at which a shock first appears. Clearly, the shock develops at the point in the wave where the slope  $\dot{r}$  is positive (i.e., at the head of the wave in time) and a maximum—i.e., at a point of inflexion. It might be supposed that for a positive pressure pulse such as produced by a rebounding cavity, a shock always occurs, because the condition Eq. (7.3) can always be satisfied by taking  $r$  to be large enough. However, if  $\dot{r}$  is everywhere small, the required value of  $r$  becomes enormous, which means that in practice there will be no shock. The effects of dispersion by viscosity and heat conduction will eventually cancel the very gradual tendency to build up a shock; for, although the magnitude of these effects on spherical waves is extremely small, they depend on  $r$  in contrast to  $\log r$  for the latter effect (13).

We are now in a position to estimate the practical conditions under which a rebounding cavitation bubble will give rise to a shock. The maximum value of  $\dot{r}$  is required; and as a first approximation it is sufficient to take  $R^2 \ddot{R}$  for  $\dot{r}$ . We assume for simplicity that the pressure inside the bubble is given by  $P = R^{-3}$ , where  $P$  is the maximum pressure and  $R$  the minimum radius (this assumption implies an adiabatic compression with  $\gamma = 5$ ; it is found that other values of  $\gamma$  do not significantly change the end results of the present calculation). By a straightforward method along the same lines as the calculations at the end of Section 3, the maximum of  $\dot{r}$  is estimated to be  $\dot{r}_{\max} = 0.6 \sqrt{P_0 R_0^3}$ . Next, values of  $\ddot{R}$  and for

water are substituted in Eq. (7.3). Hence, we deduce that the condition for a shock to be formed at radius  $r$  in water is

$$P_m = 13.6 \cdot 10^6 (r/R)^{2/3} \text{ kilobars.} \quad (7.4)$$

The value of  $R$  in Eq. (7.4) is nearly the same as  $R_m$ , but it is really unimportant which value precisely is considered. The following table shows some values of  $P_m$  just satisfying Eq. (7.4), given as a function of  $r/R$ :

$r/R$	$10^{-8}$	$10^{-7}$	$10^{-6}$	$10^{-5}$	$10^{-4}$
$P_m$ (kilobars)	1.9	2.1	2.3	2.7	3.1

We see that the necessary value of  $P_m$  varies very little over orders of magnitude of  $r/R$ . This table indicates a good practical criterion for shocks to form within "reasonable distances": this is simply that the maximum pressure in the bubble should be at least about 2 or 3 kilobars. If  $P_m$  is much smaller than this, shock waves are unlikely to be detectable, both because dispersion may overcome the tendency towards shock formation and because anyway the pressure wave will be of extremely small amplitude at the distance where a shock might appear.

As a check on this calculation, we observe from Fig. 2 that for value of  $P_m$  around 2 kilobars the maximum velocity of the bubble is still reasonably small compared with the sound velocity. Therefore compressibility of the water will not have any important effect on the bubble motion; and so the estimate of  $r(t)$  from the incompressible-fluid theory is probably quite adequate.

After a shock is initiated, it develops rapidly since its velocity is less than for a continuous wave of the same amplitude; thus, the shock is continually "fed" by wavelets arriving from behind. In the present problem, it would be feasible to account for the progress of a shock after incipience by using the methods given by Whitham (10).

## 8. CONCLUSION

The present theoretical work is intended to throw some further light on the physical mechanism of the collapse of cavitation bubbles and the noise arising therefrom. It has been shown that the theory of cavity collapse in compressible liquids can with advantage be developed by means of the Lighthill-Whitham technique of coordinate perturbation, successive approximations being obtained in powers of the parameter  $1/\rho_0$ . For the hypothetical case of an empty cavity, the approximate theory admits the interpretation that the collapse is terminated at a finite radial velocity; and although this is now believed to be an incorrect theoretical result, it is nevertheless true that the "imperfect" theory provides a uniformly valid physical approximation, since the finite terminal velocity is a reasonable representation of the apparently true fact that only a limitingly small part of the overall energy is carried right to the centre of collapse (in other words, most of the energy is stored in a compressive wave before the collapse ends).

In reality the concluding stages of a "severe" collapse (i.e., where the cavity has a negligible gas content) will be greatly affected by compression of the enclosed vapour and by other effects which have not been included in the present theory. But, in the manner suggested above, compressibility of the water may have enfeebled the ending of the collapse before the latter effects become important, so that they play an insignificant role in the overall mechanism. By similar considerations, the

possibility of a complete collapse without rebound from a certain minimum cavity size now appears fairly reasonable. Of course, as soon as the collapse is completed, a strong shock wave will be formed (the shock will probably originate from the centre; but as it expands it rapidly becomes independent of the "inner core" left unexplained by the simple theory); and this shock wave will have a rarefaction phase behind it which might re-open a cavity. The question whether or not rebounds occur in usual circumstances remains one of the most debatable topics in cavitation studies. In the author's experiments, no evidence has ever been found of a complete collapse without any rebound. Several other experimenters have, however, reported such evidence.

Another aspect of cavitation which has been considered concerns the case of a comparatively mild collapse. It has been shown that even a gas-filled bubble can generate a shock wave if the pressure of the gas rises beyond a certain limit at the instant of maximum compression when the rebound begins. Experiments by the author have revealed cases of incipient shock formation; and the observations appear to support the theoretical estimate of the critical conditions, although a precise comparison has not so far been achieved.

Finally, I feel this is an appropriate place to acknowledge my indebtedness to the British Admiralty, which has supported my work on cavitation for a number of years. In particular, I should like to express my gratitude to Dr. Jackson, Dr. Vigoureux, and Dr. Byard of the Royal Naval Scientific Service, whose advice and encouragement on many occasions in the past have greatly sustained my interest in cavitation.

## APPENDIX

The methods given earlier in this paper were shown to lead to what is very probably an incorrect answer to the theoretical question of how the collapse of an empty cavity is terminated. In view of the results of Mr. Hunter's calculations with EDSAC II, this question has been reconsidered by him along different lines, and as some progress has been made since the date of the meeting in Washington, it seems worthwhile to include the following summary of what has been done so far.

Suppose the collapse ends at  $r = 0$ , and suppose the velocity  $-R$  of the cavity does in fact increase without bound as  $R \rightarrow 0$ . The pressure just inside the liquid then also increases indefinitely; and since the sound velocity  $c$  increases with pressure, eventually the situation develops where the value  $c_0$  right at the cavity wall is insignificant compared with the values of  $c$  inside the liquid. It is therefore reasonable to assume that the motion very near the centre is the same as that of a gas flowing into a vacuous spherical cavity; for the gas the value of  $c$  is actually zero at the boundary of the cavity, in contrast to the "insignificant" value  $c_0$  which the liquid still possesses at zero pressure. Thus, the liquid motion contains an inner core which tends to the solution of this corresponding gas-dynamical problem in the limit as  $R \rightarrow 0$ .

For such a gas flow there is a "similarity solution" (i.e., a "progressive wave") of the type considered by Guderley (26) and others in studies of strong spherical and cylindrical shock waves (see Courant and Friedrichs (27), Chapter 6C, for a general account of the subject). We take the motion of the contracting inner boundary to follow the simple power law  $R = A(t-t_0)^{-1/3}$ , where  $A$  and  $t_0$  are positive constants, and assume a solution of the form

$$u = \frac{1}{r} U(\eta), \quad c = \frac{1}{r} C(\eta), \quad (A1)$$

where  $\eta = r/R = r A(t-t_0)^{1/3}$ . The inclusion of a minus sign in the expression for  $c$  makes  $C \rightarrow 0$  a positive quantity over the whole flow, since  $c$  is necessarily positive. In the

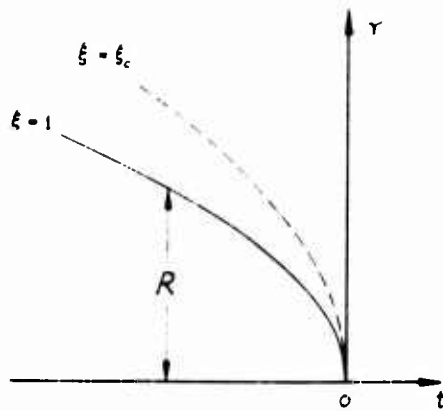


FIG. A1 - The locus of the boundary  $\xi = 1$  and the "critical characteristic"  $\xi = \xi_c$  in the  $(r, t)$ -plane.

$(r, t)$ -plane, the lines  $\xi = \text{const}$  spread from the origin as illustrated in Fig. A1, the inner boundary being  $\xi = 1$ . The boundary conditions are  $U(1) = 1$  and  $C(1) = 0$  at the inner boundary  $r = R$ , and also  $U(\infty) = C(\infty) = 0$ .

As shock waves are absent, the flow can be taken to be isentropic; hence,  $p/\rho^\gamma$  is constant everywhere and  $c$  is proportional to  $p^{(\gamma-1)/2\gamma}$ . To apply the solution of the gas-dynamical problem to the cavitation problem, we shall take  $\gamma = 7$ , recalling the approximate homentropic equation of state for water  $p + B/\rho^\gamma = \text{const}$ , where  $B = 3000$  bars (in effect, the present argument assumes that inside the central core of the liquid motion, pressures become much larger than  $B$ ).

Now, there is a particular line in the  $(r, t)$ -plane which, if it occurs inside the flow, has a crucial role in the determination of the solution Eq. (A1)—as it does in shock-wave theory (26). This is the  $\xi_c$ -line whose slope  $dr/dt$  is  $u - c$ , and which is therefore a characteristic curve passing through the origin (see Fig. A1). Hence, according to Eq. (A1), we have

$$U_c = C_c = 1, \quad (\text{A2})$$

where  $U_c$  and  $C_c$  denote the values of  $U$  and  $C$  at  $\xi_c$ . Also, the relevant characteristic equation (see p. 46 in (27)) for isentropic flow can be put in the form

$$k \frac{dc}{dt} - \frac{dc}{dt} - \frac{2cu}{r} = 0, \quad (\text{A3})$$

in which  $k = 2/\gamma - 1$  and the differentiations are performed along the characteristic, i.e., along  $dr/dt = u - c$ . The substitution of Eq. (A1) into Eq. (A3) now leads, with the use of Eq. (A2), to

$$2U^2 - (1 - k)(1 - U)^{-1} U_c + U^{-1} - 1 = 0. \quad (\text{A4})$$

Some important properties of the solution are implied directly by this quadratic equation for  $U_c$ .

We wish particularly to know the possible values of  $\xi_c$  in this problem, since from them the asymptotic behaviour of a collapsing cavity in a liquid might be inferred. The first possibility which need be considered is that  $\xi_c = 1$ . This value clearly is admissible according to Eq. (A4) whose roots become  $U_c = 0, 1$ , indicating that there is no "critical characteristic" inside the flow; or rather it could be said that the characteristic has become  $\xi = 1$  and thus coincides with the boundary  $\xi = \xi_c$ . For

$\xi = 1$ , the velocity  $UR$  is constant, as are all velocities along rays  $r/t = \text{const}$  in the  $(r, t)$ -plane. This case would therefore be relevant to the cavitation problem if the terminal velocity of collapse were finite yet very large compared with  $c$ . Courant and Friedrichs ((27), p. 431) have noted that the present gas-dynamical problem does have a solution with  $\xi_c = 1$ , at least for the value  $\gamma = 1.4$  appropriate to air. On

further investigation, however, it appears there is no solution applicable to the cavitation problem. This fact can most easily be demonstrated as follows.

When the expressions Eq. (A1) are inserted into the dynamical and continuity equations for spherical isentropic flow (see (27), p. 37) and use is made of the fact that  $d\phi/de = k/c$ , we obtain the equations

$$(U+1)U'' + k(U+C') = U^2 + (1+U)U' + kC^2 \quad (A5)$$

$$C(U' + k(U+1)C') = C' + (3+k)U' + k^{-1} \quad (A6)$$

We recall that  $U(1) = 1$  and  $C(1) = 0$ ; hence, for  $\gamma = 1$ , we find from Eq. (A6) that

$$U'(1) = \frac{3}{1+k} \quad (A7)$$

and from Eqs. (A5) and (A7) we find that

$$k(C'(1))^2 = U'(1) + U''(1) = \frac{3(k+2)}{(k+1)^2} \quad (A8)$$

This result shows that for a real solution it is necessary that  $k \geq 2$ , which means that  $\gamma \geq 2$ . With  $\gamma = 7$  as at present, there is therefore no solution with  $\gamma = 1$ .

Further investigation shows that there is only one admissible value of  $\gamma = 1$ ; but there appears to be no simple way of calculating this value. However, a lower limit to  $\gamma$  can at once be specified on consideration that Eq. (A4) must have real roots. With  $k = 1.3$ , corresponding to  $\gamma = 7$ , the conditions for real roots become

$$\gamma^2 - 7\gamma + 3 \geq 0 \quad (A9)$$

By means of some fairly simple analysis, details of which we shall omit here, one may conclude that the actual value of  $\gamma$  is only slightly greater than the value in Eq. (A9). But, to obtain  $\gamma$  accurately, the following course is necessary.

From Eqs. (A5) and (A6), a differential equation can be obtained in which  $U$  and  $C$  occur, respectively, as independent and dependent variables and in which  $e$  is absent. This has the form

$$\frac{dC}{dU} = f(C, U) \quad (A10)$$

where  $k$  and  $\gamma$  are involved as parameters in the function  $f$  of  $C$  and  $U$ . It turns out (which implies  $C = 1 - U$ ; see Eq. (A2)) corresponds in general to a singularity of this differential equation; and Eq. (A4) accordingly assumes the role of a condition on the parameters  $k, \gamma$  which is necessary for a physically realistic solution. The correct value of  $\gamma$  can apparently only be found by substituting trial values in Eq. (A10) and observing whether corresponding solution meets all the requirements of the physical problem (this procedure recalls the work of Guderley (26)). As the solutions to Eq. (A10) can be found only by numerical integration, the task of finding  $\gamma$  entails a great deal of computation. But this work has been done by Mr. Hunter at Cambridge; and for  $\gamma = 7$  he has determined the value of  $\gamma$  at about 0.5552.

Thus it appears fairly well established what the asymptotic behaviour should be in the cavitation problem if the terminal velocity of collapse is in fact infinite. Note

that the above value of  $\gamma$  implies that  $\gamma \sim R \ln R \sim R^{0.801}$  as  $R \rightarrow 0$ , this exponent being  $\gamma^{-1} = 1$ . However, it has not been proved that the terminal velocity is infinite; this has been inferred only because the results of the machine computation seem to indicate it to be so.

The total energy of the gas flow considered above is found to be infinite; but this fact is not necessarily inconsistent with our application to the cavitation problem, since only the motion very near the centre is supposed to be the same in the two cases. Actually, a very important conclusion with respect to the cavitation problem follows on considering how the energy of the gas flow is distributed. With  $\gamma = 7$  and  $\epsilon = 0.5552$ , it can be shown that in the limit as  $R \rightarrow 0$  the total kinetic and compressional energy within a sphere of radius  $r$  is proportional to  $r^{1.29}$ . Thus, evidently the energy of the liquid motion also is spread away from the centre of collapse, there being no concentration of energy at the centre (as happens in the case of incompressible flow) despite the infinite velocity which occurs there. The physical significance of this fact was noted earlier in this paper.

## REFERENCES

1. Fitzpatrick, H.M., and Strasberg, M., "Hydrodynamic Sources of Sound," p. 241 in "Symposium on Naval Hydrodynamics," Sherman, F.S., editor, Nat. Acad. Sci.-Nat. Res. Council, Publ. 515, Washington, 1957
2. Benjamin, T. Brooke, "Noise from Cavitation Generated by Vibrating a Mass of Water," Abs. in "Programme of the 55th Meeting of the Acoust. Soc. Am. (1958)
3. Mellen, R.H., "Ultrasonic Spectrum of Cavitation Noise in Water," J. Acoust. Soc. Am. 26:356 (1954)
4. Mellen, R.H., "An Experimental Study of the Collapse of a Spherical Cavity in Water," J. Acoust. Soc. Am. 28:447 (1956)
5. Gilmore, F.R., "The Growth and Collapse of a Spherical Bubble in a Viscous Compressible Liquid," Calif. Inst. Tech., Hydromechanics Lab., Report No. 26-4 (1952)
6. Flynn, H.F., "Collapse of a Transient Cavity in a Compressible Liquid," Harvard University, Acoustics Res. Lab., Tech. Mem. No. 38 (1957)
7. Lighthill, M.J., "A Technique for Rendering Approximate Solutions to Physical Problems Uniformly Valid," Phil. Mag. (7)40:1179, (1949). See also ref. (25).
8. Whitnam, G.B., "The Propagation of Spherical Blast," Proc. Roy. Soc. A, 203:571 (1950)
9. Whitham, G.B., "The Propagation of Weak Spherical Shocks in Stars," Comm. Pure Appl. Math. 6:397 (1953)
10. Whitham, G.B., "On the Propagation of Weak Shock Waves," J. Fluid Mech. 1:290 (1956)
11. Lord Rayleigh, "On the Pressure Developed in a Liquid During the Collapse of a Spherical Cavity," Phil. Mag. 34:94 (1917)
12. Harrison, M., "An Experimental Study of Single-Bubble Cavitation Noise," Taylor Model Basin Report No. 815 (1952). See also J. Acoust. Soc. Am. 24:776 (1952)

13. Benjamin, T. Brooke, "Cavitation in Liquids," Ph.D. Dissertation, University of Cambridge (1954)
14. Knapp, R.T., and Hollander, A., "Laboratory Investigations of the Mechanism of Cavitation," Trans. A.S.M.E. 70:419 (1948)
15. Bromwich, T.J.I'a., "An Introduction to the Theory of Infinite Series," 2nd Ed., p. 174 (see particularly Example 5), London:Macmillan (1926)
16. Benjamin, T. Brooke, Contribution to the discussion following Ref. (1).
17. Lamb, H., "The Early Stages of a Submarine Explosion," Phil. Mag. 45:257 (1923). See also Ref. (18), 91.
18. Lamb, H., "Hydrodynamics," Cambridge University Press, 6th Ed. (1932)
19. Cole, R.H., "Underwater Explosions," Princeton University Press (1948)
20. Plesset, M.S., "Dynamics of Cavitation Bubbles," J. Appl. Mech. 16:277 (1949)
21. Noltingk, B.E., and Neppiras, E.A., "Cavitation Produced by Ultrasonics," Proc. Phys. Soc. B, 63:674 (1950); 64:1032 (1951)
22. Robinson, R.B., and Buchanan, R.H., "Undamped Free Pulsations of an Ideal Bubble," Proc. Phys. Soc. B, 45:893 (1956)
23. Herring, C., "Theory of Pulsations of a Gas Bubble Produced by an Underwater Explosion," OSRD Report No. 236 (1941); also in "Underwater Explosion Research," Vol. II, Washington, D.C., Office of Naval Research (1950)
24. Trilling, L., "The Collapse and Rebound of a Gas Bubble," J. Appl. Phys. 23:14 (1952)
25. Tsien, H.S., "The Poincare-Lighthill-Kuo Method," Advances in Appl. Mech. 4:281 (1956)
26. Guderley, G., "Starke kugelige und zylindrische Verdichtungsstosse in der Nahe des Kugelmittelpunktes bzw. der Zylinderachse," Luftfahrtforschung 19:302 (1942)
27. Courant, R., and Friedrichs, K.O., "Supersonic Flow and Shock Waves," New York:Interscience (1948)

NOTE ADDED IN PROOF. A complete study of the asymptotic theory referred to in the Appendix is presented in a paper by C. Hunter, "On the Collapse of an Empty Cavity in Water," J. Fluid Mech. 8:211 (1960).

\* \* \* \* \*

## DISCUSSION

C. A. Gongwer (Aerojet General Corporation)

At Aerojet we have been able to generate a transient bubble of four-foot maximum diameter which is a true cavitation bubble, i.e., one with negligible permanent



T. B. Benjamin

gas content. Because it's so large, the time scale is expanded and we can take a lot of time studying it. I would estimate from movies, that the velocity of collapse is on the order of several hundred feet per second. What gas is present is possibly air which is drawn out of the water. It becomes incandescent on recompression and there is a flash. This is possibly the source of the luminescence occasionally observed in cavitation experiments. When the bubble becomes small it looks like a "porcupine" in that sharp spikes extend radially from it. There is debris in and on the surface of the bubble which is overtaken by this large, collapse acceleration and is left behind projecting like radial spikes all over the bubble.

The bubble center is 5.5 feet deep and 10 feet away. The charge is about an ounce of this non-gassing explosive.

Figures D1 and D2 are representative pictures of the bubble at maximum size and near the final collapse.



Fig. D1 - Maximum expansion of Alclo charge, reel 10031, time = 50 ms, bubble radius = approx. 4 inches

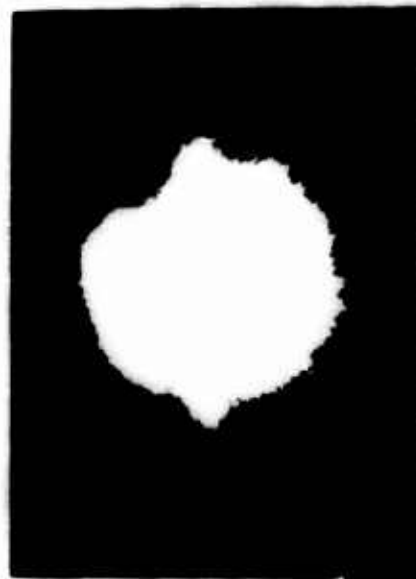


Fig. D2 - Near final collapse of Alclo charge, reel 10031, time = 95 ms, bubble radius = approx. 4 inches

This bubble lasts about one-tenth of a second, and one sees a little jet extending upward with a few bubbles in it. This is because the integrated displacement (vs time) of the bubble provides an upward impulse to the water comprising the virtual mass.

The implosion shock is of the same order as that produced by the explosion. The collapsing bubble (see Fig. 2) has sharp projections on it, sticking out radially like quills on a porcupine as it comes together. One sees a little residual burning, but when the luminescence disappears there is virtually no gas. For our purposes the bubble is empty.

### Pressure Waves from Collapsing Cavities

There is enough dissolved air on the surface of the 4-foot bubble in a layer of water 5/1000 of an inch thick to supply what appears to be the residual gas. This bubble is about 4 feet in diameter. It represents a potential energy at this stage of approximately 150,000 foot-pounds.

Further analysis of the film gives the radius-time curves, shown in Fig. D3, plus a derived curve of pressure vs. time in Fig. D4. This data was analyzed by Mr. J. Levy of Aerojet. Further work is being done on the explosive to reduce even further the amount of residual gas and thus approximate more closely the conditions presented in Dr. Benjamin's paper.

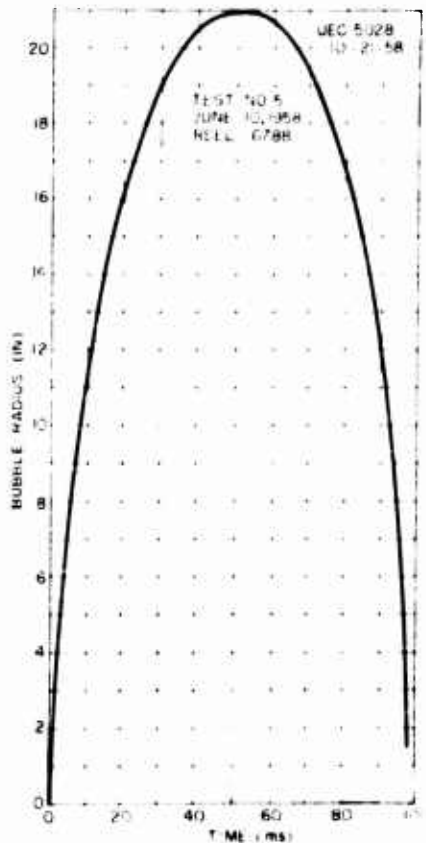


Fig. D3 - Bubble radius vs. time, 1 oz. Alcho. finger, depth 5.5 feet.

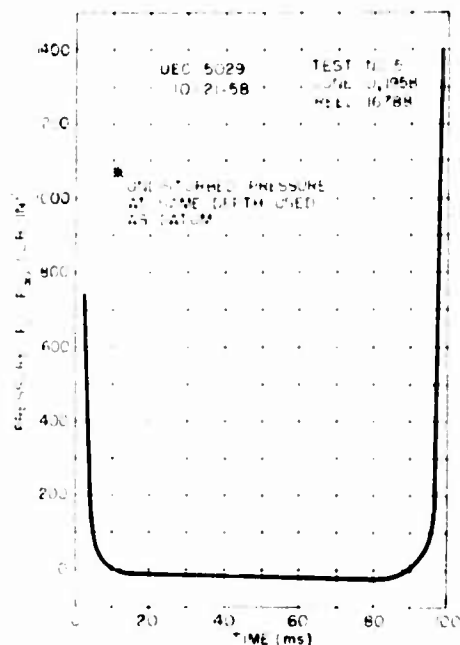


Fig. D4 - Bubble pressure vs. time, 1 oz. Alcho. finger, depth 5.5 feet.

F. S. Burt (Admiralty Research Laboratory)

With respect to the question as to whether or not rebound follows the collapse of a vapor cavity, it may be worth while referring to some experimental work which was carried out at the Admiralty Research Laboratory in 1952 by Mr. A. L. Kendrick. In these experiments, single vapor cavities were initiated by a nucleus of permanent gas produced electrolytically - the instability being induced thermally.

T. B. Benjamin

Photographs taken with a high-speed camera at the rate of 16,000 frames per second showed that any rebound that existed was extremely small. However, several well-defined rebounds could be observed when appreciable quantities of permanent gas were introduced into the cavity.

M. S. Plesset (California Institute of Technology)

Dr. Benjamin's paper contains several remarks which are somewhat obscure and puzzling. I refer to the discussion on the collapse velocity of a bubble and to the remarks about the development of a shock before the end of collapse. In connection with the latter, I was interested to see the remark that "the machine calculations organized by Mr. Hunter have indicated that no shock is in fact formed up to the instant when  $R = 0$ ." The author has also made a very questionable point to the effect that his analysis reveals an error in the Kirkwood-Bethe approximation which has been applied to this problem.

Dr. Benjamin has apparently not given much consideration to the numerical integrations of the compressible equations of bubble collapse which were carried out some years ago. One of these was made by A. J. R. Schneider<sup>\*</sup> up to a bubble collapse velocity corresponding to a Mach number of 2.2. A summary of these calculations has been given in the paper by F. R. Gilmore<sup>†</sup> which is referred to by Dr. Benjamin. A numerical integration of the compressible equations was also performed subsequent to Schneider's calculation by Dr. Gilmore. (Gilmore's results have been reported in the Proceedings of the First Symposium on Naval Hydrodynamics.)<sup>‡</sup> Both Schneider's calculations and those made by Gilmore show rather good agreement between the numerical integrations and the results obtained from the Kirkwood-Bethe hypothesis. As expressed by Gilmore, "the calculated bubble-wall velocity agrees within 6 percent with that given by the analytical theory (based on the Kirkwood-Bethe hypothesis) over the calculated range of 0.2 to 4.9 times the velocity of sound in water. The inward velocity thus appears to increase with the radius to the minus one-half power as the radius becomes small, instead of with the minus first power given by the acoustic theory or the minus three-halves power given by the incompressible theory."

T. Brooke Benjamin

Apart from expressing admiration for the resources of Aerojet, I wish to make only one minor comment upon the exciting experiments described by Dr. Gongwer. This is that the buoyancy effects are probably not duplicated by typical small cavitation bubbles owing to the great differences in respective values of the gravitational scale factor  $P_0 / \rho R_0$ , where  $P_0$  is the environmental pressure and  $R_0$  is a linear measure of bubble size. Otherwise Dr. Gongwer's bubble appears to provide a most effective model of a cavitation bubble.

<sup>\*</sup>A. J. R. Schneider, "Some Compressible Effects in Cavitation Bubble Dynamics," Thesis, California Institute of Technology, 1949.

<sup>†</sup>F. R. Gilmore, "The Growth or Collapse of a Spherical Bubble in a Viscous Compressible Liquid," Hydrodynamics Laboratory Report No. 20-1, California Institute of Technology, 1952.

<sup>‡</sup>Symposium on Naval Hydrodynamics, Sept. 24-28, 1950, Publication 515, National Academy of Sciences - National Research Council, Washington, D. C. (See in particular p. 320 and p. 280.)

Mr. Burt has done a valuable service in drawing attention to A. L. Kendrick's experiments, which I have long regarded as an important contribution to cavitation studies and which deserves wide recognition. It is hoped that a full account of these experiments may yet be published, even after so many years have passed since the work was done.

I hope that the several changes incorporated in the final draft of my paper will help to allay some of the misgivings felt by Prof. Plesset. But I still fail to see what is questionable about my remark quoted in Prof. Plesset's third sentence: I still do not find it in any way directly obvious that the shock could not form shortly before—rather than immediately at—the instant of final collapse of an empty cavity, even though I fully accept the evidence of the machine calculations that it does not. Prof. Plesset's comment seems to imply that this fact is self-evident.

Again, I see nothing questionable about my demonstration of the second-order error in the Kirkwood-Bethe approximation. This error certainly exists, though in the paper I have not considered exactly how important it may be. I also purposely refrained from making a critical examination of the theories which, as Prof. Plesset mentions, his two colleagues have worked out on the basis of the Kirkwood-Bethe approximation. The principal aim of my paper was merely to show how better approximations than this one can be made, so that a theory of cavity collapse can be developed on a more secure basis. As one definite criticism, however, I may point out that since the Kirkwood-Bethe approximation becomes wildly inaccurate for highly supersonic flows with velocities approaching infinity, particularly near the centre where the effects of spherical divergence are largest, the asymptotic law of velocity variation referred to by Prof. Plesset is obviously a spurious result. If the collapse velocity does become infinite, the correct law can only be established by some self-consistent asymptotic theory such as the one outlined in the Appendix to my paper.

\* \* \* \* \*

# NEW DEVELOPMENTS IN THE THEORY OF SUPERCAVITATING FLOWS

Marshall P. Tulin

*Office of Naval Research, London*

## INTRODUCTION

Cavity flows in fluids occur in nature under a variety of circumstances. The least sophisticated of these are the cases where the flowing fluid is a heavy liquid such as water or a volatile fuel, and when the cavity is filled with a light gas such as air or steam or volatilized fuel. The gas may be supplied externally as in the case of ventilated flows such as occur when a surface-piercing strut proceeds at such high speeds through water that a cavity forms behind it into which rushes air from the atmosphere, or the gas may be supplied by vaporization of the flowing fluid due to flow-induced reduction of pressure. This is called cavitation and commonly occurs when hydrofoils, ships' screws, hydraulic machines, or fuel pumps are driven too fast, or when the pressure of the approaching fluid is originally too low. These cases are least complicated because the pressure of the gas in the cavity is nearly constant and known in advance. Most of the recent interest in cavity flows has been motivated by problems of cavitation.

It is, of course, fortunate that the external flow may so often be considered non-viscous; when this is not the case complications naturally ensue. In fact very little is known about the effect of viscosity on cavity flows. As an interesting extreme case, very viscous flows involving gas cavities in fluids occur sometimes in oil bearings into which atmospheric air is sucked, and when gas is forced up through oil-filled soil. Such interesting problems have recently been studied by Sir Geoffrey Taylor and Phillip Saffman at the Cavendish Laboratory and will be discussed at this symposium by the latter.

Perhaps most sophisticated of all cavity flows are those involving homogeneous fluids which "separate" from the obstacle around which they flow. It will be remembered that the original infinite-wake theory of Kirchhoff was intended to deal with such a flow past a bluff obstacle. The difficulty in dealing with these flows lies in the fact that although the pressure in the cavity may be roughly constant it is not known in advance. But that difficulty is not insuperable, as an interesting illustration demonstrates. Professor M. J. Lighthill (1) has treated the problem of a bluff two-dimensional obstacle placed in the path of the flow along a flat plate. It is known that a "dead-water" region forms ahead of such an obstacle. Postulating constancy of

*Note:* The author wishes to express appreciation to the Office of Naval Research for its encouragement and those arrangements which have made it possible for him to write this paper while employed at ONR.

pressure in the dead-water, it may be shown that forward extent of that region depends on the pressure therein, as does the pressure distribution ahead of it. Lighthill reasoned that the boundary layer on the plate must just separate at the beginning of the dead-water, and he was thus able, by matching boundary layer behavior and dead-water pressure, to determine the latter, and show how it depends on the extent of the plate ahead of the obstacle and the state of the boundary layer on the plate. Separated flows of all kinds abound in nature, and it is probably not too much to hope that cavity flow theory will soon be put to further use in providing understanding of some of them. Particularly tempting and important problems involve bluff-body flame holders and stalled cascades, about which Mr. Cornell will speak at this symposium.

Most of the recently devised theory of supercavitating flows applies directly to problems of truly cavitating or ventilating flows and it is those problems that have most benefited by timely recent progress. Indeed, as will be revealed here by Professor Lerbs, and by Mr. Tachmindji and Mr. Morgan the application of low-drag hydrofoil sections to the design of supercavitating propellers was carried out successfully at the David Taylor Model Basin immediately the theory was available in early 1954, with the consequence that the possibility of operating ships' screws efficiently at such high speeds that considerable cavitation occurs was for the first time conclusively proved. At the same time the mental barrier that had existed in designers' minds as regards the safe and efficient use of hydrofoils at very high speeds was also lowered. Indeed, many of us now take for granted the eventual existence of ships' screws, hydrofoil boats, and hydrofoil-equipped aircraft, all operating with supercavitating or ventilated sections. For this change in atmosphere we are in great part indebted to theoretical developments.

In retrospect, the most significant feature of these recent developments has been their concern with lifting hydrofoil sections, a complete departure from the wartime trend which emphasized bodies of revolution such as torpedoes. In fact there now exist reasonably adequate mathematical tools to deal with lifting problems of considerable complexity. The fact that so much use has been made of linearized theory requires no apology. It is very fortunate that so many practical engineering configurations are reasonably slender. It should also be noted that experimental studies have provided much valuable information concerning lifting hydrofoils under cavitating conditions; the tests performed between 1955 and 1957 in the Hydrodynamics Laboratory of the California Institute of Technology and in the Langley Laboratory of the NACA are particularly to be noted.

In the papers to follow, the behavior of supercavitating hydrofoils in a variety of situations will be discussed. I have on different occasions in the past discussed my own results for blunt struts and lifting foils, including the particular possibility of designing for low drag (2-4). For my part now I would like to give some new results for several different and varied cavity flow problems. The topics involved are the cavity flow past smooth two-dimensional struts with unspecified cavity detachment points; effects of high speed on cavity flows past blunt struts; and the three-dimensional cavity flow past slender delta wings.

I am sure that the speakers to follow me will provide both a thorough review of their recent advances in the general field of cavity flows and a thorough discussion of practical applications. It was my interpretation of my role here that I try to say something about the future. I have thus chosen these diverse and what I hope are provocative topics. I hope that I will be excused if they have not been dealt with as conclusively as one might wish.

# THE SUPERCAVITATING FLOW PAST SLENDER STRUTS

In the first application of linearized theory to problems of supercavitating flows, I considered the case of slender blunt-based struts of such shape that the point of detachment of the cavity was necessarily at the very end of the strut. In that way the problem of determining an unknown detachment position was avoided. The case considered was of practical interest, however, and it was possible to reduce the problem of calculating cavity shapes and drags to one of quadratures. Later the problem of minimum drag struts was considered; I gave some reasons for preferring a simple parabolic shape.

Now I would like to show how linearized theory may be used in the more general case of slender struts whose cavity detachment point is unknown at the outset, and to present some results for struts of simple shape.

The pertinent two-dimensional steady flow, symmetric about the  $x$ -axis, is shown schematically in Fig. 1. The wetted boundary of the smooth strut and the cavity wall are continuous streamlines, the cavity wall being in addition a surface of constant pressure.

The point of detachment is not known in advance. However, something can be said about the behavior of the flow there in the case where the flow is truly cavitating. The curvature of the cavity just at the detachment point cannot be infinite and curved towards the body, lest it intersect the body; nor can it be infinite and curved away from the body, lest the pressure in the stream just away from that point be less than the cavity pressure. Nor can the curvature of the streamline at the point of detachment undergo a finite jump, for it is well known that the pressure cannot be constant along a streamline in the neighborhood of such a discontinuity. As has long been known then, the cavity in a cavitating flow must have just the curvature of the smooth body at the detachment point. It can in addition be stated that since the cavity must be convex (from the outside), the body itself must be convex at the point of detachment.

The condition of continuous curvature is just sufficient to allow solution of the present problem, when used together with the conditions imposed in the earlier

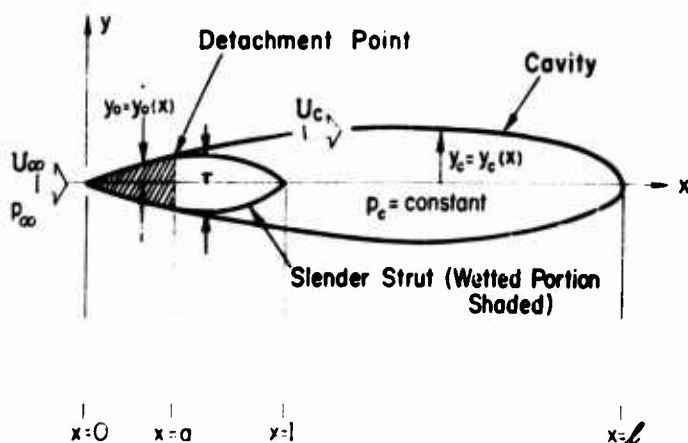
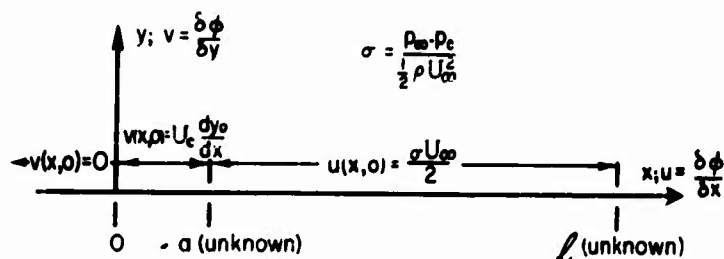


Fig. 1. Supercavitating flow past a slender strut

linearized problem in which the detachment point was known in advance. For struts considered here (third-degree polynomials), only one convex solution is found for each strut. It seems clear that the smoothness and convexity condition, while necessary, are not sufficient to yield a physically meaningful solution representing the infinite cavity past a truly cavitating body, for it need only be supposed that a very small but very sharp bump be placed near the nose of such a body. Surely a convex cavity with continuous curvature at detachment will still exist with a detachment point close to its previous position, despite the fact that the local pressures near the sharp bump will fall far below the cavity pressure. The struts considered here do not, of course, have small sharp bumps on them. When slender enough they have in fact monotonic curvature, increasing in some cases, decreasing in others. For those cases where the wetted body is convex and the curvature is nondecreasing (i.e., the convexity is nondecreasing) it seems likely that with smooth detachment the flow is a truly cavitating one, for it has been shown (5) that such is the case for bodies of nondecreasing convexity (accolades). Some of the struts considered here are not of that type however, and it must only be hoped that the flows produced are meaningful. No verification is attempted through computation of the pressures on the forebody. Interestingly enough it is found that for some of these struts which have monotonically decreasing curvature two smooth cavities exist: one detaching forward and initially convex, the other detaching aft and concave at detachment. The latter is clearly meaningless with regard to cavitation problems.

The pertinent linearized problem here involves the determination, subject to the conditions illustrated in Fig. 2, of a harmonic function  $\phi$ , the potential of the perturbation velocity, and at the same time, of the proper cavity detachment point and cavity length, these being unknown in advance.

The determination of the cavity shape for arbitrary detachment point was, in fact, made in the earlier work on blunt-based struts. The method employed involved the determination of the unknown source distribution for the cavity through inversion of the well known integral equation of incompressible thin airfoil theory.



$\phi$  is harmonic and symmetric about  $y=0$ .

Cavity Closure Condition:  $\int_0^l v(x,0) dx = 0$ .

Continuous Slope and Curvature at Detachment:  $\left. \begin{array}{l} \frac{dy_0(a)}{dx} = \frac{dy_c(a)}{dx} \\ \frac{d^2 y_0(a)}{dx^2} = \frac{d^2 y_c(a)}{dx^2} \end{array} \right\}$

Fig. 2 Linearized boundary value problem



The results are given below:

$$2U_c \frac{dy_c}{dx} = U_c \frac{y_c}{x-a} = U_c \frac{y_c}{x-a} \int_a^x \frac{dy_c}{dt} \frac{dt}{x-t} = \frac{1}{a-t} \text{ and } \frac{U_c}{2U_c} = \int_a^x \frac{dy_c}{dt} \frac{dt}{a-t} \text{ dt}$$

where

$$\frac{U_c}{U_c} = 1 + \frac{1}{2}$$

For a given strut shape  $y = y(x)$ . The first of these expressions may be differentiated to yield the cavity curvature; and thus may the detachment point  $a$  be determined by imposing the condition of smooth curvature there. For cavitation numbers other than zero, the second expression, stating that the cavity is closed, must simultaneously be used.

The actual exploitation of these relations may not be simple because of complicated quadratures, but if only very long cavities ( $a \gg 1$ ) and simple struts (polynomial shapes) are considered, results are readily obtained.

For very long cavities:

$$2U_c \frac{dy_c}{dx} = \frac{U_c}{x-a} = \frac{U_c}{x-a} \int_a^x \frac{dy_c}{dt} \frac{dt}{x-t} = \frac{1}{a-t} \text{ and } \frac{U_c}{U_c} = 4 \int_a^x \frac{dy_c}{dt} \frac{dt}{a-t} \text{ dt}$$

For struts of the shape,  $y = b + a_1x + a_2x^2 + a_3x^3$ , then,

$$2U_c \frac{dy_c}{dx} = \left\{ \frac{U_c}{x-a} + \frac{2U_c b}{x-a} \left[ (2a_1 + 4a_2x + 6a_3x^2) \tan^{-1} \left| \frac{x-a}{x-a} \right| \right] \right. \\ \left. + \frac{U_c}{x-a} (4a_2 + 6a_3x + 4a_3x^2) \right\}$$

and, differentiating to obtain the curvature,

$$2U_c \frac{dy_c^2}{dx^2} = \frac{1}{x-a} \left[ -\frac{U_c}{2} + \frac{2U_c b}{x-a} \left\{ -\frac{a}{2x} (2a_1 + 4a_2x + 6a_3x^2) - (2a_2 + a + 3a_3x + 2a_3x^2) \right\} \right. \\ \left. + \frac{2U_c b}{x-a} (6a_3x + a) + \frac{2U_c b}{x-a} \tan^{-1} \left| \frac{x-a}{x-a} \right| (4a_2 + 12a_3x) \right]$$

The smooth curvature condition is consequently satisfied only when  $a$  satisfies the relation:

$$1 + \frac{1}{2} = \frac{1}{a} (a_1 + 4a_2a + 8a_3a^2)$$

The other necessary relation which follows from the cavity closure condition is

$$1 + \frac{1}{2} = \frac{1}{a} (2a_1 + 8a_2a + 16a_3a^2)$$

These two relations may fortunately be combined to give simple formulas relating (a) detachment point to strut shape and cavitation number, and (b) cavity length to the same quantities. These are:

$$\left( (1 + \frac{1}{2}) 4a_3 \right)^2 = (a_1 + 4a_2a + 8.3 a_3a^2) (2a_1 + 8.3 a_2a + 16.5 a_3a^2) \\ (2a_1 + 8.3 a_2a + 16.5 a_3a^2) \\ (a_1 + 4a_2a + 8a_3a^2)$$

In the case of zero cavitation number and infinite cavity length, the detachment point is given by the vanishing of the quadratic,  $a_1 + 4a_2a + 8a_3a^2$ , and is independent of the strut thickness. The coefficients  $a_1$ ,  $a_2$ ,  $a_3$ , which define a strut, cannot be chosen independently of one another. If  $a_1$  is zero, then  $a_2$  may be taken as unity; in order for the strut ordinate to vanish at  $t = 0, 1$  then  $a_3 = -1$ . If  $a_1$  is not zero then it may be chosen as unity and again for a strut spanning the interval  $0, 1$  it must be that  $a_2 = -(a_3 + 1)$ ; a one parameter family of struts results. It may be shown that these struts are segments of the third-degree polynomial whose zeros are at  $(0, 1, 1/a_3)$ ; the coefficient  $a_3$  must then be less than unity.

The position of the detachment point is plotted against the parameter  $a_3$  in Fig. 3. For values of  $a_3$  between 1 and 3.4, two detachment points are found. The forward point, falling where the body is convex, may have physical meaning, but the after one clearly does not as the body is concave there; only the forward point is plotted in Fig. 3. The fact is illustrated, however, that at least for very slender bodies, the continuous curvature condition is not sufficient in itself to guarantee truly cavitating flows.

Calculations have been made to determine the movements of detachment point with  $\sigma$ . These indicate that the point moves aft very slowly with increasing cavitation number, and that its position depends on the strut thickness. If  $\tau$  is the ratio of strut maximum thickness to strut chord, and  $\Delta$  is the displacement of the detachment point forward of its position for zero  $\sigma$ , the approximate results hold that  $\Delta$  is proportional to the square of the ratio of  $\sigma$  to  $\sigma_0$  and that the cavity length  $\lambda$  is inversely proportional to  $\sigma$ . The calculated constants of proportionality for three different struts are shown in Fig. 4.

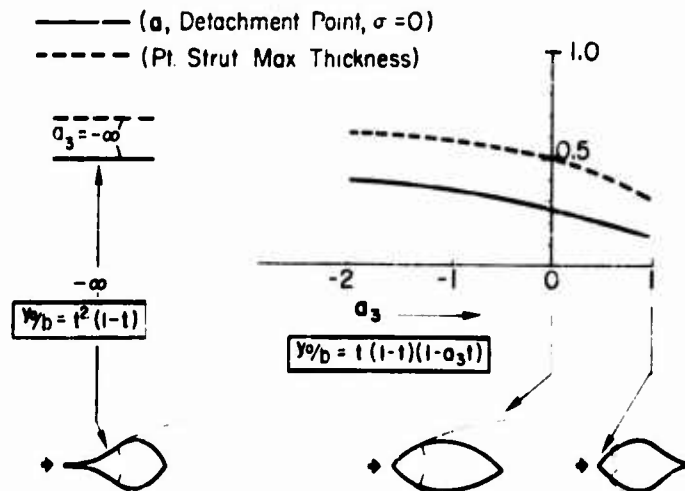
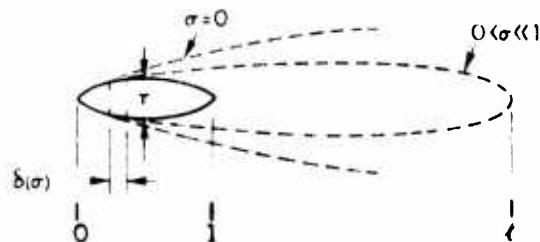


Fig. 3. Cavity detachment point.



$$\sigma \ll 1: \quad \delta = k_1 \left( \frac{\sigma}{T} \right)^2; \quad l = \frac{k_2}{\delta}.$$

$\alpha_3$	$k_1$	$k_2$
$-\infty$	0.025	0.067
0	0.029	0.083
+1	0.008	0.034

Fig. 4 - Cavity length and detachment point,

The resistance of any strut, the detachment point having been determined, may be obtained using the result of previous work. Neglecting terms of order  $\sigma^2$ , the drag coefficient based on maximum strut thickness  $T$  is

$$C_D = \frac{2}{\pi} \left[ \int_0^1 \left( \frac{dy}{dt} - \frac{dt}{a-t} \right)^2 dt \right].$$

The theory indicates that the very slow forward movement of the detachment point contribute only terms of order higher than  $\sigma^2$  to the drag integral, so that just as for blunt-based struts:

$$C_D \approx C_D(0) + 1 \cdot \sigma^2.$$

The drag coefficients ( $\sigma = 0$ ) of the polynomial struts considered here are shown in Fig. 5. The conclusion might be drawn that blunt noses are harmful to resistance; this is certainly the case for the family considered here. However, the superiority of parabolic struts has been shown before. In order to put the present results in proper perspective, the shapes and drags of three struts which cover the entire range of those considered here are compared with three other struts from outside the family in Fig. 6. These are a symmetric diamond strut, a symmetric strut with parabolic nose and tail, and a blunt parabolic strut.

All of these results concerning drag and position of detachment point may be boldly presented as no experimental results for two-dimensional struts seem to be available (although some results for bodies of revolution are available; see Eisenberg (6)). It would clearly be worthwhile for someone to carry out pertinent tests.

Finally, implications of some of the results obtained here with regard to the uniqueness of smooth cavity flows past closed struts may be stated. First: as mentioned before, it was found that for certain of those struts whose curvature is monotonically decreasing two smooth cavities were found, one concave at detachment, the other convex. Second: struts given by higher degree polynomials (than three)

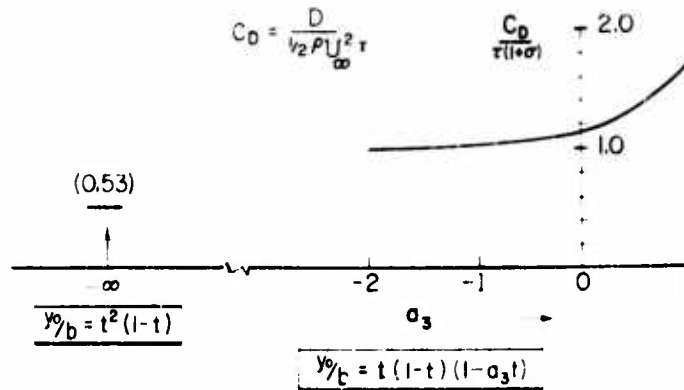
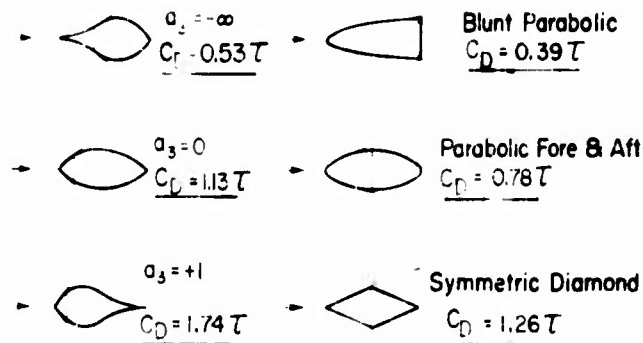


Fig. 5 - Drag of polynomial struts



*Note that the strut  $a_3 = -\infty$  is just the strut  $a_3 = +1$  but turned around*

Fig. 6 - Comparison of strut drags

may very well yield more than two smooth cavity flows, for it is clear that the position of detachment satisfies an algebraic equation of one degree less than the degree of the polynomial defining the strut. It would be interesting to see whether a strut could be found for which more than one smooth and convex cavity flow presents itself.

#### HIGH-SPEED EFFECTS ON SYMMETRIC CAVITY FLOWS

It is probably not too frivolous an undertaking to try to say something about cavity flows in compressible fluids, for the successful and general application of cavity flow information to the study of gas flows with "dead-water" wakes such as may exist in the case of bluff-body flame holders and stalled cascades will certainly require some understanding of the effects of high speed. In addition, problems of

symmetric cavity flows should be tempting to the students of compressible fluids for not only are they relatively simple flows, but they are flows with finite drag at subsonic speeds. The subject is, indeed, not a new one. For certain polygonal obstacles including single wedges, the infinite-wake flow for zero cavitation number may be determined exactly (for Mach numbers at least as great as unity) through the use of a suitable hodograph method, for then the transformed boundaries of the flow are known, the boundary conditions imposed thereon are linear, as are the transformed gas-dynamic equations. Students of transonics have been particularly interested in this possibility and attempts at making calculations for wedge forebodies have been made by Inai (7) and Mackie and Pack (8). Most recently, Helliwell and Machie (9) have treated the flow past slender wedges trailing free streamlines with sonic velocity thereon; they used von Karman's transonic approximations and Roshko's free streamline model.

In the absence of exact results of sufficient detail or even of the pertinent transonic solution, the use of a suitably modified Prandtl-Glauert rule to extrapolate incompressible results for low cavitation number flows past suitably slender forebodies, the cavity detachment point being known, seems particularly inviting.

For suitably low cavitation numbers, even an unslender body will possess a very slender cavity, since the thickness ratio of the latter is, at least in an incompressible flow, proportional to  $\frac{1}{M_\infty^2}$ . The Mach number of the flow in the vicinity of these slender cavities will be very close to the Mach number corresponding to the cavity pressure coefficient. This cavity Mach number,  $M_c$ , will generally be greater than free stream Mach number,  $M_\infty$ , except in the case of an infinite cavity when they will be equal. No matter how slender the forebody, therefore, the streamwise perturbation of the free stream does not tend to vanish, but, instead, approaches on the body and cavity a constant value equal to  $(M_c - M_\infty)$ . The proper linearization of the nonlinear gas-dynamic equations is, then,

$$(1 - M_c^2) \frac{\partial^2 \phi}{\partial x^2} + \frac{\partial^2 \phi}{\partial y^2} = 0$$

and the Prandtl-Glauert rule must be suitably modified.

As implied above, this linearized equation must be a very good approximation for slender bodies because of the cavity enforced uniformity of the near flow field. For still another reason, the Prandtl-Glauert rule seems especially useful: according to linearized theory (2), it is a consequence of D'Alembert's paradox that the cavitation drag of the forebody must be identical with the "nose drag" of the end of the cavity (which in turn depends only on the radius of curvature of that nose). Jones and van Dyke (10) have recently shown (but not rigorously) that the Prandtl-Glauert rule is particularly applicable to the estimation of nose drag. In fact they have shown that even though it may fail to predict exactly the distribution of pressures, the P-G rule does extrapolate the overall drag of a parabolic half body exactly for Mach numbers up to one. All of which implies that were the shape of the cavity behind a given slender forebody known for all Mach numbers, the drag could be estimated without error for zero  $C_d$  and with small error for suitably small  $C_d$ . Unfortunately the changing shape of the cavity is not known in advance, but must be estimated; hence the use of the P-G rule involves unknown errors. However, as remarked previously, the cavity enforced uniformity of the perturbation flow gives reason to hope that nonlinear distortions of the cavity shape which are not predicted by the P-G rule will be limited in importance to very high subsonic Mach numbers and that this completely linear theory has a large range of applicability. Confirmation of this speculation awaits the solution of the pertinent transonic problem.

Figure 7 shows the cavity flow in the real physical plane (on the left) and in the affinely transformed incompressible flow plane (on the right). The primed quantities refer to the incompressible transformed plane. The application of the P-G rule is well discussed by Sears (11) and only results for the case of cavity flows are presented here. Certain results for incompressible cavity flows presented by Tulin (2) are also utilized without derivation.

Important results are that the drag increases with Mach number as

$$\frac{1}{\sqrt{1-M_c^2}} \quad (1-M_c^2)^{-1/2}$$

and that the cavity becomes more slender as  $(1-M_c^2)^{-1/2}$ , the length increasing as  $(1-M_c^2)^{-1}$  and the thickness as  $(1-M_c^2)^{-1/2}$ . All of these quantities may be readily determined for a given forebody utilizing the available incompressible theory. Some results are summarized below:

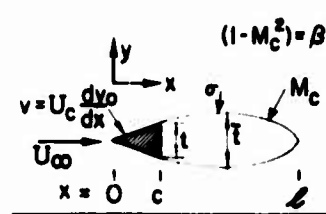
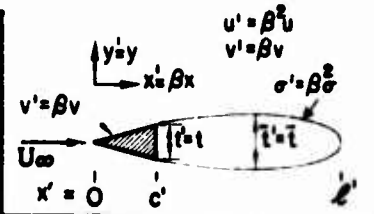
COMPRESSIBLE	TRANSFORMED INCOMPRESSIBLE
 <p> <math>(1-M_c^2)^{-1/2} = \beta^2</math>  <math>v = U_c \frac{dy}{dx}</math>  <math>U_\infty</math>  <math>x = 0 \quad c \quad l</math>  <math>y = 0 \quad t</math>  <math>M_c</math> </p>	 <p> <math>u' = \beta^2 u</math>  <math>v' = \beta v</math>  <math>\sigma' = \beta^2 \sigma</math>  <math>U_\infty</math>  <math>x' = 0 \quad c' \quad l'</math>  <math>y' = 0 \quad t'</math>  <math>M' = 0</math> </p>
$M = M_\infty$	$M' = 0$
$(1-M_c^2) \phi_{xx} + \phi_{yy} = 0$	$\phi'_{xx} + \phi'_{yy} = 0$
$D' = \beta^2 D$	$D' = \beta^2 D$
$C_D = \frac{D}{\frac{1}{2} \rho U_\infty^2 t} = \frac{C_D'}{\beta^2}$	$C_D' = \beta^2 C_D(M) = \frac{2(1+\sigma')}{t'} \left[ \int_0^{x'} \frac{dy'}{dx'} \frac{dy'}{dx'} \right]^2$ $C_D' \left( \frac{M \neq 0}{\sigma = 0} \right) = \beta C_D' \left( \frac{M=0}{\sigma=0} \right)$ $C_D' \left( \frac{M \neq 0}{\sigma \neq 0} \right) = [1 + \beta^2 \sigma] \beta C_D' \left( \frac{M=0}{\sigma=0} \right)$ $= [1 + \beta^2 \sigma] \beta \frac{C_D' \left( \frac{M=0}{\sigma \neq 0} \right)}{[1 + \sigma]}$ $= [1 + \beta^2 \sigma] \beta \frac{C_D \left( \frac{M=0}{\sigma \neq 0} \right)}{[1 + \sigma]}$ $= \beta^2 C_D \left( \frac{M \neq 0}{\sigma \neq 0} \right)$
$C_D(M; \sigma) = C_D \left( \frac{M=0}{\sigma=0} \right) \frac{[1 + \beta^2 \sigma]}{\beta [1 + \sigma]}$	
$l'/t' = \frac{8}{\pi} \frac{C_D \left( \frac{M=0}{\sigma=0} \right)}{\pi \sigma^2 \beta^2}$	$l'/t' = \frac{8}{\pi} \frac{C_D'}{\sigma'^2} \quad \sigma \ll 1$

Fig. 7 - The Prandtl-Glauert transformation, cavity flows

# New Developments in the Theory of Supercavitating Flow

$$C_D = 1 - C_D(M_\infty) = \frac{2}{\sqrt{1 - M_\infty^2}} \left[ \int_0^1 \frac{dy_0}{dx} \frac{dx}{1 - x^2} \right]^2$$

where  $C_D$  is based on the strut maximum thickness,  $T$ , and where  $y_0$  is the ordinate of the strut, which is itself of unit length.

$$C_D = 1 - \frac{8T}{\sqrt{1 - M_\infty^2}} C_D(0,0)$$

where  $\ell$  is the cavity length.

$$C_D = 1 - \frac{4T}{\sqrt{1 - M_\infty^2}} C_D(0,0)$$

where  $\bar{T}$  is the maximum thickness of the cavity.

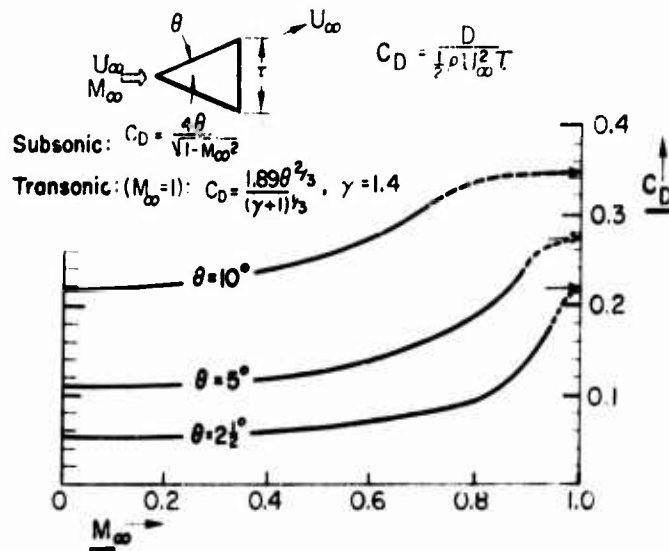
The P-G rule predicts infinite drag for sonic cavity Mach numbers and transonic theory must be invoked before such speeds are reached. As previously noted, Helliwell and Mackie (9) have considered the case of slender wedges trailing free streamlines with sonic velocity thereon. According to their results, the drag coefficient,  $C_D$ , of a wedge of semi-apex angle equal to  $\alpha$  is, when  $C_D$  is based on wedge total thickness and when the base pressure is taken into account:

$$C_D = \frac{1.89 - 2.3}{(\alpha + 1)^{1.3}}$$

which result implies that the Mach number distribution on the wetted portion of the wedge is insensitive to changes in free stream Mach number; this effect is not really surprising as, in the case considered, the velocity at the apex and shoulder of the wedge are fixed and independent of  $M_\infty$ . If the Mach number on the free streamline is not fixed as unity but is instead taken as equal to  $M_\infty$  ( $\alpha = 0$ ), then the reason for the insensitivity of the wedge Mach number distribution to  $M_\infty$  is partially removed. It is conjectured that, in fact, the wedge Mach number distribution would in that case be closely proportional to  $M_\infty$ . The drag coefficient of the wedge would then be relatively insensitive to  $M_\infty$  for subsonic Mach numbers close to unity (since  $C_D = 4\alpha / (1 - M_\infty^2)$ ). It would be interesting to verify this conjecture by actual calculation using transonic theory.

The estimated drag of slender wedges of semi-apex angle, 2-1/2, 5, and 10 degrees with infinite trailing cavities,  $\alpha = 0$ , are presented in Fig. 8; the ratio of specific heats,  $\gamma$ , is assumed to be 1.4.

These brief considerations have been undertaken mainly to discover some effects of speed on simple cavity flows, but it is well that they serve at the same time to indicate for the symposium record the existence of the interesting transonic theory for cavity flows. It is worthwhile to note that a very recent pertinent paper by Nonweiler (12) contains the interesting result that a half-body whose ordinates vary as  $x^{2/5}$  has a sonic surface velocity everywhere, except at the nose, when the free stream speed is sonic. This gives hint that the asymptotic form of infinite cavities at sonic speed will be of the form  $x^{2/5}$ ; the result of Jones and van Dyke (10) shows, of course, that the asymptotic form of cavities for all subsonic speeds must be  $x^{1/2}$ , and that a different form must obtain at sonic speed.

Fig. 8 - The drag of slender wedges,  $\alpha = 0$ 

#### SUPERCAVITATING FLOW PAST SLENDER DELTA WINGS

Without implying that interesting and important problems\* do not remain to be investigated, it may be said that the behavior of two-dimensional, thin, lifting foils with full cavitation in steady unbounded flow is now fairly well understood. Despite the very considerable work that has been devoted to two-dimensional problems, however, there do not seem to exist any theoretical results pertaining particularly to the behavior of three-dimensional lifting wings with full cavitation. It is true that the direct application in practice of standard aspect ratio corrections to the case of lightly loaded propellers has so far given satisfaction, but no attempt to rationalize the procedure, even for the simple case of a high or moderate aspect ratio plane wing, has been made.

When the wing cavity length is somewhat shorter than the span of the wing, no difficulties would seem to present themselves in the direct extension of lifting line results, but when the cavity is longer than the span then even the forces on the high aspect ratio foil may very well be affected not only by the decreased effective angle of attack due to the trailing vortex system, but also by the difference, due to the finite span of the cavity, between the two-dimensional and actual cavity shapes. For a given cavitation number, clearly the cavity at mid-span must become fatter for decreasing cavity aspect ratio. It is not clear now to what order this fattening of the trailing cavity will affect the lift on the foil, and it is this very point which requires future clarification.

In the extreme case of very low aspect ratio (or slender) supercavitating wings, the flow pattern becomes primarily dependent on the "tip" effects, and different

\*For instance, the behavior of airfoils of conventional shape (rounded nose, sharp tail) for which the cavity detachment point varies with  $\alpha$  and is not known in advance.



considerations apply than in the case of moderate aspect ratio wings. This extreme case is, however, very interesting in its own right and seems to offer a special opportunity to study three-dimensional cavities. Some considerations of the flow past slender supercavitating wings, in particular past the mathematically tractable flat delta wing, are now presented.

As is well known, it is possible to visualize the flow past lightly loaded, low aspect ratio wings having thin cross-sections and fully wetted, as a changing two-dimensional flow in the transverse plane being convected with the main stream. The theory for such purely lifting slender wings allows, even for incompressible flows, no downstream effects to be propagated upstream. If the slender body has significant thickness, however, the flow at a particular point on the body does depend on the shape of the body everywhere else. If the body is smooth and slender and its shape known in advance, the slender body theory reduces the problem of finding the flow to one of quadrature (for the thickness effects) plus a set of two-dimensional potential problems, the normal derivatives of the potential being specified. Thus is the problem solved.

In the present case, and characteristic of cavity flow problems, the cavity thickness is not known in advance. Instead the pressure on that part of the top of the wings just under the cavity is specified. This pressure has, in general, contributions from both the thickness effects and the transverse flows. Unfortunately, adequate boundary conditions in the transverse flow planes are not really known in advance, but must be determined through consideration of the interaction between thickness effects and transverse flows and their additive effect on the wing pressure distribution. This involves a complicated procedure.

In the case of flat, slender, deltas the possibility exists that the supercavitating flow past such wings is essentially conical. The determination of the transverse flow and longitudinal thickness distribution may then be simplified. In the present analysis it is shown that an almost conical flow may be found for all cavitation numbers; the flow being more conical at the apex of the delta than at the trailing edge. Let it be stated in advance that the cavity, which is itself conical in shape, does not cover all of the wing top in any case but as the cavitation number decreases, grows from the leading (or side) edge region until at  $\infty$  it covers all of the wing top except for a wedge-shaped region along the wing centerline which region is wetted by a sort of re-entrant jet flow. The theory, in fact, imposes a very special relationship between the cavity shape and the amount of fluid in the impinging jet. The cavities carried off downstream are assumed to take up such a shape that the pressure within them has the proper value, and they are assumed to have an important influence on the flow over the wing only at the trailing edge where, of course, the flow cannot be truly conical. The effect of these cavities, diminishing toward the apex, will at any rate only be such as to change the ambient pressure field equally on the top and bottom of the wing and it is here neglected.

The flow about a flat, slender delta wing of apex angle  $\alpha$ , inclined at an angle of attack  $\theta$ , operating at cavitation numbers both very large ( $\sigma \rightarrow 0$ ) and very small ( $\sigma \rightarrow 1$ ) is shown schematically in Fig. 9. It is these extreme cases for which numerical results are provided in the present paper. Some assumptions about the flow are already introduced into the figure. These are that (a) the flow over the wing is assumed to be similar in the various transverse planes - and thus conical, and (b) the conical cavity envelops only part of the upper surface of the wing.

Some of the nomenclature to be used is illustrated in Fig. 10.

For simplicity, a delta wing of unit length has been chosen.

Diagram illustrating the addition of magnetic fluxes in a cavity. The diagram shows a 3D coordinate system with axes labeled  $x$ ,  $y$ , and  $z$ . A vector  $n\Phi$  points into a shaded plane. The plane is divided into two regions by a line, with vectors  $\Phi_1$  and  $\Phi_2$  pointing into it. The total flux  $\Phi$  is shown as the vector sum of  $\Phi_1$  and  $\Phi_2$ . A box at the bottom contains the equation  $\Phi_1 + \Phi_2 = \Phi$ .

$$(X \times Y) \cap U = \bigcup_{i=1}^n (X_i \times Y_i) \cap U$$

For small angles of attack, the vertical velocity on the bottom of the wing is constant and equal to  $v_{\text{bottom}}$ . Thus

1. 1. 1.

everywhere on the bottom of the wing. The available boundary conditions have now been stated.

For sufficiently slender bodies (13):

$$\Phi(x, y, z) = \Phi(x, z; x) + f(x)$$

where

$$\Delta \Phi = \Delta \Phi \Phi = 0$$

and

$$f(x) = \frac{U_0}{4} \int_{-\infty}^{\infty} \frac{\Phi(x_1)}{x - x_1} dx_1 + \frac{1}{2} \int_{-\infty}^{\infty} \frac{\Phi(x_1)}{x - x_1} dx_1$$

The term  $\Phi(x, z; x)$  will be recognized as the two-dimensional flow in the transverse  $(x, z)$  plane while the  $f(x)$  is a flow due to thickness.

The two-dimensional potential may be expressed in terms of a contour integral around the boundary of the body in the transverse plane (Green's Theorem). For small angles of attack, the cavity thickness is also small and the integration may thus be made around the projection of the wing and cavity on the horizontal plane (i.e., along the top and bottom of a symmetric slit in the  $z$  axis). Then

$$\Phi(x, z; x) = \frac{1}{2} \oint \left( \frac{1}{z - z'} - \frac{1}{z - z''} \right) \Phi(z - z')^2 + x^2 dz'$$

The assumption that the flow is conical over the wing leads, through consideration of the above integral and the definitions  $x = 2x/s$ ,  $z = 2z/s$ , to the following:

$$\Phi(x, z; x) = \Phi(x) + \frac{s(x)}{2} \Phi(y, z)$$

where

$$\Phi(x) = \frac{U_0 s(x)}{4} + \frac{s(x)}{2} + \int_{-1}^1 \frac{\Phi(y, z)}{x - y} dy$$

and  $\Phi(y, z)$  is harmonic. The latter represents the two-dimensional flow in the non-dimensionalized cross-flow planes.

The fact that the two-dimensional flow  $\Phi$  makes a contribution to the total flow which is only a function of  $x$  (the term  $\Phi(x)$ ) is especially to be noted.

The boundary conditions now become:

On the bottom of the wing,

$$\frac{\partial \Phi}{\partial y} = 0$$

and, on the part of the wing top covered by the cavity ( $z = 1$ ),

$$\frac{p}{\rho} = \frac{U_0^2}{2} - \frac{1}{2} (x^2 + y^2) = \frac{1}{2} \left( z^2 - r^2 \right),$$

In order that this condition be satisfied,

$$z = \frac{r}{\sqrt{2}} = \text{constant}$$

and

$$f'(x) + g'(y) = \text{constant}.$$

However it may readily be shown, utilizing the definitions of  $f$  and  $g$  given earlier, that near the apex of the delta ( $x \rightarrow 0$ ),

$$f'(x) + g'(y) = \frac{U_0^2 k}{2} \oint_{\Gamma} \frac{dz}{z} = 0$$

where  $k$  is defined such that  $S(x) = 2k \oint_{\Gamma} \frac{dz}{z}$ , ( $S(x)$  is the contour integral of  $\frac{1}{z}$  in a transverse plane.)

Thus, in order for the flow to be conical as assumed and still to contain a constant pressure region, the contour integral of  $\frac{1}{z}$  (or  $\frac{1}{z^2}$ ) in the transverse plane must be identically zero. If a growing cavity exists at all then, the outflow in the transverse plane that it will cause must be accompanied by an inflow just sufficient to make the net source flow in the transverse plane null. The inflow may be imagined to go into two symmetrically placed re-entrant jets. It is just this situation which was anticipated in Figs. 9 and 10. The present theory does not, of course, allow a detailed discussion of the behaviour of the flow in the vicinity of the juncture of cavity and wetted region on the top of the wing. It is believed nevertheless that the theory will reproduce the general features of the real flow.

The new condition has been obtained that the flow in the transverse plane cannot be source-like, or

$$\int_{\Gamma} \frac{dz}{z} = 0.$$

Since  $f$  and  $g$  are then identically zero,

$$\frac{z}{\sqrt{2}} = \frac{U_0}{\sqrt{2}} \quad \text{for } x = 0, \quad z = 1.$$

Since  $z$  must be symmetric with respect to  $z$ ,

$$z = \frac{U_0}{\sqrt{2}} + U_{0,2} \frac{z^2}{\sqrt{2}} + \dots$$

or

$$\frac{z}{\sqrt{2}} = U_{0,2} \frac{z^2}{\sqrt{2}} + \dots \quad z = 0$$

$$\frac{z}{\sqrt{2}} = U_{0,2} \frac{z^2}{\sqrt{2}} + \dots \quad z = 0.$$



M. P. Tatin

It is easily shown that  $A_1$  is pure imaginary, and that

$$\frac{1}{1 - 2} \frac{1}{U_\infty S^2(1)} = iA_1.$$

If  $w$  is the complex velocity in the transverse plane, and  $z = 1/Z$ , then

$$\frac{1}{1 - 2} \frac{1}{U_\infty S^2(1)} = \frac{1}{2} \frac{d^2}{dz^2} (0).$$

Incidentally, the condition that

$$\int_{-1}^1 \frac{1}{z} dz = 0$$

becomes

$$\frac{d}{dz} = 0 \quad 0.$$

The boundary value problem illustrated in Fig. 11 is more easily solved by considering the complex velocity  $w(z)$  in a transformed plane,

$$1 - z^2 = \zeta^2.$$

The reason for this is that the problem in the  $z$  plane has no symmetry about the plane on part of which the boundary conditions are stated, whereas the  $\zeta$  plane has been chosen in order that it be symmetric about the  $\zeta$  plane on the whole of which either  $u$  or  $v$  are specified. The problem for  $w(\zeta)$  is illustrated in Fig. 12.

The proper solution to the problem posed in Fig. 12 may be found by inspection. It is

$$w(\zeta) = iU_\infty \left( 1 - \frac{1}{2} \right) + iU_\infty \left( 1 - \frac{1}{2} \right) \int \frac{\zeta - \zeta_0}{1 - \zeta^2} d\zeta_0.$$

The first two terms on the right represent the appropriate flow past the two plates  $A - BB'$  and  $CC' - D$  having zero horizontal velocity on that part of the  $\zeta$  axis outside

of the plates. The third and most complicated term on the right represents a distribution between  $BB'$  and  $CC'$  of elemental vortices of strength  $2U_\infty$ , each in the presence of the two plates (i.e., having null vertical velocities in that part of the  $\zeta$  axis where the plates exist).

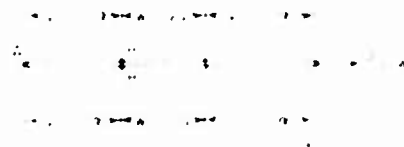
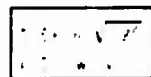


Fig. 12. Flow field in the  $\zeta$  plane.

The two parameters  $\alpha$  and  $\beta$  yet remain to be simultaneously determined. Very complicated quadratures unfortunately appear, especially in the evaluation of  $\alpha$  at the wing leading edge. For the purpose of this paper we shall be satisfied

with having described the appearance of these conical flows and with certain approximate results for the cases of very high ( $\sigma \rightarrow 1$ ) and very low ( $\sigma \rightarrow 0$ ) cavitation numbers. These cases correspond, respectively, to the cases of very short leading edge cavities and cavities covering the entire delta upper surface except in the immediate neighborhood of the wing centerline.

( $\sigma \rightarrow 1$ ). The following asymptotic results for high cavitation number regime may be derived making use of various conditions and results previously given herein. The tedious calculations are omitted.

The nondimensional width,  $\delta$ , of the cavity measured in the transverse plane from the wing leading edge to the inboard end of the cavity is

$$\delta \approx \left( \frac{\sigma}{2} \right)^2.$$

The lift coefficient for a delta is increasingly reduced by cavitation and equals

$$C_L = \frac{1}{2} \rho U^2 S^2 (1 - \frac{\sigma}{2}) \approx \frac{1}{2} \rho U^2 S^2 \left( 1 - \frac{\sigma}{2} \right).$$

As the region of cavitation vanishes ( $\sigma \rightarrow 0$ ) the lift approaches, as it should, that of a fully wetted delta wing according to linear slender body theory.

It is to be noted that the effect of cavitation is to reduce the lift, but that the effect only appeared in terms of the order of  $\sigma^2$ . It is well known that other nonlinear effects associated with separated vortices (which may exist above the top of the wing) will alter the lift to the order of  $\sigma^2$ ; these effects serve to increase rather than decrease the lift on the wing. Their nature will certainly be affected by the possibility of cavitation, but their existence can probably not be ignored in any proper theory. This fact should be kept in mind when comparing the present theory (without separated vortices) with actual experiments. In particular, the reduction of linear lift through cavitation may not be nearly as severe for small angles of attack as the present theory predicts - due to the compensating effect of separated vortices which tend to increase the lift above the linear prediction.

According to present theory, the transverse velocity on short bubbles is, as might have been otherwise deduced, simply related to  $\sigma$  and  $\delta$ :

$$v \approx \left( \frac{\sigma}{2} \right)^{1/2}.$$

( $\sigma \rightarrow 0$ ). As the cavitation number is decreased the cavities cover more and more of the wing, but always with a re-entrant flow along the centerline. Whether this re-entrant jet actually wets the wing or is somehow dissipated before doing so is problematical, but, at any rate, almost all of the top surface of the wing will be at the pressure in the cavity. The transverse velocity on the very wide bubbles depends only on the wing angle of attack:

$$v \approx \left( \frac{\sigma}{2} \right)^{1/2}.$$

The lift for this case of asymptotically small cavitation numbers is related to the cavity width:

$$C_L = \frac{1}{2} \rho U^2 S^2 (1 - \frac{\sigma}{5}) \approx \frac{1}{2} \rho U^2 S^2 \left( 1 - \frac{\sigma}{5} \right).$$

where, it will be remembered,  $2b$  is the width of the wetted portion of the wing top - or to look at it in another way, the width of the re-entrant jet. The actual relationship between  $L$  and  $b$  is of great interest, but has not been obtained here. Presumably  $L/b$  becomes very small as  $C_v \rightarrow 0$ , with the implication that at  $C_v = 0$  a wing of given geometry develops approximately 4-10 of its fully wetted linear lift. Full cavitation is then just a little more effective in reducing lift than is planing; it may be recalled (14) that the lift of a slender delta surface planing on smooth water is

$$\frac{1}{2} \rho U^2 b^2$$

just one-half of its fully wetted linear lift.

The drag,  $D$ , of the cavitating delta is simply  $L \cdot C_v$ , i.e.,

$$D = 0.5 \rho U^2 b^2 C_v$$

It may be shown that one-half of this drag is associated with the kinetic energy in the vortex wake (induced drag), the other half, then, being due to cavitation.

Generally speaking, the cavitation drag increases with cavity volume; thus the problem of minimizing cavitation drag for a given lift is equivalent to the problem of minimizing the volume of the cavity. Even without deriving a theory for the supercavitating flow past a more general slender wing it is clear that the same sort of planforms and cambers which reduce spraydrag for slender planing surfaces will be effective in the present case. Thus, reduced cavity sizes and drags (relative to the uncambered delta) should be obtained with surfaces whose planform curvature is concentrated on the forward portion of the surface, and whose (positive) camber is concentrated aft; for example, a surface whose planform shape is of the form  $y = ax^{1/2}$  and whose bottom surface shape is  $z = bx^3$ .

The results described above which relate the lift on the delta wing to the cavity width are displayed in Fig. 13. Except in the case of very high cavitation numbers ( $C_v > 1$ ) the relation between cavity width and other physical parameters has not been given. In place of an exact theoretical prediction of the variation of lift on a given delta, only a rough estimate based on the asymptotic results obtained here is presented in Fig. 14. The highly nonlinear behavior of the lift as a function of angle of attack is especially to be noted; it is, of course, a consequence of the widening of the cavities as the angle of attack increases, the cavitation number being fixed.

It is to be hoped that the near future will provide experimental results for slender supercavitating wings such as the deltas considered here, with the consequence that our understanding of these complex and interesting flows may be very much broadened.

## SUMMARY

The three separate topics discussed here concern the cavity flow past smooth two-dimensional struts with unspecified cavity detachment points; effects of high speed on cavity flows past blunt struts; and the three-dimensional cavity flow past slender delta wings. The use of linearized theory is emphasized.

The dependence of cavity detachment point on strut shape and cavitation number ( $C_v$ ) is studied. It is shown that for small  $C_v$  the detachment point motion is rearward



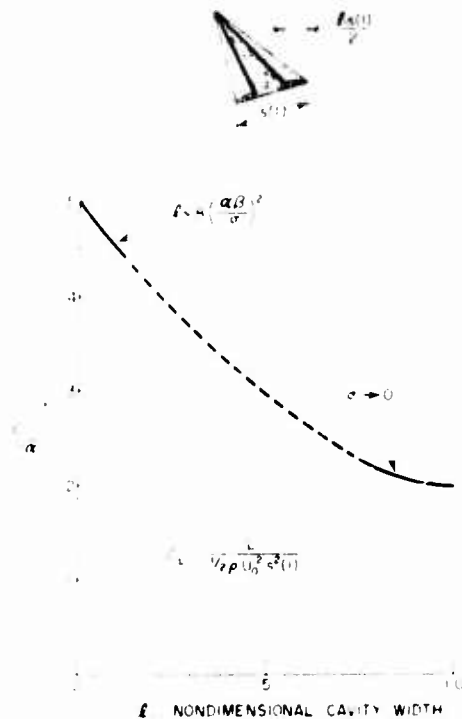


Fig. 13 - Lift on cavitating delta wing as a function of cavity width

and of the order  $M^{-2}$ . The drag of a family of struts is calculated and the dependence of resistance on strut shape discussed. Some interesting indications concerning the non-uniqueness of the Helmholtz flow past closed struts are revealed.

A Prandtl-Glauert rule for the estimation of Mach number effects on cavity flows past blunt struts is derived. For infinite cavities ( $\sigma = 0$ ) it is shown that the cavity drag varies inversely as  $1 - M^2$ . For finite cavities the length is shown to vary inversely as  $(1 - M^2)$ , while the maximum cavity breadth varies inversely as  $1 - M^2$ . The situation for transonic speeds is very briefly discussed.

The flow past slender delta wings is studied under the assumption that it may be considered conical. Theory is developed for a flow involving cavities which spring from the leading edges and cover a part of the top of the wing. Results are obtained for the two separate asymptotic cases in which the cavitation number is either very small or very large. The width of the cavities on the wing upper surface increases with decreasing  $\sigma$  and the lift decreases. It is shown that the upper surface never becomes completely enveloped in a cavity, even for  $\sigma = 0$ . Finally, the lift of a fully cavitating wing ( $\sigma = 0$ ) is estimated to be approximately  $4/10$  of its fully wetted lift.

M. P. Tulin

$$C_L = \frac{L}{\frac{1}{2} \rho U_0^2 s^2 (1)}$$

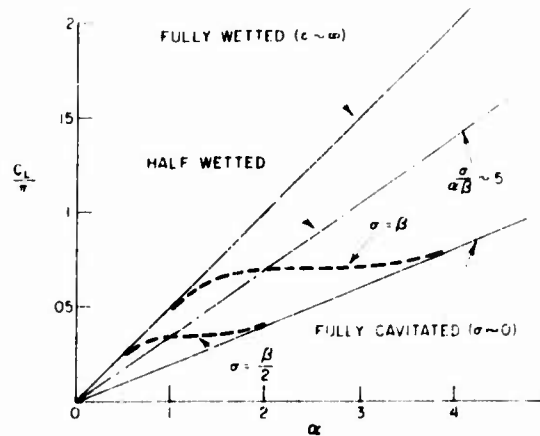


Fig. 14 - Estimated lift on cavitating delta

#### REFERENCES

1. Lighthill, M.J., Proc. Roy. Soc. A, 217:344 (1953)
2. Tulin, M.P., David Taylor Model Basin Report 834, 1953
3. Tulin, M.P. and Burkart, M.P., David Taylor Model Basin Report C-638, 1955
4. Tulin, M.P., Proc. NPL Symp. on Cavitation in Hydrodynamics, London: Her Majesty's Stationery Office, 1955
5. Leray, J., Commentarii Math. Helv. 8:149-180, 250-263 (1935)
6. Eisenberg, P., David Taylor Model Basin Report 712, 1950
7. Imai, I., J. Aero. Sci. 19:496 (1952)
8. Mackie, A.G. and Pack, D.C., J. Rat. Mech. Anal. 4:177 (1955)
9. Helliwell, J.B. and Mackie, A.G., J. Fluid Mech. 3:93 (1957)
10. Jones, R.T. and van Dyke, M.D., J. Aero. Sci. 25:171 (1958)
11. Sears, W.R., "General Theory of High Speed Aerodynamics," Princeton University Press, part C, p. 81, 1954
12. Nonweiler, T.R.F., J. Fluid Mech. 4:140 (1958)
13. Heaslet, M.A. and Lomax, H., NACA TN 2900, 1953
14. Tulin, M.P., Schiffstechnik 4:125 (1957)

# DISCUSSION

E. H. Handler (U. S. N. Bureau of Aeronautics)

As a consequence of the work by Marshall Tulin of the Office of Naval Research and Virgil Johnson of the National Advisory Committee for Aeronautics, the Bureau of Aeronautics has awarded a contract for the design, construction, installation, and evaluation of a Gruenberg, supercavitating, hydrofoil system mounted on a JRF-5 seaplane. While the hydrofoil boat operates at essentially a fixed trim angle, the hydrofoil airplane must trim up many degrees during the actual process of take-off or alighting. The Gruenberg system, with the foil just aft of the center of gravity, is ideal for seaplane use. The forward planing, or feeler, skis are a low-speed stabilizing device and a high-speed safety device.

The JRF-5 airplane will fly within a year and the results will be published by the Bureau of Aeronautics.

E. Müller (Max-Planck Institut für Strömungsforschung)

The Max-Planck Institut für Strömungsforschung is currently performing experiments with delta wings for cavitation numbers ranging from 0.02 to 0.13. The flat delta wing with an apex angle of 60 degrees has been tested, and drag and lift were measured as functions of the angle of attack and cavitation number. The shape of the wing is quite similar to the shape of the bodies assumed by Mr. Tulin but, as he has said, his work is for an apex angle of not more than 30 degrees, while our work is for an apex angle of 60 degrees. Thus, the results cannot be compared, but experiments with the same bodies as were considered by Mr. Tulin will be made in the near future.

L. M. Milne-Thomson (Brown University)

As Mr. Tulin observes, no account is taken in his paper of viscosity or gravity. In regard to the effect of gravity, I would like to indicate a method of approach which, as far as I know, has been overlooked in the literature.

Consider an inviscid liquid in steady irrotational flow under gravity. Fritz John<sup>1</sup> has given the following equation for a surface of constant pressure, assuming the  $y$ -axis to be vertically upwards:

$$z''(t) + 1/2 (z'(t))^2 = S(t) + z'(t),$$

Here  $t$  is a certain parameter and  $S(t)$  is an arbitrary real function. To each specific problem there belongs a specific function  $S(t)$  which, if we could divine its form, would solve the problem. The integration of the above equation can be effected by finding a complementary function and a particular integral. This observation would be completely trivial, were it not for the fact that in many problems we know the complementary function  $z_0$  in advance. Take the case of a jet from an orifice in a flat plate in the absence of gravity—a well-known Helmholtz problem. Here

<sup>1</sup>Communics. Pure and Appl. Math., 6:497-503 (1953).

Mr. P. Tulin.

$$Z'(\eta) = (1 - S(\eta)) Z_0'(\eta)$$

which determines  $S(\eta)$  insofar as  $\psi(\eta)$  is independent of  $\eta$  in the gravity problem. This is a matter for investigation in each case.

If we now regard  $\eta$  as a function of an auxiliary parameter,  $\xi$ , we can integrate the full equation in the form

$$Z'(\xi) = Z_0'(\xi) + \frac{1}{2} \frac{U^2}{V^2} (1 - f(\xi))$$

where  $f(\xi)$  is a determinate function and  $\eta = \eta(\xi)$  at the edge of the orifice. This equation reduces to  $Z'(\xi) = Z_0'(\xi)$  when  $U = 0$ , and gives

$$Z(\xi) = Z_0(\xi)$$

at the edge of the orifice. It remains to see whether the condition at infinity is satisfied.

Thus, in the case of an orifice of breadth  $2a$  and a vertically downwards jet, this condition is satisfied when

$$U^2 = \frac{2}{3} \frac{av}{r}$$

where  $r$  is the skin velocity on the jet in the Helmholtz problem.

W. A. Clayden (Armament Research and Development Establishment)

Concerning Mr. Tulin's work on cavity detachment, we have noticed in our work with cavitating spheres at ARDE that the flow does not separate tangentially to the surface, but separates with a non-zero angle which may be well over 90 degrees. I think that this effect has also been studied by other workers in more detail.

We have also performed some tests on yawed cavitating cones which may be considered to behave in a manner similar to slender delta wings, and the cavities have been kidney-shaped, or distorted ellipses, in cross section before rolling up into a pair of vortices as predicted by Mr. Tulin's calculations.

I should like to take a few minutes to tell you of the work on cavitating wedges that has been done at ARDE by my colleague, A. D. Cox. He considered the following two cases:

1. An inclined wedge with non-zero cavitation number. The mathematical model used is the familiar re-entrant jet at the rear of the cavity and a subsidiary leeward cavity. This work is an extension of the zero cavitation number case.

2. A generalized image-model for non-zero cavitation number and zero incidence in which the cavity is closed on another wedge of arbitrary angle. It is shown that the standard image-model of Plesset and Shaffer and the dissipative model of Roshko are special cases of the generalized model. The model may also be applied to include a representation of the familiar jet flow at the rear of the cavity.

W. G. Cornell (General Electric Company)

In regard to the first problem wherein, for a given strut, one is able to find, by Mr. Tulin's method, the detachment point of the cavity and the cavity itself, I have a slight philosophical problem. It seems to me that one is getting something for nothing by obtaining all this information without considering boundary layers and turbulence.

Also, I wish to express great pleasure in seeing this consideration of compressibility effect in cavity flows.

B. R. Parkin (California Institute of Technology)

In connection with Mr. Tulin's two-dimensional solution, I wish to cite some experimental results<sup>4</sup> which are quite old, and which are familiar to Mr. Tulin and perhaps to other members of this symposium also. These measurements concern the role of surface tension and viscosity in the inception of cavitation on a smooth symmetrical body.

About five years ago, R. W. Kermeen and I investigated the nature of the separation zone on a blunt, axially-symmetric body just after the cavity flow had become established. Although we did not investigate the flow in detail we did obtain some magnified motion pictures and still photographs which showed the shape of the small cavities near their point of attachment on the body. These photographs indicate that such cavities originate in the boundary layer. They are shaped somewhat as shown in the schematic diagram of Fig. D1.

The boundary-layer and displacement thicknesses are shown in Fig. D1 so that we may judge the effect of the changing velocity of the water in the boundary layer upon the shape of the liquid-vapor interface. The water has zero velocity on the body and its velocity increases continuously as one progresses from the surface of the body to the main flow. From the shape of the free streamline in the neighborhood of the cavity leading edge it is evident that the flow does not separate from the body in accordance with the assumption commonly employed in potential problems which involve flow separation. In view of the fact that this difference is found in the boundary layer flow on the body, even for those cases in which very large cavities are attached to the body, its effect upon the overall flow should be small, once the location of the separation point is established. Therefore it does seem that Mr. Tulin's solution should give a valid picture of the flow in the large when the point of separation corresponds closely to that which one would observe in practice. Because of the physical evidence discussed above one might ask if Mr. Tulin's theoretical solution, although mathematically determinate, must always give results which correspond to those obtained in an actual flow; might not there still be some ambiguities remaining to be resolved? If one were to adopt the most pessimistic view, as a believer in cause and effect, he might even suppose that it would be necessary to trace the whole history of the inception process in order to fix the position of a separation point on the body. One may certainly hope that less-stringent measures would be required.

4. Parkin and R. Kermeen, "Incipient Cavitation and Boundary Layer Interaction on a Streamlined Body," California Institute of Technology Hydrodynamics Laboratory, Report No. 504, Dec. 1953.

5. Kermeen, McCrea, and Parkin, "Mechanism of Cavitation Inception and the Related Scale Effects Problem," *Trans. ASME*, 77(Nov. 4) 533 (1955).

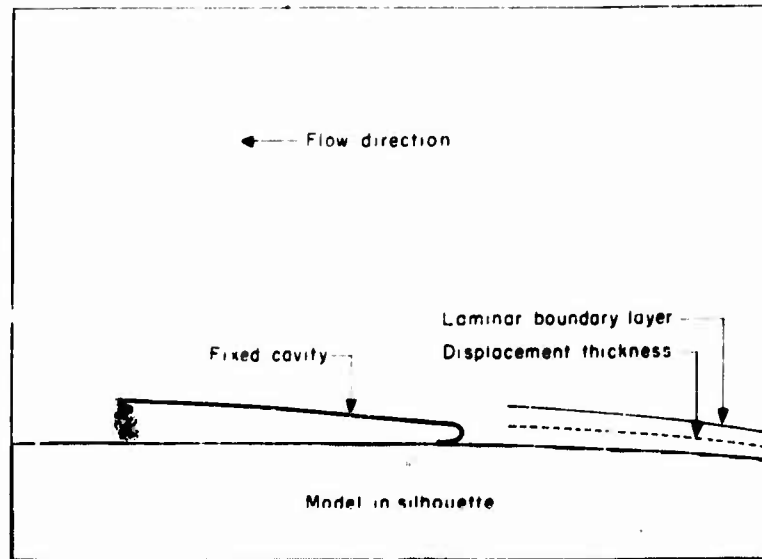


Fig. D1 - Vapor cavity attached to the surface of a smooth body

## M. Tulin

Mr. Cornell's philosophical problem is old as far as potential flow theory is concerned. One can read about previous attacks on the problem within the framework of potential flow theory, ignoring any effects of viscosity and surface tension. The problem has been formulated, more-or-less, in the same way as in my linearized version, and in a few cases it has been solved. There is a very good discussion of the problem by Birkhoff and Zarantonello. I did touch on the question of the uniqueness of these flows. The sufficiency of the condition of smooth detachment is also discussed. There is no conclusive statement to be made about it, but I think this condition of smooth detachment is sufficient for the bodies that have been tried. It gives one a meaningful problem; I have only linearized its formulation.

Now, I should have said a few words about the possibility that this may be fantasy, because we just don't know enough about the role played by viscosity and surface tension in disturbing the detachment point. This is a very good problem. The way I might wiggle out of it is this: I try to show how, using linearized theory and the usual linear condition for an ideal fluid, one can solve the problem for slender bodies.

When we know enough about the effects of viscosity or surface tension, then we still presumably must solve some potential flow problems. Perhaps they will be something like Lighthill's problem, where he achieves a matching between the boundary layer behavior ahead of the plate on the body and the constant pressure flow. If so, then one still needs to solve a potential flow problem to calculate the pressures on the body and determine where the boundary layer separates, or where viscosity or surface tension is involved, and include its effects.

This is definitely a subject for future research, both experimental and theoretical.

\* \* \* \* \*

# JETS, WAKES, AND CAVITIES

Garrett Birkhoff  
*Harvard University*

My talk today is intended as a sequel to the reviews made by Cox and Maccoll and by Gilbarg at the 1956 Naval Hydrodynamics Symposium (1). Whereas "hydroballistics" can be loosely considered as a branch of engineering, and "free streamline theory" as a branch of pure mathematics (specifically, of potential theory), my talk will be from the standpoint of the applied mathematician.\* My primary concern is thus to survey mathematical methods for predicting accurately the behavior of real jets, wakes, and cavities—especially the latter, which are the central theme of this part of the present Symposium.

If my tone is that of the "cautious critic" (1, p. 233), it is because I think a careful (not, I hope, agonizing!) reappraisal will help us to discern profitable lines of future work. In this vein, I shall point out a number of specific questions which seem tractable by available methods, provided the necessary interest, ability, and financial support are available.

I shall not try to offer any new and major challenges to intellectual giants; such men usually seek out their own problems. The level of the problems is intended to be that of high-level Ph.D. theses in applied mathematics; this is perhaps the highest level on which research can be systematically planned.

In Gilbarg's review (1), attention was focused almost exclusively on two problems of pure potential theory, which may be roughly defined as follows.

**Helmholtz Problem:** Given stationary obstacles, walls, etc., having fixed boundaries, find those irrotational, incompressible, steady flows bounded by streamlines which (piecewise) either coincide with these boundaries, or are free (i.e., at constant velocity).

In the Helmholtz Problem, it is understood that the flow behavior at large distances is specified. If we refer to solutions of the Helmholtz problem as "Helmholtz flows," then the second problem is the following.

**Helmholtz-Brillouin Problem:** Find those Helmholtz flows past given fixed boundaries, in which the maximum velocity is assumed along all free boundaries.

Before I discuss the physical significance of these problems, I shall survey some purely mathematical questions not covered adequately at the 1956 Symposium (1).

(Note: This work was done under Contract Nona-13600(4) with the Office of Naval Research.  
In the sense of Sydney Goldstein (2).)

## MATHEMATICAL RIGOR

Though not always attainable in applied mathematics, rigor is desirable—and one should always have a clear idea of the extent to which it has been achieved. Contrary to an impression which seems widespread among physicists and engineers, not even all pure mathematics is equally rigorous. Far from being exceptional, free streamline theory seems to be especially confused today on this fundamental issue. I should like to begin, therefore, with some questions of rigor.

### Plane Flows

Even in the simplest case of plane Helmholtz flows, only a few results have been rigorously established. For example, the class of all Helmholtz flows has been rigorously determined, with full generality, only for the case of a single flat plate.\* Determinations in other cases involve topological assumptions (usually tacit) about flow separation. Though these assumptions are very plausible, the analysis in the section called Cavity Separation will show that they are actually rather arbitrary.

If the flow topology is assumed known, then plane Helmholtz flows past polygonal fixed boundaries can be treated rigorously by classical methods. In the case of curved fixed boundaries it is, however, much more difficult to establish existence and uniqueness theorems. In this connection, I recall that the first rigorous general existence theorem for the Dirichlet problem was not given until 1899. This was 50 years after Kelvin and Dirichlet had attempted to found the theory on a nonrigorous minimum principle,<sup>1</sup> and 150 years after potential theory had been usefully applied to solve problems in mathematical physics.

Existence and uniqueness theorems for flows with free streamlines are very much harder to establish. Though Levi-Civita, M. Brillouin, and Villat discerned some of the most important facts in the decade 1904-15, and succeeded in formulating them mathematically,<sup>2</sup> in the two-dimensional case, the first rigorous proofs were obtained by Weinstein and Leray in the decade 1925-35. I cannot overestimate the technical difficulty of these proofs; as extended by Kravtchenko, Huron, and others so as to cover more general cases, they run to at least 1000 pages of close and delicate mathematical reasoning. Moreover Leray has informed me that at least one extension (Oudart) is not complete.

In spite of all this work, even the Helmholtz problem has not been solved in all cases; especially little is known about the existence and uniqueness of plane jets from asymmetric nozzles. What is more striking, the only solid obstacle for which the Helmholtz-Brillouin problem has been solved, is the circular cylinder! However, I would not advise any applied mathematician to try to extend these results.

### Thin Hydrofoils

More fruitful, it seems to me, would be the rigorous justification of Tulin's "linearized theory" of thin hydrofoils, dealt with elsewhere in this volume. The brilliant applications of Tulin's approximation to engineering design problems should

\* E. H. Zarantonello, *J. de math. pures et appl.*, 33:276-80 (1954).

<sup>1</sup> See G. D. Kellogg, "Potential theory," Ch. XI, 1.

<sup>2</sup> As a singular nonlinear integral equation, to which we will recur in the next section, see Ref. 3, Ch. VII, for an exposition of some of the more accessible results. Further references are given there.



blind us to the fact that it involves all the usual assumptions of the pure mathematician—and an additional linearization as well.

The successful correlation of Tulin's formulas with those of Levi-Civita (3, Ch. V'), besides rigorizing the linearization, should have two other useful consequences. First, it should give better estimates of the errors involved in linearization, and on how to correct them. Second, it might indicate improved ways to solve the integral equations to which Levi-Civita's formulas lead—including especially the determination of parameters.

#### Axially Symmetric Case

The methods mentioned above do not give any information about the axially symmetric case, of the greatest importance for hydroballistics. One is, of course, free to conjecture that natural analogs of existence and uniqueness theorems, proved for symmetric plane flows, will also hold for axially symmetric space flows. But such freewheeling conjectures, however suggestive, are not a part of science.

It was therefore most gratifying when what may be termed the "Stanford School" (Garabedian, Lewy, Schiffer, Spencer, Gilbarg, and Serrin) obtained positive results for axially symmetric space flows also. The technical brilliance of their achievements can hardly be overestimated—even after making due allowance for contributions by Riabouchinsky, Lavrentiev, Polya-Szegő, and others to the basic methods involved. However, brilliance does not imply infallibility, and the time has come for sober appraisal of what has actually been proved.

The existence proofs of Garabedian et al. (4) are based on the synthesis of a variational principle due to Riabouchinsky, Steiner symmetrization as recently exploited by Polya-Szegő, and a principle of analytic continuation due to H. Lewy. The details are again delicate and highly technical—even in the plane case, when use can be made of Schiffer's technique of interior variations.

Though I have not myself studied all the details, I have given considerable thought to many aspects of the proofs, and have discussed them with other competent analysts. On the basis of this thought and discussion, it is my impression that only the case of finite cavities has been worked through completely. For infinite cavities, I think many details must be supplied before the proof sketched in (4) can be accepted as rigorous. A complete and clearly expounded proof for infinite cavities would be very valuable.

Weinstein has called my attention to a much simpler difficulty regarding the uniqueness proofs of Gilbarg and Serrin, with particular reference to the conditions under which "starlikeness of the obstacle implies starlikeness of the free streamline." In the plane, this can be proved rigorously; in the axially symmetric case, its proof by Serrin (5) depends on a plausible principle of potential theory, which has however itself never been rigorously proved. Thus, in the axially symmetric case, a rigorous proof of uniqueness has only been given within the class of flows with starlike free streamlines—contrary to what is implied in Ref. 3, p. 96.

\*Of course, one would expect a quadratic correction term, which could be estimated by a single exact calculation.

In this connection, see E. Ruzenski, Tech. Rep. 67, Applied Math. Statistics Lab., Stanford Univ., Aug. 1957. A proof of uniqueness for the "Indholter-Brillouin problem" (6) (proof, as yet, not a fully remarkable contribution).

In thinking about this difficulty, I have come to realize that the appeal in Ref. 3, p. 96, to Levinson's theorem (6) about the asymptotic shape of axially symmetric infinite cavities requires that one also assume Levinson's hypotheses. Basically, one must use these to prove the existence of a similarity transformation of one free boundary, making it lie entirely outside the other—except at one or more points of tangency—so as to make Lavrentieff's comparison method rigorously applicable. Presumably, Levinson's hypotheses and "starlikeness" can be combined into one elegant (and plausible) assumption; this would certainly seem worth doing.

In the same vein, statements have recently been made about free streamlines under gravity, which seem to me not rigorously proved. I shall comment on these later in connection with the paper by Taylor and Saffman in this volume.

## NUMERICAL METHODS

The recent development of high-speed digital computing machines, with multiplication times of a millisecond or less, has enormously increased the class of economically computable formulas. The impact of this development on applied mathematics is incalculable because it is economically computable formulas that the applied mathematician requires.

Unfortunately, effective rigor in this area is hardly ever achieved, in the sense that rigorous error bounds are usually far too pessimistic. In practice, errors are usually estimated by repeating the calculations with doubled mesh length. This sometimes gives a reliable estimate of the truncation error; in other cases, the significance of the estimate so obtained is only statistical.

I shall now discuss some numerical methods which have been successfully applied to free streamline problems, with special reference to their mathematical accuracy and their potentialities for further development, using high-speed computing machines. In specifying mathematical accuracy, I mean of course the agreement with exact solutions of analytically defined Helmholtz problems—always assuming that these problems have been "well set" in the sense of existence and uniqueness. Some aspects of physical accuracy will be discussed in the following sections.

### Integral Equation Methods

Perhaps the most highly developed integral equation method concerns the solution of plane Helmholtz problems by discretization of equivalent singular, nonlinear integral equations. This method has been described in Ref. 8, reviewed in Ref. 3, pp. 215-219, and briefly criticized in Ref. 1, pp. 224-225. The integral equations are those of Levi-Civita and Villat, mentioned in the preceding section.

For symmetric flows past obstacles having curvature of constant sign, very consistent results have been obtained with this method. There is even a rigorous theory\* of its convergence (9), though the assumptions involved are not easy to interpret. This is not to say that error bounds have been calculated, or even that error estimates are available. However, the method always gives a potential flow with free streamlines past an obstacle whose shape differs slightly from that of the given obstacle. Therefore to get error estimates, it would suffice to solve the following problem.

\*In particular, the singularity at the separation point causes no difficulty, contrary to the assertion in Ref. 1, p. 224.

**Problem:** Given two functions defining the curvature  $K = K_i(\psi)$  as functions of the slope  $\psi$ ,  $i = 1, 2$ , estimate the changes in the flow pattern and pressure distribution due to  $\Delta K(\psi) = K_1(\psi) - K_2(\psi)$ .

The method involved is capable of various extensions. Thus, various classical problems involving plane flows with free streamlines under gravity, and straight fixed boundaries, can also be transformed into nonlinear integral equations (3, Ch. VIII, §11). Though the singularities involved are nastier than in the case treated in Ref. 3, the problem should be tractable.\* We had also originally hoped to apply simple modifications of the method, to calculate asymmetric flows and compressible flows in the Chaplygin approximation (3, p. 191). Adaptations of the method to jet calculations should also be feasible.

By using slope-length equations  $\psi = \theta(\zeta)$  in place of curvature-slope relations  $K = K(\psi)$ , one can interpret plane cavity flows past obstacles having points of inflection (curvature of variable sign) in terms of integral equations (3, p. 136). It would be interesting to perfect a technique for solving such integral equations numerically; in principle, this would seem not too difficult.†

#### Thin Hydrofoils

An especially timely extension would be to the calculation of asymmetric cavity flows past thin hydrofoils, such as are considered elsewhere in this volume by Drs. Tulin, Johnson, Timman, Cohen, and Di Prima. Such calculations would give a clearer idea of the correction to be made for finite thickness. Conversely, a study of methods effective for the linearized approximation might suggest more effective methods for solving the exact nonlinear equations.

The general case of a smooth asymmetrical hydrofoil in an infinite stream involves three parameters (3, Ch. VI, §7):  $M$ ,  $T_0$ ,  $\psi_0$ . These are presumably determined by the pitch angle of the hydrofoil and the two points of flow separation—though the relation between these and the location  $\psi_0$  of the stagnation point may be hard to determine, unless the hydrofoil has a sharp leading edge. The angle of pitch should presumably be carried as a free parameter in calculations—but the angles  $\psi_1$ ,  $\psi_2$  of flow separation or the condition of "smooth separation" used to eliminate the other two parameters.

For fixed  $M$ ,  $T_0$ ,  $\psi_0$ , the iterative methods described in Ref. 3, Ch. IX, should converge rapidly, provided the hydrofoils involved have a sharp leading edge, since the curvatures involved (hence  $M$ ) are then small. However, for nonconvex hydrofoils, one would presumably have to use the Villat integral equation.

#### Axially Symmetric Case

Even more valuable would be the perfection of numerical techniques for solving axially symmetric Helmholtz problems. Two approaches to this problem are

\*For one case, see Ref. 7 and P. Garabedian, Proc. Roy. Soc. (London) A241:769-80 (1957). The radius of curvature at the bubble vertex seems hard to determine accurately.

†Persons interested in this problem should consult with Dr. Hans Bremermann of Stanford University, who spent some time on it.

‡Perhaps not, if the curvature had constant sign on each side of the stagnation point. Alternatively, one could treat the first six coefficients  $a_0, a_1, \dots, a_5$  of the Levi-Civita function  $\psi(\zeta)$  as free parameters.

§Especially because no analytical solution is known.

reviewed in Ref. 1. In both approaches "certain similarity principles between ... two-dimensional and three-dimensional problems are involved" (1, p. 222).

Approaches based on assumed analogies between plane and axially symmetric flows have long been used to make engineering estimates. For cavity flows, the recent assumptions of Plesset and Shaffer are perhaps best known. The evidence reviewed in Ref. 1, pp. 225-227, shows again that such estimates have a purely engineering significance.

#### Variable Dimension Number

The preceding analogy can also be put on a scientific basis, as first shown by Garabedian (10). The correct approach is to consider one-parameter families of flows satisfying

$$U_{xx} + \frac{p}{y} U_y + U_{yy} = V_{xx} - \frac{p}{y} V_y + V_{yy} = 0 \quad (1)$$

in  $p + 2$  dimensions, with  $p$  a continuous parameter. This idea of considering flows in fractional dimensions,\* which would not normally occur to a physicist or engineer, illustrate the practical value of pure mathematical abstractions.

Garabedian's methods and conclusions are summarized in Ref. 3, pp. 288-289, except that Gilbarg fails to emphasize Garabedian's plausible but arbitrary interpolation with respect to  $p$  ( $p + 2$ ). Because of this arbitrariness, though I believe that Garabedian has obtained genuine estimates for corrections to the widely quoted results of Plesset and Shaffer (and of Trefftz for jets), I am not convinced that these estimates can be relied on beyond  $\pm 30$  percent.

It would be very valuable if Garabedian could extend his method so as to obtain asymptotic estimates of the relative length  $l/d$  and diameter  $d_m/d$  of cavities behind discs of diameter  $d$  as functions of the cavitation number  $Q$ . The extension to other obstacle shapes seems to involve formidable difficulties.

#### Difference Equation Methods

Most promising, in my opinion, are attempts to calculate Helmholtz flows approximately, by covering the domain involved by a fine mesh, and replacing the Laplace equation over this mesh by a suitable difference equation. In both the plane and axially symmetric case, this procedure (with due attention to boundary conditions) leads to vector equations  $Au = f$  involving well-conditioned symmetric matrices. Clearly, such equations are most tractable for small domains—e.g., for flows having finite cavities in finite channels. By way of contrast, the methods based on integral equations and variation of the dimension number  $n = p + 2$  are most effective for infinite cavities in an unbounded stream. Therefore, their ranges of application are essentially complementary: neither is to be thought of as a substitute for the other.

#### Relaxation Methods

The approximate numerical solution of Helmholtz flow problems, through approximating difference equations, was first accomplished (using hand "relaxation methods")

\*Previously applied to other problems by Beltrami, Bers and Gelbart, and Weinstein (Trans. Am. Math. Soc. 63: 342-354 (1948), where earlier references are given).

by Sir Richard Southwell and Miss Vaisey (11), in an important pioneer paper. Though not mentioned in Ref. 1, Ref. 11 seems to deserve further study at the present time, for two reasons.

First, many of the approximate solutions obtained in Ref. 11 can now be compared with results obtained by other methods, and this will give a better idea of the truncation errors involved—a subject about which little information is now available.\* Thus, such a comparison is possible for the two-dimensional Borda mouthpiece in a channel: Example 1 of Ref. 11 is tractable analytically as described in Ref. 3, Ch. V, §8. Though a numerical parameter (ratio of mouthpiece width to channel width of  $1/6$ ) must be determined a posteriori in the exact analytical formulas, the amount of work involved is not really great. Again, as to the cusped cavity behind a circular cylinder, treated as Example 10 in Ref. 11, one can use the formulas of Ref. 3, Ch. VI, §10, to reduce the problem to the solution of a nonlinear integral equation involving two parameters  $M$  and  $Q$ , connected by an implicit relation. For one value of  $Q$ , this equation and the relation have been solved numerically (8, Case 22a); it would be interesting to make a comparison with the relaxation solutions† for  $Q = 0.234, 0.562, \dots$ , as well as for the infinite cavity of zero drag.

Analytically, the various plane flows with free streamlines under gravity treated in Ref. 11 as Examples 4-8 are also reducible to mildly singular integral equations, which should be tractable by iterative numerical methods, as explained above.

Second, the numerical labor required to "relax" has been so shortened in many cases with the help of ultrafast computing machines, that it seems reasonable to hope that this will also be true of the "free streamline" flows treated in Ref. 11. The general procedure followed, in both hand and machine computations, is to solve a sequence of problems involving fixed boundaries, which are adjusted by successive trials until the condition of constant velocity is met on the (then) free streamline. Since the difference equations are the same, the only question is as to how effectively one can substitute regimented automation for free human intuition.‡

Very substantial contributions to the automatic solution of Helmholtz problems are embodied in Ref. 12. Using a square mesh, to which the successive overrelaxation (extrapolated Liebmann) method of Young and Frankel is ideally adapted, "Riabouchinsky" flow past a disc in a channel was treated on the NORC at Dahlgren.

Surprising though it may seem, the NORC calculations did not give results which were clearly better than those previously obtained by Miss Vaisey (3, p. 232). In fact, no convergence proof or error estimate is available for either method, and somewhat variable results were obtained by both, so that the problem is still unsolved. I should like to make some specific comments in this connection; I understand that Dr. Arms of the Naval Proving Ground also has some ideas. I believe that reconsideration of convergence speed and truncation errors, in the light of these comments and ideas, would make a successful attack possible in the near future, using new and more powerful machines.

\*Even for solutions of the Dirichlet problem; the case of free boundaries is much more difficult!

†See R.V. Southwell, "Relaxation Methods in Theoretical Physics," Oxford, p. 226, 1946. A concise revision of much of Ref. 11 is presented in pp. 212-26.

‡Human intuition has many advantages of flexibility—as in the easy introduction of local mesh refinements suggested by experience.

§Thus, with the PDQ-03 Bettis Code, and rectangular meshes (with independent spacings in  $x$  and  $y$ ), in rectangular domains, fixed boundary problems involving 7500 points can be solved on the IBM-704 in 10 to 15 minutes!

Perhaps the major computational difficulty centers around the (mild) separation singularity. The square mesh usually used in Ref. 12 is not well adapted to treating the local behavior near this singularity.\* Successive overrelaxation is also compatible with rectangular subdivisions with unequal spacings, which could be used to concentrate mesh points near the separation point. On the other hand, the type of local mesh refinement used in Ref. 11—which seems better adapted to the problem—does not satisfy Young's property A: that net-points can be divided into "red" and "black" points, such that adjacent net-points have opposite colors. Other mesh refinements having property A might be tried, such as those sketched in Fig. 1.

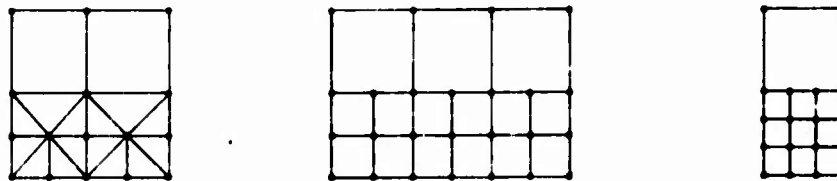


Fig. 1 - Mesh refinements having property A

One alternative would be to apply second-order Richardson or Chebychev polynomial methods to meshes having local refinements of the kind used in Ref. 11. Though these methods require twice as much storage and computing time with a square mesh† as successive overrelaxation, I am sure they are still much faster (using ultrafast machines) than hand computation. Or, one could try successive overrelaxation, hoping that it would converge rapidly even without theoretical justification.‡ As a third alternative, one could use linear interpolation during mesh transitions, as proposed by Arms.

#### PHYSICAL RIGOR

Solutions of the Helmholtz problem are in equilibrium under inertial forces and, in the case of wakes, under gravity. Unfortunately, as realized by Helmholtz himself (1868), this equilibrium is very unstable in single-phase flow. Gravity is neglected in representations of (two-phase) cavity flows, but the equilibrium is much more stable (14, p. 54). Moreover viscous forces, turbulence, surface tension, evaporation, air content, and impurities in solution are neglected in any case.

It is obviously important to know how best to approximate physical reality by Helmholtz flows, and also how to allow for the various forces neglected. I reviewed this question ten years ago;§ in ideal cavitation, one might expect to observe the nominal equation of state (3, p. 7)

$$p = p_v \quad \text{if } p < p_v \quad (2a)$$

$$p = p_v \quad \text{if } p \geq p_v \quad \text{elsewhere.} \quad (2b)$$

\*A local analytical expansion was generally used instead of local mesh refinement.

†R.S. Varga, *J. Soc. Ind. Appl. Math.* 5:39-46 (1957)

‡Such justification may actually be implicit in recent work by Kahan and Varga. (Comment of Dr. Young.)

§G. Birkhoff, *Proc. 7th Int. Congress Appl. Mech.*, London, 2:7-16 (1948), also Ref. 14, p. 51 and Ref. 3, Ch. I. The use of Eqs. (2a) and (2b) goes back at least to Riabouchinsky, Demtchenko, Ackeret, and Wang (1926-32).

If inertial forces alone are considered, this equation leads naturally to the Helmholtz-Brillouin Problem.\*

#### Reentrant Jet Models

Unfortunately, one can show that Helmholtz-Brillouin flows past a single obstacle necessarily involve infinitely long cavities and zero cavitation number  $Q$ , whereas real cavities have finite length and positive  $Q$ ! To avoid this paradox, it is customary to use the Riabouchinsky and reentrant jet models, and to take

$$Q = \frac{p_n - p_c}{\frac{1}{2} \rho v^2}$$

as an empirical constant. (Here  $p_n$  is the local ambient pressure;  $p_c$  is the (mean) cavity pressure, which is  $p_v$  in ideal cavitation.)

These models give almost identical predictions for drag and cavity dimensions in two-dimensional flow.† However, it is very hard to find accurate published statements about the conformity of such models and reality; usually, authors are content to mention the qualitative occurrence of reentrant jets.

This is partly due, of course, to the limited practical interest of two-dimensional cavity flow, and partly to experimental difficulties. Anyway, the most frequently seen comparisons refer to integrated, artificially rotated (Plesset-Shaffer) pressure distributions on wedges for ideal Bobileff flows, as compared with drag measurements on cone heads in water tunnels. Since the theoretical interpretation of the calculated drag coefficients is obscure, these comparisons have questionable scientific significance.

The published experimental values  $C_D(Q) = 0.55 \pm 0.40$  for flow past a circular cylinder agree, at  $Q = 0$ , with the numerical value calculated by Brodetsky. It would seem desirable to redo these experiments, and to check the values for  $Q \neq 0$  against calculations recently performed on the MANIAC.

But agreement between calculated and measured values of  $C_D(Q)$ , however useful, does not tell the whole story. Especially in cases where, as with cones, the separation point is determined by a sharp corner, such agreement is almost built in. As observed nearly 15 years ago by L. B. Slichter, the difference between the stagnation and separation pressures outside the boundary layer is fitted by the choice of  $Q$ . Again, the pressure distribution is a convex even function in most cases treated. One can therefore expect fair engineering estimates of  $C_D(Q)$ , without knowing much about the flow as a whole. Especially good estimates may be expected when, as with cones (following Armstrong (1, pp. 226-227)), one can match the local pressure distribution near the vertex and the separation point to a higher order.

\*Gillberg (1, p. 285) calls Helmholtz-Brillouin flows "physically acceptable," but this seems to me a confusion of physics with metaphysics, because of all the physical variables neglected.

†First observed by D. Gillberg and R. A. Anderson, *J. Appl. Phys.* 19:157-60 (1948); see also Ref. 3, Plate II. The prediction of  $Q$  is an important unsolved problem. [Reference 1, p. 227, and B. Perrin and M. S. Plesset, pp. 251-261 of the Riabouchinsky Jubilee Volume, Publ. Sci. Tech. Min. de l'Air, Paris, 1954. Garabedian's calculations for a disc are more significant.]

‡G. Birkhoff, H. H. Goldstone, and E. H. Zarantonello, *Rend. Sem. Mat. Torino* 13:205-235 (1954), esp. Case 23a. An unpublished rough check of Martyrer's data was made by the late R. L. Knapp around 1947. (See the next footnote.)

Approximate agreement between theoretical and measured values of  $C_D(Q)$  does not, in any case, imply agreement as regards separation angle, cavity size, or behavior at the rear end of the cavity. In particular, I think that the differences between ideal and "reentrant jets" has been insufficiently emphasized.

Thus, I take exception to the phrase "observed experimentally" in Ref. 1, p. 286, line 13. In spite of Fig. 16 on p. 230, I doubt that Fig. 15 of Ref. 1, p. 230, accurately represents the flow of Fig. 14 on p. 229. Whereas ideal reentrant jets are irrotational and steady, most real reentrant jets have vorticity and are unsteady. This seems especially likely for very small cavities, like that of Fig. 14. Again, as shown conclusively by Swanson and O'Neil (1, p. 230) (see also the paper by Campbell in this volume) one loses axial symmetry at the rear end of long cavities behind axially symmetric obstacles. This is because of gravity.

#### Cavity Size

In principle, the preceding models give unambiguous predictions as regards relative cavity diameter  $d_m/d$  and length  $l/d$ , as functions of the cavitation number  $Q$ . Until these functions have been calculated effectively, one cannot ascertain the correctness of these predictions. My guess is that, for small  $Q$ , the predicted  $d_m/d$  will turn out to be too big, and the predicted  $l/d$  much too big because of the neglect of gravity. This is, of course, important for some aspects of hydrofoil design; I would guess that linearized "thin hydrofoil" cavity theory would be subject to the same trend (again, for very long cavities).\*

It seems reasonable to expect that the correction will begin to be large when the twin vortices, first observed by Swanson and O'Neil (1, p. 230), are a dominant feature at the rear end of the cavity. In this connection, one should consult Campbell's paper again.

Similarly, in the case of water entry of missiles, the Froude number  $F = v^2/gd$  has always been supposed to be the primary variable determining similitude (e.g.,  $d_m/d$  and  $l/d$ ). Since  $F$  and  $Q$  have very different dimensional dependence, while  $v$  and  $d$  can be varied independently,  $F$  and  $Q$  can hardly both determine  $d_m/d$  and  $l/d$ .

To clarify the above questions, I think more accurate measurements of  $(p_a - p_c)$  will be needed than are now available.

#### Wake Models

Before World War II, potential flows with free streamlines were taken as models for "wakes" (and for homogeneous jets<sup>†</sup>) in hydrodynamics, with only vague qualifications. This was in spite of the extreme instability of the free streamlines, already known to Helmholtz himself. As a result of this instability, viscosity and turbulence have an accentuated importance for wakes—though gravity, fortunately, has only a hydrostatic effect. It is therefore especially challenging to try to approximate real wake behavior by models involving potential flow.

\*Some experimental data bearing on the above remarks may be found in Rpt. E-73.6 of the Caltech Hydrodynamics Lab. by R.L. Ward, and in Project Rpt. 59 of the St. Anthony Falls Hydraulic Lab. by E. Silberman.

†As shown in Cornell's paper in this volume, good predictions of contraction coefficients  $C_c$  for jets can often be had. Cf. the last line of Ref. 3, Ch. 5, § 7.



Since the pressure in real wakes, as in cavities, is below the ambient pressure  $p_\infty$ , it is natural to try to represent the flow outside them by the Riabouchinsky and reentrant jet models. Again, considerable success in estimating pressure distributions with such models is possible (3, p. 28, Fig. 3) in cases where the separation point is fixed by a sharp corner. However, unlike cavities, wakes have irregular and unstable boundaries. Hence, though the models with "dead water" wakes are in nominal near equilibrium when  $R \rightarrow 1$ , real wakes are in fact highly turbulent.

A better model for real wakes is probably provided by an old discontinuous potential flow model of Joukowski, with variable  $Q \neq 0$ , recently discussed by Roshko\* and Eppler.† In this model, the wake or "cavity" terminates in a strip bounded by fixed parallel streamlines, thus predicting an asymptotically constant displacement thickness downstream, as seems reasonable (3, p. 266). It would be interesting to compare this model (for the right  $Q$ ) with Flachbart's photographs of the wake behind a flat plate, and to see whether agreement was also better locally than for the Riabouchinsky model (3, p. 356). Moreover, comparisons of the predicted with real displacement thickness  $2(Q)$  and pressure coefficient distribution  $C_p(x, y, Q)$  would be interesting, as functions of the Reynolds number  $R$  too! (This plays no role in the Roshko-Eppler model.) Finally, it would be interesting to make similar comparisons for curved obstacles; calculations could be made by the methods of Ref. 3, Ch. VI.

In any event, the Roshko-Eppler model seems a definite improvement on earlier, otherwise analogous models† with  $Q = 0$ , as regards simulation of flow outside the wake.

The pressure recovery which is observed in real wakes is also obtained by another model, recently suggested by Batchelor.‡ This model, which has some metaphysical plausibility as a representation of asymptotic behavior when  $R$  approaches infinity, involves the assumption of constant vorticity in the wake "bubble." In the light of observed wake instability for  $R \rightarrow 50$ , however, it seems obvious that neither of the above models resembles physical reality at all, within the wake itself (except possibly in supersonic flow). Similar objections apply to the Karman "vortex street" model for periodic wakes (3, Ch. XIII), even in the most favorable range of Reynolds numbers, though with much less force.

### Impact Forces

More critical comparisons between theory and experiment are also desirable, as regards the "impact forces" arising during the first half-diameter of entry of a missile into water. This important subject was reviewed briefly in Ref. 1, pp. 216-20, but with emphasis on favorable comparisons. I should like to record my opinion, that unfavorable comparisons should receive equal emphasis—I see no reason why such comparisons should be taboo.

For instance, consider Ref. 17, p. 403, Fig. 1, which gives the impression that all is sweetness and light. A more careful study shows that the "experimental points" plotted there represent averages of variable observations, which decrease by factors 1.5 to 3.5. Obviously, in such cases, the "experimental"  $k$  will depend on the interval of averaging—and Watanabe's data disagree dimensionally with the formula  $F \propto A y^2$  predicted by Wagner's similarity argument.

\*A. Roshko, *J. Aer. Sci.* 22:124-132 (1955).

†R. Eppler, *J. Rat. Mech. Anal.* 3:591-644 (1954).

‡See Ref. 13, and references given there to earlier work of Prandtl, Schmiedgen, Squire, and others. Also see R. von Mises, "Theory of flight," p. 101.

*J. Fluid Mech.* 1:177-90 and 1:388-98 (1956). This model is remotely reminiscent of Föppel's old model of a vortex-pair (3, p. 263).

In the above case, I would guess that the discrepancy is due to experimental difficulties, but this question should be settled scientifically and not by prejudice. In the cases of the "expanding lens" and other pseudo-mathematical models also reviewed favorably in Ref. 1, the theory rests on a less firm foundation\* and critical comparisons with observation of all "theoretical" predictions seems especially needed.

## CAVITY SEPARATION

It is well known (1, pp. 224, 234, 285) that the prediction of the separation point for cavity flow past smooth obstacles is especially difficult, and that potential flows past analytic profiles have their only singularity there. However, it is not clear to what extent or how viscosity, turbulence, and surface forces affect separation.

In Ref. 1, pp. 224, 295, Maccoll and Imai point to boundary layer theory as the key to the problem. I shall discuss this suggestion below, showing in particular that a laminar boundary layer theory implies a unique separation point.

For wakes, observed pressure distributions do not indicate a unique separation point (16, pp. 422, 497); the separation point is strongly turbulence dependent.

### Low Velocity Effects

As shown by Eisenberg (15, pp. 10-11), the same is true of cavities at large  $Q$ : the problem is the old one of predicting conservation of the liquid-gas balance in the cavity. In a similar vein, it is known that cavity formation is drastically delayed by spinning spheres,<sup>†</sup> because of boundary layer turbulence. Again (14, p. 63), Slichter has observed a downward refraction of spheres at low speeds, when entering water at angles of 20 degrees with the horizontal, at moderate speeds, and explained this as due to the effect on separation of insufficient ventilation. Finally, Worthington himself observed effects on separation of the surface condition ("wettability")—effects recently confirmed by May.<sup>‡</sup>

As regards cavities, all these anomalies occur at relatively low velocities. I therefore repeat my suggestion (made in 1948) that solutions of the Helmholtz-Brillouin problem should give good indications of the separation angle as a function of  $Q$  for cavities behind slowly decelerating macroscopic missiles, in the range 150 fps  $< v < 1400$  fps (Mach number  $M < 0.3$ ).

At lower speeds, one should expect delayed separation and other scale effects. Thus viscosity and surface tension, in combination, will make the cavity separate at a finite angle, and not tangentially. An approximate computation of this contact angle, as a function of the variables involved, would be very instructive.

### Separation Curvature

Actually, the Helmholtz-Brillouin problem was first formulated to avoid the mathematical indeterminacy in the separation point which would otherwise arise for

\*Even the calculations of Hillman, reported in Ref. 17, are subject to the general truncation error uncertainty I discussed earlier.

†H. Wayland and F.G. White, Proc. Symposium Fluid Mech. Heat Transfer, Stanford, pp. 51-64, 1949.

‡A. S. May, J. Appl. Phys. 22:1219-1222 (1951); Ref. 3, p. 326. For the case of circular struts, see Wetzel's paper in this volume.

Helmholtz flows past smooth obstacles. To solve it, Brillouin postulated that the free streamline curvature must be finite at the separation point (3, p. 139)—now called the condition of "smooth separation" (1, p. 285). Villat related this condition to the solution of the Levi-Civita integral equation (3, p. 139), and also assumed that this condition, of a lowest order singularity possible in potential flow, actually determined the separation of flow.

The condition of smooth separation has always seemed to me without physical basis; I cannot see why nature should abhor infinite pressure gradients. If infinite curvature is ruled out, then so is Kirchhoff-Bobyleff flow past a flat plate! My view seems to have been shared by von Mises and Schmieden who, as recalled in the previous section, proposed the "wake of zero drag" as a first approximation to wake flow with turbulent boundary layer. Indeed, it seems obvious to me that separation should entail both a mathematical and a physical singularity; thus boundary layer theory (cf. *infra*) even predicts a jump in slope at the separation point (16, p. 57, Fig. 22).

Much more reasonable is the condition for ideal cavitation, corresponding to the nominal equation of state (Eqs. 2a and 2b) which leads to the Helmholtz-Brillouin problem if inertial forces alone are considered.

Though significant deviations from Eqs. (2) can occur under exceptional conditions (3, Ch. XV), variations of one atmosphere in pressure change the pressure coefficient  $C_p = (p - p_a) / \frac{1}{2} \rho v^2$  by less than 0.03, if  $v = 200$  fps, and by less than 1 percent if  $v = 400$  fps. Hence, in such cases, the Helmholtz-Brillouin problem is a priori very reasonable. Even air-filled and vapor-filled cavities should behave similarly, since we have  $p_v < p < p_a$  under these circumstances.\*

Unfortunately, the Helmholtz-Brillouin problem is not easy to solve mathematically, and one seldom knows whether it has a unique solution.

### Boundary Layer Theory

I agree with Drs. Maccoll and Imai (1, pp. 224, 295) that the influence of viscosity on the separation point should first be studied using boundary layer theory. This theory makes it obvious why separation must occur behind the point of minimum pressure—i.e., why the Helmholtz-Brillouin problem predicts separation too far forward. It also suggests a way of improving agreement between theory and observation (a "viscosity correction"). Experimental data can be corrected by displacing the liquid-solid and liquid-gas interfaces outward by an easily calculated displacement thickness  $\delta^*(s)$ . It would be interesting to study the resulting potential flows as solutions of the Helmholtz-Brillouin problem for the displaced fixed boundary. Perhaps this would explain the discrepancy noted in Ref. 1, p. 224.

On the other hand, I do not think that boundary layer theory is an adequate substitute for Eqs. (2), as suggested by Imai.<sup>†</sup> I do not even agree that, according to boundary layer theory, the asymptotic curvature must be finite. Why should not a

\*It seems unlikely that one can attain cavity overpressure by "hyperventilation"—i.e., that forcing air into the cavity will make  $Q < 0$ . Cf. Proc. First Symp. Appl. Math. Am. Math. Soc., p. 1, 1949; Ref. 14, p. 58; Proc. 7th Int. Congress Appl. Mech., London, 2:12 1948.

<sup>†</sup>Ref. 1, p. 295; and J. Phys. Soc. Japan 8:399-402 (1953).

brief adverse pressure gradient, followed by a mild singularity\* inducing separation with infinite curvature, be compatible with conventional boundary layer theory?

It is attractive to speculate that the separation point can be located by combining free streamline and boundary layer theory, as follows. Consider the one-parameter family of cavity flows, with variable separation point, which is possible if the maximum velocity occurs before separation—as suggested by boundary layer concepts. Then find which flow is compatible with the usual boundary layer separation criteria. This could probably be calculated numerically, in the case of a circular cylinder, and I think such a calculation would be very desirable.

However, it is clear that such a calculation will predict a fixed separation point, independent of the flow velocity. For, inside the boundary layer, the equations are invariant under the group<sup>†</sup>

$$x \rightarrow x, \quad y \rightarrow y + t, \quad u \rightarrow u, \quad v \rightarrow v + t u \quad (t > 0). \quad (3)$$

Outside the boundary layer, the flow scales inertially (14, p. 97), completing the verification.

#### REFERENCES

1. Sherman, F.S., editor, "Symposium on Naval Hydrodynamics," Nat. Acad. Sci.-Nat. Res. Council, Publ. 515 pp. 215-40 and 281-96 Washington, 1957
2. Goldstein, S., "The Place of Applied Mathematics in Higher Education and Research," Technion Year Book, 1950
3. Birkhoff, G. and Zarantonello, E.H., "Jets, Wakes and Cavities," New York:Academic Press, 1957
4. Garabedian, P.R., Lewy, H., and Schiffer, M., "Axially Symmetric Cavitation Flow," Annals of Math. 56:560-602 (1952)
5. Serrin, J.B., J. Rat. Mech. Anal. 2:563-575 (1953)
6. Levinson, N., "On Asymptotic Shape of Cavity. . .," Annals of Math. 47:704-730 (1946)
7. Birkhoff, G. and Carter, D., "Rising Plane Bubbles," J. Rat. Mech. Anal. 6:769-780 (1957)
8. Birkhoff, G., Goldstine, H.H., and Zarantonello, E.H., "Calculation of Plane Cavity Flows Past Curved Obstacles," Rend. Sem. Mat. Torino 13:205-224 (1953)
9. Zarantonello, E.H., "A Constructive Theory for the Equations of Flows with Free Boundaries," Collectanea Math., Barcelona, 5:175-225 (1952)
10. Garabedian, P.R., "Calculation of Axially Symmetric Cavities and Jets," Pac. J. math. 6:611-684 (1956)

\*I know of no exhaustive mathematical study of the nature of the singularity at a separation point.

†As well as under the group of Ref. 14, p. 127, (25\*), which is useful in finding self-symmetric solutions.

Jets, Wakes, and Cavities

11. Southwell, R.V. and Vaisey, G., "Relaxation Methods Applied to . . . 'Free' Streamlines," Phil. Trans. A240:117-161 (1946)
12. Young, D.M. Jr., et al., "Computation of an Axially Symmetric Free Boundary Problem on NORC," Naval Proving Ground Report V1413, Dahlgren, Va., 1955
13. Imai, I., J. Phys. Soc. Japan 8:399-402 (1953)
14. Birkhoff, G., "Hydrodynamics: A Study in Logic, Fact, and Similitude," Princeton, 1950 (Revised edition 1960)
15. "Cavitation in Hydrodynamics," Symposium at Nat. Phys. Lab. Teddington (1955), London:Her Majesty's Stationery Office, 1956
16. Goldstein, S., editor, "Modern Developments in Fluid Dynamics," Oxford, 2 vols. 1938
17. Shiffman, M. and Spencer, D.C., Comm. Pure Appl. Math. 4:379-418 (1951)

\* \* \* \* \*

# CAVITY FLOWS OF VISCOUS LIQUIDS IN NARROW SPACES

Sir Geoffrey Taylor and P. G. Saffman  
*University of Cambridge*

\* \* \* \* \*

This communication is concerned with the motion of the interface between two immiscible viscous fluids contained in the narrow space between two closely spaced surfaces. One of the fluids may be of negligible viscosity and density, corresponding to the case of a cavity. When the surfaces are fixed, parallel, and plane, the configuration is known as a Hele-Shaw apparatus.

The penetration of a viscous fluid into a more viscous fluid contained in a straight-sided channel in a Hele-Shaw apparatus is discussed under certain simplifying assumptions about the physical conditions at the interface. These are that the pressure change on crossing the interface is constant, and that the sheets of the more viscous fluid left behind after the interface has passed are of constant thickness. The problem is not unique, possessing a singly infinite family of solutions, and some analytical features of the solution which single out a particular flow are described.

\* \* \* \* \*

## INTRODUCTION

Taylor (1) has shown, and Lewis (2) has verified experimentally, that the surface between two superposed fluids of different densities and negligible viscosities which are accelerated in a direction perpendicular to their interface is stable or unstable to small deviations according as the acceleration is directed from the more dense to the less dense fluid or vice versa. If the fluids are confined within a long tube or channel, a final steady state appears to be attained in which a long bubble or finger of the less dense fluid advances along the tube whilst the more dense fluid drains away round the sides. This situation occurs when a vertical tube filled with fluid is closed at the top and opened at the bottom to the atmosphere. The steady motion of large bubbles or cavities rising through inviscid liquids in tubes and channels has been studied experimentally and theoretically; see, for example, Davies and Taylor (3); Garabedian (4), where other references may be found.

Saffman and Taylor (5) have shown that analogous phenomena occur when two superposed immiscible viscous fluids are forced with uniform velocity through a Hele-Shaw cell, that is, between two closely spaced, fixed parallel sheets. When the

interface between the two fluids is straight and perpendicular to the direction of motion, a steady uniform motion is theoretically possible; but it can be shown that the interface is unstable to small deviations when the direction of motion is from the less viscous to the more viscous fluid (i.e., when the less viscous drives the more viscous) and stable when the more viscous pushes the less viscous. Actually this statement is strictly true only when the plates bounding the cell are horizontal, or the fluids have the same densities, so that the stabilizing or destabilizing effects of gravity are not important. When gravity effects have to be considered, the statement holds if the uniform velocity with which the fluids move through the cell is greater than a certain critical velocity (which may be negative) depending upon the density difference. However, when the plates are very close together or the fluids are very viscous, the pressures required to drive the fluids will be large compared with the hydrostatic pressure so that gravity may effectively be neglected even if the plane of the cell is vertical.

The instability was demonstrated experimentally and the motion into which the instability develops was observed. This consists of the penetration of the more viscous fluid by "fingers" of the less viscous one in a way analogous to the later stages of the instability of accelerated interfaces as reported by Lewis. A characteristic feature of the later stages of the growth of "instability" into "fingers" is the tendency of the fingers to space themselves so that the width of the fingers and the columns of more viscous fluid between them are of approximately the same breadth. Another characteristic feature was the inhibiting effect on the growth of its neighbours by any finger which gets ahead of them. These features are shown in the three photographs of Fig. 1 in which air was used to drive glycerine downwards through a Hele-Shaw cell consisting of two vertical rectangular sheets of flat glass 0.09 cm apart. The first photograph (a) was taken shortly after the beginning of the motion and shows the instability in its initial stages. The second photograph (b) was taken

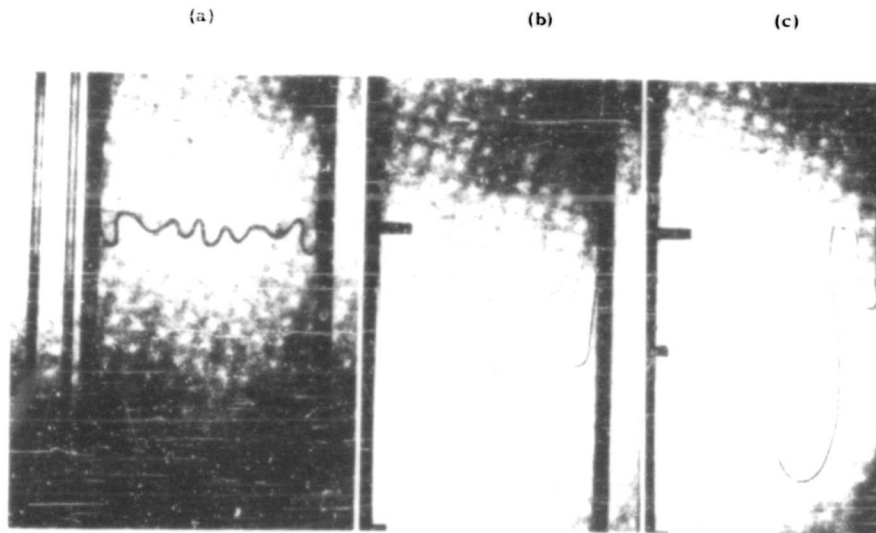


Fig. 1 - The development of the instability of an air-glycerine interface. The air is above and the glycerine below; the direction of motion is downwards. (a) An early stage, (b) a later stage, (c) a later stage than (b).

at a later stage of the instability (not the same experiment) and shows the tendency of the fingers to be separated by a distance approximately equal to their width. The third photograph (c), taken at a still later stage with another experiment, shows the inhibiting effect, because the three fingers on the right-hand side of this photograph all started to grow at the same time but the middle finger, which was slightly larger than its neighbours, has almost completely inhibited the growth of the others and has spread laterally.

In attempting to understand the mechanics of the formation and propagation of fingers from an unstable interface, the authors were led to the consideration of a single finger of fluid, or a cavity, propagating steadily through a channel of fixed width in a Hele-Shaw cell containing a more viscous fluid. Actually, it appears that if the superposed fluids with an unstable interface are confined within a sufficiently long parallel-sided channel in a Hele-Shaw cell, then "instability" finally develops into such a motion with the penetrating finger of less viscous fluid in the middle of the channel and a certain fraction of the channel width. Thus this problem will be closely related to the rise of an air bubble through a long vertical channel, closed at the top and open to the air at the bottom, in a Hele-Shaw cell, i.e., between two closely spaced sheets.

#### THE ANALYTICAL DESCRIPTION OF THE MOTION OF TWO IMMISCIBLE FLUIDS IN A HELE-SHAW CELL

For a viscous fluid moving between two closely spaced, fixed, parallel plates, the components of the mean velocity across the stratum are given by (see, for example, Lamb (6))

$$u = \frac{-b^2}{12\eta} \left( -\frac{\partial p}{\partial x} + g \right), \quad v = \frac{-b^2}{12\eta} \frac{\partial p}{\partial y}, \quad (1)$$

where  $b$  denotes the (small) distance between the plates,  $p$  the pressure (assumed constant across the stratum),  $\eta$  the density and  $g$  the viscosity of the fluid, and  $g$  the acceleration due to gravity. The plane of the plates is here taken as vertical,  $x$  and  $y$  are coordinates measured in the plane of the plates with the  $x$ -axis taken vertically upwards (the  $y$ -axis is therefore horizontal), and  $u$  and  $v$  are the components of the mean velocity averaged across the stratum in the  $x$ - and  $y$ -directions, respectively. The case in which the plates bounding the cell are horizontal is obtained by putting  $g = 0$ .

The mean velocity field is two dimensional and can be derived from a velocity potential

$$\phi = \frac{-b^2}{12\eta} (p + g x).$$

By virtue of the equation of continuity,  $\nabla^2 \phi = 0$  and there exists a stream function which is the harmonic conjugate of  $\phi$ , so that the complex potential  $\phi + i\psi$  is an analytic function of  $x + iy$ . (This result was used by Hele-Shaw (7) for the purpose of demonstrating the streamlines in the irrotational flow of an inviscid liquid in two dimensions.)

Consider now the motion of the interface between two immiscible fluids of viscosities  $\eta_1, \eta_2$  and densities  $\rho_1, \rho_2$ , and suppose the direction of motion of the interface is away from fluid 2 towards fluid 1; i.e., fluid 2 drives fluid 1. For a cavity flow,  $\rho_2$  and  $\eta_2$  will be zero, but for the moment we shall suppose this is not necessarily



so. Now fluid 1 is not necessarily completely expelled or replaced by fluid 2; a film of fluid 1 may wet the plates and adhere to them whilst a tongue of fluid 2 advances along the middle of the gap between the plates. The thickness of this tongue is a fraction,  $\tau$  say, of the gap between the plates and it may be expected that  $\tau$  will depend upon the viscosities of the fluids, the velocity of advance of the tongue, and the interfacial tension.

That is, the motion may be, in fact, a combination of two different types of cavity flow. There is that flow viewed by an observer standing in front of the cell looking in a direction perpendicular to the plates; he sees the motion of the two-dimensional interface between two regions, one occupied by fluid 1 and the other by fluids 2 and (possibly) 1, and is observing in fact the projection, on the plates bounding the cell, of the boundary of the region containing fluid 2. The velocity of the interface he sees is actually the velocity of the tip of the tongue between the plates. On the other hand, an observer standing at the side and looking between the plates (assuming this is possible) sees the penetration of a viscous fluid between two closely spaced parallel plates by a tongue of another viscous fluid, and this cavity flow, although schematically similar to the first, is in fact governed by different equations, namely those of slow creeping motion which reduce to the biharmonic equation for two-dimensional flow, whereas the first type of cavity flow may be described (under assumptions formulated below) by solutions of Laplace's equation. The two flows are not independent, but, by making plausible assumptions about the thickness of the tongue, it is possible to analyse the motion as seen by an observer standing in front, and this communication is concerned with cavity flows regarded from this viewpoint.

Suppose first that one fluid completely expels the other so that  $\tau = 1$ . In this case the tip of the meniscus viewed by an observer in front represents an interface completely separating the two fluids. Also, the streamlines which would be seen by this observer if the fluids were marked are those of the mean velocity field. The mean velocity across the stratum of fluid 1 ahead of the interface can be derived from the velocity potential

$$\phi_1 = (b^2/12) \phi_1 (p + \rho_1 g x)$$

and that of fluid 2 from

$$\phi_2 = (b^2/12) \phi_2 (p + \rho_2 g x),$$

where  $\phi_1$  and  $\phi_2$  both satisfy Laplace's equation. Since  $b$  is small, the width of the projection of the meniscus onto the plates is small compared with the length scale of the mean motion, and the interface may be regarded as a sharp line. It follows from continuity that the component of mean velocity normal to the interface is continuous across it and is equal to the velocity of the interface normal to itself; i.e.,

$$\phi_1 n = \phi_2 n, \quad \text{or} \quad \phi_1 = \phi_2 \quad (2)$$

at the interface, where  $n$  is differentiation in the normal direction.

The authors (5) have given some evidence to show that, in cases likely to be met with in cavity flows of this type,  $\tau$  may be within 1-1/2 percent of unity. However, the conditions determining the value of  $\tau$  and the mechanics of the second type of cavity flow are far from being fully understood, and the assumption  $\tau = 1$  will not be reasonable in all the cases likely to be encountered. On the other hand, it appears that the thickness of the tongue may be sensibly constant for some cases, and if this is so it transpires that it is possible to analyse the motion in a way similar to the case  $\tau = 1$ .

Suppose now that the thickness of the tongue is constant. The interface can now be identified with the tip of the tongue. Ahead of the tongue, the mean velocity is given by Eq. (1); behind the interface, the velocity distribution across the gap between the plates can be worked out making the same approximation used in calculating Eq. (1) that velocity gradients in directions parallel to the plates are small compared with those in the perpendicular direction and that the pressure is constant across the gap. The mean velocities in the tongue and the layers adhering to the plates can be shown to be derivable from velocity potentials which satisfy Laplace's equation, and continuity considerations at the interface give a boundary condition between the velocity potentials on each side. It can then be shown that the interface moves as if it were an interface completely separating two imaginary fluids of different viscosities and densities, one of which completely expels the other, i.e., for which  $\tau = 1$ . For the case in which a viscous fluid is penetrated by a cavity (i.e.,  $\tau_2 = \tau_1 = 0$ ), the motion of the interface is the same as if a fluid of viscosity  $\tau_1$  and density  $\rho_1 \cdot (1 - \tau_1)(1 - \tau_1^2)^{1/2}$  were completely expelled, the pressures in the two flows being the same.

In other words, the case  $\tau = \text{constant}$  is equivalent, for the purposes of mathematical analysis, to  $\tau = 1$ . The analysis will henceforward be based on the assumption that  $\tau = \text{constant}$ , since otherwise a simple description of the motion is not possible; so that it is sufficient in fact to consider only the case  $\tau = 1$  without loss of generality. The available evidence indicates that this is a reasonable assumption, but further work remains to be done.

To complete the description of the equations governing the flow, it is necessary to know what is the pressure drop across the interface. If the fluid wets the plane surfaces, it might be expected that under static conditions the pressure drop would be  $T(2/b + 1/R)$ , where  $R$  is the radius of curvature of the projection, on the plane of the plates bounding the cell, of the meniscus. When the fluids are moving, the pressure drop across the interface may depend upon a variety of physical circumstances which are not yet understood. The simplest assumption we can make is that the pressure drop has the same value as in the static case and hence that

$$p_2 - p_1 = \frac{T}{R} = \text{constant} \quad (3)$$

on the interface. Further, the pressure gradients in the viscous fluid are of order  $u/12b^2$ , where  $u$  is the velocity of the interface, so that if  $T/R = uR/12b^2$ , i.e.,  $uR^2/(12Tb^2) = 1$  (which is likely to be the case if the motion is not very slow), it seems reasonable to neglect  $T/R$  and take the boundary condition at the interface as

$$p_2 = p_1 = \text{constant} = 0, \text{ say.} \quad (4)$$

The pressure inside a cavity is effectively zero, so that for cavity flows the boundary condition in this case is  $p = 0$  at the surface of the cavity.

#### THE PENETRATION OF A CAVITY INTO A CHANNEL

The authors (5) have investigated the propagation of a finger of fluid through a straight parallel-sided channel in a Hele-Shaw cell containing a more viscous liquid. They showed that when the fluid in the finger has negligible viscosity, and hydrostatic pressures can be ignored, and it is assumed that the viscous fluid is completely expelled, i.e.,  $\tau = 1$  (or, as is mathematically equivalent,  $\tau = \text{const.}$ ), and the pressure is assumed constant on the interface, i.e., Eq. (4) is used, then the potential and stream function of the mean velocity (across the stratum) of the viscous liquid satisfy the boundary conditions:

$$v_x \text{ as } x \rightarrow \infty$$

where  $v$  denotes the uniform mean velocity of the fluid at infinity ahead of the finger;

$$v = V \text{ on } y = 1,$$

since the walls of the channel which are taken as  $y = \pm 1$  are streamlines of the mean velocity (edge effects which occur at walls in the Hele-Shaw cell and invalidate Eq. (1) within distance  $b$  of them are neglected);  $\psi = 0$  on the interface, by virtue of Eq. (4); and (assuming the finger is symmetrical about the centre line of the channel)

$$v_y \text{ on } x = 0 = 0,$$

where  $v$  is the velocity of propagation of the finger. The solution of this free boundary problem was shown to be

$$x + iy = \frac{z + i}{V} + \frac{2}{\pi} (1 - \epsilon) \log \frac{1}{2} \left[ 1 + \exp \frac{-\pi(z + i)}{V} \right], \quad (5)$$

and the velocity of the finger is related to the mean velocity at infinity by

$$V = v, \quad (6)$$

where  $\epsilon$  is the fraction of the channel width occupied by the finger after the nose has passed; i.e.,  $2\epsilon$  is the distance between the straight sides of the finger. The equation of the interface is the image of  $\psi = 0$  and is easily seen to be

$$x = \frac{1 - \epsilon}{\pi} \log \frac{1}{2} (1 + \cos \pi y). \quad (7)$$

It was pointed out further that the case in which the fluid in the finger has a non-zero viscosity and hydrostatic pressures are not neglected can be reduced to this case, provided the same simplifying assumptions, namely those embodied in Eqs. (2) and (4), are made about the physical conditions at the interface. In particular, the equation of the interface is still given by (7). For the case of a cavity rising through a vertical channel in a vertical cell, the relation between the velocities is

$$v = V + (12/b^2)(1 - \epsilon)g,$$

$V = 0$  corresponds to the case in which the channel is closed at the top, and the velocity of rise is then

$$v = 1 + \frac{12}{b^2} \epsilon.$$

Now there is nothing in the analysis which leads up to Eqs. (5), (6), and (7) which specifies the value of  $\epsilon$ , the fraction of the channel occupied by the finger after the nose has passed. That is, if only the conditions at infinity in front of the cavity are specified, the mathematical problem does not appear to possess a unique solution and there is an infinity of possible shapes for the interface, each with a different velocity of penetration. (It is worth noting that, according to the analysis, the family of possible shapes is independent of the physical properties of the fluids.) The calculated shapes for  $\epsilon = 0.2, 0.5$ , and  $0.8$  are shown in Fig. 2.

It was noted recently by Garabedian (4) that the analogous free-boundary problem of an air bubble rising through a vertical tube or channel containing an inviscid

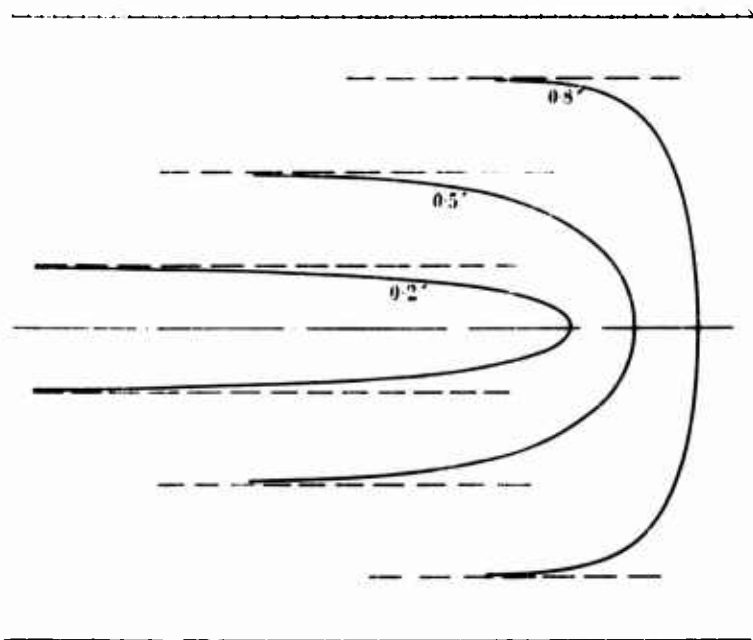


Fig. 2 - Calculated profiles with  $\lambda = 0.2, 0.5, 0.8$  for a finger propagating through a channel

liquid also does not possess a unique solution. It is nice to be able, in the present, much easier, problem, to demonstrate explicitly a singly infinite family of solutions.

This motion was investigated experimentally using a variety of fluids. In the first series of experiments, a finger of air was blown through a channel containing glycerine and photographs were taken of the interface. It was found that the value of  $\lambda$  for several experiments was within 2 percent of 0.50. The observed shapes of the interface were compared with the calculated shape with  $\lambda = 0.50$ , and the agreement was found to be very good. In Fig. 3 the line is the photographed interface and the circles are surrounding points calculated from Eq. (7) with  $\lambda = 1/2$ . This agreement seems to justify the assumed boundary conditions.

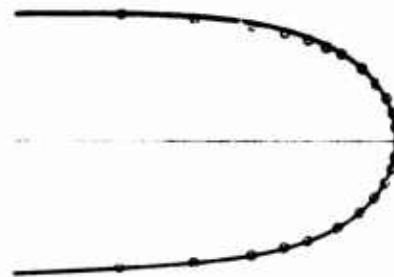


Fig. 3 - Comparison between an observed profile and the interface calculated from Eq. (7) with  $\lambda = 1/2$

The question now arises why in practice the finger with  $\lambda = 1/2$  is singled out from the infinity of theoretically possible solutions. It might be thought that a hypothesis of a maximum or minimum rate of energy dissipation might single out a

unique value of  $\lambda$ , but this in fact is not so, since it is easily seen that for given conditions ahead of the finger the rate of energy dissipation is independent of  $\lambda$ .

Further experiments were carried out in order to see whether  $\lambda$  depended upon the ratio of the viscosities of the fluids inside and outside the finger or upon any other of the physical properties of the fluids. These experiments showed that it was often possible to obtain very uniform fingers (Fig. 4 shows an example with water penetrating a narrow channel filled with an oil), and that the value of  $\lambda$  was always close to 1/2, provided that the speed of the finger was not too slow.

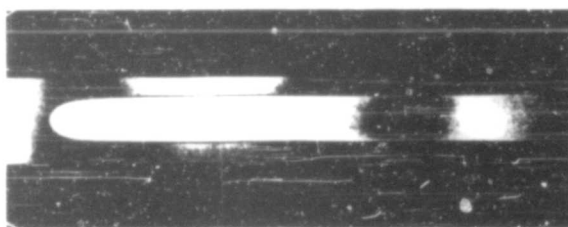


Fig. 4 - A photograph showing a uniform finger of water penetrating a channel filled with oil

At low speeds, the value of  $\lambda$  increased from 0.5 to the limit 1.0 as the velocity tended to zero, but it was found that the wider forms did not conform to the corresponding profiles calculated from Eq. (7) with the same value of  $\lambda$ . This indicated that surface tension, or some equivalent surface stress, was affecting the shape of the interface, and that the boundary condition (Eq. 4) is not applicable when  $u$  is too small (as is indeed to be expected according to the previous discussion). Restricting attention to the case of cavity flows in which the viscosity of the fluid in the finger is negligible, it would then be expected on dimensional grounds that the value of  $\lambda$  in a channel of given shape would be a function of  $\mu U/T$  only, when the fluid wets the flat sides of the channel. The results of some experiments are shown in Fig. 5 and justify this expectation.

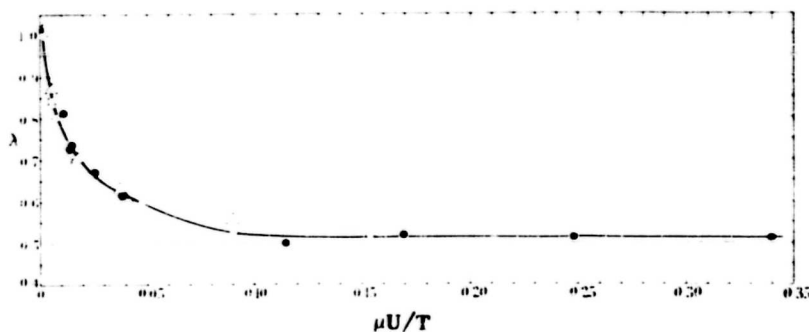


Fig. 5 - Dependence of  $\lambda$  on  $\mu U/T$

The value of  $\gamma$  rapidly decreases to  $1/2$  as  $U/T$  increases, i.e., as the effect of interfacial stress in determining the shape of the interface becomes less important in comparison with that of the viscous stress. This indicates that when the physical conditions are such that the boundary condition (Eq. 4) is a reasonable representation of the actual physical conditions at the interface, then the only one of the infinity of possible shapes given by Eq. (7) that can actually occur is that for which  $\gamma = 1/2$ , a conclusion which is supported by the evidence of Fig. 3.

The authors (5) were unable to put forward any theoretical reason for this deduction from observation. Further work still in progress has not yet succeeded in accounting for this phenomenon, but a number of mathematical results, which however lack an obvious physical significance, have been discovered which single out  $\gamma = 1/2$ . These will be described in the following section.

#### SOME MATHEMATICAL RESULTS WHICH DISTINGUISH $\gamma = 1/2$

1. The first result is of a geometrical character. Consider the area between the surface of the cavity, its asymptotes  $y = \pm \frac{1}{2}$ , and the tangent at the vertex of the finger. This area is, according to Eq. (7),

$$A = 2 \int_0^{\frac{1}{2}} x dy = \frac{2(1-\gamma)}{\gamma} \int_0^{\frac{1}{2}} \log \frac{1}{2} \left( 1 + \cos \frac{\gamma y}{1-\gamma} \right) dy$$

$$= \frac{4}{\gamma} \log 2 \cdot (1-\gamma)$$

Hence, the arbitrary criterion that  $A$  is a maximum gives  $\gamma = 1/2$ !

2. An exact unsteady solution, under the same simplifying assumptions about the physical conditions at the interface, has been discovered (8) which represents the change with time of the interface between a cavity and a viscous fluid in a channel in a Hele-Shaw cell. Initially, the shape of the interface is such that it is almost flat and extends right across the channel; as the time becomes large, the shape tends to that of a long finger propagating steadily through the channel. That is, the solution represents the growth of a finger from a flat interface which is disturbed initially in a particular way; by reflecting in the channel walls we have a solution for the growth of equal and equally spaced fingers from an unstable interface.

There is a singly infinite family of these unsteady solutions corresponding to different values of the ratio of the width of the final finger and that of the channel; this parameter is denoted by  $\gamma$ . It was shown that the shape of the interface for each value of  $\gamma$  is obtained by eliminating the real variable  $s$  from

$$x + iy = s + \frac{2}{\gamma(1-\gamma)} \log \frac{1}{2} \left\{ 1 + a(\tau) e^{-i\gamma s} \right\} = \text{constant},$$

where  $a(\tau)$  is a function of the time  $\tau$  which is small when  $\tau = 0$  and which tends to one as  $\tau \rightarrow \infty$  (giving Eq. (7) in the limit). It was also shown that

$$\log(1-a) = -\frac{\tau}{(1-\gamma)} \quad \text{as } \tau \rightarrow \infty,$$

so that the rate at which  $a \rightarrow 1$ , which corresponds intuitively with the rate at which the final asymptotic state is attained, is a minimum when  $\gamma = 1/2$ , thus distinguishing the finger which is half the width of the channel.

Actually, this result is puzzling, since it might intuitively be expected that the actual shape would correspond to a maximum rate of formation.

3. Consider the mean (two-dimensional) velocity field in a channel due to the supposition of a uniform mean velocity  $V_2$  and a "source" of strength  $2V_2$ , i.e., a source of viscous fluid which gives rise to a (two-dimensional) distribution of mean velocity whose magnitude is  $V_2/r$  near the source and radially outwards. Using the notation from the preceding section, it is easily seen that the complex potential  $\phi(z)$  is related to  $z = x + iy$  by

$$v_z = \frac{v}{\gamma} \log \left( 2 \sinh \frac{1}{2} z \right) = \frac{v}{\gamma} \log (e^{z/2} - 1), \quad (8)$$

At  $z = 0$ , the mean velocity is zero, at  $z = \infty$  the mean velocity is uniform of magnitude  $V$ .

The equation of the equipotential  $\phi = 0$  is

$$x = \frac{1}{2} \log 2 + \frac{1}{2} \log \frac{1}{2} \left( 1 + \cos \frac{\pi}{2} \right),$$

and, on it,  $\gamma = 2\gamma_0$ . Hence, the mean velocity field in a channel due to a "source" of strength  $\gamma$  moving with velocity  $2V$  and a uniform mean velocity  $1/2 V$  is identical with the mean velocity field in a viscous fluid being driven through the channel by a finger whose width is half that of the channel (provided the conditions at the interface may be represented by the simplifying assumptions), which is a mathematical feature to distinguish  $\gamma = 1/2$ .

All the flows with  $\alpha = 1/2$ , that is, for all combinations of viscosities, densities, and various values of  $\tau$ , can be so obtained by a superposition of a uniform stream and a moving source of appropriate magnitudes. Zhuralev (8) has pointed out that two-dimensional cavity flows in a porous medium (which is mathematically analogous to flow in a Hele-Shaw cell) may be constructed by a suitable superposition of sources and sinks and he refers to the solution (Eq. 8). It is, in fact, possible to demonstrate that the flows with  $\alpha = 1/2$  can be constructed in a similar way, but it turns out that the system of sources required is much more complicated involving line sources and line dipoles instead of the simple source which suffices for  $\alpha = 1/2$ .

4. Before we give the next feature, it is first necessary to describe briefly a stability investigation. The stability to small disturbances of the interface of a cavity penetrating a channel was investigated theoretically since it was thought that this might throw some light on the occurrence of  $\alpha = 1, 2$  in practice. Taking the origin at a point fixed in space (and neglecting hydrostatic pressures), the steady mean motion is given by ( $t$  denotes time)

$$Z_n = \sqrt{V} \cdot U^{(n)} \cdot \sqrt{2} \cdot (1 - \log \frac{1}{2} (1 + e^{-\frac{1}{2} V}))^{-1/2}, \quad V = U^{(n)} \cdot U^{(n)}, \quad (5)'$$

where the  $\frac{1}{2}$  term arises because the origin is fixed in space and not fixed relative to the bubble as in the derivation of Eq. (5), and  $\dot{z}$  is taken as a function of  $\theta$ , so that in fact we are working in the potential plane. Suppose the motion is slightly disturbed, so that it is given by

*J. J. O'Neil*, *University of Illinois at Chicago*

where  $\epsilon$  is small. The conditions that the disturbance vanishes at infinity and that the walls of the channel are streamlines are  $x_1 \rightarrow 0$  as  $x \rightarrow \pm \infty$  and  $y_1 = 0$  on  $x = \pm V$ , respectively. If we assume that the boundary conditions at the interface are unaltered, i.e., the interface is taken as  $y = 0$  and the value of  $t$  is supposed to remain unaltered, then it can be shown that the condition satisfied by  $x_1$  and  $y_1$  on the interface is

$$\frac{x_1}{V} + \frac{1}{2} \frac{x_1}{V} + \frac{1}{V} \frac{\sin(\epsilon \cdot V)}{1 + \cos(\epsilon \cdot V)} - \frac{y_1}{V} = 0 \quad \text{or} \quad y_1 = 0,$$

to the first order in  $\epsilon$ . It is then easy to show that

$$x_1^{(n)}(x, y, t) = e^{n \cdot V \cdot t} \sum_{r=0}^n a_{rn} e^{-r \cdot V \cdot t}$$

satisfies all the necessary conditions, and that any disturbance which leaves the straight sides unaltered at  $t = 0$  (i.e., which vanishes as  $x \rightarrow \pm \infty$ ) can be expressed as a sum of disturbances of this type. The  $a_{rn}$  are real constants determined by a set of simultaneous equations. Since the amplification factor is positive, the conclusion of this analysis is that all possible shapes calculated using Eq. (7) are unstable; a conclusion which is manifestly wrong (see, for example, Fig. 4).

This indicates that surface tension, or some other effect of interfacial stress, must stabilize the motion in some way, even when  $U \cdot T$  is large, and that it is not legitimate to discuss the stability under the same simplifying assumptions about the physical conditions at the interface which were used in calculating the steady motion. To explain why surface tension can be neglected in calculating the steady shape, but yet is apparently important in its effect on the stability, is a problem which has not yet been resolved. Partly, the difficulty is that our knowledge of the actual physical conditions at the interface is limited, though it is hoped that further work will clarify this, and also throw light on the mechanism which selects the value of  $\epsilon$ . It should be noted that, along the straight sides of the finger, the velocity of the fluid is exponentially small so that  $U \cdot T$ , where  $U$  is a local velocity, must eventually be small; and the surface tension effect may be expected to be large relative to the viscous stress along the straight sides, although it will still be small relative to the viscous stresses at the nose.

In this connection, a mathematical feature which distinguishes  $\epsilon = 1/2$  of the stability analysis given above may possibly be relevant. If we express the velocity potential and stream function in terms of the physical coordinates in the region of the straight sides of the finger (i.e., as  $x \rightarrow \pm \infty$ ), it can be shown that the perturbation of the pressure behaves as

$$e^{2(1-\epsilon)x} \cos \frac{(1-\epsilon)y}{2(1-\epsilon)} f(t) + e^{2(1-\epsilon)x} \cos \frac{(1-\epsilon)y}{2(1-\epsilon)} g(t) + O\left(\frac{3-\epsilon}{2(1-\epsilon)}\right)$$

where  $f(t)$  and  $g(t)$  are exponentially growing functions of the time. It so happens that  $f(t) = 0$  for any disturbance when  $\epsilon = 1/2$ , but the physical significance of this is not yet clear.

#### MOTION OF A FINITE BUBBLE IN A CHANNEL

In a further attempt to find an explanation for  $\epsilon = 1/2$ , we were led to the theoretical consideration of the steady motion through a channel in a Hele-Shaw cell of a



bubble of finite area bounded by a closed curve symmetrical about the centre line of the channel, under the same assumptions about the physical conditions at the interface as were used for calculating the shape of the long fingers. Restricting attention to the case in which the fluid in the bubble is of negligible viscosity and hydrostatic pressures can be neglected, a solution is required of the free boundary problem formulated earlier in this paper, except that the interface has now to be closed instead of infinite. For brevity we shall omit the analytical details and confine ourselves to quoting the final result.

It may be verified that

$$z = \frac{4(U-1)}{U} \tanh^{-1} \left[ \frac{\tan \frac{1}{2} \pi y}{\tan \frac{1}{2} \pi x} \left\{ \tanh^2 \frac{1}{2} \pi x - \left( \tanh^2 \frac{1}{2} \pi x + \tan^2 \frac{1}{2} \pi y \right)^{1/2} \right\} \right]$$

gives the velocity potential and stream function of the mean velocity when a finite bubble bounded by the curve

$$x = \frac{2(U-1)}{U} \tanh^{-1} \left[ \sin^2 \left( \frac{1}{2} \pi y \right) - \cos^2 \left( \frac{1}{2} \pi y \right) \tan^2 \left( \frac{1}{2} \pi y \right) \right]^{1/2}$$

moves steadily with velocity  $U$ , the velocity at infinity ahead of and behind the bubble being uniform and equal to unity. The bubble is symmetrical about its centre, its length is

$$L = \frac{4(U-1)}{U} \tanh^{-1} \sin \left( \frac{1}{2} \pi U \right) \quad \text{say,}$$

its maximum width is  $2$ , and its area is

$$A = \frac{16(U-1)}{U^2} \tanh^{-1} \tan^2 \left( \frac{1}{4} \pi U \right) \quad \text{S, say.}$$

If  $U \rightarrow 1$ , keeping  $U$  fixed, the area of the bubble tends to  $0$ , and it is easily shown that we can recover Eqs. (5) and (7). This is, of course, only to be expected since a long finger may clearly be regarded as the front of a large bubble. It is clear that the motion is mathematically not unique. For a bubble of given area and for given conditions at infinity, there is again a singly infinite family of mathematically possible shapes.

When  $U$  is small compared with one and  $U$  remains finite, the dimensions of the bubble are small compared with the width of the channel, so that this is the case of the motion of a small bubble. The equation of the interface reduces to

$$\frac{x^2}{(U-1)^2} + y^2 = 1$$

so that a small bubble is (according to the analysis) an ellipse of axis ratio  $U-1$ , where  $U$  is really the ratio of the velocity of the bubble to the velocity at infinity. When  $U = 2$ , the interface is circular.

Now the analysis has so far been based on the assumption that the pressure drop across the interface is given by Eq. (4). For small bubbles, surface tension is likely to be of some effect, in which case the pressure drop is more likely to be given by Eq. (3). It is worth noting that the above solution for small bubbles is valid exactly

using the boundary condition (3) when the bubble is circular. Furthermore, the effect of surface tension may be expected to tend to reduce the length of the perimeter and make a small bubble circular; and we should therefore expect the motion of a small bubble to be physically unique with the bubble circular and moving with twice the velocity at infinity (if  $\epsilon \ll 1$ ).

Visual observations of small bubbles indicate that they are indeed circular when sufficiently small. When larger, they are often pear shaped with a rounded front and pointed back; some, on the other hand, seem to be ovoid with the sharper end pointed in the direction of motion. These latter shapes are not predicted by the analysis and are probably due to the physical conditions at the retreating interface over the back of the bubble being different from those at the front; there is, however, no clear evidence on this point. When the dimensions of the bubble become comparable with the width of the channel, the front of the bubble resembles closely that of a long finger, but the shape at the back is different, for probably the same reason.

Returning to the exact solution for a bubble of arbitrary size, a particular shape is singled out by making the arbitrary hypothesis that  $U$  should be a minimum for a bubble of given size. It is easily seen that this gives  $U = 2$ . When the bubble is small, the circular bubble is singled out; when the bubble is large, i.e.,  $U \gg 1$ , this gives  $\lambda \approx 1/2(1)$  and in the limit the finger which is half the width of the channel.

The product  $U$  of the velocity of the bubble and its maximum width does not have a clear physical significance, although it may be identified intuitively with the rate at which fluid is pushed aside by the bubble. Attempts to give this result a sound physical basis have so far failed.

#### REFERENCES

1. Taylor, Sir Geoffrey, Proc. Roy. Soc. A201:192 (1950)
2. Lewis, D.J., Proc. Roy. Soc. A202:81 (1950)
3. Davies, R.M. and Taylor, Sir Geoffrey, Proc. Roy. Soc. A200:375 (1950)
4. Garabedian, P.R., Proc. Roy. Soc. A241:423 (1957)
5. Saffman, P.G. and Taylor, Sir Geoffrey, Proc. Roy. Soc. A245:312 (1958)
6. Lamb, H., "Hydrodynamics," 6th Ed., Section 330, Cambridge University Press
7. Hele-Shaw, H.J.S., Trans. Instn. Nav. Archit. Lond. 40:21 (1898)
8. Saffman, P.G., Quart. J. Mech. Appl. Math., p. 146, Vol. XII, Part 2 (May 1959)
9. Zhuralev, P.A., Zap. Leningr. Gorn. In-ta. 33:54 (1956)

\* \* \* \* \*

# DISCUSSION

G. Birkhoff (Harvard University)

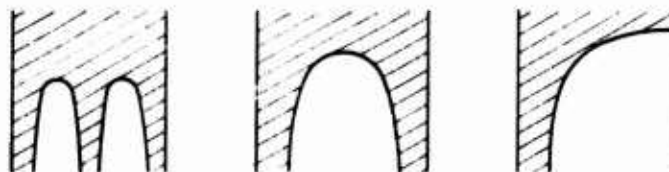
I agree that surface tension is probably an important stabilizing factor in the experiments considered, especially for shorter wavelengths as in the experiments of Lewis (1950) on ordinary Taylor instability. In analyzing the experimental data, it would be interesting to tabulate the dimensionless parameter

$$\Delta V / (\mu \cdot \gamma) g d^2 = F \cdot (1 - \alpha^2) R_p$$

This, roughly, expresses the ratio: (viscous pressure gradient)/(gravity pressure gradient), if  $d$  is the plate spacing (about 0.09 cm). A casual inspection of Fig. 13 of Saffman-Taylor (1958) suggests that, perhaps, gravity might explain the marked deviation from (17).

As regards  $\alpha$ , it would be interesting to see how stable the value  $\alpha = 1/2$  was against its initial width, which could be controlled by forcing an air bubble into a channel from a narrow orifice. It would also be interesting to see how stable the centering of the bubble about the channel axis was, by forcing air from an orifice near one edge. Further, it would be interesting to know how stable the bubble shape is against small variations in  $d$ . For example, if the plates are not parallel how great is the tendency for the bubble to migrate towards the side where the spacing is greater?

Finally, I should like to mention that the first demonstration of non-uniqueness in such problems was made by Carter and myself<sup>\*</sup> using simple considerations of symmetry (see sketch). I should also like to record my personal impression that Garabedian's discussion is not rigorous. As this point has been explained<sup>†</sup> I shall not discuss it further here.



P. G. Saffman

With regard to Professor Birkhoff's first comment, the plane of the Hele-Shaw apparatus was horizontal in most of the experiments. The dimensionless parameter  $\Delta V / (\mu \cdot \gamma) g d^2$  is not relevant to these experiments, and in particular the deviation shown in Fig. 13 from the calculated shapes is not capable of being explained by gravity effects. Indeed, the same family of shapes is given by the analysis irrespective of whether the plane of the apparatus is vertical or horizontal although the

<sup>\*</sup>G. Birkhoff and D. Carter, Appendix D of Rep. LA-1927 of the Los Alamos Scientific Labs.

<sup>†</sup>G. Birkhoff and D. Carter, Arch. Ratl. Mech. Anal. 6:769-780 (1957).

velocity field is different. For example, in the case when the viscosity of the fluid inside the finger is negligible, the velocity of the fluid outside adjacent to the straight sides of the finger is at rest relative to the plates if the plane of the apparatus is horizontal, but not if it is vertical.

Systematic information on the stability of (12) against changes in the initial conditions or small variations in  $d$  is not available. It should be noted that  $\lambda$  is expected to be a function of the spacing  $d$ , as well as of  $Re$ .

In connection with the sketches shown by Professor Birkhoff, we should like to mention that we have found exact solutions in closed form\* giving asymmetric finger shapes, and there is a whole series of these shapes which go continuously from the symmetrical one shown in the middle sketch to the shape shown in the third sketch.

---

\*G. I. Taylor and P. G. Saffman, (to appear, 1959) Quart. J. Mech. Appl. Math.

\* \* \* \* \*

# UNSTEADY SUPERCAVITATING FLOWS

T. Y. Wu

*California Institute of Technology*

## INTRODUCTION

The problem of unsteady flows with wake formation of with separated free streamlines has recently stimulated some research interest. To fix ideas, consider the flow past a plate with its broad side facing the stream and oscillating about a fixed point as shown in Fig. 1. The flow separates from the plate at points A and A', and we can adopt the hypothesis that the free streamlines AB and A'B' bound a region, called the wake or the cavity, of constant pressure  $p_c$ , which may be different from the pressure at infinity,  $p_\infty$ . In the absence of the unsteady motion, the streamlines of constant pressure in this incompressible irrotational flow imply streamlines of constant velocity. However, the velocity on the free streamlines in an unsteady flow is no longer constant since the pressure depends also on the time-rate of change of the local velocity field, and furthermore, the unsteady motion of the body causes vorticity of varying strength to be shed from the body and carried downstream along the free boundaries. When the plate inclination decreases to a small angle with the undisturbed flow, the wake may disappear, the two vortex sheets then coalesce into a single sheet, and the flow becomes that considered in the unsteady airfoil theory. Thus the unsteady flow with wake formation differs from the airfoil theory essentially by the presence of two vortex sheets instead of one, and the problem is thereby considerably complicated.

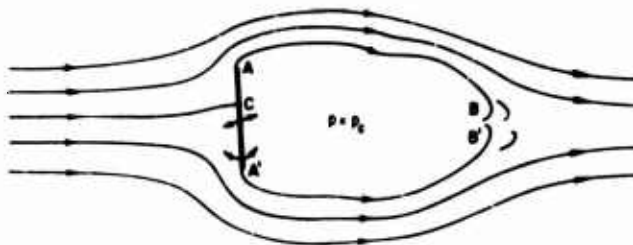


Fig. 1 - Flow past a plate

Aside from these conspicuous points, other new features may arise in the problem of the unsteady motion with wake formation; they may be basically different from the corresponding features characterizing the steady cavity flows and hence are pertinent to the general formulation of the problem. One of these features is the possibility for the volume of a finite or infinite wake to vary with time. For cavity flows of an incompressible liquid surrounding a vapor cavity, it is obvious that, when the

volume of the vapor cavity changes, the conservation of mass and conservation of volume of the entire flow become incompatible because of the difference in the liquid density and the vapor density. Consequently, any variation of the cavity volume must come from a source distribution whose net strength depends on the time rate of change of the cavity volume. A direct consequence of this source distribution in a two-dimensional flow of infinite extent is that it generates a pressure field which is logarithmically singular at infinite distances. Thus it is clear that the change in the cavity volume depends on the flow conditions imposed at infinity. More precisely, the cavity volume will change if the flow at infinity is of a source type, and it will not change if otherwise. Physically this can be seen as follows. Consider an obstacle moving through an incompressible liquid contained in a rigid container, large enough to make the wall effects negligible. After the cavity trailing behind the body is established, e.g., by removing the liquid through openings of the container and by allowing the obstacle to move fast enough, the container is then assumed to be perfectly rigid and free from leakage. Then, as the velocity of the obstacle changes in time, the cavity, whether still attached to or detached from the obstacle depending on the later state of the motion, certainly cannot change its volume. On the other hand, if the liquid has a free surface above the obstacle, then the cavity volume may change with the velocity of the motion. Therefore, in order to make the problem completely specified and the solution uniquely determinate, the condition of the velocity and pressure at infinity must also be given as functions of the time. For simplicity, we shall confine ourselves in this work to the case in which the flow at infinity is source-free, and hence the cavity volume will remain constant. However, it should be remarked here that the generalization of this argument to the case of separated flow in air would be open to question; for in this case of one-phase flow, the fluid inside the wake may actually consist of fluid particles originally outside due to the turbulent mixing in the unsteady motion. In any case, if the fluid particles outside a cavity essentially remain outside, then one may assume that the wake or cavity does not change in volume. This is perhaps a reasonable assumption when the unsteady part of the motion is only a small perturbation of a basic steady flow.

Another question about the unsteady wake flow is whether the wake pressure may vary with time. For a liquid flow with a vapor-gas cavity, the thermal process of changing phase on the free boundary and the process of any gas diffusion across the boundary may be regarded to be almost instantaneous with respect to the unsteady motion. Furthermore, the inertia of the vapor or gas inside the cavity has negligible effect on the outer flow because of the large difference in density of the two phases. Hence, for this case at least, the assumption of constant pressure in the cavity is as realistic as for the steady motion. On the other hand, the same assumption, when applied to a separated flow of a single-phase medium, such as air, seems somewhat questionable, because the unsteady motion of the body imparts acceleration to the fluid both outside and inside the cavity, and they respond in turn with the same inertia. However, the assumption of constant pressure in the wake may still be retained as the first approximation. The effect of gravity, which arises in the two-phase flows, is neglected here as usual.

In the following we shall first describe the particular case when the time and space variables can be separated. Next, the hydrodynamic motion shortly after an unsteady motion is introduced will be considered. The discussion will then be concentrated on the case in which the unsteady part of the motion is only a small perturbation of the basic steady flow. Two methods of approach will be described. For a blunt body with a wide wake, the small perturbation is made on the velocity potential; whereas, when the body-wake system is very thin, the acceleration potential is employed. In the former case, the acceleration potential of course also exists, but it is not divergence free. Consequently the value of using it is greatly reduced.

## FINITE CAVITIES WITH CONSTANT SHAPE

In 1949 Von Kármán (1) treated an accelerated flow normal to a flat plate which is held fixed in an inertial frame such that with given acceleration of the flow, the flow will separate from the plate to form a closed wake of constant shape behind the plate (Fig. 2). This incompressible, irrotational flow has a velocity potential of the form

$$\Phi(x, y, t) = U(t) \cdot \psi(x, y) \quad (1)$$

where  $x$  and  $y$  are the Cartesian coordinates in the flow plane, fixed with respect to the plate and with the  $x$ -axis parallel to the undisturbed uniform stream, and  $t$  is the time. The pressure is given by

$$p = -\rho \left( \frac{dU}{dt} \right) \psi - \frac{1}{2} U^2 (\text{grad } \psi)^2 - C(t). \quad (2)$$

Here,  $\psi$  is a harmonic function of  $x$  and  $y$ , and satisfies the following boundary conditions:

- (i) at infinity  $\psi_x = 1, \quad \psi_y = 0$
- (ii) on the plate  $\psi_x = 0$
- (iii) on the free boundary of the wake,  $p = p_0 = \text{const.}$

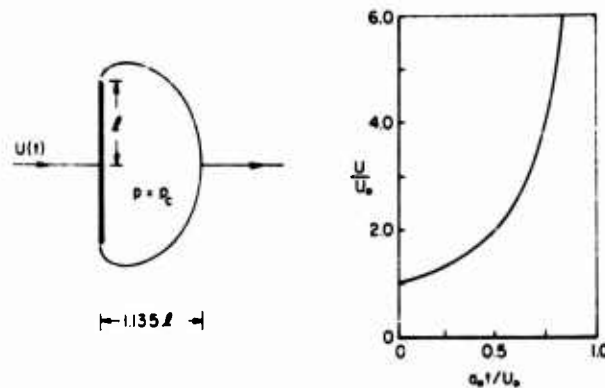


Fig. 2 - Accelerated flow past a fixed plate forming a closed wake of constant shape

The only boundary condition that involves  $t$  is (iii). Hence  $\psi$  will not depend on  $t$ , as assumed, when and only when the two time factors in Eq. (2) are proportional to each other; that is,

$$k = a U^2 = -\frac{1}{2} U^2 \quad (4)$$

where  $k$  is a real constant,  $a(t) = U^2(t)$ ,  $a_0 = a(0)$ , and the initial velocity of the flow at infinity  $U(0)$  is assumed to be positive but otherwise arbitrary. Then condition (iii) becomes

T. Y. Wu

$$(\text{grad } \psi)^2 + 2k\psi = 0 \quad \text{on the free boundary.} \quad (5)$$

The arbitrary constant  $k$  is determined such that the problem of  $\psi$  with conditions (3i), (3ii), and (5) possesses a solution. Now Eq. (4) has the general integral

$$U(t) = U_\infty \left( 1 - \frac{a_0 t}{U_\infty} \right)^{-1} \quad (6)$$

which characterizes the flow velocity at infinity. Von Kármán obtained the solution of  $\psi$  for a particular case in which the two branches of the free boundary of the wake meet and close the cavity at a stagnation point, and showed that a closed wake of constant shape is possible only when the "Froude number"

$$U^2/a_0 = U_\infty^2/a_0 \cdot \left[ \left( \frac{\pi}{2} + 1 \right)^{1/2} + \frac{1}{2} \arccos \left( \frac{\pi}{2} + 1 \right) \right]^{-1} = 0.599 \quad (7)$$

where  $a_0$  is the half-width of the plate. It can be seen that when the flow at infinity obeys (6) and (7), the velocity on the free boundary decreases from  $3.11 U$  at the separation point to zero at the rear. This is the only case for which a stagnation point can occur on a free boundary of constant pressure.

Writing  $w = iF/dz$ , with  $z = x + iy$  and  $F$  the complex potential, we see that  $F/w$ , and hence  $z$  as determined from  $dF/w$ , is evidently independent of  $t$  by virtue of (1). It then follows that the wake shape is constant in time. In fact the rear end of the wake is at a distance  $1.135 a_0$  from the plate (see Fig. 2). Furthermore, the pressure coefficient defined by

$$C_p = (p - p_\infty) \frac{1}{\frac{1}{2} \rho U^2}$$

is also independent of  $t$  by (2) and (4), and so is the acceleration coefficient

$$C_a = \frac{D}{Dt} \left( \text{grad } \psi \right) \frac{1}{\frac{1}{2} \rho U^2}.$$

This flow is thus also characterized by having  $C_p$  and  $C_a$  constant in time. It therefore follows that the drag coefficient has a fixed value which can be verified to be

$$C_D = \text{Drag} / U^2 = 10.48. \quad (8)$$

The magnitude  $m' = \text{drag}/\text{acceleration}$  may be called the cavity-induced mass; then by (7) and (8),

$$m' = U^2 \cdot C_D/a_0 = 6.26 a_0^2. \quad (9a)$$

If the flat plate had undergone an acceleration  $a$  normal to the flow without wake formation (a postulated Dirichlet flow), then the induced mass would be

$$m'_0 = \frac{1}{2} \rho a_0^2. \quad (9b)$$

Thus,

$$m'/m'_0 = 1.995. \quad (9c)$$

As pointed out by Tan (2), the law of motion (Eq. 6) for preserving the wake pattern (with Eq. 7 as a special case) is general and unique. The law is general in the



sense that it applies to any body shape with well-defined separation points, provided there exists a solution for  $\phi$ . The law is unique because no other fluid motion will produce such a preserved pattern of the wake flow. For the case of the flat plate, the class of flows characterized by (Eq. 6) has been investigated by Gilbarg (3). It was shown that only under (Eq. 7) the flow (which is that given by Von Kármán) has a stagnation point in the rear, whereas for other values of acceleration obtained from the solution of  $\phi$ , the cavity shapes all have cusps at the rear. Another type of the flows in this case was discovered to contain a doubly covered cavity subregion (3); these flows were considered as physically unrealistic. The case of polygonal obstacles was also treated by Gilbarg (3).

It should be remarked that the wake flow generated by a flat plate accelerating broadwise through the fluid which is otherwise at rest in an inertial frame is a problem different from the present one since the pressure equation in this case assumes a different form.

### SUDDEN ACCELERATION OF CAVITY FLOWS

It is of importance to note an essential difference between the unsteady flows with and without free boundaries. In the determination of the velocity field of the unsteady potential flows without a free boundary, the time appears only as a parameter since no knowledge about the time rate of change of the physical quantities is required in the problem. Only when the pressure field is calculated does the effect of unsteady motion explicitly appear (through the term  $\phi_t$  in the Bernoulli equation). On the other hand, when the wake is present, the flow will depend on its previous time history, because the explicit role of the time enters the problem through the boundary conditions on the free surface. However, when a basic steady wake flow is given a sudden acceleration, there will be no past history of any time-varying disturbances at the moment of the application of this sudden change. Therefore, the problem of finding the flow characteristics at the initial instant of the unsteady cavity flow is expected to be not any more complicated than the general unsteady flow without a cavity. For this reason we shall first consider the initial stage of the reaction of a cavity flow to the sudden acceleration of a rigid boundary in contact with it.

Let  $\phi(\vec{x})$  be the velocity potential of an established steady cavity flow past a stationary rigid body. Suppose now the body is given a sudden acceleration  $a$  at time  $t = 0$  in the direction opposite to the undisturbed flow, say. Then the velocity potential for small  $t > 0$  will assume the form (4)

$$\phi(\vec{x}, t) = \phi(\vec{x}) + at A(\vec{x}) + O(t^2). \quad (10)$$

The quantity  $A$  will be referred to as the "initial acceleration potential" for unit acceleration. Since  $\phi$  of the resulting flow and  $\phi$  of the basic steady flow are both harmonic functions, it follows that

$$\Delta A = 0. \quad (11)$$

From the momentum equation we see at once that the pressure will assume the form

$$P(\vec{x}, t) = p(\vec{x}) + p_1(\vec{x}) + O(t), \quad p_1 = -\rho a A(\vec{x}), \quad (12)$$

where  $p(\vec{x})$  described the pressure field of the original steady flow, and  $p_1$  is the pressure generated by the sudden acceleration.

From the boundary condition that the relative normal velocity on the rigid body must vanish,  $\Phi_{,n} = a t n_1$ , where  $\vec{n}$  is the unit normal vector on the body and  $n_1$  its component along the direction of undisturbed flow. Since the displacement of the rigid body is  $O(t^2)$ , this boundary condition can be applied on its undisturbed position. Hence, at  $t = 0^+$ , we have from (10),

$$A_{,n} = -n_1 \quad \text{on the rigid boundary.} \quad (13a)$$

By hypothesis, the pressure in the cavity remains constant. Hence, at  $t = 0^+$ , we have from (12)

$$A = 0 \quad \text{on the free boundary.} \quad (13b)$$

Furthermore, since this sudden acceleration of the body cannot affect the flow at infinity, we require that

$$A \rightarrow 0 \quad \text{as } |x| \rightarrow \infty \quad \text{in the flow.} \quad (13c)$$

The acceleration potential  $A$  is then uniquely determined by (11) and conditions (13a)-(13c). It may be noted that  $A$  depends on the basic steady flow through condition (13b), in which the location of the free boundary must be specified.

#### Sudden Acceleration of a Helmholtz Flow

A simple interesting case is the sudden acceleration of a flat plate in the Helmholtz flow, which has been treated recently by Gurevich (5). The steady Helmholtz flow past a plate set normal to the stream is given by the solution

$$z = \frac{4}{\pi} \left[ \frac{2w}{(1-w^2)^2} + \frac{w}{1-w^2} + \tanh^{-1} w \right] \quad (14)$$

in which the origin of  $z = x + iy$  is chosen at the plate center,  $\tau$  is the half-width of the plate, the region of the complex velocity  $w = u - iv$  is  $u \geq 0$  and  $w \leq 1$ , and  $w = 1$  at  $z = \tau$ . The parametric representation of the free boundary is obtained by letting  $w = \exp(-i\theta)$ , since we have there  $w = 1$ . The boundary condition of  $A$  on the plate is now

$$A_{,x} = -1 \quad \text{on } x = 0, \quad |y| \leq \tau. \quad (15)$$

The solution of (11) satisfying conditions (15), (13b), and (13c), with the free boundary determined from (14), is readily obtained. It is conveniently expressed as

$$\frac{dG}{dw} = \frac{8i}{(4-w^2)^3} \left[ \frac{(1-w^2)^2}{(1-w^2)^3} \log \frac{1+ix}{1-iw} - \frac{i}{1-w^2} + (\dots) \frac{iw(1-w^2)}{(1-w^2)^2} \right]$$

where  $G = A + iB$ ,  $B$  is the conjugate harmonic function of  $A$ , and the real part of gives the solution of the problem.

The additional drag due to the sudden acceleration of the plate can be shown to be

$$D_1 = \int_{-\tau}^{\tau} p_1 dy = \rho \int_{-\tau}^{\tau} A dy = 1.6896 \rho a^2 \tau^2. \quad (16)$$

## Unsteady Supercavitating Flows

In this case the initial value of the cavity-induced mass, defined by  $D_1 a$ , is

$$m' = D_1 a = 1.6396 \cdot a^2 \quad \text{at } t = 0^+. \quad (17)$$

The ratio of  $m'$  to the induced mass  $m'_0$  of (9b) is therefore

$$m' / m'_0 = 1.6896 \approx 0.5377 (7.13). \quad (18)$$

The result that this ratio is less than unity may be explained in that the cavitated side of the plate, being located in the region of a constant pressure, has no capacity of imparting kinetic energy to the exterior flow.

It may be recalled that the induced mass of an unsteady flow without a cavity or other free boundaries has always the same value whether the flow in the past has been steady or not. However, this is certainly not the case in the presence of free boundary for the reason previously given. Consequently, the present analysis is applicable only to the initial instant when the original steady cavity flow is subjected to a sudden change. Even though its application is limited, this theory nevertheless gives us some general idea about the reaction of a cavity flow to a sudden change of state.

## Basic Steady Flows with a Finite Cavity

Since the steady flow will be the basic reference on which the small unsteady perturbations are to be superimposed, the use of the simplest possible representation of the basic flow will obviously facilitate the analysis of the problem. There are several mathematical potential flow models proposed to give a good representation of the steady cavity flows, such as the Riabouchinsky image model, the reentrant jet model, and a third one which will be called here the dissipation wake model, as investigated independently by Joukowski, Roshko, and Eppler. The physical significance underlying these models and the accuracy of their results in estimating the flow quantities in comparison with the experimental observations have been discussed elsewhere (e.g., see Refs. 4 and 6 and the references cited therein).

For a simple example of the dissipation wake model, consider the case of a flat plate set normal to an otherwise uniform flow, with the physically realistic situation of cavity pressure  $p_c$  less than  $p_\infty$ . The flow in the physical space is represented by this model as shown in Fig. 3. According to this model, the flow separates from the plate at points A and A', and becomes parallel to the undisturbed flow at D and D', the

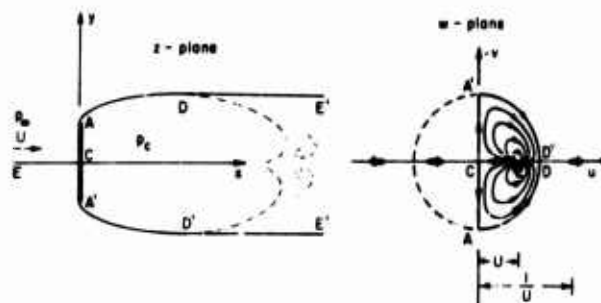


Fig. 3 - Example of flow according to the dissipation wake model

location of which can be determined from the theory. The wake pressure in between  $AB$  and  $A'D'$  takes the assigned value  $p_c$ , and the flow further downstream of  $B$  and  $D'$  is supposed to be dissipated in such a way that the pressure increases gradually from  $p_c$  back to  $p_\infty$  in a strip parallel to the flow at infinity. Outside the approximated wake the flow is assumed to be everywhere irrotational. Thus, from the complex potential

$$f(z) = \phi(x, y) + i\psi(x, y) \quad (19)$$

the complex velocity  $w$  can be derived as

$$w(z) = df/dz = u + iv = qe^{-i\alpha} \quad (20)$$

where  $q$  and  $\alpha$  are the magnitude and direction of the velocity. The pressure is given by

$$p = p_\infty - \frac{1}{2} \rho U^2 + \frac{1}{2} \rho q^2 \quad (21)$$

By hypothesis,  $p = p_c$  on  $AD$  and  $A'D'$ ; hence we have there  $q = q_c = 1$  by normalization. Then, in terms of  $p_c$  and  $q_c = 1$ ,

$$U = q_c(1 - \sigma)^{-1/2} = (1 - \sigma)^{-1/2}, \quad \sigma = (p_\infty - p_c)/\frac{1}{2} \rho U^2 \quad (22)$$

where  $\sigma$  is called the cavitation number, an important parameter of the flow. Since  $p_c = p_\infty$ , then  $\sigma = 0$  and  $U = 1$ . Also by hypothesis, along  $DE'$  and  $D'E'$ ,  $\sigma = 0$ , while  $q$  decreases from unity back to the free-stream value  $U$ .

The boundary condition of  $f(z)$  is that  $\psi = 0$  on  $ECADE'$  and on  $ECA'D'E'$ . In view of the qualitative shape of the streamlines  $\psi = \text{const.}$  near the point  $w = U$  in the  $w$ -plane, it is obvious that  $f$  must have there a singularity of the form  $(w - U)^{-1/2}$ . Hence the boundary condition on  $\psi$  can be satisfied exactly by using the method of images, first reflecting  $(w - U)^{-1/2}$  into the unit circle and then into the line  $u = 0$ , to give

$$f = B \left( \frac{1}{w - U} - \frac{1}{w + U} - \frac{U^{-2}}{w - U^{-1}} + \frac{U^{-2}}{w + U^{-1}} \right) \quad (23)$$

where  $B$  is a real constant. Hence

$$z = \int_0^w \frac{df}{dw} dw = \frac{2B}{U} \left[ \frac{(U^2 - U^{-2})w}{(w^2 - U^2)(w^2 - U^{-2})} - \frac{1}{U} \tanh^{-1} \frac{w}{U} + U \tanh^{-1}(Uw) \right]. \quad (24)$$

If  $a$  is the half-width of the plate, so that  $z = ia$  at  $w = -i$ , then  $B$  is determined by the relation

$$a = \frac{2B}{U} \left\{ \frac{1 - U^2}{1 + U^2} + \frac{1}{U} \left[ 2 - (1 + U^2) \tanh^{-1} U \right] \right\}. \quad (25)$$

The drag coefficient of this flow is readily obtained from the above solution

$$C_{D_0} = \frac{\text{Drag}}{\frac{1}{2} \rho U^2} = 2 \left\{ \frac{U^3}{1 + U^2} + \frac{U^2}{1 - U^2} \left[ 2 - (1 + U^2) \tanh^{-1} U \right] \right\}^{-1}. \quad (26)$$

For small values of  $\alpha$ , (26) may be expanded to yield

$$C_{D_n} = \frac{2\alpha}{4} \left[ 1 + \frac{\alpha^2}{6(4 - \alpha^2)} \right] \quad (26')$$

which provides a good approximation of (26) within 2 percent error for  $\alpha < 1$ . The above result (26) agrees with the result of Riabouchinsky's model or of the reentrant jet model within 0.5 percent for  $\alpha = 1$  (or  $0.707 \sqrt{U/q_c} = 1$ ). In some other known cases of inclined or curved (or polygonal) obstacles, the result yielded by using this model has been found also to be in good agreement with the experiments (6, 7).

Equations (24) and (25) are Roshko's solution (8), which here has been rederived conveniently by the image method. For the general case of the steady cavity flow past an inclined obstacle with small curvature, it is possible to generalize this method with linearization of the curvature. The same problem solved by using Riabouchinsky's model or the reentrant jet model would be considerably more complicated. Because of the simplicity of the mathematical details generally involved in the dissipation model relative to the other models, this model is preferred here for representing the basic flow.

#### The Effect of Cavity Size on Accelerated Cavity Flows

Consider now the problem of the sudden acceleration of a flat plate in a cavity flow characterized by the cavitation number  $\sigma$  as defined by (22). By using the dissipation model, the solution of the basic steady flow is given by Eqs. (23)-(25). When the plate is accelerated with acceleration  $a$ , opposite to the undisturbed flow, the initial acceleration potential  $\Lambda$  again obeys the boundary conditions (13b), (13c), and (15). By the conformal transformation

$$z = \frac{2B}{U} \frac{1 - w^2}{1 + w^2}, \quad w = i, \quad (27)$$

the entire flow region is mapped onto the upper half  $w$ -plane, with the plate lying on  $y = 0$ ,  $|x| < 1$  and the cavity boundary at  $y = 0$ ,  $|x| > 1$ . Again, with  $G = \Lambda + iB$ , condition (13b) may be written as

$$\operatorname{Re} \frac{dG}{dw} = \frac{\Lambda}{U} = 0 \quad \text{on } y = 0, \quad |x| > 1. \quad (28)$$

On the plate, by making use of condition (15), we have

$$\operatorname{Im} \frac{dG}{dw} = \operatorname{Im} \frac{dG}{dz} \frac{dz}{dw} = \frac{y}{U} \frac{\Lambda}{x} = -y \quad \text{on } y = 0, \quad |x| < 1 \quad (29a)$$

where the value of  $-y$  on the plate can be calculated from (23) and (27), to give

$$-y = \frac{2B}{U} \left( \frac{1 - w}{1 + w} \right) \left[ \sqrt{1 - w^2} - \sqrt{1 - \left( \frac{1 - w^2}{1 + w^2} \right)^2} \right] \quad \text{for } |x| < 1. \quad (29b)$$

The solution of this mixed boundary value problem, prescribed by (28) and (29), is

$$\frac{dG}{dw} = \frac{1}{\sqrt{1 - w^2}} \int_{-1}^1 \left( -\frac{y}{x} \right) \frac{\sqrt{1 - w^2}}{\sqrt{1 - \xi^2}} d\xi \quad (30)$$

with  $y$  given by (29b).

T. Y. Wu

The additional drag due to the sudden acceleration of the cavitated plate can be calculated from

$$D_1 = \int_{-1}^1 p_1 dy = -\sigma \int_{-1}^1 A \frac{dy}{dz} dz = -\sigma \int_{-1}^1 y(z) \frac{\sigma A}{4z^2} dz.$$

Substituting (29b) and (30) into the above expression and evaluating the integrals for small values of  $\epsilon$ , one obtains

$$D_1 = 1.6896 \cdot \sigma \epsilon^2 [1 + 0.269 \epsilon^2 + 0.075 \epsilon^4 + 0.049 \epsilon^6 + O(\epsilon^8)] \quad (31)$$

where

$$\epsilon = \frac{1 - U^2}{1 + U^2} = \frac{1 - \sigma}{2 + \sigma}.$$

In the practical range of interest, the cavitation number  $\sigma$  is generally not large, hence  $\epsilon$  is always appreciably less than unity. Consequently (31) may be used to cover a wide range of  $\sigma$ . For  $\sigma = 1$  in particular, (31) may be approximated by

$$D_1 = 1.6896 \cdot \sigma \epsilon^2 [1 + 0.067 \epsilon^2 (1 - \sigma) + O(\epsilon^4)]. \quad (32)$$

As  $\sigma \rightarrow 0$ , this result reduces to the previous solution, Eq. (16).

It is of interest to note that the effect of the cavitation number on the part of the drag due to sudden acceleration, denoted by  $D_1$ , starts with the term of  $O(\epsilon^2)$ ; hence  $D_1$  increases at a much slower rate than the steady part of the drag,  $D_0$  (see Eq. 26'), with increasing  $\sigma$ .

#### PERTURBATION OF UNSTEADY PLANE FLOWS PAST BLUNT BODIES WITH FINITE CAVITIES

Since the general case of the unsteady wake flow having a large time-varying part is virtually unsolved, we shall first consider the special case of the small unsteady perturbations superimposed on the basic steady flow past a blunt body. It is convenient to formulate this latter problem by dividing the flow into two parts, namely, (a) the basic steady flow, the problem of which is in general nonlinear, and (b) the small unsteady perturbations, the problem of determining them to be linearized. This method of approach has already been used in several recent works on this general subject. A scheme of small perturbations of the basic steady flows has been applied by Ablow and Hayes (9) to treat two unsteady free surface flows: the hollow vortex and the problem of the Borda mouthpiece. The problem of unsteady flow past curved obstacles with an infinite wake has been treated by Woods (10-12), applying small perturbations to the basic Helmholtz-Kirchhoff flow. Here this method will be generalized to the case of finite cavities.

Suppose for  $t < 0$  the rigid body in the cavity flow is given an unsteady motion of small amplitude. The small perturbation assumption then implies that for  $t > 0$  the complex potential, complex velocity, and the pressure of the resulting flow may be expressed as

$$\begin{aligned} F(z, t) &= F_0(z) + F_1(z, t), \\ W(z, t) &= dF/dz = w_0(z) + w_1(z, t) = Q e^{-i\omega t}, \\ P(x, y, t) &= P_0(x, y) + p_1(x, y, t) \end{aligned} \quad (33)$$

in which  $f_0(z)$ ,  $w_0(z)$ , and  $p_0(x, y)$  represent the basic steady flow, which, as was discussed in the section "Basic Steady Flows with a Finite Cavity," are assumed to be known here. The time-dependent perturbations  $f_1$ ,  $w_1$ , and  $p_1$  are assumed to have moduli much smaller than those of the basic flow, except possibly at some isolated points. Consequently, relations among the flow quantities are assumed to hold only to the first order in the small perturbations. Here, the space variable  $z$ , following the Eulerian description, is not perturbed. It is further noted that  $f_1(z, t)$  and  $w_1(z, t)$  are both analytic functions of  $z$  for every  $t$  and continuously differentiable in  $t$  if the motion of the rigid body has a continuous time derivative. The pressure equation is now

$$\frac{\partial p_1}{\partial t} + \frac{1}{2} Q^2 = C \quad (34)$$

where  $\gamma_1$  is the real part of  $f_1$ ,  $Q = |w|$ , and  $C$  may be taken as a constant.

To apply the boundary conditions, it is convenient to introduce the new variables:

$$\gamma_1 = \gamma_1 + i\gamma_2 = \log \frac{w_1}{w_0} = \log \frac{Q_1}{Q_0} + i(\Theta - \Theta_0). \quad (35a)$$

Hence, to the first-order terms,

$$\gamma_1 = -\log \left( 1 + \frac{Q - Q_0}{Q_0} \right) = -\frac{Q - Q_0}{Q_0}, \quad \Theta - \Theta_0 = \gamma_2 \quad (35b)$$

so that  $\gamma_1$  represents the percentage change in the velocity magnitude, and  $\gamma_2$  denotes the change in the flow angle, both with respect to the basic flow (see Fig. 4). Thus,  $\gamma_1$  is an analytic function of  $z$ , and hence of any analytic function of  $z$ , and  $\gamma_1$  is a small quantity of the first order. The equation for the pressure disturbance, from (21) and (34), is

$$\frac{\partial p_1}{\partial t} + \frac{1}{2} Q^2 = 0. \quad (36)$$

The boundary conditions of the perturbed flow may be stated as follows:

1. In general, the motion of the rigid boundary consists of a small translation and a small rotation. Let  $(x_0, y_0)$  be a point on the rigid boundary in the basic flow; then its perturbed position may be expressed as

$$\begin{aligned} X &= x_0 + \epsilon(t) + \eta(t)v_{0y} \\ Y &= y_0 + \epsilon(t) + \eta(t)x_{0y} \end{aligned} \quad (37)$$

where  $\epsilon$ ,  $\eta$ , and  $\eta$  are arbitrary functions of  $t$  with small magnitudes. From this expression, the perturbation velocities  $q_n$  and  $q_s$  of the flow normal and tangential to the rigid surface are readily obtained. Since the motion is infinitesimal, the value of  $(q_n, q_s)$  at  $(X, Y)$  may be approximated by their value at  $(x_0, y_0)$ . Doing so, we have, to the first order in  $q_n$  and  $q_s$ ,

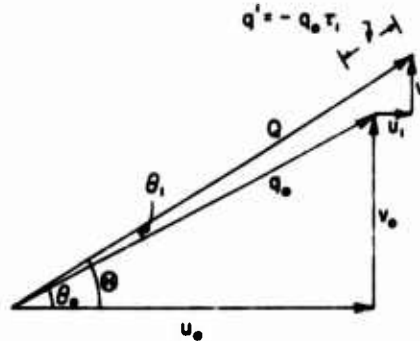


Fig. 4 - Unsteady flow expressed as a perturbation on the basic steady flow

$$\tau_1 = \tan^{-1} \frac{q_n}{q_0} = \frac{q_n}{q_0} \quad \text{on the unperturbed rigid surface} \quad (38)$$

where  $q_n$  is the component of the velocity  $(\dot{x} = v_0 + y_0 \dot{\tau}_1, \dot{y} = u_0 + x_0 \dot{\tau}_1)$  normal to the rigid surface. Hence  $\tau_1$  is known over the rigid boundary.

2. Over the free boundary, the pressure everywhere in the unsteady cavity wake is assumed to retain its value in the basic flow. Hence, to the first order of approximation,

$$p_1 = 0, \quad \text{over the unperturbed free boundary.} \quad (39)$$

Hence (33) becomes

$$\frac{d\tau_1}{dt} - q_0^2 \tau_1 = 0 \quad \text{over the free boundary.}$$

Let  $s$  be the arc length along a streamline; then from

$$Q = \frac{\partial \Phi}{\partial s} = \frac{\partial}{\partial s} (\phi_0 + \phi_1) = q_0 + \frac{d\tau_1}{ds}, \quad \text{or} \quad \frac{d\tau_1}{ds} = \frac{Q - q_0}{q_0} = -\tau_1$$

we can write the above equation as

$$\frac{d}{ds} (q_0^2 \tau_1) + \frac{d\tau_1}{dt} = 0 \quad \text{on the unperturbed free boundary.} \quad (40)$$

This equation may also be written as

$$\left( \frac{d}{dt} + q_0 \frac{d}{ds} \right) (q_0^2 \tau_1) = 0$$

which expresses the fact that, for any disturbance in  $\tau_1$  due to the unsteady motion of the rigid boundary, the quantity  $q_0^2 \tau_1$  is convected downstream along the free boundary with the basic flow, unchanged in magnitude. In particular, it can be asserted at once that for any  $t > 0$ ,  $\tau_1 = 0$  over the portion of the free boundary for  $s \geq s_c$ , where  $s_c$  is given by

$$t = \int_0^{s_c} ds / q_0.$$

Since  $q_0$  is a known function of  $s$ , the above condition reduces the problem to that of determining the value of  $\tau_1$  at the points of separation. The physical significance of  $q_0^2 \tau_1$  can be shown to be the vorticity variation due to the unsteady motion, and the above condition is actually the statement of the conservation of vorticity. It can also be seen that the disturbance in  $\tau_1$  will generate a surface wave along the free boundary; this surface wave is sustained by the velocity field of the flow in much the same way as the wavy water jet emitted from an oscillating garden hose.

3. At  $z = \infty$ , we further require that the perturbation does not change the flow direction and pressure at infinity; that is,

$$(a) \quad \tau_1 \rightarrow 0 \quad \text{as} \quad |z| \rightarrow \infty \quad (41a)$$

$$(b) \quad p_1 \rightarrow 0 \quad \text{as} \quad |z| \rightarrow \infty. \quad (41b)$$



Furthermore, by Kelvin's circulation theorem, the unsteady motion cannot, for any finite  $t$ , result in a net vortex at infinity; that is,

$$(c) \quad \text{Re} \oint_{\Gamma} w_1(z, t) dz = 0 \quad \text{for } t < \infty \quad (42)$$

where  $\Gamma$  is a closed contour with  $|z| \rightarrow \infty$ . It is not difficult to show that these conditions (a)-(c) imply that the perturbation flow at infinity has no net source or vortex and  $w_1 \rightarrow 0$  as  $|z| \rightarrow \infty$  at most be

$$w_1 = O(z^{-3/2}) \quad \text{as } |z| \rightarrow \infty. \quad (43)$$

The problem of determining  $w_1(z, t)$  with the above boundary conditions of a mixed type (i.e., with  $\phi_1$  given over a part of the boundary and  $\tau_1$  governed by (40) over the remaining part) can in principle be solved, sometimes conveniently with application of the Laplace transform. Such a detail, however, will be omitted here. Because many of the functions that appeared in the numerical calculation of the general problems are not yet tabulated, a few relatively simple cases have been carried out. Woods (10) treated an interesting example - the problem of a flat plate in the basic Helmholtz flow undergoing an impulsive motion and a harmonic motion. The result shown in Fig. 5 corresponds to the case when the velocity of the plate is increased impulsively from  $U$  to  $(21/20)U$  for the time period  $\tau = 2$  and is then reduced back to  $U$ .

#### UNSTEADY CAVITY FLOWS PAST THIN BODIES: ACCELERATION POTENTIAL

For the case of unsteady cavity flows past slender or thin bodies the method of using the acceleration potential is readily applicable, provided the body-cavity system remains slender in the flow motion. Thus the rigid body under consideration will be a thin body of small thickness and camber, held at a small angle to the flow and with the finite cavity extending downstream of the body. The unsteady motion may consist of a translation and a rotation, both of small amplitude. It is further assumed that (a) in the absence of the unsteady motion, a steady cavity of finite size has already been established, with cavitation number  $\sigma > 0$  and hence  $U$  and  $\eta_c$  related by (22), and that (b) the unsteady motion is again only a small perturbation of the basic flow. Because the body-cavity system is very thin, it is reasonable to expect that the flow is perturbed by the system only slightly from the uniform state, and the problem may therefore be linearized with respect to the uniform flow, taking the steady and unsteady part as a whole. Based on this approach, a few cases of interest have been treated by Parkin (13) and Wu (14).

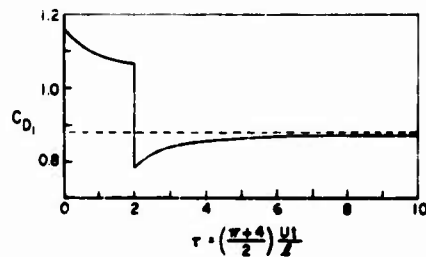


Fig. 5 - Result of impulsively increasing the velocity of a flat plate in the basic Helmholtz flow from  $U$  to  $(21/20)U$  for the time period  $\tau = 2$

#### The General Formulation

It is of interest to note that, unlike the thin airfoil theory, there are in this problem two characteristic velocities instead of one:  $U$ , the characteristic velocity near infinity, and  $U_c$ , the other characteristic velocity in the basic steady flow near the

cavity. Since the flow quantities near the body and cavity are of direct interest, it is convenient to take  $q_c$  as the reference for the entire velocity field.

The flow outside the body-cavity system is governed by

$$\frac{d\dot{q}}{dt} + (\dot{q} \cdot \nabla) \dot{q} = -\frac{1}{\rho_c} \nabla p, \quad (44)$$

When the motion is steady, this equation can be integrated to give (21), and hence the relation (22) between  $U$  and  $q_c$  follows. For the unsteady flows in general, (44) implies that the acceleration vector has a scalar potential  $\phi(x, y, t)$  such that

$$\dot{q} = \frac{d\dot{q}}{dt} + (\dot{q} \cdot \nabla) \dot{q} = q_c^2 \text{grad } \phi, \quad (45)$$

where

$$\phi = (\Gamma - p_c) / q_c^2. \quad (46)$$

In the above, the constant cavity pressure  $p_c$  and the constant velocity  $q_c$  on the cavity of the basic flow are chosen for convenience. For definiteness, we take the Cartesian coordinates  $(x, y)$  in the flow plane, with the planar body-cavity system lying over a certain region of the  $x$ -axis, and write the total velocity as

$$\dot{q} = q_c (1 + u, v) \quad (47)$$

so that  $(u, v)$  represents the nondimensional perturbation velocity.

Now we shall introduce the small perturbation assumption that the flow is only perturbed slightly from a uniform state  $(q_c, 0)$  so that  $|u|, |v| \ll 1$  almost everywhere in the flow and all quantities of second and higher order in  $(u, v)$  may be neglected. Then (45) is linearized to yield

$$\frac{\partial u}{\partial x} + \frac{1}{q_c} \frac{\partial u}{\partial t} + \frac{\partial v}{\partial y} = \frac{\partial v}{\partial y} + \frac{\partial v}{\partial t} + \frac{\partial v}{\partial x}. \quad (48)$$

Hence from the continuity equation  $\text{div } \dot{q} = 0$ , it follows that

$$\nabla^2 \phi = 0. \quad (49)$$

The above formulation can of course be extended to three-dimensional cavity flows past slender bodies as well. It may also be noted that while the acceleration potential  $\phi$  defined by (45) always exists (even in the flows past blunt bodies),  $\phi$  satisfies the Laplace equation (49), to the first-order terms, only in the planar or slender flows.\*

For two-dimensional problems, (49) implies the existence of a conjugate harmonic function  $\psi(x, y, t)$  such that

$$\frac{\partial \phi}{\partial x} = \frac{\partial \psi}{\partial y}, \quad \frac{\partial \phi}{\partial y} = -\frac{\partial \psi}{\partial x}. \quad (50)$$

\*For the case of cavity flows past blunt bodies as treated in the previous section, writing  $\dot{q} = \dot{q}_0(x, y) + \dot{q}_1(x, y, t)$  and assuming  $\dot{q}_1 = \dot{q}_0$ , one readily observes that  $\nabla^2 \phi = 4(u_0 \phi_{1x} + v_0 \phi_{1y})$  which is in general not zero; hence the merit of using  $\phi$  in that case is greatly reduced.

Hence, the complex acceleration potential  $G = u + iv$  must be an analytic function of  $z = x + iy$  at any time instant:

$$G(z, t) = u(x, y, t) + i v(x, y, t). \quad (51)$$

This potential  $G$  is related to the complex velocity  $w = u - iv$  by

$$\frac{dG}{dz} = \left( \frac{1}{q_c} \frac{\partial}{\partial t} + \frac{\partial}{\partial z} \right) w(z, t). \quad (52)$$

It may further be noted that although  $w(z, t)$  is still an analytic function of  $z$  for all  $t$ , it is in general not regular everywhere inside the flow, because vortex sheets may be shed continuously from the body due to its unsteady motion, whereas  $G(z, t)$ , with its real part corresponding to the pressure, will certainly be regular there. It is for this reason that the analysis is simpler with the direct use of  $G(z, t)$ .

The boundary conditions of this problem are as follows:

1. At upstream infinity, where the disturbances are required to die out,  $P = P_\infty$  and  $v = 0$ . Hence from (46), (22), and (48),

$$G = -\frac{1}{2(1-\sigma)} \quad \text{at } z \rightarrow -\infty. \quad (53)$$

2. The cavity pressure is assumed to remain constant,  $P = P_c$ . Hence by (46), we have on the cavity boundary

$$G = 0 \quad (54)$$

which, after linearization, may be applied on the portion of the  $x$ -axis that is the projection of the cavity boundary from above or from below. This condition is valid as long as the intermediate portion of the cavity boundary does not reattach to the solid surface. For simplicity, the body length is normalized to unity so that it occupies the region  $0 \leq x \leq 1$  and the cavity extends from certain known separation points to  $x = \sigma(t)$ ,  $\sigma > 1$  or  $\sigma < 1$ . The value  $\sigma(t)$  is determined as a part of the problem for given cavitation number  $\sigma$ , or vice versa.

3. The motion of the wetted rigid boundary may be described in general by

$$y = h(x, t) \quad (55)$$

with  $h = 1$  for all  $t$ , and the motion is limited to such a type that the wetted portion of the boundary always remains being wetted. Then the  $y$ -component of the flow at the rigid surface, in the linearized nondimensional form, is

$$v(x, 0, t) = \frac{1}{q_c} \frac{\partial h}{\partial t} + \frac{\partial h}{\partial x}, \quad 0 \leq x \leq 1. \quad (56)$$

Hence from (48) and (52), on  $0 \leq x \leq 1$ ,

$$\frac{\partial}{\partial x} (x, 0, t) = -\left( \frac{1}{q_c} \frac{\partial}{\partial t} + \frac{\partial}{\partial x} \right) v(x, 0, t) = -\left( \frac{1}{q_c} \frac{\partial}{\partial t} + \frac{\partial}{\partial x} \right)^2 h(x, t). \quad (57)$$

Here, again, both the above conditions may be applied on the projection of the wetted rigid surface on the  $x$ -axis. The integral of  $v$  in terms of  $\sigma$  may be obtained from (57) as

$$v(x, 0, t) = \int_{-\infty}^{\infty} H\left(0, t - \frac{|x|}{c}\right) d\tau, \quad H(x, y, t) = \frac{1}{\pi} \phi(x, y, t) \quad (58)$$

provided, of course, the integral converges. In this integral the condition that  $v = 0$  at  $x = \infty$  is used. It may be emphasized that the solution satisfying the boundary condition on acceleration (57) will also satisfy the boundary condition on velocity (56), provided (58) satisfies (56) also.

4. The condition that the cavity boundary and the wetted rigid surface must form at every instant a closed contour enclosing a constant cavity volume may be expressed by

$$\oint_C v(x, 0, t) dx = \text{Im} \oint_C w(z, t) dz = 0, \quad \text{for all } t \quad (59)$$

where  $C$  is a contour enclosing the boundary of the body and the cavity.

5. The Kutta condition for the lifting problem, fully cavitating or not, is that

$$G(z, t) \text{ is regular at the trailing edge for all } t. \quad (60)$$

This completes the formulation of the problem. With the cavitation number  $\kappa$  given and the motion of the wetted boundary prescribed, the cavity length  $\ell(t, \kappa)$  and the complex acceleration potential  $G(z, t, \kappa)$  satisfying these conditions can, at least in principle, be found.

#### Hydrodynamic Force and Moment

Since  $G(z, t, \kappa)$  is an analytic function of  $z$  for all  $t$ , regular everywhere outside the body-cavity system, the expansion of  $G$  near  $z = \infty$  must assume the form

$$G(z, t, \kappa) = a_0 + ib_0 + \frac{a_1 + ib_1}{z} + \frac{a_2 + ib_2}{z^2} + \dots \quad (61)$$

in which the coefficients  $a_n, b_n$  may depend on  $t$  and  $\kappa$ . From (53) it follows that

$$a_0 = -\frac{1}{2(1 + \kappa)}, \quad b_0 = 0. \quad (62)$$

These two conditions and condition (59) in general determine the cavity length  $\ell(t, \kappa)$  since they contain no other unknowns except  $\ell$  and  $\kappa$ .

It is of interest to analyze the singularities of the solution  $G(z, t, \kappa)$ . From the boundary conditions imposed it is not difficult to see that for  $\kappa > 0$  (and hence  $\ell(t, \kappa) < \infty$ )  $G(z, t, \kappa)$  may admit singularities only at the leading edge of the rigid body and at the rear end of the cavity. Near the cavity end  $z = \ell$ , we take a path  $\gamma_\ell$  encircling the point  $z = \ell$  from the lower to the upper side of the cavity boundary; then  $\arg(z - \ell)$  increases by  $2\pi$  along  $\gamma_\ell$ . Since on the lower surface,  $\kappa = 0$  and  $\ell < 0$  (it can be seen from (48) and (50) that near  $z = \ell$ ,  $u_x = -v_x$  and  $v$  is positive) and on the upper surface,  $\kappa = 0$  and  $\ell > 0$ , the image point in the  $G$ -plane of the point  $z$  on  $\gamma_\ell$  describes in the  $G$ -plane a path along which  $\arg G$  decreases by  $\pi$ , provided along this path  $\kappa \rightarrow 0$  (so that  $\ell \rightarrow \ell_c$ ). Then it follows from the theorem of conformal transformation that

# Unsteady Supercavitating Flows

$$G(z, t, \kappa) = K(t)(z - z_0)^{-1/2} [1 + O(z - z_0)^{1/2}] \quad \text{near } z = z_0(t) \quad (63)$$

where  $K$  is a real coefficient which may depend on  $t$ . One may interpret this result by saying that the detailed structure of the wake behind the cavity, often represented by an image of the rigid body or a reentrant jet in the nonlinear problems, is now collapsed to a point singularity in planar cavity flows. This singular behavior of the solution also facilitates the calculation of the drag force.

If a sharp leading edge in a lifting flow is wetted on both sides, then it is known in the airfoil theory that

$$G(z, t, \kappa) = C_1(t) z^{-1/2} [1 + O(z)^{1/2}] \quad \text{near } z = 0. \quad (64)$$

However, if the leading edge is cavitated on one side, then an argument similar to the above leads to the conclusion that

$$G(z, t, \kappa) = C_2(t) z^{-1/4} [1 + O(z)^{1/4}] \quad \text{near } z = 0. \quad (65)$$

The leading edge singularity is thus weaker than in the former case.

From the above solution it is readily found that the lift coefficient is given by (14)

$$C_L = \frac{\text{Lift}}{\left(\frac{1}{2} \rho U^2\right) (\text{chord})} = 4 \kappa (1 + \kappa) b_1(t, \kappa) \quad (66)$$

where  $b_1$  is defined in (61). Similarly, the moment coefficient about the leading edge, positive in the nose-up sense, is

$$C_M = \frac{\text{Moment}}{\left(\frac{1}{2} \rho U^2\right) (\text{chord})^2} = 4 \kappa (1 + \kappa) b_2(t, \kappa). \quad (67)$$

The calculation of the drag coefficient is more complicated. However, it can be shown (14) that for  $\kappa(t) > 1$ ,

$$C_D = 2\pi(1 + \kappa) K^2 - (\nu + \nu^*)_{\kappa=1} C_L + \frac{2(1 + \kappa)}{\eta_c} \oint_B \left[ v_t \int_0^x \mu(\tau, y, t) d\tau - \mu h_t \right] dx \quad (68)$$

where  $K$  is defined in (63) and  $B$  denotes the contour enclosing the rigid surface only. For  $\kappa < 1$ , the first term on the right side should be halved.

## Oscillating Hydrofoil at $\kappa = 0$

An interesting example of the theory, treated by Parkin (13), is that of a flat plate held at a small angle of attack  $\alpha_0$ , fully cavitated with an infinite cavity ( $\kappa = 0$ ), and performing a small plunging oscillation normal to the undisturbed flow. The hydrofoil motion is given by

$$y = h_0 c e^{j\omega t} \quad 0 \leq x \leq c \quad (69)$$

where  $c$  is the chord of the plate,  $h_0$  is the nondimensional amplitude,  $j = \sqrt{-1}$  is the imaginary unit for the time motion, and  $\omega/2\pi$  is the frequency. The solution obtained by Parkin gives

$$C_L = \frac{\pi}{2} \left\{ \alpha_0 + \left[ \frac{9}{16} k^2 - jkW(k) \right] h_0 e^{j\omega t} \right\} \quad (70)$$

where  $k = \omega c/U$  is the "reduced frequency" based on the full chord, and  $W(k)$  is a special function which is plotted in Fig. 6. The term  $\alpha_0/2$  gives the steady part of the lift as experienced by an inclined lamina in the Helmholtz flow. The second term with  $9k^2/16$ , being independent of the forward speed when the lift coefficient is converted to the lift force, represents the contribution of the apparent mass to the lift. The last term accounts for the influence of the cavity upon the lift. On the other hand, the unsteady lift on a flat plate airfoil without separation is

$$C_L = \frac{\pi}{2} \left\{ \alpha_0 + \left[ \frac{1}{4} k^2 - jkC\left(\frac{k}{2}\right) \right] h_0 e^{j\omega t} \right\} \quad (71)$$

where  $C(k/2)$  is the Theodorsen circulation function. A comparison of these results shows that the apparent mass of an inclined flat plate with an infinite cavity is only 9/16 the apparent mass of the plate in fully wetted flow. Furthermore, as plotted in Fig. 6,  $W(k)$  is quite different from  $C(k/2)$ . This is probably due to the wake structure and the presence of two vortex sheets instead of one single sheet as in the airfoil problem.

Rewrite (70) as

$$C_L = \frac{\pi}{2} \alpha_0 + 2\pi \left( \alpha_1 + j\alpha_2 \right) h_0 e^{j\omega t} \quad (72)$$

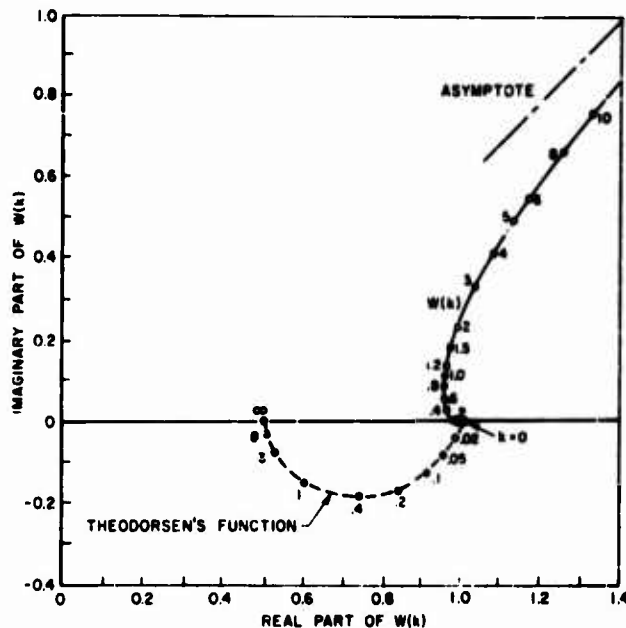


Fig. 6 - Special function in Eq. (70)

# Unsteady Supercavitating Flows

with

$$\gamma_1 = \frac{\pi}{4} \left[ \frac{\eta}{16} k^2 + k \operatorname{Im} W(k) \right], \quad \gamma_2 = -\frac{\pi}{4} k \operatorname{Re} W(k).$$

The quantity  $\gamma_1$  is usually called the "stiffness derivative," and  $\gamma_2$  the "damping derivative." In flutter problems it is the sign of  $\gamma_2$  in a certain degree of freedom which determines whether the motion in that degree of freedom is damped or not by the hydrodynamic forces. The damping derivative  $\gamma_2$  is plotted in Fig. 7, with its value in the fully wetted flow shown for comparison. The same problem with more general locations of the upper separation point has been treated by Woods (11) by using the method described in the section "Perturbation of Unsteady Plane Flows Past Blunt Bodies with Finite Cavities;" his result for the present case agrees exactly with this theory. A comparison with the case of the fully wetted flow shows that there is a loss of damping for plunging oscillation in the cavity flow. In fact, as

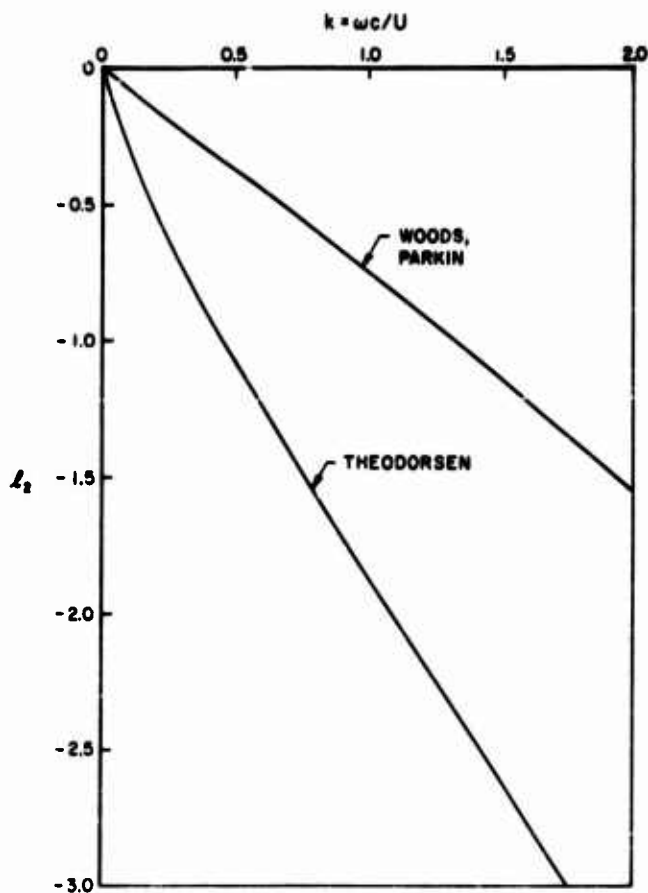


Fig. 7 - Plot (top curve) of the damping derivative  $\gamma_2$  of Eq. (72), compared with the corresponding quantity for flow without separation.

shown by Woods, when the flow is allowed to separate from different locations on the upper surface of the plate, in almost all frequency ranges there is a loss of damping effect for both plunging and pitching oscillations, and this loss increases with increasing extent of flow separation. It was also predicted by Woods that a fully stalled airfoil pivoted at its midchord would tend to flutter in the frequency range  $0.4 < k < 1.6$  in our notation.

#### Supercavitating Slender Wedge in Plunging Oscillation

Another example is the problem of a supercavitating slender wedge of half vertex angle  $\gamma$  performing a vertical plunging oscillation. The instantaneous position of the wedge surface is given by

$$h(x, t) = h_0 e^{i\omega t} \quad \text{on } y = 0, \quad 0 \leq x \leq 1. \quad (73)$$

It has been found (14) that the lift and moment experienced by the cavitated oscillating wedge have the same expression as those experienced by an oscillating airfoil, except that the reduced frequency for  $\gamma = 0$  is  $k = c/\eta_c$  instead of  $c/U$  as for the fully wetted flow. The drag exerted on the cavitated wedge due to the cavity formation, however, is now

$$C_D = \frac{8\gamma^2}{\pi} (1 + \gamma) \frac{1}{1 - \gamma} + 2(1 + \gamma) h_0^2 k^2 C^2\left(\frac{k}{2}\right) e^{2j\omega t} \quad (74)$$

where  $k = c/\eta_c$ ,  $C(k/2)$  is the Theodorsen function, and  $\gamma$  is cavity length given by the relation

$$\frac{\gamma}{2(1 + \gamma)} = \frac{1}{2} \left( \frac{2}{1 - \gamma} + \log \frac{1 - \gamma}{1 + \gamma} \right). \quad (75)$$

The first term in (74) gives the drag coefficient of the basic cavity flow over the wedge, while the last term expresses the contribution of the unsteady motion.

#### REFERENCES

1. Von Kármán, T., *Annali di Matematica Pura ed Applicata*, Series 4, 29:247-249 (1949); reprinted in "Collected Works of Theodore Von Kármán," London: Butterworths Scientific Publications. Vol. 4, pp. 396-398, 1956
2. Tan, H.S., *Quart. Appl. Math.* 12:78-80 (1954)
3. Gilbarg, D., *Z. ang. Math. Phys.* 3:34-42 (1952)
4. Birkhoff, G., and Zarantonello, E.H., "Jets, Wakes and Cavities," New York: Academic Press, 1957
5. Gurevich, M.I., *Prikl. mat. mekh.* 16:116-118 (1952)
6. Wu, T.Y., *J. Math. Phys.* 35:236-265 (1956)
7. Parkin, B.R., *J. Ship Research* 1:34-56, 1958



8. Roshko, A., NACA Technical Note 3168, 1954
9. Ablow, C.M. and Hayes, W.D., "Perturbation of Free Surface Flows," Tech. Rept. 1, Applied Mathematics, Brown University, 1951
10. Woods, L.C., Proc. Roy. Soc. (London) A229:152-180 (1955)
11. Woods, L.C., Proc. Roy. Soc. (London) A239:328-337 (1957)
12. Woods, L.C., Proc. Roy. Soc. (London) A229:235-250 (1955)
13. Parkin, B.R., "Fully Cavitating Hydrofoils in Nonsteady Motion," Engineering Division Report 85-2, California Institute of Technology, 1957
14. Wu, T.Y., "A Linearized Theory for Nonsteady Cavity Flows," Engineering Division Report 85-6, California Institute of Technology, 1957

\* \* \* \* \*

#### DISCUSSION

B. R. Parkin (California Institute of Technology)

I would like to put a question to Professor Wu concerning his first topic, that is, his elucidation of the theory of Von Kármán. As Professor Wu has mentioned, the coordinate system is chosen in such a way that, being fixed to the body, it is not an inertial frame of reference, and thus it introduces a pressure gradient at infinity, noticed throughout the flow. I would appreciate Professor Wu's indicating the bearing of this pressure gradient at infinity on the values of the coefficients which he quoted from Von Kármán's work. Would these coefficients and the cavity shape be any different from those which would obtain if the liquid at infinity had been at rest?

P. Kaplan (Stevens Institute of Technology)

My comment is concerned with the application of Wu's results, and results to follow, in the general field of naval hydrodynamics. In particular, the requirements of supercavitating devices, which are being emphasized, are such that they have thin sections, combined with great sensitivity of the hydrodynamic forces to the camber. This makes the problem of hydroelasticity appear important for high-speed operation. The forces on the oscillating supercavitating foil are also essential for the study of flutter, and I am happy that Dr. Wu has mentioned the applicability of some of his results to this problem.

T. Y. Wu

In reply to Dr. Parkin's question, I wish to say that the wake flow generated by a flat plate accelerating broadwise through the fluid, which is otherwise at rest in an

inertial frame, is a problem different from that treated by Kármán. In this case one may take a coordinate system fixed with respect to the fluid at infinity so that at infinity the velocity is zero and the pressure is equal to  $p_\infty$ , a constant. Then the plate will be moving with acceleration  $a$ . If the shape of the free boundary may still be constant in time, then when the condition of constant pressure is applied on the moving free boundary, one has a different expression for the pressure equation.

Next, I wish to give a uniqueness proof with respect to the leading-edge singularity,  $z^{-3/4}$  or  $z^{-1/4}$ . The first time I looked at the 3/4-power singularity I thought this singularity may be ruled out by the argument that the energy is not integrable at the leading edge. Though this statement is true, I was not too happy with this answer. Then I looked for other physical requirements and found a satisfactory one. I imposed another condition, namely that the pressure outside of the solid body and the cavity wake must not be less than the pressure in the cavity. That is,

$$u = R|w|^2 - \frac{1}{2} C_p \geq 0 \quad \text{in the flow field.}$$

Suppose that the solution of  $w$  has, in the neighborhood of the leading edge, the expansion

$$w = iAz^{-3/4} + iBz^{-1/4} + O(z^{1/4})$$

where  $A, B$  are two real coefficients so that  $u = 0$  on the cavity. Then, with  $z = re^{i\theta}$ , we have near  $r = 0$ ,

$$u = Ar^{-3/4} \sin(3\theta/4) + Br^{-1/4} \sin(\theta/4) + O(r^{1/4}).$$

From this result we notice that the term  $\sin(3\theta/4)$  will change sign, whereas the term  $\sin(\theta/4)$  will not, as  $\theta$  changes from 0 to  $2\pi$ . Since the first term violates this physical condition on the minimum pressure, we must therefore have  $A = 0$ .

My own viewpoint with respect to the existence of the flow source is as follows. Suppose we have a two-dimensional cylinder and let it pulsate with its radius  $R$  as a function of  $t$  in a uniform stream of velocity  $U$ ; then, the velocity potential is

$$\phi(r, \theta, t) = U(r + R^2/r) \cos \theta + RR' \log r,$$

so that we have now a source of strength  $2RR'$  which depends on the rate of change of the cross section of the cylinder. For the problem of unsteady cavity flows, however, it seems that the physical requirement must be imposed that the pressure be finite at infinity. Otherwise, we would require an infinite amount of energy, and hence an infinite time, to create such a flow. Thus the question arises: Why don't we let the cavity volume grow and have an infinite pressure at infinity? At the first sight it seems to me that the affirmative is not the case. One flow model which avoids the flow source at infinity is that, when the volume of the cavity near the body changes, there will be a wake which becomes thinner or fatter in the opposite sense.

In regard to the philosophical question about the physical background of these flow models and their agreement with experiments, I have the following point of view: We realize that all the wake flows are the end product of the real fluid effect. In order to solve the problem in an easy way, however, we want to keep the potential problem as a possible approximation by making some mathematical assumptions, which we call mathematical models. If any mathematical model gives a good approximation of the flow quantities near the solid body, so that we can predict very accurately

#### Unsteady Supercavitating Flows

the total hydrodynamic forces on the body, then, as far as I am concerned, the model should be quite acceptable. However, we should not expect that the simple model is also capable of providing a good description of the complicated wake flow downstream. The problem of the wake flow in the wake is entirely different from those considered here and I believe one cannot obtain a good result without considering the viscous effect, vortex shedding, the turbulent mixing, and so forth.

Several experimental results have been available for a few special cases of the cavity flow past a flat plate inclined at a small angle. These results give substantial support to these mathematical models. With respect to the present linearized model, there are certain features which are different from the nonlinear cases. Here, again, the validity of this model depends on its agreement with future experiments.

\* \* \* \* \*

# THE INFLUENCE OF DEPTH OF SUBMERSION, ASPECT RATIO, AND THICKNESS ON SUPERCAVITATING HYDROFOILS OPERATING AT ZERO CAVITATION NUMBER

Virgil E. Johnson, Jr.  
*Langley Research Center  
National Aeronautics and Space Administration*

The linearized theory for infinite depth is applied to design two new low-drag supercavitating hydrofoils. The linearized solution for the characteristics of supercavitating hydrofoils operating at zero cavitation number at finite depth is also accomplished. The effects of camber determined from the linear theory are combined with the exact nonlinear flat-plate solution to produce nonlinear expressions for the characteristics of arbitrary sections. The resulting theoretical expressions are corrected for aspect ratio by conventional aeronautical methods. Agreement between theory and experiment is found to be good for the lift coefficient, drag coefficient, center of pressure, and location of the upper cavity streamline. The theory is used to compare the maximum lift/drag ratios obtainable from various cambered sections of equal strength. At an aspect ratio of 3 and a depth of 1 chord, a five-term section with  $C_{L,d} = 0.1$  has a maximum L/D of 10.5. However, the maximum L/D is not greatly dependent on the type of camber since a circular arc section of  $C_{L,d} = 0.1$  has a maximum L/D of about 9.5. It is concluded from the analysis that for operation at a depth greater than about 1 chord, a lift/drag ratio of about 10 is close to the maximum value that can ever be attained on a single hydrofoil supported with one strut and operating at zero cavitation number.

## INTRODUCTION

One of the missions of the Hydrodynamics Division of the National Aeronautics and Space Administration is to find means of improving the takeoff and landing performance of seaplanes, particularly in rough water. The desirability of using an auxiliary lifting surface such as a hydro-ski for reducing seaplane hull loads and improving rough water performance has been established. It is possible that hydrofoils with higher aspect ratio and thus higher efficiencies could be superior to the hydro-ski; however, only the low-aspect-ratio planing hydro-ski has so far been successfully applied as landing gear to modern high-speed aircraft. This is because the conventional hydrofoil presents problems not experienced by a hydro-ski.

As a hydrofoil nears the free surface (during a takeoff run) the low pressure side of the foil almost always becomes ventilated from the atmosphere. This phenomenon results in a severe and usually abrupt loss in lift and reduction in the lift/drag ratio. For conventional airfoil sections the loss in lift may exceed 75 percent. The speed at the inception of ventilation depends on the angle of attack and depth of submersion; but, except for very small angles of attack and relatively low takeoff speeds, the inception speed is usually well below the takeoff speed of the aircraft.

Even if the ventilation problem is overcome by using small angles of attack and incorporating "fences" or other devices for suppressing ventilation, the onset of cavitation presents a second deterrent to the use of conventional hydrofoils at high speeds. The loss in lift accompanying cavitation of conventional airfoil sections is not abrupt, but the ultimate reduction in lift and lift/drag ratio is comparable to that of ventilated flow. Even thin airfoil sections of small design lift coefficient enter this cavitating regime of poor lift/drag ratios at speeds in excess of about 80 knots.

Since the takeoff speed of supersonic aircraft may be in the range of 150 to 200 knots, lifting surfaces with cavitating or ventilating characteristics superior to those of conventional airfoil sections are desirable. Fortunately the theoretical work of Tulin and Burkart (1) has shown that superior configurations do exist, and they have selected a cambered configuration for operation in cavitating or ventilated flow which has two-dimensional lift/drag ratios at its design angle of attack and zero cavitation number about six times that of a flat plate. If such a cambered foil can be induced to ventilate at very low speeds, while the aircraft hull still supports most of the load, a stable and efficient takeoff run may be possible. This new philosophy is to design for operation with a cavity; whereas in the past the philosophy has been to try to avoid cavitation and ventilation. The situation is very definitely one of, "If you can't beat it, join it."

The present paper is concerned with some theoretical and experimental work on supercavitating hydrofoils which has been carried out during the last few years at the Langley Research Center, Langley Field, Virginia, of the National Aeronautics and Space Administration. A large percentage of the information contained in this paper has been previously published as Refs. 2 and 3. However, since these reports have only recently been declassified, the principal results contained in them are reviewed, although in some places details are omitted. The purpose of the investigation has been to determine the characteristics of practical supercavitating hydrofoils; therefore the effects of aspect ratio, depth of submersion, and hydrofoil thickness are subjects of particular interest. The theoretical portion makes frequent use of the linearized theory for cavitating flows developed in Ref. 1 and extends this theory to include the problem of hydrofoils which operate in a ventilated condition near the free surface. Conventional aeronautical corrections for finite span are employed. The theoretical results obtained are compared with a variety of experimental data obtained in the towing tanks of the NASA. These tanks include the new high-speed facility which is presently capable of speeds up to 175 fps and which will soon be capable of speeds nearing 260 fps.

## SYMBOLS

- A aspect ratio  
 $A_n, A_n$  coefficients of sine-series expansion of vorticity distribution on equivalent airfoil section, that is,

$$\gamma(x) = 2V \left( A_0 \cot \frac{\theta}{2} + A_1 \sin \theta + A_2 \sin 2\theta + \cdots + A_n \sin n\theta \right)$$

# Supercavitating Hydrofoils Operating at Zero Cavitation Number

where

$$A_n = \frac{2}{\pi} \int_0^\pi \frac{dy}{dx} \cos n\alpha \, d\alpha$$

$$A_0 = -\frac{1}{\pi} \int_0^\pi \frac{dy}{dx} \, d\alpha + \frac{1}{2} + A'_0$$

$A_n, B_n, A'_0, B'_0$  coefficients of sine-series expansion of vorticity distribution on hydrofoil section

$\alpha$  distance from equivalent airfoil leading edge to center of pressure in chords

$B_n, B'_0$  coefficients of cosine series defining location of image vortex in airfoil plane using  $Z = z + \bar{z}$  transformation

$b$  parameter defining location of spray at infinity in  $z$  plane (see Ref. 4)

$C_D$  total drag coefficient,  $D/\rho S$

$C_f$  skin-friction drag coefficient,  $D_f/\rho S$

$C_L$  total-lift coefficient,  $L/\rho S$

$\bar{C}_L$  total-lift coefficient of equivalent airfoil section,  $\bar{L}/\bar{\rho} \bar{S}$

$C_{L,1}$  lift coefficient exclusive of crossflow,  $L_1/\rho S$

$C_{L,c}$  crossflow lift coefficient,  $L_c/\rho S$

$C_m$  pitching-moment coefficient (about the leading edge),  $M/\rho S c$

$\bar{C}_m$  pitching-moment coefficient of equivalent airfoil section (about the leading edge),  $\bar{M}/\bar{\rho} \bar{S} \bar{c}$

$\bar{C}_{m,3}$  third-moment coefficient of equivalent airfoil section (see Ref. 1),  $\bar{M}_3/\bar{\rho} \bar{S} \bar{c}^3$

$C_N$  resultant-force coefficient on arbitrary section,  $F/\rho S$

$C_{N,f}$  resultant-force coefficient of flat plate,  $F/\rho S$

$C_n, C_0$  coefficients of sine-series expansion of vorticity distribution on equivalent airfoil section at arbitrary depth using  $Z = z + \bar{z}$  transformation

$C_p$  pressure coefficient,  $(p - p_\infty)/\rho$

$c$  chord

$D$  total drag force

$D_f$  drag force due to skin friction

$d$  leading edge depth of submersion

- E Jones' edge correction, ratio of semiperimeter to span (see Ref. 5)
- F resultant force
- f distance from hydrofoil leading edge to stagnation point in chords
- g acceleration due to gravity
- L total lift force
- $L_c$  lift force due to crossflow
- $L_1$  lift force exclusive of crossflow,  $L - L_c$
- $\bar{r}$  perpendicular distance from hydrofoil reference line to upper cavity streamline
- M moment about leading edge
- $\bar{M}_3$  third moment about leading edge,  $2 \int_0^c p(x) x^3 dx$
- m  $C_L$
- p pressure, lb/sq ft
- $p_c$  pressure within cavity, lb/sq ft
- $p_o$  pressure at mean depth of hydrofoil, lb/sq ft
- $p_v$  fluid vapor pressure, lb/sq ft
- q free-stream dynamic pressure,  $\frac{1}{2} \rho V^2$
- R cavity ordinate - aspect ratio correction factor
- S area, sq ft
- s span, ft
- u perturbation velocity in X-direction
- V speed of advance, fps
- v perturbation velocity in Y-direction
- X, Y coordinate axes
- x distance from leading edge along X-axis
- $x_{c.p.}$  distance from leading edge to center of pressure of hydrofoil
- $\alpha$  geometric angle of attack measured from reference line radians unless otherwise specified
- $\alpha_c$  angle-of-attack increase due to camber, radians unless otherwise specified
- $\alpha_1$  induced angle of attack, radians unless otherwise specified

# Supercavitating Hydrofoils Operating at Zero Cavitation Number

- $\alpha_c$  angle between hydrofoil chord line and reference line, positive when chord line is below the reference line, radians unless otherwise specified
- $\alpha'$  angle of attack measured from hydrofoil chord line,  $\alpha' = \alpha - \alpha_c$ , radians unless otherwise specified
- $\Gamma$  circulation, strength of single vortex
- $\theta$  central angle subtending chord of circular-arc hydrofoil
- $\delta$  spray thickness at infinite distance downstream
- $\epsilon$  deviation of resultant force vector from normal to hydrofoil reference line
- $z$  complex airfoil plane,  $z = x + iy$  plane
- $\eta$  ordinate in the  $z$  plane
- $\tau$  parameter defining distance along airfoil chord,  $x = c/2 (1 - \cos \tau)$
- $\rho$  mass density, lb-sec<sup>2</sup>/ft<sup>4</sup>
- $\tau$  abscissa in the  $z$  plane
- $\sigma$  cavitation number,  $(p_0 - p_c)/\rho$
- $\sigma_i$  cavitation number at inception
- $\gamma$  correction factor for variation from elliptical plan form
- $\psi$  angle between spray and horizontal
- $\omega$  vorticity
- $f(\cdot)$  indicates "function of," for example,  $C_{N,f(\cdot)}$   $C_{N,f(\cdot + \cdot)}$  also  $(\cdot)$  sometimes used
- $Z = X + iY$
- $\phi = \tan^{-1} \frac{C_D}{C_L} = \phi + i$

## Subscripts

- $e$  effective
- $0$  zero depth of submersion
- $t$  total
- $\infty$  infinite depth of submersion
- c.p. center of pressure
- $c$  due to camber
- $A_0$  due to  $A_0$

Barred symbols refer to equivalent airfoil section and unbarred symbols refer to the supercavitating hydrofoil section.



## DESCRIPTION OF SUPERCAVITATING FLOW

The parameter defining cavity flow is  $\sigma = (p_o - p_c) / q$  where  $p_o$  is the pressure at the mean depth,  $p_c$  is the pressure within the cavity, and  $q$  is the dynamic pressure. The magnitude of  $\sigma$  for the condition at which cavitation is incipient is defined by the particular value  $\sigma_i$ . If  $\sigma$  is reduced below  $\sigma_i$ , cavitation becomes more severe; that is, the cavitation zone extends over a larger area. When a hydrofoil operates at sufficiently low values of  $\sigma$ , the cavity formed may completely enclose the upper or suction surface and extend several chords downstream, as shown in Fig. 1a. The re-entrant flow formed at the rear of the cavity is caused by the necessity for constant pressure along the cavity streamline. When the cavity is sufficiently long so that the re-entrant flow is dissipated without impinging on the body creating the cavity as shown in Fig. 1a, the flow is defined as supercavitating. Theoretically, if the cavitation parameter is reduced to zero the cavity formed will extend to infinity.

Low values of cavitation number, and thus supercavitating flow, may be obtained by increasing either velocity or cavity pressure or both. At a constant depth and water temperature,  $\sigma$  for normal vapor-filled cavities is dependent only on the velocity, since  $p_o - p_c$  is then  $p_o - p_v$  and is constant.

If part or all of the boundary layer of a configuration is separated, the eddying fluid in the separated region can be replaced by a continuous flow of lighter fluid such as air (6,7). Regulation of the amount of air supplied will control the cavity pressure and thus the length of the cavity formed. If the quantity of air supplied is very large, the cavity pressure will approach the ambient pressure  $p_o$  and a very long cavity will result even at low stream velocities.

The ventilation of surface-piercing hydrofoils is therefore a supercavitating flow due to large quantities of air supplied from the atmosphere to separated flow on the suction surface of the foil. Supercavitating flow as a result of ventilation also occurs when a non-surface-piercing hydrofoil of moderate aspect-ratio operates near the free surface (Fig. 1b). As pointed out in Ref. 8, air is entrained in the trailing vortices and drawn to the suction side of the foil, causing a long trailing cavity to completely enclose the foil upper surface and extend far downstream. The ventilated-type cavity described in Ref. 8 differs in shape from those formed in deeply submerged flow because of the proximity of the free surface. It is similar to planing, with the spray forming the upper surface of the cavity. Since the cavity pressure is

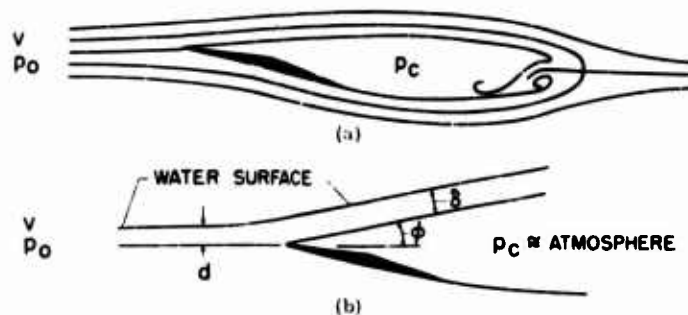


Fig. 1 - Definition sketch: (a) supercavitating flow at finite cavitation number ( $\sigma > 0$ ), (b) supercavitating or ventilated flow near the free surface ( $\sigma > 0$ )

## Supercavitating Hydrofoils Operating at Zero Cavitation Number

approximately the same as the ambient pressure (at small depths of submersion), the cavitation number for this type flow is nearly zero. The present paper is concerned with the theoretical predictions of the characteristics of practical hydrofoils operating in the ventilated or zero-cavitation-number regime.

### FORCES AND MOMENTS

#### Two-Dimensional Theory

**Flat Plate, Infinite Depth**—The characteristics of a two-dimensional inclined flat plate in an infinite fluid, operating at zero cavitation number, have been obtained by Kirchhoff and Rayleigh (9). The resultant force on the plate is given by the well-known equation

$$C_{N,f} = \frac{2\pi \sin^2 \alpha}{4 + \pi \sin^2 \alpha} \quad (1)$$

**Flat Plate, Finite Depth**—Similar work was performed by A. E. Green (4,10) to include the effect of the free surface (but neglecting gravity). The solution is necessarily obtained in terms of spray thickness  $b$  rather than the more useful depth of submersion and is given as two parametric equations in terms of the parameter  $\theta$ :

$$C_L = C_{N,f} \cos \alpha + \frac{2(b - \frac{1}{2}b^2 - \frac{1}{2}) \sin \alpha \cos \alpha}{D} = m, \quad (2a)$$

$$D = b - \frac{\cos^2 \theta}{D} \quad (2b)$$

where

$$D = (b - \frac{1}{2}b^2 - \frac{1}{2}) \sin \alpha + \frac{1}{\pi} \left[ 2 \cos \alpha + (b \cos \alpha - 1) \ln \frac{b-1}{b+1} \right].$$

This result is plotted as the variation of  $m$  with  $b/c$  for various angles of attack in Fig. 2.

Although gravity is neglected in Green's solution, the forces on the plate can still be obtained in terms of  $b/c$  from Eq. (2) if the Froude number  $v^2/gc$  is large. On the other hand, the relationship between the spray thickness and the actual leading edge depth of submersion cannot be determined from Green's two-dimensional analysis. However, in the practical case, at small angles of attack the depth of submersion and spray thickness may be taken as identical even at relatively shallow depths. From Fig. 2 it may be seen that for depths greater than about 1 chord the depth and spray thickness may be considerably different without affecting the value of  $m$ . Thus at depths greater than about 1 chord the assumption that  $b/c = d/c$  is adequate in determining the forces. However at large angles of attack and shallow depths a better relationship is needed between  $b/c$  and  $d/c$  if adequate accuracy is to be maintained. No theoretical solution for the relationship has been obtained. However, to give an idea of the relationship between these variables, experimentally obtained lines of constant  $b/c$  for an aspect ratio-1 flat plate are shown in Fig. 2. Experience has shown that these lines are sufficiently accurate for determining the value of  $m$  for moderate aspect ratios. The lines of constant  $d/c$  were faired to a value of  $\alpha = 90$  degrees obtained from the equation

$$b/c = d/c + 1/c \quad (3)$$

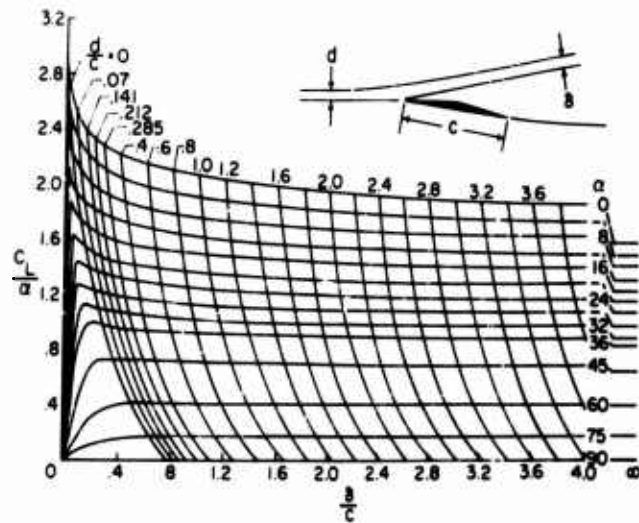


Fig. 2 - Green's solution for the lift-curve slope of a two-dimensional flat plate (with approximate lines of constant  $d/c$ )

where  $f/c$  is the dimensionless distance from the leading edge to the stagnation line. The distance  $f/c$  can be obtained from Green's work and for  $\alpha = 90$  degrees is

$$\frac{f}{c} = \frac{1}{2} + \frac{1}{2} \ln \left( \frac{b}{b-1} \right) - \frac{b^2-1}{2} \sin^{-1} \left( \frac{1}{b} \right) \quad (4)$$

$$- (b - \frac{1}{2}b^2 - 1) \ln \left( \frac{b+1}{b-1} \right)$$

where  $b$  has been previously defined in Eq. (2). Equation (3) is based on the assumption that the stagnation line for the condition  $\alpha = 90$  degrees is parallel to the undisturbed water surface.

**Linearized Solution for Cambered Sections at Infinite Depth**—The case of cambered surfaces at infinite depth can theoretically be analyzed in two dimensions by the method of Levi-Civita (10). However, like many conformal mapping problems the method is very difficult to apply to a particular configuration and only a few specific solutions have been obtained. Among these is the work of Rosenhead (11) and Wu (12). Although the solution of Wu is applicable in principle to arbitrary sections, it has been carried out only for the circular arc. A particular advantage of Wu's solution is that it includes the effects of nonzero cavitation number.

The most useful treatment of cambered surfaces is the linearized theory of Tulin and Burkart (1) which is readily applicable to any surface configuration (with positive lower surface pressures) as long as the angle of attack and camber are small. The principal results of this linearized theory are summarized below.

The supercavitating hydrofoil problem in the  $Z$  plane is transformed into an airfoil problem in the  $\bar{Z}$  plane by the relationship  $\bar{Z} = \bar{z}$ . Denoting properties of the equivalent airfoil with barred symbols and those of the hydrofoil with unbarred symbols, the following relationships are derived:

# Supercavitating Hydrofoils Operating at Zero Cavitation Number

$$\frac{dy}{dx}(x) = \frac{1}{x} \frac{dy}{dx}(x^2) \quad (5)$$

$$u(x) = u(x^2) \quad (6)$$

$$C_L = C_m = 2 \left( A_0 + A_1 - \frac{A_2}{2} \right) \quad (7)$$

$$C_D = 1.8 + (C_L^2) + 2 \left( A_0 + \frac{A_1}{2} \right)^2 \quad (8)$$

$$C_m = C_{m,3} = \frac{1}{32} (5A_0 + 7A_1 - 7A_2 + 3A_3 - A_4 - 2) \quad (9)$$

The coefficients  $A_n$  are the thin airfoil coefficients in the sine series expansion of the airfoil vorticity distribution

$$\gamma(x) = 2V \left( A_0 \cot \frac{\theta}{2} + \sum_{n=1}^{\infty} A_n \sin n\theta \right) \quad (10a)$$

where

$$x = \frac{1}{2} (e^{\theta} + 1 - \cos \theta) \quad (0 \leq \theta < \pi) \quad (10b)$$

and can be found for a given configuration from the following equations:

$$A_0 = -\frac{1}{\pi} \int_0^{\pi} \frac{dy}{dx} d\theta = -\frac{1}{\pi} \int_0^{\pi} \frac{dy}{dx} d\theta = A'_0 \quad (11a)$$

$$A_n = \frac{2}{\pi} \int_0^{\pi} \frac{dy}{dx} \cos n\theta d\theta \quad (11b)$$

The first term in equation (10a), that is, the  $A_0$  term, is the vorticity due to angle of attack and the second term is that due to camber. In order to isolate the effects of camber,  $A_0$  will be considered zero. Any section profile derived on this basis will also, for convenience, be orientated with respect to the  $\bar{x}$ -axis in such a manner that  $A'_0 = 0$ . From Eq. (9a) these conditions require that  $\alpha$  also be equal to zero. Thus, the derived orientation is defined as the zero-angle-of-attack case.

When  $A_0$  is set equal to zero, the hydrofoil lift drag ratio for a given lift coefficient is obtained from Eqs. (7) and (8) as follows:

$$\frac{C_L}{C_D} = \frac{\left( A_1 - \frac{A_2}{2} \right)^2}{A_1^2 + 4} = \frac{1}{2C_L} \left( 1 - \frac{A_2}{2A_1} \right)^2 = \frac{1}{2C_L} \quad (12)$$

Obviously, for maximum lift drag ratio,  $-A_2/A_1$  must be as large as possible. However, if the assumed condition that a cavity exists only on the upper surface is to be real, the vorticity distribution given by Eq. (8) must be positive in the interval  $0 \leq \theta \leq \pi$ ; that is, the pressure on the hydrofoil lower surface must be positive over the entire chord, otherwise a cavity will exist on the lower surface. Thus, for

maximum hydrofoil lift/drag ratio,  $-A_2/A_1$  must be as large as possible and still satisfy the condition

$$\gamma(\bar{x}) = 2V \sum_{n=1}^{\infty} A_n \sin n\pi \leq 0 \quad (0 \leq \bar{x} \leq 1) \quad (13)$$

**Tulin-Burkart Section**—With the stipulation that the vorticity distribution is defined by only two terms in Eq. (13), Ref. 1 finds the optimum relationship between  $A_1$  and  $A_2$  as  $-A_2/A_1 = 1/2$ . This results in a hydrofoil configuration given by the equation

$$\frac{y}{c} = \frac{A_1}{2} \left[ \left( \frac{x}{c} \right) - \frac{8}{3} \left( \frac{x}{c} \right)^{3/2} - 4 \left( \frac{x}{c} \right)^2 \right] \quad (14)$$

From Eq. (7) the design lift coefficient (that is, for  $\alpha = 0$ ) for this section is

$$C_{L,d} = \frac{5\pi A_1}{8} \quad (15)$$

and the lift/drag ratio for this condition as obtained from Eq. (12) is

$$\frac{L}{D} = \frac{25}{4} \left( \frac{\pi}{2C_L} \right) \quad (16)$$

Since  $\pi/2C_L$  represents the lift/drag ratio of a flat plate, the configuration given by Eq. (14) has a lift/drag ratio 25/4 times as great as that of the flat plate. When the hydrofoil given in Eq. (14) is operated at an angle of attack, the lift/drag ratio becomes

$$\frac{L}{D} = \frac{\pi}{2} \left( \frac{1}{5\pi} + \frac{2}{5\pi} C_{L,d} \right) \quad (17)$$

In Ref. 1 it is pointed out that configurations superior to the one given by Eq. (14) are possible. In Ref. 2 two such superior configurations are selected.

**Three-Term Section**—If the vorticity distribution given by Eq. (10) is assigned three terms, it is shown in Ref. 2 that the optimum vorticity distribution for low drag is

$$\gamma(\bar{x}) = 2V A_1 \left( \sin \pi \bar{x} - \sin 2\pi \bar{x} + \frac{1}{2} \sin 3\pi \bar{x} \right) \quad (18)$$

The shape of the hydrofoil corresponding to Eq. (18) is

$$\frac{y}{c} = \frac{A_1}{10} \left[ 5 \left( \frac{x}{c} \right) - 20 \left( \frac{x}{c} \right)^{3/2} + 80 \left( \frac{x}{c} \right)^2 - 64 \left( \frac{x}{c} \right)^{5/2} \right] \quad (19)$$

By using Eq. (7), the lift coefficient of this hydrofoil becomes

$$C_L = \frac{\pi}{2} \left( \frac{3A_1}{2} \right) \quad (20)$$

or for  $\alpha = 0$  the design lift coefficient is

$$C_{L,d} = \frac{3\pi A_1}{4} \quad (21)$$

The following drag coefficient may be obtained by using Eq. (8):

$$C_D = \frac{\pi}{2} \left( 1 + \frac{A_1}{2} \right)^2 - \frac{\pi}{2} \left( 1 + \frac{2C_{L,d}}{3\pi} \right)^2. \quad (22)$$

For  $\alpha = 0$ , the lift/drag ratio is

$$\frac{L}{D} = 9 \left( \frac{\pi}{2C_L} \right). \quad (23)$$

This value is nine times as large as that for a flat plate and 1.44 times as large as the value for the hydrofoil of Ref. 1 where  $L/D = 25/4 (\pi/2C_L)$ . The following lift/drag ratio may be obtained for finite angles of attack by dividing Eq. (20) by Eq. (22)

$$\frac{L}{D} = \frac{1 + \frac{2}{3\pi} C_{L,d}}{\left( 1 + \frac{2C_{L,d}}{3\pi} \right)^2}. \quad (24)$$

**Five-Term Section**—Another hydrofoil section which theoretically has lower drag than either of the previously discussed profiles can be obtained by assigning the following value to Eq. (10)

$$(x) = 2V A_1 (\sin x - 4/3 \sin 2x + 4/3 \sin 3x - 2/3 \sin 4x + 1/3 \sin 5x). \quad (25)$$

The shape of the hydrofoil corresponding to Eq. (25) is

$$\frac{y}{c} = \frac{A_1}{315} \left[ 210 \left( \frac{x}{c} \right) - 2,240 \left( \frac{x}{c} \right)^3 + 12,600 \left( \frac{x}{c} \right)^5 - 30,912 \left( \frac{x}{c} \right)^7 + 35,840 \left( \frac{x}{c} \right)^9 - 15,360 \left( \frac{x}{c} \right)^{11} \right]. \quad (26)$$

By using Eq. (7), the lift coefficient of this hydrofoil may be given as

$$C_L = \frac{\pi}{2} \left( 1 + \frac{5A_1}{3} \right) \quad (27)$$

or for  $\alpha = 0$  the design lift coefficient is

$$C_{L,d} = \frac{5\pi A_1}{6}. \quad (28)$$

The following drag coefficient is obtained by using Eq. (8):

$$C_D = \frac{\pi}{2} \left( 1 + \frac{A_1}{2} \right)^2 - \frac{\pi}{2} \left( 1 + \frac{3C_{L,d}}{5} \right)^2 \quad (29)$$

and for  $\alpha = 0$  the lift/drag ratio is

$$\frac{L}{D} = \frac{100}{9} \left( \frac{\pi}{2C_L} \right). \quad (30)$$

This lift/drag ratio is about 11 times as large as the value for a flat plate and nearly twice as efficient as the configuration of Ref. 1.

V. E. Johnson, Jr.

For finite angles of attack,

$$\frac{L}{D} = \frac{1 + \frac{2}{3} C_{L,d}}{\left(1 + \frac{3}{5} C_{L,d}\right)^2} \quad (31)$$

**Circular-Arc Section**—Because of the geometrical simplicity of the circular-arc profile, it is desirable to include its characteristics so that the circular arc may be compared with the other low-drag sections. Denoting the central angle subtending the chord as  $\alpha$  and using the chord line as the reference axis, the coefficients for the circular arc determined from the linearized theory are

$$A'_0 = -\frac{\alpha}{8} \quad (32a)$$

$$A_1 = \frac{\alpha}{2} \quad (32b)$$

$$A_2 = -\frac{\alpha}{8} \quad (32c)$$

$$A_n = 0 \quad (n > 2). \quad (32d)$$

Since for the reference axis used,  $A'_0$  is negative, positive lower-surface pressures cannot possibly be realized near the leading edge unless the angle of attack is increased at least to the point where  $\alpha = \pi/8 = 0$ . Because  $A'_n = 0$  for  $n > 2$  and  $A_1 \sin \alpha + A_2 \sin 2\alpha$  is everywhere positive in the interval  $0 \leq \alpha \leq \pi$ , the condition  $\alpha = \pi/8 = 0$  is sufficient to specify positive pressures over the entire chord of the hydrofoil. A convenient way of treating the circular-arc section to make it comparable to the other low-drag sections is to reorient its reference line an angle  $\pi/8$  above the chord line so that for this orientation  $A'_0 = 0$  and  $\alpha = 0$ . Using this new reference line the lift coefficient of the circular-arc section is

$$C_L = \frac{\pi}{2} \left(1 + \frac{9}{16}\right) \quad (33)$$

or for  $\alpha = 0$  the design lift coefficient is

$$C_{L,d} = \frac{9\pi}{32} \quad (34)$$

The following drag coefficient is obtained by using Eqs. (8) and (34):

$$C_D = \frac{\pi}{2} \left(1 + \frac{1}{4}\right)^2 = \frac{\pi}{2} \left(1 + \frac{8}{9} C_{L,d}\right)^2 \quad (35)$$

and for  $\alpha = 0$  the lift/drag ratio is

$$\frac{L}{D} = \frac{81}{16} \frac{1}{2C_{L,d}} \quad (36)$$

This lift/drag ratio is about 5 times as large as the value for a flat plate and almost as great as the Tulin-Burkart section.

For finite angles of attack

$$\frac{L}{D} = \frac{1 + \frac{2}{\pi} C_{L,d}}{\left(1 + \frac{8}{\pi} C_{L,d}\right)^2} \quad (37)$$

**Comparison of Sections**—The shape of the four sections discussed in the preceding paragraphs are shown for comparison in Fig. 3a. The pressure distribution on these sections is presented in Fig. 3b. It may be noted that the location of maximum pressure moves rearward with increase in the ratio  $-A_2/A_1$ .

The lift/drag ratio given by Eqs. (17), (24), (31), and (37) are compared in Fig. 4. The great improvement over the  $L/D$  of a flat plate offered by positively cambering the lower surface and operating at the design angle of attack is most encouraging. However, a comparison at what amounts to a fictional design angle of attack is not justified. It is obvious from a structural standpoint that hydrofoils with any strength must be operated at finite angles of attack (corresponding to the dashed lines in Fig. 4). Thus the maximum lift/drag ratio for any section depends on the minimum angle at which it can be operated with a cavity from the leading edge. A meaningful comparison of the hydrofoil sections just discussed is not possible unless the influence of the upper surface of the hydrofoil is also included, for it is this surface which controls the maximum lift/drag ratio of the section. Assuming infinite speed and thus zero cavitation number, it is clear that if any portion of the upper surface becomes wetted, the lift will decrease and the drag increase. Thus, a knowledge of the profile of the given hydrofoil upper surface combined with the location of the upper cavity streamline at various angles of attack will permit the prediction of the angle of attack at which the maximum lift/drag ratio will occur. Only on the basis of maximum lift/drag ratio can the best supercavitating hydrofoil be selected. A comparison of the various sections based on calculated cavity streamline locations and hydrofoil thickness is presented in the last section of this paper.

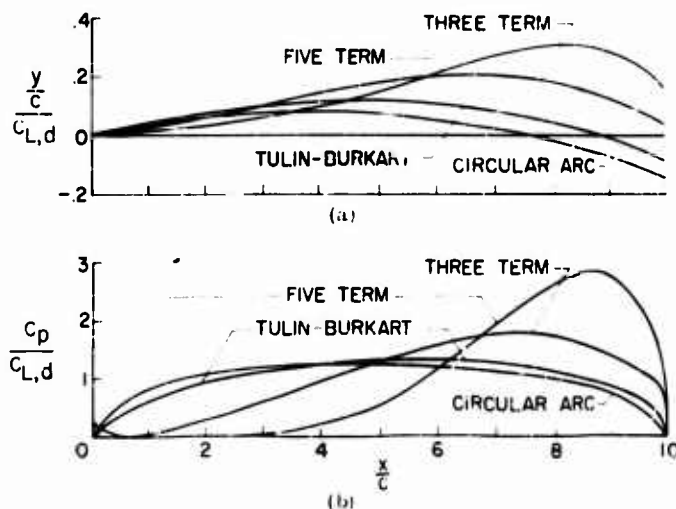


Fig. 3 - Shape and pressure distribution of four low-drag supercavitating hydrofoils;  $\alpha = 0$ ; infinite depth: (a) lower surface profile, (b) pressure distribution



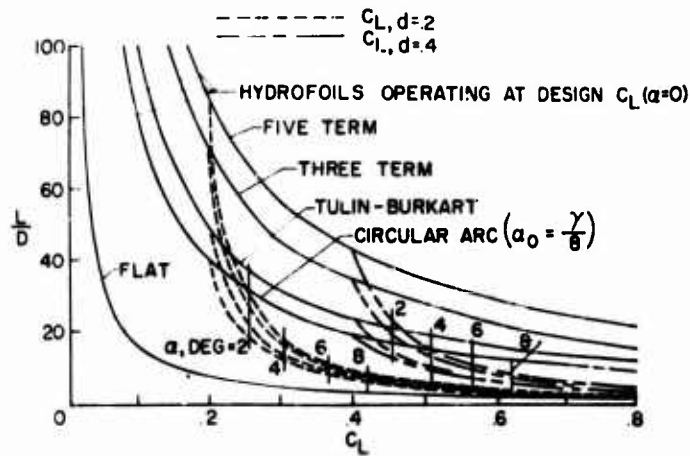


Fig. 4 - Lift/drag ratios for low-drag hydrofoils calculated from two-dimensional linearized theory

The practical use of the formulas presented in the preceding discussion is also limited by the assumptions made in their derivation. In fact, the restrictions imposed by the assumptions of the linearized theory prevent its use in the calculation of the characteristics of hydrofoils suitable for use as aircraft landing gear. Here, because of the high hydrofoil loads on necessarily thin hydrofoils the aspect ratio may be as low as 1 or 2. Also the hydrofoil must operate near the free water surface and in some instances at large angles of attack. Thus, the effects of these variables on the characteristics of supercavitating hydrofoils (particularly of cambered sections) is needed. Much of this information can be obtained by additional application of the linearized theory combined with certain modifications to the two-dimensional theory discussed in preceding paragraphs.

#### Modifications of Infinite Depth Theory

**Nonlinear Equation for Lift at Infinite Depth**—If  $\alpha = 0$  refers to the reference line which makes  $A_1 = 0$ , then Eq. (7) may be written as

$$C_L = \frac{\pi}{2} \left( \alpha + A_1 - \frac{A_2}{2} \right) \quad (38)$$

where  $\alpha_c$  is the effective increase in angle of attack due to camber ( $A_1 - A_2/2$ ). Thus, the solution for cambered hydrofoils is merely the flat-plate linearized solution with  $\alpha$  replaced by  $\alpha + \alpha_c$ . This is exactly analogous to the influence of camber on airfoils in an infinite fluid where there is an effective increase in angle of attack due to the camber. By carrying this procedure further, and by applying it to the resultant force rather than the lift, the nonlinear solution of Rayleigh becomes applicable to arbitrary configurations simply by replacing  $\alpha$  by  $\alpha + \alpha_c$ ; that is,

$$C_N = \frac{2\pi}{4} \sin(\alpha + \alpha_c) \quad (39)$$

The lift will then be

$$C_L = \frac{2\pi \sin(\alpha + \epsilon_c)}{4 + \pi \sin(\alpha + \epsilon_c)} \cos \alpha. \quad (40)$$

In Eq. (40),  $\epsilon_c = \alpha + \epsilon$ , where  $\epsilon$  denotes the deviation of the resultant-force vector from the normal to the hydrofoil reference line. For large values of  $\alpha$ ,  $\epsilon$  is small compared with  $\alpha$  and  $\cos(\alpha + \epsilon) \approx \cos \alpha$ . When  $\alpha$  is very small,  $\epsilon$  is a maximum and will almost always be less than about 3 degrees, for which the cosine is very nearly 1 or  $\cos(\alpha + \epsilon) \approx \cos \alpha \approx 1$ . Therefore,  $\cos \alpha$  in equation (38) may be replaced by  $\cos(\alpha + \epsilon)$  with little loss in accuracy and great gain in simplicity. Equation (40) then becomes

$$C_L = \frac{2\pi \sin(\alpha + \epsilon_c)}{4 + \pi \sin(\alpha + \epsilon_c)} \cos \alpha. \quad (41)$$

For a circular-arc hydrofoil of central angle  $\gamma$ , it has been shown in Eq. (33) that  $\epsilon_c = (9/16)\gamma$ . It has also been shown that for the circular arc the reference line must be chosen at an angle  $\alpha_0$  to the chord line so that  $A'_0 = 0$ . The result obtained by substituting  $\epsilon_c = (9/16)\gamma$  into Eq. (41) is compared in Fig. 5 with the linear solution of Tulin and Burkart (Eq. 38) and the nonlinear solution of Wu (12) for two circular-arc profiles. The agreement of Eq. (39) with the more exact solution of Wu is good over the entire range of angle of attack from 0 to 90 degrees. Similar agreement is expected for any configuration of small camber.

The successful modification of the Rayleigh equation to include cambered configurations leads at once to a similar modification of the solution of Green. However, in this case the argument for replacing  $\alpha$  by  $\alpha + \epsilon_c$  is very weak unless the section coefficients which determine  $\epsilon_c$  are known as a function of the depth of submersion.

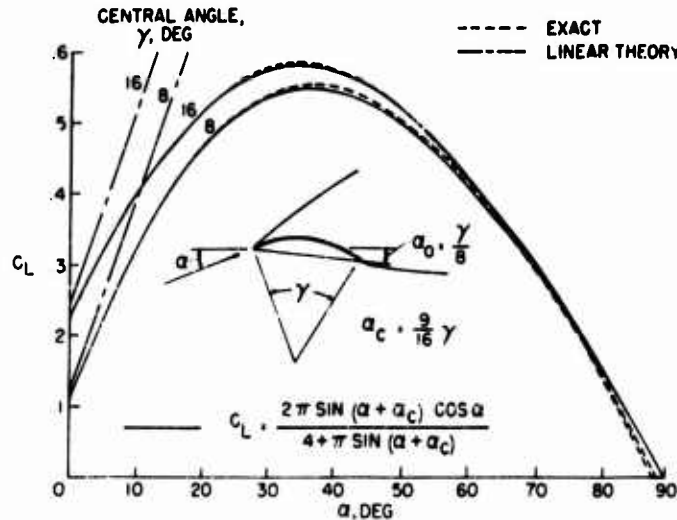


Fig. 5 Two-dimensional theories for the lift coefficient of a circular-arc hydrofoil at infinite depth

**Linearized Solution for Lift of Cambered Sections at Finite Depth**—An examination of the linearized expressions for the lift coefficient of arbitrary foils at infinite depth and at zero depth reveals that both the lift-curve slope and the increase in angle of attack due to camber do change with depth of submersion. At infinite depth the linearized expression for lift coefficient is given by Eq. (33). At zero depth the lift coefficient must be one-half the fully wetted value obtained from thin-airfoil theory as pointed out in Ref. 13; that is,

$$C_{L,0} = \pi \left( A_{0,h} + \frac{A_{1,h}}{2} \right) \quad (42)$$

where  $A_{0,h}$  and  $A_{1,h}$  are the thin-airfoil coefficients of the section in the hydrofoil plane and are given by the expressions

$$A_{0,h} = \frac{1}{\pi} \int_0^\infty \frac{dy}{dx} dx \quad (43a)$$

$$A_{1,h} = \frac{2}{\pi} \int_0^\infty \frac{dy}{dx} \cos \theta dx \quad (43b)$$

For the Tulin-Burkart section at zero angle of attack these values may be determined as

$$A_{0,h} = 0.227 A_1 \quad (44a)$$

$$A_{1,h} = 1.151 A_1 \quad (44b)$$

Thus, from Eqs. (38) and (42) it is seen that, for a flat plate at small angles, the lift coefficient goes from  $\pi/2$  at infinite depth to  $\pi/4$  at zero depth (as given by Greer.), whereas for the Tulin-Burkart section at zero angle of attack these values are  $\pi(1.25 A_1)/2$  at infinite depth and  $\pi(0.802 A_1)$  at zero depth. Although the flat-plate lift coefficient doubles in going from infinite to zero depth, the ratio is only 1.28 for the cambered section. The important point to note is that the value of  $C_L$  for the Tulin-Burkart section changes from  $1.25 A_1$  to  $0.802 A_1$ .

It is now desirable to determine  $C_L$  for finite depths of submersion. This can be accomplished by modifying the linearized theory of Ref. 1 to include the effects of the free water surface.

**Rigorous Solution**—The effect of the free water surface may be obtained by finding the transformation which will map the free water surface, the hydrofoil, and the cavity streamlines into the real axis of an auxiliary or equivalent airfoil plane denoted as the  $\bar{z}$  plane to distinguish from the  $z$  plane used at infinite depth. The transformation required is

$$\bar{z} = \frac{z^2}{4d} (1 - 1/n - 1) \quad (45)$$

where  $d$  is the depth of submersion of the leading edge, or more exactly the spray thickness  $\delta$ . The  $z$  plane and its transformation in the  $\bar{z}$  plane are shown in Fig. 6. In the linearized theory developed in Ref. 1 points of corresponding perturbation velocities  $u$  and  $v$  remain constant in the transformation; therefore, the boundary conditions shown in the  $z$  plane are shown in the  $\bar{z}$  plane in their corresponding locations. The potential flow problem shown in the  $\bar{z}$  plane is exactly the thin airfoil

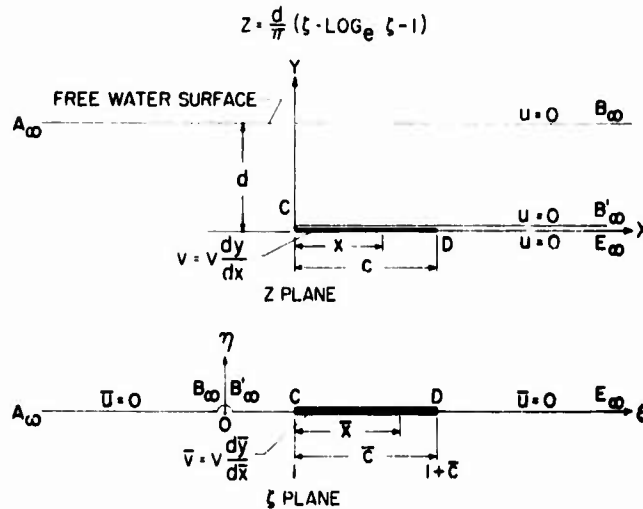


Fig. 6 - Transformation of hydrofoil at finite depth to equivalent airfoil

problem. It is well known that the thin airfoil problem can be solved by distributing vortices along the chord so that the condition  $v = (dy/dx)V$  is satisfied (14). The desired distribution of vorticity is  $\gamma(x)$  as given in Eq. (8). With  $\gamma(x)$  known,  $u(x)$  and  $v(x)$  are known. These values of  $u$  and  $v$  on the airfoil are exactly the same as the values of  $u$  and  $v$  on the hydrofoil if the relationship between  $x$  and  $\bar{x}$  satisfies the equation

$$x = \frac{d}{c} \bar{x} - \ln(1 + \bar{x}) \quad (46)$$

Equation (46) is obtained directly from Eq. (45) by noting that  $\bar{x} = 1 + x$ . Dividing Eq. (46) through by  $c$  gives

$$\frac{x}{c} = \frac{1}{c} \frac{d}{c} \bar{x} - \ln(1 + \bar{x}) \quad (47)$$

When  $\frac{x}{c} = 1$ ,  $\bar{x} = c$ , therefore

$$\frac{d}{c} = \frac{1}{c} - \ln(1 + c) \quad (48)$$

Using Eqs. (47) and (48) the relationship between  $x/c$  and  $\bar{x}/c$  may be determined for both positive and negative values of  $x/c$ . It can be seen in Fig. 6b that negative values of  $x/c$  correspond to points in front of the airfoil which in turn are related to points on the upper cavity streamline. The relationship between  $x/c$  and  $\bar{x}/c$  is presented in Fig. 7. With the aid of Fig. 7 and a knowledge of thin-airfoil theory the solution to the supercavitating hydrofoil problem at finite depth is easily determined. The word easily refers to the comprehension of the solution; the actual labor is considerably involved because of the necessity to frequently resort to plotting curves and employing a planimeter.

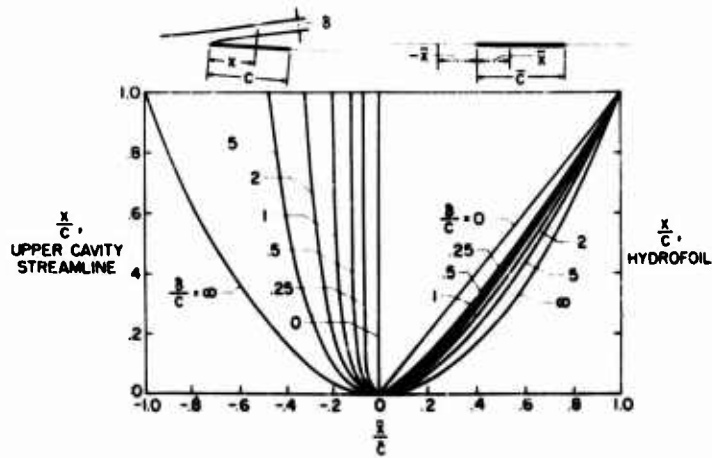


Fig. 7 - The influence of depth of submersion on the relationship between points in hydrofoil and equivalent airfoil planes

The procedure for determining the pressure distribution and thus the forces and moments on a hydrofoil at arbitrary depth is as follows:

1. The shape of the hydrofoil is known as  $y = y(x)$  and thus

$$\frac{dy}{dx} = \frac{dy}{dx}(x) \quad \text{or} \quad \frac{dy}{dx}\left(\frac{x}{c}\right).$$

2. The slope of the equivalent airfoil at the point  $x/c$  is exactly the same as the slope of the hydrofoil  $dy/dx(x/c)$  when  $x/c$  and  $x/c$  are related as shown in Fig. 7. Thus  $dy/dx(x/c)$  is found.

3. The vorticity distribution on the airfoil is then obtained from Eqs. (8) and (9).

4. The perturbation velocity  $u$  in terms of the vorticity  $\gamma$  is given by the equation

$$u\left(\frac{x}{c}\right) = \frac{1}{2} \gamma\left(\frac{x}{c}\right) \quad (49)$$

Thus the velocity  $u(x/c)$  is determined at every point along the airfoil.

5. The perturbation velocity  $u(x/c)$  on the hydrofoil is exactly the same as the velocity  $u(x/c)$  if  $x/c$  and  $x/c$  are related as shown in Fig. 7. Thus the velocity  $u(x/c)$  is determined.

6. Step 5 also determines the linearized pressure coefficient since  $C_p$  is given by the equation

$$C_p = \frac{p - p_\infty}{q_\infty} = 2 \frac{u}{V_\infty}$$

or

$$C_p \left( \frac{x}{c} \right) = A_0 \cot \frac{\theta}{2} + \sum A_n \sin n\theta \quad (50)$$

where  $\theta$  is related to  $x/c$  by Eq. (10b) and Fig. 7.

7. With a knowledge of  $C_p(x/c)$  the lift, drag, and moment coefficients are determined as

$$C_L = \int_0^1 C_p \left( \frac{x}{c} \right) d \frac{x}{c} \quad (51a)$$

$$C_D = \int_0^1 C_p \left( \frac{x}{c} \right) \frac{dy}{dx} d \frac{x}{c} \quad (51b)$$

$$C_m = \int_0^1 C_p \left( \frac{x}{c} \right) \frac{x}{c} d \frac{x}{c} \quad (51c)$$

**Approximate Solution**—The calculations by the rigorous method outlined above were so cumbersome that the solution by this method was abandoned when an approximate method was discovered. The approximate method continues with the simple transformation  $\bar{Z} = -\bar{Z}$  used in Ref. 1. The advantage of the simpler transformation is that if the vorticity distribution in the presence of the water surface can be determined in the  $\bar{Z}$  plane, the simple Eqs. (7) and (9) for the lift and moment coefficient will still be applicable. It is shown in Ref. 3 that the influence of the free surface on the equivalent airfoil in the  $Z$  plane can be approximated by locating a singular vortex in the position shown in Fig. 8. The strength of this vortex  $\Gamma_1$  is equivalent to the total circulation about the airfoil. Using the model shown in Fig. 8 and equating

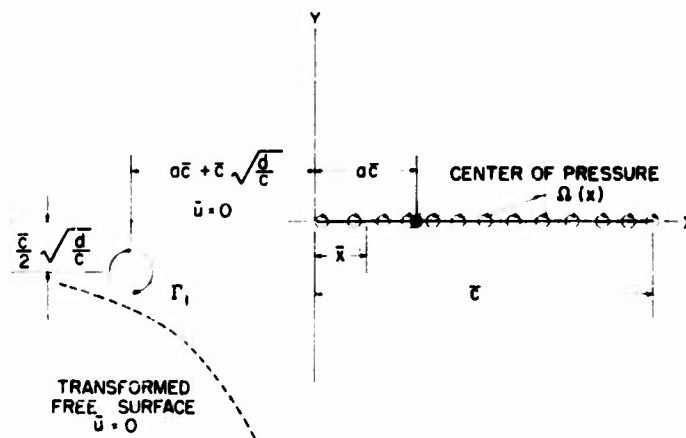


Fig. 8 - Linearized model for calculating the effect of depth of submersion on the vorticity distribution of the equivalent airfoil section using the  $\bar{Z} = -Z$  transformation

the airfoil slope at the point  $x$  to the streamline slopes induced by the sum of the airfoil vorticity and the image vortex; the airfoil vorticity was determined in Ref. 3 as

$$\gamma(x) = 2V \left( C_0 \cot \frac{\pi x}{2} + \sum_{n=1}^{\infty} C_n \sin n\pi x \right) \quad (52)$$

where

$$C_0 = \frac{A_0(4 + B_1) + A_1 B_0}{4 + B_1 - 2B_0} \quad (53a)$$

$$C_1 = \frac{2A_1(2 - B_0) - 2A_0 B_1}{4 + B_1 - 2B_0} \quad (53b)$$

$$C_n = A_n - \frac{(2A_0 + A_1)B_n}{4 + B_1 - 2B_0} \quad (53c)$$

The  $B$  coefficients are given in Fig. 9 in terms of the center of pressure location  $ac$  where  $a$  is given by the equation

$$a = \frac{\frac{1}{4} C_0 + C_1 - \frac{C_2}{2}}{C_0 + \frac{C_1}{2}} \quad (54)$$

The  $A$  coefficients (Eqs. 53) are the section coefficients for infinite depth.

The  $C$  coefficients are computed by iteration; that is, a value of  $a$  is assumed, the  $B$  coefficients are obtained from Fig. 9, and the  $C$  coefficients determined from Eqs. (53). If the value of  $a$  determined from Eq. (54) does not agree with the original assumption, the procedure should be repeated.

If the  $C$  coefficients are determined for the case of  $i$  or  $A_0 = 0$ , the ratio of the lift coefficient due to camber at finite depth to the lift coefficient due to camber at infinite depth may be determined from the following equation:

$$\left( \frac{C_L}{C_{L,\infty}} \right)_{i=0} = \frac{C_0 + C_1 - \frac{C_2}{2}}{A_1 - \frac{A_2}{2}} \quad (55)$$

The values of  $(C_L/C_{L,\infty})_{i=0}$  given by Eq. (55) for the four sections of interest are presented in Fig. 10.

The true linearized lift-curve slope  $m$  for finite depths of submersion in the equation  $C_L = m(\alpha + \alpha_{cr})$  is that shown in Fig. 2 for  $i = 0$ . Therefore, the effective angle of attack due to camber  $\alpha_{cr}$  is obtained from the following relationship:

$$\frac{m}{2} = \frac{m_{i=0}}{2} \left( \frac{C_L}{C_{L,\infty}} \right)_{i=0} \quad (56)$$

Supercavitating Hydrofoils Operating at Zero Cavitation Number

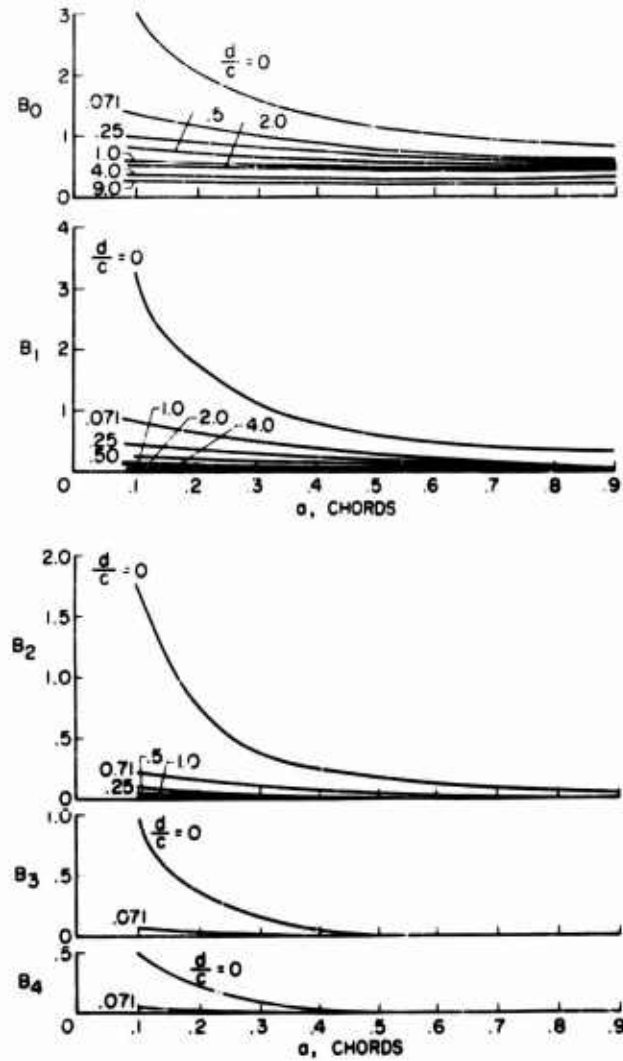


Fig. 9 - The B coefficients (a)  $B_0$  and  $B_1$ , (b)  $B_2$ ,  $B_3$ , and  $B_4$

Thus

$$\frac{t_c}{t_{c,0}} = \frac{C_L}{2m_{(c=0)} C_{L,0}}$$

Values of  $t_c/t_{c,0}$  are plotted against  $t_c$  in Fig. 11 for the Tulin-Burkart, the circular-arc, and the three-term and five-term sections.



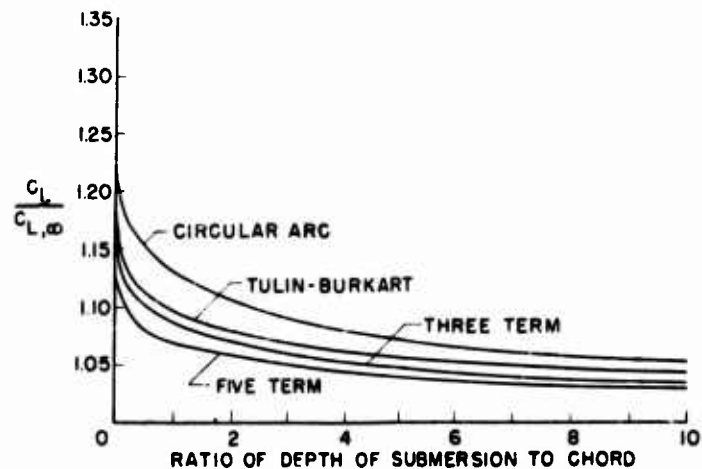


Fig. 10 - Influence of depth of submersion on the lift coefficient of cambered sections operating at the design angle of attack ( $\alpha = 0$ )

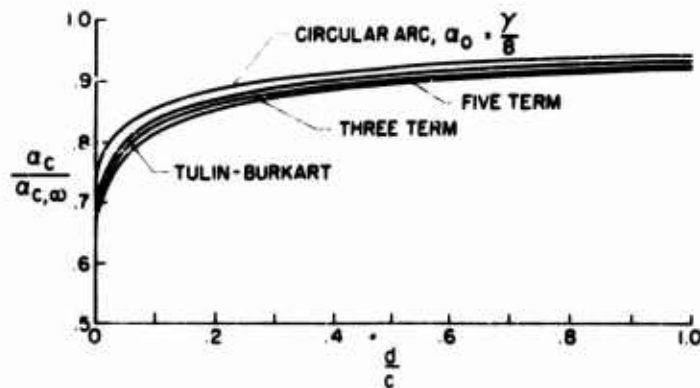


Fig. 11 - Influence of depth of submersion on the effective angle of attack of cambered sections operating at the design angle of attack ( $\alpha = 0$ )

Equation (57) is obviously limited by the linearizing assumptions made in its derivation. An important limitation is due to the assumption that the free surface is always horizontal and thus  $\alpha_c = \alpha_{c,\infty}$ . At small depth/chord ratios and particularly for large magnitudes of camber the free water surface is not horizontal and  $\alpha_c \neq \alpha_{c,\infty}$ . Thus, for small values of  $\frac{d}{c}$  and large magnitudes of camber the values of  $\frac{\alpha_c}{\alpha_{c,\infty}}$  given in Fig. 11 are probably too low.

**Nonlinear Equation for Lift at Finite Depth**—With a knowledge of the angle of attack due to camber  $\alpha_c$  at finite depths of submersion, Green's solution is now modified to include camber by treating the effective angle of attack as  $\alpha = \alpha_c$ , where  $\alpha_c$  is

obtained from Fig. 11. This is exactly the method used in modifying the Rayleigh equation to obtain the nonlinear approximation for the lift coefficient at infinite depth. With this assumption, the resultant-force coefficient for a cambered hydrofoil at any positive depth of submersion is obtained in terms of the spray thickness  $\delta/c$  from Eqs. (2) as

$$C_N^{(1)} = C_{N,f}^{(\alpha + \alpha_c)} \quad (58)$$

Equation (58) states that the resultant force on a cambered section is approximated by replacing  $\alpha$  in Green's solution for a flat plate by the effective angle of attack  $\alpha + \alpha_c$ . It will be shown that the resultant force will deviate only slightly from the normal (as previously pointed out for the condition of infinite depth) and therefore

$$C_L^{(1)} = C_{N,f}^{(\alpha + \alpha_c)} \cos \alpha \quad (59)$$

**Three-Dimensional Theory at Finite Depth—Lift**—The flow about a supercavitating hydrofoil may be constructed by a suitable combination of sources and vortices. The vortices contribute unsymmetrical velocity components and lift; the sources contribute symmetrical components which provide thickness for the cavity but no lift. For a finite span the vortices cannot end at the tips of the foil, and a system of horseshoe vortices must be combined with the sources to describe the flow. If it is assumed that the influence of finite span on the two-dimensional lift coefficient is due to the effects of the trailing vorticity, then the resulting effect of aspect ratio is exactly the same as for a fully wetted airfoil. Jones (15) gives the lift of a fully wetted elliptical flat plate as

$$\bar{C}_L = \frac{1}{E} 2\pi(\alpha - \alpha_i) \quad (60)$$

where  $E$  is the ratio of semiperimeter to the span and  $\alpha_i$  is the induced angle of attack caused by the trailing vorticity. Thus the effect of aspect ratio is to decrease the two-dimensional lift curve slope by a factor  $1/E$  and to decrease the effective angle of attack by an increment  $\alpha_i$ . Therefore for the finite aspect ratio supercavitating hydrofoil at infinite depth Eq. (38) is modified to give

$$C_{L,1} = \frac{1}{E} 2\pi(\alpha + \alpha_c - \alpha_i) \quad (61)$$

or more generally for finite depth, Eq. (59) becomes

$$C_{L,1} = \frac{1}{E} C_{N,f}^{(\alpha + \alpha_c - \alpha_i)} \cos \alpha \quad (62)$$

where for rectangular plan form of aspect ratio  $A$ ,  $E = (A + 1)/A$  and

$$\alpha_i = \frac{C_{L,1}}{A} (1 + \gamma) \quad (63)$$

where  $\gamma$  is a correction for plan form (see Ref. 14).

Another effect due to finite aspect ratio is the concept of additional lift due to crossflow (5,16). This crossflow lift is assumed due to the drag on the hydrofoil contributed by the component of free-stream velocity normal to the hydrofoil. In the present case of zero cavitation number, the crossflow drag coefficient is the Rayleigh value, 0.88. Since this lift is caused only by the spanwise flow (flow around the ends of the plate) it is also modified to account for the aspect ratio by the Jones' edge

correction, 1/E. Since only the spanwise flow is considered, E is now the ratio of semiperimeter to chord. Because the flow being considered is normal to the plate, the induced angle for this flow is zero. Thus for a flat plate, the crossflow lift  $C_{L,c}$  is

$$C_{L,c} = \frac{1}{A+1} 0.88 \sin^2 \alpha \cos \alpha. \quad (64)$$

No experimental or theoretical information on the crossflow lift of cambered surfaces is available in the literature. In order to approximate this component the following assumptions are made: (a) the crossflow force acts normal to the hydrofoil chord line, and (b) the effective direction of the free stream on the plate is altered by the increase in angle of attack due to camber  $\alpha_c$ . Thus, the crossflow lift on cambered sections is assumed to be

$$C_{L,c} = \frac{1}{A+1} 0.88 \sin^2(\alpha' + \alpha_c) \cos \alpha' \quad (65)$$

where  $\alpha' = \alpha + \alpha_c$ , in which  $\alpha_c$  is the inclination of the chord line to the reference line of the section (positive if the chord line is below the reference line), and  $\alpha_c$  is obtained from Fig. 11 for the depth of interest.

The total lift on a finite aspect ratio hydrofoil operating near the free water surface is therefore obtained by adding Eq. (65) to Eq. (62) to give

$$C_L(\alpha) = \frac{A}{A+1} C_{n,f}(\alpha + \alpha_c - \alpha_i) \cos \alpha + \frac{1}{A+1} 0.88 \sin^2(\alpha' + \alpha_c) \cos \alpha'. \quad (66)$$

In view of the very approximate nature of Eq. (65) it is desirable to examine the effect of this crossflow term on the total-lift coefficient. For a Tulin-Burkart, aspect-ratio-1 section ( $A_1 = 0.2$ ) operating at  $d/c = 0.071$  the ratio of the calculated crossflow lift,  $C_{L,c}$ , to the calculated total lift was 0.157 at  $\alpha = 4$  degrees and 0.283 at  $\alpha = 20$  degrees. For a five-term section with  $A_1 = 0.075$ , aspect ratio = 3, and  $d/c = 0.071$ , the ratio has been calculated at 0.014 at  $\alpha = 4$  degrees and 0.072 at  $\alpha = 20$  degrees. Thus any inaccuracies in the crossflow lift as computed by Eq. (65) will appreciably affect the total-lift coefficient at large angles, small aspect ratios, and large cambers. On the other hand at higher aspect ratios and small cambers, errors in the crossflow component do not greatly influence the total calculated lift.

Equation (66) may be written in terms of the slope  $m$  (given in Fig. 2) as

$$C_L = \frac{A}{A+1} m(\alpha + \alpha_c - \alpha_i) \frac{\cos \alpha}{\cos(\alpha + \alpha_c - \alpha_i)} + \frac{1}{A+1} 0.88 \sin^2(\alpha' + \alpha_c) \cos \alpha' \quad (67)$$

where  $\alpha_c$  is obtained from Fig. 11 for the depth-chord ratio of interest and  $\alpha_i$  is obtained from Eq. (63). In Eq. (63)  $C_{L,1}$  is the first term in Eq. (67). Equation (67) is solved by iteration and the convergence is quite rapid.

**Drag**—The drag coefficient of a supercavitating hydrofoil of finite aspect ratio operating at zero cavitation number and finite depth of submersion is

$$C_D = C_{L,1} \tan(\alpha + \epsilon) + C_{L,c} \tan \alpha' + C_f \quad (68)$$

where  $C_{L,1}$  is the first term in Eq. (67) and  $\epsilon$  is the deviation of the resultant-force vector from the normal. For a flat plate  $\epsilon = 0$ ,  $\alpha' = \alpha$ , and thus  $C_D = C_L \tan \alpha + C_f$ . For cambered surfaces similar to the circular-arc or Tulin-Burkart section,  $\epsilon$  becomes very small at large angles of attack and may be neglected; however, at small

angles of attack, the effect of  $\epsilon$  on the drag coefficient cannot be neglected. An approximation to the value of  $\epsilon$  can be made by determining its value from the two-dimensional linearized solution and then modifying the result for the case of finite angles of attack and aspect ratio. Either the rigorous or approximate methods of obtaining the linearized drag coefficient may be used. Using the approximate method of determining the influence of the free water surface on the equivalent airfoil in the  $\bar{z}$  plane, it is shown in Ref. 3 that the value of  $\epsilon$  may be determined from the following equation.

$$\frac{(C_1 - 2C_2) A_1 + (2C_0 + 2C_1 + C_4) A_2 - A_4 C_2}{4 \left( C_0 + C_1 - \frac{C_2}{2} \right)} \quad (69)$$

where the  $C$  coefficients are obtained from Eqs. (53). The value of  $\epsilon$  given by Eq. (69) is adequate only for the case of small angle of attack and camber and depth chord ratios larger than about 1. For large angles of attack, large camber, and finite aspect ratio, it is pointed out in Ref. 3 that an effective depth of submersion  $(d/c)_e$  should be used in determining the  $C$  coefficients in Eq. (69). The value of  $(d/c)_e$  is the value of  $d/c$  on the  $\epsilon = 0$  line in Fig. 2 corresponding to the value of  $m = m_e$  where

$$m_e = \frac{C_L}{C_{L,1}} = \frac{m^{1/2} + \frac{1}{2} \left( \frac{C_1 - C_2}{C_0 + C_1 - \frac{C_2}{2}} \right)}{m^{1/2} + \frac{1}{2} \left( \frac{C_1 - C_2}{C_0 + C_1 - \frac{C_2}{2}} \right)} \quad (70)$$

The value of the  $C$  coefficients are then determined for  $(d/c)_e$  and  $A_0 = \alpha - \alpha_1$ . It has been found after several calculations that the value of  $\epsilon$  is not greatly affected by the depth of submersion.

**Center of pressure**—The linearized expression for the center of pressure of a finite-aspect-ratio, supercavitating hydrofoil operating at zero cavitation number and finite depth of submersion is

$$x_{c.p.,1} = \frac{C_{m,1}}{C_{L,1}} = \frac{1}{16} \frac{5C_0 + 7C_1 - 7C_2 + 3C_3 - \frac{C_4}{2}}{\left( C_0 + C_1 - \frac{C_2}{2} \right)} \quad (71)$$

where the  $C$  coefficients are determined at the effective depth of submersion given by Eq. (70) and for  $A_0 = \alpha - \alpha_1$ . Superimposed on this flow is the crossflow component of lift which is assumed to be distributed uniformly over the chord and acting in a direction normal to the chord line. Thus, the distance from the leading edge to the center of pressure of the crossflow-lift component  $x_{c.p.,c}$  is given by

$$x_{c.p.,c} = 0.5c \quad (72)$$

Admittedly, this assumption is crude and accurate only for a flat plate. For cambered surfaces the crossflow will not be uniformly distributed and for low-drag cambered sections such as the five-term section the crossflow is probably concentrated on the rearward portion of the hydrofoil.

By combining Eqs. (71) and (72) the center of pressure of the combined flows is, therefore,

$$x_{c.p.} = \left( \frac{C_{L,1}}{C_L} x_{c.p.,1} + 0.5 \frac{C_{L,c}}{C_L} \right) c \quad (73)$$

As in the case of  $C_D$ , a few calculations reveal that a fair approximation for  $x_{c.p.,1}$  is obtained by using  $C_{D,1} = C_{D,2}$  and  $C_{D,2} = A_{D,2}$  in Eq. (71).

#### Comparison Between Theory and Experiment

**Lift**—In Fig. 12 the lift coefficient as given by Eq. (67) is compared with experimental data obtained on four different hydrofoils operating ventilated near the free surface. These models were

1. Flat plate, aspect-ratio-1,  $d/c = 0.071$
2. Tulin-Burkart section,  $C_{L,d} = 0.392$ , aspect-ratio-1,  $d/c = 0.071$
3. Five-term section,  $C_{L,d} = 0.392$ , aspect-ratio-1,  $d/c = 0.141$
4. Five-term section,  $C_{L,d} = 0.196$ , aspect-ratio-3,  $d/c = 0.141$ .

The models were tested in Langley tank No. 2 at speeds between 20 and 80 fps and in the high-speed facility at speeds up to 180 fps. All force and moment coefficients obtained in the ventilated condition were found to be independent of speed. It may be seen that the experimental lift coefficients obtained were in excellent agreement with the theory.

In Fig. 13 the theory is compared with experimental data obtained on the four models at an angle of attack of 20 degrees operating ventilated for a range of depths of submersion. Again the theory is in excellent agreement with the data. It should be noted that the depth of submersion over the range of  $d/c$  from 0 to 1.0 has only a small effect on the value of  $C_L$ , particularly for the highly cambered model 3. The greatest influence of depth is found for the flat plate where the lift coefficient at zero depth is about 25% greater than that calculated for the infinite depth.

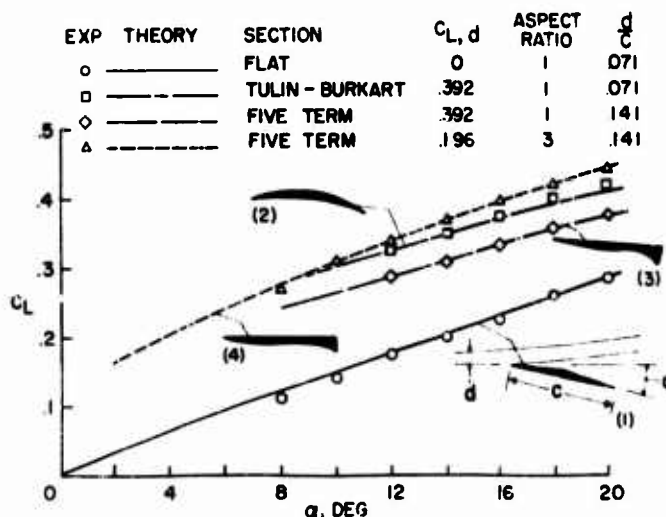


Fig. 12 - Lift coefficients of four low-aspect-ratio hydrofoils

# Supercavitating Hydrofoils Operating at Zero Cavitation Number

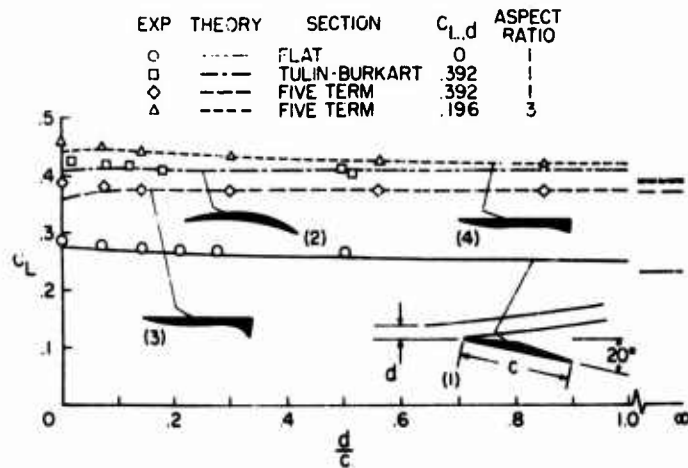


Fig. 13 - The influence of depth of submersion on the lift coefficient of four low-aspect-ratio hydrofoils ( $\alpha = 20$  degrees)

**Drag**—In Fig. 14 the drag coefficients of the four models obtained from experiment are compared with the theoretical values computed from equation (68). The agreement is excellent except for the highly curved model 3. The deviation between theory and experiment for model 3 is attributed to the inability of the linearized theory to accurately predict the pressure distribution when the camber is so gross. On a shape such as the five-term section only a small error in pressure distribution can greatly influence the drag without appreciably affecting the lift.

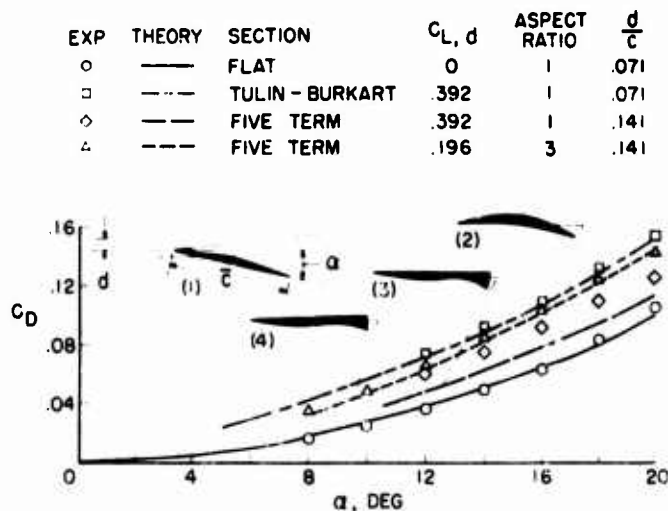


Fig. 14 - Drag coefficient of four low-aspect-ratio hydrofoils (excluding friction)

**Center of Pressure**—In Fig. 15 a comparison is made between the centers of pressure determined from Eq. (73) and those obtained experimentally on the four models. The theory is in good agreement with the data obtained on models 1 and 2, and about 10% too low on models 3 and 4.

#### LOCATION OF UPPER CAVITY STREAMLINE

The desirability of operating as near the design lift coefficient as possible is obvious from Fig. 4. Therefore, the minimum angle at which a hydrofoil with a finite thickness can operate with a cavity from the leading edge is needed. The angle can be determined by determining the location of the upper cavity streamline. The minimum angle at which this upper cavity streamline clears the upper surface of a hydrofoil of finite thickness is the angle desired. An approximate solution for the location of the cavity streamline is derived in the following analysis.

#### Two-Dimensional Theory-Arbitrary Depth

**Green's Exact Solution for Flat Plate**—The equation of the upper cavity streamline for a two-dimensional flat plate may be obtained from the solution of Green as

$$x = \frac{1}{(b - \cos \psi)} \left[ \cos \psi (t - 1) - (1 - b \cos \psi) \ln \frac{t - b}{b - 1} \right] \quad (74)$$

$$t = \frac{\sin \psi}{(b - \cos \psi)} \left[ t^2 - 1 + b \ln (t + t^2 - 1) - b^2 - 1 \ln \left( \frac{b t - 1 + b^2 - 1}{t - b} (t^2 - 1) \right) \right] \quad (75)$$

where  $x$  is distance from the leading edge along the plate,  $\psi$  is the perpendicular distance from the lower surface of the plate to the cavity streamline, and  $\psi$  is the spray

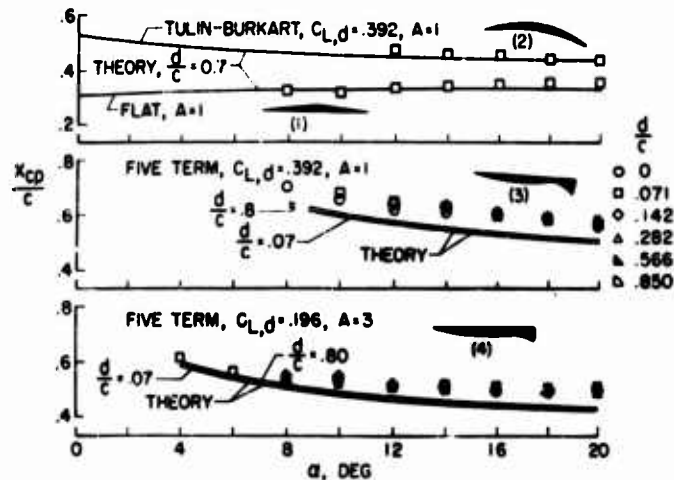


Fig. 15 - Location of center of pressure for four low-aspect-ratio hydrofoils

thickness. For a selected value of  $\alpha$ ,  $b$  is known from Eq. (2b). Thus  $\eta$  or  $\eta/c$  for a given  $x/c$  may be obtained by using the equations

$$\frac{x}{c} = \frac{x}{c} + \frac{1}{2} \left( \frac{\eta}{c} \right)^2 + \frac{1}{2} \left( \frac{\eta}{c} \right)^2 \quad (76)$$

and Eq. (75) for various values of the parameter  $\alpha$ . The cavity streamline computed in this manner for several angles of attack and spray-thickness-to-chord ratios are presented in Fig. 16. The subscript  $A_0$  on  $(\eta/c)_{A_0}$  is to indicate cavity ordinate due to angle of attack. It can be seen in Fig. 16 that for finite depths the cavity streamline rapidly approaches a straight line. The angle between this line and the plate is denoted as  $\beta$  and is given in Ref. 4 as

$$\beta = \frac{b \cos \alpha - 1}{b + \cos \alpha} \quad (77)$$

The magnitude of  $\beta$  is shown for each streamline in Fig. 16. In Fig. 10 it may be seen that the cavity ordinate varies almost linearly with angle of attack for angles less than about 8 degrees. The value of  $(\eta/c)_{A_0}$  or more generally  $(\eta/c)_{A_0}/A_0$  can be readily obtained and is given in Fig. 17. The value of  $(\eta/c)_{A_0}/A_0$  for infinite depth is the same as the linearized result obtained in Ref. 1. Figure 17 shows that the cavity ordinates at a depth of about 0.5 chord are nearly twice as great as those obtained at infinite depth.

**The Linearized Solution for Cambered Sections**—In order to determine the cavity ordinates for a cambered section it is necessary to use the rigorous linearized solution previously discussed in the section on forces and moments. The problem of obtaining the hydrofoil cavity ordinates is simple in principle. All that is required is to find the vertical velocity perturbations  $v(x/c)$  ahead of the equivalent airfoil shown in Fig. 6. The value of  $v$  is needed because from it the value of  $\eta$  on the hydrofoil cavity streamline can be found. Since the linearized slope of the cavity streamline  $dy/dx$  is  $v/V$ , the shape of the cavity is determined.

The procedure for determining the vorticity distribution on the airfoil is exactly the same as the first three steps given in the procedure for determining the linearized solution for the forces and moments. The value of  $v(x/c)$  can be determined by integrating the increments of  $v$  induced at a point  $-x/c$  due to the distributed vorticity given by Eqs. (10) and (11). Obviously this integration becomes very complicated, particularly if there are many terms in  $A_n \sin n\alpha$ . The problem can be simplified however by dividing the velocity  $v$  into two parts,  $v_{A_0}$  and  $v_c$ , where  $v_{A_0}$  is the component contributed by the first term  $A_0 \cot \alpha/2$ , and  $v_c$  the component contributed by the camber terms,  $A_n \sin n\alpha$ . Thus the final nondimensional cavity ordinates  $\eta/c$  will be broken down into two components  $(\eta/c)_{A_0}$  and  $(\eta/c)_c$  such that

$$\eta/c = (\eta/c)_{\text{total}} = (\eta/c)_{A_0} + (\eta/c)_c \quad (78)$$

The distance  $\eta$  is measured from the reference line of the section along a line normal to the reference line. There are two advantages to dividing the vorticity into its angle of attack and camber components. First, the value of  $(\eta/c)_{A_0}$  is known from Green's solution and has been given in Fig. 16. The linearized version is shown in Fig. 17. Thus, half the job is done if  $A_0$  is known or can be determined.

It is now important to review the meaning of the coefficient  $A_0$ . The angle of attack is measured from the orientation which makes  $A_0 = 0$  when the depth is infinite. At this orientation and infinite depth

$$A_0' = -\frac{1}{\pi} \int_0^\pi \frac{dy}{dx} d\theta = 0 \quad (79)$$



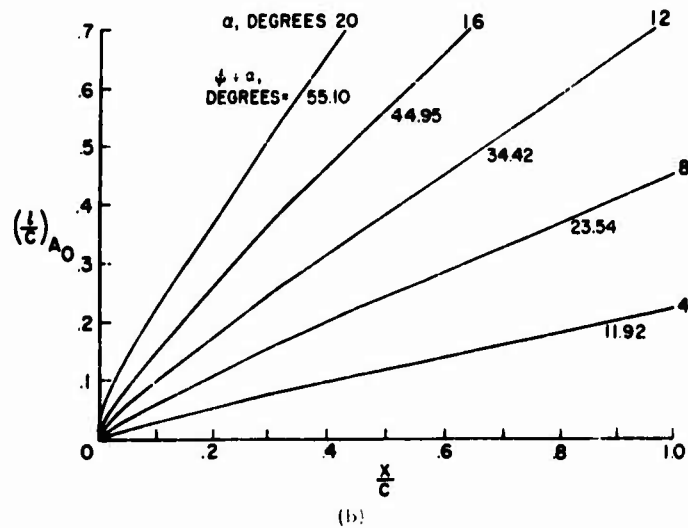
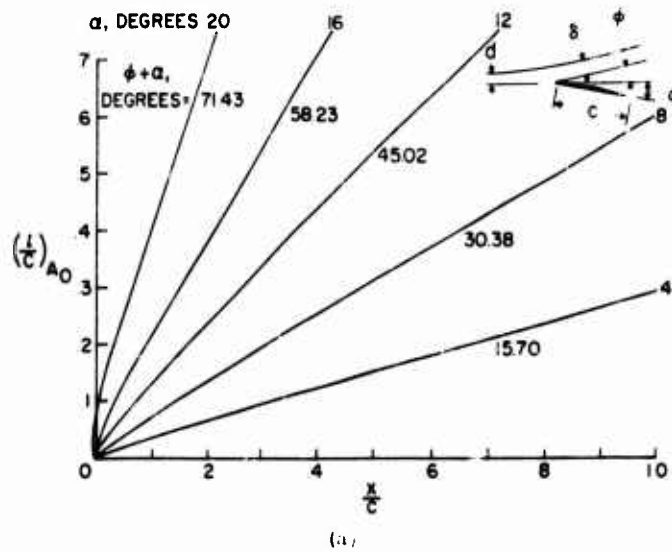
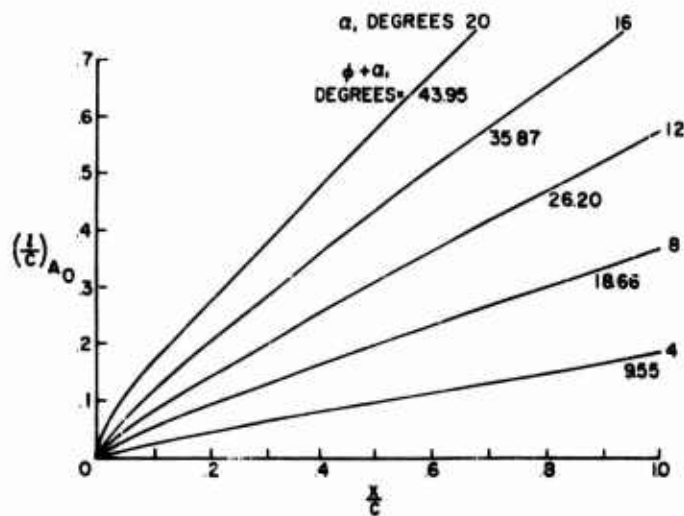
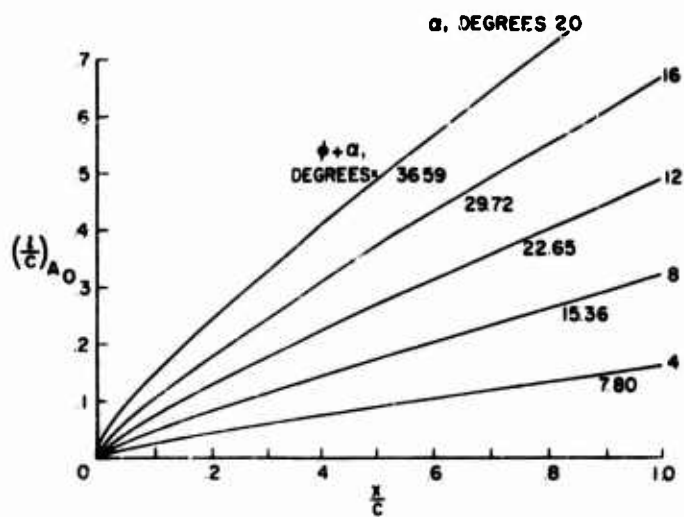


Fig. 16 - Green's solution for the upper cavity streamline of a flat plate. (a)  $\delta/c = 0.25$ , (b)  $\delta/c = 0.50$ , (c)  $\delta/c = 1.0$ , (d)  $\delta/c = 2.0$ , (e)  $\delta/c = 5.0$ .

Supercavitating Hydrofoils Operating at Zero Cavitation Number



(c)



(d)

Fig. 16 (Continued) - Green's solution for the upper cavity streamline of a flat plate. (a)  $\delta/c = 0.25$ , (b)  $\delta/c = 0.50$ , (c)  $\delta/c = 1.0$ , (d)  $\delta/c = 2.0$ , (e)  $\delta/c = 5.0$ .

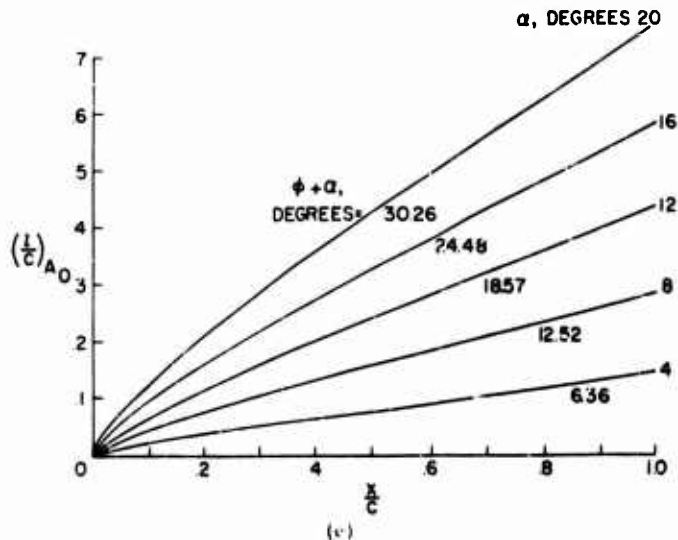


Fig. 16 (Continued) - Green's solution for the upper cavity streamline of a flat plate. (a)  $\delta/c = 0.25$ , (b)  $\delta/c = 0.50$ , (c)  $\delta/c = 1.0$ , (d)  $\delta/c = 2.0$ , (e)  $\delta/c = 5.0$ .

and for angles of attack measured from this reference orientation,  $A_0 = 0$ . However if the angle of attack is measured from this reference line at finite depths it is found that the value of  $A_0' \neq 0$ . This means that at finite depths there is an induced angle of attack  $A_0'$  due to the camber. The magnitude of  $A_0'$  is directly proportional to the slope of the foil and thus to  $C_{L,cl}$ . The calculated value of  $A_0' / C_{L,cl}$  is given in Fig. 18 for the four sections of interest for a range of depth-chord ratios. To obtain the value of  $(1/c)A_0$ , one obtains  $A_0'$  from Fig. 18 and  $A_0$  by adding  $\alpha$ ; that is,  $A_0 = \alpha + A_0'$ . Then  $(1/c)A_0$  is obtained from Fig. 16 or 17.

The second reason for dividing the vorticity distribution into the  $A_0$  and camber contributions is that the  $A_0 \sin n$  contribution usually has only small strength near the leading edge. In fact for low-drag sections, it is desirable to distribute the vorticity as near the trailing edge as possible. Thus the velocity induced at points ahead of the airfoil due to the  $A_0 \sin n$  or camber contribution may be adequately approximated by concentrating the entire camber vorticity at one point, the center of pressure  $x_1$ , as shown in Fig. 19. The value of  $x_1$  is given by  $\bar{C}_m / \bar{C}_L$  or

$$x_1 = \frac{(A_0 + A_1 - \frac{A_2}{2})}{A_0 + \frac{A_1}{2}} \quad (80)$$

The strength of the singular vortex can be obtained from the equations

$$L_c = \rho V C_{L,c/2} V^2 = A_1 c \frac{1}{2} V^2.$$

Therefore

$$A_1 = 2cV \quad (81)$$

# Supercavitating Hydrofoils Operating at Zero Cavitation Number

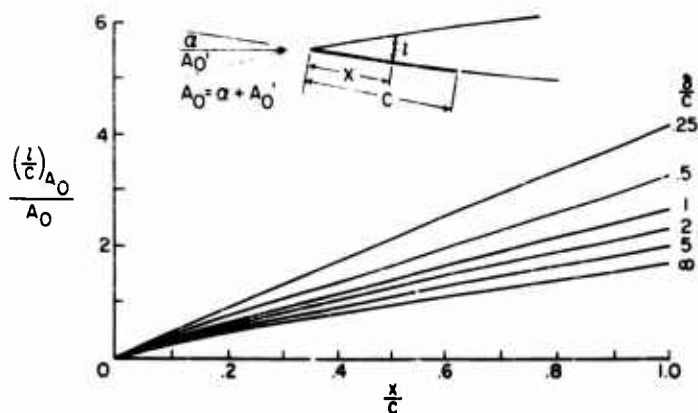


Fig. 17 - The linearized solution for cavity ordinates due to angle of attack

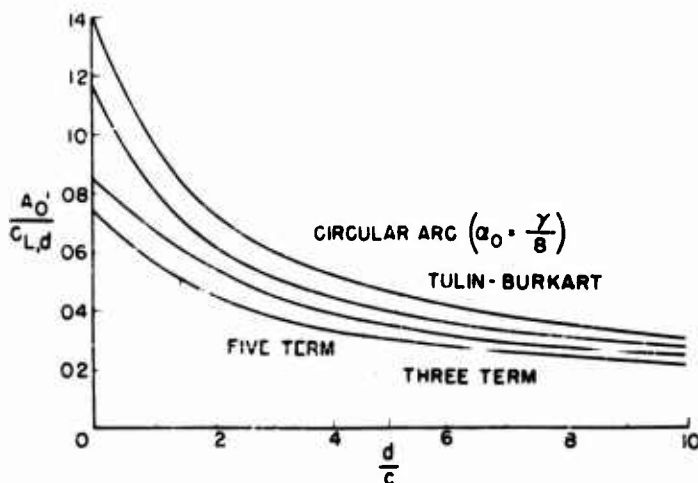


Fig. 18 - The influence of depth of submersion on the angle of attack induced by camber

The velocity induced at a point on the  $x$  axis due to  $c$  is therefore

$$v = \frac{c}{2} \frac{A_1}{(a-c-x)} = \frac{c}{2} \frac{A_1}{(a-x-c)} = \frac{c}{2} \frac{A_1}{(a-x-c)} \quad (82)$$

The velocity  $v$  in front of the airfoil at a point  $-x/c$  is exactly the same as  $v$  on the cavity streamline if the relationship between  $-x/c$  and  $x/c$  given in Fig. 7 is maintained. Thus  $v = V$  and therefore the slope of the cavity streamline due to camber  $dy/dx (x/c)$  is known. Integrating  $dy/dx$  from the leading edge to a point  $x/c$  gives

$$\left( \frac{y}{c} \right) = \int_0^{x/c} \frac{dy}{dx} \left( \frac{x}{c} \right) d \left( \frac{x}{c} \right) \quad (83)$$

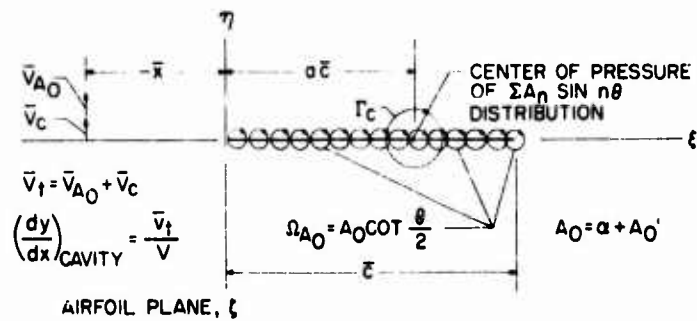


Fig. 19 - Linearized model for calculating upper cavity streamline at arbitrary depth

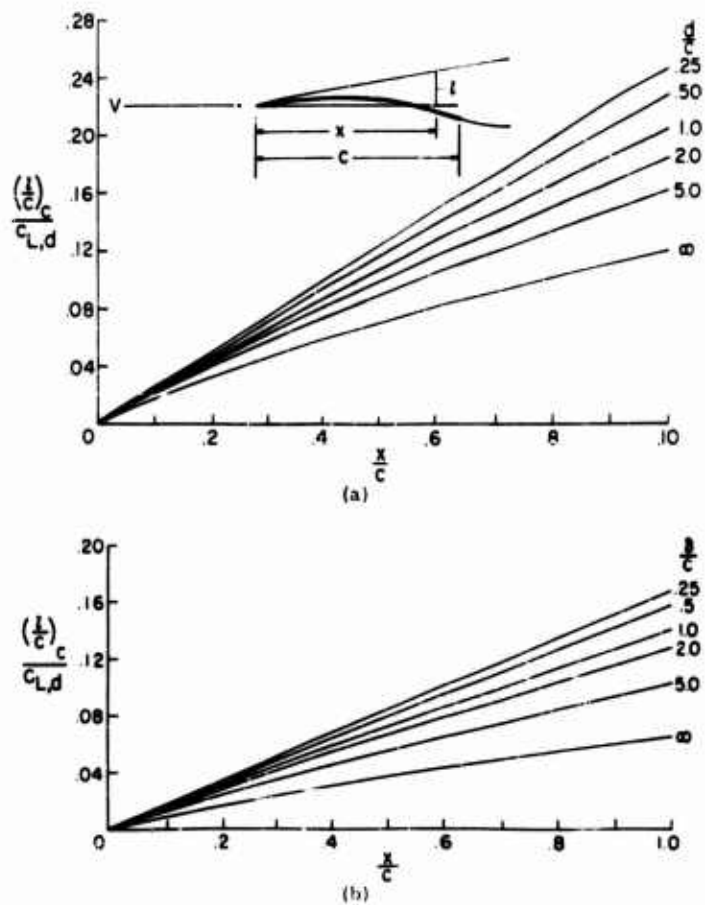


Fig. 20 - The influence of depth of submersion on the cavity ordinates due to camber: (a) circular-arc hydrofoil ( $z_0 = 8$ ), (b) Tulin-Burkart hydrofoil

Therefore, since  $dy/dx = (x/c) \sqrt{v/v_c}$ , and  $v = v_c$ , combining Eqs. (82) and (83) gives

$$\left(\frac{y}{c}\right)_c = \frac{A_1}{4} \int_0^{x/c} \left(1 - \frac{x}{c}\right) dx \quad (84)$$

where  $x/c$  takes on negative values and the relationship between  $-x/c$  and  $x/c$  is found in Fig. 7. Since  $C_{L,d}$  is a function of  $A_1$ , then  $(y/c)_c C_{L,d}$  can be determined from Eq. (83). The magnitude of  $(y/c)_c C_{L,d}$  as a function of the depth/chord ratio is presented in Fig. 20 for the four sections of interest. Thus the total ordinates of the upper cavity streamline are obtained for the two-dimensional hydrofoil operating at zero cavitation number and arbitrary depth by using Figs. 16, 18, and 20 and Eq. (78).

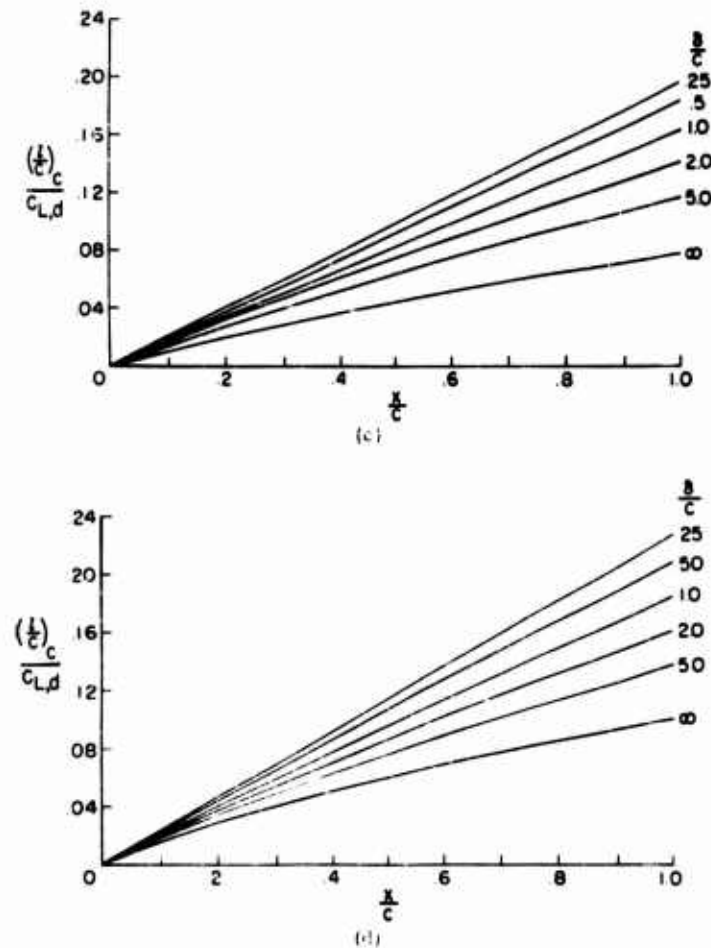


Fig. 20 (Continued) - The influence of depth of submerison on the cavity ordinates due to camber: (c) three-term hydrofoil, (d) five-term hydrofoil

## Correction for Finite Aspect Ratio

Equation (82) shows that the cavity ordinates are directly proportional to the circulation on the equivalent airfoil and thus the circulation of the hydrofoil. Therefore, if the hydrofoil circulation is reduced from its two-dimensional value by finite span, the cavity ordinates must also reduce. Another argument for this decrease in cavity ordinates is that if the two-dimensional drag coefficient is reduced because of finite aspect ratio the maximum cavity thickness must also decrease as pointed out in Ref. 17. It is now assumed that for finite aspect ratios the cavity ordinates will be reduced from the two-dimensional value in proportion to the reduction in  $C_{L,1}$ . This reduction occurs in two places, first because of the reduced angle  $\alpha_i$  and because of the reduced lift-curve slope  $m$ . More specifically, assuming the cosine terms are about equal to unity, the first term of Eq. (67) can be written as

$$C_{L,1} = \frac{A}{A+1} m_{(\alpha+\alpha_c-\alpha_i)} (\alpha-\alpha_i) + \frac{A}{A+1} m_{(\alpha+\alpha_c-\alpha_i)} \alpha_c \quad (85)$$

where the subscripts on  $m$  indicate the angle at which  $m$  is determined on Fig. 2. If  $\alpha_c$  is broken into two components  $A'_0$  and  $\alpha'_c$ , that is,  $\alpha_c = A'_0 + \alpha'_c$ , Eq. (85) becomes

$$C_{L,1} = \frac{A}{A+1} m_{(\alpha+\alpha_c-\alpha_i)} (\alpha + A'_0 - \alpha_i) + \frac{A}{A+1} m_{(\alpha+\alpha_c-\alpha_i)} \alpha'_c \quad (86)$$

The value of the cavity ordinates at infinite aspect ratio and angle  $\alpha + A'_0 - \alpha_i$  is

$$(\alpha'_c)_{total} = (\alpha'_c)_{(A_0-\alpha_i)} + (\alpha'_c)_c \quad (87)$$

where  $(\alpha'_c)_{(A_0-\alpha_i)}$  is determined from the nonlinear solution of Green and  $(\alpha'_c)_c$  from the linearized theory. Therefore the effective lift-curve slope at infinite aspect ratio and angle  $A_0 - \alpha_i$  is  $m_{(A_0-\alpha_i)}$  for the first term in Eq. (87) and  $m_{(\alpha=0)}$  for the second term. Thus at finite aspect ratio the corrected cavity ordinates are

$$(\alpha'_c)_{total} = \frac{A}{A+1} \frac{m_{(\alpha+\alpha_c-\alpha_i)}}{m_{(A_0-\alpha_i)}} (\alpha'_c)_{(A_0-\alpha_i)} + \frac{A}{A+1} \frac{m_{(\alpha+\alpha_c-\alpha_i)}}{m_{(\alpha=0)}} (\alpha'_c)_c \quad (88)$$

or

$$(\alpha'_c)_{total} = R_{A_0} (\alpha'_c)_{(A_0-\alpha_i)} + R_c (\alpha'_c)_c \quad (89)$$

where

$$R_{A_0} = \frac{A}{A+1} \frac{m_{(\alpha+\alpha_c-\alpha_i)}}{m_{(A_0-\alpha_i)}}$$

$$R_c = \frac{A}{A+1} \frac{m_{(\alpha+\alpha_c-\alpha_i)}}{m_{(\alpha=0)}}$$

The preceding analysis assumes that the induced angle  $\alpha_i$  is constant over the span. Since  $\alpha_i$  actually varies over the span, except for the case of elliptic loading, the cavity ordinates will also vary over the span. This effect can be included by using the appropriate spanwise distribution of  $\alpha_i$  determined from finite span airfoil theory (14). Also the influence of the crossflow component of flow on the cavity ordinates has been assumed to be negligible. However, near the tips the cavity shape is largely determined by the crossflow. For example, at zero aspect ratio the cavity is entirely determined by crossflow. Thus, it seems that the true cavity shape is determined at the tips by the crossflow and at the center by the main flow; the cavity shape in between is some transition between the two extremes.

## Comparison Between Theory and Experiment

Figure 21a shows an aspect ratio one flat plate operating at a depth of 0.05 chord and an angle of attack of 16 degrees. The plate had 3 pins located along the span so that the upper ends of the pins were 0.34 chords rearward of the leading edge and 0.17 chords from the lower surface of the plate. These pins were spaced 0.021, 0.198, and 0.375 chords from the right tip of the plate. From the photograph the cross section of the cavity may be estimated as shown by the solid line in Fig. 21b. The horizontal dashed line is the calculated location based on a uniform distribution of  $\alpha_i$ . The other dashed curve is the calculated streamline assuming the airfoil induced angle distribution for a rectangular plan form (14). It may be noted that near the tips the cavity shape is primarily due to crossflow, whereas near the center the calculated value based on the more nearly exact distribution of induced angle of attack is nearly correct if the draw-down due to the strut is overlooked. The cavity shape based on uniform induced angle distribution is about 20 percent too low.

In Fig. 22 the calculated cavity shapes based on uniform  $\alpha_i$  are presented for two aspect-ratio-one hydrofoils operating at  $d/c = 0.5$ . It may be seen in Fig. 22a that for the flat plate the calculated streamline at an angle of attack of 4 degrees just touches the upper surface of the model. If it is assumed that the speed is sufficiently high so that no significant negative pressure coefficient can exist in the flow field, and if the forward portion of the upper surface is wetted and positive pressures occur, then the lift will decrease. Thus it may be concluded from the calculations that the maximum value of the lift/drag ratio for this flat plate hydrofoil should occur at the 4-degree angle of attack. Experimental data obtained at speeds up to 180 fps reveal that the forward portion of this flat-plate hydrofoil does become wetted at an angle of attack of about 4 degrees. The maximum lift/drag ratio also occurred at an angle of attack of about 4 degrees.

The hydrofoil section shown in Fig. 22b has a lower surface conforming to the Tulin-Burkart profile with  $C_{L,d} = 0.392$ . The details of the upper surface may be found in Ref. 3. The calculated location of the cavity streamline is shown for angles of attack of 4, 8, and 12 degrees. It may be noted that the calculated streamlines are almost identical with those shown in Fig. 22a for the flat plate. The reason that both foils have about the same theoretical cavity streamline location is peculiar to the

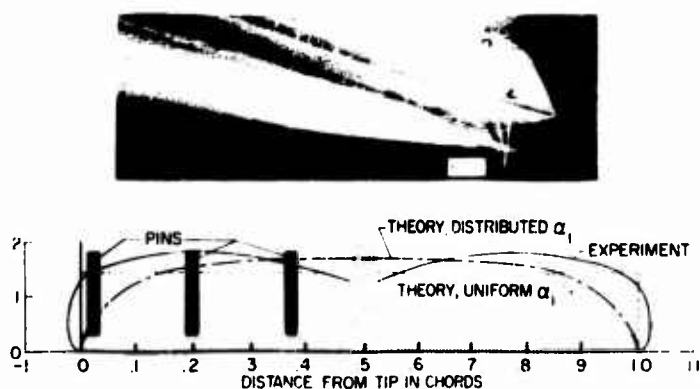


Fig. 21 - Cavity cross section for flat plate; aspect ratio, 1;  $d/c = 0.5$ ;  $\alpha = 16$  degrees: (a) view of ventilated flow, (b) section at 0.34 chord from leading edge



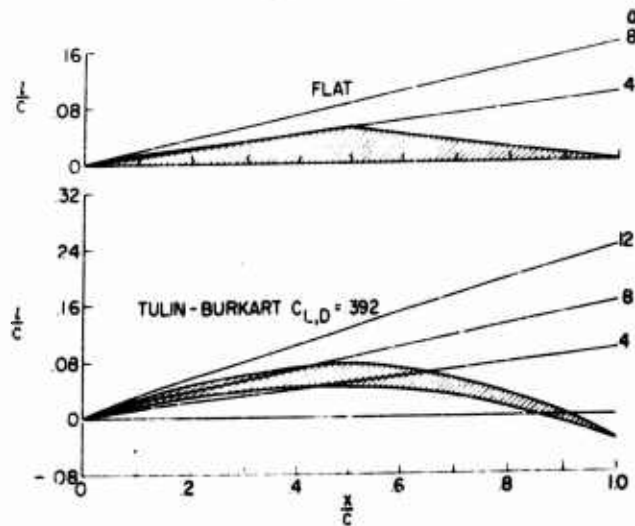


Fig. 22 - Calculated cavity shapes for flat and cambered models; aspect ratio,  $i$ ;  $d/c = 0.5$

aspect ratio of 1. There are two compensating effects due to camber which cause this similarity in streamlines. The cambered foil cavity ordinates are increased because of the foil curvature, but simultaneously the camber causes increased lift at a given angle which produces a greater induced angle of attack. The greater induced angle of attack results in a decrease in cavity ordinates, thus effectively cancelling out the increased ordinates contributed by the foil curvature. Experimental data on both foils were in agreement with this theoretical phenomenon; in fact, at a 20-degree angle of attack the flat-plate cavity streamline obtained from both theory and experiment was slightly higher than that obtained for the cambered model.

Figure 22b indicates that ventilation from the leading edge of the cambered model will not be possible at angles less than about 10 degrees. Experiments conducted in ventilated flow up to speeds of 180 fps were in excellent agreement with this prediction; that is, at angles less than 10 degrees the forward portion of the upper surface was wetted. However, the maximum lift/drag ratio of the cambered model occurred at an angle of attack of about 7 to 8 degrees. The fact that the lift/drag ratio continued to increase even with the upper surface wetted is attributed to the curvature of the upper surface and finite speed. At a speed of 175 fps it is possible to support a negative pressure coefficient as low as -0.07. Thus, it is possible at finite speeds for the upper surface to add to the lift and possibly decrease the drag. Theoretically at higher speeds the maximum lift/drag ratio will occur closer to the predicted 10-degree angle of attack.

#### THEORETICAL COMPARISON OF PRACTICAL LOW-DRAG SECTIONS

The experimental data given in the preceding section indicate that a reliable approximation to the cavity streamline location on high-speed moderate-aspect-ratio surfaces can be obtained theoretically. Using the theory developed, it is now possible to determine the best of the four section shapes (circular-arc, Tulin-Burkart, three-term, and five-term) when operating under practical conditions. The operating

condition chosen for comparison was at a depth of submersion of 1 chord and an aspect ratio of 3. The structural characteristics of the section were arbitrarily chosen as (a) thickness ratio  $t/c = 0.03$  at 0.2 chord from the leading edge and (b)  $t/c = 0.04$  at the chordwise location of the maximum lower surface ordinate. The leading edge and these control points were assumed to be connected by straight lines and the upper surface rearward of the latter control point was taken as parallel to the reference line of the section. Because of the almost uniform gradation of the various characteristics of the four sections, only the extremes, the circular-arc and five-term section, were compared.

Over the range of cambers from  $C_{L,d} = 0$  to 0.3, the calculated cavity streamlines first touched the upper surface of the assumed hydrofoil sections at the 0.2-chord control point. Thus the second point at the maximum lower surface ordinate did not influence the maximum lift/drag ratio of the sections. The friction drag coefficient was estimated to be 0.004. Using Eqs. (67) and (68), the lift and drag coefficients of the sections were calculated. A plot of lift/drag ratio versus lift coefficient is presented in Fig. 23. Also shown in Fig. 23 is the line denoting the minimum angle at which the control point at 0.2 chord just clears the calculated cavity streamline. The area above this line is shaded to indicate that these regions are not attainable under the design conditions. The important result shown by these plots is that either type of camber can give higher maximum lift/drag ratios than the flat plate. The optimum amount of camber for both hydrofoils correspond to a value of  $C_{L,d}$  of about 0.1. The optimum lift coefficient is about 0.175 for both sections. The hydrofoil cross sections shown in the top of Fig. 23 are for  $C_{L,d} = 0.1$  oriented at the minimum angle of attack revealed by the analysis. The analysis as presented in Fig. 23 also shows that the five-term section is superior to the circular arc. The maximum values of the lift/drag ratios are 10.5 and 9.5 for the five-term and circular-arc sections respectively. Although L/D of the five-term section is slightly higher than that of the circular arc, it is not twice as high as predicted from the two-dimensional theory.

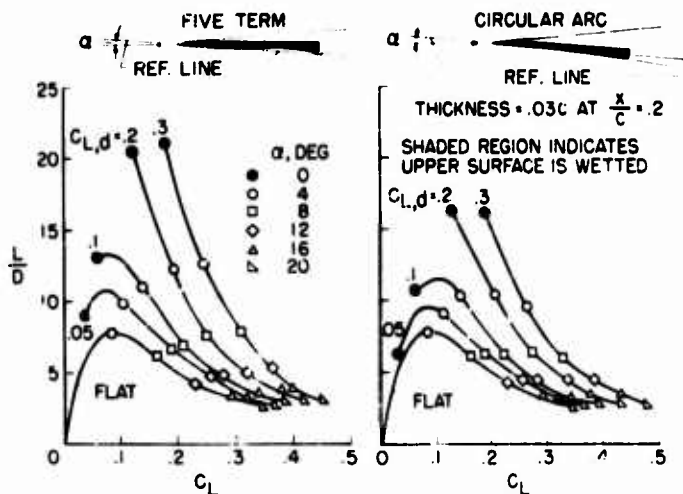


Fig. 23 - Theoretical lift/drag ratios of five-term and circular-arc hydrofoils; aspect ratio, 3;  $d/c = 1.0$

The thickness distribution chosen for the analysis is not conservative, but a bare minimum. Structurally, an aspect ratio of 3 is close to the maximum when the hydrofoil is supported by a single strut. Therefore, the calculated maximum lift/drag ratio of about 10 at a lift coefficient of 0.18 is very near the optimum that can be obtained on a single supercavitating hydrofoil supported on one strut and operating at zero cavitation number. More severe structural requirements than those imposed in the present analysis will reduce the maximum attainable lift/drag ratio.

#### CONCLUDING REMARKS

In conclusion, it may be stated that the concept of combining the linearized effects of camber with nonlinear flat-plate theory has proved satisfactory. The results of a comparison of this theory, corrected for aspect ratio, with experimental data obtained on four low-aspect-ratio sections may be summarized as follows.

1. The theoretical lift coefficient was in excellent agreement with experimental data.
2. The theoretical drag coefficient was in excellent agreement with experimental data on all models except the highly cambered five-term section whose  $C_{L,d} = 0.392$ . The disagreement is attributed to the inability of linearized theory to accurately predict the pressure distribution when the curvature is very great.
3. The theory predicts centers of pressures slightly low for the five-term section; however, the agreement may be improved by taking the center of pressure of the crossflow component rearward of the mid-chord.
4. Theoretical cavity shapes based on a uniform induced angle of attack are in good enough agreement with experiment to warrant their use in engineering calculations.

Using the theory presented and selecting sections of similar structural geometry, it is shown that the highest lift/drag ratio that can be obtained on a ventilated hydrofoil supported by a single strut at depths of 1 chord or more is about 10. The best section for optimum lift/drag ratio is the five-term design; however, the camber profile may range from the five-term to the circular arc with only about a 10 percent change in the maximum lift/drag ratio.

#### REFERENCES

1. Tulin, M.P., and Burkart, M.P., "Linearized Theory for Flows About Lifting Foils at Zero Cavitation Number," Rept. C-638, David W. Taylor Model Basin, Navy Dept., Feb. 1955
2. Johnson, V.E., Jr., "Theoretical Determination of Low-Drag Supercavitating Hydrofoils and Their Two-Dimensional Characteristics at Zero Cavitation Number," NACA RM L57G11a, 1957
3. Johnson, V.E., Jr., "Theoretical and Experimental Investigation of Arbitrary Aspect Ratio, Supercavitating Hydrofoils Operating Near the Free Water Surface," NACA RM L57I16, 1957
4. Green, A.E., "Note on the Gliding of a Plate on the Surface of a Stream," Proc. Cambridge Phil. Soc. XXXII(pt. 2):248-252 (May 1936)

Supercavitating Hydrofoils Operating at Zero Cavitation Number

5. Shuford, C.L., Jr., "A Theoretical and Experimental Study of Planing Surfaces Including Effects of Cross Section and Plan Form," NACA TN 3939, 1957
6. Perry, B., "Experiments on Struts Piercing the Water Surface," Rept. E-55.1 (Contract N123s-91875), C.I.T., Hydrod. Lab., Dec. 1954 (available from ASTIA as AD No. 56179)
7. Eisenberg, P., "On the Mechanism and Prevention of Cavitation," Rept. 712, David W. Taylor Model Basin, Navy Dept., July 1950
8. Wadlin, K.L., Ramsen, J.A., and Vaughan, V.L., Jr., "The Hydrodynamic Characteristics of Modified Rectangular Flat Plates Having Aspect Ratios of 1.00, 0.25, 0.125 and Operating Near a Free Water Surface," NACA Rep. 1246, 1955 (supersedes NACA TN's 3079 by Wadlin, Ramsen, and Vaughan and 3249 by Ramsen and Vaughan)
9. Lamb, H., "Hydrodynamics," reprint of sixth ed. (first American ed.) Dover Publications, 1945
10. Milne-Thompson, L.M., "Theoretical Hydrodynamics," 2nd ed., MacMillan and Co., Ltd., 1949
11. Rosenhead, L., "Resistance to a Barrier in the Shape of an Arc of Circle," Proc. Roy. Soc. (London) A117(No. 777):417-433 (Jan. 2, 1928)
12. Wu, T. Yao-tsu, "A Free Streamline Theory for Two-Dimensional Fully Cavitated Hydrofoils," Rept. 21-17 (Contract N6onr-24420), C.I.T., Hydrod. Lab., July 1955
13. Wagner, H., "Planing of Watercraft," NACA TM 1139, 1948
14. Glauert, H., "The Elements of Airfoil and Airscrew Theory," 2nd ed., Cambridge Univ. Press, 1917 (reprinted 1948)
15. Jones, R.T., "Correction of Lifting Line Theory for the Effect of the Chord," NACA TN 817, 1941
16. Flax, A.H., and Lawrence, H.R., "The Aerodynamics of Low-Aspect Ratio Wings and Wing-Body Combinations," Rept. CAL-37, Cornell Aero. Lab., Inc., Sept. 1951
17. Tulin, M.P., "Supercavitating Flow Past Foils and Struts," Proceedings of a Symposium on Cavitation in Hydrodynamics, National Physical Laboratory, Sept. 14-17, 1955

\* \* \* \* \*

# DISCUSSION

D. Savitsky (Stevens Institute of Technology)

I would like to congratulate Mr. Johnson on accomplishing a most clever combination of established aerodynamic and hydrodynamic results to develop practical solutions for a most difficult hydrodynamic problem. As is typical for semi-empirical approaches, the approximations used can often times be questioned and more refined approximations suggested. However, the choice is usually the author's to make and if the calculated results agree with data then he's chosen correctly.

Working within the framework developed by Mr. Johnson, I would like to address myself to the subject of the two-dimensional cavity shape associated with the design lift coefficient at various depths of submersion. The design lift coefficient is, as usual, that existing for the "shock-free" entry condition. The study of the cavity shape is, by far, the most pressing one since the intersection of the cavity with the foil's upper surface is the strongest obstacle in the way to achieving the very high lift-drag ratios which are potentially possible with super-cavitating hydrofoils.

In Fig. 20 of Mr. Johnson's paper a plot is shown of the influence of depth of submersion on the cavity ordinates due to the circulation developed by a cambered foil when operating with shock-free or design lift coefficient at infinite draft. It is seen in Fig. D1 that for a fixed value of circulation the cavity opens up as the free water surface is approached. Now it can be shown from Johnson's work that the design angle (shock-free) of attack for a given cambered section decreases with decreasing submersion while the design lift coefficient remains essentially constant. Using this result then, Fig. D1 can be interpreted as representing the cavity shape relative to the horizon when a given circular-arc hydrofoil is maintained at a constant design lift coefficient by reducing the geometric chord line angle of attack when approaching the free-surface. Superposed on Fig. D1 is a circular arc hydrofoil

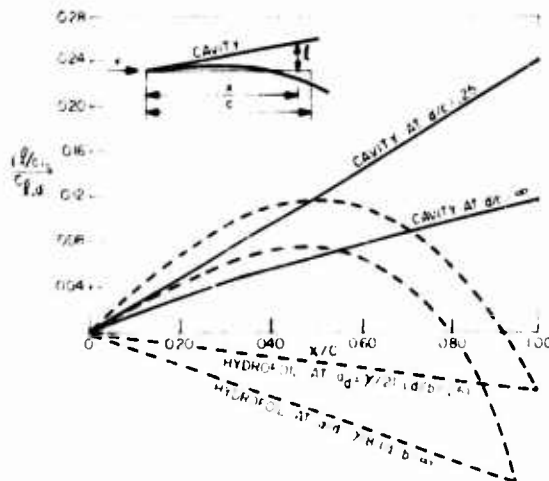


Fig. D1 - Cavity ordinates for circular-arc hydrofoil--Johnson's results

## Supercavitating Hydrofoils Operating at Zero Cavitation Number

oriented to the design angle of attack for  $d/c = 1$  and  $d/c = .25$ . It is seen that the intersection of the cavity with the hydrofoil is, within engineering accuracy, very nearly the same for the entire range of submersion.

Figure D2 shows the collapsed results and points up that the cavity interaction with the hydrofoil can be represented by one curve for all depths of submersion when the foil is maintained at design lift coefficient. In effect then, while the cavity does open up as the free-surface is approached, we rotate the foil into the cavity as the geometric angle of attack is decreased to maintain the design lift coefficient.

Hence, the problem of the cavity shape is equally obstructive at all drafts and whatever can be done to alleviate the cavity interference problem at one draft should probably hold at other drafts.

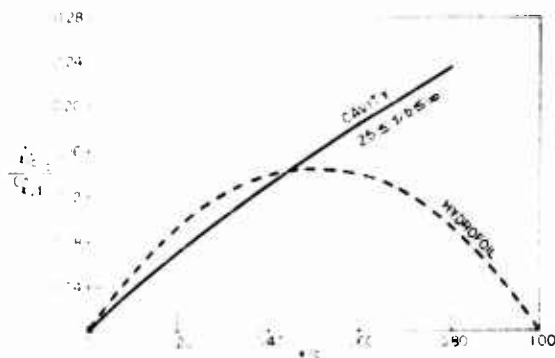


Fig. D2 - Cavity ordinates for circular-arch hydrofoil--collapsed results for hydrofoil at design angle of attack corresponding to each draft

M. C. Eames (Naval Research Establishment, Halifax)

I think I am correct in saying that Mr. Johnson's paper presents more information of use to the practical designer than can be found in any single paper on conventional hydrofoils. That this has been accomplished so rapidly in this new field of supercavitating hydrofoils is a remarkable achievement.

I would like to supplement Mr. Johnson's introduction from the point of view of the surface ship - as opposed to that of the aircraft.

It is well known that the limit on speed resulting from cavitation on conventional hydrofoils implies a corresponding size limit due to the so-called "square-cube" law. That is to say, as the size of craft is increased, retaining a constant design speed, the required size of the hydrofoils increases rapidly, and the weight associated with the hydrofoils soon becomes a prohibitive proportion of the total displacement.

Attempts at delaying cavitation to higher speeds are of limited value because they imply lower lift coefficients, and hence, again, large hydrofoils.

Thus to the surface ship designer, the successful development of supercavitating hydrofoils offers the possibility - at least - of radical increases in the size of vessel for which hydrofoil support is feasible. There will be serious engineering problems involved in the design of large hydrofoil ships, but there no longer appears to be any fundamental objection to increasing size.

Undoubtedly the most important contribution made by the NACA work is the concept of using a fully-ventilated cavity. Prior to this development, three regimes of design were recognized. Below a speed of about 40 knots, cavitation presented no problems provided reasonable lift coefficients were used, and it is fair to say that no problems remain in the design of hydrofoil craft up to this order of speed - accepting the size limitations that I have referred to. By careful foil selection it is possible to delay the onset of cavitation to about 60 knots, still retaining reasonable lift coefficients, but in this regime difficulties begin to be encountered in rough water. This is because the range of angle of attack over which cavitation free operation can be obtained is very limited. Moreover, with the type of section required here, the onset of cavitation is not a gradual process, but can be as sudden and abrupt as complete ventilation.

Above 60 knots it was thought that super-cavitation would take over. At this speed a fully developed vapour cavity would be feasible, but there remained the problem of ensuring that this would not ventilate.

Mr. Johnson's solution to this problem—refusing to solve it—is one of those delightfully simple touches that characterize a major technical breakthrough. Not only does the "super-ventilating" foil, if I may use this term, solve the problem of stabilizing the cavity in the presence of a free surface, but it also means that the transition from conventional to super-cavitating operation can be made at a much lower speed. It is likely that the troublesome "cavitation delaying" hydrofoils required for operation in the 40-60 knot range have no place in future developments.

As many of you will be aware, the Naval Research Establishment in Halifax has been concerned with the development of hydrofoil craft in the 40-60 knot range of speeds, and this new concept is therefore of very great interest to us.

In the course of our work, in addition to the R-100 "Massawippi" and R-103 "Bras d'Or" hydrofoil craft, which have received a fair amount of publicity, we have developed a new research vehicle, known as the "R-X", which we intend to use for an investigation into the practical application of "super-ventilating" foils for surface craft.

The new R-X is not intended to represent a scale model of any possible operational prototype. It was designed as a basic research vehicle with the capability of exploring a wide range of hydrofoil configurations and types. A full description is out of place here, but it is felt that some of the unusual features which make this craft particularly suitable for fundamental studies will be of interest.

Figure D3 provides a general view of the 3-ton boat. The important feature of the 25-foot plywood hull is the aluminum rail (A) which runs the full length of each gunwale. By means of a slide attachment the main foil mounting structure (B) can be positioned at any point on the length of the hull. In Fig. D3, a three-point, two-leading, configuration is shown fitted. For a four-point, or tandem, configuration a second identical structure can be mounted aft.

Figure D4 shows a close-up of one of the main foil units. The mounting structure consists of a rigid athwartships beam (C), which is pivoted to the gunwale slides (D)

Supercavitating Hydrofoils Operating at Zero Cavitation Number

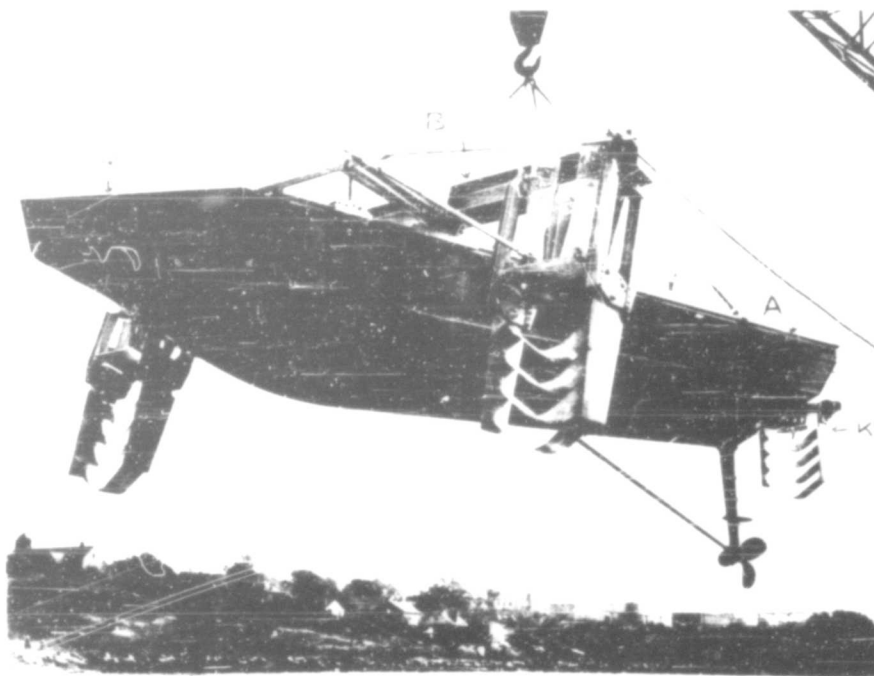


Fig. D3 - The R-X research craft

port and starboard. Change of rake or fine adjustment of incidence can be accomplished by means of a screw thread (E). Rigid cantilevers (F) can be clamped to the beam in any athwartships position thus providing for alteration of foil track, and of the span of individual foil units. The frames (G) which carry the foil struts are connected to the rigid cantilevers (F) only by way of dynamometer elements (H). There are four such elements to each strut, enabling lift, drag and cross force to be independently measured and recorded. This, and other instrumentation is currently being developed.

For three-point configurations, the stern unit (Fig. D3, K) is mounted on a telescopic tube fitted into the stern of the hull. By this means the fore and aft position of the stern unit can be varied over a distance of 5 feet. This is sufficient to investigate configurations in which the stern foil supports between 10 percent and 33 percent of the all-up weight without changing the foil base length. Figure D5 is a close-up of the stern unit, showing the telescopic tube (L), the steering bearings (M) and the mounting beam (N). The foil struts are attached by clamps (O), thus allowing for units of different span, while the beam (N) can be tilted for adjustment of rake or incidence by a screw thread device not visible in this view. The beam assembly is attached to the steering bearings only by way of four dynamometer elements (P).

For three point, one-leading, or "canard," configurations the telescopic tube can be removed from the stern of the craft, and fitted in the bow. This necessitates



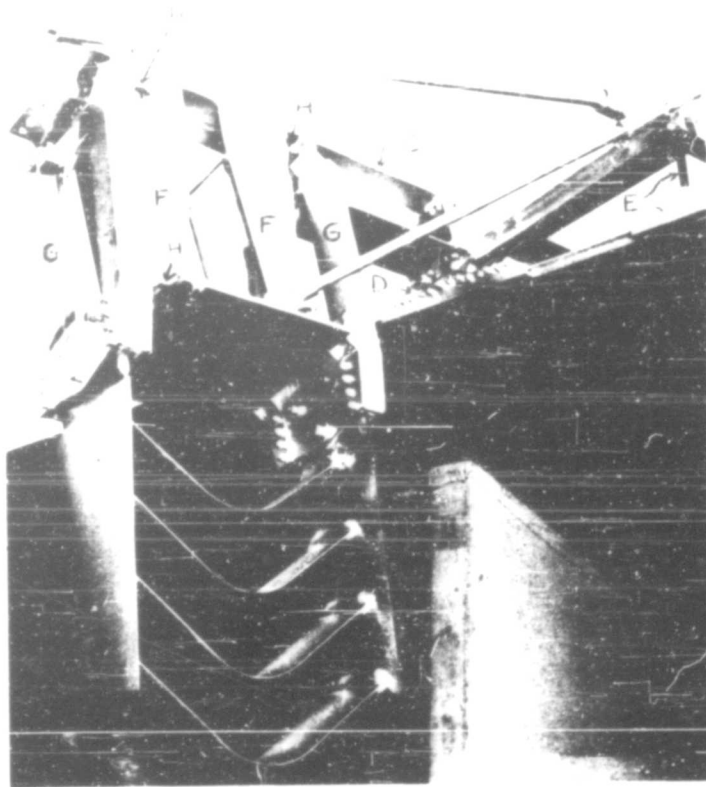


Fig. D4 - One of the main foil units

removal of the false bow (Fig. D3, Q), and steering would then be accomplished by turning the bow unit. The same mounting structure is used for the bow unit.

The craft is being powered by conventional means to provide a speed of at least 40 knots with a minimum lift-to-drag ratio of 5; instrumentation will include the recording of thrust, torque, r.p.m., pitch, roll, vertical accelerations and foil unit forces on a time base. A strut unit for measuring altitude, speed and angle of yaw is also being developed.

It is felt that the versatility of this craft is unique and that although "teething troubles" will no doubt be encountered, due to attempting to fit a quart into a pint pot, its potential value for extending laboratory experiments on ventilated hydrofoils to actual operating conditions is high.

# Supercavitating Hydrofoils Operating at Zero Cavitation Number

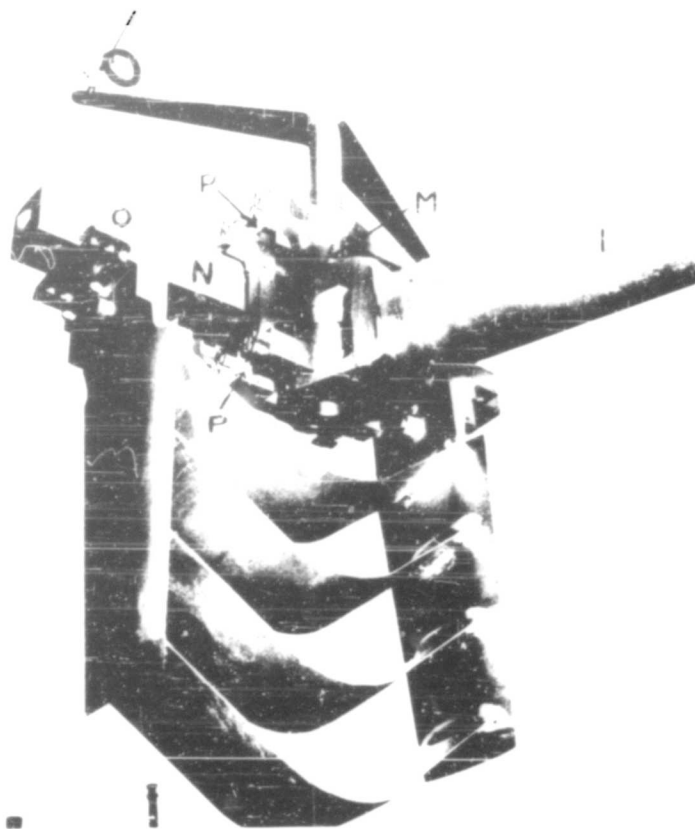


Fig. D5 - The stern foil unit

**P. Ward Brown (Stevens Institute of Technology)**

There is such a great wealth of information in Mr. Johnson's paper, and so many novel ideas scattered liberally throughout it, that it is perhaps ungracious to comment in any other way than by prolonged applause.

Nonetheless, I would like to discuss the method of calculating lift at finite depth. Mr. Johnson develops an ingenious, but approximate, linear solution for the lift of a supercavitating hydrofoil at finite depth. In order to improve the approximation he calculates the approximate lift at finite depth with a design angle of attack for infinite depth. Through this calculated point he draws a line having the slope given by Green's non-linear theory<sup>2</sup> at finite depth and design angle of attack for finite depth. It would seem to be more correct to calculate the lift at finite depth and at the design angle of attack for finite depth, and then to use the slope given by Green's theory.

<sup>2</sup>A.E. Green, "Note on the Gliding of a Plate on the Surface of a Stream," Proc. Camb. Phil. Soc., 52:248-252 (1956).

The difference between these two approaches for a circular-arc foil is shown in Fig. 1 and 2, for the case of zero depth. The lift curve for infinite depth is shown for reference.



Fig. D6 - Effect of depth on lift coefficient - Johnson's method

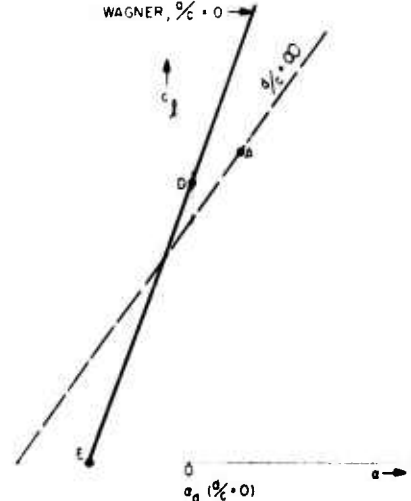


Fig. D7 - Effect of depth on lift coefficient - proposed method

Figure 1 shows Johnson's method. Point B is the lift calculated for zero depth at the design angle of attack for infinite depth and the line BC has the slope given by Green. The alternate method is shown in Fig. 2. Point D is calculated for zero draft and at the design angle of attack for zero draft. Again, DE has the slope given by Green but gives a different intercept on the lift axis.

It is interesting to note that the line DE given by the second method is exactly that predicted by Wagner<sup>†</sup> and the very small change in design lift coefficient with depth may also be noted. In fact according to Wu's non-linear theory<sup>‡</sup> the design lift coefficient of a circular-arc hydrofoil at infinite depth is exactly the same as the design lift coefficient given by Wagner for zero depth.

It seems that the lift at finite depth might be written as follows;

$$C_l = c_l(\alpha_d) + \alpha_d(c_l) + C_{l0} \quad (1)$$

where the slope,  $c_l(\alpha_d)$ , and the design angle of attack,  $\alpha_d$ , are both functions of the draft-chord ratio,  $d/c$ , (as given by Green and Johnson, respectively) and the design lift coefficient,  $C_{l0}$ , is independent of draft.

<sup>†</sup>H. Wagner, "Planning of Watercraft," NACA TM 1139, 1948.

<sup>‡</sup>L.Y. Wu, "A Free-Streamline Theory for Two-Dimensional Fully Cavitated Hydrofoils," C.I.T. Hydro Lab, Rep. No. 44-07, April 1955.

It is not always necessary to correct for depth effects. Recently at the Experimental Towing Tank, Stevens Institute of Technology, under contract with the Office of Naval Research, the lift and drag of a fully ventilated, surface-piercing, dihedral hydrofoil, has been measured. Analysis of the experimental results shows that after eliminating aspect ratio effects there is no residual depth effect. Thus a surface-piercing, dihedral foil has an effective draft-chord ratio of infinity. The tests also confirmed the linear slope,  $\pi/2$ , of the lift curve up to 16, but there was no fall off in lift as predicted by Wu's non-linear theory. However, the experimental design lift coefficient was only 70 percent of that predicted by the linear theory. The results of these tests will be published shortly.\*

Hirsh Cohen and R. C. DiPrima

In reply to Marshall Tulin, we would like to say that we are in agreement with his remarks. What we were trying to point out was simply that the linearized theory that has been used to estimate boundary effects does give the correct qualitative effects, but does not, at least in the cases considered here (the  $15^\circ$  half angle wedge, and the flat plate at angle of attack of  $12^\circ$ ), give the accuracy of a non-linear theory.

The question of slotted wall tunnels has been brought up by Dr. Silverleaf and by Prof. Silberman. It seems to us that judging from the results presented in this paper, little effect on force coefficients is to be expected. It seems reasonable to expect the results for force coefficients to lie between those for solid-wall and free-jet test sections. On the other hand, blockage effects on cavity dimensions are of some interest. For a given model and tunnel size, lower cavitation numbers may be obtained with a slotted wall tunnel. It certainly seems worthwhile to make blockage studies for the slotted wall case. There seems to be need of some caution in using such test sections, as proven by the instability problems experienced at A.R.L. The possibility of cavity-slotted wall instability interactions should be looked into.

Professor Silberman has raised a point which has, indeed, troubled us. He remarks that for very low cavitation numbers the drag on the  $15^\circ$  and  $12.5^\circ$  wedges is lower in the free jet than the drag predicted in an infinite stream by the exact theory. But this is borne out in his experiments only by the single point,  $C_D = 0$ . The linear theory predicts that the drag in a free jet will be lower than in the infinite stream at all cavitation numbers. One feels that this should also appear in the experimental results. If there is an abrupt rise in the drag as the cavitation number increases from zero it certainly should not become greater than the infinite stream value.

\*P.W. Brown, "The Force Characteristics of Surface-Piercing, Fully Ventilated, Dihedral Hydrofoils," S.I.T., E.T.T. Rep. No. 698. (To be published).

\* \* \* \* \*

# WALL EFFECTS IN CAVITATING FLOWS

Hirsh Cohen and R. G. DiPrima  
*Rensselaer Polytechnic Institute*

## INTRODUCTION

In this paper we would like to review some recent work on cavity flows in bounded regions. In particular we shall consider the effects of solid walls and free surfaces on finite cavity flows. While our discussion will not, of course, be all inclusive, we hope it will be sufficiently comprehensive to make certain general conclusions about boundary effects.

There are three major points of distinction to be made in the general problem we have chosen to discuss. The first is the geometry of the flow. It is natural to distinguish between symmetric flows past symmetric bodies and unsymmetric flows past symmetric or unsymmetric bodies. The second point concerns the types of boundaries to be considered. The boundaries which are of interest are those which confront the experimentalist in testing devices — water tunnel walls or free jet surfaces — and those which provide interference in actual applications. These would include free surface effects on cavitating bodies traveling near the surface and the interference of solid bodies such as hulls near cavitating bodies. Finally, we shall emphasize in this discussion finite cavity flows. There is a famous and abundant literature dealing with cavities or wakes of infinite length. Obviously, infinite cavities will seldom be encountered in testing procedures or anywhere else. The infinite cavity theory does form, however, an interesting and often useful limiting case and it will be pertinent to make reference to many of the results. The need for a finite cavity model is obvious for physical reasons and has been met in several ways mathematically. All of these finite cavity flow models have been employed in discussing boundary effects and their use will be related here.

Most of the discussion to follow deals with two-dimensional flows. Few studies have been made of three-dimensional boundary effects. The three-dimensional cavity flow theories that have been available to the present time have been extremely difficult to use. The results for bounded flows that are available, which are referred to later in detail, are obtained by an indirect method.

For the cases reviewed and discussed in this paper, one of the more interesting conclusions seems to be that the presence of boundaries does not greatly alter the force coefficients acting on cavitating bodies, providing the same cavitation conditions can be attained with and without boundaries.\* This statement must be carefully

---

Note: The research presented in this paper was sponsored by the Office of Naval Research.

\*This conclusion seems to confirm in part the statement of the Principle of the Stability of the Pressure Coefficient suggested by Birkhoff, Plesset, and Simmons (1).

understood; for bodies placed within solid wall boundaries, blockage effects are often very large and do not allow for great freedom in modeling the cavitation conditions in an unbounded medium.

Our discussion will follow the following outline: A general formulation of the bounded cavity flow problem is given. The need for, and the particular characteristics of, the various finite cavity flow models are discussed and the general linearized problem is set out. Also, a study of the effects of a free surface on a wedge traveling parallel to it, given recently by DiPrima and Tu, is mentioned briefly (2). The effects of solid walls are then taken up in detail. The various theoretical and experimental results for both symmetric and unsymmetric flows are compared. A similar discussion of free jets is given, followed by some comparisons of flows in solid channels, jets, and in an unbounded stream for the two-dimensional case. Finally, a brief discussion is given of bounded, axially symmetric flows.

#### FORMULATION OF THE TWO-DIMENSIONAL PROBLEM

The general problem under consideration is that presented in rather compact form in Fig. 1. The solid body  $B$  is located in the bounded region  $D$ , which contains an incompressible, nonviscous fluid whose velocity at upstream infinity ( $x \rightarrow -\infty$ ) is  $U_\infty$ . Attached to  $B$  at the known points  $S_1$  and  $S_2$  is a constant-pressure region  $C$ , the cavity. The pressure in the cavity,  $p_c$ , the pressure,  $p_\infty$ , corresponding to  $U_\infty$ , and the constant fluid density,  $\rho$ , define the cavitation number  $\sigma = (p_\infty - p_c) / (1/2) \rho U_\infty^2$ . The boundary of the combination  $B$  and  $C$  is a streamline. A distance in the  $x$  direction may be associated with each of  $B$  and  $C$  (a chord,  $c$ , and a cavity length,  $l$ ). The boundaries of  $D$  are the streamlines  $\psi_u$  and  $\psi_l$ . The leading edge of  $B$  is at distances  $h_u$  and  $h_l$  from  $\psi_u$  and  $\psi_l$ , respectively. Besides being streamlines, a second condition is required on  $\psi_u$  and  $\psi_l$ . In the free jet case the pressure is constant and known; in the solid wall case the lines themselves are given.

Unfortunately, as is well known, a satisfactory solution to the problem just sketched does not exist except under special conditions, even for  $h_u$  and  $h_l$  both infinitely large. If one is willing to accept cavity shapes concave to the flow with  $p_c < p_\infty$  or to consider cavities of infinite length, a solution may be found within classical potential theory. This is essentially the content of a "non-existence" theorem of Serrin (3). This theorem, then, implies that finite cavities of the shape required are not available from the classical theory. The bounded infinite cavity case, the Kirchhoff-Helmholtz theory, has been taken up at some length by various authors. The work of Réthy (4), Valcovic (5), and von Mises (6) is discussed by Birkhoff, Plesset, and Simmons (1). Actually, a certain amount of prior credit seems to fall to Joukowski (7) who considered virtually all of the cases taken up by the other

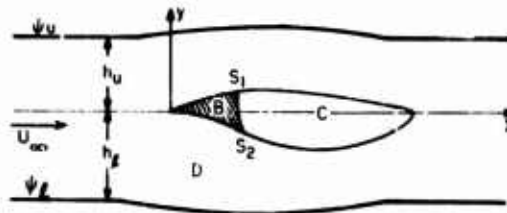


Fig. 1 - General two-dimensional cavity flow problem

authors plus several not discussed by them. It is important to observe that as the cavity becomes infinitely long the cavitation number  $\sigma$  may or may not approach zero. If the streamlines  $\psi = 0$  and  $\psi = \psi_0$  represent solid walls at downstream infinity, then  $\sigma$  approaches a limiting value  $\sigma_0$ , and the water tunnel is effectively blocked by the body and its infinite downstream appendage. On the other hand, if either  $\psi = 0$  or  $\psi = \psi_0$ , or both of them, represent free surfaces at downstream infinity,  $\sigma$  approaches zero as the cavity length becomes infinitely long.

We turn now to a discussion of the finite cavity models. The fundamental element supplied by the exact finite cavity flow models is a mechanism for explaining dissipation near the downstream end of the cavity. The Riabouchinsky model achieves this by setting an image body symmetrically located downstream from the forebody. The re-entrant jet theory allows the free streamline to reverse direction at the rear of the cavity and flow toward the forebody. The transition flow model provides a gradual "dissipation" downstream of a constant-pressure region along streamlines whose direction is prescribed. These models all prove to be useful and to give comparable results. An excellent description of them and a comparison of their usefulness is given in a paper by Wu (8). Further details will not be related here. A common difficulty of these models is that they are not very flexible as to the shape of the forebodies which can be handled with enough facility to produce computable data. The cases which have been discussed, even for unbounded flows, are virtually limited to straight-line boundaries. Furthermore, the Riabouchinsky and re-entrant jet theories are additionally complicated for unsymmetrical problems; the transition flow model does not have this difficulty. All of the flow models mentioned have been used to describe bounded flows; the results of these analyses will be related in subsequent sections.

Because of the difficulties associated with these models it would appear useful to consider a non-exact model. Tulin (9) has applied the ideas of thin airfoil theory to finite cavity flows to obtain a linear cavity flow theory. The linearization is in terms of a slenderness ratio or a small angle of attack and involves the usual introduction of perturbation velocities. The conditions along solid contours and constant-pressure surfaces are expressed in terms of these velocities. Instead of trying to satisfy conditions along the body or the unknown constant-pressure surfaces, the boundary conditions are satisfied on a known mean chord line. A condition which insures that the body-cavity juncture is closed and another condition, either providing a smooth body-cavity juncture or a smooth flow at the trailing edge of the foil, seem to be sufficient to yield a useful flow theory.

If the linearized theory is applied to the problem of Fig. 1, the problem becomes a mixed analytic function theory problem defined over the strip bounded by  $\psi = 0$  and  $\psi = \psi_0$  and exterior to the cut along the  $x$ -axis. (See Fig. 2.) The cut will represent the

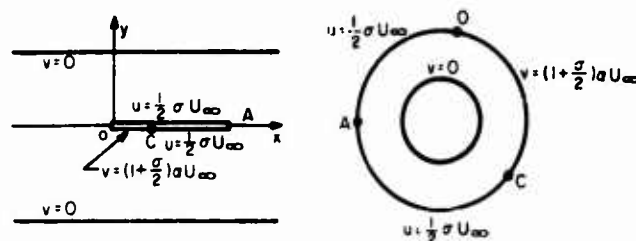


Fig. 2 - Linearized cavity flow for a lifting foil between solid walls

distance from the leading edge to the end of the cavity for the case of fully cavitating flow. For partially cavitating flow (the cavity closing on the body), the cut will be the mean chord length of the body. It is clear that unless there is symmetry about the  $x$ -axis or the cavity is infinitely long we are faced with solving a mixed boundary value problem in a multiply connected domain.

The general problem can be represented as one defined over the annulus shown in Fig. 2 with either the perturbation velocities  $u$  or  $v$  prescribed on the inner circle\* and  $u$  and  $v$  prescribed in alternate segments on the outer circle. Furthermore, certain continuity and singularity conditions are imposed on the complex velocity function on the outer circle. It would seem as though this is just the type of problem to be handled in very general form by the methods of Muskhelishvili (10). As it turns out, however, there are difficulties in finding the analytic continuations of the analytic functions needed in the Muskhelishvili method. This is also pointed out by Woods (11) and in fact, Woods has developed an alternative approach to such boundary value problems. The original cut strip of Fig. 2 may be mapped to a periodic array of rectangles, periodic in both vertical and horizontal directions, by elliptic mapping functions. Then, using a Cauchy integral method, Woods (12,13) has given a formulation for fully wetted foils between porous walls which can be easily extended to the cavity flow problem. In the limiting cases, the porous walls of the Woods theory become solid or constant-pressure surfaces. An examination of this method, now underway at R.P.L., for both fully cavitating and partially cavitating flows, shows, as Woods has warned, that the expressions obtained for such required relations as those between  $\psi$  and  $\chi$  and for  $C_L$  and  $\psi$  are very difficult to handle. However, if the walls are far from the body it appears possible to achieve some results.

Using the same mapping to the periodically repeated rectangles, Timman (14) has considered the problem of an oscillating airfoil between solid walls by finding appropriate Green's functions. In adopting his method for the bounded cavity flow problems, we find that the partial cavity flow past a lifting flat plate between solid walls requires the solution of the following rather interesting integral equation:

$$\int_{2K}^{2K+\pi\ell} \alpha(\zeta) \operatorname{sn}(\zeta) H(\zeta, \tau) d\zeta = - \left\{ \frac{2K\ell}{1 + \ell^2/2} \operatorname{sn} \tau + \int_{2K+\pi\ell}^{4K} \alpha(\zeta) \operatorname{sn}(\zeta) H(\zeta, \tau) d\zeta + \int_0^{2K} \alpha(\zeta) \operatorname{sn}(\zeta) H(\zeta, \tau) d\zeta \right\},$$

where  $K(k)$  is the complete elliptic function of the first kind,  $\alpha$  is the local inclination of the forebody, and  $\pi\ell$  represents a cavity dimension. The kernel  $H(\zeta, \tau)$  is a singular kernel with an analytic term and has the form

$$H(\tau, \eta) = \cot \frac{\pi(\tau - \eta)}{4K} + 4K \sum_{m=1}^{\infty} \frac{q^m}{1 - q^m} \sin \frac{m\pi(\tau - \eta)}{2K},$$

\*If  $u$  and  $v$  refer to different types of boundaries,  $u$  and  $v$  will be specified on separate portions of the inner circle.



Here  $q$  is the elliptic integral nome,  $q = \exp(-\pi K'/K)$ . The modulus  $k$  is a function of channel height and the body and cavity dimensions. The unknown function,  $\chi(\cdot)$ , is related to the cavity slope in the constant-pressure region. This singular integral equation may be reduced to a Fredholm equation with regular kernel by the methods of Carleman and Muskhelishvili but this is not a very attractive procedure. One may also do a perturbation solution starting from the case  $q = 0$ , which corresponds to the walls at infinity, as the zero-order solution. This is, in fact, the method which has been adopted and is now being calculated. It can be seen that, although analytic methods are available and some are being used, the general linearized boundary value problem set forth above has not been solved. Furthermore, it can be anticipated that its general solution will be of such complexity that usable data will be hard to obtain. The bounded finite cavity problems that have been treated successfully to date by the use of the linearized method are those which can be reduced to a potential problem in a simply connected domain, either by the use of symmetry or the linearization of a transition flow model. (See for instance 15, 16, 17, 18 & 19.) The results obtained in these cases will be discussed later.

In this connection, DiPrima and Tu have recently used the linearized theory to consider the problem of a fully cavitating symmetric wedge placed under a free surface or a solid wall (2). Since the problem is unsymmetric, it is necessary to use a distribution of vortices, as well as sources and sinks to represent the flow potential. The distributions are coupled by two simultaneous integral equations. By perturbing in terms of a parameter,  $\delta =$  chord length over twice the distance from the free surface to the vortex of the wedge, it is possible to find a first approximation for  $C_L$ . Further, it was observed that for small  $\delta$  the effect of the wall or free surface on the  $\sigma - \ell$ , and  $C_D - \sigma$  relations was  $O(\delta^2)$ . It is interesting to note that in this problem, if the approximate body boundary condition introduced by Tulin is used, the term of order  $\delta$  in the expansion of  $C_L$  is identically zero. It was found that the  $C_D - \sigma$ , and  $\sigma - \ell$  relations were insensitive to the approximate body boundary conditions, but that  $C_L$  was very sensitive to any changes in the approximate conditions imposed on the body. The results of this analysis are more fully discussed in Ref. 2.

## SOLID WALL CHANNELS

Earlier in this paper, reference has been made to solutions for two-dimensional cavity flows in solid wall tunnels. We would now like to consider these in detail. In the following discussion, we adopt the notation:  $T$  is the maximum width of the body,  $c$  is the chord length,  $\ell$  is the cavity length,  $h$  is the width of the jet or channel,  $n$  is half the maximum cavity width,  $\gamma$  is the half wedge angle, and  $\alpha$  is the angle of attack for lifting foils. Further, if  $D$  is the drag per unit span, the drag coefficient  $C_D$  is defined as  $D/(1/2)\rho U_\infty^2 T$ , and if  $L$  is the lift per unit span, the lift coefficient  $C_L$  is defined as  $L/(1/2)\rho U_\infty^2 c$ .

The finite cavity problems which have been considered theoretically are the flat plate set perpendicular to the walls and the flow, slender wedges placed symmetrically in the channel, and lifting foils at small angles of attack placed anywhere between the walls. The first of these problems were considered by Gurevich (20), who made use of the re-entrant jet model; and by Birkhoff, Plesset, and Simmons (21), who employed the Riabouchinsky model. Slender symmetric bodies have been studied by Cohen and Gilbert (22) using the linearized theory, and lifting foils have been considered by a linearized transition flow model in a paper by Cohen, Sutherland, and Tu (19). For all of these cases except the last, there are infinite cavity solutions given by the exact Kirchhoff-Helmholtz theory.

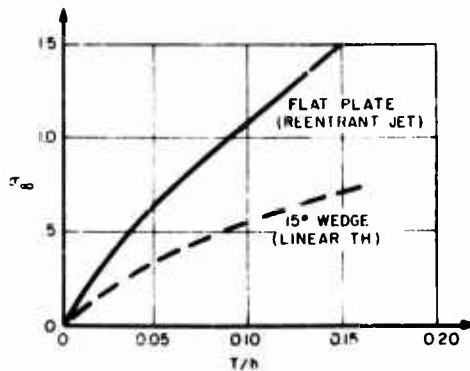


Fig. 3 - The dependence of blockage cavitation number on  $T/h$

One of the central problems in water tunnel testing of cavity flows is the blockage problem. As the cavitation number decreases, the cavity lengthens and eventually a large portion of the channel downstream from the body becomes a deadwater region. For a given ratio of body height to channel width,  $T/h$ , cavitation numbers below  $\sigma_{b,c}$ , the cavitation number at which an infinite cavity would result, are not attainable. Thus, not all cavity flow conditions can be modeled in a water tunnel.

In Fig. 3,  $\sigma_b$  has been plotted against  $T/h$  for the flat plate and for a 15-degree half-angle wedge. These curves give an indication of how drastic the blockage is, and one can

expect that the wall effects on cavity length and width will be similarly large. This is borne out in the calculations made by Gurevich and by Cohen and Gilbert as shown in Figs. 4, 5, 6, and 7.

The other consideration of importance is the effect of the tunnel width on the relation between drag coefficient and cavitation number. For the flat plate, Gurevich has calculated  $C_D$  vs  $\sigma$  for small values of  $T/h$  and finds that all of the values lie on virtually one curve, independent of  $T/h$  (Fig. 9).<sup>\*</sup> Now, for each value of  $T/h$ , there will be a minimum cavitation number,  $\sigma_{b,c}$ , corresponding to an infinite cavity. If one plots  $C_D$  for these values of  $\sigma$  ( $T/h$  increases as  $\sigma_{b,c}$  increases) even these minimum  $C_D$  values fall on the single curve mentioned above.

There are at present no exact model results for the symmetric wedge in a solid wall channel. The linear theory results of Cohen and Gilbert are shown in Fig. 8 and will be discussed presently in connection with the experimental data.

There are experimental results for both of the symmetric flows mentioned above. Waid (23) has carried out a set of tests with flat plates and small angle wedges. For the flat plate with a  $T/h$  ratio of 0.027 the experimental points agree well with the curve given by Plesset and Shaffer (24) who used the Riabouchinsky model for a flat plate in an unbounded stream (Fig. 9). Also shown is the curve given by Gurevich. The re-entrant jet theory seems to give a slightly better fit than the unbounded flow results in the partial cavitation region.

The Plesset and Shaffer results also give an excellent fit to the experimental data for the 15-degree wedge, with  $T/h = 0.027$  (Fig. 8). As can be seen, the linear theory data lie consistently above the exact theory and, in this case, the experimental data. This overestimation seems to occur generally, as has been pointed out by Wu (25). In the present case, we have again plotted a curve showing the value of  $C_D$

<sup>\*</sup>We have replotted Gurevich's curve using data from the figure in his paper; hence it is possible that the curve in Fig. 9 may be very slightly inaccurate.

Waid uses the term partial cavitation to mean that the cavities are filled with a rapidly moving combination of bubbles and water. In the figures such cavities are denoted by a solid circle.

# Wall Effects in Cavitation Flows

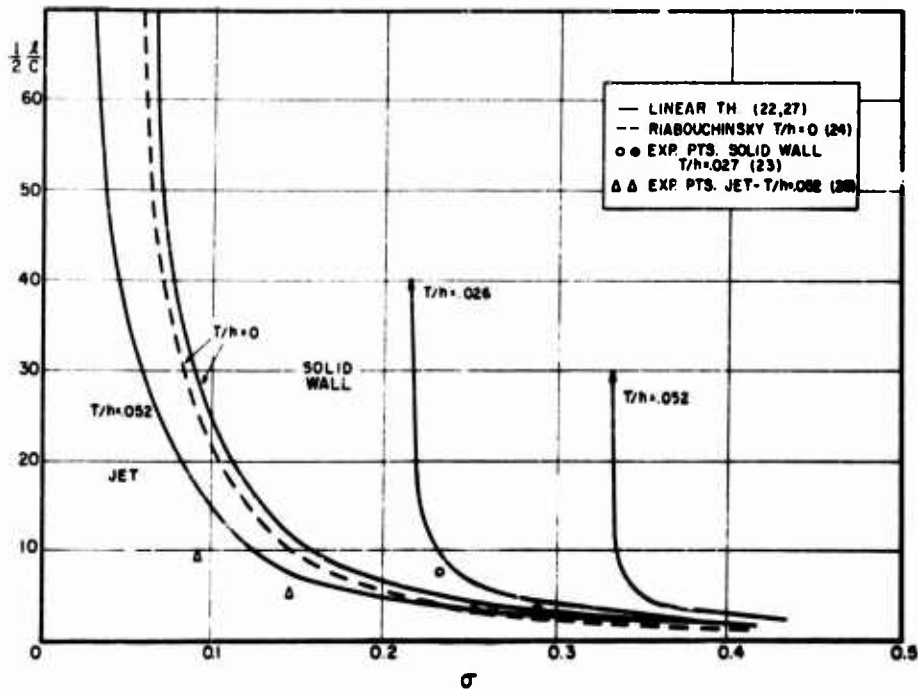


Fig. 4 - The dependence of cavity length on cavitation number for a 15-degree wedge

at the  $\sigma_{\infty}$  corresponding to any given value of  $T/h$ , the infinite cavity curve. These values of  $C_D$  will be the minimum attainable for the given value of  $\sigma$ . We have also plotted  $C_D$  as a function of  $\sigma$  for  $T/h = 0$ , the unbounded stream result. If one takes  $\sigma$  constant, then only those values of  $C_D$  lying between the two curves can be obtained by changing  $T/h$ . If one takes  $T/h$  constant, a curve can be drawn beginning at the  $\sigma_{\infty}$  value corresponding to  $T/h$  and lying always between the curves for  $T/h = 0$  and for the infinite cavity condition. Thus, although the linear result does overestimate the drag at any given value of  $\sigma$ , it gives a qualitative confirmation to the idea that the change in force coefficient is indeed small for fixed cavitation number.

One must keep in mind, however, that the boundaries do invoke limitations on the cavitation numbers. Waid has measured values for  $C_D$  just below  $\sigma = 0.2$  for the 15-degree wedge and these must be very long cavities since Cohen and Gilbert obtain  $\sigma_{\infty} = 0.212$  as the blockage cavitation number for the 15-degree wedge with  $T/h = 0.026$ .

For cavity width, Gurevich's results obviously follow the data more faithfully than the Plesset and Shaffer result for the unbounded flow (Fig. 7). Gurevich has computed widths and lengths for rather high values of cavitation number ( $\sigma > 0.5$ ) which is strange, but it appears that his results give the proper correction for Waid's data. For the 15-degree wedge, the Cohen and Gilbert data also seem to give the proper correction (Fig. 6).

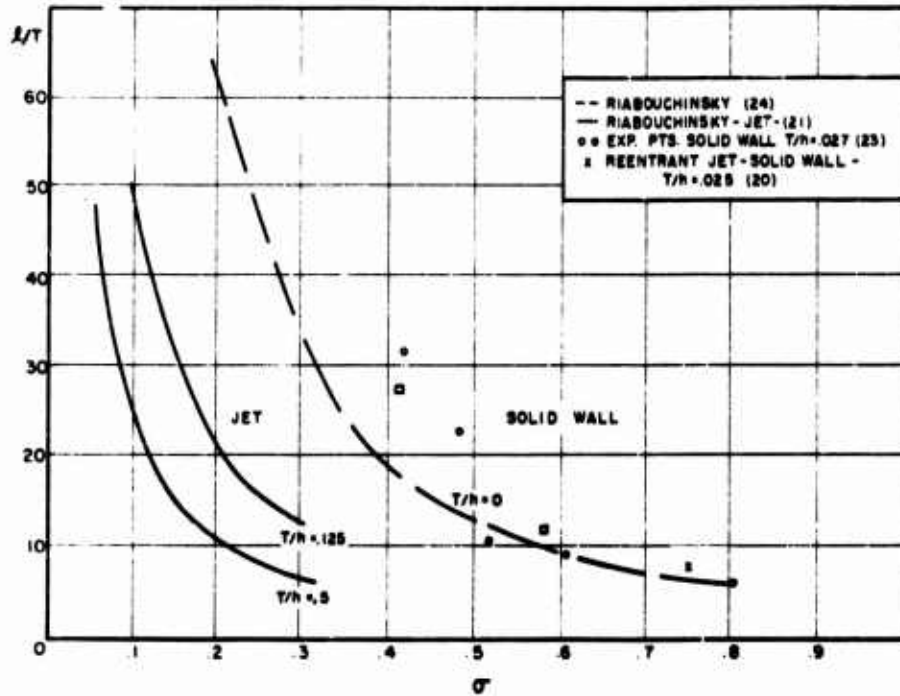


Fig. 5 - The dependence of cavity length on cavitation number for a flat plate

Unfortunately, Gurevich's calculations are not very useful for cavity length comparisons. The values of  $\sigma$  used are so large that they fall in the partial cavitation range (Fig. 5). Gurevich's results are given in explicit form and may be extended with some labor. The Plesset and Shaffer unbounded flow results are compared with Wald's data in Fig. 5. For the 15-degree wedge, the wall effect curves given by Cohen and Gilbert again seem to give the right correction (Fig. 4). The magnitude of the correction is large here; for  $\sigma = 0.3$ ,  $T/h = 0.026$ , the correction to the Plesset and Shaffer unbounded flow results is about 50 percent and becomes larger as  $\sigma$  decreases.

Thus far, we have considered only symmetrical flows. When a thin foil is placed inside a water tunnel at an angle of attack, the flow is obviously no longer symmetrical. In order to avoid the mathematical difficulties which arise for the multiply-connected domain involved in this finite cavity flow, a linearization of the transition flow model was used by Cohen, Sutherland, and Tu (19).

The general solution was obtained for any ratio of  $h_0/h_1$  (see Fig. 1). Three special cases were considered in detail for the flat plate foil. In the first, the foil is located midway between walls ( $h_0 = h_1$ ). The lift coefficient is obtained as a function of cavitation number as shown in Fig. 10 for the particular case,  $\alpha = -6$  degrees; curves were plotted for several values of  $c/h$ . On the same graph we have shown the result for  $h_0/h_1 = h_2/h_1$ , and the results for the case of the infinite cavity. For the range of cavitation numbers shown, the wall effects which lie between the two bounding curves are, indeed, small. If a choice of  $c/h$  is made, one begins at

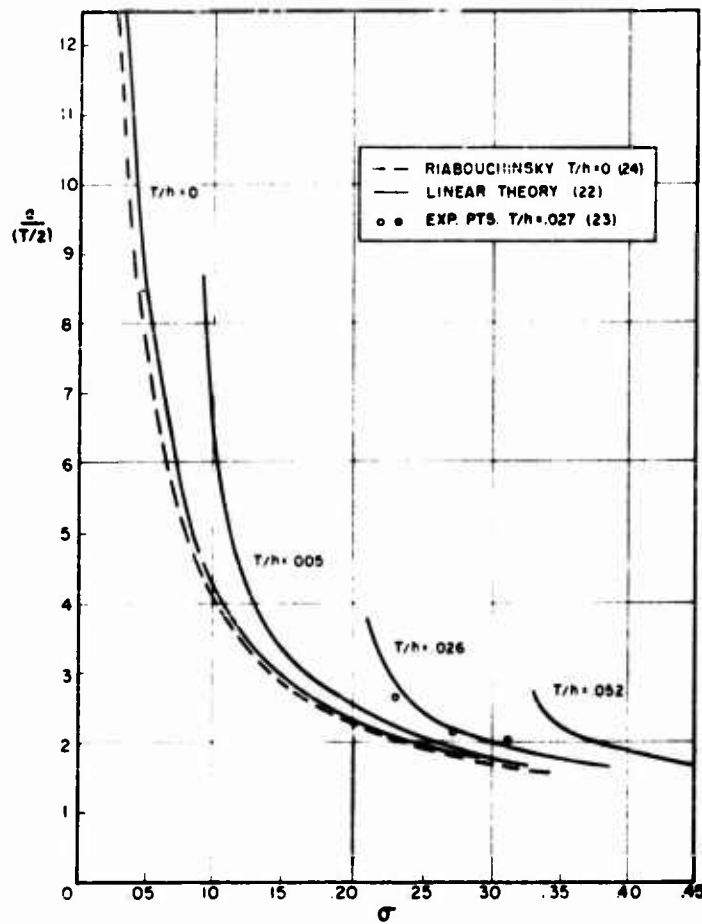


Fig. 6 - The dependence of maximum cavity width on cavitation number for a 15-degree wedge in a channel

the proper value of  $\sigma_c$  on the infinite cavity curve and proceeds along the  $C_L$  vs  $\sigma$  curve as is shown in Fig. 10. Also shown in Fig. 10 is a curve of  $\sigma_c$  vs  $c/h$  for  $h_c = h_{01} = h/2$ .

Parkin (26) has considered lifting flat plates experimentally. For the 12-degree flat plate, his data are given in Fig. 11 along with Wu's transition model theory results (8) for the unbounded stream and the results for the bounded flow using the linearized transition model (19). Here again the linear theory overestimates the force coefficient; however, it does predict only a small change in  $C_L$  for fixed  $\sigma$  with varying  $T/h$ .

The second case considered in Ref. 19 describes the flow behavior when  $h_c \rightarrow 0$  or  $h_{01} \rightarrow \infty$ ; i.e., the lifting foil near the upper or lower wall. For infinite cavities,

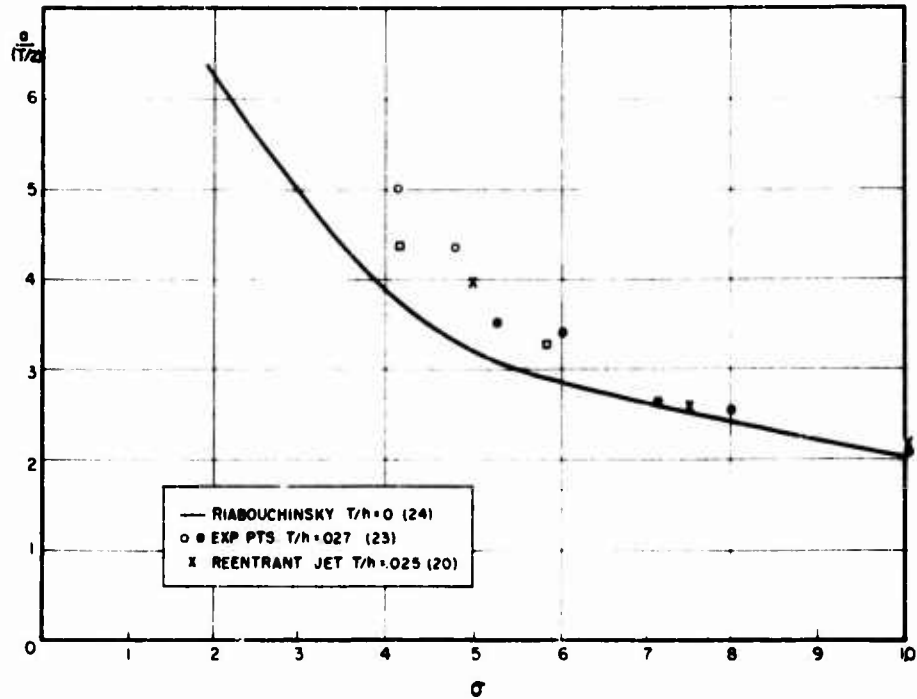


Fig. 7 - The dependence of maximum cavity width on cavitation number for a flat plate in a channel

the effect of the nearness to one wall is shown in Fig. 12. The lift coefficient for both  $h_0, h_\infty \rightarrow \infty$  in the linear theory is  $C_L = 2$ . In the case where the foil is close to the upper wall, the lift coefficient decreases as the distance from the wall decreases. On the other hand, when the foil is close to a lower wall, the lift coefficient increases as the distance from the wall decreases. It should be kept in mind, however, that these results are for the infinite cavity case with  $\sigma = 0$  (since for either  $h_0$  or  $h_\infty$  infinite there is no blockage cavitation number). The relation between  $C_L$  and  $\sigma$  for values of  $\sigma$  greater than zero has been obtained (19) for this case but has not yet been computed.

It would seem that the latter results may be of interest in observing the effect of larger bodies, such as ships' hulls, on hydrofoil characteristics. To our knowledge no experiments have been carried out on such problems.

#### THE FREE JET

Finite cavity flow in a jet seems to present a more difficult mathematical problem than the solid wall case just discussed. The preliminary results from the method of L. C. Woods mentioned previously lead to complicated expressions for the desired quantities. The linear transition flow model, although applicable, leads to hyper-elliptic integrals which are cumbersome to use and evaluate. The cases which have

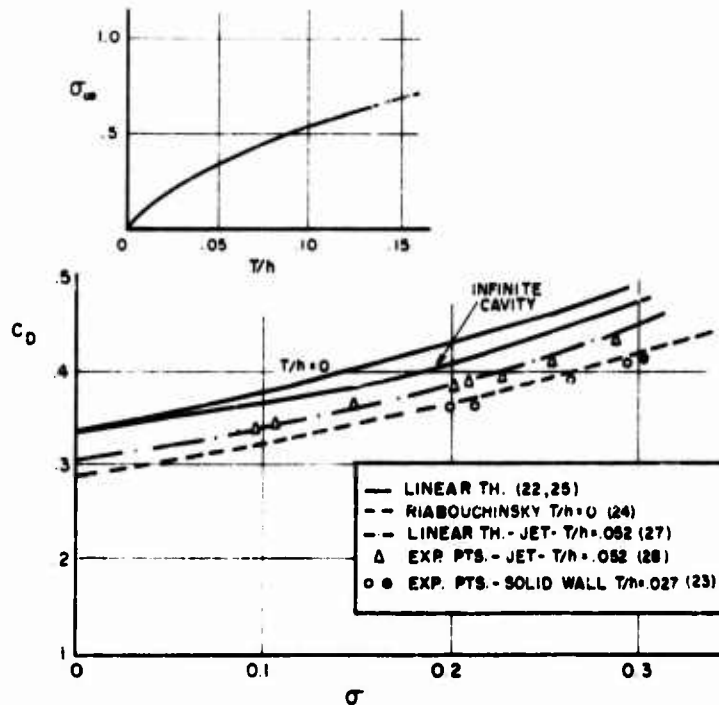


Fig. 8 - The dependence of the drag coefficient on cavitation number for a 15-degree wedge

been studied theoretically are the flat plate perpendicular to the flow direction in terms of the Riabouchinsky model by Birkhoff, Plesset, and Simmons (21), and the slender symmetrical body by Cohen and Tu (27) using the linearized theory.

The exact expressions obtained by Birkhoff, Plesset, and Simmons are very involved and, as far as we know, no calculations have been made from them. As a matter of fact, no curves or data of any kind are given in the paper. Using the approximate expressions appropriate for small cavitation numbers also derived in the paper, we have calculated the relations between  $C_D$ , cavity length, and the cavitation number. These are shown in Figs. 5 and 9 and for several values of  $T/h$ . As can be seen, a boundary correction is predicted here not only in the case of the changing cavity length, but also for the force coefficient.

Cohen and Tu have used the linearized theory to carry out calculations for the case of a 15-degree wedge. The effect on  $C_D$  of changing  $\sigma$  in a jet with  $T/h = 0.052$  at infinity is shown in Fig. 8. These results are compared with unbounded flow results for the wedge obtained by Plesset and Shaffer (24) and also with unbounded flow results from the linear theory. In addition, the experimental results of Silberman (28) are shown. The linear theory in this case seems to give the right correction and the agreement with experiment is good. Silberman was able to obtain data at  $\sigma = 0$  by venting the cavity to the upstream pressure. Here the linear theory fails, but the Kirchhoff-Helmholtz theory results of Siao and Hubbard (29) are not far off.

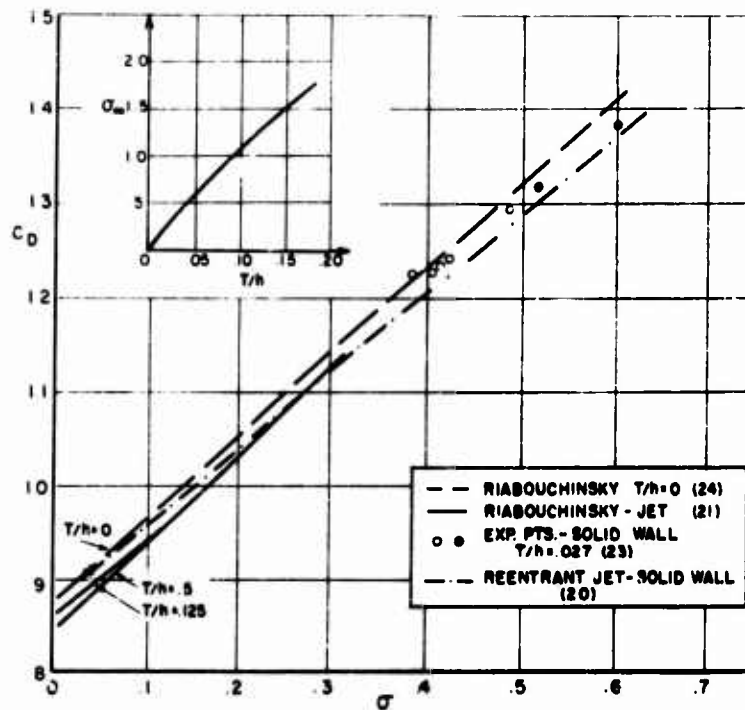


Fig. 9 - The dependence of the drag coefficient on cavitation number for a flat plate

For the cup (or scoop channel) and the circular cylinder with a ratio of body width to jet width of 0.0375, the experimental results for  $C_D$  are in good agreement with the theoretical predictions for an unbounded flow (30). For this value of  $T/h$ , it appears that the boundary effects on  $C_D$  for these bodies are negligible.

In the case of the lifting flat plate in the jet, experimental data have been compared with unbounded flow solutions. The agreement between the experimental results and the theoretical values obtained by Wu (8) using the transition flow model are quite good for cavitation numbers above 0.15. The values of  $C_L$  predicted by Wu (16) using the linearized theory lie consistently above the experimental data. The results for the drag coefficient are not in such good agreement. It is impossible to say whether this can be attributed to a boundary effect, since there are no computations for a lifting plate in a jet.

As for cavity dimensions, the jet boundary corrections given for the decrease of cavity length with diminishing jet width by Cohen and Tu for a symmetric wedge are confirmed by the experimental results (Fig. 4). The fit is not as close as for the force coefficient data but shows clearly the direction of the correction. Silbermann has also compared cavity lengths for a lifting foil with those obtained theoretically for the unbounded stream flow by Wu (8) using the transition model and Tulin (15) using the linear theory. Both theories give reasonable agreement for  $\sigma$  greater than 0.1 but are not consistent with the experimental data for  $\sigma$  less than this value.



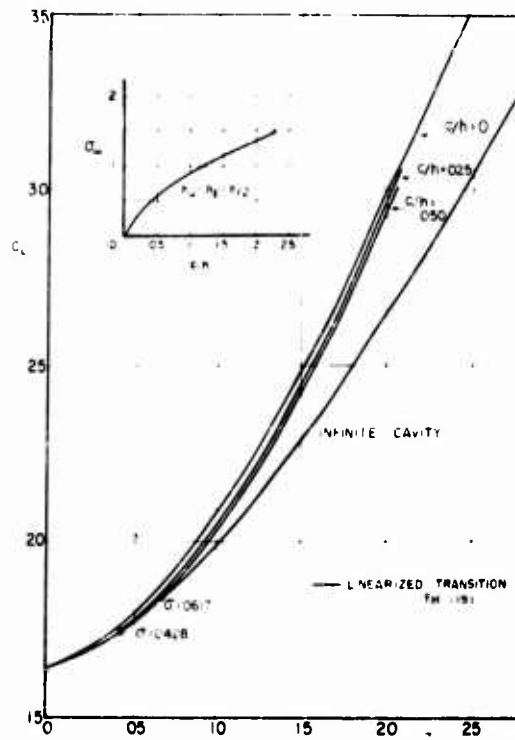


Fig. 10 - The dependence of the lift coefficient for a flat plate at angle of attack 6 degrees in a channel on cavitation number ( $\sigma_0 = p_\infty / \rho U^2 - h/2$ )

### SOME COMPARISONS AND OBSERVATIONS

We have given separately the details of the effects of solid walls and of free jet boundaries or force coefficients and cavity dimensions in some particular bounded flow problems. In the present section we would like to compare these effects. We will then discuss the theoretical and experimental data presented thus far on two-dimensional flows and offer some observations based on the examples considered.

For the purpose of comparison we have chosen the 15-degree wedge. If one begins with an unbounded stream flowing past the wedge, the cavity length can increase from zero to infinity as the cavitation number decreases to zero as shown in Fig. 4. For a jet bounded by constant-pressure streamlines, the same is true, although the cavity length is always smaller at any given value of  $\sigma_0$ . On the other hand, if the flow is bounded by solid walls, the cavity length increases at a more rapid rate than in the unbounded stream and attains infinite length at the blockage value  $\sigma_{0b}$ . For a given cavitation number, say for example  $\sigma_0 = 0.35$ , there may be as much as 100 per cent difference in cavity lengths for the same size wedge in a jet and a tunnel of the same height ( $F/b = 0.052$ ). More important, however, is the fact that cavities of very long lengths may be modeled in a solid wall tunnel at high cavitation numbers if desired and at low cavitation numbers in a jet if this is desirable.

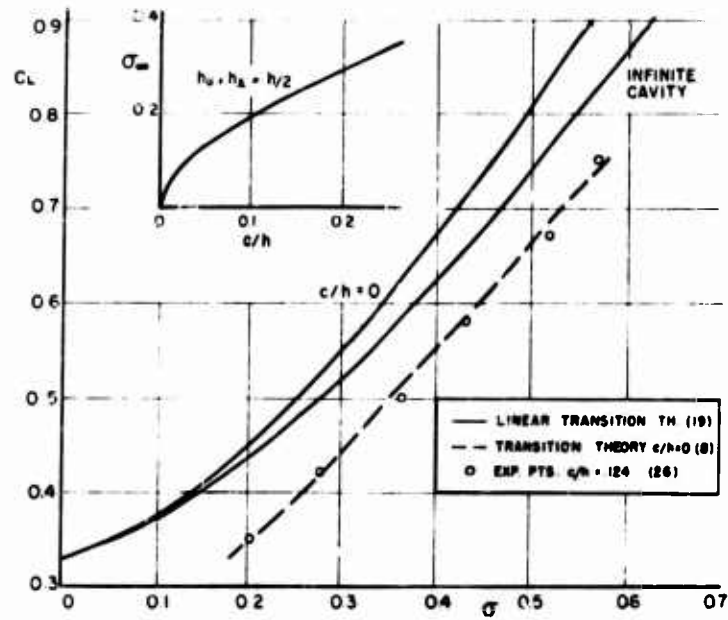


Fig. 11 - The dependence of the lift coefficient for a flat plate at angle of attack 12 degrees in a channel on cavitation number ( $h_u = h_d = h/2$ )

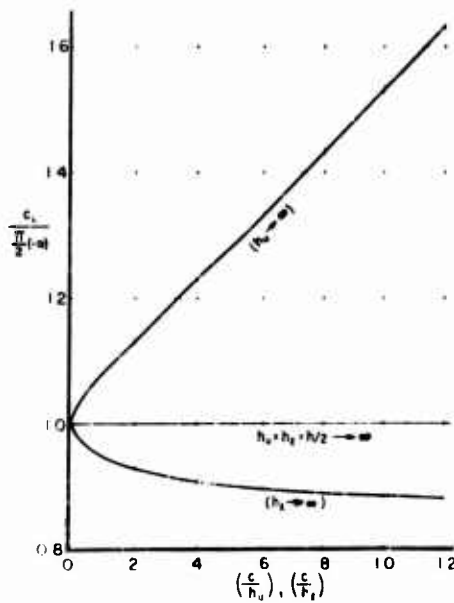


Fig. 12 - The dependence of the lift coefficient of an inclined flat plate in a channel on chord-wall height ratio for the case of one wall at infinity and cavitation number zero

Cavity width behavior in the jet and solid wall channel is similar to that of cavity length. In channels at blockage cavitation numbers, the cavity width has its maximum value. These, of course, are strongly limited by the tunnel height so that continuity of flow may be maintained. In the jet, the cavity may have any width, becoming infinite as  $\sigma$  approaches zero.

In comparing the drag coefficient for the wedge in the solid wall channel and in a jet, it must be kept in mind that the linear theory seems consistently to overestimate the force coefficient. The value of  $C_D$  predicted by the linear theory for the unbounded flow lies above that predicted by the Riabouchinsky model. If one remains within the framework of the linear theory, however, for a given value of  $\sigma$ , the value of  $C_D$  is lower in the jet than in the solid wall channel and both of these lie below the value predicted by the linear theory for the unbounded stream (Fig. 8). Actually, the experimental values for the solid wall channel lie below these linear results and, it will be recalled, coincide with the exact Riabouchinsky model results for the unbounded stream. On the other hand, the experimental results for the wedge in the jet coincide with those predicted by the linear theory. It would almost appear as though the solid walls do not affect the drag; whereas the jet boundaries do. The effect of the jet boundaries for the flat plate case (Fig. 9) is the same, although there is experimental verification for the wedge only. It is very important to keep in mind, however, that the solid wall channel does not allow the modeling of all cavitation conditions. For the experimental case cited in this report where  $T_h = 0.027$ , the minimum cavity number for the 15-degree wedge is 0.212 and for the flat plate it is 0.3. Thus there is a rather severe limitation on the use of solid wall tunnels for low cavitation number testing.

These comparisons serve to point up the more interesting results of the present survey. First of all, the experimental results of Waid (23), together with the theoretical analyses of Gurevich (20) and Plesset and Shaffer (24) for the symmetrical flows past flat plates and wedges, confirm the idea that the drag coefficient is insensitive to boundary changes in solid wall channels, providing  $\sigma$  is held constant. The linear theory provides the same result qualitatively for the wedge flow and also for the unsymmetrical flow past a flat plate foil in a solid wall channel. The linear theory results for these cases seem characteristically to overestimate the force coefficient when compared with the experiments. For the lifting flat plate foil the unbounded stream results given by Wu (8) using the non-linear transition flow model provide excellent agreement with the water tunnel data, further strengthening the remarks made on the insensitivity of the force coefficient. This observation seems to confirm at least a portion of Birkhoff's Principle of the Stability of the Pressure Coefficient (1).

The theoretical and experimental results examined do not yield quite such consistent results in the case of the free jet. Small boundary effects on  $C_D$  are predicted by the theory for the wedge and the flat plate and, in the case of the 15-degree wedge, are observed. On the other hand, fairly good agreement results when unbounded stream values of  $C_D$  are compared with the experimental values for a lifting flat plate in the jet.

Thus, in only one case do the experiments show the need for boundary corrections for  $C_D$ . It might be pointed out, however, that these experiments were run at the highest value of  $T_h$  of all those reviewed. Furthermore, and even more important, these  $C_D$  comparisons are made on the basis of constant cavitation number. The blockage computations show how difficult it is to obtain the cavitation conditions necessary to reproduce the  $C_D$  values in an unbounded stream. If one is tempted to discard wall effect computations because of the excellent agreement for  $C_D$  values with unbounded stream results, it is important to remember that one must also measure

blockage effects. Blockage formulas may be obtained which involve  $C_D$ ,  $\beta$ , and  $T_h$  by rather elementary means (see Ref. 1) but it is more convenient to have  $\beta$  and  $T_h$  related independently from  $C_D$ . Such a relation requires the solution of the bounded flow problem.

Besides the flows bounded by two free streamlines or two walls, flows near a single boundary have been discussed. There appears to be no experimental data for these cases, although it would be useful. When the lifting foil is near a solid wall above the foil, the lift coefficient decreases as the foil nears the wall and increases when the foil nears a solid wall below the foil. Further theoretical work on these single wall cases is probably necessary.

Note: After this paper has been completed, the authors obtained a copy of the original Simmons report (35) from which much of the Birkhoff, Plesset, and Simmons paper (21) has been derived. The original report gives the results of a limited number of numerical computations for the flat plate in a channel or a jet which are not included in the published paper (21). In particular, for the case of the flat plate in a channel, the dependence of  $\beta$  on  $T_h$  and  $C_D$  on  $\beta$  given by Simmons verifies the results of Gurevich (20) mentioned earlier. For this same case, in order to compare the theoretical results with the experimental results of Waid (23), the following points have been computed from Simmons' data:  $T_h = 0.025$ ,  $\beta = 0.416$ ,  $\beta T = 27.5$ ,  $\beta T = 4.35$ ; and  $T_h = 0.0295$ ,  $\beta = 0.578$ ,  $\beta T = 12$ ,  $\beta T = 3.25$ . (Due to the complexity of the computations it is impractical to determine the complete dependence of  $\beta T$  and  $\beta$  on  $T_h$  for non-zero values of  $T_h$ .) These points are indicated in Figs. 5 and 7 by small squares; they agree well with the experimental results for  $T_h = 0.027$ .

#### AXIALLY SYMMETRIC BODIES

The literature on boundary effects on axially symmetric cavity flows is extremely limited. In contrast to the recent analytic and numerical studies that have been made of the unbounded flow past a disk,<sup>2</sup> the theory of bounded, axially symmetric cavity flows rests on a combination of plausible assumptions based on physical observation.

Reichardt (33,34) observed that for an unbounded stream, certain cavity characteristics were approximately functions of  $\beta$  only; i.e., they were essentially independent of body shape. In particular, the fineness ratio,  $\beta/2a$ , ( $a$  now refers to maximum cavity radius) and the drag coefficient based on maximum cavity radius,  $K_D = 2D/U_\infty^2 \pi a^2$ , depend on  $\beta$  only; and further, the drag coefficient based on wetted frontal area,  $\beta K_D$ , can be written as  $C_D = C_D(0)(1 - \beta)$  where  $C_D(0)$  is the drag coefficient at  $\beta = 0$ . Thus if  $C_D(0)$ , the  $\beta/a$  relation, and the  $K_D - \beta$  relation are known, one can compute  $a/b$  and  $\beta/b$  for given values of  $\beta$ .

The  $\beta/a$  relation, and the  $K_D - \beta$  relation can be obtained analytically by assuming that the flow around a cavity can be represented by an axial source-sink distribution. The constant pressure condition on the closed stream surface will, of course, be only approximately satisfied. That such a method will give meaningful results is a consequence of the "non-dependence" of  $\beta/a$  and  $K_D$  on changes in the body shape. For an unbounded flow, Simmons (35) has used a source-sink distribution of linearly varying strength to determine the above relations. The value of  $C_D(0)$  can be taken as the experimental value, or may be computed by assuming that the pressure distribution on the axially symmetric body is the same as on the equivalent two-dimensional body.<sup>3</sup>

<sup>2</sup>In particular, the work of Garabedian (31,32) should be mentioned.

<sup>3</sup>The latter method, while inaccurate, does give values of  $C_D(0)$  which are not too much in error for the case of a circular disk.

The methods discussed above have been extended by Campbell and Thomas (36) to the axially symmetric cavity flow in a solid wall tunnel of radius  $R$ . In order to compute  $a/b$  and  $c/b$  for this case, it is necessary to make the additional assumption that  $C_D(1 + \dots)$  is insensitive not only to changes in  $\dots$  but also to the presence of boundaries. The results for the cavity dimensions are similar to the two-dimensional case; for a given value of  $\dots$ , both  $a/b$  and  $c/b$  increase as  $b/R$  increases.

A relation between  $\sigma_c$  and  $b/R$  can be obtained by simple continuity and momentum considerations, and the above assumption on  $C_D$ . This relation is shown in Fig. 13 for the case of a circular disk. For a given value of  $T/h = b/R$  it is clear from Fig. 13 that the limiting cavitation number is much less for axially symmetric flow than for two-dimensional flow. However, a better measure of blockage for this case is the ratio of body cross-section area to tunnel cross-section area  $(b/R)^2$ . If  $\sigma_c$  is plotted against  $(b/R)^2$ , the resulting curve is closer to the  $\sigma_c$  vs  $T/h$  curve for the two-dimensional case. Even so,  $\sigma_c$  for the axially symmetric case is less than for the two-dimensional case.

The case of an axially symmetric cavity in a circular free jet or tunnel has been considered by Armstrong and Tadman (37) who also used the source-sink methods mentioned earlier. One of their conclusions is that for small values of  $\dots$  and  $\dots/2R$  the fractional decrease, based on the unbounded flow, in cavity length and width in a jet and the fractional increase in a solid wall tunnel due to the boundaries are proportional to  $(\dots/2R)^3$ . The corrections in a tunnel are roughly four times as large as the correction in a free jet.

Since these analyses are based on assumptions on the role of  $C_D$ , they do not, of course, yield any information about the drag coefficient.

As far as we could ascertain, there is no experimental work on boundary effects on cavity dimensions which could be used to check these theories, with the exception of the study of Self and Ripken (38) in a free jet tunnel. However, their conclusions are that the cavity dimensions are insensitive to changes in the position of the boundary. This is somewhat surprising in view of the above discussion, and the known large effect that boundaries have on cavity dimensions in two-dimensional flow.

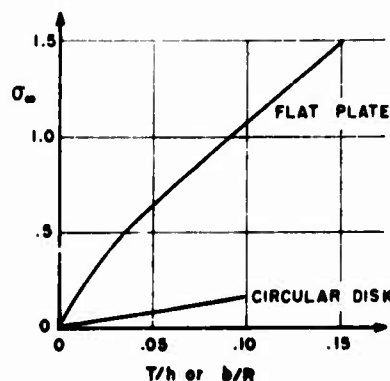


Fig. 13 - The dependence of blockage cavitation number on  $b/R$  for a circular disk

## REFERENCES

1. Birkhoff, G., Plesset, M., and Simmons, N., "Wall Effects in Cavity Flow-I," *Quar. Appl. Math.*, 2, 8 (1950), pp. 151-168
2. DiPrima, R.C. and Tu, Yih-O, "Surface Effects on the Supercavitating Flow Past a Symmetric Wedge," R.P.I. Math. Rep. 17, Rensselaer Polytechnic Institute, Troy, July 1958

3. Serrin, J.B., "Existence Theorems for Some Hydrodynamical Free Boundary Value Problems," Jour. Rat. Mech. and Anal. 1, 1 (1952)
4. Réthy, M., "Strahlformen Incompressibler Reibungsloser Flüssigkeiten," Math. Annalen 46 (1895), pp. 249-272
5. Valcovici, V., "Über Discontinuerliche Flüssigkeitsbewegungen mit Freien Strahlen," Thesis Göttingen (1913)
6. Von Mises, R., "Berechnung von Ausfluss und Überfallzahlen," Zeits. VDI 61 (1917), 447-452, 467-473, 493-497
7. Joukowski, N.E., "A Modification of Kirchhoff's Method of Determining a Two-Dimensional Motion of a Fluid, Given a Constant Velocity Along an Unknown Streamline," Collected Papers, Vol. III, Moscow, 1936, 195-365
8. Wu, T.Y., "A Free Streamline Theory for Two-Dimensional Fully Cavitated Hydrofoils," Jour. Math. and Phys., 3, 35 (1956), pp. 236-265
9. Tulin, M.P., "Steady Two-Dimensional Cavity Flows About Slender Bodies," David Taylor Model Basin Report 834, May 1952
10. Muskhelishvili, N.I., Singular Integral Equations, P. Noordhoff, N.V. Groningen-Holland, 1953
11. Woods, L.C., "On Harmonic Functions Satisfying a Mixed Condition with an Application to the Flow Past a Porous Wall," Appl. Sci. Res., Ser. A, 6, No. 5-6 (1957), pp. 351-364
12. Woods, L.C., "Subsonic Plane Flow in an Annulus or a Channel with Spacewise Periodic Boundary Conditions," Proc. Roy. Soc. of London, A, 229 (1955), pp. 63-85
13. Woods, L.C., "On the Lifting Aerofoil in a Tunnel with Porous Walls," Proc. Roy. Soc. of London A, 242 (1957), pp. 341-254
14. Timman, R., "The Aerodynamic Forces on an Oscillating Aerofoil Between Two Parallel Walls," App. Sci. Res., No. 1, Vol. A3 (1951), pp. 31-58
15. Tulin, M., "Supercavitating Flow Past Foils and Struts," Symposium on Cavitation in Hydrodynamics, Nat. Phys. Lab., Teddington, England, 1955
16. Wu, T.Y., "A Note on the Linear and Non-Linear Theories for Fully Cavitated Hydrofoils," Hydrodynamics Laboratory Report No. 21-22, Cal. Inst. of Tech., August 1956
17. Acosta, A.S., "A Note on Partial Cavitation of Flat Plate Hydrofoils," Report No. E-19.9, Hydrodynamics Laboratory, Cal. Inst. of Tech., October 1955
18. Gevurst, A.J. and Timman, R., "Linearized Theory of Flow with Finite Cavities About a Wing," Rapport 7, Technische Hogeschool, Institute voor Toegepaste Wiskunde, Delft
19. Cohen, H., Sutherland, C.D., and Tu, Yih-O, "Wall Effects in Cavitating Hydrofoil Flow, Jour. Ship Res., 3, 1 (1957), pp. 31-40

20. Gurevich, M.I., "Symmetrical Cavitation Flow Around a Flat Plate Situated Between Parallel Walls," *Bull. of Acad. of Sci. of USSR*, No. 4 (1946)
21. Birkhoff, G., Plesset, M., and Simmons, N., "Wall Effects in Cavity Flow-II," *Quar. Appl. Math.*, 4, 9 (1952), pp. 413-421
22. Cohen, H. and Gilbert, R., "Two-Dimensional, Steady, Cavity Flow About Slender Bodies in Channels of Finite Breadth," *Jour. Appl. Mech. Trans. ASME*, 79 (1957), pp. 170-176
23. Waid, R.L., "Water Tunnel Investigations of Two-Dimensional Cavities," *Hydrodynamics Laboratory Report No. E-73.6*, Cal. Inst. of Tech., Sept. 1957
24. Plesset, M.S. and Shaffer, P.A., Jr., "Cavity Drag in Two and Three Dimensions," *Nav. Ord. Report 1014*, NOTS 131, October 1949
25. Wu, T.Y., "A Simple Method for Calculating Drag in the Linear Theory of Cavity Flows," *Engineering Division Report No. 85-5*, Cal. Inst. of Tech., August 1957
26. Parkin, B.R., "Experiments on Circular-Arc and Flat-Plate Hydrofoils," *Jour. Ship Research*, 4, 1 (1958), pp. 34-57
27. Cohen, H. and Tu, Yih-O, "A Comparison of Wall Effects on Supercavitating Flows Past Symmetric Bodies in Solid Wall Channels and Jets," *Proc. of Ninth Internal Cong. Appl. Mech.*, Brussels, 2 (1956), pp. 359-370
28. Silberman, E., "Experimental Studies of Supercavitating Flow About Simple Two-Dimensional Bodies in a Jet," *St. Anthony's Falls Hydraulic Laboratory Report No. 59*, Univ. of Minnesota, April 1958
29. Siao, T.T. and Hubbard, P.G., "Deflection of Jets. I. Symmetrically Placed V-Shaped Obstacle," *Free Streamline Analyses of Transition Flow and Jet Deflection*. State Univ. of Iowa, Bull. No. 35, pp. 33-44, 1953
30. Birkhoff, G. and Zarantonello, E.H., *Jets, Wakes and Cavities*, Acad. Press Inc., New York, N.Y., p. 148, 1957
31. Garabedian, P.R., "The Mathematical Theory of Three-Dimensional Cavities and Jets," *Bull. Amer. Math. Soc.*, 62, No. 2 (1956), pp. 219-236
32. Garabedian, P.R., "The Calculation of Axially Symmetric Cavities and Jets," *Pacific Jour. of Math.*, 6 (1956), pp. 611-689
33. Reichardt, H., "The Laws of Cavitation Bubbles at Axially Symmetric Bodies in a Flow," *Ministry of Aircraft Production Reports and Translations No. 766* (1946)
34. Reichardt, H., "The Physical Laws Governing the Cavitation Bubbles Produced Behind Solids of Revolution in a Fluid Flow," *Ministry of Supply TPA3/TIB Translation G.D.C. No. 10/5678T* (1945)
35. Simmons, N., "The Geometry of Liquid Cavities with Especial Reference to the Effects of Finite Extent of the Stream," *Ministry of Supply, A.D.E. Report 17/48* (1948)
36. Campbell, I.J. and Thomas, G.E., "Water Tunnel Boundary Effects on Axially Symmetric Fully Developed Cavities," *Admiralty Res. Lab./R1/G/HY/18/1* (1956)

37. Armstrong, A.H. and Tadman, K.G., "Wall Corrections to Axially Symmetric Cavities in Circular Tunnels and Jets," Ministry of Supply A.R.E. Report No. 7/52 (1953)
38. Self, M.W. and Ripken, J.F., "Steady-State Cavity Studies in a Free-Jet Water Tunnel," St. Anthony's Falls Hydraulic Laboratory Report No. 47, Univ. of Minnesota, July 1955

\* \* \* \* \*

## DISCUSSION

E. Silberman (University of Minnesota)

I have had the pleasure of carrying on a stimulating correspondence with one of the authors, Dr. Cohen, in connection with our two-dimensional free-jet cavity studies at the St. Anthony Falls Hydraulic Laboratory of the University of Minnesota. The comments in the paper are in agreement with our own experience and ideas, on the whole. However, one point could stand amplification.

The statement by the authors that force coefficients appear to be insensitive to boundary conditions is apparently correct for blunt bodies at all cavitation numbers. The following figures comparing experimental data obtained in a free jet at  $T_h = 0.0375$  with results from unbounded fluid-flow theory and closed-tunnel data illustrate this point (these are data referred to, but not shown by the authors). Figure D1 is for the cup (or scoop) channel and compares data with theory. Figure D2a is for the circular cylinder at small cavitation numbers, comparing data with theory also. Figure D2b is for the cylinder at larger cavitation numbers, comparing free-jet data with closed-tunnel data obtained by Martyrer.\*

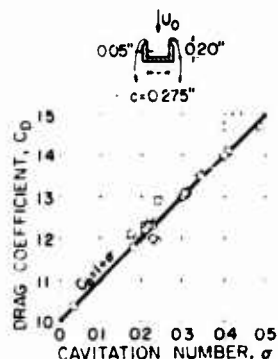


Fig. D1 - Effect of cup channel on drag coefficient

On the other hand, bodies with sharp leading edges, when operated in a free jet at small cavitation numbers (that is, at cavitation numbers generally below those obtainable in a closed tunnel), experience significantly smaller force coefficients than in unbounded fluid. Theoretical results at zero cavitation number, illustrated by Fig. D3 for the flat plate, confirm this statement.

The following three figures show pertinent experimental data: Fig. D4 presents drag coefficient data for the 15-degree semiangle wedge in a free jet; it contains much of the information shown in the authors' Fig. 8, but an experimental point obtained at zero cavitation number has been included, as well as the theoretical result at zero cavitation number (indicated by an arrow). The solid line in the figure represents the linear theory

\*E. Martyrer, "Kraftsmessungen an Widerstands Körpern und Flügelprofilen in Wasserstrom bei Kavitation," pp. 268-286 in "Hydromechanische Probleme des Schiffsantriebs," Ed. by G. Kempf and E. Foerster, Hamburg (1932).



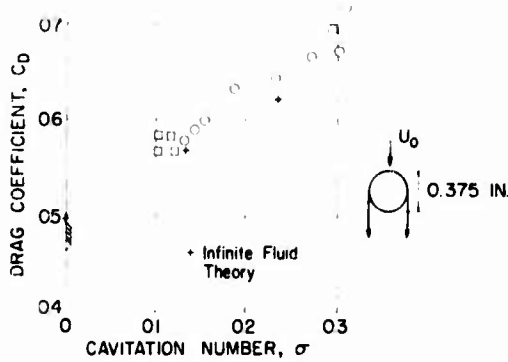


Fig. D2(a) - Effect of circular cylinder (for small  $\sigma$ ) on drag coefficient

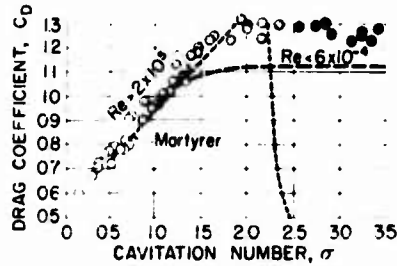


Fig. D2(b) - Effect of circular cylinder (large  $\sigma$ ) on drag coefficient

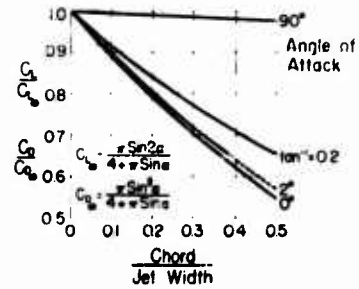


Fig. D3 - Effect of flat plate (at  $\alpha = 0$ ) on drag coefficient ( $C_D$ ) and lift coefficient ( $C_L$ ) at various angles of attack

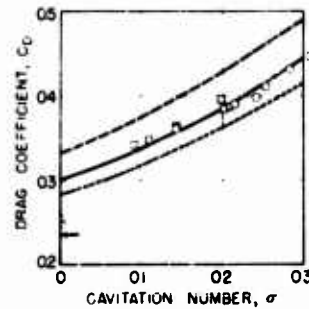


Fig. D4 - Effect of 15-degree semiangle wedge on drag coefficient

for the free jet while the broken line represents Wu's linear theory for infinite fluid and the dotted line represents the infinite fluid solution by the Riabouchinsky model. Figure D5 gives similar information for a 12.5-degree semiangle wedge. The free-jet linear theory is not available for this case. Figure D6 contains data for two inclined flat plates in a free jet. The unbounded fluid result is represented by the solid line taken from Wu's nonlinear theory. This solid line also represents closed-tunnel data obtained by Parkin at cavitation numbers exceeding the minimum for the tunnel (as shown in the authors' Fig. 11). The arrows again represent the theoretical results for the free-jet flow at zero cavitation number. It appears that the free-jet coefficients approach the unbounded-flow coefficients only at some finite cavitation number well in excess of zero.

A comment also appears in order regarding the authors' final statement referring to experimental data for three-dimensional cavities. It should not

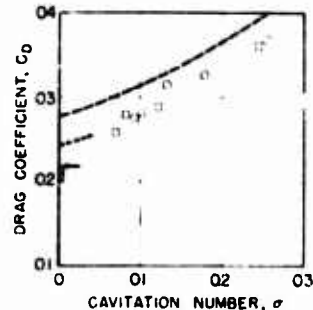


Fig. D5 - Effect of 12.5-degree semiangle wedge on drag coefficient

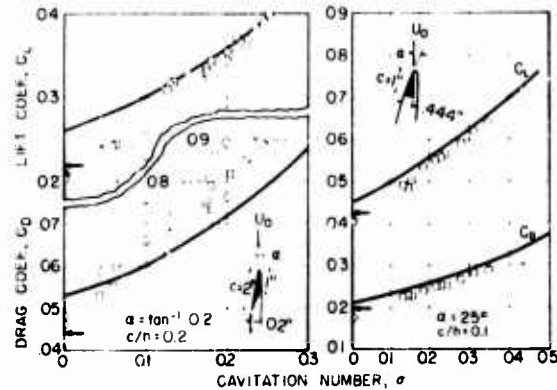


Fig. D6 - Effect of flat plates on drag coefficient ( $C_D$ ) and lift coefficient ( $C_L$ ) compared with results of Wu and Parkin (solid line)

seem surprising that shape effects on three-dimensional cavities in a free jet are very small or even nonmeasurable as compared to those on two-dimensional cavities. Nevertheless, it should be noted that the experimental work by Self and Ripken was performed in a free-jet tunnel with a contact window touching the jet for its full length and closing an eighth of the jet circumference (45 degrees). The tunnel might thus be considered slotted wall rather than free jet. Self and Ripken performed a limited experiment using two contact windows opposite each other and enclosing a quarter of the circumference. Close inspection of their data shows a small but systematic increase in cavity length for the more closed section. There are, incidentally, some interesting problems associated with cavity flows in slotted-wall tunnels, both two- and three-dimensional.

#### A. Silverleaf (National Physical Laboratory)

In addition to the work described here, I am particularly interested in several cases which are not mentioned and do not appear to have been studied. In hydrofoil work in the Lithgow Tunnel at N.P.L. we have been using slotted-wall test sections, and I feel that these configurations have advantages outweighing the difficulties they introduce. We are interested in three cases: first, the two-dimensional foil in a two-dimensional slotted-wall section having solid sides and slotted top and bottom; second, three-dimensional foils, or wings, in slotted-wall and in closed-throat sections; third, two-dimensional foils in a section with solid sides, slotted bottom, and a free surface, such as might be incorporated in a free-surface water tunnel or circulating water channel.

At N.P.L. we hope to complete within the next eighteen months some comparative tests with the same foils in a number of different test sections in a water tunnel and in an open towing tank. Using forced or artificial cavitation I think we can obtain better experimental data on wall correction coefficients than if the work is carried out only in a tunnel.

W. A. Clayden

As Professor DiPrima suggested, A. H. Armstrong at ARDE extended the work of Simmons and computed the cavity size and drag of a flat plate as a function of cavitation number and blockage ratio for a free jet. In our work we measured the cavity length for various two-dimensional flat plates in our free-jet tunnel. Armstrong's boundary corrections were then applied. This had the effect of collapsing the results onto one curve which is in close agreement with the theoretical curve obtained by Perry, Plesset and Shaffer. A similar result was obtained for the widths of the cavities as well, although, since the blockage correction is considerably less, the effect is not so striking.

M. P. Tulin (Office of Naval Research)

Professor DiPrima has made a general remark about the validity of linearized theory. It should be stated in defense of such theory that questions of agreement between linear and non-linear theory must certainly depend upon the angle of attack, the camber, and the thickness of the bodies producing the flow, as well as upon their shape. For example, the force and moment predictions made by a linearized theory for the case of a flat plate hydrofoil become asymptotically exact as the angle of attack approaches zero. At the same time the linearized theory becomes increasingly awry as the angle of attack is made larger. As is well known then, the case for linearized theory may thus be made as bright or as gloomy as one wishes, all depending on the angle-of-attack ranges chosen for discussion.

The important fact exists that linearized theory is proving quite satisfactory in an increasing number of important applications to very practical engineering problems.

R. Timman (Technische Hogeschool, Delft)

Dr. DiPrima mentioned the Winterhall correction we had been doing for some years previously. We got the exact solution in the integrals. It turned out, however, that if we wanted to have numerical results it was somewhat more convenient to work with integral equations and do the thing numerically.

Of course, one can go back one step and introduce integral equations along the walls. I think that would be sufficient unless the walls are too close to the hydrofoil.

Hirsh Cohen and R. C. DiPrima

In reply to Marshall Tulin, we would like to say that we are in agreement with his remarks. What we were trying to point out was simply that the linearized theory that has been used to estimate boundary effects does give the correct qualitative effects, but does not, at least in the cases considered here (the 15-degree, half angle wedge, and the flat plate at angle of attack of 12-degree), give the accuracy of a non-linear theory.

The question of slotted-wall tunnels has been brought up by Dr. Silverleaf and by Prof. Silberman. It seems to us that judging from the results presented in this paper, little effect on force coefficients is to be expected. It seems reasonable to expect

the results for force coefficients to lie between those for solid wall and free-jet test sections. On the other hand, blockage effects on cavity dimensions are of some interest. For a given model and tunnel size, lower cavitation numbers may be obtained with a slotted-wall tunnel. It certainly seems worthwhile to make blockage studies for the slotted-wall case. There seems to be need of some caution in using such test sections as proven by the instability problems experienced at A.R.L. The possibility of cavity-slotted-wall instability interactions should be looked into.

Professor Silberman has raised a point which has, indeed, troubled us. He remarks that for very low cavitation numbers the drag on the 15-degree and 12.5-degree wedges is lower in the free jet than the drag predicted in an infinite stream by the exact theory. But this is borne out in his experiments only by the single point,  $\sigma = 0$ . The linear theory predicts that the drag in a free jet will be lower than in the infinite stream at all cavitation numbers. One feels that this should also appear in the experimental results. If there is an abrupt rise in the drag as the cavitation number increases from zero, it certainly should not become greater than the infinite stream value.

\* \* \* \* \*

# **SOME AERODYNAMIC CAVITY FLOWS IN FLIGHT PROPULSION SYSTEMS**

William G. Cornell  
*Engineering Consultant - Aerodynamics*  
*Jet Engine Department*  
*General Electric Company*

\* \* \* \* \*

Some examples are given of the application of the Helmholtz-Kirchhoff free-streamline theory of incompressible potential flow, along with mixing calculations, to the practical estimation of separated gas flows occurring in several configurations taken from flight propulsion systems. Configurations considered are the perforated plate, the compressor-blade cascade, the vee-gutter flameholder, the target-type thrust reverser, the butterfly valve, and the perforated combustor liner. Results include cavity shape, drag force and total-pressure loss. The theoretical predictions are compared to experimental results in most cases and reasonable agreement is found in the areas wherein the theoretical assumptions are justifiable. The effects of compressibility and scale are discussed.

\* \* \* \* \*

## **INTRODUCTION**

In the development of modern air-breathing flight propulsion systems, powered by aircraft gas turbines and ramjets, certain internal aerodynamic problems arise due to the occurrence of separated flow, viz., streamlines which separate as a result of boundary layer action from the contours of immersed bodies or passage walls. Similar hydrodynamic problems arise in the fuel and propellant systems of liquid rocket engines.

In such separated flows, "dead water" regions are formed downstream of the points of separation of the fluid from the solid boundaries. Within the separated regions the fluid is more or less at rest relative to the moving fluid nearby. The separated regions may be styled as "aerodynamic cavities" in allusion to the true cavity flows in hydrodynamics, where gas filled cavities occur in similar liquid flows. In some cases, the separated flow is designed for (e.g., the separation regions of hot gas behind bluff-body flame holders in aircraft gas turbine and ramjet combustion systems). In other cases, the separated flow is not desired, but occurs under certain operating conditions (e.g., the separation regions of air behind stalled axial-compressor blades in aircraft gas turbines operating at off-design conditions).

In order to obtain optimum designs of the configurations in question, it is desired prior to model tests to predict the characteristics of the separated flow fields. The desired results are usually overall results rather than the complete details of the flow field (e.g., force on and geometry of separated region behind an immersed body, angular deflection and mass flow of a jet of gas, average total-pressure loss of gas flowing through a passage).

In cases where flow velocities are low (incompressible flow) and the flow configuration is made of or can be approximated by solid surfaces composed of linear elements, along with separated streamlines upon which static pressure is constant, and where the streamwise cavity length is long compared to configurational element size, the desired results are conveniently obtained by application of the free streamline method originated by Helmholtz (1) and Kirchhoff (2) and perfected by Michell (3) and others. The method assumes an infinitely long cavity with steady, two-dimensional, body-force-free, potential flow of an incompressible, nonviscous fluid. As a result one obtains immersed-body force, separated region geometry, jet deflection, and mass flow. Mixing calculations then yield total-pressure loss in passage flow cases. With good approximation, certain three-dimensional flows can be treated by consideration of "equivalent" two-dimensional flows having the same "cross-sectional" areas for flow. In passage flow cases with higher flow velocities, the compressibility effect can be accounted for at least approximately by a compressible generalization of the mixing calculation, if theory or experiment is available for estimation of the geometry of the separated flow region. Scale effects (viscosity effects) may be neglected in cases where the separation points are fixed by sharp edges and where the fluid-friction forces in the average streamwise direction are negligible. In other cases, the qualitative nature of the scale effect may be estimated, as discussed elsewhere in the paper.

## PHYSICAL CONCEPTS OF FREE STREAMLINE FLOWS

Early work (2) on free streamline flows included the case of a small sharp-edged orifice in an infinite plate and the case of a flat plate normal to an unbounded stream. In the former case, the theoretical contraction coefficient agreed well with experimental values obtained on both two-dimensional slits and round holes (4). In the latter case, the theoretical drag coefficients were found to be far lower than experimental values (5). This discouraging result impeded further practical applications of the method for many years.

At the root of the large difference between the two cases is the difference between two basic types of flow: (a) The relatively restricted flow of a jet through an opening, as in the case of the sharp-edged orifice, and (b) The relatively unrestricted flow of a free stream over an obstacle, as in the case of the flat plate. In the latter case, instability of the free boundary, small asymmetries, entrainment, etc., cause small motions in the cavity, the velocities of which cannot be neglected relative to the free stream velocity. In the former case, velocities likewise occur in the cavity, but are more nearly negligible relative to the large velocity of the jet. Thus, the fundamental assumption of a stagnant cavity is more justifiable in the case of the orifice than in the case of the plate and consequently there is better agreement between theory and experiment. This important point can be understood best by considering the two cases in question as limiting cases of the more general case shown in Fig. 1. The general case may be considered as a cascade consisting of an infinite number of sharp-edged flat plates of breadth  $b$ , spaced apart by spacing  $t$  along a line normal

<sup>1</sup>See Nomenclature at end of text for definition and the units of all letter symbols.

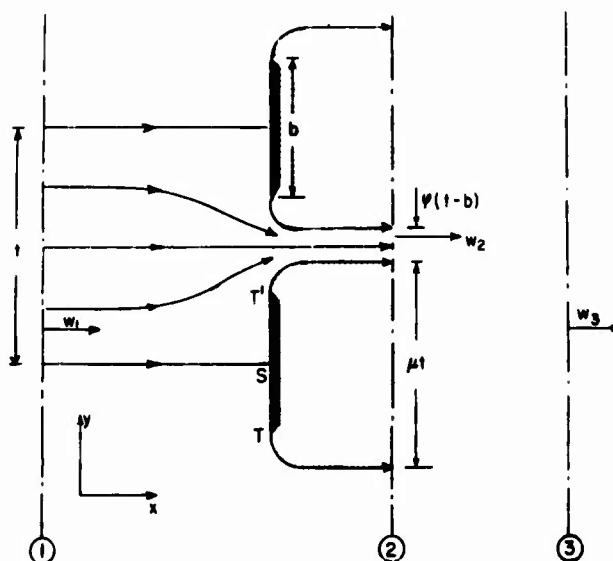


Fig. 1 - Model for flow in slat cascade

to the uniform parallel flow infinitely far upstream of the plates. The upstream flow at Section 1 in Fig. 1 has velocity  $w_1$ . Alternately, this case may be considered as an infinite number of sharp-edged orifices of opening  $t - b$ , spaced apart by spacing  $t$ . Separation regions or cavities extend infinitely far downstream and are enclosed by the free streamlines originating from the sharp edges  $T$  and  $T'$  of the solid boundaries. The static pressure is assumed to be constant at the downstream value on the free streamlines and within the cavity. Under the assumptions used, the fluid velocity is then constant on the free streamlines and discontinuously drops to zero in the cavity. Infinitely far downstream at Section 2, the cavities have width  $t$  and are interspersed with jets of velocity  $w_2$  and breadth  $\mu(t - b)$ , or alternately,  $\mu t(1 - b/t)$ , where  $\mu$  is the "contraction coefficient" for the orifice case. The model is completed by visualization of a mixing region between Section 2 and Section 3, where a uniform parallel flow of velocity  $w_3$  exists. The basic geometric parameter of the configuration is  $b/t$ . The case of the single plate is obtained by  $b/t \rightarrow 0$ , viz.,  $t \rightarrow \infty$ . The case of the single orifice is obtained by  $b/t \rightarrow 1$ , viz.,  $b \rightarrow \infty$ . In the general case of  $0 < b/t < 1$ , the jet velocity  $w_2 = w_1$  by reason of continuity of flow, the ratio  $w_2/w_1$  increasing as  $b/t$  increases. Thus, the validity of the stagnant cavity assumption increases as  $b/t$  increases, a result which is borne out by comparison of theory and test.

Therefore, internal flow configurations having cavities enclosed by jets having a velocity relatively high compared to the upstream velocity are particularly amenable to free streamline analysis. Since there is interest in other configurations (notably single bluff bodies) in which this is not the case, and since hydrodynamic cavities are frequently of finite length, numerous other theoretical methods based on various models of the flow have been developed in order to obtain better agreement between theory and experiment. Among these should be noted the model of Riabouchinsky (6) which employs a downstream "reflection image" of body and cavity, the model of Gilbarg and Rock (7) which has a finite cavity "ventilated" upstream into another

"Riemann sheet," and the model of Roshko (8) which uses an infinite cavity having linear boundaries far downstream. All of these models suffer from the requirement that either the drag coefficient or the pressure within the cavity be known from experiment in order that the flow model can be defined. A model proposed by Weinig (9) utilizes free streamlines which terminate in "winding points" in order to account somewhat for free boundary instability. Tulin (10) developed a "linearized" theory for relatively slender bodies. Any of these models can be used to improve the results of free streamline analysis of single bluff body or finite cavity cases, although analytical difficulties are sometimes large. The fact that such a large variety of models gives good results demonstrates the fact that the exact shape of the cavity does not affect the results too strongly.

The effect of compressibility and scale are discussed later in the paper.

#### ANALYTICAL METHODS FOR DETERMINATION OF FREE STREAMLINE FLOWS

The classical method for solution of free streamline problems grew<sup>12</sup> under the efforts of Helmholtz (1), Kirchhoff (2), Michell (3), Planck (13), Christoffel (14), Schwarz (15), and Rayleigh (16) to the presently accepted method as delineated for example by Lamb (17) and especially well by Milne-Thomson (18). Thus, a flow field comprising linear solid boundaries and separated free streamlines is represented in the "physical" or  $z = x + iy$  plane by a Laplacian net of streamlines ( $\Psi = \text{constant}$ ) and potential lines ( $\Phi = \text{constant}$ ), described by the complex potential  $W = \Phi + i\Psi$ . The complex velocity of flow is given by  $u - iv = U \frac{dW}{dz}$ , where  $U$  is an arbitrary reference velocity. Thus,  $W$  may be used as a position variable to define a "hodograph" or  $\zeta$  plane having the real coordinate  $u/U$  proportional to  $u$ , the  $x$  component of physical plane velocity, and the imaginary coordinate  $-v/U$  proportional to the  $y$  component. Likewise, a "logarithmic hodograph" or  $\Pi = \ln \zeta$  plane may be defined, having the position variable  $\Pi = \ln(u^2 + v^2)^{1/2} + i \tan^{-1}(v/u)$ . Accordingly, the free streamlines in the  $z$  plane may be conformally transformed to circles about the origin in the  $\Pi$  plane and lines parallel to the imaginary axis in the  $\zeta$  plane. Likewise, the linear solid boundaries transform to rays from the origin in the  $\Pi$  plane and lines parallel to the real axis in the  $\zeta$  plane. Thus, the physical flow configuration in the  $z$  plane may be studied in terms of the relatively simpler configurations of circular arcs and rays in the  $\Pi$  plane and of straight lines in the  $\zeta$  plane.

The physical problem involves the determination of the complex potential  $W(z)$ , the complex velocity  $u - iv$  and finally the static pressure  $p$  from the Bernoulli relation  $p + (1/2)\rho(u^2 + v^2) = \text{constant}$ . The relation  $W(z)$  is obtained indirectly through an auxiliary variable  $\zeta$  so defined that the  $\zeta$  plane is a half-plane on the real axis of which is mapped the polygonal boundary of the flow field in the  $\Pi$  plane, by means of the Schwarz-Christoffel transformation function. Also mapped on the  $\zeta$  plane is the (rectangular) polygonal boundary of the flow field in the  $W = \Phi + i\Psi$  plane. Thus, the relations  $\Pi(\zeta)$  and  $\zeta(W)$  are obtainable from the mappings. Then, the relation  $z(\zeta)$  is obtainable by integration as  $z(\zeta) = (1/U) \int \zeta^{1/2} dW(\zeta) / d\zeta d\zeta$ . Finally, having  $\Pi(\zeta)$ ,  $\zeta(W)$ , and  $z(\zeta)$ , there is obtained, at least implicitly,  $W(z)$  and, therefore,  $u(z)$  and  $p(z)$ .

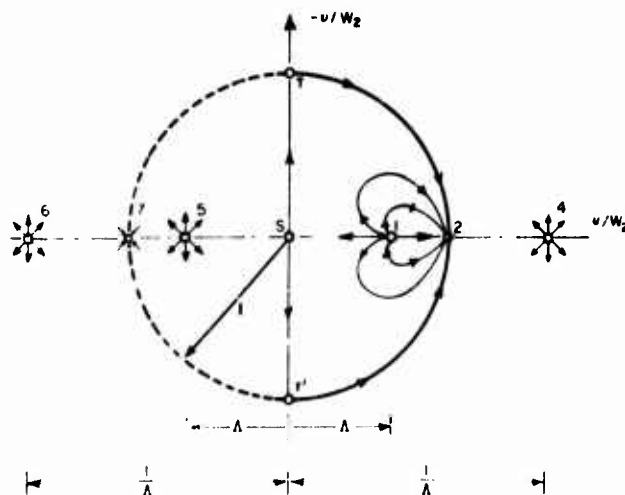
The "classical" method just described can be used in any free streamline problem, although there is no guarantee that a closed-form solution can be obtained, since

<sup>12</sup>See McNown (11) and Barkhoff (12) for interesting historical discussions of the method and its practical application.  
The convention  $W = \Phi + i\Psi$  is used herein.



### EXAMPLE OF THE SLAT CASCADE

The flow field in the  $x$  plane is shown in Fig. 2, and may be physically deduced to be so as follows: The flow in each strip of width  $t$  in the  $z$  plane maps into the



395

unit semicircle in the  $\zeta$  plane. All streamlines (total volume of flow =  $w_1 t$ ) emanate from the point  $\zeta_1 = \lambda$ , the transformed image of the line  $z_1 = -b$ , and terminate in the point  $\zeta_2 = 1$ , the transformed image of the line  $z_2 = 0$ . The plate surfaces TT' map into the imaginary axis. The free streamlines T2 and T'2 map into the unit semicircle. All streamlines of the flow in the  $z$ -plane strip map into streamlines contained within the  $\zeta$  plane semicircle. The mapping is repetitive in that each  $z$ -plane strip maps into the same  $\zeta$ -plane semicircle.

The nature of the flow at  $\zeta_1$  is that of a source of strength (volume flow)  $w_1 t$ , while at  $\zeta_2$  there must exist a double sink of strength  $2w_1 t$ . This follows from consideration of the symmetric nature of the  $\zeta_1$  flow and from the requirement that the imaginary axis and the unit semicircle be streamlines of the  $\zeta$ -plane flow. The latter requirement further demands the existence of the sources (strength  $w_1 t$ ) at  $\zeta_4$ ,  $\zeta_5$ , and  $\zeta_6$  and the double sink (strength  $2w_1 t$ ) at  $\zeta_7$ . The "reflection singularities" added in the  $\zeta$  plane are without (or on) the boundary of the unit semicircle and hence do not imply nonphysical image singularities in the  $z$ -plane flow. Finally, all required boundary conditions in the  $z$ -plane and  $\zeta$ -plane flows are satisfied and the  $\zeta$ -plane flow field is given by the complex potential due to the six singularities as

$$W(\zeta) = (w_1 t / 2\pi) \left[ \ln(\zeta^2 - \lambda^2) + \ln(\zeta^2 - 1/\lambda^2) - 2 \ln(\zeta^2 - 1) \right]. \quad (1)$$

The complex velocity of the  $\zeta$ -plane flow field is then given by

$$dW/d\zeta = (w_1 t / 2\pi) \left[ 2\zeta(\zeta^2 - \lambda^2) + 2\zeta(\zeta^2 - 1/\lambda^2) - 4\zeta(\zeta^2 - 1) \right]. \quad (2)$$

The derivative of the transformation function  $z(\zeta)$  is then given by

$$\frac{dz}{d\zeta} = \frac{dW/d\zeta}{dW/dz} = \frac{dW/d\zeta}{w_2} = \frac{(w_1 t / 2\pi w_2) \left[ 2\zeta(\zeta^2 - \lambda^2) + 2\zeta(\zeta^2 - 1/\lambda^2) - 4\zeta(\zeta^2 - 1) \right]}{1} \quad (3)$$

which equation may be integrated to yield

$$z = (w_1 t / 2\pi) \left\{ \frac{1}{\lambda} \ln \frac{\zeta - \lambda}{\zeta + \lambda} + \lambda \ln \frac{\zeta - 1/\lambda}{\zeta + 1/\lambda} - 2 \ln \frac{\zeta - 1}{\zeta + 1} \right\} + C_1 \quad (4)$$

where  $C_1$  is an arbitrary constant of integration. Equation (4) is the transformation function  $z(\zeta)$  linking points in the  $z$  and  $\zeta$  planes.

The  $\zeta$ -plane parameter  $\lambda$  may now be evaluated from use of the physical condition that the plate breadth  $b$  is given by the relation

$$b = (1/\pi) (z_T - z_{T'}), \quad (5)$$

Substituting (4) in (5) with  $\zeta_T = i$  and  $\zeta_{T'} = -i$ , yields the relation

$$b = (1/\pi) \left[ 1 - \lambda^2 + 2 \ln \frac{1 - \lambda^2}{1 + \lambda^2} + \ln \frac{1 - \lambda^2}{1 + \lambda^2} \right] \quad (6)$$

which gives the parameter  $\lambda = w_1/w_2$  implicitly in terms of the blockage  $b/t$ . Thus, the  $\zeta$  plane is completely determined for a chosen  $z$ -plane geometry  $b/t$ , and the  $z$ -plane complex velocity  $u + iv = w_2$  can be determined at any point. In particular, at the point  $\zeta_1$ , the complex velocity is  $u_2 + iv_2 = w_1/\lambda$ .

Continuity of flow in the  $x$ -plane requires that

$$w_2(1 - \lambda)t = w_1 t \quad (7)$$

so that

$$\lambda = 1 - \Lambda \quad (8)$$

is obtained for the cavity width parameter and  $\Lambda(b, t)$  is obtained from (6) and (8).

The result may be expressed in terms of the contraction coefficient defined geometrically by

$$C_c = (1 - \lambda)(1 - b/t) \quad (9)$$

which yields  $\Lambda(b, t)$  from (6), (8), and (9).

The drag force per unit span  $D$  on one of the slats may be expressed as a non-dimensional drag coefficient  $C_D = D / (1/2) \rho w_1^2 b$  as

$$C_D = (1 - \Lambda)^2 (t/b) \Lambda^2 \quad (10)$$

from application of the momentum principle to one strip of fluid of breadth  $t$  and from consideration of the Bernoulli relation for the lossfree flow between Sections 1 and 2. Then, (6) and (10) yield  $C_D(b, t)$ .

The total-pressure loss  $\Delta p_T = p_{T1} - p_{T3}$  may be calculated under the assumption of constant momentum mixing of the jets and cavities at Section 2 to yield a uniform stream of velocity  $w_3 = w_1$  at Section 3. Thus, applying the momentum principle and the continuity principle to the fluid between Sections 2 and 3 and noting that  $p_{T2} = p_{T1}$  as assumed, it follows that the total-pressure loss coefficient  $\Delta p_T / (1/2) \rho w_1^2$  is given by

$$(1 - \Lambda)^2 \Lambda^2 \quad (11)$$

so that (6) and (11) yield  $\Delta p_T(b, t)$ .

Plots of velocity ratio  $\lambda$ , contraction coefficient  $C_c$ , drag coefficient  $C_D$  and loss coefficient against blockage  $b/t$  are shown in Figs. 3a-3d, compared to two- and three-dimensional (same blockage) experimental data on various configurations. Figure 3a shows the theoretical prediction for  $\lambda(b, t)$  compared to experimental data of Betz and Petersohn (20) for the cases of water discharging into air (circled points) and air into air ( $\times$  points). It will be noted that the former tests agree most closely with theory. Figure 3b compares the theoretical  $\Lambda(b, t)$  with pipe orifice water tests of Weisbach (21) and axisymmetric nozzle air tests of Grey and Wilsted (22). The two-dimensional theory is compared to the three-dimensional data at the same blockage  $b/t$ . Figure 3c shows the theoretical prediction for

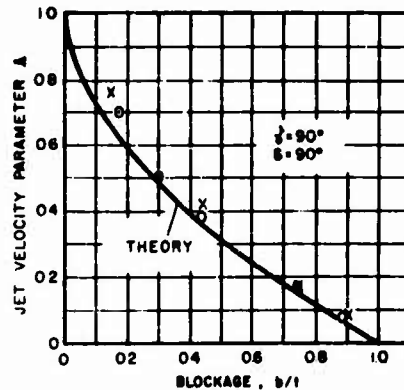


Fig. 3a - Comparison of theory and experiment for jet velocity parameter of slat cascade

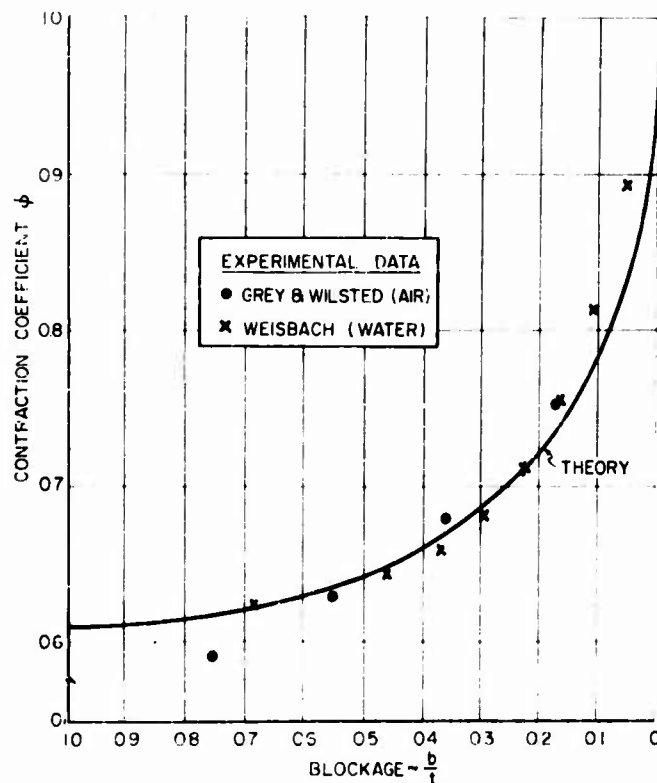


Fig. 3b - Comparison of theory and experiment for contraction coefficient of slat cascade

$C_D(w_1 w_2)^2$ , or drag coefficient based on jet velocity head, compared to air tests of Langer (23), who measured slat forces with a two-component balance. Figure 3d compares the theoretical (16) to the test results of various investigators (24) on perforated plate strainers, ribbon screens, and strip screens. The test results agree reasonably well with the theory, especially at high solidity or blockage  $b/t$ , for which cases the stagnant cavity assumption is most valid. Generally, experimental values of  $\phi$ ,  $1 - \lambda$ ,  $C_D$ , and  $\sigma$  are less than theory predicts, undoubtedly due in part to the lack of perfect sharpness of the experimental plate edges.

#### THE STALLED CASCADE OF ARBITRARY STAGGER

In off-design performance analysis of axial-flow compressors for aircraft gas turbines, it is important to be able to predict the performance of blade rows operating in stalled condition. A simple model (19) of a blade row is the two-dimensional cascade of infinitesimally thin flat plates shown in Fig. 4 and characterized geometrically by solidity  $\lambda$  and stagger  $s$ . The configuration is a generalization of that of the slat cascade ( $\lambda = 90^\circ$ ,  $s = 0$ ) previously discussed and may be analyzed by a similar method.

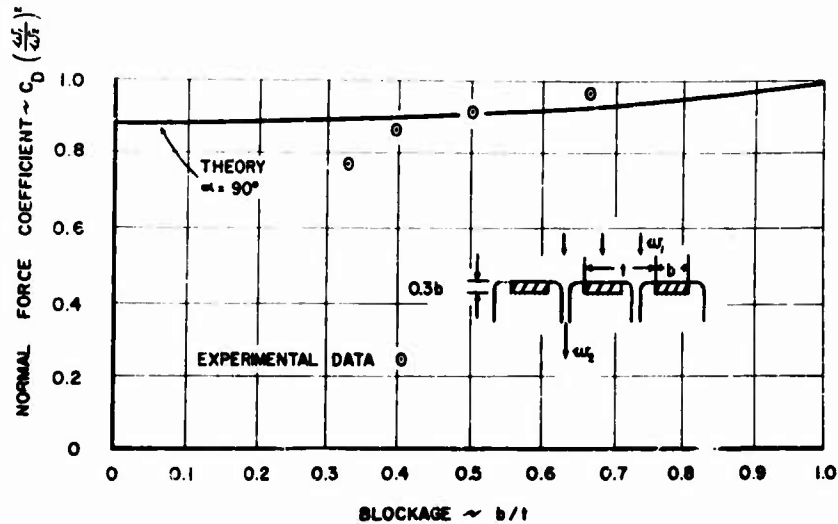


Fig. 5c - Comparison of theory and experiment for normal-force coefficient of slat cascade

In the generalized case, the flow is complicated by the fact that the cascade causes a deflection  $\alpha_1 = \alpha_2$  of the jets, while the mixing of jets and cavities causes a further deflection, to yield an overall deflection  $\alpha_1 = \alpha_3$ . The situation is conveniently visualized in terms of the conventional "velocity triangle" of the cascade, as shown in Fig. 5. It is noted that  $w_1$  and  $w_3$  have equal  $x$  components (normal to cascade axis) as a result of continuity of flow, while  $w_2$  and  $w_3$  have equal  $y$  components (along cascade axis) as a result of momentum considerations. The conventional "vector mean velocity"  $w_r$  and its inclination  $\alpha_r$  are defined such that

$$2 \tan \alpha_r = \tan \alpha_1 + \tan \alpha_3 \quad (12a)$$

$$w_r = w_1 \cos \alpha_1 \cos \alpha_r \quad (12b)$$

The free streamline analysis of Betz and Petersohn (20) yields the jet velocity parameter  $\lambda = w_1/w_2$  and the jet flow angle  $\alpha_2$  as functions of cascade geometry  $b/l$  and  $\alpha$  and of angle of attack  $\alpha_1 = \alpha$ . The cavity width parameter  $\lambda$  then follows from consideration of continuity of flow as

$$\lambda = 1 - A \cos \alpha_1 \cos \alpha_2 \quad (13)$$

Analysis of the mixing of jets and cavities (19) then yields the overall cascade performance. Thus, the final velocity  $w_3$  and its inclination  $\alpha_3$  are obtained from continuity and momentum consideration as

$$w_3/w_2 = \sin \alpha_2 / [1 + (1 - \lambda)^2 \tan^2 \alpha_2]^{1/2} \quad (14a)$$

$$\tan \alpha_3 = \tan \alpha_2 (1 - \lambda) \quad (14b)$$

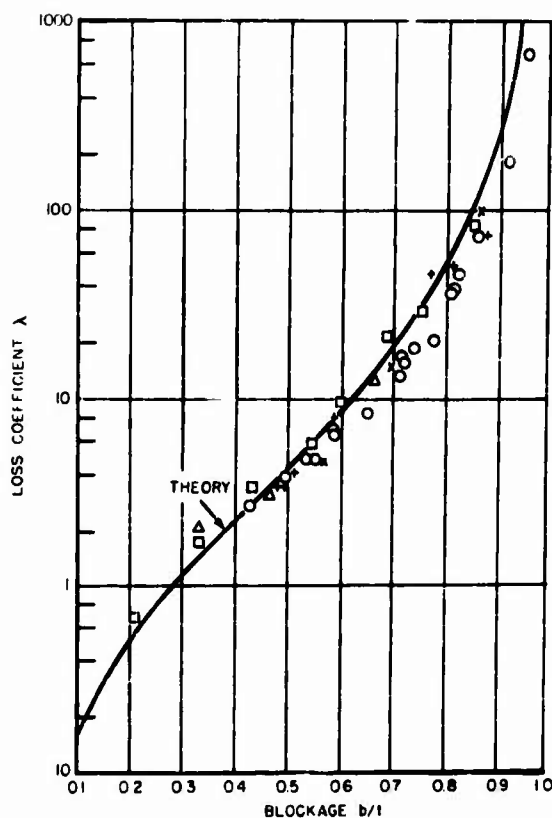


Fig. 3d - Comparison of theory and experiment for total-pressure loss coefficient of slat cascade

The vector mean velocity  $w$ , and its inclination  $\alpha$ , are then obtained from (12) and the overall changes in static and total pressure are obtained from continuity and momentum considerations as

$$(P_3 - P_1) / (1/2) \rho w^2 = \cos^2 \alpha \left\{ 2 - (1 - \cos^2 \alpha) - \sec^2 \alpha (1 - \lambda^2) \lambda^2 \right\} \quad (15a)$$

$$(P_{T1} - P_{T3}) / (1/2) \rho w^2 = \cos^2 \alpha - 2(1 - \cos^2 \alpha)^2, \quad (15b)$$

The force  $N$  on each plate is normal to the plate and may be expressed in terms of a normal force coefficient  $C_N = N / (1/2) \rho w^2$ , referred to  $w$ . Then, conventionally, the total plate force may be resolved into the lift  $L$  and drag  $D$  forces, respectively normal and parallel to  $w$ . Then, the lift and drag coefficients are given by

$$C_L = L / (1/2) \rho w^2 = C_N \cos(\alpha - \beta), \quad (16a)$$

$$C_D = D / (1/2) \rho w^2 = C_N \sin(\alpha - \beta), \quad (16b)$$

The normal force coefficient  $C_N$  is obtained from momentum considerations as

$$C_N = (\cos^2 \alpha_1 - \cos^2 \alpha_2) (1 - \lambda^2) + \sin^2 \alpha_1 (1 - \lambda^2) \lambda^2 + 2 \cos \alpha_1 \sin \alpha_2 (1 - \lambda^2) + (1 - \lambda^2) \sin^2 \alpha_2 (1 - \lambda^2) \quad (17)$$

Then, (16) and (17) may be used to obtain  $C_L$  and  $C_D$ .

Typical theoretical results (19) are shown in Figs. 6a-6c for the case of the stagger  $\alpha = 30^\circ$  and the angle of attack  $\alpha = 0$ . Companion results for  $\alpha = 0$  (turbine case) are given in Ref. 19. Figure 6a shows the relation among jet velocity ratio  $\lambda$ , jet turning angle  $\alpha$ , solidity  $l/t$ , and angle of attack  $\alpha$ . Figure 6b shows the relation among overall turning  $\alpha$ , loss coefficient  $\lambda$ ,  $l/t$ , and  $\alpha$ . Figure 6c shows the "polar diagram" where lift coefficient  $C_L$ ,  $C_L/(a_1 a)^2$  is plotted as a function of drag coefficient

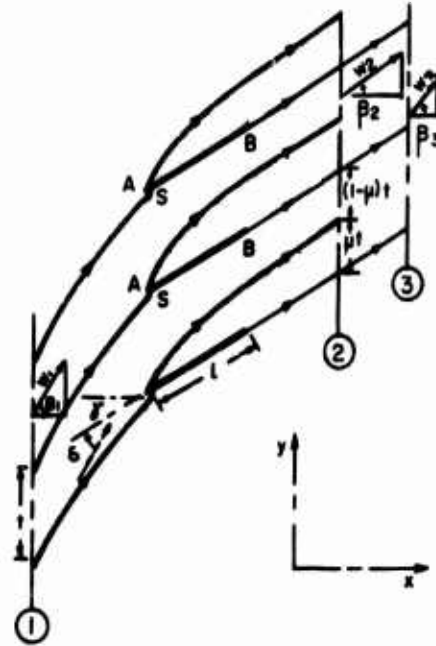


Fig. 4 - Model for flow in stalled cascade of stagger

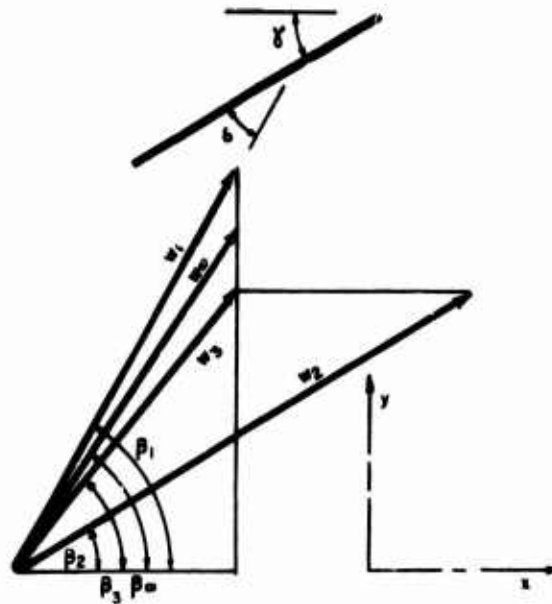


Fig. 5 - Velocity triangle for stalled cascade

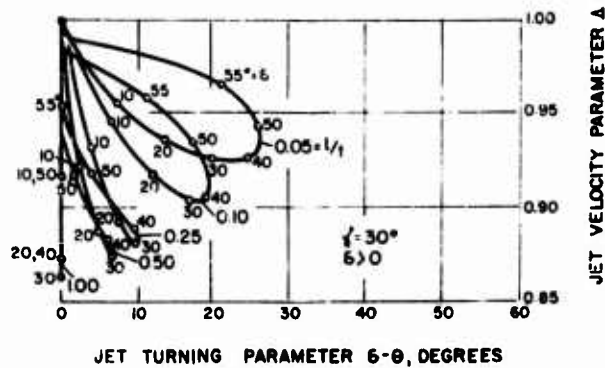


Fig. 6a - Theoretical jet turning angle and jet velocity parameter of stalled cascade

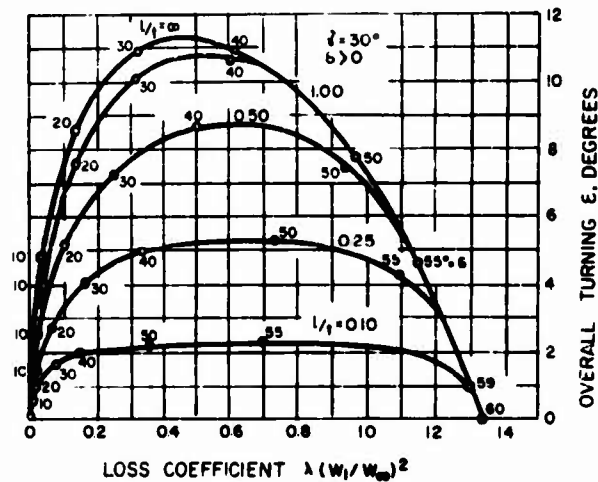


Fig. 6b - Theoretical overall turning angle of stalled cascade

$C_D = C_D(w_1/w_\infty)^2$  for various  $l/t$  and  $\gamma$ . Figures 7a and 7b show comparisons of the theoretical results with experimental results of various investigators. Figure 7a compares the theoretical predictions of  $\lambda$  and  $\epsilon$  with experimental air test data of Betz and Petersohn (20) for  $l/t = 1.2$ , inlet angle  $\gamma_1 = 0$ , and various stagger  $\gamma$ . Figure 7b shows theoretical normal-force coefficient  $C_N(w_1/w_\infty)^2$  for various solidity  $l/t$ , and several values of angle of attack  $\alpha$  and stagger  $\gamma = 90^\circ$ , compared to air test results of Langer (23). Experimental values of  $\lambda$  and  $\epsilon$  exceed theoretical predictions, the discrepancy undoubtedly being due in part to the lack of perfect edge sharpness. The low values of normal-force coefficient at low incidence probably imply the lack of fully developed stall. The force coefficient comparison shows improvement in agreement between theory and test as solidity increases, a trend shown by other experimental data on  $\lambda$  and  $\epsilon$  (19).



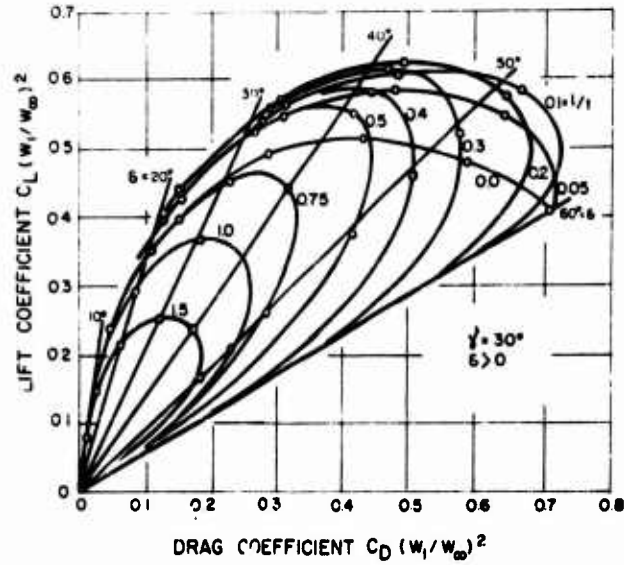


Fig. 6c - Theoretical lift-drag polar of stalled cascade

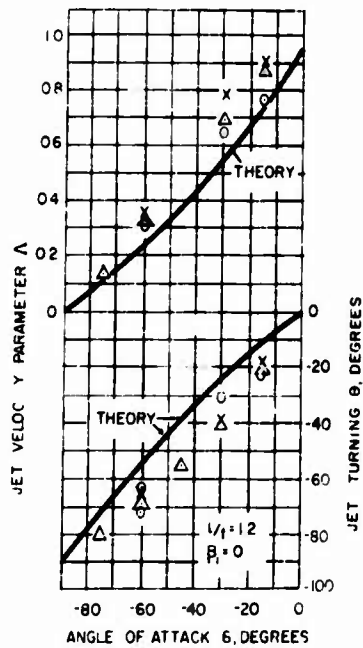


Fig. 7a - Comparison of theory and experiment for jet velocity parameter and jet turning angle of stalled cascade of 1.2 solidity and zero inlet angle

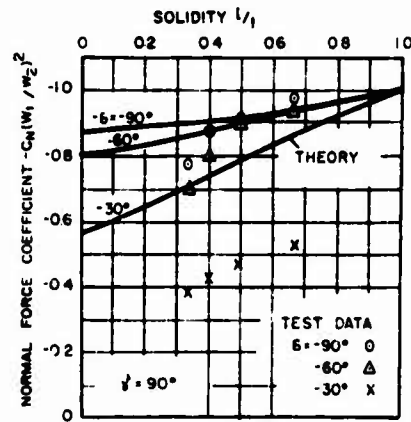


Fig. 7b - Comparison of theory and experiment for normal-force coefficient of stalled cascade of 90 stagger

## THE VEE-GUTTER FLAMEHOLDER

In afterburners of aircraft gas turbine power plants and in ramjet combustors, various bluff bodies are used as flameholders, the downstream cavities being used to stabilize combustion. A typical configuration is composed of concentric rings of vee cross-section. A simple model (25) is the two-dimensional vee-gutter cascade shown in Fig. 8. The configuration may be considered to be a generalization of the slat cascade ( $\alpha = 90^\circ$ ), with the additional geometrical variable of gutter-included half-angle  $\alpha$ . The desired results are again the cavity width parameter  $\beta$ , the drag coefficient  $C_D$  and the total-pressure loss coefficient  $\zeta$  for a chosen cascade geometry given by blockage  $b/t$  and half-angle  $\alpha$ .

The configuration of the vee-gutters and cavities is aerodynamically equivalent, under the assumptions made, to the two-dimensional contraction of wall angle  $\alpha$  and area ratio  $1 - b/t$ . The contraction was analyzed by von Mises (26), utilizing the classical method, in order to obtain the contraction coefficient  $C_c = (1 - \beta)/(1 - b/t)$  as a function of  $b/t$  and  $\alpha$ , a result useful in the prediction of flow through conical exhaust nozzles (same area ratio) of turbojet engines. The theoretical results of von Mises (26) are shown in Fig. 9 in terms of  $C_c$  as a function of  $b/t$  and  $\alpha$ .

Then, as in the case of the slat cascade, drag coefficient  $C_D$  and loss coefficient  $\zeta$  are calculated (25) as functions of  $b/t$  and  $\alpha$  by application of the continuity and momentum principles. The theoretical results are shown in Figs. 10a and 10b. In Figs. 11a-11c, the theoretical results are compared (25) to experimental results of various investigators. Figure 11a compares theoretical values of wake width to pitch ratio  $\beta$  for various half-angle  $\alpha$  and blockage  $b/t$  to experimental results of Grey and Wilsted (22) for air tests of conical nozzles. The experimentally determined contraction coefficients are expressed in terms of equivalent values of  $\beta$  for the comparison. Figure 11b shows theoretical drag coefficient  $C_D/(w_1 w_2)^2$  for  $\alpha = 140.5^\circ$  and various  $b/t$  compared to experimental data of Langer (23) from air tests. Figure 11c compares the theoretical prediction for loss coefficient  $\zeta$  for  $\alpha = 45^\circ$  and various  $b/t$  with air and combustion gas test results of Noreen (27) on two-dimensional single-gutter flameholder models. In general, theory and experiment compare best at high blockage  $b/t$ .

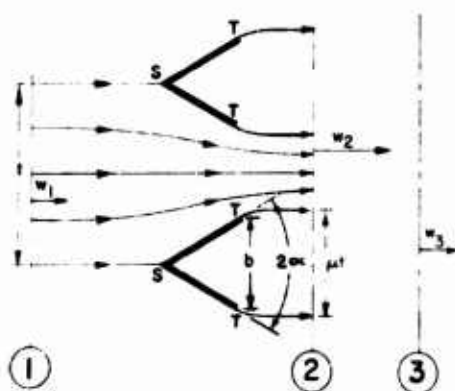


Fig. 8 - Model for flow in vee-gutter cascade

## THE TARGET-TYPE THRUST REVERSER

In order to slow down jet aircraft upon landing, without decreasing engine rotative speed so much that large engine acceleration times would be required should landing plans be abandoned, a variety of jet thrust spoilers and reversers have been investigated. One type of jet thrust reverser is the target type, in which an obstacle of concave form on the upstream face is inserted across the jet in order to deflect the jet upstream, thereby providing some reverse or negative thrust. For design purposes, it is desired to obtain the shape of and velocity in the deflected jet as a function of target geometry, so that effectiveness of thrust reversal may be studied.

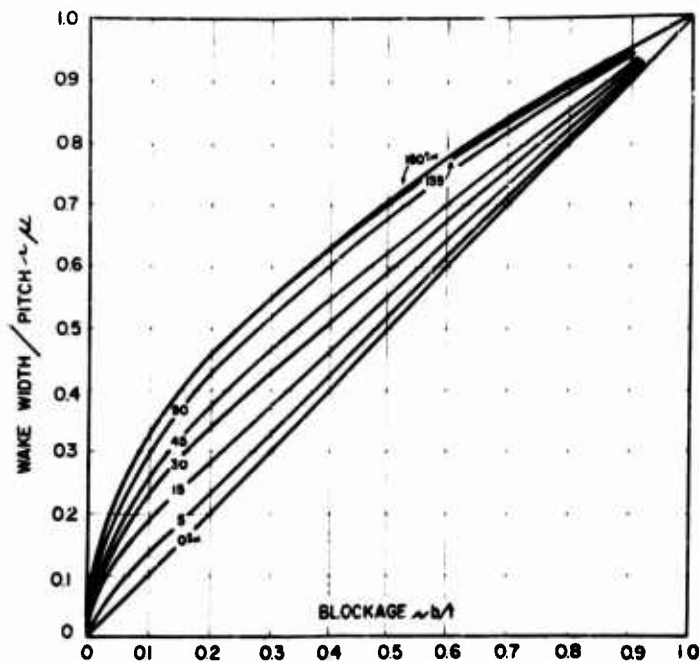


Fig. 9 - Theoretical wake width to pitch ratio of vee-gutter cascade

Considering a cylindrical thrust reverser of internal diameter  $D$  and axial length  $c$ , positioned symmetrically across a jet of diameter  $d$ , the equivalent two-dimensional configuration is shown in Fig. 12. The model reverser has axial length  $c$  and breadth  $b$ , the upstream jet breadth being  $a$ , where  $c/a = c/d$  and  $b/a = (D/d)^2$  define the equivalence of the two- and three-dimensional configurations. The initial jet of breadth  $a$  and velocity  $u_1$  splits into two symmetrical jets of width  $a/2$  and velocity  $u_1$ , since the jets are bounded by the free streamlines along which the velocity is taken as constant. The desired result is the jet deflection angle  $\theta$  as a function of target and jet geometry  $b/a$  and  $c/a$ . Sarpkaya (28) has analyzed the configuration by the classical method in order to study the flow in water turbine "scoop" buckets. The theoretical results are shown in Fig. 13, compared to three-dimensional test data of Siao and Hubbard (29) and De Haven (28) taken with water jets in air. The check between theory and test is best at low  $b/a$  and low  $c/a$ , suggesting that frictional effects may be responsible for the lack of better agreement.

A similar analysis may be made of a conical target of internal diameter  $D$  and included angle  $2(\theta - \phi)$  positioned symmetrically across a jet of diameter  $d$ . The equivalent two-dimensional configuration, shown in Fig. 14, has breadth  $b$  and included angle  $2(\theta - \phi)$ , the jet breadth being  $a$ , where  $b/a = (D/d)^2$  defines the equivalence. The desired result is jet deflection angle  $\theta$  as a function of target and jet geometry  $b/a$  and  $\phi$ . Siao and Hubbard (29) analyzed the model configuration by the classical method in order to study water turbine bucket flows. Their theoretical results are shown in Fig. 15, compared with results of their three-dimensional experiments on water jets in air. Measured deflection angles are lower than predicted and increasingly so at larger  $b/a$ , presumably due mostly to the effect of friction and possibly also to the lack of perfect sharpness of test plate edges.

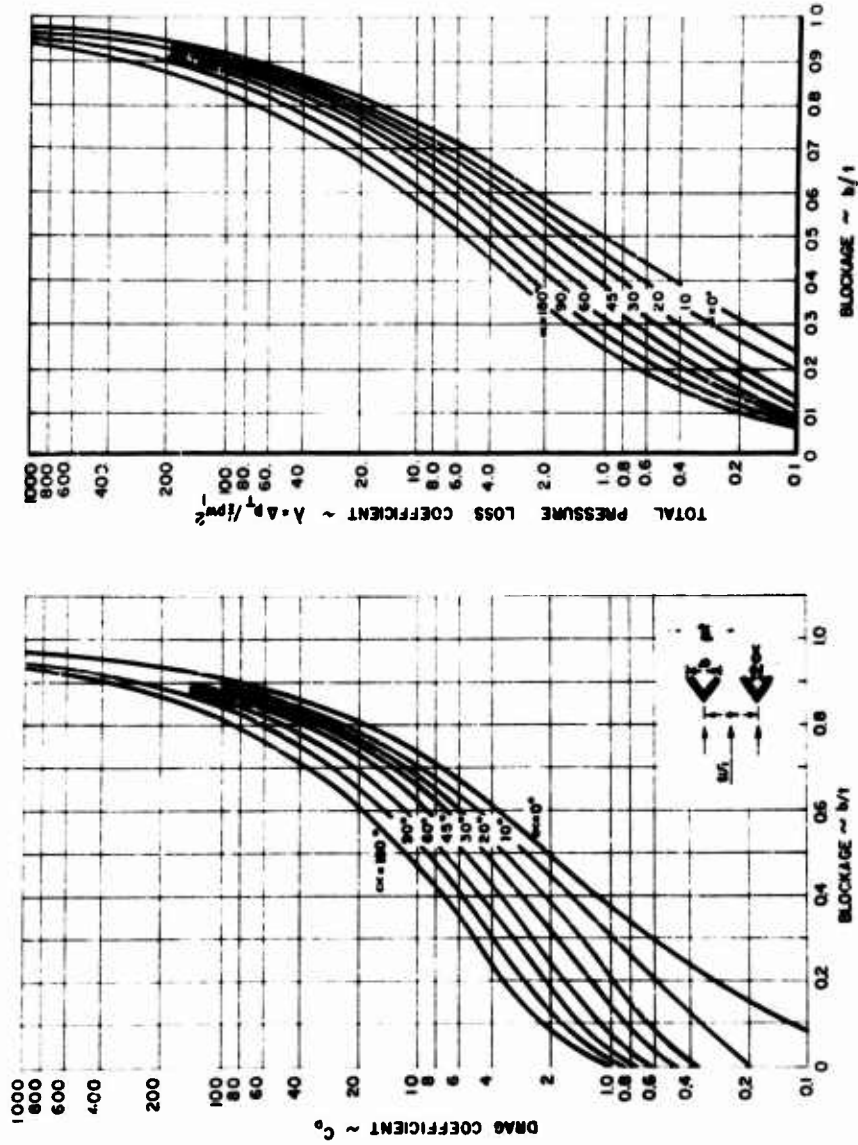


Fig. 10b - Theoretical total-pressure loss coefficient of vee-gutter cascade

Fig. 10a - Theoretical drag coefficient of vee-gutter cascade

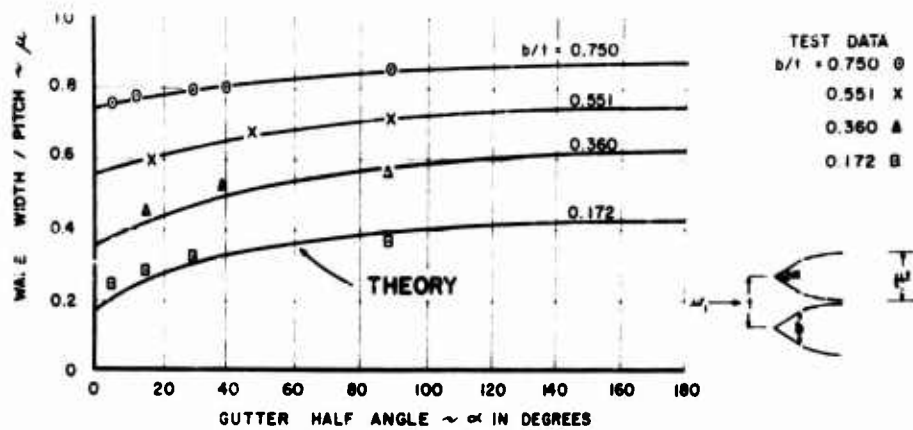


Fig. 11a - Comparison of theory and experiment for wake width to pitch ratio of vee-gutter cascade

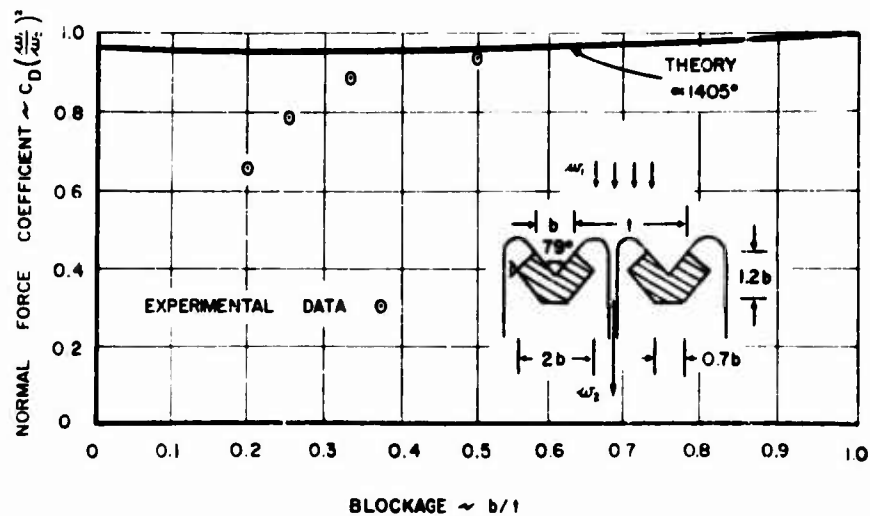


Fig. 11b - Comparison of theory and experiment for normal-force coefficient of vee-gutter cascade of  $140.5^\circ$  half-angle

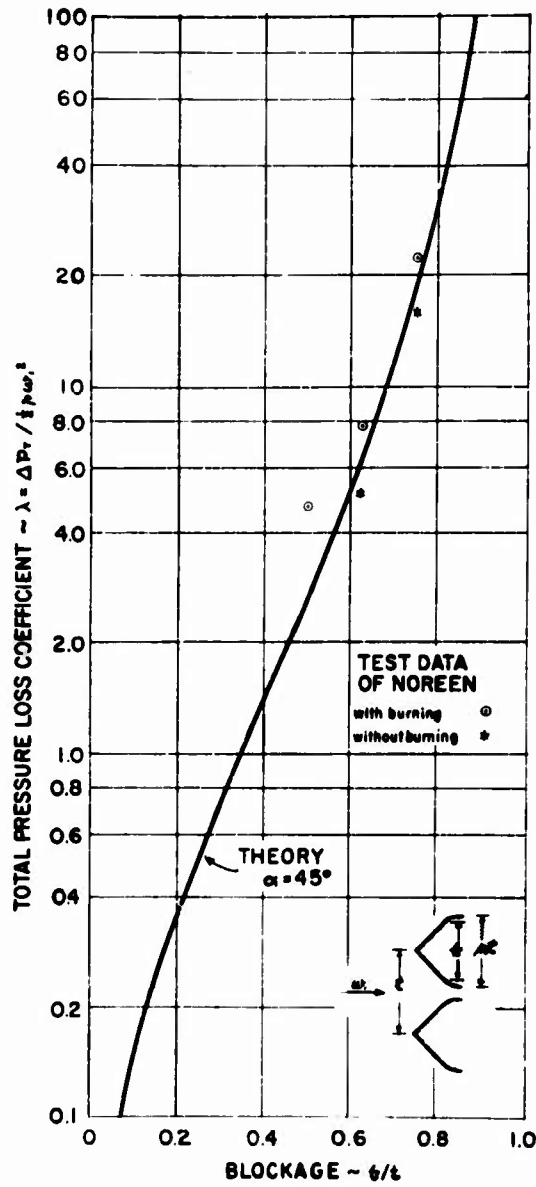


Fig. 11 - Comparison of theory and experiment for total-pressure loss coefficient of vee-gutter cross-section of 45° half-angle

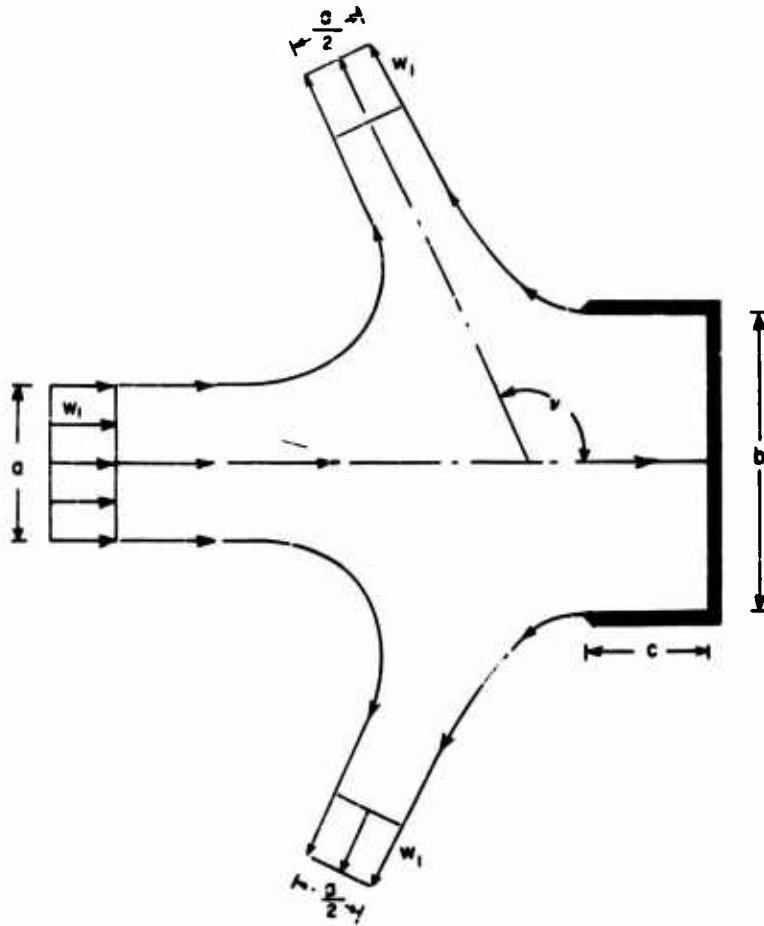


Fig. 12 - Model for flow over cylindrical thrust reverser

From the point of view of thrust reverser effectiveness, viz., largest deflection angle for smallest target size, the results of the two configurations show that thrust reversal ( $\approx 90^\circ$ ) begins at  $b/a = 2$ , smaller targets giving  $\approx 90^\circ$ . Little additional deflection is obtained above about  $b/a = 4$ . For the cylindrical target, increasing axial length much above about  $b/a = 1.5$  gives little additional deflection. For the conical target, the included half-angle  $\alpha$ , must be less than  $90^\circ$  in order to get reversal. As  $\alpha$  is decreased from  $90^\circ$ , deflection increases at a decreasing rate. Generally speaking, the conical target requires greater axial length than the cylindrical target, for the same diameter and deflection angle, making the latter preferable because of smaller size and weight.

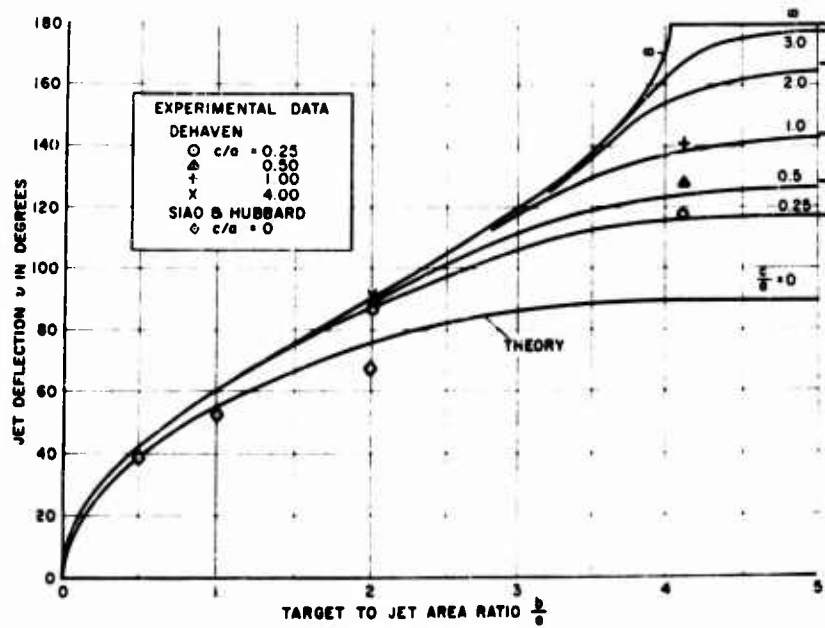


Fig. 13 - Comparison of theory and experiment for jet deflection angle of cylindrical thrust reverser

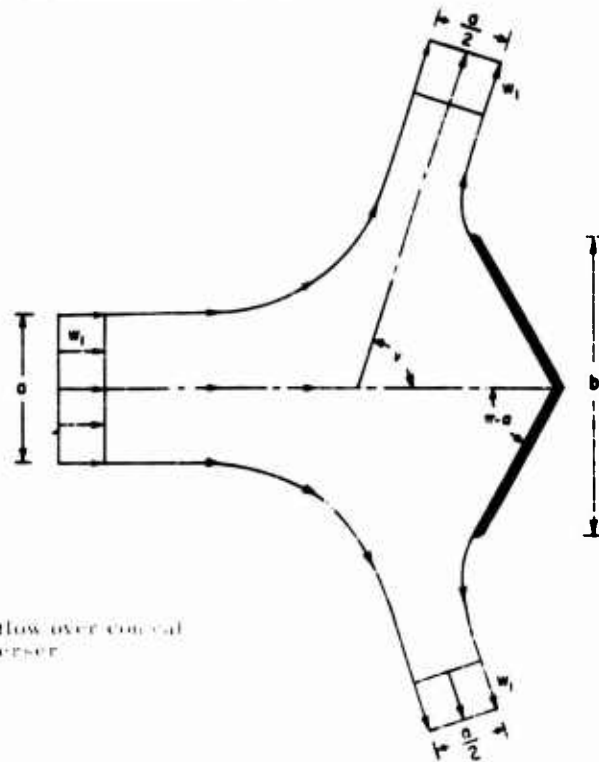


Fig. 14 - Model for flow over conical thrust reverser



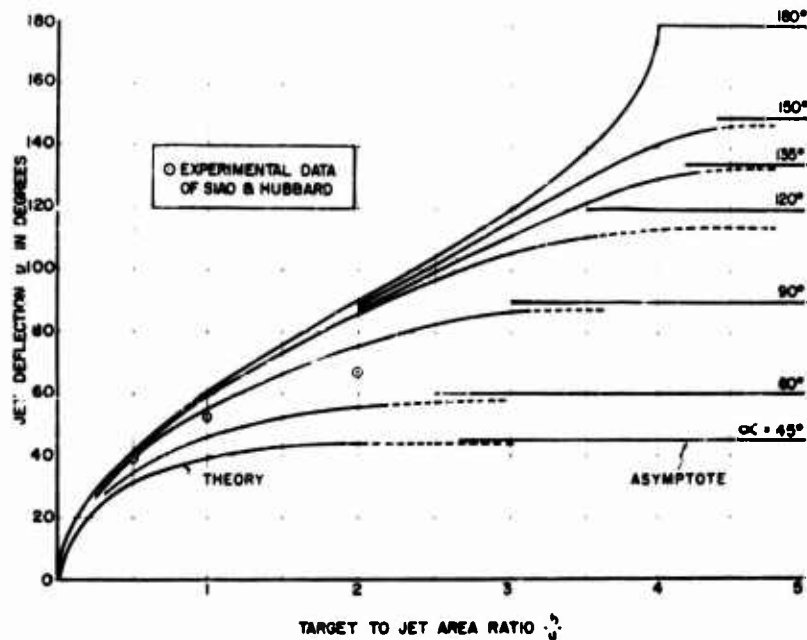


Fig. 15 - Comparison of theory and experiment for jet deflection angle of conical thrust reverser

## THE BUTTERFLY VALVE

Butterfly or damper valves are frequently used as flow regulators in liquid rocket engine piping, aircraft gas turbine control system piping, and aerodynamic test facility ducting. It is desirable to predict the flow characteristics and total-pressure losses of such valves, as well as the forces acting on the regulating plates. A two-dimensional model of a butterfly valve is shown in Fig. 16. A plate of breadth  $t$  is placed in a channel of the same breadth making an angle  $\alpha$  with the channel axis. Gaps of breadth  $(1/2)(t - (1/2)t(1 - \sin \alpha))$  exist at each side of the plate. A cavity is formed behind the plate, having breadth  $t - (1/2)t(1 - \sin \alpha)$  infinitely far downstream from the plate. The asymmetry of the configuration causes different breadths  $t/2$  and  $t/2$  of the jets outside of the cavity. The velocity  $u_2$  exists in both jets, assuming uniform static pressure at Section 2. The "average" contraction coefficient of the valve may be regarded as  $(1/2)(C_{c1} + C_{c2})$ .

Ehrich (30) made an approximate analysis of the model configuration by treating the flow in two parts as shown in Fig. 17. The two approximate component configurations have unknown upstream breadths respectively equal to  $t/2$  and  $t/2$ , where  $t/2 + t/2 = t$ ; otherwise boundary conditions are the same. Then, Ehrich recognized that the configurations of Fig. 17 were equivalent to von Mises' (26) two-dimensional contractions (or, likewise, the author's (25) vee-gutter cascades). Thus the contraction coefficients  $C_{c1}$  and  $C_{c2}$  may be obtained as  $C_{c1} = (s_1^2 / (1 - s_1^2))$  and  $C_{c2} = (s_2^2 / (1 - s_2^2))$ , where  $s_1^2 = 1 - (t/2)^2$  and  $s_2^2 = 1 - (t/2)^2$  are respectively the blocked area ratios of the two approximate configurations and  $\alpha_1$  and  $\alpha_2$  are the wall angles. Then, the contraction coefficient  $(1/2)(C_{c1} + C_{c2})$  is obtained in terms of valve closure angle  $\alpha$ . Ehrich

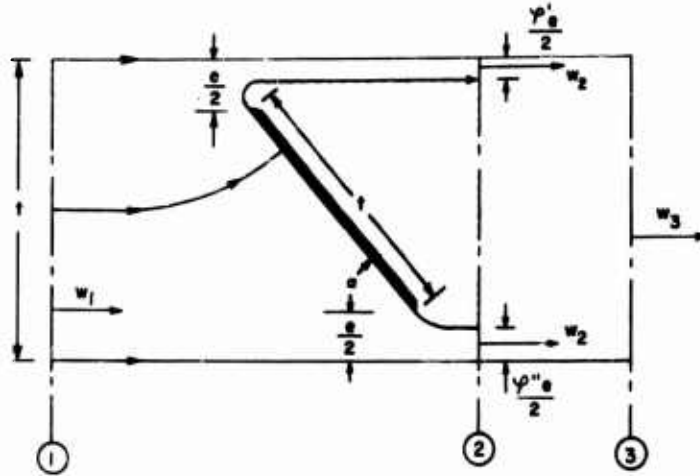


Fig. 16 - Model for flow in butterfly valve

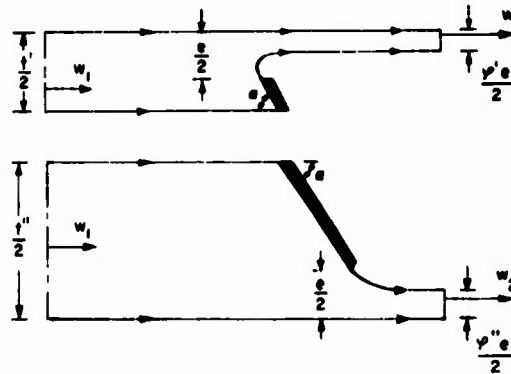


Fig. 17 - Approximate model for flow in butterfly valve

obtained the (normal) force acting on the valve plate by consideration of momentum and continuity, in terms of component axial and lateral force coefficients as:

$$C_{Ax} = F_{Ax} / 1.2 \rho V_1^2 = 2 \cos^2 \alpha \sin^2 \alpha \left( 1 - \frac{1}{2} \right)^2 \quad (18a)$$

$$C_{Ay} = F_{Ay} / 1.2 \rho V_1^2 = 2 \cos^2 \alpha \sin^2 \alpha \left( 1 - \frac{1}{2} \right)^2 \cot \alpha \quad (18b)$$

where  $\alpha = 1 - \sin \alpha$ . Thus, the valve force is obtained as a function of valve closure  $\alpha$ .

The total-pressure loss across the valve may be obtained by assuming complete mixing of the cavity and jets to yield a uniform flow of velocity  $V_3 = V_1$  at Section 3

as shown in Fig. 16. Thus, from continuity and momentum considerations (as in the case of the slat cascade analysis), the total-pressure loss coefficient is given by

$$(p_{T1} - p_{T3}) / (1/2) \rho V_1^2 = \left\{ 2 \left( \frac{C_d}{C_c} \right)^2 - 1 \right\} \quad (19)$$

which yields  $C_d$ .

Figures 18a and 18b show the theoretical results of contraction coefficient and loss coefficient as functions of valve closure angle  $\alpha$ . The theoretical loss coefficient is compared to three-dimensional test data of Weisbach (31), with the latter being largest, presumably because of the approximation introduced in the analysis (compare vee-gutter cascade results).

Other interesting valve configurations analyzed by Ehrich (30) include flapper, needle, orifice plate, gate, and spool valves.

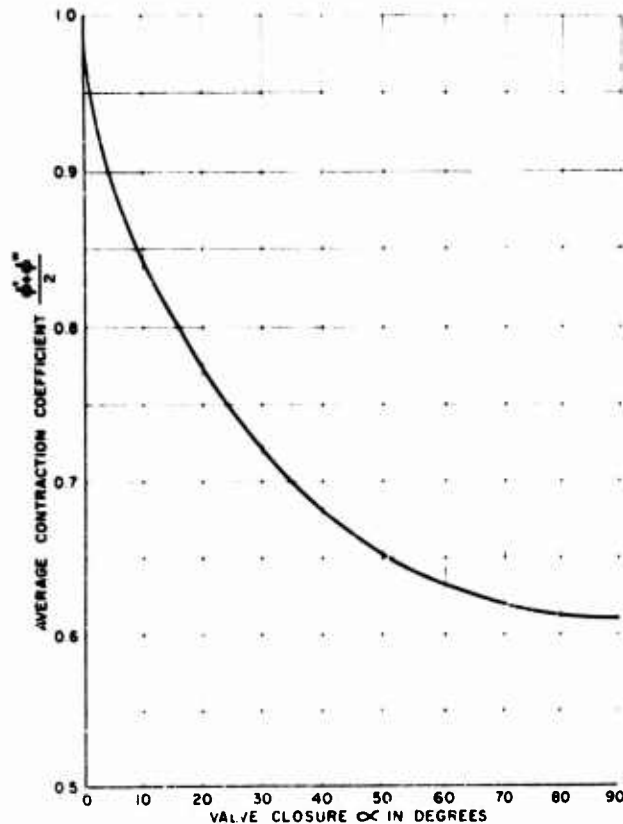


Fig. 18a Theoretical contraction coefficient as a function of valve closure angle.

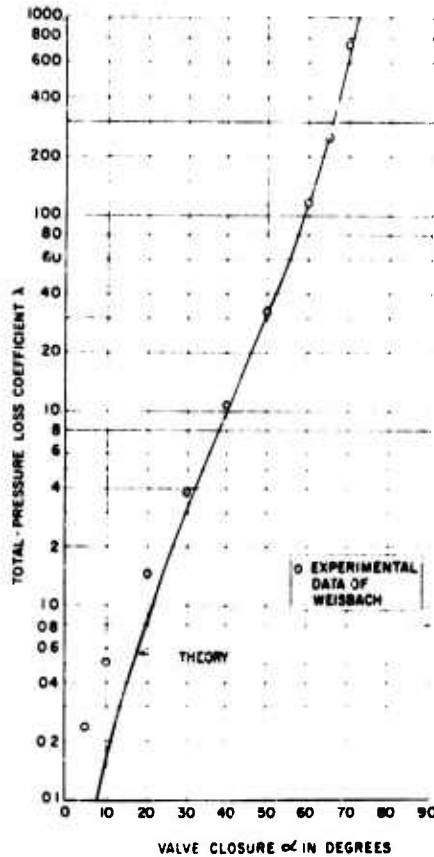


Fig. 18b - Comparison of theory and experiment for total-pressure loss coefficient of butterfly valve

flowing axially in the annular space between the cylinders enters the inner cylinder through the perforations, is mixed with fuel, and burned, leaving downstream. Thus, there is considerable practical interest in the flow of air through a sharp-edged opening in a wall having air flow along it. It is desired to predict the flow through the opening and the "penetration" (described by flow angle) of the jet into the downstream space. McNown and Hsu (32) have studied the model shown in Fig. 19. A two-dimensional channel of breadth  $g$  has uniform velocity  $w_1$  at infinity. A slot of breadth  $t$  in one wall forms a jet having area  $t$  and velocity  $w_2$  at infinity. The jet is deflected through an angle  $\phi$  relative to the upstream flow at Section 1. The remainder of the flow passes out of the channel with velocity  $w_4$  at Section 4 at infinity. It is desired to predict the contraction coefficient  $C_c$  and the jet deflection angle  $\phi$  for various slot/channel breadth ratios  $t/g$  and various amounts of jet flow as characterized by the velocity ratio  $w_4/w_1$ . McNown and Hsu obtained the solution by the classical method. The theoretical results are shown in Fig. 20, where  $C_c$  and  $\phi$  are shown as functions of  $t/g$  and  $w_4/w_1$ .

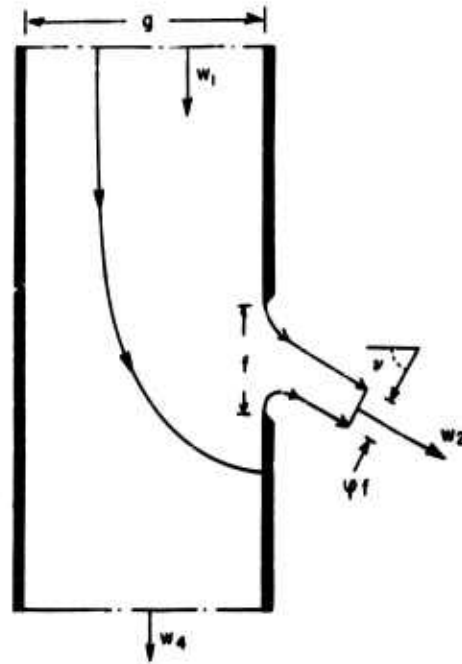


Fig. 19 - Model for flow in perforated combustor liner

#### THE PERFORATED COMBUSTOR LINER

In primary combustion systems for aircraft gas turbines the combustor configuration usually consists of one or more cylindrical containers, each having a concentric inner cylinder perforated with various holes, slots, and louvers. Air

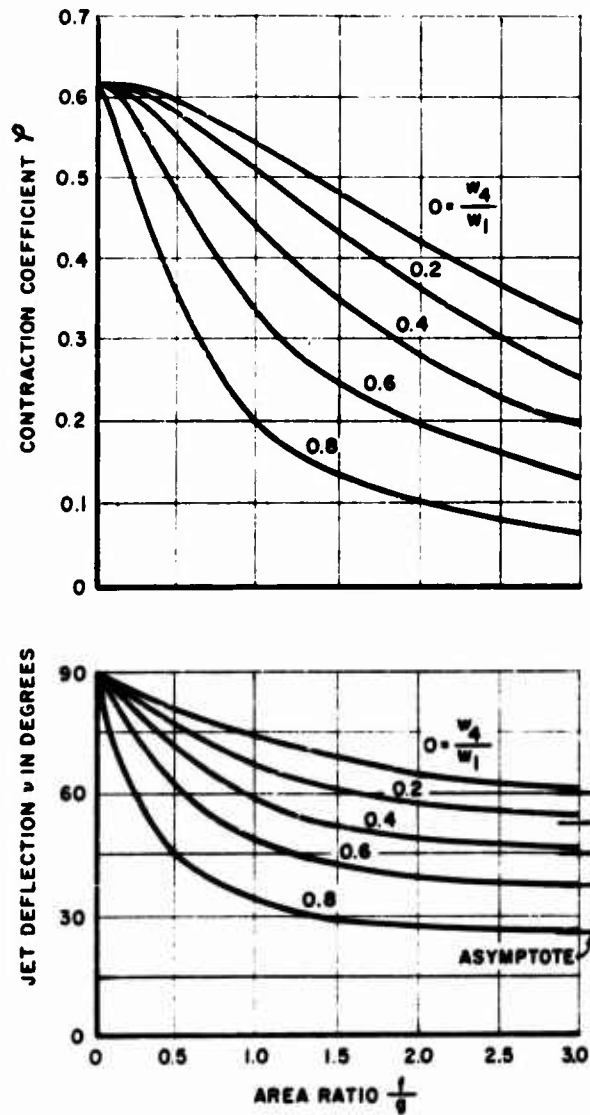


Fig. 20 - Theoretical contraction coefficient and jet deflection angle of perforated combustor liner

Ehrich (33) analyzed a different case having combustion interest, wherein air is fed through a sharp-edged slot into a parallel flow which is directed along the wall. For the case of equal total-pressures of the two streams, the surface of separation between the streams was calculated, as well as the free streamline separating the jet from the downstream solid boundary. Qualitative agreement was obtained between theoretical jet shapes and those obtained experimentally.

## COMPRESSIBILITY EFFECTS IN AERODYNAMIC CAVITY FLOWS

The various solutions discussed above assume incompressible flow and yield reasonable results as long as this and the other assumptions are justifiable. However, in cases of high blockage or high inlet Mach number (ratio of flow velocity to velocity of sound) or both, results are a strong function of Mach number, since very high velocities then occur in the jets. In such cases, the compressibility effect is important. Analytical methods are not available for handling the general case. However, for specific configurations, solutions can be made in a manner entirely similar to the incompressible calculations.

An example of a compressible case is that of the slat cascade, treated by the author (24) in the study of flow through sharp-edged screens. In this case, the contraction coefficient  $C_c$  was estimated as a function of blockage  $b/t$  and jet Mach number  $M_1$ . The estimation of  $C_c$  was based on air test data on conical flow nozzles, taken over a range of nozzle pressure ratios. Then, compressible mixing calculations yielded the theoretical results shown in Fig. 21, where loss coefficient  $C_L$  is shown as a function of inlet Mach number  $M_1$  for various blockages  $b/t$ . The loss coefficient  $C_L$  rises with  $M_1$  for a given  $b/t$ , as might be physically expected. A subsonic flow limit curve is shown, the locus of conditions such that  $M_2 = 1$ . The curves are shown dashed beyond this limit because they are extrapolations, the one-dimensional mixing calculations used being invalid in this region. Further, additional shock waves will occur in supersonic jets. The curves are terminated by the envelope curve labeled "upper bound for choke," the locus of conditions such that sonic velocity exists across the entire opening of breadth  $t/b$ . Actual choking conditions will obtain somewhere between the subsonic flow limit and the upper bound for choke. Additional calculations could be made to yield compressible drag coefficients for the slat cascade.

A comparison of theoretical predictions of loss coefficient  $C_L$  with experimental results (24) is shown in Fig. 22, for air tests of two perforated plates. Reasonable agreement is found between theory and test.

## SCALE EFFECTS IN AERODYNAMIC CAVITY FLOWS

In cases where separation points are definitely fixed by the geometry (sharp edges) and where fluid-friction forces in the average streamwise direction acting on solid surfaces are negligible, e.g., the slat cascade, little scale effect is found (24). At very low Reynolds numbers (based on upstream velocity  $V_1$  and slat breadth  $t$ ), the loss coefficient  $C_L$  may be expected to fall and then rise again as the Reynolds number is decreased, and likewise for the drag coefficient  $C_D$ . The contraction coefficient  $C_c$  may be expected to rise and then fall again as the Reynolds number falls, similar to the case of the single sharp-edged orifice.

In cases where separation points are geometrically fixed, but fluid-friction forces in the average streamwise direction are not negligible, e.g., the tee-gutter cascade, some scale effect is to be expected. At low Reynolds numbers, the loss coefficient  $C_L$  may be expected to rise with falling Reynolds number, and likewise for the drag coefficient  $C_D$ . The contraction coefficient may be expected to fall with falling Reynolds number, similar to the case of the rounded flow nozzle.

In cases where the separation points are not geometrically fixed and fluid-friction forces in the average streamwise direction are not negligible, e.g., a cascade of cylinders, a large scale effect is to be expected. As in the case of the single circular cylinder, the locations of the separation points will vary with the Reynolds

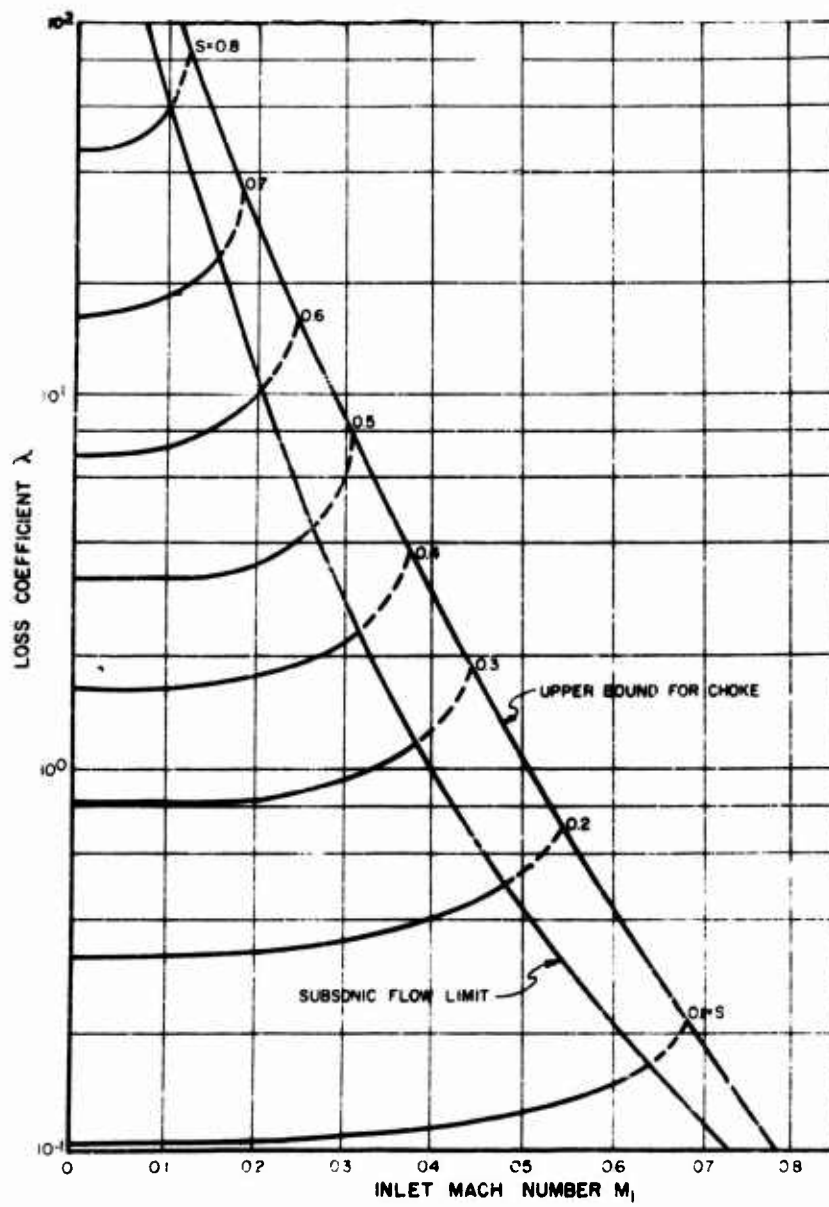


FIG. 2.1. Theoretical incompressible total-pressure loss coefficient of flat-plate or perforated plate.

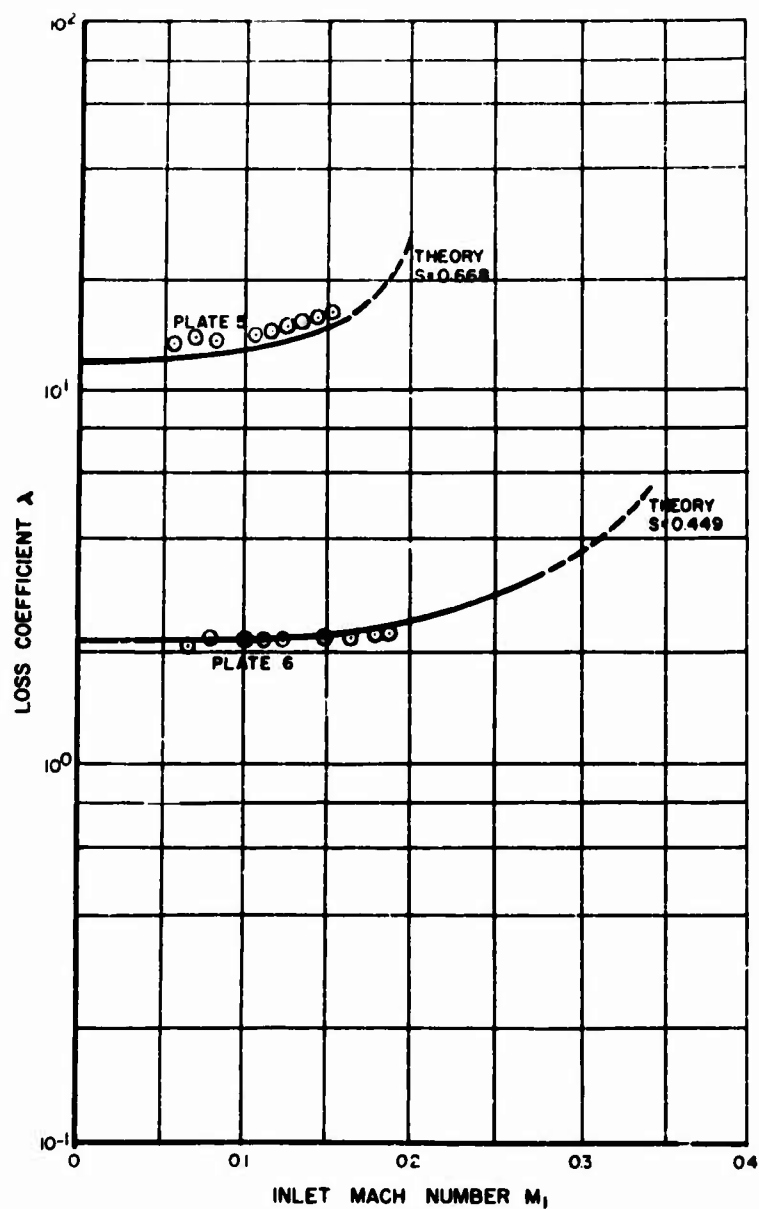


Fig. 22 - Comparison of theory and experiment for compressible total-pressure loss coefficient of perforated plates



number and, possibly, the entire character of the flow will likewise vary. For example, experimental data on round-wire screens (24) show a strong increase in drag coefficient  $C_D$  as the Reynolds number decreases in the region of low Reynolds numbers.

## CONCLUSIONS

In aerodynamic cavity flows, viz., long cavities or wakes of relatively low velocity trailing behind solid obstacles in gas flows, reasonable results can be obtained in predicting cavity shape, drag force, and total-pressure loss by use of the free streamline method of Helmholtz-Kirchoff, along with mixing calculations, if the flow velocities are low enough to justify the assumption of incompressible flow, solid surfaces can be approximated by linear elements, the Reynolds number is not too low, and jet velocities adjacent to the cavities are high enough to justify the assumption of a stagnant cavity.

Results can be obtained for higher velocity flows, if the effect of compressibility on cavity shape can be estimated analytically or otherwise. Scale effect (Reynolds number effect) will not be large in cases where the separation points (cavity inception) are fixed by sharp edges and where one may neglect the fluid-friction forces in the average streamwise direction on the solid surfaces. In other cases, the qualitative nature of the scale effect may be estimated.

## ACKNOWLEDGMENT

The author is indebted to Mrs. Barbara Emmons for preparation of the present manuscript.

## NOMENCLATURE

- $a$  = jet breadth upstream of thrust reverser (ft)
- $b$  = breadth of configuration element in direction transverse to upstream flow direction (ft)
- $c$  = axial depth of cylindrical thrust reverser (ft)
- $C_D$  = drag force coefficient, referred to upstream velocity head
- $C_L$  = lift force coefficient, referred to upstream velocity head
- $C_N$  = normal force coefficient, referred to upstream velocity head
- $D$  = drag force per unit span length (lb/ft)
- $\theta$  = opening of butterfly valve, measured normal to valve axis (ft)
- $t$  = breadth of bleed slot in wall of combustor liner (ft)
- $w$  = breadth of channel upstream of bleed slot in combustor liner (ft)
- $\gamma = \sqrt{\gamma - 1}$

- $l$  = chord of flat plate cascade (ft)
- $L$  = lift force per unit span length (lb/ft)
- $H = \zeta + i\eta$  = non-dimensional complex position variable in the logarithmic hodograph plane
- $M$  = Mach number
- $N$  = normal force per unit span length (lb/ft)
- $p$  = static pressure (lb/ft<sup>2</sup>)
- $p_T$  = total-pressure (lb/ft<sup>2</sup>)
- $s$  = blocked area ratio of butterfly valve or perforated plate
- $t$  = pitch or spacing between configuration elements (ft)
- $u$  =  $x$  component of fluid velocity (ft/sec)
- $U$  = reference velocity (ft/sec)
- $v$  =  $y$  component of fluid velocity (ft/sec)
- $w$  = fluid velocity (ft/sec)
- $W = \phi + i\psi$  = complex potential (ft<sup>2</sup>/sec)
- $x$  = abscissa in the physical plane (ft)
- $y$  = ordinate in the physical plane (ft)
- $z = x + iy$  = complex position variable in the physical plane (ft)
- $Z$  = complex position variable in the auxiliary half-plane (ft)
- $\beta$  = included half-angle of vee-gutter cascade or valve closure angle of butterfly valve or external half-angle of conical thrust reverser
- $\gamma$  = fluid angle measured relative to normal to cascade axis
- $\delta$  = stagger angle of flat plate cascade
- $\alpha = \alpha_1 - \alpha_2$  = angle of attack in flat plate cascade
- $p_T = p_{T1} - p_{T2}$  = total-pressure loss (lb/ft<sup>2</sup>)
- $\theta = \theta_1 - \theta_2$  = overall deflection angle of flat plate cascade
- $\zeta = (\phi + i\psi)/U$  = nondimensional complex position variable in the hodograph plane
- $\theta = \theta_1 - \theta_2$  = jet deflection angle of flat plate cascade

# Aerodynamic Gravity Flows in Flight Propulsion Systems

- $\epsilon = \frac{p_T}{\rho_1} (1 - \frac{w_2^2}{w_1^2}) =$  total-pressure loss coefficient, referred to upstream velocity head
- $\lambda = \frac{w_1}{w_2} =$  velocity ratio
- $\mu =$  cavity breadth as a fraction of pitch  $t$
- $\theta =$  jet deflection angle of thrust reverser or combustor liner
- $\kappa =$  contraction coefficient (jet breadth as a function of configuration aperture breadth)
- $\rho =$  fluid mass density (slug/ft<sup>3</sup>)
- $\Phi =$  potential function (ft<sup>2</sup>/sec)
- $\Psi =$  stream function (ft<sup>2</sup>/sec)

## Subscripts

- $ax =$  subscript referring to axial force in butterfly valve analysis
- $lat =$  subscript referring to lateral force in butterfly valve analysis
- $1 =$  subscript referring to conditions infinitely far upstream of configuration
- $2 =$  subscript referring to conditions infinitely far downstream of configuration
- $3 =$  subscript referring to conditions after mixing of jets and cavities
- $4 =$  subscript referring to conditions downstream of bleed slot in combustor liner
- $\infty =$  subscript referring to vector mean velocity in flat plate cascade

## REFERENCES

1. Helmholtz, H., "Ueber diskontinuierliche Fluessigkeitsbewegungen," Monatsberichte Akademie der Wissenschaften, Berlin, 1868, pp. 215-228; also, Philosophical Magazine, November 1868
2. Kirchhoff, G., "Zur Theorie freier Fluessigkeitsstrahlen," Crelle's, Journal fuer Mathematik 70:289-298 (1869)
3. Michell, J.H., "On the Theory of Free Streamlines," Philosophical Transactions of the Royal Society (London) A181:389-431 (1890)
4. Trefftz, E., "Ueber die Kontraktion kreisfoermiger Fluessigkeitsstrahlen," Zeitschrift fuer Mathematik und Physik 64:34-61 (1916); also, Dissertation, Strassburg, 1913
5. Flachsbart, O., "Messungen an ebenen und gewoelbten Platten," Ergebnisse der Aerodynamisch Versuchsanstalt zu Goettingen, IV Lieferung, 1932, pp. 96-100.

6. Riabouchinsky, D., Proceedings of the London Mathematical Society 19:206-215 (1921)
7. Gilbarg, D., and Rock, D.H., Naval Ordnance Laboratory Memorandum No. 8718, 1945
8. Roshko, A., "A New Hodograph for Free-Streamline Theory," National Advisory Committee for Aeronautics Technical Note 3168, July 1954
9. Weinig, F.S., "Computation of Drag in Separated Flow by Use of Rolling Up Free Streamlines," Proceedings of the 9th International Congress for Applied Mechanics, Brussels, 1957, Vol. 1, pp. 215-220
10. Tulin, M.P., "Steady Two-Dimensional Cavity Flow about Slender Bodies," David Taylor Model Basin Report 834, May 1952
11. McNowen, J.S., "Elements of Free-Streamline Theory," in "Free-Streamline Analyses of Transition Flow and Jet Deflection," State University of Iowa, Studies in Engineering, Bulletin 34, 1953, pp. 3-14
12. Birkhoff, G., "Hydrodynamics - A Study in Logic, Fact and Similitude," Princeton University Press, 1950, pp. 40-76
13. Planck, M., "Zur Theorie der Fluessigkeitsstrahlen," Annalen der Physik und Chemie 21:499-509 (1884)
14. Christoffel, E.B., "Cal Problema delle Temperature Stazionarie e la rappresentazione di una Data Superficie," Annali di Matematica, Series 2, 1:95-103 (1867)
15. Schwarz, H.A., "Notizia sulla rappresentazione conforme di un'area ellittica sopra un'area circolare," Annali di Matematica, Series 2, 3:166 (1869)
16. Lord Rayleigh, "Notes on Hydrodynamics," Philosophical Magazine, December 1876
17. Lamb, H., "Hydrodynamics," 6th ed., New York:Dover (reprint) 1945
18. Milne-Thomson, L.M., "Theoretical Hydrodynamics," 2nd ed., New York:Mac-Millan, 1950
19. Cornell, W.G., "The Stall Performance of Cascades," Proceedings of the Second U.S. National Congress of Applied Mechanics, Ann Arbor, Michigan, 1954, pp. 705-713
20. Betz, A., and Petersohn, E., "Anwendung der Theorie der freien Strahlen," Ingenieur-Archiv 2:190-211 (1931); see also National Advisory Committee for Aeronautics Technical Memorandum 667, 1932
21. Weisbach, J., "Die Experimental-Hydraulik," Freiberg:Engelhardt, 1855
22. Grey, R.E., and Wilsted, H.D., "Performance of Conical Jet Nozzles in Terms of Flow and Velocity Coefficients," National Advisory Committee for Aeronautics Technical Note 1757, November 1948
23. Langer, R., "Bremswirkung von Windschutzgittern," Ergebnisse der Aerodynamischen Versuchsanstalt zu Goettingen, IV Lieferung, 1932, pp. 138-141

24. Cornell, W.G., "Losses in Flow Normal to Plane Screens," Transactions of the American Society of Mechanical Engineers 80(No. 4):791-799 (1958)
25. Cornell, W.G., "The Flow in a Vee-Gutter Cascade," Transactions of the American Society of Mechanical Engineers 78(No. 3):573-580 (1956)
26. von Mises, R., "Berechnung von Ausfluss- und Ueberfallzahlen," Zeitschrift des Vereines deutscher Ingenieure 61(No. 21):447-452 (1917); 61(No. 2):469-474 (1917); and 61(No. 23):493-498 (1917)
27. Norcen, A.E., unpublished, 1954
28. Sarpkaya, T., "Deflection of Jets - Symmetrically Placed U-Shaped Obstacles," in "Free-Streamline Analysis of Transition Flow and Jet Deflection," State University of Iowa, Studies in Engineering, Bulletin 35, 1953, pp. 45-53
29. Siao, T-T, and Hubbard, P.G., "Deflection of Jets - Symmetrically Placed V-Shaped Obstacles," in "Free-Streamline Analysis of Transition Flow and Jet Deflection," State University of Iowa, Studies in Engineering, Bulletin 35, 1953, pp. 33-34
30. Ehrich, F.F., "Some Hydrodynamic Aspects of Valves," American Society of Mechanical Engineers, Paper No. 55-A-114, November 1955
31. Merriman, M., "Treatise on Hydraulics," 8th ed., New York:Wiley, 1907, pp. 216-217
32. McNow, J.S., and Hsu, E-Y, "Application of Conformal Mapping to Divided Flow," Proceedings of the First Midwestern Conference on Fluid Dynamics, May, 1950, Ann Arbor:Edwards, 1951, pp. 143-155
33. Ehrich, F.F., "Penetration and Deflection of Jets Oblique to a General Stream," Journal of the Aeronautical Sciences 20:99-104 (1953)

\* \* \* \* \*

## DISCUSSION

G. Birkhoff (Harvard University)

This is an excellent review of the favorable side of the ledger, as regards predictions of real wake behavior from mathematical solutions of the Helmholtz Problem. Perhaps in Dr. Cornell's discussion of general conformal mapping methods more emphasis might have been put on the parameter problem: in most cases, the greatest difficulty comes in determining the auxiliary constants (parameters) of the Schwarz-Christoffel transformations involved.

I was unable to understand clearly the "constant momentum mixing" hypothesis used, and wonder if it is mathematically equivalent to the following naive method of calculation. Let two parallel streams of equal density  $\rho$ , thicknesses  $\tau_1$ ,  $\tau_2$ , and velocities  $v_1$ ,  $v_2$ , mix as they flow downstream under Helmholtz instability. The

W. G. Cornell

mean downstream velocity,  $v_o = (T_1 v_1 + T_2 v_2) / (T_1 + T_2)$ , should be regarded as zero relative to this, by the Bernoulli equation

$$p_1 + \frac{1}{2} \rho (v_1 - v_o)^2 = p_2 + \frac{1}{2} \rho (v_2 - v_o)^2.$$

In 1943, I suggested this method of calculation to the late John von Neumann as a basis for calculating wake underpressure (in this case,  $T_2 = 1$  and  $v_o = v_2$ ). He pointed out that for most cases (though not for a broadside flat plate) it seriously over-estimated the wake underpressure.

M. Tulin (Office of Naval Research)

Has there been any application of cavity-flow models to the prediction of flameout?

W. G. Cornell

With respect to flameout, I would say no. So far, most applications have been to predict so-called dry losses in the flameholders which are put in to stabilize combustion.

\* \* \* \* \*

# MECHANICS OF VENTILATION INCEPTION

Kenneth L. Wadlin

*Langley Aeronautical Laboratory  
National Advisory Committee for Aeronautics*

\* \* \* \* \*

The research programs conducted by NACA in connection with ventilation are reviewed to provide examples of ventilation and to indicate some significant parameters influencing its inception. It is shown that low pressure is not a sufficient requirement for ventilation but that separation of the boundary layer is also required. The influence of the free water surface on boundary layer separation is presented as a determining factor involved in ventilation inception. An image system is presented for a surface-piercing strut to indicate the manner in which the free water surface may influence separation of the boundary layer and therefore the inception of ventilation.

\* \* \* \* \*

## INTRODUCTION

Ventilation is an interesting and important subject which has been associated with seaplane hull steps for some time. However, only recently with the renewed interest in hydrofoils and the advent of hydro-skis has much effort been made to understand it. By ventilation is meant the entrance of air from the atmosphere to low pressure areas on lifting surfaces or bodies operating in water. The NACA interest in ventilation has been primarily in connection with seaplane hull steps, hydrofoils and hydro-skis. However, ship hulls, rudders and propellers are also susceptible to this phenomenon. When ventilation occurs, areas which previously were experiencing low pressures are subjected to the relatively high atmospheric pressure or pressures approaching atmospheric pressure. This results in significant changes in the flow patterns and the force characteristics of the elements involved. These force changes may result only in a simple change in static equilibrium. However, in many cases the flow reverts to the unventilated condition before equilibrium is reached and instability occurs. Such instabilities may be manifested as porpoising or skipping of a seaplane and heaving, yawing, or stumbling of a hydro ski or hydrofoil equipped craft. It therefore becomes important to define those areas where ventilation may be expected in order to avoid them or to make modifications to provide a stable transition from the unventilated to the ventilated condition.

Ventilation is also of interest in connection with supercavitating hydrofoil, since the fully ventilated condition is analogous to the zero cavitation number case. As a matter of fact data for the zero cavitation number case are obtained in NACA experimental investigations by inducing ventilation. The lift-drag ratios of hydrofoils designed for supercavitating flow are generally depreciated if operated in the fully

wetted condition. Therefore early ventilation may be of interest for efficiency as well as stability reasons when supercavitating hydrofoils are required for high-speed applications. This paper presents a review of some of the work done by NACA in connection with the ventilation of hydrofoils, hydro-skis, and struts. A possible explanation of the cause of ventilation inception is also developed.

### EXAMPLES AND EFFECTS OF VENTILATION

On surface-piercing hydrofoils and struts ventilation generally occurs, as might be expected, by air entering along the hydrofoil from the water surface. Experimental studies in connection with this type of ventilation have been carried out by several investigators (see Refs. 1-5). Figure 1 is an example of such a hydrofoil that has ventilated. The photograph is of a surface-piercing dihedral hydrofoil having an NACA 64 A series airfoil section. It can be seen that the ventilated area extends from the water surface to a point near the tip of the hydrofoil. Ventilation in this case started at the water surface and rapidly extended toward the tip of the hydrofoil. The cavity is open to the atmosphere and is very long.

On fully submerged lifting surfaces, however, ventilation occurs through the trailing vortices. Ventilation of this type has been investigated by NACA in connection with experimental studies of hydro-skis operating in the fully submerged condition (6-8). Such ventilation resulted in large and sudden changes in the force characteristics of the hydro-ski and thus stimulated further investigation of the subject. The development of the vortex type of ventilation and the resulting flow changes are shown schematically in Fig. 2. Air enters the low pressure area in the core of the trailing tip vortices at a point some distance aft of the lifting surface and travels up the vortex core to a point which draws closer to the lifting surface as the speed is increased. This continues until the aerated portion of the vortex contacts the surface and the flow separates completely from the leading edge of the surface and complete ventilation occurs. Photographs of two phases of this process are shown in Fig. 3. The surface shown is a flat plate having an aspect ratio of 0.25. The upper photograph shows the flow after the low pressure in the vortex core has vented to the atmosphere. The air appears to enter the vortex at the turbulent area at the base of the roach and extends to a point well forward but not in contact with the plate. The lower



Fig. 1 - Photograph of a surface-piercing hydrofoil ventilated to the atmosphere



#### Mechanics of Ventilation Inception

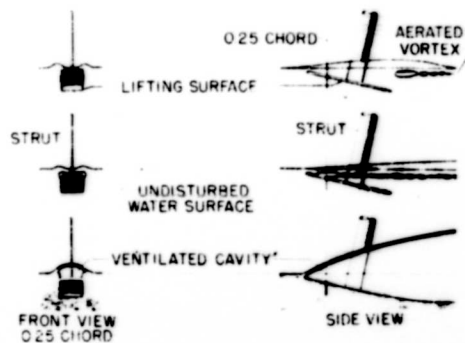


Fig. 2 - Development of vortex ventilation

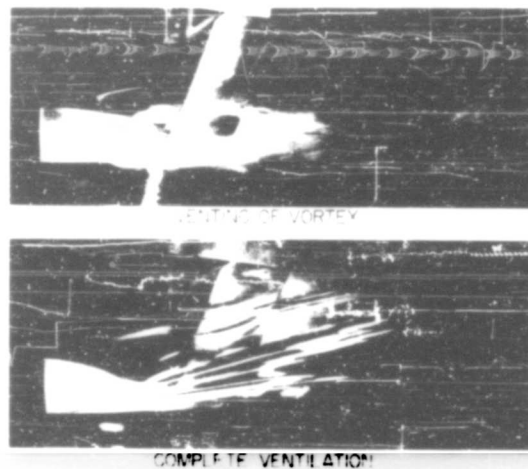


Fig. 3 - Photographs showing the development of vortex ventilation of an aspect-ratio-0.25 flat plate

photograph shows the flow after the aeration of the vortex core had moved progressively forward until it contacted the plate and complete ventilation occurred.

The influence of such ventilation on the lift of the plate is shown in Fig. 4. The lift increased with speed with no noticeable influence of the vortices becoming aerated at speeds below 70 feet per second. However at 70 feet per second when ventilation occurred the lift immediately dropped to a much lower value.

#### PARAMETERS INFLUENCING VENTILATION INCEPTION

It is apparent from Fig. 4 that the effects of ventilation can be quite important in any particular application of lifting surfaces. Therefore it is important to know when

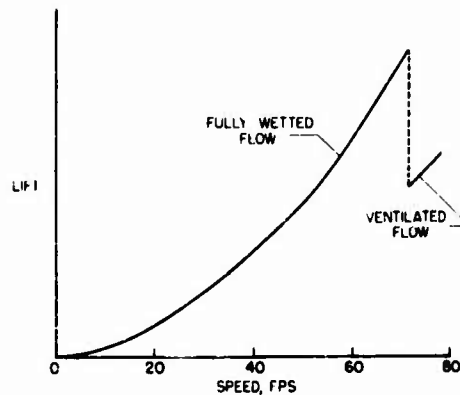


Fig. 4 - Influence of vortex ventilation on the lift of a submerged flat plate having an aspect ratio of 0.25

ventilation may be expected to occur. Figure 5 presents the ventilation inception boundaries for the surface considered in the previous figures. These boundaries define the speed at which ventilation occurred for a given angle of attack for several depths of submersion. The boundaries divide into two definite areas. At the high angles of attack the ventilation inception speed is almost independent of the angle of attack. However, the change in inception speed with depth of submersion is appreciable, increasing rapidly with increasing depth of submersion. At the lower angles of attack this is reversed. Here the incipient ventilation speed is significantly affected by the angle of attack. However, the change with depth of submersion is reduced to a small value. From these tests it appeared that ventilation inception was influenced by, if not the direct result of, boundary layer separation. It appeared that ventilation at high angles might be related to stall or turbulent separation. The ventilation at low angles appeared to be related to laminar separation near the leading edge.

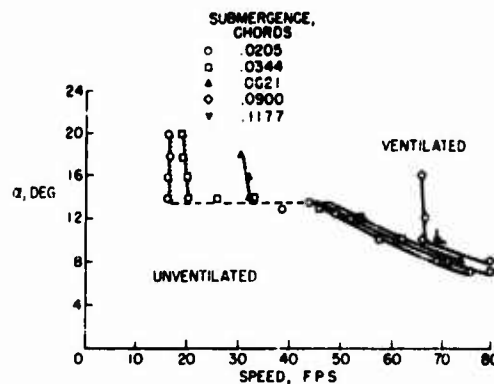


Fig. 5 - Ventilation boundaries for a submerged flat plate having an aspect ratio of 0.25

# VENTILATION-SEPARATION RELATIONSHIP

When ventilation inception is assumed to be associated with boundary layer separation, it immediately, as do all boundary layer problems, becomes a complex problem. The simplest case of ventilation is that of the surface-piercing strut. This case will be considered in an effort to gain some understanding of the ventilation-separation relationship.

For blunt-trailing-edge bodies such as cylinders intersecting the water surface there appears to be a definite relationship between the depth of ventilation and the Froude number based on the depth of submergence. This is shown in Fig. 6 where data presented by Wetzel in Ref. 4 have been replotted. The Froude number, based on the depth of submergence, at which cylinders of diameters ranging from 0.031 to 2.00 inches ventilated to the bottom are presented for varying depths of submergence. It can be seen that beyond a depth of submergence of about 2 inches the Froude number based on the depth of submergence at which ventilation occurred was about 1.7. This is a value which has also been found by others (5,9). The relationship between the base pressure coefficient at the lower end of the strut and this Froude number is  $C_{p,B} = 2 / (F_h)^2$ . Figure 6 therefore indicates that at submergence depths greater than 2 inches the pressure coefficient at the tip was constant. However at depths less than 2 inches the pressure coefficient at the tip decreased rapidly. This is as would be expected since as the lower tip of the cylinder approaches the water surface it approaches a constant pressure or free stream velocity boundary and therefore a  $C_p$  of zero. Since the pressure coefficient is decreasing, it is necessary for the speed or Froude number to be increased to provide the dynamic pressure head required to overcome the static water head.

Though this relationship between the pressure coefficient and the Froude number based on the depth of submergence applies to the bluff sections such as cylinders, flat plates, or wedges, this is not the case for streamline sections. This is demonstrated in Fig. 7 which was presented in Ref. 10. The strut shown has a chord of 4 inches and an NACA 66<sub>4</sub>-021 airfoil section at zero angle of attack. It penetrated the water surface to a depth of 8 inches and was being towed at a speed of 75.8 feet per second. Extensive cavitation can be seen which approached to within about 0.75 inch of the water surface. The presence of cavitation indicates low pressures approximating

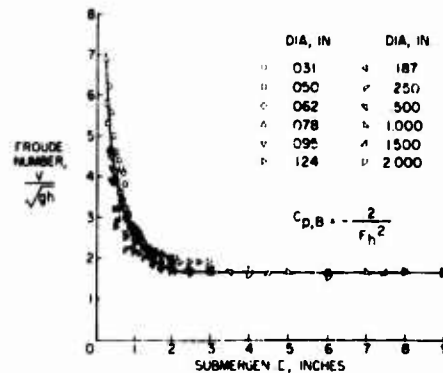


Fig. 6 - Froude number at which ventilation occurs for surface-piercing cylinders at various depths of submergence

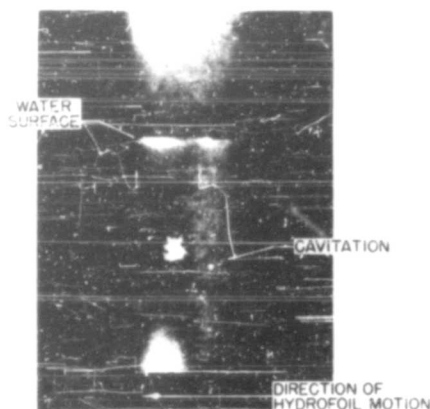


Fig. 7 - Photograph of surface-piercing strut cavitating yet not ventilating

vapor pressure within 0.75 inch of the water surface. Such pressures correspond to water heads of over 30 feet and yet no tendency toward ventilation was apparent. Such observations lead to the conclusion that the turbulent wake behind the cylinder provided low energy paths through which air could enter the low-pressure regions. In the case of the airfoil section the flow about the foil was smooth and of high energy with no turbulent wake in its immediate vicinity and therefore no low energy path through which the air could enter. Of course, such sections do ventilate at higher angles of attack. In such cases the chordwise pressure gradient may have pressure peaks near the leading edge followed by an adverse pressure gradient which could result in boundary layer separation and susceptibility to ventilation.

#### EXPERIMENTAL FLOW STUDIES

In an effort to correlate the presence of separation with the occurrence of ventilation, an oil-flow technique developed at NACA by Donald Loving was used. The technique was developed for use in air but worked as well in water. It consists of putting a thin film of oil on the surface to be investigated and then towing it at a constant speed. The oil tends to wipe off more rapidly in high-energy attached flow and turbulent areas than it does in low-energy separated areas. This results in a greater concentration of oil in the separated areas. The oil pattern is highly visible under ultraviolet light which causes the oil to fluoresce. Figure 8 is a photograph of a typical oil pattern obtained on an unventilated surface piercing hydrofoil having an NACA 64 series section. Above the water surface the oil moved toward the trailing edge. Below the water surface the oil accumulated in the center portion of the chord and was wiped clear in the vicinity of the leading and trailing edges. A laminar separation bubble is indicated by the accumulated oil. As indicated by the sketch the accumulation of oil was due to the forward motion of the boundary layer at the aft end of the bubble moving the oil forward rather than permitting it to be swept downstream by the turbulent flow aft of the bubble.

Figure 9 is a photograph of the same model where air was artificially introduced into the area which the oil pattern indicated to be separated. The air remained in an

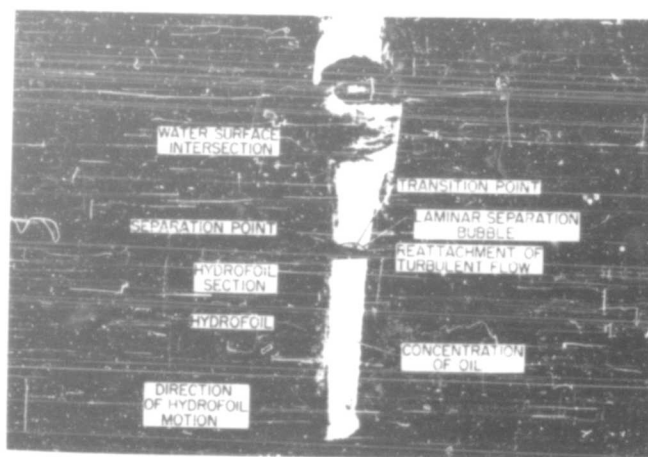


Fig. 8 - Photograph of oil flow pattern showing laminar separation bubble

area whose forward portion closely resembles that of the laminar bubble indicated by the oil-flow pattern shown in Fig. 8. This indicates that ventilation will occur if the foil has a separated flow region and air can get to this region. However, ventilation did not occur naturally in Fig. 9 but was induced by disturbing the water surface in the vicinity of the foil leading edge. When the disturbance was removed the cavity closed at the water surface as can be seen by close inspection of the photograph. The air in the cavity was then entrained by the water and the cavity gradually dissipated until fully wetted flow was again attained. The fact that the foil had separated flow regions of low pressure on it and still did not ventilate naturally or even maintain

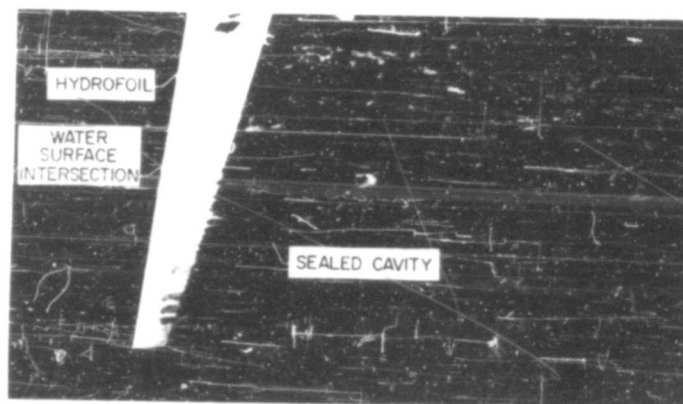


Fig. 9 - Photograph of ventilation of the laminar separation bubble

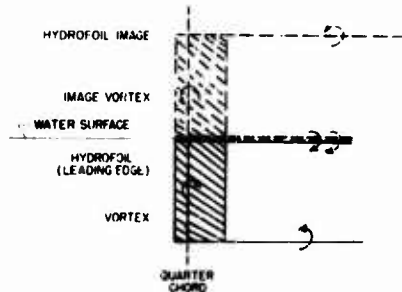


Fig. 10 - Horseshoe vortex system which satisfies the boundary conditions for a surface-piercing strut

ventilation after initial ventilation was induced indicates that the separated region did not extend to the water surface. This could be expected since separation of the boundary layer is strongly influenced by pressure gradients, and the water surface has no such gradient since it is a constant pressure boundary.

#### MATHEMATICAL MODEL

In an effort to gain some insight as to the extent to which the proximity of the water surface might retard separation the method of images was employed. The image system shown in Fig. 10 was set up to satisfy the condition of constant pressure at the free water surface. A single horseshoe vortex was substituted for the hydrofoil. The bound vortex was located at the quarter-chord and the trailing vortices were located at the tip and at the water surface. The image vortex was located in a similar manner except above the water surface. The vorticity of the image was of opposite rotation as that of the hydrofoil vortex. Such a simplified image system cannot be expected to calculate the flow accurately, especially in areas close to the vortices. However flow directions calculated in the vicinity of the leading edge should provide an indication of the distribution of the load along the span.

Figure 11 presents the spanwise distribution of the parameter  $(\frac{W}{V})(\frac{C_L}{2\pi})$  which defines the flow direction at the leading edge of the hydrofoil, where  $W$  is the flow velocity normal to the undisturbed stream velocity  $V$  and  $C_L$  is the lift coefficient of the hydrofoil. It can be seen that the angle of flow rapidly decreases in the vicinity of the water surface, becoming zero at the water surface. Since this flow angle is an indication of the loading, it indicates that the loading also becomes zero at the water surface. As the loading approaches zero, the chordwise pressure gradient must also approach zero and thereby reduce the tendency of the boundary layer to separate. The fact that the chordwise pressure gradient at the water surface is zero would indicate that separation would never occur at the water surface and therefore ventilation would never occur. This is a limitation of the mathematical model. Another limitation of

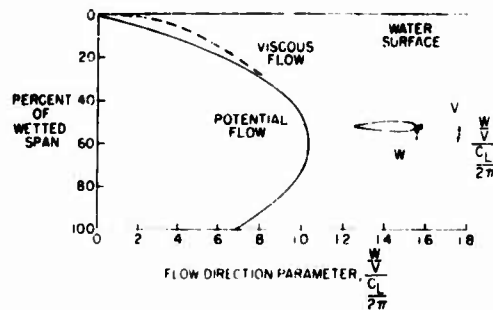


Fig. 11 - Flow direction at the leading edge of a surface-piercing strut obtained by using the method of images

the mathematical model is that it does not account for the effect of speed which is quite apparent in experimental investigations. Both of these deficiencies result from the fact that the mathematical model assumes potential flow.

#### EFFECT OF VISCOSITY

Efforts to understand the intimate details of the mechanics of ventilation inception have not been extensive. As a result no definite conclusions have developed as to the manner in which the separation at the water surface, which ultimates in ventilation, occurs. It is believed, however, that the usual concept of inviscid irrotational flow outside the boundary layer is not adequate near the water surface, especially in the vicinity of the leading edge of the hydrofoil. In such a case there would be an interaction between the two flows which could result in substantial changes in the pressure gradients and flow. Thus both separation at the water surface and the influence of speed could be explained as a result of such an interaction. Referring back to Fig. 11 it will be noted that since the parameter  $(W/V)(C_L/2\pi)$  is an indicator of the flow angle and loading, it is also an indicator of the perturbation velocity. Viscosity will alter the distribution of this velocity. This is particularly true when the velocity gradients are large. The shear forces due to viscosity tend to average the velocities. That is, the lower velocities in the region close to the water surface will be increased over those predicted by potential flow, while the higher velocities at the greater depths would be reduced. The effect near the surface is of interest in the case being considered. The dashed curve on Fig. 11 is intended to indicate this change in perturbation velocity. It can be seen that though the perturbation velocity approaches zero in the proximity of the water surface, its velocity gradient is greatest there and the effect of viscosity is to increase this gradient. These high velocity-gradients in the vicinity of the water surface are conducive to eddies which would provide low-energy paths to the separated areas farther below the water surface. Since these velocity gradients will increase with stream velocity, the tendency for eddies to form will increase with increasing stream velocity. This is a possible explanation for the influence of velocity on the inception of ventilation which is so apparent in experimental investigations.

#### CONCLUDING REMARKS

Some understanding of the mechanics of ventilation inception has been gained in that it has been shown that low pressure is not a sufficient requirement for ventilation but that separation of the boundary layer is also required. It has also been found that separation of the boundary layer is greatly retarded by the presence of the free water surface. However further investigation will be necessary before the mechanism of this retardation and how it is influenced by speed is understood and a means of calculating boundaries for the inception of ventilation can be developed.

#### REFERENCES

1. Breslin, John P. and Skalak, Richard, "An Exploratory Study of Ventilated Flows About Yawed Surface-Piercing Struts," ETT, SIT Rep. 668, 1957
2. Perry, Byrne, "Experiments on Struts Piercing the Water Surface," CIT Rep. E-55.1, 1954
3. Kiceniuk, Taras, "A Preliminary Experimental Study of Vertical Hydrofoils of Low Aspect Ratio Piercing A Water Surface," CIT Rep. E-55.2, 1954

K. L. Wadlin

4. Wetzel, J.M., "Experimental Studies of Air Ventilation of Vertical, Semi-Submerged Bodies," St. Anthony Falls Hydraulic Laboratory, U. of Minn., 1957
5. Hay, Donald A., "Flow About Semi-Submerged Cylinders of Finite Length," Princeton University, 1947
6. Wadlin, Kenneth L., Ramsen, John A., and Vaughan, Victor L., Jr., "The Hydrodynamic Characteristics of Modified Rectangular Flat Plates Having Aspect Ratios of 1.00, 0.25, and 0.125 and Operating Near A Free Water Surface," NACA Rep. 1246, 1955
7. Vaughan, Victor L., Jr., and Ramsen, John A., "Hydrodynamic Characteristics Over a Range of Speeds Up to 80 Feet Per Second of a Rectangular Modified Flat Plate Having an Aspect Ratio of 0.25 and Operating at Several Depths of Submersion," NACA TN 3908, 1957
8. Ramsen, John A., "An Experimental Hydrodynamic Investigation of the Inception of Vortex Ventilation," NACA TN 3903, 1957
9. Hoerner, S.F., "Some Characteristics of Spray and Ventilation," Bath Iron Works Corporation, 1953
10. Coffee, Claude W., Jr., and McKann, Robert E., "Hydrodynamic Drag of 12- and 21-Percent-Thick Surface Piercing Struts," NACA TN 3092, 1953

\* \* \* \* \*

## DISCUSSION

H. Saunders (Capt., U.S.N., Ret.)

It seems a pity to me that the use of the single word "ventilation" to signify all aspects of the entrance of air to a region of negative differential pressure in or around or below the water surface has spread so widely within the last few years. This word "ventilation," like everything else, has its proper place in the universe and, if we are to judge by Webster, "ventilation" is something which indicates that air is entering where it is desired or needed. It is most confusing to have the word used also for a situation where the air is definitely detrimental. To cover this second phase we have used the expression "air leakage."

If you don't know whether the air is a good thing or not, then you can speak of "aeration."

J. P. Breslin (Stevens Institute of Technology)

I would like to touch briefly on a few of the highlights which were revealed by an exploratory study<sup>1</sup> which was conducted at the Stevens Institute Experimental Towing

<sup>1</sup>J.P. Breslin and R. Skalak, "An Exploratory Study of Ventilated Flows About Yawed Surface-Piercing Struts," ETT Report No. 658, October 1957.



Tank (SETT) under support of the Hydrodynamics Laboratory of the NACA. Some of these results corroborate the findings on ventilation inception as given by Mr. Wadlin and others are offered as additional facts which may be of interest to those who would like to be able to estimate the forces on a ventilating body.

The SETT tests were made with two vertical surface-piercing struts, one being a symmetrical, 2.5-inch circular-arc section and the other a 3-inch cambered section (NACA 4412) which has a nearly flat pressure side. Three modes of inception were found:

- 1) by ingestion of air through momentarily developed "Rankine" vortices in the unsteady, separated flow attending stall conditions at large angles of yaw (Fig. D1),
- 2) through aeration of the trailing vortex developed by the lower tip, and
- 3) through the action of a slight disturbance applied at the suction side near the leading edge at the juncture with the free surface when underway at speeds and angles of yaw well below those for which ventilation occurred spontaneously at stalling conditions.

The first mode was observed in quite some detail through the use of a motion picture camera.

The discovery of the high sensitivity of the flow to slight disturbances (mode 3 above) led to an investigation of the boundary layer by the NACA which was very effectively carried out through the use of the oil-ultra-violet light technique described in the paper. Similar observations at SETT also revealed regions of laminar separation and re-attachment of the boundary layer which are sealed from the free surface by a relatively thin strip of nonseparated flow over the length of the chord at the juncture with the streaming free-surface. This strip is nonseparated because of the near-zero longitudinal pressure gradient imposed by the presence of the free surface. Momentary rupture of this seal permits air to replace the separated fluid and a new flow phase is thereby initiated. The presence of a laminar separation (which, incidentally, does not always give rise to noticeable anomalies in the side-force curve)

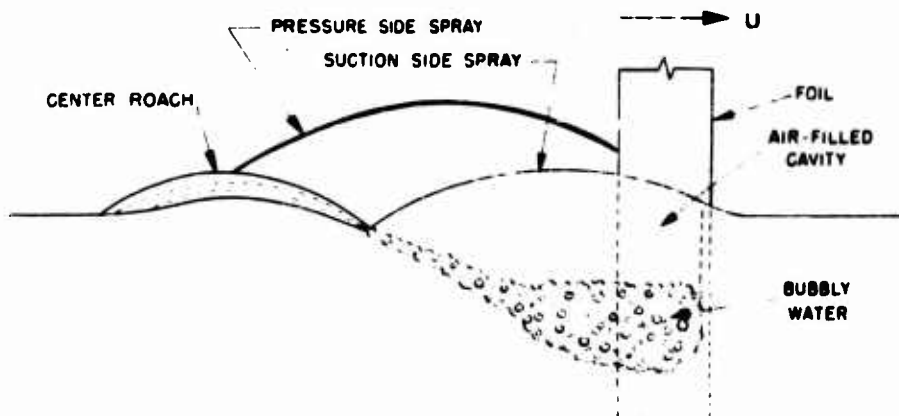


Fig. D1 - Partial cavity formed at low Froude numbers and large angles of attack

is a consequence of the low Reynolds numbers at which small models are tested. It is therefore advisable for towing tanks to take measures to insure turbulent boundary layers in any experiment in which ventilation inception conditions are being sought. It is expected that at high Reynolds numbers the susceptibility to ventilation by disturbances around the leading edge at angles of attack well below stall will be small if there are no regions of separation present.

However, attention is invited to the observed fact that once a ventilated flow is developed it is very stable and will persist down to small angles of yaw (or side-force coefficients) as may be seen in a typical set of data from the SETT tests shown in Fig. D2. The ventilated cavity will collapse at conditions beyond that for natural closure only if some means of inhibiting the supply of atmospheric air is applied. Conditions for natural closure of cavities were observed and these are shown in Fig. D3. It appears that a sufficient condition for the existence of full ventilation on the tested models is given by

$$C_L = \frac{5}{F_{0.2}^2} - \frac{5gh}{U^2} \quad \gamma_{cr} = 3. \quad (D1)$$

However, for operation at  $C_L$  values above this, ventilation will not be easily generated unless boundary layer separation exists. In the absence of such separation it is expected that a rather large disturbance is necessary to develop the other possible flow below stall, viz., full ventilation.

It has been noted, without elaboration by the author, that a fully ventilated flow is analogous to the flow about the same body at zero cavitation index. This is true only at "infinite" Froude number. At finite Froude numbers there appears to be a very plausible connection between the flow in a section of a ventilated flow and that about the corresponding section in a two-dimensional cavitation flow. The conditions which must be imposed in order that these flows be similar can be obtained as follows:

For any point on the wall of a three-dimensional ventilated cavity ( $p = p_a$ ), we have

$$\frac{v_z^2}{F^2} = \frac{v_z^2}{F^2} = 2 \left( \frac{u_z}{U} \right)^2 + \left( \frac{u_z}{U} \right)^2 + \left( \frac{v_z}{U} \right)^2 + \left( \frac{w_z}{U} \right)^2 \quad (D2)$$

and

$$\frac{w_z}{U} = x \quad (D3)$$

On the wall of a two-dimensional vapor cavity ( $p = p_v$ ), we have

$$\frac{v_z^2}{F^2} = \frac{v_z^2}{F^2} = 2 \left( \frac{u_z}{U} \right)^2 + \left( \frac{u_z}{U} \right)^2 + \left( \frac{v_z}{U} \right)^2 \quad (D4)$$

Here:

$z$  is the vertical distance below the free surface to the point on the ventilated cavity wall (negative downward),

$F$  is the "submergence" Froude number,

$g$  is the acceleration of gravity.

# Mechanics of Ventilation Inception

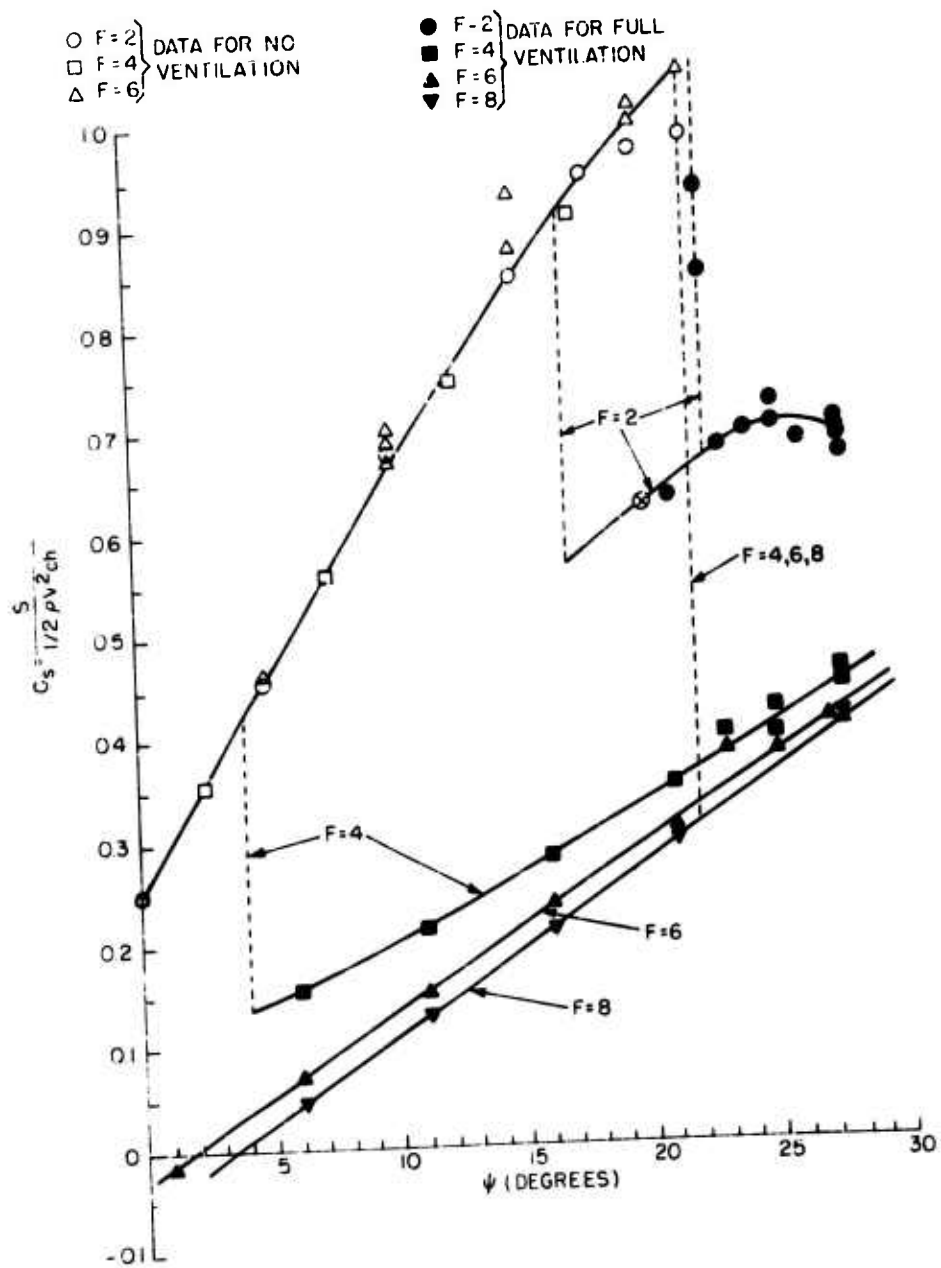


Fig. D2 - Side force coefficients

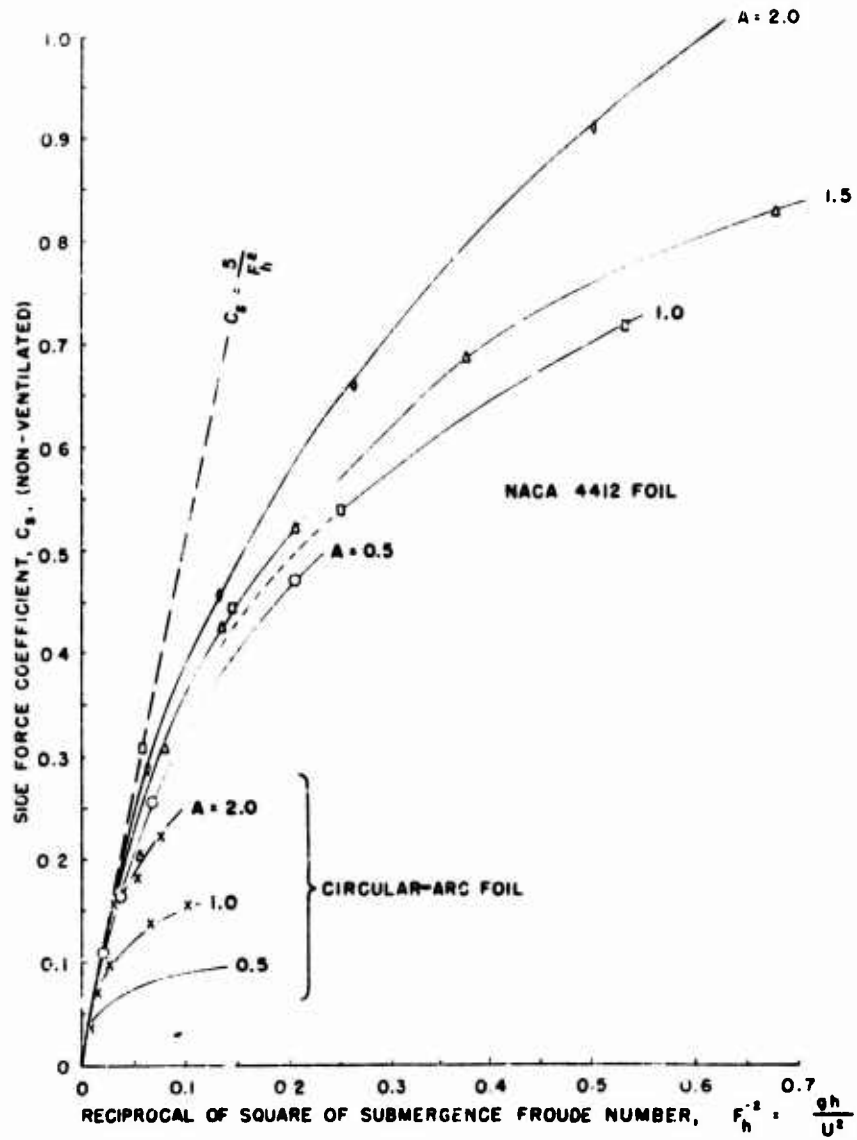


Fig. D3 - Side-force coefficient bounds, below which ventilated cavities are not sustained, as a function of submergence Froude number

$U$  is the free-stream speed, or speed of advance,

$u, v, w$  are  $x$ -,  $y$ -, and  $z$  components of velocities produced by presence of body and cavity in three dimensions,

$x, y, z$  are coordinate axes taken in such a way that the free stream is parallel to the negative  $x$ -axis and the  $z$ -axis is positive upward,

$p_\infty$  is the reference pressure at infinity,

$p_v$  is the vapor pressure,

$p_a$  is the atmospheric pressure, and

$\sigma$  is the cavitation index.

For points which are not near the extremities of the ventilated cavity, i.e., where  $x$  is negligible, the flows may be expected to be quite similar. Thus, the flows may be matched if we take

$$\frac{u}{U} = \frac{2}{F_h^2} + \frac{2x}{U^2} - h \cdot \frac{z}{U^2} < 0, \quad (D5)^{16}$$

which certainly imposes the condition that  $u_2 = u_3$  in all regions where the quadratic terms are negligible.

Employing this relationship a bit freely leads to a formulation for the effective two-dimensional side-force coefficient of a ventilated strut as

$$C_{s_2}(\dots, F_h) = \frac{1}{h} \int_0^h C_{L_2}(\dots) dz \quad (D6)$$

which through use of (D6) yields

$$C_{s_2}(\dots, F_h) = \frac{F_h^2}{2} \int_0^2 \bar{C}_{L_2}(\dots) d\bar{z} \quad (D7)$$

$$\bar{C}_{L_2}(\dots) \text{ for } 0 \leq \bar{z} \leq \frac{2}{F_h^2}$$

where  $C_{L_2}$  is the two-dimensional lift of the cavitating section, and  $\bar{C}_{L_2}$  is the mean of  $C_{L_2}$  between the limits 0 and  $2/F_h^2$ . (It is clear that for  $F_h \rightarrow \infty$ ,  $C_{s_2} = C_{L_2}(\dots, 0)$ .)

To account for aspect-ratio effects, in the main, we arrive at the side-force coefficient for finite span (3-dimensions) in the form:

$$C_{s_3} = \frac{C_{s_2}(\dots, F_h)}{E + \frac{a_2^2}{A}} = \frac{C_{L_2}(\dots, F_h)}{E + \frac{a_2^2}{A}} \quad (D8)$$

<sup>16</sup>This result was obtained by Perry<sup>†</sup> who did not, however, indicate restrictions imposed by three-dimensional effects.

<sup>†</sup>B. Perry, "Experiments on Struts Piercing the Water Surface," Cal. Tech. Hydrodynamics Lab. Report E-55-1, December 1954.

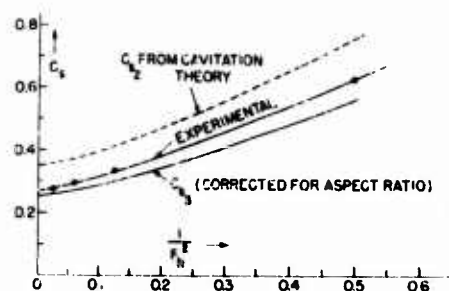


Fig. D4 - Measured and computed side-force coefficients for fully ventilated strut

aspect ratio 2.0 and yaw angle  $\alpha = 20$  degrees yields the curves shown in Fig. D4. It is seen that the dependence of the side-force coefficient upon Froude number is well represented over the entire test range by the use of the cavitation analogy. It is also clear how large  $F_{11}$  must be before the flow may be likened to that at zero cavitation index ( $\sigma = 0$ ).

F. S. Burt (Admiralty Research Laboratory)

At A.R.L. we had the advantage of a preview of Dr. Wadlin's paper, but we are not entirely convinced of the proposition that boundary layer separation is needed before ventilation can begin. It seems rather like the problem of which came first, the chicken or the egg. You can just as easily argue that low pressure produces ventilation which produces separation as the proposition that separation causes ventilation. In fact, Fig. 5<sup>†</sup> of Wadlin's paper, showing the ventilation boundary, could quite well be explained at the lower incidences, without necessarily postulating the existence of a laminar bubble at the lower incidences, by saying that lower incidences produce lower peak suction; hence, higher speeds would be necessary to produce given values of suction. Whether the flat plate used to obtain the data in Fig. 5 had a laminar bubble would depend largely on the nose shape of the leading edge, and no details of this are given. It would be of interest to know if this particular section has been tested in a wind tunnel and the existence of the laminar bubble under these conditions has been demonstrated. The oil picture of the strut in Fig. 8 would appear to show the laminar bubble, but it would be of interest to know what the Reynolds number of the tests were and whether they tied up with the Reynolds number at which ventilation occurred.

The author suggested that the surface-piercing foil could be considered as the simplest case of ventilation, yet he showed that the effect of the free surface flow conditions are such as to inhibit the prime requisite for ventilation, namely, the free entry of the air. It would seem to be much simpler to consider a fully submerged foil and to repeat the result of Fig. 5 to see if there is any similarity in the test points at the lower incidences.

<sup>†</sup> T. T. Wu, "A Free-Streamline Theory for Two-Dimensional Fully Cavitated Hydrofoils," Calif. Tech. Hydrodynamics Lab. Report 21-17, July, 1955.

<sup>‡</sup> All figure numbers are from Wadlin's paper.

where

$E$  is the Jones' edge-correction factor which is computed as perimeter less the chord length at the water surface divided by twice the span,

$\alpha_2$  is the cavitating section lift-slope at  $\sigma = 0$ ,

$A$  is the geometric aspect ratio,

and  $\alpha_0$  is the angle of zero lift.

Evaluation through the use of Wu's\* results for the lift of a cavitating plate in the case of the NACA 4412 strut at

P. DuCane (Vosper, Ltd., England)

Referring to the type of flow described in Wadlin's Fig. 2, I have recently observed what would seem to be a rather unusual example of such flow - at least it is an example which has not been seen previously and the explanation of which, it must be confessed, was not immediately obvious.

During the course of functioning trials in the case of an installation of roll damping fins aboard a fast type of round form torpedo boat of the Swedish Navy we were employing the technique known as "forced rolling" to test the installation. This consists of reversing the signal from the controlling gyros in such a manner that the fins will at all times be ordered to increase the roll velocity rather than to reduce it, which is the normal "modus operandi" of such installations.

In this way a roll amplitude is built up each side of the vertical, the magnitude of which is dependent upon the fin forces developed as well as the natural damping of the hull and its statical stability expressed in the form GM.

Such forced rolling is a useful test of many features of the installation, especially if heavy weather is required for a trial and is liable to lead to much delay before the desired conditions are realized.

While observing the mechanism in the engine room we were informed from a deck that "jets" of spray were emerging from the surface by the fins. The "jets" emerged as the fin neared the surface and rose to some ten or fifteen feet for a few seconds while the ship was heeled to the maximum away from the side from which the spray was emerging.

It should be understood that in "forced rolling" the fin will still be trying to lift the ship even as it approaches the surface as in Fig. D5. It therefore seems quite reasonable to suppose that a flow approximating that shown in the lower illustration of Wadlin's Fig. 2 causes this spray to emerge in the manner and at the angle described.

This type of flow associated with a submerged lifting foil approaching the surface is sometimes referred to as Green's flow or Green's solution. It will be interesting to measure the change in lift as the surface is approached and ventilation occurs.

T. Kiceniuk (California Institute of Technology)

Mr. Wadlin's finding that low pressure is necessary, but not sufficient, to induce ventilation behind a surface-piercing body corroborates the findings made in the Free-Surface Water Tunnel at the California Institute of Technology.<sup>††</sup> Figures D6 and D7, taken from these earlier reports, show some details of the flow which may give added insight to the mechanism for ventilation inception. The electronic flash photographs reveal what appear to be ventilated vortices shed downstream of the model. These vortices provide a feasible mechanism for the deep penetration by air into the body of a dense liquid in motion. These photographs, as well as visual observations, indicate that real understanding of this problem must await careful and

B. Pomeroy, "Experiments on Struts Piercing the Water Surface," CII Hydro. Lab. Report No. E-55-1, Dec. 1951.

†† E. Kiceniuk, "A Preliminary Experimental Study of Vertical Hydrofoils of Low Aspect Ratio Piercing a Water Surface," CII Hydro. Lab. Report No. E-58-1, Dec. 1954.

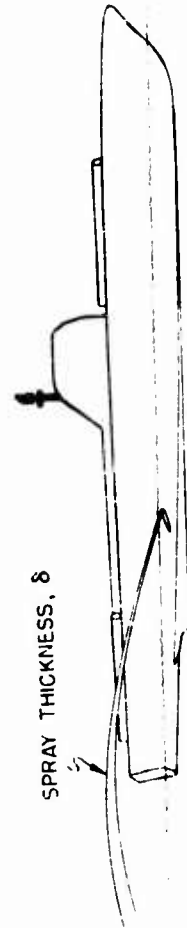
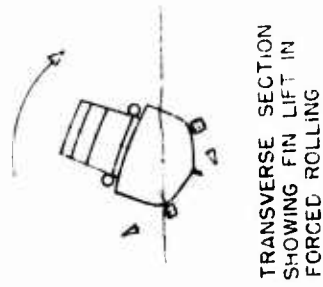


Fig. D5 - High-speed patrol craft in forced rolling showing Green's flow, from leading edge of fin, developing lift



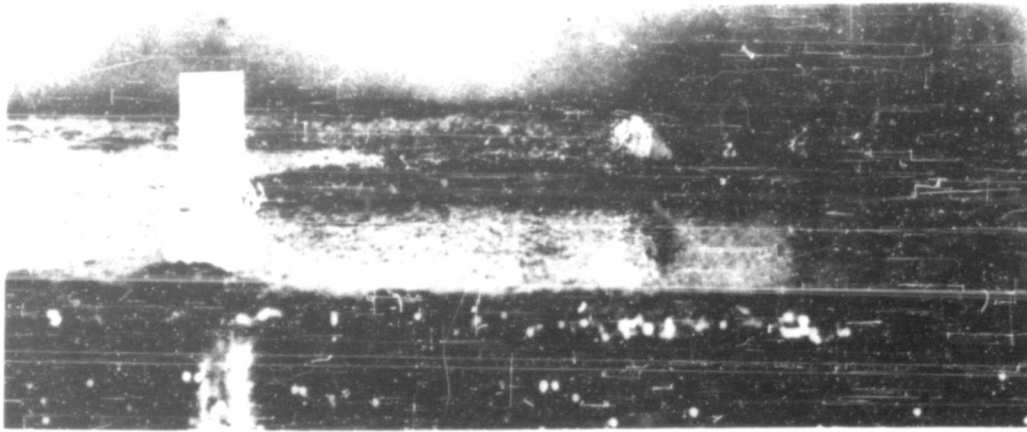


Fig. D6 - Electronic flash photograph of the ventilation behind a surface-piercing body

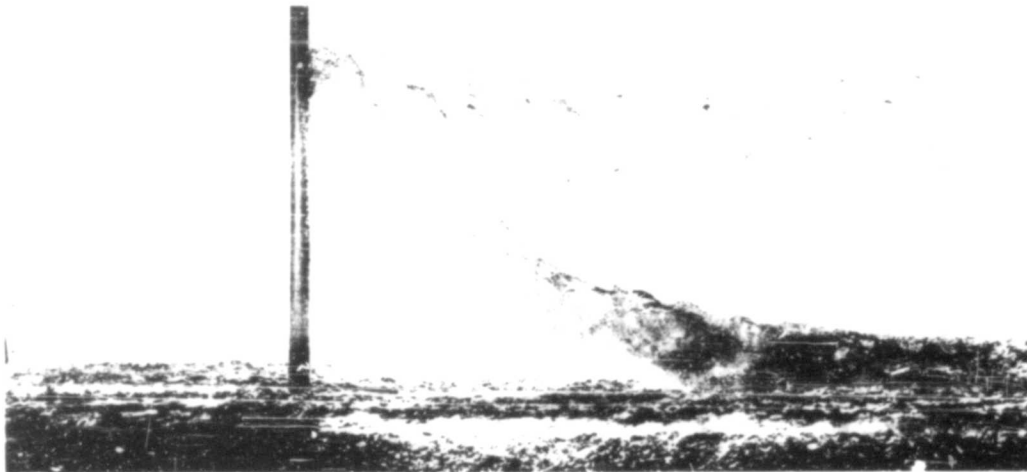


Fig. D7 - Electronic flash photograph of the ventilation behind a surface-piercing body showing possible vortices

detailed observations and measurements of the physical processes taking place in the wake of the body. The use of time-averaged measurements such as the usual pressure coefficient, for example, may be irrelevant in a separated flow situation where the instantaneous low pressures existing at a point on the body or within a vortex core triggers the ventilation. High-speed photographs taken in the wake region of surface-piercing bodies may reveal other phenomena which must be reconciled with any proposed theory.

The vortices in Fig. D7, if they are indeed vortices, are being shed at a frequency which compares very well with those computed by Roshko\* for a bluff body.

#### B. Perry (California Institute of Technology)

In answer to Mr. Burt's question, some unreported experiments performed a few years ago in the Free Surface Tunnel at the California Institute of Technology may be of interest. In connection with experiments on air-inflated cavity flow on

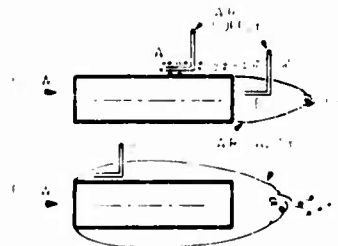


Fig. D8 - Introduction of air at various points near a body in a flow stream

cylindrical bodies with flat noses, we tried to induce a full cavity flow by introducing air through a probe at various points. We found that air introduced several diameters aft of the nose, as at A in Fig. D8, was swept away as bubbles, while the introduction of air at B opened an air cavity attached to the rear of the body as shown. Only by putting the air supply probe forward to a location such as C, i.e., into a zone of viscous separation, could a full cavity be formed. Once established, however, the cavity could then be supplied with air with the probe placed anywhere inside it. As I recall it, the flow velocity was of the order of 15 fps and the body diameter was about 2 inches. These tests seem to be in complete agreement with the ideas put forward here by Mr. Wadlin, and earlier by Hoerner.

With the mechanism of ventilation now understood, at least in a general way, it may be pertinent to consider an inherent difficulty which faces the designer of high speed craft. If any zone of potential ventilation is available, some inadvertent disturbance to the flow may cause a cavity to open up which will then, so to speak, provide its own passage for air supply. Since this may cause a catastrophic change in flow pattern, one is led to the conclusion that in many instances the only safe design procedure will be to assume that ventilation will occur.

#### M. C. Eames (Naval Research Establishment, Halifax)

The essential connection between ventilation and a separated boundary layer, or wake, has been suspected for some time. It is perhaps unfortunate that a newcomer to the subject might obtain the impression that this was being claimed as an original idea. Actually, in Ref. 9 of Wadlin's paper, for example, Hoerner refers to "an accumulation of boundary-layer material and a negative pressure within the separated region" as prerequisite for ventilation.

To my mind the extreme value of the more recent work lies in the experimental approaches which have been developed to demonstrate this relation. The use of an oil film is a particularly nice technique, and the results are most gratifying.

There is one point to which I should like to add emphasis. Experience in the full-scale operation of hydrofoil craft suggests that significant retardation of ventilation

\* R. P. Roshko, On the Structure and Shedding Frequency of Two-Dimensional Bluff Body Vortices, NACA TN 5608, July 1964.

#### Mechanics of Ventilation Inception

by the influence of the constant-pressure water surface can only be obtained under laboratory conditions. In openwater even the smallest ripples appear to be sufficient to initiate ventilation at the water surface. This of course is an advantage to full-scale operation since ventilation proceeds smoothly as speed is increased. The explosive type of phenomenon which results when large negative pressures are supported in calm water and subsequently tripped by a small disturbance could represent a very dangerous situation for a hydrofoil craft.

The fact that only a small disturbance is necessary would appear to add circumstantial evidence to Mr. Wadlin's ingenious explanation of the mechanism behind surface ventilation. The high velocity gradients in the vertical direction provide a highly unstable situation requiring little deviation of the surface to initiate powerful eddying and thus give rise to the requisite low energy paths.

Finally, I would like to ask Mr. Wadlin whether he has carried out any experiments using anti-ventilation "fences." In an "ad hoc" search for the smallest effective fence we have found that on a particular section designed for uniform pressure distribution it is only necessary to extend the fence over the leading 50 percent of the chord. (Maximum thickness occurs at 50 percent chord.) I would have expected most of the low energy paths to exist behind this, and therefore the success of the half-fences surprises me. Perhaps Mr. Wadlin could clarify my thinking on this point.

\* \* \* \* \*

# VENTILATION OF BODIES PIERCING A FREE SURFACE

J. M. Wetzel

*St. Anthony Falls Hydraulic Laboratory  
Minneapolis, Minnesota*

\* \* \* \* \*

Experimental studies were conducted at the St. Anthony Falls Hydraulic Laboratory to investigate the scale-effect problem associated with the ventilation of vertical, semisubmerged cylindrical rods and streamlined lifting surfaces. Two types of ventilation--creeping or partial and a flash or delayed vent formation--have been observed for these shapes. Data for the large-diameter rods can be correlated with the Froude number and submergence ratio, whereas uncoated rods of small diameter require consideration of several parameters. The use of Teflon-coated rods improved the Froude number correlation for the rods of small diameter.

Ventilation of vertical, lifting struts is primarily a function of velocity, yaw angle, submergence, and strut shape. Ventilation data of several strut shapes at high yaw angles can be correlated with the Froude number based on chord

\* \* \* \* \*

## INTRODUCTION

As a surface-piercing body moves through a liquid, at a certain velocity an air pocket will form that will expose part or all of the rear portion of the body to the atmosphere. The formation of this pocket of atmospheric air will be called ventilation, although in some references it is also referred to as air leakage. Knowledge of the inception and mechanism of ventilation is of considerable importance as ventilation creates a distinct change in the hydrodynamic characteristics of the body.

To investigate the ventilation phenomena, it was considered desirable to conduct experimental studies on models and extrapolate the model data to prototype conditions by means of suitable modeling parameters. During the course of model tests on inclined, streamlined bodies piercing a free surface, it was found that a scale effect existed; i.e., the extrapolated data from the model did not agree with the data from the prototype. As scale effect is a serious design problem, an additional series of tests was initiated to study the ventilation of elementary body shapes, such as circular cylinders in a vertical position. In these tests with circular cylinders, the effect of gravity, surface tension, and viscous forces on ventilation was investigated.

The studies were later extended to include vertical, yawed struts of streamlined shape. This paper summarizes the results of this series of tests, which were part of a fundamental research program conducted at the St. Anthony Falls Hydraulic Laboratory under the sponsorship of the Office of Naval Research.

## GENERAL CONSIDERATIONS

A relatively large amount of data has been published on the flow about semi-submerged cylinders of finite length. Hay (1) has done considerable work in this field, although his primary interest was the resistance of cylinders rather than the mechanics of ventilation or the scale effect associated with ventilation. However, some of the data presented can be extrapolated to a useful form for comparison purposes. Several papers are also available from NASA (2) and the California Institute of Technology (3,4) regarding ventilation of streamlined shapes in the presence of a free surface; the latter papers describe preliminary tests on struts.

In general, two distinct types of ventilation on a vertical, semisubmerged body can be observed: (a) a "creeping" or partial ventilation where the air pocket gradually increases in depth with increasing velocity, and (b) a "flash" ventilation or "delayed vent formation" where the air pocket forms very suddenly at a certain velocity, with little or no previous depression being observed behind the body. The size, submergence, and orientation of the body will generally determine which type of ventilation will normally occur.

In the case of the vertical, yawed strut, ventilation can usually be obtained for a given angle by increasing the velocity of the strut. For high yaw angles, as the velocity is increased to a certain value (which is dependent on foil shape and submergence) a pocket opens on the suction side but does not extend completely to the bottom of the strut. A relatively large amount of aerated water is present in the lower portion of the pocket. As the velocity is further increased, the pocket will eventually extend to the bottom of the strut and full ventilation is attained.

For the low yaw angles, air enters the suction side of the strut suddenly, creating a very marked change in the lift force. The water separates completely from the strut near the leading edge and forms a rather well-defined spray sheet. If the velocity of the strut is reduced slowly, the sheet will not reattach itself until a relatively low velocity is obtained, indicating a considerable hysteresis effect. The yaw angle that separates the partial and delayed ventilation is primarily dependent on strut shape but may change slightly with submergence. By consideration of well-known modeling parameters, it is possible to correlate ventilation data for various body sizes and submergences, although best results are obtained for the creeping ventilation.

## EXPERIMENTAL FACILITIES

The studies were conducted in a circular steel tank of 10-foot diameter and 2-foot depth. The tank was equipped with a rotating-arm mechanism as shown in Fig. 1. The rotating arm was driven by a 5-hp hydraulic motor through a Vickers transmission, with fluid at high pressure being provided by a hydraulic test stand. Such an arrangement provides a wide range of velocities up to a velocity of about 20 fps with an arm length of 3.5 feet. The maximum velocity is restricted because of excessive turbulence and waves created by the moving body. The velocity was determined by a calibrated flowmeter on the hydraulic test stand and also by a tachometer generator driven by a gear fastened to the drive shaft of the arm mechanism. The rotating arm

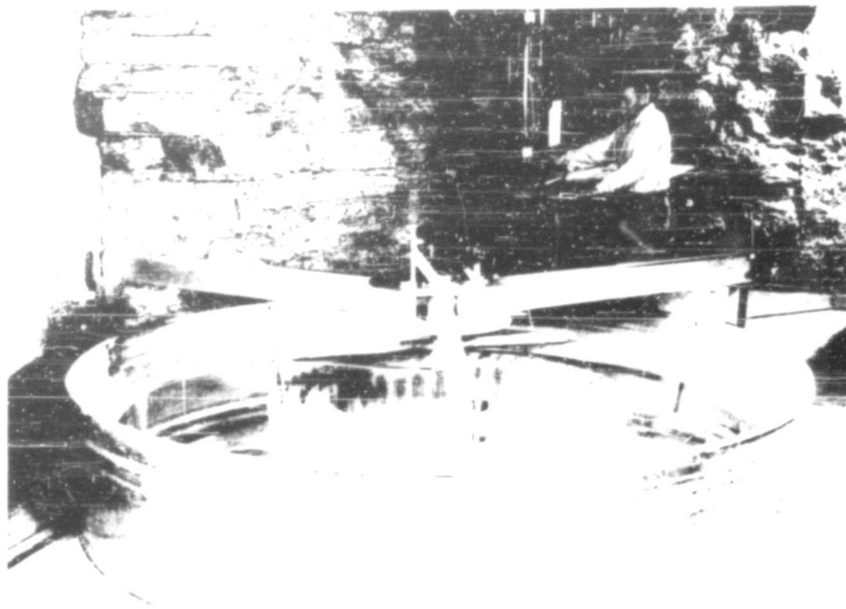


Fig. 1 - Photograph of rotating-arm tank

can be adjusted to various lengths, and the outer end is constructed to receive a variety of test-body shapes.

The circular, impermeable beach absorber placed around the circumference of the tank is very effective in absorbing the waves created by the moving test body for velocities under 20 fps. A 5-foot-diameter permeable wave filter constructed of hardware cloth has been placed in the center of the tank to reduce wave action further. The magnitude of the circulation, or swirl, created by the motion of the body through the water was small, but in some cases was taken into consideration, particularly for the streamlined, lifting struts. A sufficient period of time elapsed between runs for the circulation and excessive turbulence to be dissipated before the next test was begun.

Cylindrical rods with nominal diameters from  $1/32$  inches to 2 inches were tested at various submergences. Several of the rods were covered with a coating of Teflon (tetrafluoroethylene resin) sprayed to a 1-mil thickness; these rods will hereafter be referred to as Teflon rods. A summary of the rod diameters and rod materials used in the study is given in Table 1. All the rods had smooth surfaces, and the ends were machined perpendicular to their longitudinal axes. For the Teflon rods, the coating completely covered the submerged portion of the rod, including the milled end.

Table 1

Rod Diameters (in.)  
and Materials Used

Steel	Brass	Lucite	Teflon
0.031	0.124	1.500	0.052
0.050	0.187	2.000	0.064
0.062	0.250		0.127
0.078	0.500		0.254
0.095	1.000		0.503
			0.753

The streamlined struts used in the ventilation studies were of NACA 0012 and NACA 0024 profiles. Two- and 3-inch chord struts were available for the NACA 0012 section, and a 2-inch chord for the NACA 0024 section. The foils were made of aluminum with a special milling cutter, hand finished and polished. An NACA 0012 strut of 2-inch chord sprayed with Teflon was also used for the tests. The strut was fastened to a mounting bracket attached to the end of the arm. The bracket was constructed to permit adjustment of the yaw angle (to within  $1/2$  degree) and submergence.

#### EXPERIMENTAL PROCEDURE

Data were taken by visual observation of the complete ventilation to the bottom of the body, and the velocities for this condition were noted. Repeat tests have indicated that this point could be observed accurately and data could be reproduced satisfactorily. Cylindrical rods with nominal diameters of less than  $1/4$  inch were braced to reduce lateral vibrations. Most of the rods were tested in tap water and also in water with altered surface tension and viscosity. The surface tension was reduced by addition of commercial detergents, such as Alconox or A11. By varying the concentration of detergent, the surface tension could be reduced from about 72 to 35 dynes/cm (0.00495 to 0.0024 lb/ft). The solutions were carefully mixed, and surface tension measurements were made several times during the test by the ring method, using a Du Noüy tensiometer. The viscosity was changed by heating the water with heating coils placed on the bottom of the tank. With this method, the kinematic viscosity could be reduced by a factor of nearly one-third.

With the struts, a submergence and a yaw angle were set for a particular shape and the velocity increased in small increments until complete ventilation was attained. The occurrence of complete ventilation was determined visually with little difficulty. Attempts were made to obtain the data for smooth-water conditions in the tank; therefore, in most cases boom rotations were confined to one or two. A brief series of spot checks was made with the towing carriage to verify the data taken in the rotating-arm facility.

#### DISCUSSION OF RESULTS—CIRCULAR CYLINDERS

##### Effect of Froude Number

The velocities for complete ventilation were used to compute the Froude number based on either the rod submergence,  $H$ , or the rod diameter,  $D$ . Data showing the relationship of the Froude number and a dimensionless submergence ratio,  $H/D$ , for the uncorded rods are plotted in Figs. 2 and 3. The vertical broken line is taken from results by Hay (1). His results indicate that the ventilation velocity for certain rod submergences and diameters can be computed with sufficient accuracy by  $V_{\text{crit}}/gH = 1.7$ . The St. Anthony Falls data, particularly for the larger rods at all but the smallest submergences, appear to verify Hay's data. Data for the smaller diameter rods do not agree so well except at the large submergence ratios; a definite scale effect exists for the lower submergence ratios when plotted in this manner. The Froude number of approximately 1.7 must be approached from the decreasing side before complete ventilation of either basic type would occur for most of the rods tested.

# Ventilation of Bodies Piercing a Free Surface

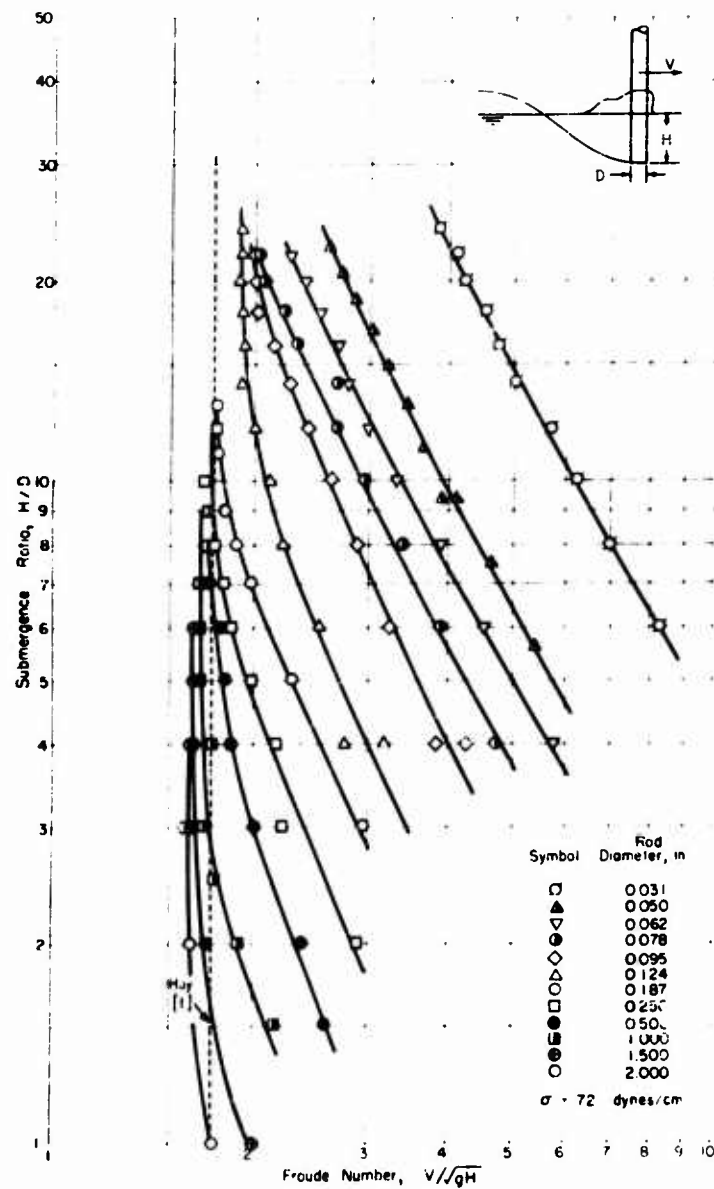


Fig. 2 - Rod ventilation as function of Froude number based on submergence



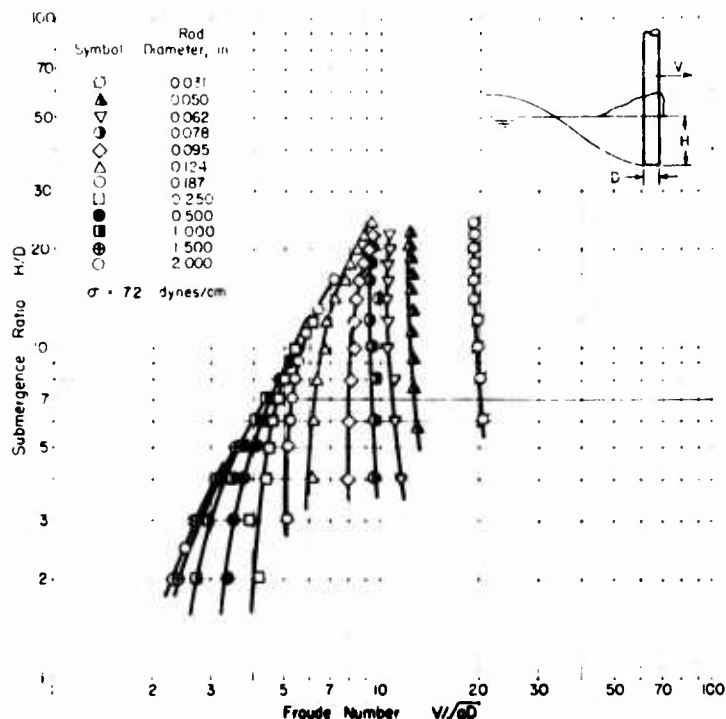


Fig. 3 - Rod ventilation as function of Froude number based on diameter

Figure 3 illustrates the same data plotted as a function of the Froude number based on diameter. For the smaller rods, the ventilation Froude number is nearly independent of the submergence ratio, i.e., for a rod of given diameter, the velocity for complete ventilation remains essentially constant. As the rod diameter increases the same trend is true, but over a smaller range of submergences (low submergences). During the tests it was observed that the ventilation of the small-diameter, uncoated rods occurred in general as flash ventilation, with an increasing tendency for creeping ventilation as the diameter and submergence increased. For the large rods, no flash ventilation was observed. Relating this observation to the data of Fig. 3 it is apparent that the velocity for creeping ventilation is dependent upon the submergence ratio, whereas the velocity for flash ventilation is relatively independent of the submergence ratio.

#### Effect of Weber-Number Correction

As the data for all rod diameters and submergences were not successfully correlated with the Froude number, it was decided to determine the significance of surface tension. The effect of surface tension on ventilation was investigated by adjusting the surface tension of the water to maintain a constant ratio of the Froude number to the Weber number for a particular group of rod diameters ( $\frac{F_r^2}{We_r}$ , where  $\eta_r$  = diameter ratio and  $\gamma_r$  = kinematic capillarity ratio). Rods with nominal diameters

of less than 1/4 inch were used more extensively in these tests, as the small-diameter rods exhibited a relatively large-scale effect. The results of this study are shown in Figs. 4 and 5. As shown in Fig. 4 for the smaller rods, a reduction of surface tension decreases the ventilation velocity to some extent, but the reduction is not sufficient for satisfactory data correlation. For example, consider the data for the 0.095-inch rod in Fig. 4. Two sets of data are shown for this diameter; one set (solid symbol) represents data for a lowered surface tension, the other (open symbol) represents data taken with tap water. The latter set of data is included to compare directly the effect of lowering the surface tension on the ventilation velocity for a rod of given diameter. To satisfy the assumption that surface-tension forces are significant (constant Froude/Weber number ratio), the data for the 0.095-inch rod and  $\sigma = 42$  dynes/cm (closed symbol) should agree favorably with the data for the 0.125-inch rod in tap water with  $\sigma = 72$  dynes/cm. It is evident that this assumption is not completely correct, as the data do not form a common curve. The reduced surface tension did not lower the ventilation velocity of the 0.095-inch rod sufficiently to make the Froude numbers equal. Figure 5 contains data for larger diameter rods. It is evident that surface tension has less effect on the ventilation velocity, particularly for the larger submergences. This is in agreement with the Froude number correlation previously found for the larger diameter rods.

#### Effect of Reynolds-Number Correction

To scale the inertia, viscous, and gravity forces simultaneously, it was necessary to maintain a constant ratio of the Froude and Reynolds number ( $D_r = \frac{V^2}{\nu}$ , where  $\nu$  = kinematic viscosity ratio). This was accomplished by adjusting the viscosity of the water in the tank as described previously. Again the smaller diameter rods were used, as ventilation of the larger rods was correlated with the Froude number alone for most submergences. Figure 6 illustrates the typical effect of the

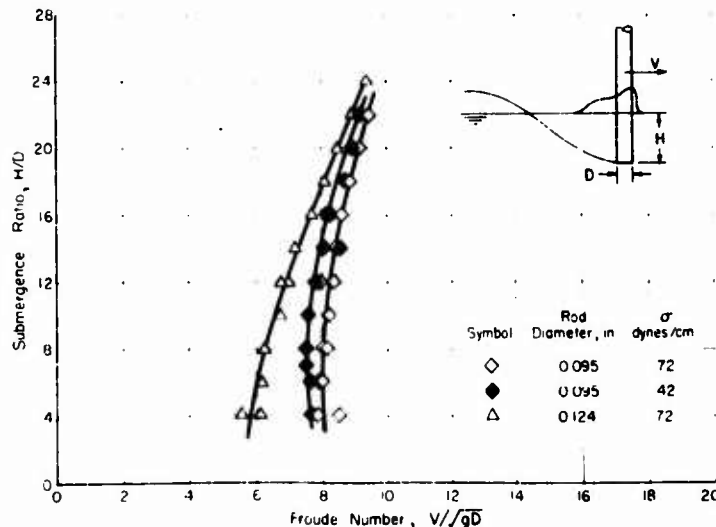


Fig. 4 - Effect of constant Froude/Weber ratio on rod ventilation (0.095-inch and 0.124-inch rods)

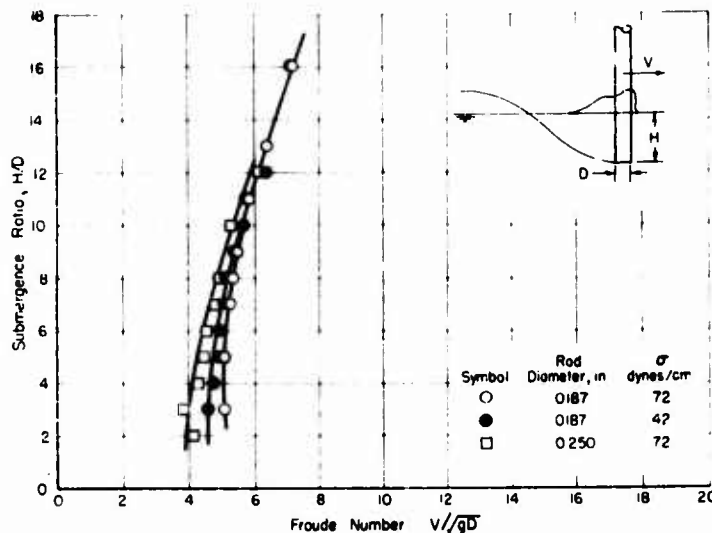


Fig. 5 - Effect of constant Froude/Weber ratio on rod ventilation (0.187-inch and 0.25-inch rods)

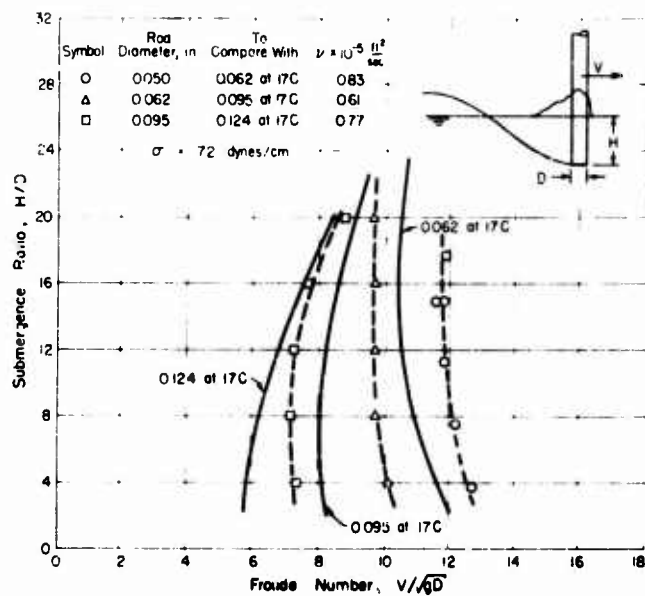
viscosity correction. For most rods two sets of data taken in water with different viscosities are shown for a particular diameter. The solid line is faired through data taken in unheated water at 17°C. The broken line is faired through data taken in water heated to maintain a constant Froude/Reynolds ratio. As an example, consider the 0.062-inch rod. The data for this rod with a lowered viscosity (open triangles) should agree favorably with the 0.095-inch rod in unheated water, as the ratio of the Froude to the Reynolds number has been kept essentially constant. It is evident that the ventilation velocity has been reduced, as shown by the broken and solid faired lines for the 0.062-inch rod, but not sufficiently to permit satisfactory Froude-number correlation with a larger diameter rod as determined from the original assumption.

#### Teflon Rods

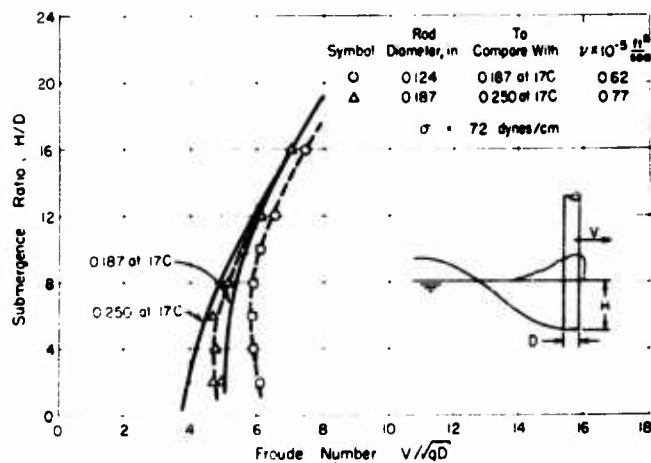
In an attempt to reduce further the existing discrepancy between data for rods of different sizes, several of the rods were coated with Teflon. Plots of faired curves of the data for the submergence ratio  $H/D$  against the Froude numbers are shown in Fig. 7. The data for rod diameters above 0.254-inch fall on essentially the same line for most submergence ratios, indicating that the Froude numbers can be considered the proper modeling parameter for these particular submergence ratios and diameters. From comparison of Fig. 7 with Fig. 2 or Fig. 3, it is evident that the use of Teflon greatly improved the Froude-number correlation.

One of the most significant ventilation characteristics of the Teflon rod was that delayed vent formation was practically nil, whereas with the uncoated rods of small diameter it was the predominating type of ventilation. It would be expected that the effect of the Teflon would become less apparent for the large rod diameters, as above 0.254 inches. This also can be noted from a comparison of the previous graphs.

# Ventilation of Bodies Piercing a Free Surface

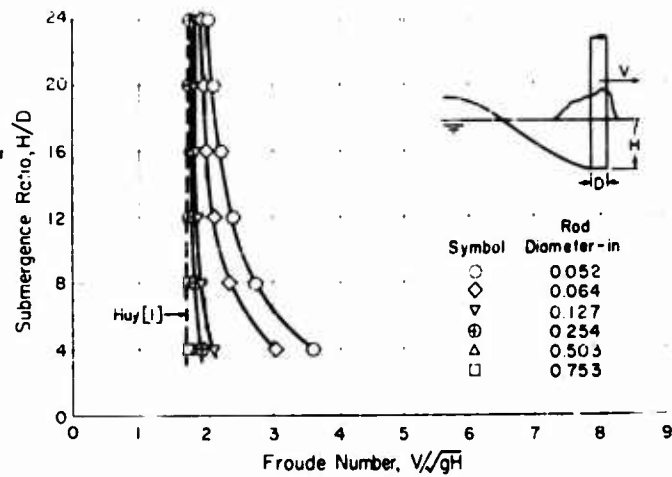


(a)

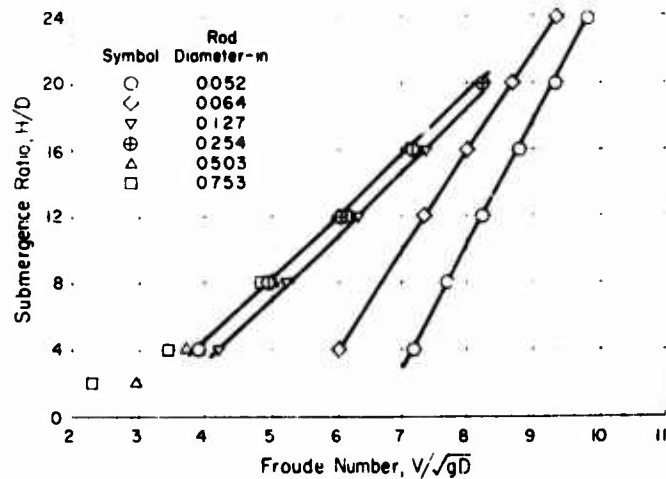


(b)

Fig. 6 - Effect of constant Froude/Reynolds  $\sigma/\nu$  on rod ventilation



(a)



(b)

Fig. 7 - Ventilation of Teflon rods as a function of the Froude number and submergence ratio

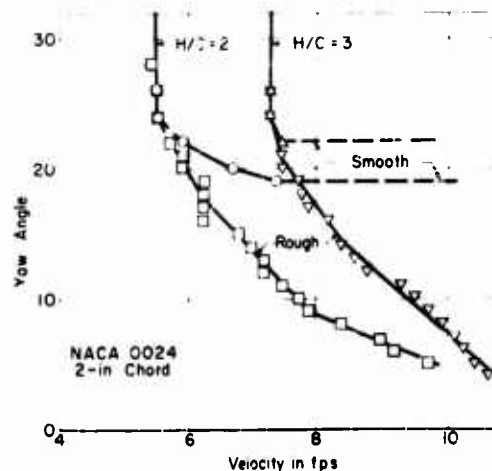
In observing the ventilation of the cylindrical rods, it was noted that a considerable hysteresis effect existed for the uncoated rods of small diameter, as is typical of flash ventilation. The Teflon rods exhibited no hysteresis, as the ventilation appeared and disappeared at essentially the same velocity. It also was found that the velocity at which the vent closes was independent of the rod material.

DISCUSSION OF RESULTS--  
YAWED STRUTS

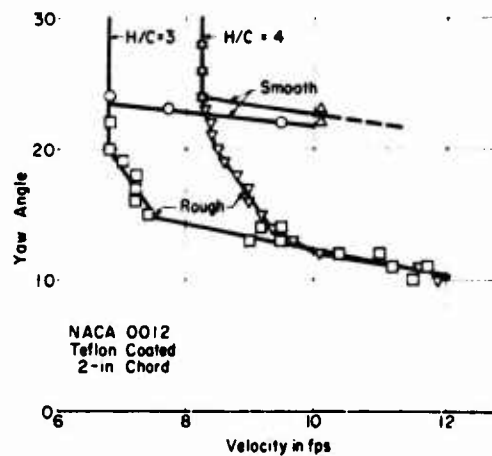
The basic data that have been obtained include the velocity for complete ventilation for a particular submergence, and yaw angle. Typical data are shown in Figs. 8 and 9 for various submergence ratios. In the course of the ventilation studies it was noted that a wide range of scatter was present for ventilation of the struts at all but the very high yaw angles. This scatter was believed to be caused by the condition of the water surface or turbulence in the rotating-arm facility. It appeared that if the foil struck any surface disturbance, provided the foil was moving at a sufficient velocity, it would immediately ventilate, even though ventilation would not occur for smooth-water conditions. It was also found that a minimum velocity could be obtained for which the strut would not ventilate under any conditions. The difference in magnitude of this minimum velocity and the velocity required for ventilation in smooth water was very considerable, the difference increasing with decreasing yaw angle. This can be readily seen from Figs. 8 and 9.

The rough-water curve represents the minimum ventilation velocities that could be obtained by forcing the ventilation to occur. The ventilation was forced by creating a disturbance through which the strut passed. It also was possible in many cases to start ventilation by creating a disturbance in the wake of the strut, thereby permitting air to enter this region and move forward to the foil. With these artificial disturbances it was possible to obtain ventilation at relatively low yaw angles, as compared to smooth water. In a sense, the difference between the rough- and smooth-water curves represents the hysteresis effect for the struts, as the forced-ventilation data are essentially the points where complete ventilation disappears.

The effect of surface tension has also been briefly investigated in the rotating-arm tank. The surface tension was lowered and repeat runs were made with the

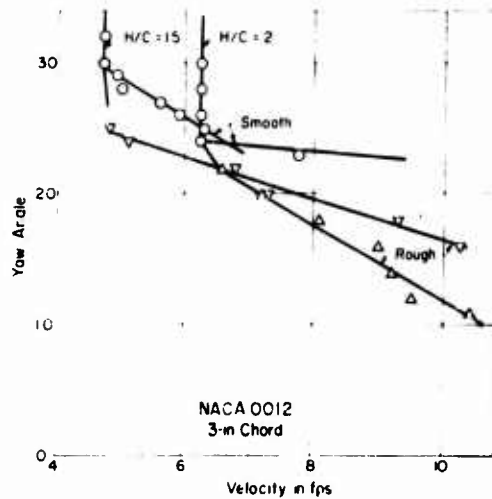


(a)

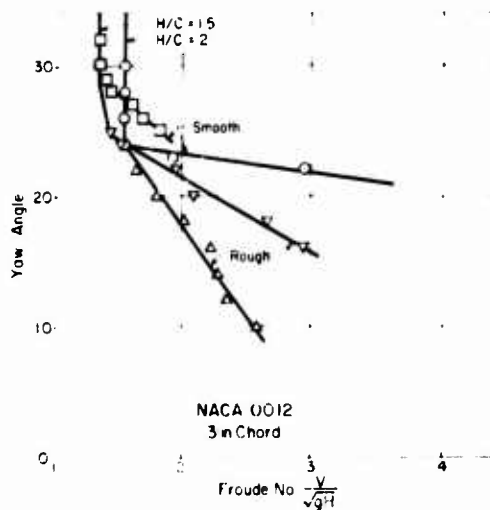


(b)

Fig. 8 - Effect of water-surface conditions on ventilation velocity (2-inch chord)



(a)



(b)

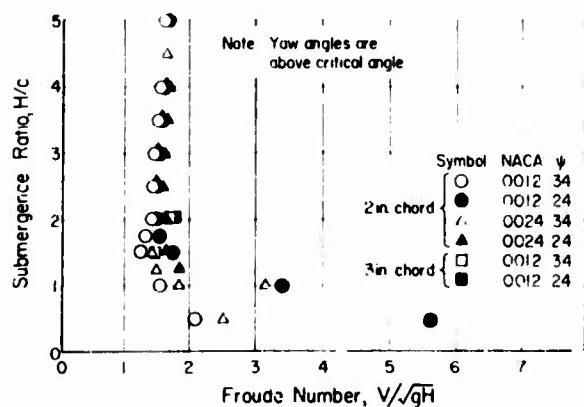
Fig. 9 - Effect of water-surface conditions on ventilation velocity (3-inch chord)

changes. The sharp break in the curve occurs over a relatively small range of yaw angles. For yaw angles below the break in the curve, ventilation was very difficult to obtain in relatively smooth water at the velocities available in the rotating-arm facility. The high-angle ventilation (angles above the break) is essentially independent of yaw angle and can be correlated by the Froude number based either on submergence

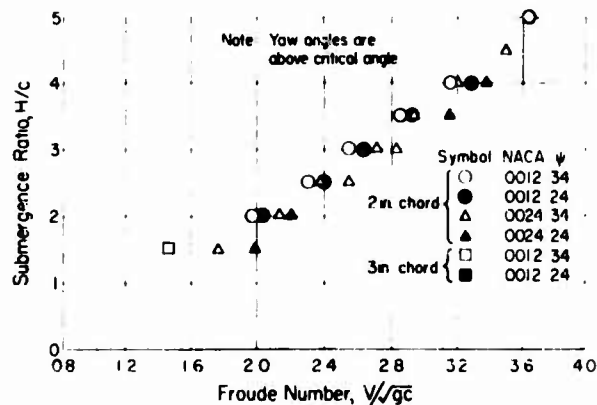
same strut geometry. In general, it appears that the ventilation velocity was reduced slightly for the sizes of struts used in the tests. However, this was rather difficult to ascertain carefully as the conditions of the water through which the strut passes have also been shown to have a very marked effect on the ventilation velocity. The reduction of surface tension did create a different pattern in the spray formation about the strut but apparently did not greatly influence the factors that are responsible for the triggering of ventilation. Surface tension may effect ventilation of surface-piercing bodies in several ways. It may permit air to leak into the low-pressure side of the strut more easily, or it may permit air to enter the wake area more easily through the trailing vortices. In both cases, it would be expected that lowering the surface tension would reduce the velocity for complete ventilation. More tests appear necessary to separate completely the effects of surface tension and rough-water or turbulent conditions on the aeration of the flow in the region of the strut.

Preliminary analysis has been directed toward correlating data for the sections utilized. Attempts at correlating data over the entire range of yaw angles have not been successful, but better results have been obtained by dividing the ventilation into two types which are determined by the yaw angle for a given strut geometry. As seen in Figs. 8 and 9 for a particular submergence ratio, the ventilation velocity is essentially constant for the high angles of yaw. As the angle is decreased, a position is found where the velocity becomes very sensitive to small angle

# Ventilation of Bodies Piercing a Free Surface



(a)



(b)

Fig. 10 - Correlation of high-angle strut ventilation data

or on chord and the submergence ratio (depth in chords). This correlation is shown in Fig. 10 for the NACA 0012 and NACA 0024 sections and for two chord sizes. Also note that the data for three foils tend to group together for the higher submergence ratios at a submergence Froude number of about 1.6. Foil thickness or shape apparently has little effect for this range of yaw angles. Struts of a rectangular cross section have been used in preliminary tests and have exhibited essentially the same properties.

Some work of a preliminary nature has been done regarding the relationship of the stall angle to high- and low-angle ventilation. A brief series of tests was conducted to measure the lift force with a dynamometer and thereby determine the wetted-flow stall angle for the particular sections. In general, it was found that the



angle that separated the two regions of ventilation was approximately the stall angle for the strut. Therefore, in the case of smooth water, it was difficult to obtain ventilation below the stall angle at the available velocities. However, if the flow pattern was disturbed by some external conditions, ventilation was achieved.

## CONCLUSIONS

Based on the tests described in the preceding sections, it is possible to derive the following conclusions:

1. Two distinct types of ventilation occurred—creeping and flash ventilation. The predominating type was determined by body size, submergence, and, for struts, angle of yaw.

2. Creeping ventilation predominated for large-diameter, uncoated rods and also for Teflon-coated rods. Flash ventilation predominated for the small, uncoated rods at all but very large submergences.

3. Creeping-ventilation data could be correlated with the Froude number and submergence ratio. In general, flash-ventilation correlation necessitated consideration of other parameters.

4. Little hysteresis effect existed for creeping ventilation. A very pronounced effect was found for flash ventilation as the formation of the air pocket was considerably delayed.

5. The two distinct types of ventilation that occurred for vertical, lifting struts were dependent on the angle of yaw. Above a certain yaw angle, ventilation was primarily a function of submergence and body shape, and the ventilation velocity was essentially independent of the yaw angle. Below this angle, the ventilation velocity became increasingly dependent on yaw angle, and less dependent on submergence. High-angle ventilation data were successfully correlated with the Froude number and submergence ratio.

## REFERENCES

1. Hay, A.D., "Flow About Semi-Submerged Cylinders of Finite Length," Princeton University, October 1947
2. Ramsen, J.H., "An Experimental Hydrodynamic Investigation of the Inception of Vortex Ventilation," National Advisory Committee for Aeronautics Technical Note 3903, April 1957
3. Kiceniuk, T., "A Preliminary Experimental Study of Vertical Hydrofoils of Low Aspect Ratio Piercing a Water Surface," California Institute of Technology, Hydrodynamics Laboratory Report E-55.2, December 1954
4. Perry, B., "Experiments on Struts Piercing the Water Surface," California Institute of Technology, Hydrodynamics Laboratory Report E-55.1, December 1954

\* \* \* \* \*

## DISCUSSION

J. P. Breslin (Stevens Institute of Technology)

This experimental investigation should be of paramount importance to all concerned with small model studies of ventilation and cavitation phenomena. Mr. Wetzel's results reveal the major effect of surface tension forces on the character and degree of ventilation of rods up to a diameter of 3/4 inch. The use of Teflon apparently prevents the development of highly curved junctures between the body and the cavity. Consequently, the relatively large surface-tension forces are avoided. Mr. Wetzel's Figs. 2 and 7(a) should be presented side-by-side and to the same scale to do justice to the remarkable difference in behavior which the use of Teflon provides.

The discovery of this large effect opens the question of the influence of surface tension on the equilibrium location of vapor cavities on curved sections and bodies. It may be that the extent of cavitation will be found to be remarkably affected since the radii of curvature at the forward cavity body juncture should be very small. Perhaps there are researchers who have done such experiments. In any event the effect of a non-wetting material will be investigated in a study of ventilation of small scale dihedral foils at the Experimental Towing Tank.

In regard to the remaining scale effects exhibited in Fig. 7(a), possibly the curvatures at the bottom of the ventilated pocket are small enough for the smallest rods to provide sufficiently large surface fractions to inhibit full cavity development. In addition, the effect of viscosity at low Reynolds numbers may also be expected to prevent scaling of the velocity distribution about the fore part of the smallest cylinders.

T. Kiceniuk (California Institute of Technology)

There were no photographs of the two regimes of operation. I was wondering if the two could be distinguished visually once ventilation was established, or whether they remained different.

Although the effect on the surface tension of the added detergent was reported, no mention was made of the contact angle between the water and the model before and after the detergent was added. Also were the surface-tension values or contact angle affected by change in water temperature which was being used to secure Reynolds Number variation?

In past studies at the C.I.T. Hydrodynamics Laboratory we tried waxing the surface of planing cylinders to determine what effect this would have on the spray-sheet formation and on the forces acting on the model. Surprisingly, the spray sheet still clung to the cylinder and trailed aft, and no significant change in the force picture could be detected.

P. Eisenberg (Office of Naval Research)

It may be of interest to reveal how Mr. Wetzel was led to examine the effects of a material such as Teflon on the surface-tension influences found to be of importance in the ventilation process. Some years ago, I was told of the discovery of a material or coating that was purported to allow slip at a fluid boundary and, therefore, to lower the frictional resistance below expected values for a hydraulically smooth

surface. The evidence cited was the remarkable acceleration of a hydroplane racing boat on which the planing surfaces had been coated with this material.

Doubting the slip hypothesis, I naturally looked for a more rational explanation of such exceptional performance. It occurred to me that, if the step in the planing surface could be ventilated at a lower speed than would normally happen, it would be possible to achieve the full-planing condition much earlier, and, therefore, to accelerate more rapidly since the hump resistance would thus have been lowered.

It was found subsequently that Teflon did indeed exhibit small, interfacial tension relative to water at the air-water interface. I believe it was Mr. Tulin, then in ONR's Mechanics Branch, who suggested that we could both test my hypothesis of the effect of a material such as the one mentioned above and, at the same time, show perhaps that the surface tension effects could be eliminated in this way, thus making it possible to test at small Froude numbers models for which ventilation phenomena are important on the prototype. We therefore arranged for Mr. Wetzel to carry out the tests described in his paper, with the results fully confirming the postulated behavior and so ably reported. We selected Teflon only because we were already acquainted with its properties in some detail.

K. L. Wadlin (National Advisory Committee for Aeronautics)

Mr. Wetzel has carried out a comprehensive study of the principal parameters influencing the inception of ventilation. The answers to many of our questions about the mechanics of the inception process are undoubtedly available in the data obtained by him. It is interesting to note that flash ventilation and hysteresis only occurred when the Reynolds number was low. Also the effects of viscosity, surface tension, and Teflon were noticeable only at low Reynolds numbers. That is, only these influenced ventilation inception when conditions were such that the flow probably was close to the transition from fully attached flow around the cylinder to separated flow. These effects then probably influenced the separation point on the cylinder, particularly in the region of the water surface. This would lead to separated regions being available to provide paths for the air as soon as the pressure gradients were sufficient to draw the air down. This results in creeping ventilation instead of flash ventilation occurs when the pressure gradient is present before separation.

E. R. Tinney (State College of Washington)

The careful experimental work performed by Mr. Wetzel has clarified many points particularly with regard to some of the "scale effects" that can be expected in laboratory tests on ventilation. The writer suggests that a different manner of presenting the data on cylinders (particularly Fig. 2 of Mr. Wetzel's paper) would add to the understanding of the ventilation phenomenon.

At incipient ventilation it is a necessary, though undoubtedly not a sufficient, condition that the pressure be atmospheric in the ventilation region. That is,

$$p_{\text{atm}} = p_{\text{atm}} + \frac{\rho V^2}{2} C_n = 0 \quad (D1)$$

from which

$$\frac{V}{v_{\text{atm}}} = \sqrt{\frac{2}{-C_n}} \quad (D2)$$

#### Ventilation of Bodies Piercing a Free Surface

For the Reynolds numbers at which the author conducted his tests ( $R_e$  between  $1.5 \times 10^3$  and  $1.5 \times 10^5$ , based on diameter), the value of  $C_p$  at a point on the cylinder 90 degrees from the line of the approaching flow is approximately -0.8 for long cylinders deeply submerged. Substituting this value into Eq. (D2) gives

$$\frac{V}{\sqrt{gH}} = 1.58. \quad (D3)$$

This value of 1.58 agrees well with the minimum value of 1.6-1.7 which the author finds as the asymptotic value for all cylinders deeply submerged.

The value of  $C_p$  is affected by the free surface to a degree that is probably dependent upon Reynolds number. It seems logical, therefore, to plot  $V/\sqrt{gH}$  as a function of Reynolds number for constant values of  $H/D$ . This is done in Fig. D1 which shows that Eq. (D3) applies for all the cylinders tested, if the Reynolds number is greater than  $5 \times 10^4$ . This provides a lower limit for laboratory tests if "scale effect" due to viscosity is to be avoided. The limiting value of Reynolds number is seen to depend on the value of  $H/D$ .

At lower values of Reynolds number an empirical relation can be developed which indicates the relative significance of both Reynolds number and submergence. This relation is

$$\frac{V}{\sqrt{gH}} = 1.6 + \frac{1.8 \times 10^6}{\left(\frac{H}{D}\right)(R_e)^{3/2}}. \quad (D4)$$

This equation is plotted in Fig. D2 together with all the data given by the author on his Fig. 2. From Fig. D2 it appears that the influences of submergence and Reynolds number on ventilation are insignificant for values of the parameter  $H/D (R_e)^{3/2}$  greater than  $10^6$ .

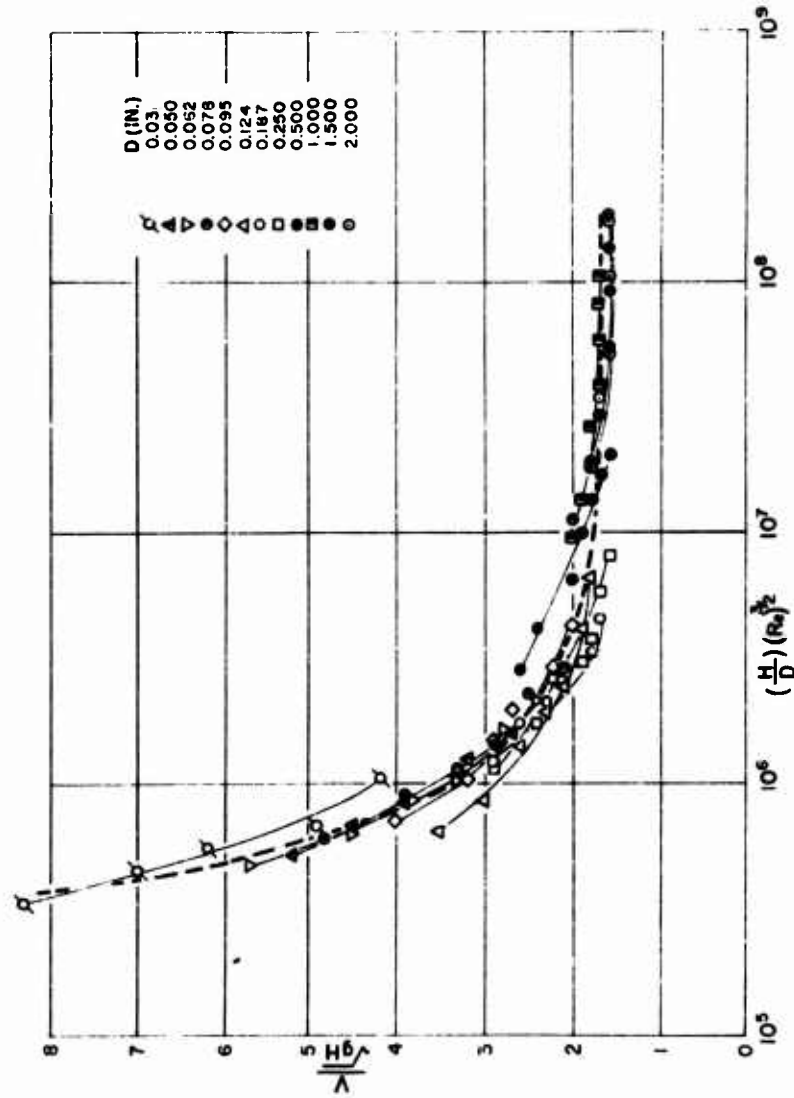


Fig. D1 - Plot of  $\frac{H}{\Delta}$  as a function of Reynolds number for constant  $D$  values

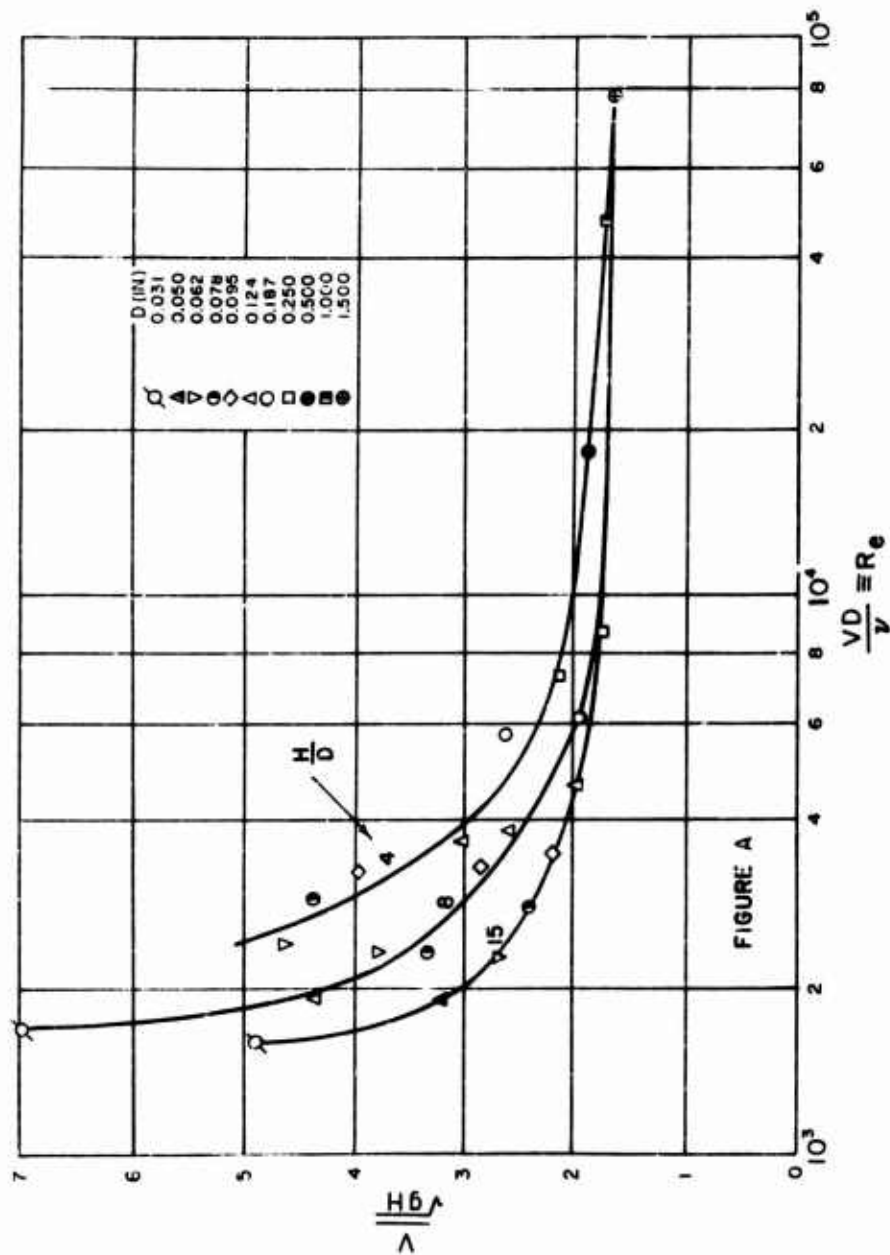


Fig. D2 - Influence of submergence and Reynolds number on ventilation

\* \* \* \* \*

# AIR ENTRAINMENT BEHIND ARTIFICIALLY INFLATED CAVITIES

I. J. Campbell and D. V. Hilborne  
*Admiralty Research Laboratory  
Teddington, Middlesex*

## INTRODUCTION

A fully developed cavity can be formed behind an obstacle moving through water either by boiling of the water in the low-pressure region round and behind the obstacle or by the injection of air behind the obstacle. The use of air injection can greatly extend the conditions of speed and free stream pressure under which well-developed cavities can be formed. The air is, of course, entrained at the rear of the cavity and left behind in the water and the air supply must be continually maintained.

The air entrainment behind artificially inflated cavities was first investigated experimentally in the Hydrodynamics Laboratory at the California Institute of Technology (1). In the Caltech experiments the cavities were formed behind a circular disc supported in a free surface water tunnel. Figure 1 shows diagrammatically how the entrainment rate was found to vary with the cavitation number, other parameters being held constant. The part of the curve where the entrainment is nearly constant was observed to correspond to a configuration in which a re-entrant jet or splash was formed at the rear of the cavity; in these circumstances it was supposed that the water entering the cavity collected air by turbulent entrainment and carried it downstream in falling back through the cavity wall. In the region in which  $Q$  increases rapidly with decreasing  $\sigma$  a pair of air-filled vortex tubes was observed trailing behind the cavity and it was supposed that the vortex cores acted as pipes along which the air was readily transported away from the cavity. From analysis of a number of such entrainment measurements it was found empirically at Caltech that the non-dimensional entrainment coefficient,  $C_{Q1}$ , correlated, although rather roughly, with the product  $\sigma F$  of cavitation number with Froude number based on disc diameter. It was also found empirically that the "twin vortex" regime held sway when  $\sigma F > 1$  and the "re-entrant jet" regime when  $\sigma F < 1$ .

A theory of air entrainment in the trailing vortex regime has been formulated by Cox and Clayden (2), who employed some of the concepts of aerofoil theory to calculate the size of the vortex cores. The theory of Cox and Clayden contains one parameter to be determined by fitting the theoretical predictions to experimental data.

The discovery at Caltech of the trailing vortex regime behind cavities and the application by Cox and Clayden at the Armament Research and Development Establishment of the concepts of aerofoil theory to this situation are the most interesting contributions which have been made to the subject of cavity gas entrainment.

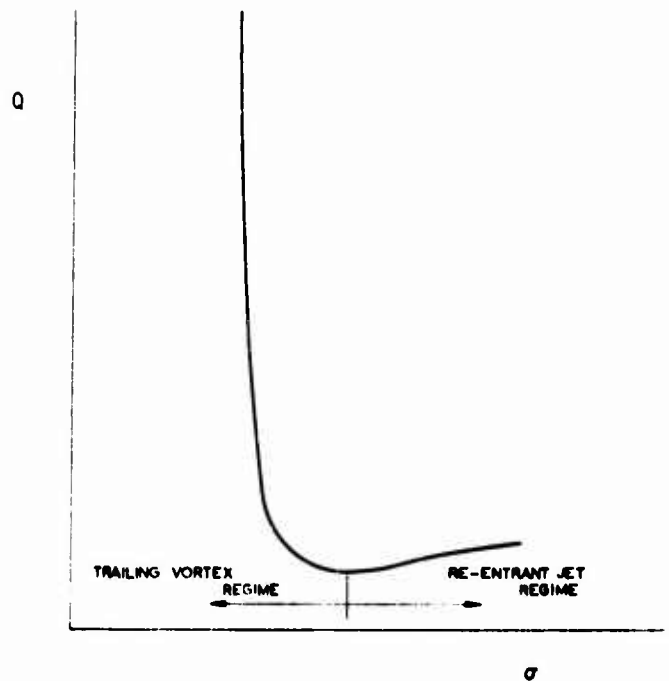


Fig. 1 - Typical entrainment curve for a cavity formed behind a given disc at a given speed

In this paper we report some air-entrainment measurements which we ourselves have made. Our experiments were very similar to those made at Caltech, but a somewhat larger range of conditions was covered. As it might be suspected that viscosity and surface tension could affect the results, the hypothesis that the entrainment depends exclusively on Froude number and cavitation number was examined in some detail. As this involved the use of models of different sizes, particular care was taken to correct for the influence of channel boundary effects.

Also we propose a modification to the theory. The theoretical model originally proposed by Cox and Clayden is not applicable to our experimental conditions. The modified theoretical model, which involves no empirical parameter,\* gives predictions of gas entrainment which are in broad agreement with our experimental results.

#### THEORETICAL DISCUSSION

Cox and Clayden (2) point out that, since the pressure in the cavity is fairly constant, there must be a difference in the velocity on the free streamlines corresponding to the difference in hydrostatic pressure at the top and bottom of the cavity.

\*We make use of some experimentally derived values of cavity dimensions but no empirical parameter which has to be evaluated from air-entrainment measurements is involved.



This gives rise to a circulation which can be evaluated. Cox and Clayden then argue that the function of the circulation is to produce a force which is equal and opposite to the buoyancy force on the bubble. This enables them to calculate the distance apart of the vortices and, thus, their inclination to the horizontal caused by the vertical velocity induced by each of them at the position of the other. They estimate the diameter of the vortex tubes from the circulation and from the condition that the pressure on their boundaries shall be cavity pressure. They then treat the vortex tubes as pipes along which the air is transported away from the cavity. In this view the air flows along each vortex tube under the action of a pressure gradient which is imposed by the hydrostatic pressure variation and so is known from the inclination of the vortices to the horizontal. The mean air velocity,  $v_m$ , in the tubes is then determined in terms of an equivalent friction coefficient,  $\lambda$ , for air flow in the vortex pipes. The coefficient  $\lambda$  is left as a parameter to be determined empirically by fitting the theoretical predictions to experimental results.

As will be seen later, application of this picture to our experimental results implies values of  $v_m/v_\infty$  which are in many cases less than unity. Velocity  $v_\infty$  is the free stream velocity, and the axial velocity of water near the vortex tubes may be supposed to be approximately  $v_\infty$  except in the immediate neighborhood of the bubble. When  $v_m/v_\infty = 1$ , the mean air velocity in each vortex pipe is equal to the axial velocity of the pipe walls. When  $v_m/v_\infty < 1$ , the pipe friction, far from restraining the air flow under the action of the hydrostatic pressure gradient, would actually aid it. In these circumstances the model of Cox and Clayden cannot be regarded as applicable. For this reason we propose a modification of the model. We suppose simply that when the model moves through unit distance, enough air has to be supplied to fill unit length of newly laid twin vortex trail. We now derive an expression for the entrainment on this basis.

Following Cox and Clayden and considering the vertical meridian plane through the cavity (Section AA of Fig. 2), we write

$$v_1^2 - v_\infty^2 = 2g(H_u - H_u)$$

where  $v_1$  and  $v_\infty$  are the velocities and  $H_u$  and  $H_u$  the hydrostatic heads of water on the upper and lower surfaces of the cavity. The circulation,  $\Gamma$ , which is set up in this way round the cavity is given by

$$\int_C v \, ds$$

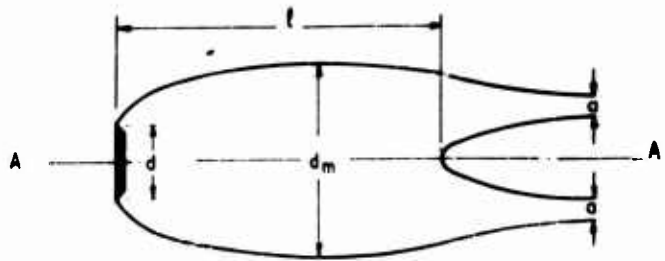


Fig. 2 - Cavity behind a disc

where  $c$  is the trace of the cavity on the vertical meridian plane. For sufficiently slender cavities this integral may be approximated as follows:

$$\int_c v(x) dx = \int_0^l (v_1 - v_u) dx$$

where the  $x$  axis is parallel to the direction of the main flow and  $l$  (see Fig. 2) is the length of the bubble. Since

$$v_1 - v_u = (v_1^2 - v_u^2) / (v_1 + v_u) = (v_1^2 - v_u^2) / 2v_u$$

then  $\int_c$  can be further approximated:

$$\int_c \frac{g}{v_u} \int_0^l (H_1 - H_u) dx$$

$$\frac{g}{v_u} \frac{1}{4} d_m^2$$

where  $C$  has been approximated by an ellipse, so that the integral then becomes the area of the ellipse.

If we neglect the inclination of the trailing vortices to the horizontal and assume that the axial velocity of the water in the neighborhood of the vortices (sufficiently far downstream) is  $v_u$ , then the transverse velocity,  $q_c$ , round the periphery of the vortex tubes is given by Bernoulli's equation. Thus

$$p_c + \frac{1}{2} (v_u^2 + q_c^2) = p_u + \frac{1}{2} v_u^2$$

i.e.,

$$q_c^2 = v_u^2$$

where  $\sigma$  is the cavitation number. In calculating  $q_c$ , Cox and Clayden allow for the inclination of the vortices and so include an additional term which has, however, only a very small influence, at least in our range of experimental conditions.

The diameter,  $a$ , of the vortex cores is then given by

$$a = \frac{1}{2} q_c$$

whence

$$a^2 = \frac{g^2 d_m^2}{16 v_u^4}$$

According to our view the volume of gas entrained per unit time is given by

$$Q = 2 \left( \frac{1}{4} a^2 \right) v_u$$

Hence the nondimensional entrainment coefficient,  $C_{Qd}$ , based on disc diameter, is given by

$$C_{Q,d} = \frac{Q}{v_o d^2} = \frac{\pi}{2} \left( \frac{a}{d} \right)^2 = \frac{\pi}{32} \frac{K^2 d^2}{v_o^4} \left( \frac{d_m}{d} \right)^2 \left( \frac{r}{d} \right)^2$$

or

$$C_{Q,d} = \frac{1}{32 F^4} \left( \frac{d_m}{d} \right)^2 \left( \frac{r}{d} \right)^2 \quad (1)$$

It is known from the experiments of Reichardt (3) on cavities formed behind a circular disc that

$$(d/d_m)^2 = 1.1$$

to a very good degree of approximation. With this approximation we can write

$$C_{Q,d} = \frac{1}{35.2 F^4} \left( \frac{r}{d} \right)^2 \quad (2)$$

The ratio  $r/d$  is also, of course, a function of  $F$  for cavities behind a circular disc and so  $C_{Q,d}$  is a function of  $F$  and  $r$ . Reichardt's experiments also show that as a rough approximation we may write

$$d/r = 0.7$$

over a limited range (say 0.04 to 0.12). If we incorporate also this approximation we find that

$$C_{Q,d} = 15.8 F^4 \quad (3)$$

This makes it intelligible that it was found possible in the Caltech work to obtain a rough correlation between  $C_{Q,d}$  and  $F$ . In fact (3) is in reasonable accord with the Caltech results at the lower rates of entrainment.

#### EXPERIMENTAL ARRANGEMENT AND PROCEDURE

The measurements reported here were made on the small water whirling arm at the Admiralty Research Laboratory; as compared with a water tunnel of normal type this equipment offers ready dispersal of entrained air and relatively small boundary wall interference. The inner radius of the channel is 3.8 ft and the outer radius 6.8 ft; in these tests the model was positioned at the 5-ft radius. For most of the tests the model was maintained at 8-1/2 in. below the surface in water depth of 18 in. In addition some measurements were also made in different depths of water and with different vertical positions for the model.

The models consisted of a number of interchangeable discs of different diameters mounted at the front end of a sting, which was in turn carried on a supporting strut (see Fig. 3). Provision was made for air to be supplied to the back of the discs and for measurements of dynamic head and cavity pressure.

A rotating seal and conduit permitted a continuous supply of air to be brought from outside the arm to the model. A second seal was used to take a direct connection to the manometer used for measuring cavity pressure. In the case of the dynamic head, which involved measuring a wide range of pressures, a strain-gauge transducer which could be placed to take advantage of the balancing effect of radial

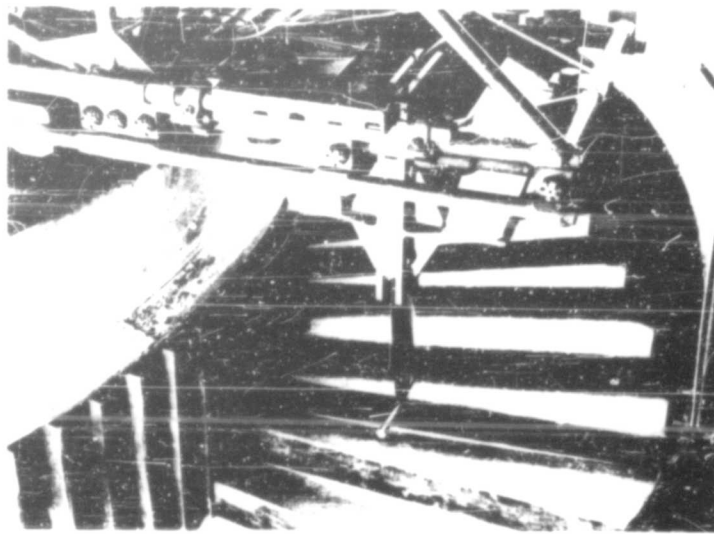


Fig. 3 - Disc (3/4 in.) mounted in position on whirling arm

acceleration was used. Pressure measurement and all filtering, metering, and control of the air supply took place off the arm.

In most cases the procedure adopted was to make a sequence of observations all at the same model speed but with differing air supply rates. Initially the air was supplied at a high rate and then the air supply valve was closed step by step, the air supply, total head, and cavity pressure being measured and the model speed checked at each stage. When eventually the cavity was on the verge of collapse, the process was reversed.

A typical example of the results obtained is given in Fig. 4. It can be seen that, as the air supply valve was closed, the cavity pressure fell steadily until a point A was reached at which a further small adjustment of the valve in the same direction caused a sharp change to conditions of lower cavity pressure as at point B. It was not found possible to hold the cavity pressure at any intermediate point by adjustment of the air supply. If the process was continued the pressure dropped until the cavity suddenly collapsed and a further large reduction in pressure occurred.

Reversing the process and re-forming a clear cavity, a similar change occurred, this time in the opposite direction and at a considerably greater rate of flow (C to D) but otherwise the results remained the same. The cavity pressure showed great sensitivity to speed fluctuation but was relatively insensitive to changes of air supply at high cavity pressures.

The right-hand section of the entrainment curve of Fig. 4 was observed to correspond to the trailing vortex regime and the left-hand section to the re-entrant jet regime. The measurements reported in this paper apply only to the trailing vortex regime. In this paper the point A has been taken as representing the transition point between the trailing vortex regime and the re-entrant jet regime.

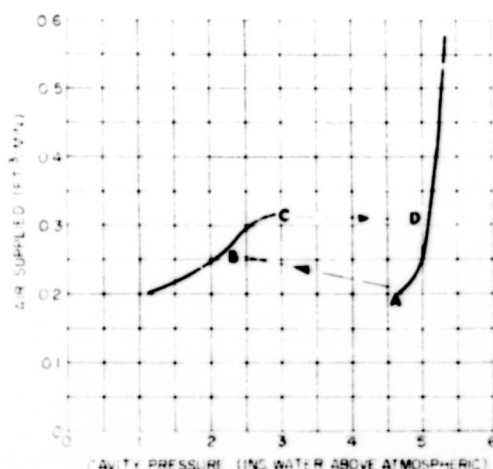


Fig. 4 - Results obtained with a 1/2-in. disc 8-1/2 in. deep with a speed of 18 fps

Figure 5 shows a photograph of a cavity with a pair of trailing vortices behind it. The appearance does not accord well with the idea of air flowing along a pipe; at least it might equally well be supposed on this evidence that the bubbles filling the tubes are simply left behind in the water.

#### DISCUSSION OF EXPERIMENTAL RESULTS

The main results are presented in graphical form in Figs. 6 to 8, where  $C_{ei}$  is plotted against  $U$  for various disc sizes and for various model speeds. Individual experimental points are not plotted; in fact a great many observations were made and these define the experimental curves shown very closely. The right-hand end of each curve in Figs. 6 to 8 corresponds to the point in Fig. 4 labeled A at which transition to the re-entrant jet regime occurs.

The results presented in Figs. 6 to 8 have already been corrected for interference effects from the free surface and the channel floor. To obtain these corrections, sets of measurements were made in various depths of water, in some cases with the model held at a fixed height above the bottom and in others with the model held at a fixed depth below the free surface. It was found that for each boundary the effect of an alteration of boundary position was to move the entrainment curve bodily parallel to the axis of  $U$  by an amount depending on the distance, expressed in model diameters, of the model from the boundary. As the effect diminishes quite rapidly with increase in distance it

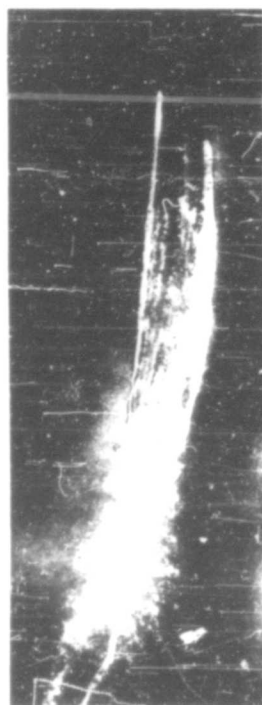


Fig. 5 - Cavity with trailing vortices

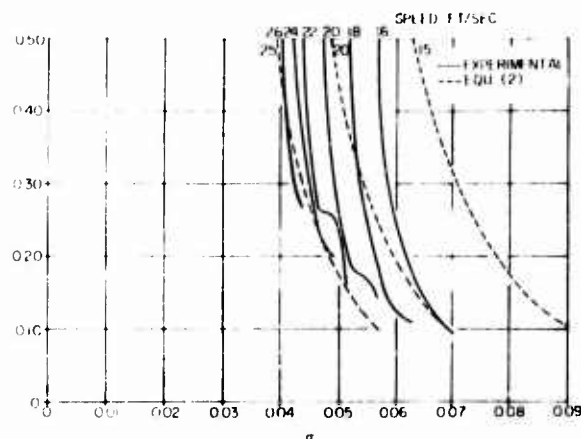


Fig. 6 - Entrainment coefficient versus cavitation number; 1/2-in. disc

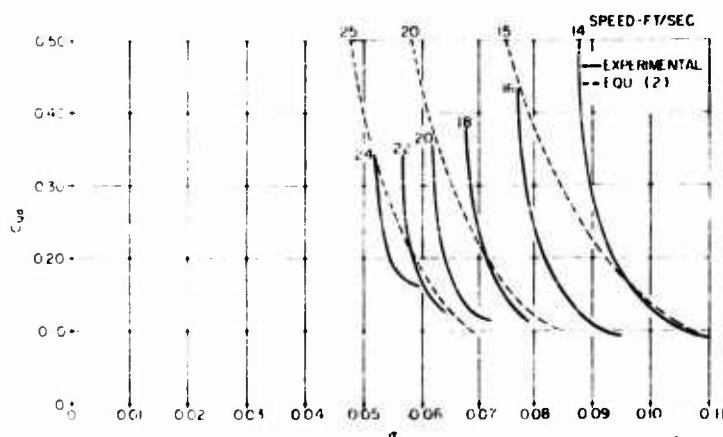


Fig. 7 - Entrainment coefficient versus cavitation number; 3/4-in. disc

was found possible to estimate the cavitation number for a given entrainment coefficient in unbounded flow,  $\sigma_u$ , and express the effect of boundary interference as the difference in cavitation numbers,  $\sigma_u - \sigma$ . The experimental results are summarized in Fig. 9. This includes measurements made at different rates of entrainment, Froude number, and Reynolds number.

The boundary effects on entrainment are presumably associated directly with the boundary effects on the geometrical configuration of the cavity. Arguing from the theory of tunnel boundary effects on cavities and from the theory of entrainment outlined above, the proximity of a free surface might be expected at a given  $\sigma$  to make smaller both the cavity and the gas supply required to maintain it. In the same way

# Air Entrainment Behind Artificially Inflated Cavities

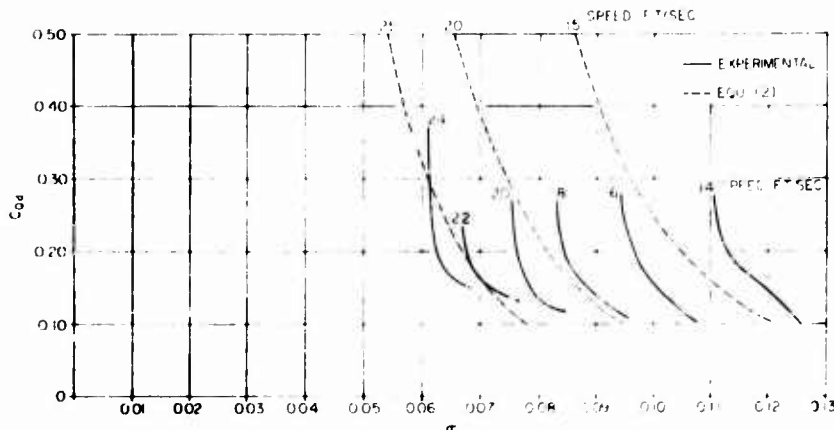


Fig. 8 - Entrainment coefficient versus cavitation number; 1-in. disc

the proximity of a fixed surface might be expected to have the opposite effect. This at least explains qualitatively what actually occurs. It should be noted in this connection that the bottom and sides of the channel, being covered with anti-swirl barriers, are a rather complex shape.

The distance of the nearest side wall from the model position was 14 times the diameter of the largest disc. Noting the effect of the bottom at this distance it was considered reasonable to regard boundary interference from the side walls as negligibly small.

Comparison between the entrainment curves obtained at the same Froude number but with different disc sizes shows that entrainment is not exclusively a function of  $F$  and  $\sigma$ . For example, the entrainment curve for the 1 2-in. disc at 18 fps is roughly parallel to the entrainment curve for the 3 4-in. disc at 22 fps but is displaced from it along the  $\sigma$  axis: these two cases correspond to the same Froude number. The effect is small but seems quite definite.

It appears that the entrainment curves (for the twin vortex regime) are bounded on the right by a value of  $\sigma$  which depends only on  $F$ . For a given value of  $F$  the entrainment curves for the larger discs lie above those for the smaller discs. Figures 10, 11, and 12 illustrate the situation.

In Fig. 10 measurements of entrainment all at the same  $\sigma$  are plotted against  $F$  for the different discs. The evidence is limited because it is difficult to select the data necessary for constructing such a diagram. The points clearly do not define a single curve but show a systematic trend of increasing entrainment with increasing disc size.

Again in Fig. 11, in which the minimum value of  $C_d$  capable of sustaining a cavity in the twin vortex regime is given as a function of  $F$  for the various discs, the data, although somewhat scattered, define fairly clearly, roughly parallel curves, one for each disc, and the value of minimum  $C_d$  for a given value of  $F$  increases with increasing disc size.

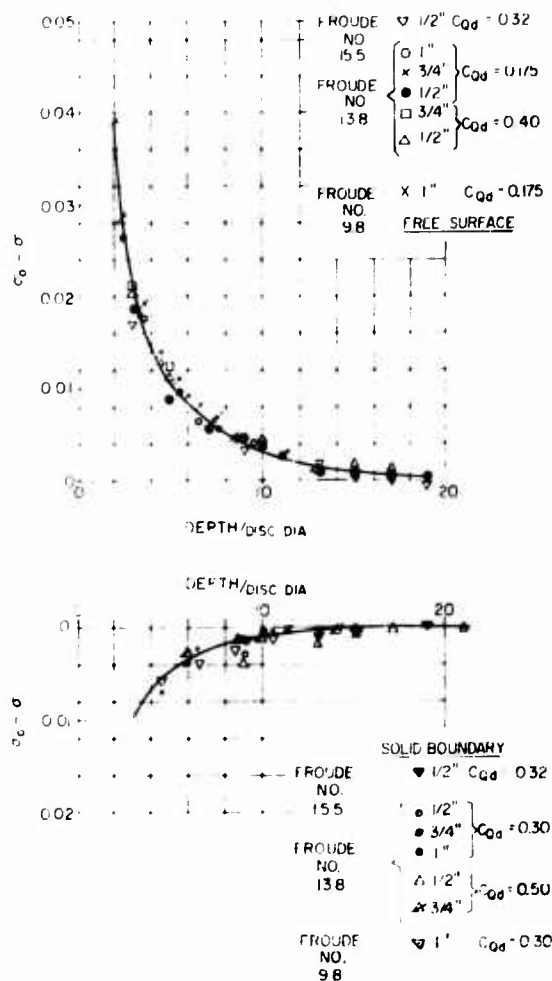


Fig. 9 - Effect of presence of channel boundaries.

In Fig. 12 the highest values of  $C_0/b$  at which a cavity with the twin vortex regime can be sustained are plotted against  $F$  for the various discs. It follows from the smallness of the scatter that  $C_0/b$  and  $F$  are the principal factors which govern the transition condition.

A few measurements were devoted to a check on the possibility that surface tension might affect entrainment. By adding enough Teepol to the water to give an 0.043 percent solution, the surface tension was reduced from 62 dynes/cm to 43 dynes/cm, i.e., by 34 percent. When the entrainment curve for a 1.2-in. disc moving at 18 fps through this solution was compared with the corresponding curve obtained with uncontaminated water, no difference could be distinguished.



# Air Entrainment Behind Artificially Inflated Cavities

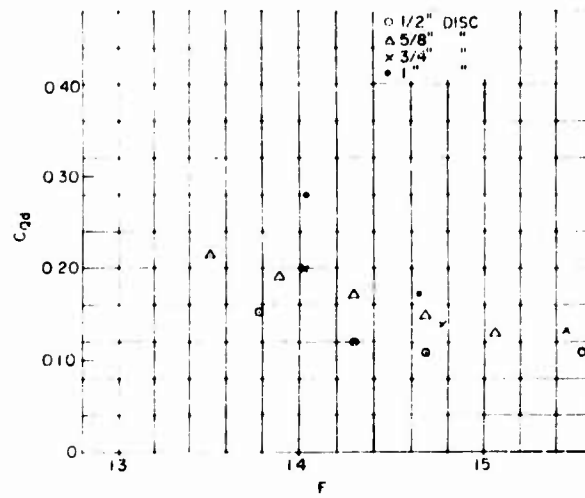


Fig. 10 - Variation of entrainment coefficient with Froude number for various disc sizes; cavitation number, 0.064

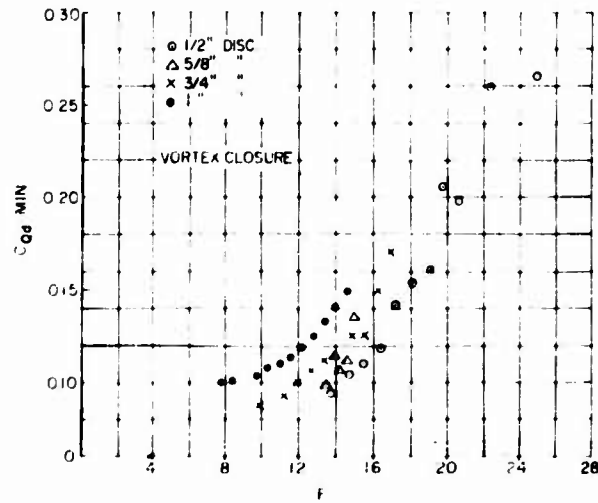


Fig. 11 - Variation of minimum obtainable entrainment coefficient with Froude number

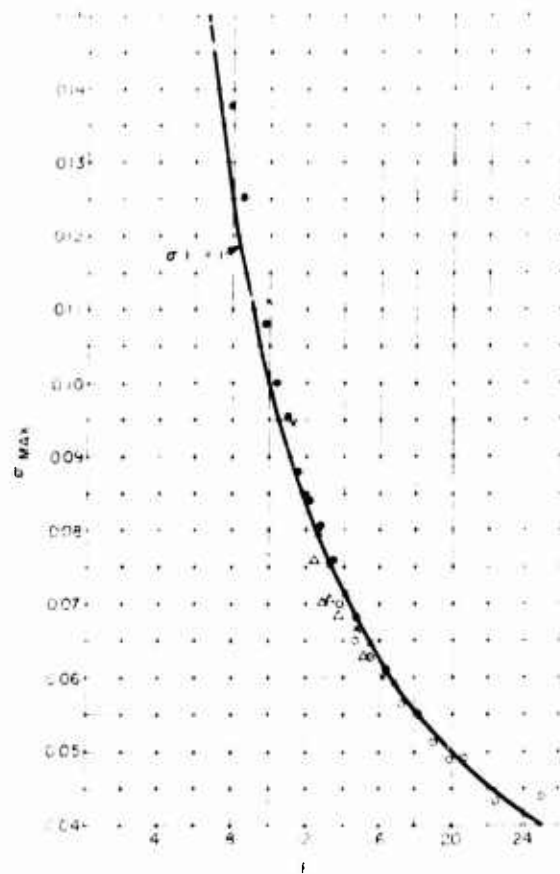


Fig. 12 - Variation of maximum obtainable cavitation number with Froude number

Accordingly it seems unlikely that the parameters, other than  $F$  and  $\sigma$ , on which  $C_{C,1}$  depends include the Weber number. The effects which we have described may possibly be Reynolds number effects; since the viscosity has not been varied, however, it is impossible to assert that this is the case.

The condition for transition from one flow regime to the other is extremely important. Once the trailing vortex regime takes over, the entrainment rate can rise exceedingly rapidly. It is of interest to note from Fig. 12 that the transition condition is quite well approximated by the rectangular hyperbola  $CF = 1$ .

Finally we compare the experimental results with the theoretical predictions. In addition to the experimentally determined curves, Figs. 6 to 8 show also some corresponding theoretical curves. These have been derived from Eq. (2) using Reichardt's values of  $\sigma$  as a function of  $F$ . It will be observed that the theory accounts for the measurements in broad outline.

# Air Entrainment Behind Artificially Inflated Cavities

The cases where the measured value of  $C_{ed}$  lies below the value given by Eq. (2) are cases which would involve values of  $v_m/v_o$  less than 1 in the model of Cox and Clayden. It is for this reason that we regard the theory of Cox and Clayden as not applicable in our range of experimental conditions. The model of Cox and Clayden may, of course, be applicable and our modified version not applicable at higher entrainment rates.

The fact that the experimental results are broadly described by a theory which predicts dependence only on  $F$  and  $h$  naturally confirms that these are indeed the main parameters on which the entrainment depends.

## ACKNOWLEDGMENT

Acknowledgment is due to the Admiralty for permission to publish this paper.

## NOMENCLATURE

- $a$  = diameter of vortex cores
- $C_{ed}$  = air entrainment coefficient based on disc diameter =  $Q/v_o d^2$
- $d$  = disc diameter
- $d_m$  = maximum diameter of cavity
- $F$  = Froude number based on disc diameter =  $v_o/(gd)^{1/2}$
- $g$  = acceleration due to gravity
- $h$  = hydrostatic head of water
- $l$  = length of cavity
- $p_o$  = free stream pressure
- $p_c$  = cavity pressure
- $Q$  = volume of air at cavity pressure entrained per second
- $q_c$  = transverse velocity at periphery of vortex core
- $v_o$  = free stream velocity
- $v_m$  = mean air velocity in vortex cores in the theoretical model of Cox and Clayden
- $\Gamma$  = circulation round vortex tubes
- $\mu$  = equivalent friction coefficient for air flow in vortex tubes in the theoretical model of Cox and Clayden
- $\rho$  = density of water
- $\sigma$  = cavitation number =  $(p_o - p_c)/\frac{1}{2} \rho v_o^2$

#### REFERENCES

1. Swanson, W.M., and O'Neill, J.P., "The Stability of an Air-Maintained Cavity Behind a Stationary Object in Flowing Water," California Institute of Technology, Hydrodynamics Laboratory (unpublished)
2. Cox, R.N., and Clayden, W.A., "Air Entrainment at the Rear of a Steady Cavity," Proceedings of the N.P.L. Symposium on Cavitation in Hydrodynamics, London: H.M.S.O., 1956
3. Reichardt, H., "The Physical Laws Governing the Cavitation Bubbles Produced Behind Solids of Revolution in a Fluid Flow," Ministry of Supply Translation G.D.C. No. 10/5678T

\* \* \* \* \*

#### DISCUSSION

W. A. Clayden (Armament Research and Development Establishment)

It was our experience also that for low values of  $C_{c,1}$  (say less than 0.5) the vortex tubes degenerated into trails of bubbles and it is presumably a consequence of the bubble formation that there are no effects of the hydrostatic pressure gradient along the vortex tubes. For a steady flow pattern to be maintained similar to that shown in the author's Fig. 6, the rate at which the bubbles entrain air must be equal to the rate at which the vortex tubes are laid down. For large air entrainment rates, however, fully formed tubes exist for some distance behind the cavity. In general,  $U_m/U_o$  will not be unity and in our experiments values up to 5 were measured.

It is perhaps worth pointing out that if these data are used to predict the trajectory of a missile, the air entrainment rate will be modified, since the circulation around the cavity which produces the vortices is proportional to  $\cos \theta$ , where  $\theta$  is the angle between the longitudinal axis of the cavity and the horizontal, and also depends upon the lift force.

K. L. Wadlin (National Advisory Committee for Aeronautics)

The authors certainly have arrived at a simple relationship for the case they considered, that is, where the cavity walls are not turbulent. It would be interesting to know if the case where the cavity walls are turbulent has been considered by them. This is of interest since there is a significant difference between the character of the cavity surface shown in the photograph and that which we experience at the NACA. The photograph indicates very smooth flow along the cavity boundaries by virtue of the glassy clearness of the cavity. Our experience, at somewhat higher speeds, has been that the cavity boundary, except for an extremely small distance near its origin, is opaque, indicating turbulence. This is true with and without gas being injected into the cavity. This may mean that at low Reynolds numbers the cavity walls do not entrain the gas but only the turbulent trailing vortices, while at the higher Reynolds

numbers the cavity walls would be a large factor in the entrainment process. It seems that the method of analysis used here might be extended to handle this case also.

I. J. Campbell and D. V. Hilborne

Mr. Clayden's remarks imply that, even when the trailing vortex regime holds sway, there are still two possible situations. In the one situation, at relatively low airflows, the air-filled vortex tubes break up into bubbles and this is the situation in our experiments. In the other situation, at high entrainment rates, fully formed tubes exist for some distance behind the cavity and that situation was realized in the experiments of Cox and Clayden. We agree with this suggestion.

We agree too with Mr. Clayden's remark that the air entrainment rate must be modified when the direction of motion is no longer normal to the direction of gravity and must depend also on the lift force. Appropriate experiments would be interesting.

With regard to Mr. Wadlin's comments it has been our experience that clear cavities are associated with the trailing vortex regime. The only opaque cavities which we have encountered have been associated with the re-entrant jet regime: in these circumstances the wall roughness arises from the re-entrant jet splashing onto the cavity wall. What happens in the re-entrant jet regime is outside the compass of the present paper. Light might be thrown on the point which Mr. Wadlin has raised by experiments with roughened discs behind which cavities in the trailing vortex regime are produced.

The authors wish to thank Mr. Clayden and Mr. Wadlin for their written contributions.

\* \* \* \* \*

# ON SUPERCAVITATING PROPELLERS

H. W. Lerbs

*Hamburgische Schiffbau-Versuchsanstalt  
Hamburg*

This little paper is an attempt to answer the question as to the efficiency of a supercavitating propeller, that is, of a propeller which is intentionally designed for full cavity flow with free streamlines from the leading and trailing edges of the sections. This question arose from time to time during my stay at the David Taylor Model Basin (DTMB) in relation with the propulsion of fast ships. One advantage of such propellers was immediately seen in reduction of erosion and there were also some indications that the noise characteristics might be improved with supercavitating propellers. An open question that remained was the magnitude of the efficiency of such a propeller. It is well known that the efficiency of a conventional propeller, i.e., of a propeller designed for operation near the limit of onset of cavitation, decreases for fully developed cavitation. This reduction becomes, in general, greater the smaller the cavitation number is. The question we were mainly confronted with was, therefore, whether or not the efficiency of a propeller which is intentionally designed for supercavitating conditions might be greater than that of a conventional propeller. It might be said beforehand that the prospect for a supercavitating propeller was unfavorable on account of those theoretical considerations which could be made before the papers by Tulin (1) and Wu (2) on the free streamline theory of fully cavitating hydrofoils were available. However, this situation became different when results from the papers just cited were applied to the propeller flow. These results have made possible a successful solution of this particular propeller problem under consideration.

In the following contribution I wish first to outline briefly the statements on the efficiency of a fully cavitating propeller which were possible prior to Tulin's and Wu's work and then give a few results when their findings are applied on fully cavitating sections to a propeller.

The older papers are connected with the names of Posdunine and Baer, Betz, and Walchner. Of these the first two are of Russian origin. These two papers are related since the problem is treated in both of them by means of methods of momentum theory. To characterize the application of this method to our problem we will restrict ourselves to the paper by Baer, which is the more complete one (3). In this paper a flow model of a cavitating propeller is assumed corresponding to Fig. 1.

The essential feature of this model is that the density of the fluid behind the screw  $\rho_1$  is assumed smaller than the density  $\rho_0$  in front of the screw. On account of the sudden change of the density at the disc not only the pressure but also the speed will change abruptly at the disc. The results which are obtained for this model when applying the laws of energy, continuity, and momentum are interesting. For instance, when such a flow is realized, a positive thrust might be generated under certain

conditions with a negative pressure jump at the disc. For the efficiency  $\eta_1$ , i.e., the efficiency in nonviscous flow, it follows that

$$\eta_1 = \frac{1 - \sqrt{1 - \frac{2}{c_T}}}{1 + \sqrt{1 - \frac{2}{c_T}}} \left( 1 - \sqrt{1 - \frac{2}{c_T}} \right)^2$$

where  $c_T = T / (\rho v_\infty^2)$  is the thrust loading coefficient. It should be noted that this expression changes over into that given by the Froude-Rankine theory if  $c_T \rightarrow 1$ . Further it is seen that  $\eta_1$  decreases if  $c_T$  increases and that  $\eta_1 \rightarrow 0$  if  $c_T \rightarrow 1$ .

The answer of this theory to our problems is incomplete for two reasons. It is firstly not possible to establish a relation between  $c_T$  and the cavitation number  $\sigma$ . However, one might guess that the ratio  $c_T$  becomes great if the cavitation number becomes small. One would then conclude that the efficiency becomes small if the cavitation number is small and goes probably to zero if  $\sigma$  goes to zero. There are, further, no indications that a supercavitating propeller as defined at the beginning behaves differently from a conventional propeller. However, such indications might not be expected from momentum theory because of the inherent assumptions on the geometry of the propeller common to all momentum theories.

It is therefore necessary to consider a supercavitating propeller from the point of view of airfoil theory which requires the polar curves of supercavitating sections to be known. An approximate theory for the lift and drag as functions of the cavitation number and the angle of attack is developed in the aforementioned paper by Betz (4). He starts out from the free streamline flow of a flat plate according to Helmholtz and Kirchhoff. From this theory the lift coefficient is approximated by  $c_L = 2$ , which is only 1/4 the lift in the usual flow without free streamlines. In a cavitating flow, the lift is greater, since the pressure of the fluid between the free streamlines is assumed in the theory by Helmholtz and Kirchhoff to equal the pressure of the undisturbed flow,  $p_\infty$ . When the free streamlines form the boundary of a cavity the pressure is smaller than  $p_\infty$  and equals the cavity pressure. From this follows an additional lift of order  $\sigma$  so that

$$c_L = 2 + \sigma$$

Then the pressure drag coefficient for a flat plate is

$$(c_D)_p = c_L \sigma$$

and the total drag coefficient is

$$c_D = (c_D)_p + c_f$$

where  $c_f$  is the frictional resistance coefficient of the pressure side of the plate. Further, the drag lift ratio is represented by

$$\frac{c_D}{c_L} = \frac{c_f}{c_L} + \sigma$$

With these relations for a fully cavitating plate, one is able to estimate the efficiency of a fully cavitating propeller. It follows from propeller theory that the efficiency is

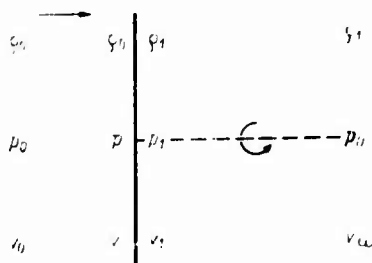


Fig. 1 - Flow model of a cavitating propeller

where  $\epsilon$  represents the losses which arise from the kinetic energy of the slipstream and  $\epsilon_d$  those from the drag of the sections. The first factor is for optimum propellers a known function of number of blades, advance coefficient, and loading coefficient. The second factor may be written

$$\frac{(1 - 2\epsilon_d)}{(1 + \frac{2}{3}\epsilon_d)}$$

where  $\epsilon_d$  is the effective mean of the drag, lift coefficients of the sections and  $\epsilon_d = \epsilon_d / \epsilon$ .

Comparison of the efficiency of two propellers, both designed for the same conditions, the one as a conventional propeller at the limit of onset of cavitation and the other one as a supercavitating propeller, amounts essentially to a comparison of  $\epsilon$ . For the propeller of an MTB (motor torpedo boat) of 43.5 knots the conventional design gave the following results:  $\epsilon_i = 0.84$ ,  $\epsilon = 0.080$ ,  $\epsilon_i = 0.444$ ,  $\epsilon = 0.837$ , and  $\epsilon = 0.703$ . Designing this propeller for equal conditions as a supercavitating propeller on a basis of Betz's theory, one obtains  $\epsilon = 0.125$  and  $\epsilon_i = 0.745$ . These latter figures depend somewhat on the choice of the lift coefficients and may be considered as an order of magnitude. This means then a loss of efficiency for the supercavitating design of about 12 percent. Since numerous other numerical results were in about the same range, one is led to conclude that a supercavitating propeller is, in general, connected with an appreciable loss of power input.

This conclusion, depends, of course, to a great deal on the accuracy of Betz's theory of fully cavitating hydrofoils. However, there was not much reason to consider this theory inadequate since tests by Walchner showed satisfactory agreement. Walchner conducted cavitation tests on series of both ogival (5) and modified ogival sections (6). The modified sections had a circular-arc suction surface and a flat pressure surface with rounded leading and trailing edges. With these modified sections the measurements have been recently repeated by Kermeen (7). His results for cavitating flow show poor agreement with those obtained by Walchner. There was in general more cavitation in Kermeen's tests at all cavitation numbers, so that the loss in lift in the latter tests is greater for the same cavitation number. The difference in forces amounts to a change in cavitation number of about 0.1. Because of these discrepancies between the experimental results, the approximations by Betz do not appear sufficient for a general application.

The same conclusion is reached by the work of Tulin and Wu. It is not the purpose of this paper to enter into these theories; only a few numerical results which are of interest for the propeller design will be given here. In Fig. 2 the pressure drag lift coefficient is shown as a function of the lift coefficient for both the flat plate and a circular-arc plate as follow from Wu's theory (8). The figure is restricted to the limit  $\sigma = 0$ . For this limit the result for the flat plate passes over into that from Raleigh's

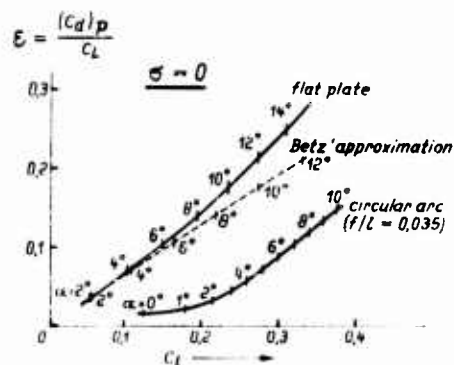


Fig. 2 - Pressure drag/lift coefficient as a function of the lift coefficient for both a flat plate and a circular-arc plate



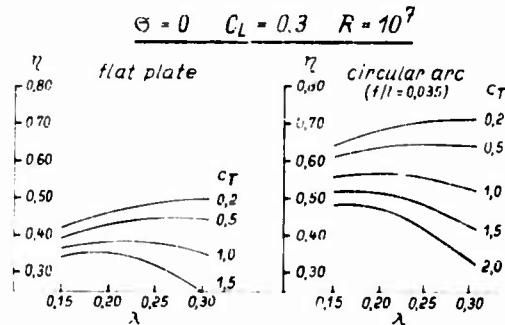


Fig. 3 - Effect of camber on propeller efficiency

theory of the oblique lamina. The figure shows clearly the considerable effect of the section camber on the drag, lift coefficient in fully cavitating flow. For a comparison, the result of Betz's approximations is included. It is seen that there is satisfactory agreement only for small angles of attack of a flat plate. This is to be expected, whereas the effect of camber does not follow from the approximation because of the inherent assumptions.

It is this latter effect, which has made it possible to successfully design a supercavitating propeller. Taking the same example of the

MTB propeller as before and calculating the efficiency for equal values of both local lift coefficient and local cavitation number, one obtains for fully cavitating circular-arc plates a mean effective drag, lift ratio  $= 0.055$  and correspondingly  $\eta = 0.87$ . As compared to the conventional propeller the supercavitating propeller designed from circular arc plates shows in this particular case a gain in efficiency of about 4 percent.

The effect of the camber of fully cavitating sections on the propeller efficiency is shown in a more general way on Fig. 3 (9). On the left side of the diagram, the efficiency of 3-bladed propellers is represented for flat plate sections, on the right side for circular sections as function of the advance coefficient and the thrust loading coefficient. To simplify, the limiting case  $\sigma = 0$  has been considered and also the lift coefficient has been assumed to equal 0.3. Similar diagrams have been calculated for different lift coefficients. Because of the first assumption, viz.,  $\sigma = 0$  the diagram gives the lower limit of the propeller efficiency which may be obtained under extreme conditions of cavitation. For cambered sections this limit is considerably greater than was formerly expected. As a consequence I think I am right in saying that the possibility is indicated for efficient propulsion of naval vessels at unlimited speed by means of a screw propeller.

Since these numerical results on the propeller efficiency depend on an experimental verification of the free streamline theories of fully cavitating sections, the papers by Parkin (10) and by Waid and Lindberg (11) are of great interest. In the first paper a flat plate and a circular-arc section are tested; in the second one a curved wedge-shaped section designed for full cavity operation by DTMB on the basis of Tulin's theory. In both of these investigations good agreement between the experimental and theoretical lift coefficients is found. The drag coefficients as measured in the latter paper, however, differ if  $\sigma = 0.2$  and  $\sigma = 0.5$ . Although the drag lift ratio and its trend are affected by the discrepancies, there is fairly satisfactory agreement for full cavity flow if the cavitation number is less than 0.2. This covers the range of cavitation numbers which is of interest for high-speed propellers. It should be mentioned that the discrepancies are not considered imperfections of the theoretical work but are attributed either to tunnel wall effect or to an incomplete evaluation of the theory.

The aforestated results for the efficiency of fully cavitating propellers, designed from proper low-drag sections, made it worth while to enter into the problem of

developing such propellers. When this decision was made, the method of propeller design on a basis of circulation theory was well advanced at DTMB. This method has been applied to fully cavitating propellers. Without going into details I only wish to mention that circulation theory has reliably worked also in this case. Many difficulties arose from the necessity to satisfy both hydrodynamic and strength conditions. Since most of the work to overcome these difficulties has been done after I had left DTMB, I hope that Mr. Tachmindji and Mr. Morgan are going to report in their paper on the further progress on this problem.

#### REFERENCES

1. Tulin, M., "Supercavitating Flow Past Foils and Struts," Symposium on Cavitation in Hydrodynamics, National Physical Laboratory, Teddington, England, 1955
2. Wu, T.Y., "A Free Streamline Theory for 2-Dimensional Fully Cavitated Hydrofoils," California Institute of Technology Report 21-17, 1955
3. Baein, A.N., "A Contribution to the Theory of the Ideal Cavitating Screw Propeller," Doklady Akad. Nauk SSSR 49:8 (1945)
4. Betz, A., "Effect of Cavitation on the Power Input of Ship Propellers," Proceedings of the Third International Congress for Applied Mechanics, Vol. 1, Stockholm, 1930
5. Walchner, O., "Measurements on Cavitating Profiles," Hydromechanische Probleme des Schiffsantriebes, Hamburg, 1932
6. Walchner, O., Report der Aerodynamischen Versuchsanstalt, Göttingen, 1934
7. Kermeen, R.W., "Water Tunnel Tests of NACA 4412 and Walchner Profile 7 Hydrofoils in Noncavitating and Cavitating Flow," California Institute of Technology Report 47-5, 1956
8. Wu, T.Y., and Perry, B., "Comparison of the Characteristics of a Hydrofoil under Cavitating and Noncavitating Operation," California Institute of Technology Report 47-4, 1955
9. Lerbs, H., and Alef, W., "The Limits of Efficiency of Fully Cavitated Propellers," Schiffstechnik, Vol. 4, 1957
10. Parkin, B.R., "Experiments on Circular Arc and Flat Plate Hydrofoils in Non-cavitating and Full Cavity Flow," California Institute of Technology Report 47-6, 1956
11. Waid, R.L., and Lindberg, Z.M., "Experimental and Theoretical Investigations of a Supercavitating Hydrofoil," California Institute of Technology Report 47-8, 1957

\* \* \* \* \*

#### EDITOR'S NOTE:

The Symposium discussion of Dr. Lerb's paper was deferred until the next paper on the same subject had been read. The joint discussion appears after the next paper

\* \* \* \* \*

# THE DESIGN AND ESTIMATED PERFORMANCE OF A SERIES OF SUPERCAVITATING PROPELLERS

A. J. Tachmindji and W. B. Morgan

*David Taylor Model Basin*

\* \* \* \* \*

This paper outlines the procedure which has been developed for the design of supercavitating propellers and the possible range of application in which such propellers can be used. This design method has been used to predict the performance characteristics of a series of supercavitating propellers and compared with specific experimental results.

\* \* \* \* \*

## INTRODUCTION

The tendency toward increasing speeds is continuously imposing design limitations on conventional propellers and is providing the impetus for new types of propulsion devices which operate satisfactorily at high speeds. A number of propulsion mechanisms (pumpjets, shrouded propellers) have been investigated with the purpose of delaying the inception of cavitation and its associated effects of erosion and performance breakdown. It becomes apparent, however, that for very high speeds (50 knots and above) suppression of cavitation becomes impossible and it is then necessary to investigate propellers which are designed to operate at low cavitation numbers.

Operation in this speed range results in the back or suction side of the blade sections being completely enclosed within a vapor cavity which originates at the leading edge of the blade and extends beyond the trailing edge. Propellers exhibiting this type of flow configuration are usually known as supercavitating propellers. It should be noted that supercavitating propellers operate completely submerged and are to be distinguished from conventional speedboat propellers which are only partially submerged.

It is the purpose of this paper to outline the procedure which has been developed for the design of supercavitating (SC) propellers and indicate the possible range of application in which such propellers can be used. Certain criteria, which have been derived from experimental information, indicate the operating conditions at which these propellers can be efficiently applied. Furthermore, owing to the somewhat lengthy design calculations and for the purposes of initial estimates it has been deemed desirable to investigate on a theoretical basis the performance characteristics of a series of supercavitating propellers. These results can then be compared with experimental results of specific propellers in order to indicate the accuracy and usefulness of this series.

# DESIGN CONSIDERATIONS

## Range of Application

The initial decision which has to be made is whether a conventional noncavitating or a supercavitating propeller is the most desirable for specific operating conditions. For conventional propellers it is desirable to have no cavitation on the blades, a condition which is impossible beyond a certain operating speed. In the case of SC propellers the vapor cavity which originates at the leading edge of the blade should collapse beyond the trailing edge in order to prevent erosion of the blades. Experimental results have indicated (1) that in order to have satisfactory supercavitating operation, the cavitation number\* of the blade section at 0.7 of the propeller radius, should be less than 0.045; and if the propeller operates at moderate speeds (35 to 50 knots), this requires a high rotational speed. The high rotational speed, however, will result in an inherently low pitch and a correspondingly low propeller efficiency.

Based on the foregoing considerations it has been possible to derive a diagram, shown in Fig. 1, which indicates the areas in which SC propellers become practical. This diagram has  $H/V_k^2$  (which is proportional to the propeller cavitation index) plotted versus the speed coefficient  $J$ , where

$$J = \frac{V_n}{nD} \quad (1)$$

and

$D$  = propeller diameter

$H$  = absolute pressure at the shaft centerline minus the cavity pressure (in feet of water)

$n$  = revolutions per unit time

$V_n$  = speed of advance

$V_k$  = speed of advance in knots.

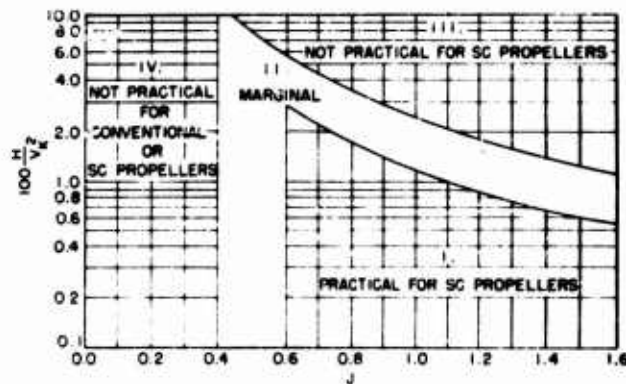


Fig. 1 - Chart of practical application of supercavitating propellers

\* See Eq. (29).

In this figure the marginal region (II) above a  $J$  of 0.6 is a region of operation in which partial cavitation will probably occur on both conventional and SC propellers. This same region below a  $J$  of 0.6 indicates an area in which the propeller efficiency will be low and should be avoided if at all possible.

Study of this diagram will indicate that the speed of advance at which supercavitating propellers become practical is relatively high. Further work has shown, however, that it is possible to decrease the speed of application by artificially increasing the cavity pressure, thus effectively decreasing the section cavitation number. This is achieved by providing an air passage from the back of the blade through which air can be sucked or injected. Such propellers are presently known as ventilated or force-ventilated propellers. For a certain cavitation index, however, it is immaterial whether the cavity is a vapor or an air-cavity and the design considerations which are outlined in this paper are expected to hold equally well in the cases of ventilated propellers. The range of application for these propellers is then only limited by the resulting pressure which can be obtained in the cavity and the operating depth of the propeller.

#### Choice of Design Parameters

The design of a SC propeller for a given set of design parameters leads to a rather complex investigation and usually results from a compromise between the hydrodynamic considerations, the acceptable stress limits and the practical limitations on propeller diameter.

The first problem considered in connection with the design of the propeller is determining the optimum diameter-rpm relationship. An estimate of this relationship can be obtained from the performance curves which are presented in this paper.

A problem of equal importance with the diameter and rpm is the selection of the number of blades. The choice should be made primarily on the basis of blade stress and vibration. If possible, the number of blades should be chosen so that the blade frequency forces do not cause resonance with any natural frequencies of the ship. As far as stress is concerned (see Appendix A) an individual investigation may be necessary in each case. Decreasing the number of blades will result in an increase in loading, section lift, and hence section thickness. The resultant stress may be either larger or smaller depending on whether the increase in loading or thickness predominate.

For SC propellers the hub diameter may be used, within certain limits, to effectively reduce the blade stress. An increase in hub size will result in an increase in blade loading, but a decrease in bending moment. Since the thickness is a function of blade loading, this increase in loading will result in an increase in thickness and a decrease, up to a certain limit, in stress. Therefore, the changes in both moment and loading will result in a decrease in stress. However, the hub size should not be increased to the point where it materially affects the propeller efficiency.

Other design parameters such as blade chord and section angle of attack are also governed by both the hydrodynamic performance and the structural characteristics of the propeller and must be investigated for a best compromise.

#### Sections

A critical feature of the design is governed by the choice of sections which are selected to operate in the supercavitating range. The work done by Tulin (2,3) in

determining the characteristics of an optimum section within a series of similar shapes, has been the foundation for predicting the characteristics of SC propellers. The results of this work coupled with the experimental investigations of the shapes of these sections (4,5) have provided information extremely useful to the designer.

The work of a number of investigators such as Wu (6), Hug (7), Cohen (8), Johnson (9,10), and others have also been used in the prediction of section characteristics. Their results, however, are essentially similar with Tulin's results within the limits of the basic assumptions. This two-dimensional work has furnished design criteria regarding angle of attack, optimum lift coefficient, and expected drag/lift ratios which are extensively used in the prediction of SC propeller performance. These design considerations are outlined in the parts of this paper describing the design procedure.

## DESIGN THEORY

In principle the operation of the SC propeller differs from a noncavitating propeller only in the type of sections used. Hence, the circulation, or lifting-line, theory applies equally well to these propellers.

Two general methods of approach can be considered. The first, developed by Goldstein (11) and extended by Tachmindji (12), deals with the optimum lightly-loaded propeller with a finite number of blades, and the second, developed by Lerbs (13), determines the circulation distribution for moderately-loaded propellers in which the condition of normality is not necessarily assumed. Comparison of the two methods has shown (14) that for the range and load distributions normally encountered in propeller designs, the differences between the two are small. Design calculations in the case of SC propellers have been made using both methods. These calculations have indicated that the circulation distribution factors and the induction factors give essentially the same result.

Based on these two basic approaches, a number of calculations have been made (15-18) which give information directly usable by the designer. From the theory of the optimum propeller, the ideal efficiency ( $\eta_i$ ) has been computed (19,20) and can be used in the case of nonoptimum propellers as a first estimate for the hydrodynamic pitch angle ( $\beta$ ).

The foregoing discussion on propeller theory has been restricted to a blade which has been replaced by a lifting line operating in a nonviscous fluid. In applying this theory to propeller design, the lifting-line considerations have to be expanded to include lifting surface and viscous effects. Ludwig and Ginzel (21) have examined the curvature of the flow at the midpoint of each section and obtained corrections to the section camber. Lerbs (22) has determined an additional correction in the form of an angle of attack due to change in curvature over the section chord.

The viscous corrections for supercavitating sections and their effect on the ideal efficiency have been derived by Morgan (23).

## DESIGN PROCEDURE

Once the propeller diameter, rpm, and hub size have been determined, the propeller can then be calculated. The design can be made either on the basis of thrust or power. Designing on the basis of thrust may be preferable since the variation of thrust between viscous and nonviscous flow is not as great as in the case of power

and the speed-resistance relationship is normally more accurately known. The following nondimensional coefficients are computed:

$$C_T = \frac{V_a}{\pi n^2 D^4} \quad (2)$$

and

$$C_P = \frac{T}{\rho D^2 V_a^2} \quad (3)$$

or

$$C_P = \frac{2 C_T}{\rho D^2 V_a^2} = \frac{550 \text{ SHP}}{\rho D^2 V_a^4} \quad (4)$$

where

$D$  = propeller diameter

$n$  = revolutions per unit time

$T$  = torque

$\text{SHP}$  = shaft horsepower

$V_a$  = thrust

$V_a = (1 - w_a)V$  = speed of advance of the propeller

$V$  = ship speed

$w_a$  = effective wake fraction

$\rho$  = mass density of fluid.

Since the propeller is calculated on the basis of a nonviscous fluid, the viscous thrust or power coefficient must be modified to their nonviscous values. An approximation for the nonviscous coefficients can be made by assuming that the hydrodynamic pitch angle ( $\theta$ ) and the drag/lift ratio ( $\lambda$ ) at 0.7 radius are average values for the propeller, then

$$C_{T_1} = \frac{C_T}{1 - 2(\theta/\lambda)_{0.7}} = (1.02 \text{ to } 1.08)C_T \quad (5)$$

$$C_{P_1} = \frac{C_P}{1 - \frac{2}{3}(\theta/\lambda)_{0.7}} = (0.85 \text{ to } 0.98)C_P \quad (6)$$

where

$$(\theta/\lambda)_{0.7} = \frac{0.7}{1} \left( \frac{1}{\lambda} \right)_{0.7} = \frac{0.7}{1} \left( \frac{1}{\lambda} \right)_{0.7}$$

0.1 is a first estimate.

With Eq. (2) and  $C_{T_1}$  or  $C_{P_1}$  from Eq. (5) or Eq. (6), the ideal efficiency  $\eta_i$  of an optimum propeller can be obtained from Refs. 19 and 20. Using this value of ideal

efficiency the first approximation to the hydrodynamic pitch angle is computed using the relation

$$\tan \phi_i = \frac{\lambda}{x} \frac{1}{\eta_i} = \frac{\tan \phi_i}{\eta_i} \frac{1}{x} \quad (7)$$

where

$x$  = nondimensional radius

$\phi_i$  =  $\arctan(\lambda/x)$  = advance angle

$\eta_i = \lambda/\eta_i$  (for a free-running optimum propeller).

For an optimum free-running propeller, the ideal efficiency  $\eta_i$  is constant along the blade. If the propeller is not optimum, then  $\eta_i$  varies along the blade and the assumption is made that the ideal efficiency at 0.7 radius is equal to that obtained from the curves.

In order to describe each propeller section, it is necessary to know the radial distribution of hydrodynamic pitch angle  $\phi_i$ , circulation  $G$ , coefficient of lift  $C_L$ , and thrust coefficient  $dC_T/dx$  or power coefficient  $dC_P/dx$ . These values are derived from the following equations:

$$G = \frac{2x}{Z} \frac{u_t}{2V_n} \quad (8)$$

$$\frac{C_L}{b} = \frac{2G \cos \phi_i}{\left( \frac{1}{\tan \phi_i} - \frac{u_t}{2V_n} \right)} \quad (9)$$

$$\frac{dC_T}{dx} = 4ZG \left( \frac{1}{\tan \phi_i} - \frac{u_t}{2V_n} \right) \quad (10)$$

$$\frac{dC_P}{dx} = 4Z \frac{G}{\tan \phi_i} \left( 1 + \frac{u_n}{2V_n} \right) \quad (11)$$

where

$$\frac{u_t}{2V_n} = \left( \frac{\tan \phi_i}{\tan \phi_i - 1} \right) \left( \frac{\tan \phi_i}{\tan^2 \phi_i - 1} \right) \quad \text{tangential induced velocity}$$

$$\frac{u_n}{2V_n} = \left( \frac{1}{\tan \phi_i} \right) \left( \frac{u_t}{2V_n} \right) \quad \text{axial induced velocity}$$

$b$  = section chord

$Z$  = number of blades

$G$  = circulation distribution factor from Ref. 16 or Goldstein factor from Ref. 15.



It should be noted that the integral of  $dC_{T_i}/dx$  or  $dC_{P_i}/dx$  along the radius should equal the design values of  $C_{T_i}$  or  $C_{P_i}$ :

$$C_{T_i} = 4Z \int_{x_h}^1 \left( \frac{1}{\tan \alpha} - \frac{u_t}{2V_n} \right) dx \quad (12)$$

and

$$C_{P_i} = 4Z \int_{x_h}^1 \frac{G}{\tan \alpha} \left( 1 - \frac{u_n}{2V_n} \right) dx \quad (13)$$

where  $x_h$  is the nondimensional hub radius.

If the propeller is an optimum propeller the difference between  $C_{T_i}$  from Eqs. (5) and (12) and between  $C_{P_i}$  from Eqs. (6) and (13) will only be within the accuracy with which  $\alpha$  can be read from the chart. For a nonoptimum propeller the above equations are equally valid, but an iteration procedure is necessary in order to determine the hydrodynamic pitch angle.

The foregoing discussion has been concerned with free-running propellers. For wake-adapted propellers the fact that the wake varies with radius must be considered. Therefore, for the design of these propellers the different coefficients are nondimensionalized on the basis of ship speed instead of speed of advance (14).

Once the desired  $C_{T_i}$  or  $C_{P_i}$  is obtained, the propeller section shape, section length, and angle of attack can be selected. For SC sections the camberline is the pressure side of the foil and the thickness is applied between the camberline and the free streamline. The maximum ordinate of the pressure side of Tulin's section (2) can be written as follows:

$$(y^+)_{max} = 0.5 \sin \alpha + (0.1128 C_L - 0.11817 \alpha) \cos \alpha \quad (14)$$

where

$y^+$  = face ordinate measured perpendicularly to the nose-tail line

$C_L$  = design lift coefficient

$\alpha$  =  $\alpha_i + 57.3$  = geometric angles of attack in radians

$\alpha_i$  = design angle of attack in degrees

$\alpha_i$  = ideal angle of attack in degrees

$c$  = chord length.

For small  $\alpha$ ,  $\sin \alpha \approx \alpha$  and  $\cos \alpha \approx 1$  and Eq. (14) reduces to

$$(y^+)_{max} = 0.5 + 0.1128 C_L - 0.01182 \alpha + 0.1553 C_L \alpha - 0.00426 \alpha^2 \quad (15)$$

The distribution of the face ordinates along the chord is given in Table 1.

The thickness of the section, measured normal to the nose-tail line, is given by

Table 1

Distribution of Face Ordinates and Coefficients for Calculating Thickness Along the Chord

x	y y <sub>max</sub>	F'	N'
0	0	0	0
0.0075	0.01888	-0.001326	0.254
0.0125	0.03244	-0.002574	0.1870
0.05	0.14189	-0.016816	0.005704
0.10	0.29150	-0.039520	0.010074
0.20	0.56636	-0.078940	0.017349
0.30	0.78458	-0.097600	0.022222
0.40	0.93187	-0.092870	0.024647
0.50	1.0	-0.071780	0.025710
0.60	0.98340	-0.037750	0.025853
0.70	0.87797	0.005940	0.025605
0.80	0.68055	0.056880	0.024660
0.90	0.38860	0.112090	0.023047
0.95	0.20650	0.139620	0.022048
1.0	0	0.166950	0.020937

$$t = F' C_L + N' \quad (16)$$

where the coefficients  $F'$  and  $N'$  are also given in Table 1. This equation gives a section slightly thicker than the theoretical cavity shape as shown in Fig. 2. Experimental results (1) have shown that this additional thickness is necessary in order to avoid leading edge vibration and does not affect its performance.

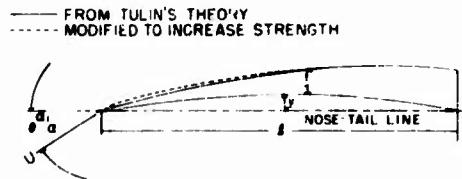


Fig. 2 - Comparison of theoretical and TMB modified thickness distribution of Tulin's SC section

One difficulty encountered in the use of cambered SC sections is pressure face cavitation. If the section is operated at too low an angle of attack for a given camber, face cavitation will occur and poor performance and possibly vibration will result. In addition, it has been shown (1,24) that a certain angle of attack is necessary for the section to have adequate strength. By analyzing a

number of experimental results, and noting that theoretically the design angle should be as small as possible in order to obtain minimum drag, the following relationships between design angle of attack  $\alpha$  and the coefficient of lift  $C_L$  has resulted:

$$\alpha = 36.5 C_L \quad \text{for } 0 < C_L < 0.0548 \quad (17a)$$

$$\alpha = 5.7 \quad \text{for } 0.0548 < C_L < 0.2 \quad (17b)$$

$$\alpha = 19 C_L \quad \text{for } 0.2 < C_L < 0.3 \quad (17c)$$

It should be noted that Eq. (17a) results in a flat-face section.

Using the above relationships between  $C_L$  and  $\alpha$ , calculations can be made for the drag/lift ratio of Tulin's section with part of the lift taken by angle of attack. These calculations have already been made (23) and the results indicate that an optimum lift coefficient for this section is approximately 0.16. This value can then be used in Eq. (9) for estimating the section chord at 0.7 radius. The blade outline can then be chosen similar to the one given in Table 2.

It is then necessary to determine the stress distribution in the propeller. (A simplified method is given in Appendix I.) In many cases it may be found that the blade outline should be adjusted until acceptable nominal stresses are obtained. This may also be accomplished by an increase in angle of attack towards the root.

Once the chord, coefficient of lift and angle of attack have been selected the face and thickness can be calculated from Eqs. (15) and (16). The face ordinates, however, must be corrected for the lifting surface effects (14) and are given by

$$(y')(\text{corrected}) = k_1 k_2 (y') \quad (18)$$

where  $k_1$  and  $k_2$  are obtained from Fig. 3 and

$$\frac{A_F}{A_0} = \frac{2Z}{\pi} \int_{x_h}^1 (1-D) dx \quad \text{expanded area ratio.}$$

The next step is the calculation of the pitch correction. There are three corrections to be considered; friction correction, effect of finite cavitation number, and correction from lifting surface effect (22). From the data available, it appears that the friction correction is small for these propellers and can therefore be neglected. The effect of finite cavitation number is combined with both the design and the ideal angle of attack into one additional angle of attack ( $\alpha_1$ ) and is given by

$$\alpha_1 = 57.3 K_c + 57.3 K_c (0.0849 C_L + 0.01512 \alpha) \text{ deg} \quad (19)$$

where  $K_c$  is obtained from Fig. (4) and the cavitation number ( $\sigma$ ) is computed for 0.7 radius, as follows:

$$\sigma_{0.7} = \frac{2gH(\sin^2 \alpha)_{0.7}}{V_n^2 \cos^2 (\alpha_1 + \alpha)_{0.7}} = \frac{2gHJ^2}{V_n^2 (J^2 + 4.84)} \quad (20)$$

where  $g$  = acceleration of gravity.

The correction for the lifting surface effect results from both free and bound vortices and again occurs as an additional angle of attack ( $\alpha_2$ ) given by

$$\alpha_2 = \alpha_1 + \alpha_2 = \alpha_1 \left[ 1 + \cos^2 \left( \frac{2}{h} - 1 \right) \right] \quad (21)$$

Table 2

Radial Distribution of Section Chord

x	r = 0.7
0.20	1.088
0.30	1.088
0.40	1.088
0.50	1.085
0.60	1.062
0.70	1.0
0.80	0.871
0.90	0.655
0.95	0.475
1.00	0

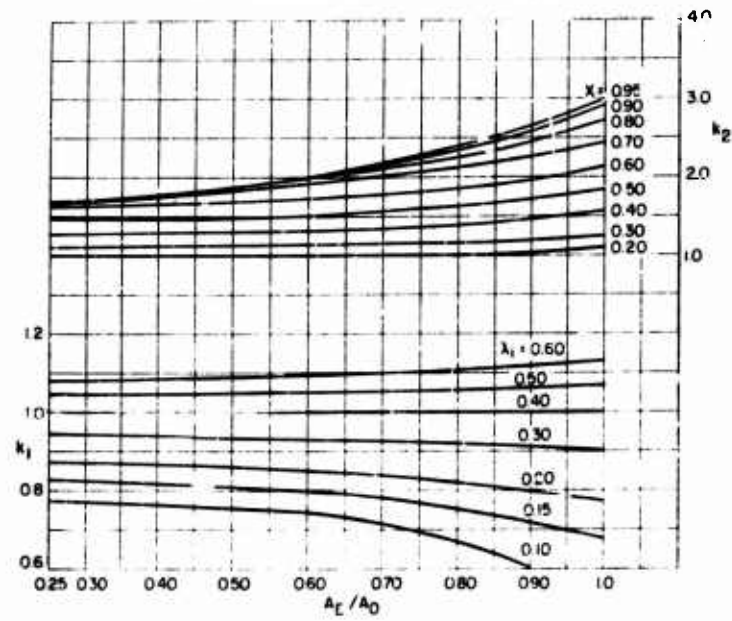


Fig. 3 Camber correction coefficients

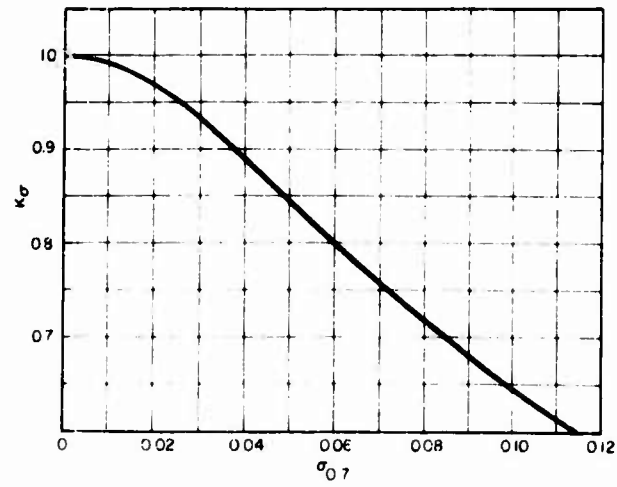


Fig. 4 - Correction to  $k_1$  for finite cavitation number

where  $h$  is from Fig. 5 and

$$h = 57.3 \left( \frac{\sin \beta_i}{2} \right) \sum_Z \left[ \frac{1}{D} \sin \alpha_i + 0.7 \cos \beta_i \cos \alpha_i + \int_{x_h}^1 \frac{G}{(F/R)^3} dx \right]$$

in which

$$(F/R)^3 = \left[ x^2 + \left( \frac{1}{D} \right)^2 + 0.49 + 2 \left( \frac{1}{D} \cos \alpha_i \cos \beta_i + 0.7 \sin \alpha_i \right) x \right]^{3/2}$$

$$G = \frac{1}{2} + \frac{2}{Z} (m-1) \quad \text{for } m = 1, 2, 3 \dots Z.$$

It should be noted that in Eq. (21) the values of  $\beta_i$ ,  $\alpha_i$ , and  $\beta_1$  are taken at the 0.7 radius and considered constant. This correction is then made at this radius and the same percentage change applied to the other radii.

$$1 + \frac{\Delta P/D}{P/D} = \frac{\tan(\beta_i + \beta_1 + \beta_2)_{0.7}}{\tan(\beta_i + \beta_1)_{0.7}}. \quad (22)$$

The final pitch is then given as

$$P/D = x \left( 1 + \frac{\Delta P/D}{P/D} \right) \tan(\beta_i + \beta_1). \quad (23)$$

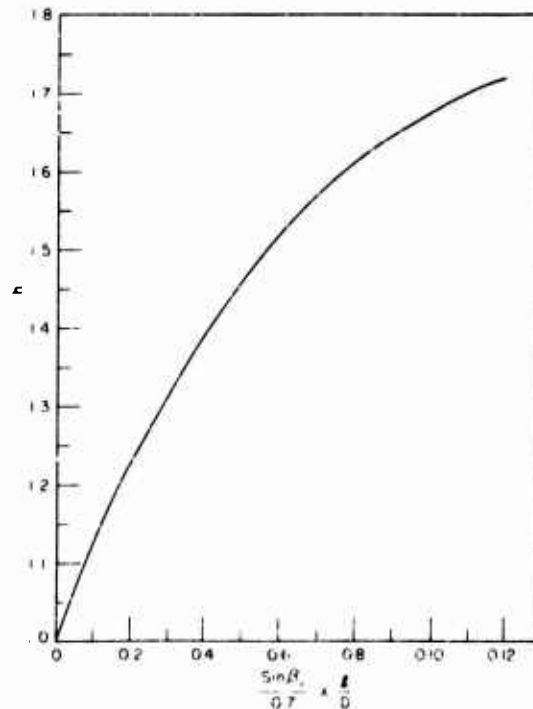


Fig. 5 - Pitch correction coefficient ( $h$ ) for  $x = 0.7$

With the calculation of the pitch, the design of a propeller is complete except for checking the ratio of  $C_T$  to  $C_P$ , or the ratio of  $C_T$  to  $C_{P_1}$  and determining the propeller efficiency. In order to make these calculations it is necessary to know the values of the drag/lift ratio along the radius. These values can be obtained from theoretical (23) or experimental (4) two-dimensional results but must be adjusted for application to propellers (1). Using the foregoing information the following equations for have been found to give satisfactory results:

$$0.795 C_L = \frac{0.569}{C_L \left( \log \frac{U}{V} \right)^{2.58}} \quad \text{for } 0 < C_L < 0.0548 \quad (24a)$$

$$(2.14 C_L + 1.13) \left[ \frac{(0.4 C_L + 0.0328)^2}{1.5708 C_L} + \frac{0.455}{C_L \left( \log \frac{U}{V} \right)^{2.58}} \right] \quad \text{for } 0.0548 < C_L < 0.2 \quad (24b)$$

$$(2.14 C_L + 1.13) \left[ 0.2025 C_L + \frac{0.455}{C_L \left( \log \frac{U}{V} \right)^{2.58}} \right] \quad \text{for } 0.2 < C_L \quad (24c)$$

where

$$U = V_a \frac{\cos(\alpha_i - \beta)}{\sin \beta} \quad \text{section inflow velocity}$$

$$\nu = \text{kinematic viscosity of the fluid.}$$

It is now possible to evaluate the thrust and power coefficient for viscous flow. This check, made at 0.7 radius, gives good results but can be made more accurately by taking into account the drag of each section. The following equations give the viscous thrust and power coefficients as a function of the radius:

$$C_T = \int_{x_h}^1 (1 - \tan \alpha_i) \frac{dC_{T_1}}{dx} dx = \int_{x_h}^1 \frac{\tan \alpha_i}{\tan \alpha_i + 1} (1 - \tan \alpha_i) \frac{dC_{P_1}}{dx} dx \quad (25)$$

and

$$C_P = \int_{x_h}^1 \left( 1 + \tan \alpha_i \right) \frac{dC_{P_1}}{dx} dx = \int_{x_h}^1 \frac{(\tan \alpha_i + 1)}{\tan \alpha_i} \frac{dC_{T_1}}{dx} dx \quad (26)$$

$C_T$  or  $C_P$  calculated from the above equations should compare closely with the design values. Also, by using Eq. (25) or Eq. (26) the power or thrust absorbed by the propeller can be calculated and the propeller efficiency is given by

$$\eta = \frac{C_T}{C_P} \quad (27)$$

## SC PROPELLER SERIES

Propeller series results are usually determined by testing a number of systematic designs and determining their characteristics. In the case of SC propellers, however, this procedure can become extremely costly and time consuming, since all propellers have to be tested over a range of cavitation numbers as well as speed coefficients. With the availability of high-speed computers such characteristics can now be predicted by means of theoretical computations, thus substantially reducing

the necessary effort required. The strength or weakness of such a method is of course dependent on the propeller theory on which it is based and the accuracy of its predictions. Calculations of this character should, therefore, be confirmed by means of experimental results in the case of specific propellers, and only then can their accuracy be completely determined. However, if the absolute value of the results is not exactly correct, such a series does provide a means of rapidly determining the relative performance gain or loss which can be obtained by a variation of parameters. Furthermore, such a theoretical series is not intended to replace the design of individual propellers, but can serve as a guide in determining the design conditions. At the present time, it is contemplated that after such conditions are determined the individual design should still be performed.

This series has been derived (25) by designing thirty propellers to cover a range of  $\sigma$  from 0.1 to 0.5 and  $C_T$  from 0.015 to 4.0 at a cavitation number  $\sigma$  of zero. Each propeller has three blades, an expanded area ratio ( $A_E/A_O$ ) of 0.5, a nondimensional hub radius of 0.2 and used Tulin's sections with the relationship between  $C_L$  and  $\sigma$  as given by Eq. (17). The Reynolds number, used in calculating the section friction drag, varied between  $9.5 \times 10^6$  and  $5.7 \times 10^7$ . The results of the calculations, at  $\sigma = 0$ , are plotted in Figs. 6 and 7 as the square root of the thrust coefficient and the square root of the power coefficient versus the speed coefficient  $J$  for various pitch ratios. On these plots are included contours of efficiency and an optimum efficiency line for a given  $C_T$  or  $C_P$ .

Once the basic design is completed for zero cavitation number the calculations are extended to include finite cavitation numbers ( $\sigma_{0.7}$ ) of the section at 0.7 radius. These calculations result in a change in pitch and are plotted in Figs. 8 and 9 as a function of  $C_T$ ,  $J$ , and  $\sigma_{0.7}$ . The final pitch is, then, given by

$$P/D = (P/D)_{\sigma=0} + (P/D)C_{\sigma} \quad (28)$$

where

$(P/D)_{\sigma=0}$  = pitch ratio from Fig. 6 or 7

$(P/D)$  = pitch correction coefficient from Fig. 8

$C_{\sigma}$  = pitch correction coefficient from Fig. 9

$\sigma_{0.7}$  = cavitation number at 0.7 radius from Eq. (20).

The maximum face ordinate at the 0.7 radius is given in Fig. 10 as a function of  $C_T$  and  $J$ . Using this ordinate and the distribution of face ordinates along the chord obtained from Table 1 it is possible to calculate the ordinates of this section. The radial distribution of chord can be obtained from Table 2, where  $r/D$  at 0.7 radius is 0.351, and the blade thickness fraction (BTF) for this propeller series can be taken from Fig. 11. Additional information for other radii, similar to that given in Fig. 10, is also given in Ref. 25.

A simplified method for calculating the stress has been derived for this propeller series, and the maximum stress (compressive) in psi at the blade root can be estimated by

$$S_c = \frac{0.65 \cdot C_T V_A^2}{144 (BTF)^2} + 0.009 \frac{C_T V_A^2}{(BTF)^2} \quad (29)$$

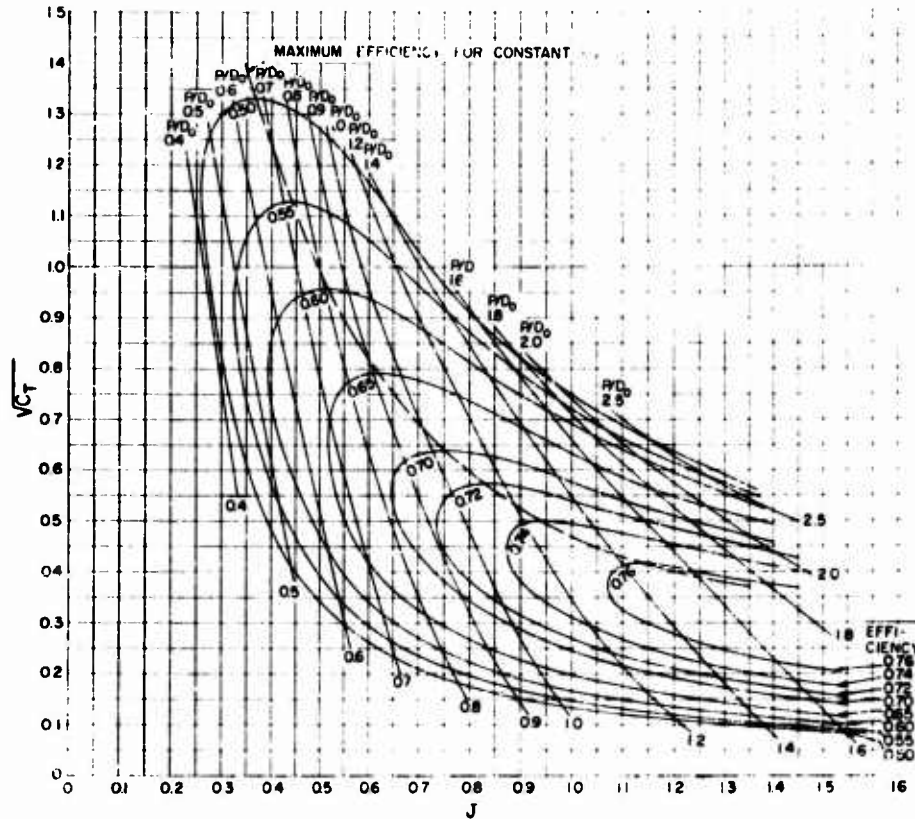


Fig. 6 -  $C_T$  -  $J$  diagram for TMB SC 3-bladed propeller series

Figures 6 and 7 can also be used to calculate the optimum rpm for a given diameter and the optimum diameter for a given rpm. As an example, the optimum rpm for the following design conditions can be obtained as follows:

$$T = 25,000 \text{ lbs}$$

$$V_a = 101.28 \text{ fps}$$

$$D = 3 \text{ ft.}$$

From Eq. (3)

$$C_T = \frac{T}{\rho D^4 V_a^2} = 0.35$$

and

$$C_T = 0.591.$$



# Design and Performance of Supercavitating Propellers

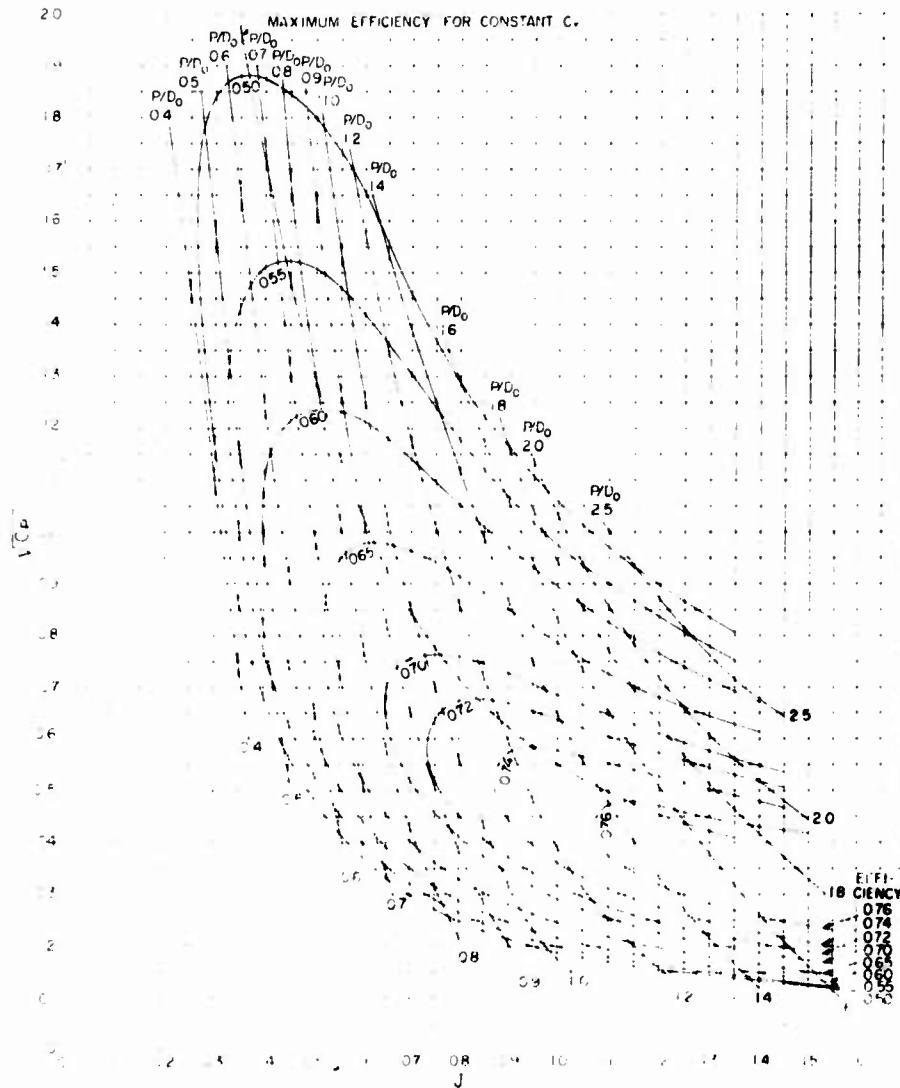


Fig. 6.  $C_p$  -  $J$  diagram for FMB SC 3 loaded propeller series

From Fig. 6, the optimum  $J$  for this  $C_p$  is 0.815; therefore, the optimum rpm is given by

$$n = \frac{60V}{\pi D} = 2485$$

The calculation of optimum diameter for a given rpm, speed, thrust, or power can be performed by assuming a diameter and calculating  $J$  and  $C_p$  or  $C_T$ . A straight line is then drawn through this point and the origin, and the maximum

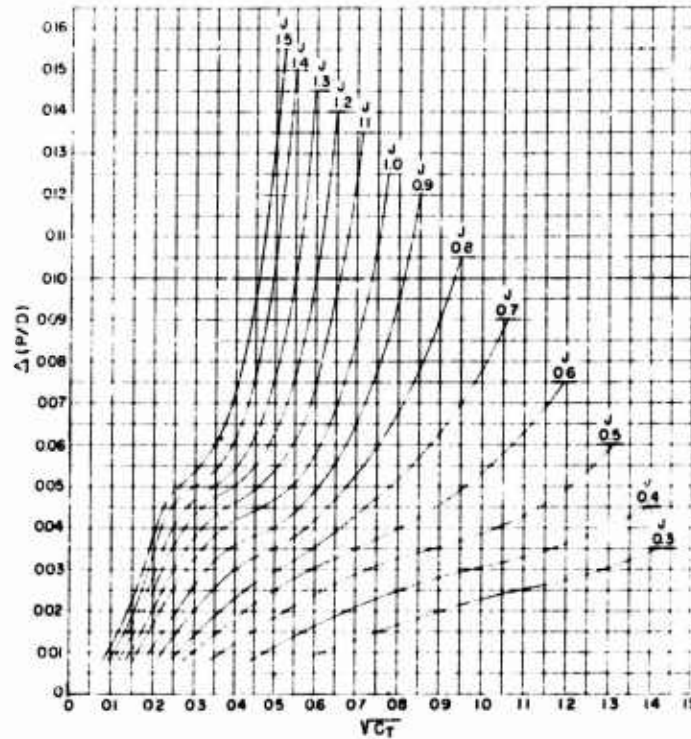


Fig 8 - Pitch correction coefficient  $\Delta(P/D)$  for finite cavitation numbers for TMB 3-bladed SC propeller series

efficiency along this line represents the point at which the diameter is an optimum. An example, for the design conditions

$$T = 18,000 \text{ lbs}$$

$$V_n = 101.28 \text{ fps}$$

$$n = 36 \text{ rps}$$

is as follows. Assume that  $D = 3$  feet. From Eq. (3)

$$C_T = \frac{T}{\rho n^2 D^4} = 0.25, \quad C_T = 0.5, \quad \text{and} \quad J = \frac{V_n}{nD} = 0.94.$$

This point is then plotted on Fig. 6 and a line is drawn through this point and the origin. The maximum efficiency along this line occurs at a  $J$  of 0.9, and the optimum diameter is

$$D = \frac{V_n}{Jn} = 3.13 \text{ feet.}$$

# Design and Performance of Supercavitating Propellers

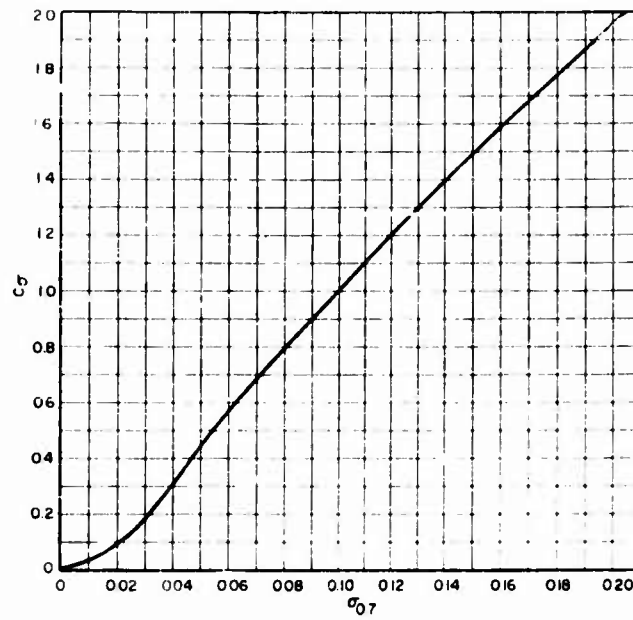


Fig. 9 - Pitch correction coefficient  $C$  for finite cavitation number for TMB 3-bladed SC propeller series

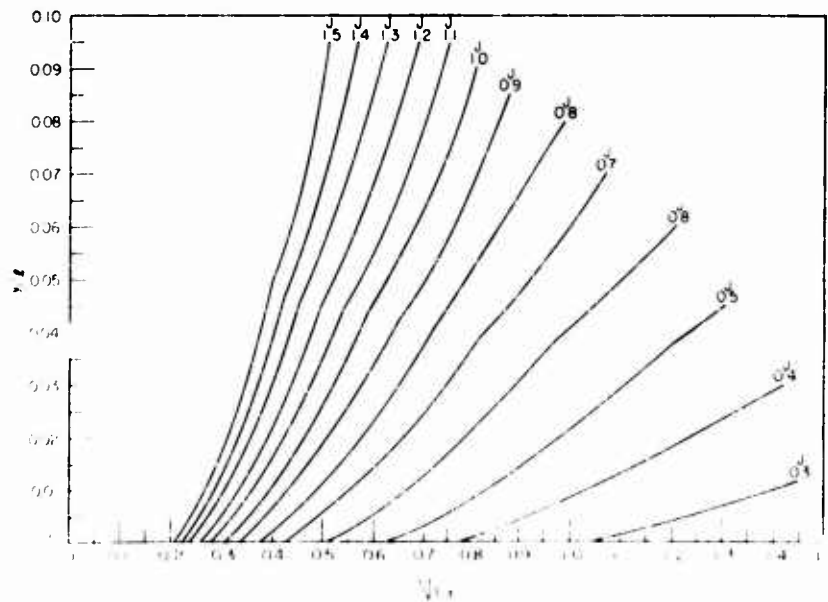


Fig. 10 - Maximum face ordinate at 0.7 radius for TMB 3-bladed SC propeller series

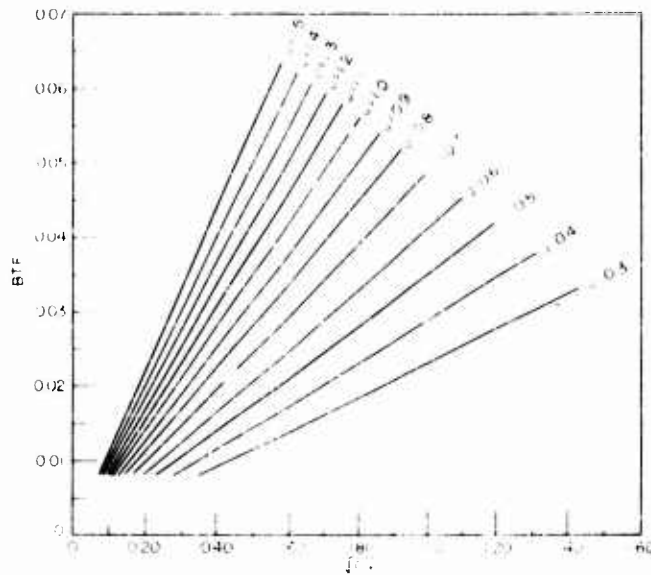


Fig. 11 - Blade thickness fraction for TMB 3-bladed SC propeller series

## EXPERIMENTAL RESULTS

A number of tests have been conducted on SC propellers that indicate the adequacy of the design method and practicability of using SC sections on propellers (1). Figure 12 gives the performance characteristics for a 3-bladed propeller designed for 50 knots, 3500 pounds thrust, and 3000 rpm with a diameter of 18 inches. Using nondimensional coefficients these conditions result in a thrust coefficient  $K_T$  of 0.140, speed coefficient  $J$  of 1.125, and cavitation number  $\sigma_0$  of 0.064. The physical characteristics of this propeller are given in Fig. 13.

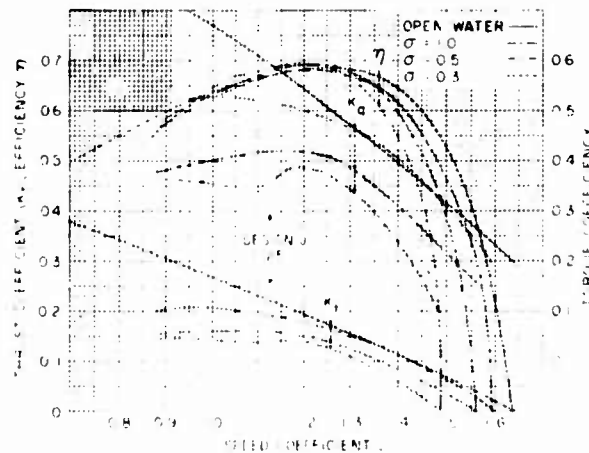


Fig. 12 - Composite plot of tests on propeller 3500

PROP NO.	DA IN	PROP IN	PROP IN	NUMBER OF BLADES	EXP BLADE AREA	EXP AREA RATIO	EXP WGT RATIO	PROJ AREA	PROJ AREA RATIO	PROJ THICKNESS FRACTION	RAKE ANGLE	ROTATION
1000	0.000	27.600	1.585	3	33.070	444	310	64.393	332	VAR	NONE	RH

PITCH CURVE - INCHES

28.116	
28.026	
27.926	
27.756	
27.601	
27.522	
27.504	
27.522	
27.558	
27.576	

EXPANDED OUTLINE

T.E. THICKNESS

MAX FACE CAMBER AND THE THICKNESS AT REF LINE

3509-RH  
3 BLADES

3680

4200

4500

3125

3125

From Fig. 12 it can be seen that this propeller gives very close to the design thrust at the design J and also develops an efficiency of approximately 68.5 percent. This propeller has nearly the same characteristics as a propeller obtained from the series previously discussed. From this series for the above design conditions,  $C_T = 0.278$  and  $J = 1.125$ , the propeller would have a  $P/D$  of 1.57 and  $\eta$  of 70 percent. It will be noted that these values are in satisfactory agreement with the experimental values.

An interesting characteristic of propellers using SC sections is shown in Fig. 14. This figure is a cross plot from Fig. 12 showing the relationship of thrust coefficient  $K_T$ , torque coefficient  $K_Q$ , and efficiency to the cavitation number at design  $J$ . This shows that while cavitation has great effect upon the thrust and torque, it has little effect upon efficiency. The fact that there is a decrease of thrust with decreasing cavitation number is not important as long as the efficiency remains constant and it is possible to meet the design conditions.

Confirmation of the validity of the charts by means of experimental results has also been performed for other propellers. These propellers, however, were 2-bladed and a correction regarding the effect of the number of blades must be introduced. Although such comparisons are not as direct as that performed above, they have indicated agreement between the experimental and predicted results to better than 3 percent.

The feasibility of supercavitating propellers in the case of high-speed application appears quite promising, particularly where they can be used to the full benefit of

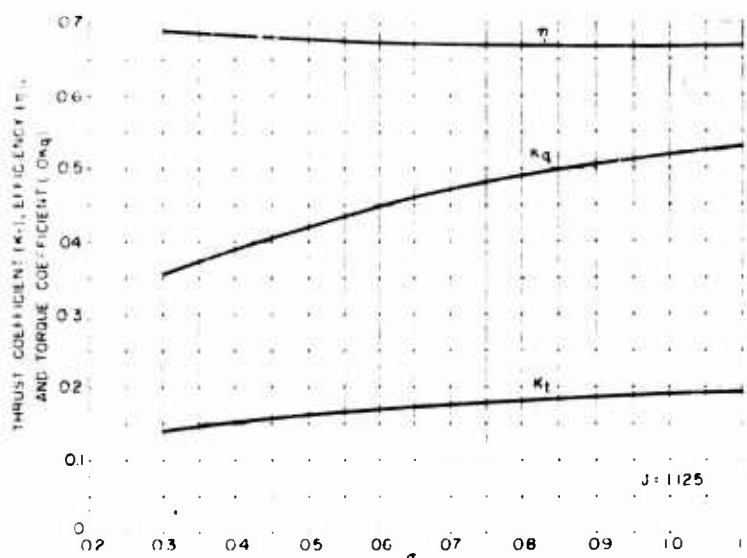


Fig. 14 - Plot of  $K_t$ ,  $K_q$ , and  $\eta$  versus  $\sigma$  for propeller 3509

their hydrodynamic performance. Their range of application may also be extended to lower speeds by the use of ventilated sections.

The design method which has been presented in this paper appears to give results which are verified by experimental confirmation. Improvements in this method, however, can be anticipated as more designs are accomplished and test results become available. The characteristics for the SC propeller series must also be confirmed by means of experimental results for specific propellers and only then can their accuracy be completely determined. It is felt, however, that the series work which has been accomplished to date will provide a method of assessing the effectiveness of the various design parameters. Furthermore, it can certainly be used as an impetus for the design of SC propellers which will exceed these performance characteristics.

#### ACKNOWLEDGMENTS

The authors wish to thank Captain E. A. Wright, Director of the David Taylor Model Basin, for permission to publish this paper. The assistance of the many members of the Propeller Branch, especially Mr. E. B. Caster, is also greatly appreciated.

#### NOTATION

- $A_t/A_o$  expanded blade area ratio  
 B/F blade thickness fraction

# Design and Performance of Supercavitating Propellers

- $C_L$  section lift coefficient  $\left( \frac{L}{\frac{1}{2} \rho V_a^2} \right)$
- $C_P$  power coefficient  $\left( \frac{2 C_h}{\pi \rho V_a^3} \right)$
- $C_{P_1}$  nonviscous power coefficient
- $C_T$  thrust coefficient  $\left( \frac{T}{\rho V_a^2} \right)$
- $C_{T_1}$  nonviscous thrust coefficient
- $C$  pitch correction coefficient
- $D$  propeller diameter
- $F'$  coefficient for determining section thickness
- $\Gamma$  nondimensional circulation per blade
- $g$  acceleration of gravity
- $H$  absolute pressure at the shaft centerline minus the cavity pressure (in feet of water)
- $h$  pitch correction coefficient
- $I_x, I_y$  blade-section-area moments of inertia
- $J$  speed coefficient  $(V_a / nb)$
- $K_q$  torque coefficient  $(Q / n^2 b^5)$
- $K_t$  thrust coefficient  $(T / n^2 b^4)$
- $k$  correction factor for finite cavitation number
- $k_1, k_2$  camber correction coefficients
- blade-section chord
- $M_t, M_{t_1}$  bending moments on blade section
- $M_{t_1}, M_{t_2}$  bending moments on blade section
- $N'$  coefficient for determining section thickness
- $n$  revolutions per unit time
- $p/b$  pitch ratio
- $Q$  torque
- $R$  maximum propeller radius

$r$	radius of any propeller blade section
$S_c$	nominal blade stress
SHP	shaft horsepower
$T$	thrust
$t$	section thickness
$U$	inflow velocity to section $\begin{bmatrix} V_a \cos \epsilon + i \\ \sin \end{bmatrix}$
$u_a$	axial component of induced velocity
$u_t$	tangential component of induced velocity
$V$	ship speed
$V_a$	speed of advance
$V_k$	speed of advance in knots
$w_a$	effective wake fraction
$x$	nondimensional radius ( $r/R$ )
$x$	fractional distance along chord measured from leading edge
$y$	pressure face ordinate
$z$	number of blades
	design angle of attack
$\gamma_1$	geometric angle of attack corrected for finite cavitation number
$\gamma_2$	angle of attack from lifting surface effect
$\gamma_3$	angle of attack for effect of bound vortices
$\gamma_4$	ideal angle of attack
	advance angle
$\gamma_5$	hydrodynamic pitch angle
$(P/D)$	pitch correction coefficient
	drag/lift ratio
	propeller efficiency
$\eta_i$	ideal propeller efficiency
	geometric angle of attack



## Design and Performance of Supercavitating Propellers

- circulation distribution factor or Goldstein factor
- advance coefficient
- $\nu$  kinematic viscosity of the fluid
- density of fluid
- cavitation number based on propeller speed of advance ( $2gH/v_a^2$ )
- cavitation number based on inflow velocity to the section at  $x$  ( $2gH/v^2$ )
- pitch angle.

## REFERENCES

1. Tachmindji, A.J., Morgan, W.B., Miller, M.L., and Hecker, R., "The Design and Performance of Supercavitating Propellers," David Taylor Model Basin Report C-807, Feb. 1957
2. Tulin, M.P., and Burkart, M.P., "Linearized Theory for Flows about Lifting Foils at Zero Cavitation Number," David Taylor Model Basin Report C-638, Feb. 1955
3. Tulin, M.P., "Supercavitating Flow Past Foils and Struts," Paper No. 16. Symposium on Cavitation in Hydrodynamics, National Physical Laboratory, Teddington, England, 1955
4. Waid, R.L., and Lindberg, Z.M., "Water Tunnel Investigations of a Supercavitating Hydrofoil," California Institute of Technology, Hydrodynamics Report No. 47-8, Apr. 1957
5. Parkin, B.R., "Experiments on Circular Arc and Flat Plate Hydrofoils in Non-cavitating and Full Cavity Flows," California Institute of Technology, Hydrodynamics Laboratory Report No. 47-6, Feb. 1956
6. Wu, T.Y., "A Free-Streamline Theory for Two Dimensional Fully Cavitated Hydrofoils," California Institute of Technology, Hydrodynamics Laboratory Report 21-17, July 1955
7. Hug, M., "Theoretical and Experimental Investigations of Forces on Cavitation Hydrofoils," Ph.D. Thesis, University of Iowa, Feb. 1956
8. Cohen, H., and Sutherland, C.D., "Finite Cavity Cascade Flow," Rensselaer Polytechnic Institute, Mathematics Report No. 14, Apr. 1958
9. Johnson, V., "Theoretical Determination of Low-Drag Supercavitating Hydrofoils and Their Two-Dimensional Characteristics at Zero Cavitation Number," NACA RML57 G11A, Sept. 1957
10. Johnson, V., "Theoretical and Experimental Investigation of Arbitrary Aspect Ratio, Supercavitating Hydrofoils Operating near the Free Water Surface," NACA RML57 I/6, Dec. 1957

11. Goldstein, S., "On the Vortex Theory of Screw Propellers," Proc. Roy. Soc. (London) 123:440 (1929)
12. Tachmindji, A.J., "The Potential Problem of the Optimum Propeller with Finite Hub," David Taylor Model Basin Report 1051, Aug. 1956, and International Shipbuilding Progress, Nov. 1956
13. Lerbs, H.W., "Moderately Loaded Propellers with a Finite Number of Blades and an Arbitrary Distribution of Circulation," Trans. Soc. Naval Architects Marine Engrs. 60:73-117 (1952)
14. Eckhardt, M.K., and Morgan, W.B., "A Propeller Design Method," Trans. Soc. Naval Architects Marine Engrs. 63:325-374 (1955)
15. Tachmindji, A.J., and Milam, A.B., "The Calculation of Goldstein Factors for Three, Four, Five and Six Bladed Propellers," David Taylor Model Basin Report 1034, Mar. 1956
16. Tachmindji, A.J., and Milam, A.B., "The Calculation of the Circulation Distribution for Propellers with Finite Hub Having Three, Four, Five, and Six Blades," David Taylor Model Basin Report 1141, June 1957, and International Shipbuilding Progress, Oct. 1957
17. Wrench, J.W., Jr., "The Calculation of Propeller Induction Factors, AML Problem 69-54," David Taylor Model Basin Report 1116, Feb. 1957
18. Morgan, W.B., "Propeller Induction Factors," David Taylor Model Basin Report 1183, Nov. 1957
19. Kramer, K.N., "Induzierte Wirkungsgrade von Best-Luftschrauben endlicher Blattzahl," Luftfahrt-Forschung, vol. 15, No. 7, NACA Technical Memorandum 884, 1939
20. Shultz, J.W., "The Ideal Efficiency of Optimum Propellers Having Finite Hubs and Finite Numbers of Blades," David Taylor Model Basin Report 1148, July 1957
21. Ludwig, H., and Ginzel, I., "On The Theory of Screws with Wide Blades," Aerodynamische Versuchsanstalt, Report 44/A/108, Goettingen, Germany, 1944
22. Lerbs, H.W., "Propeller Pitch Correction Arising from Lifting Surface Effect," David Taylor Model Basin Report 942, Feb. 1955
23. Morgan, W.B., "Optimum Supercavitating Sections," David Taylor Model Basin Report C-856, Aug. 1957
24. Morgan, W.B., "Centroid and Moment of Inertia of a Supercavitating Section," David Taylor Model Basin Report 1193, Aug. 1957
25. Caster, E.B., "TMB 3-Bladed Supercavitating Propeller Series," David Taylor Model Basin Report 1245, Aug. 1959
26. Morgan, W.B., "An Approximate Method of Obtaining Stress in a Propeller Blade," David Taylor Model Basin Report 919, Oct. 1954

## APPENDIX A

## STRENGTH ANALYSIS

At the present time there is no theory for which the stress in propellers can be adequately determined. This fact is particularly noted in the design of SC propellers where the sections are inherently thin at the leading edge. Consequently, these propellers are subject to leading edge vibration and fatigue failure. For these reasons it is necessary to use a high-strength material and a large factor of safety. From Ref. 1 it has been concluded that for a material with a 140,000-psi tensile strength the nominal stress of the SC propeller should not be over 30,000 psi.

The nominal stress at any blade section is calculated (26) from the bending moments ( $M_{x_0}$  and  $M_{y_0}$ ), the centroid ( $x_0$  and  $y_0$ ), and moment of inertia ( $I_{x_0}$  and  $I_{y_0}$ ) by the following equations:

$$\text{Stress at leading edge} = \frac{y_1 M_{x_0}}{I_{x_0}} - \frac{x_1 M_{y_0}}{I_{y_0}} \quad (A1)$$

$$\text{Stress in trailing edge on face} = \frac{y_2 M_{x_0}}{I_{x_0}} - \frac{x_2 M_{y_0}}{I_{y_0}} \quad (A2)$$

$$\text{Stress on back at maximum back ordinate} = \frac{y_3 M_{x_0}}{I_{x_0}} - \frac{x_3 M_{y_0}}{I_{y_0}} \quad (A3)$$

where, as shown in Fig. A1,  $x_1$ ,  $x_2$ , and  $x_3$  and  $y_1$ ,  $y_2$ , and  $y_3$  are used to denote the abscissas and ordinates of the leading edge, face, trailing edge, and point of maximum back ordinate, respectively, measured from the centroid of the section. In these equations a positive stress denotes tension and a negative stress denotes compression.

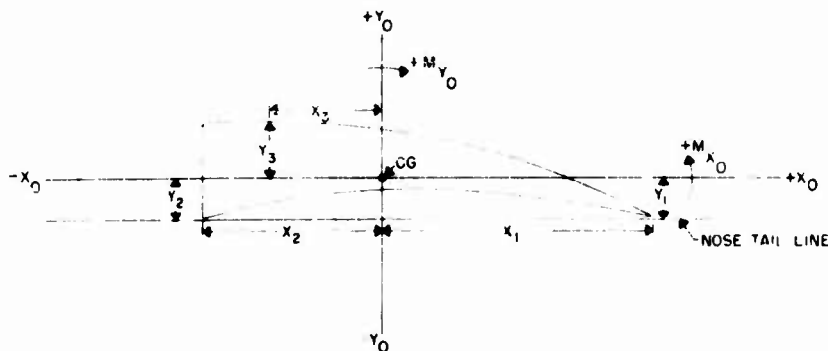


Fig. A1 - Geometric properties of a SC section

In the foregoing equations the bending moments  $M_{x_0}$  and  $M_{y_0}$  are computed from the thrust and torque moments ( $M_T$  and  $M_Q$ ) and the pitch angle  $\beta$  as follows:

$$M_{x_0} = M_T \cos \beta - M_Q \sin \beta \quad M_{y_0} = M_T \sin \beta + M_Q \cos \beta \quad (A4)$$

$$M_{V_1} = M_{T_1} \sin \alpha_1 = M_{Q_1} \cos \alpha_1 \quad M_{T_1} \sin \alpha_1 = M_{Q_1} \cos \alpha_1 \quad (A5)$$

where

$$M_{T_1} = \frac{R^3}{2Z} V_A^2 \int_{x_0}^1 (x - x_0) (1 - \tan^2 \alpha_1) \frac{dC_{T_1}}{dx} dx$$

$$= \frac{R^3}{2Z} V_A^2 \int_{x_0}^1 (x - x_0) \frac{dC_{T_1}}{dx} dx$$

$$= \frac{R^3}{2Z} V_A^2 \int_{x_0}^1 (x - x_0) \frac{\tan^2 \alpha_1}{\tan^2 \alpha_1} \frac{dC_{P_1}}{dx} dx \quad (A6)$$

$$M_{Q_1} = \frac{R^3}{2Z} V_A^2 \int_{x_0}^1 (\tan \alpha_1) (x - x_0) \left(1 + \tan^2 \alpha_1\right) \frac{dC_{P_1}}{dx} dx$$

$$= \frac{R^3}{2Z} V_A^2 \int_{x_0}^1 (\tan \alpha_1) (x - x_0) \frac{dC_{P_1}}{dx} dx$$

$$= \frac{R^3}{2Z} V_A^2 \int_{x_0}^1 (\tan \alpha_1) (x - x_0) \frac{dC_{T_1}}{dx} dx \quad (A7)$$

and  $x$  is the nondimensional radius of the section being analyzed.

The assumptions that the pitch angle  $\alpha$  in Eqs. (A4) and (A5) is equal to the hydrodynamic pitch angle  $\alpha_1$  and that the drag/lift ratio is zero in Eqs. (A6) and (A7) will have small effect on the bending moments except for heavily loaded propellers.

By comparing a number of calculations, it has been shown (24) that the term  $xM_{V_1}/I_{x_0}$  in the stress equation can be neglected for most SC sections. Therefore, only the moment of inertia  $I_{x_0}$  and the ordinates need be considered.

Also, if the relationship between  $C_1$  and  $\alpha$ , as given by Eqs. (17), is assumed, it is possible to considerably simplify the equations for stress. The equations for a flat-face section, (see Eq. 17a) are as follows:

$$\text{Stress at leading edge} = \frac{y_1 M_{x_0}}{I_{x_0}} + \frac{8.2 M_{x_0}}{3 C_1^2} \quad (A8)$$

$$\text{Stress at trailing edge on face} = \frac{y_2 M_{x_0}}{I_{x_0}} + \frac{8.2 M_{x_0}}{3 C_1^2} \quad (A9)$$

$$\text{Stress at } y_{max} = \frac{y_3 M_{x_0}}{I_{x_0}} + \frac{10.6 M_{x_0}}{3 C_1^2} \quad (A10)$$

# Design and Performance of Supercavitating Propellers

The results for the other relationships given in Eqs. (17) are more complicated and have been combined into nondimensional coefficients  $\frac{I^3 y_1}{I_{x_0}}$ ,  $\frac{I^3 y_2}{I_{x_0}}$ , and  $\frac{I^3 y_3}{I_{x_0}}$  and are plotted in Figs. (A2) and (A3) as a function of  $C_L$  and the camber corrections  $k_1$  and  $k_2$ . Using those coefficients and neglecting the last term in Eqs. (A1), (A2), and (A3), the calculations of stress for these particular SC sections are considerably simplified.

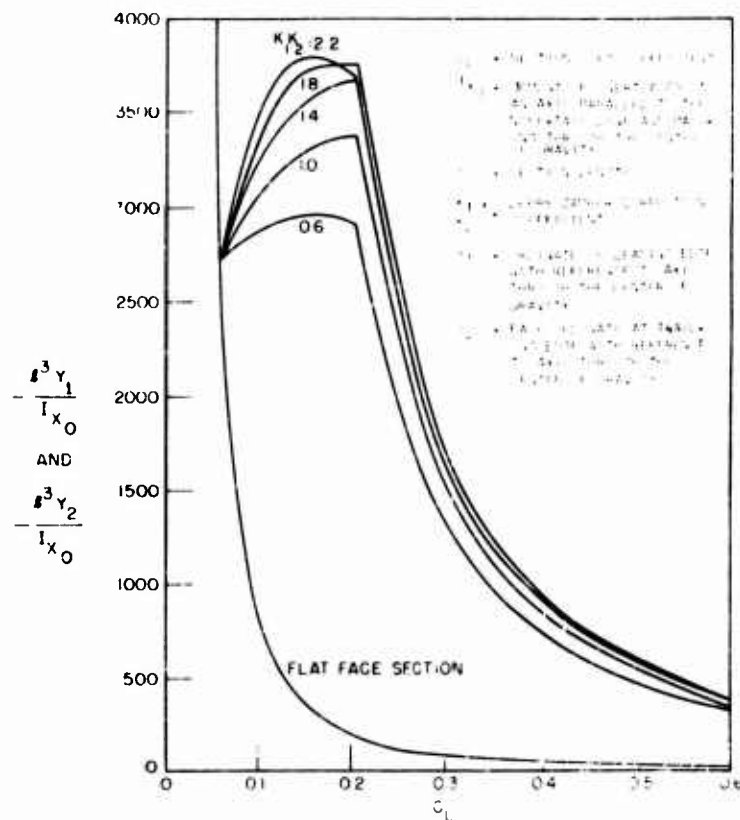


Fig. A2 - Coefficient for determining the stress of the TMB modified SC section

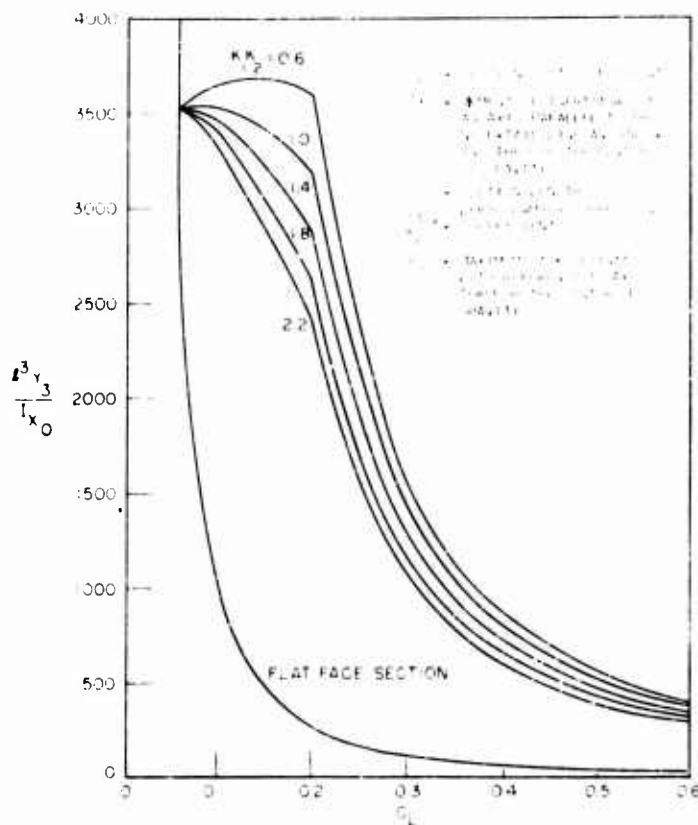


Fig. A3 - Coefficient for determining the stress of the LMB modified SC section

\* \* \* \* \*

## DISCUSSION

H. P. Rader (Vosper, Ltd., England)

The authors of the two papers have given us the benefit of their experience with supercavitating propellers which should be most useful to those interested in high-speed marine propulsion problems.

I would like to take this opportunity to mention a few characteristics of supercavitating propellers which we found during the study of the problem over the last five years.

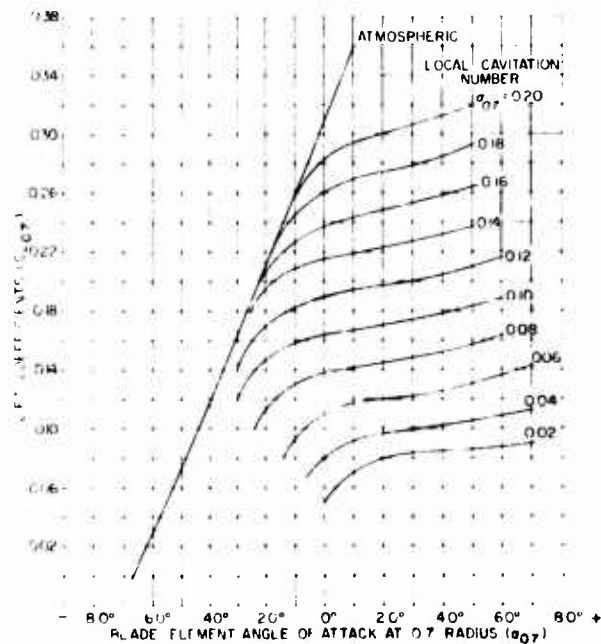


Fig. D1 - Lift coefficients of propeller blade sections at 0.7 radius as function of angle of attack ( $\alpha_{0.7}$ ) with local cavitation number ( $\sigma_{0.7}$ ) as parameter. (Typical values for good, high-speed propellers.)

The advantages of cambered blade sections from the efficiency point of view have been stressed already by Professor Lerbs. I should like to add that flat-faced blade sections are not only less efficient but also inadequate as far as lift production is concerned. Let me explain this. In Fig. D1 the lift coefficients of the equivalent blade section at 0.7 radius for various local cavitation numbers between 0.02 and 0.20 are plotted as function of angle of attack. The curves are obtained from the analysis of the results of cavitation tunnel tests of a good supercavitating propeller with highly cambered blade sections. Please note how small the gradient of these curves is in particular at the low cavitation numbers. For flat-faced blade sections all these curves would be lower and flatter. That means that it is impossible to produce two propellers of the same blade area ratio (B.A.R.), one with cambered and one with flat-faced blade sections, which will produce the same thrust at the same rate of advance even if the pitch of the propeller with the flat-faced sections is increased until it reaches practical limits. The small gradient of the lift-incidence curves is no real drawback. On the contrary, it proves to be a very useful characteristic for high-speed propellers which have to work in a nonuniform velocity field or on a shaft which is inclined relative to the inflow direction. The fluctuations or cyclic variations of the blade element lift components due to incidence changes will be much smaller for a correctly designed supercavitating propeller than for a propeller designed to be free from cavitation.

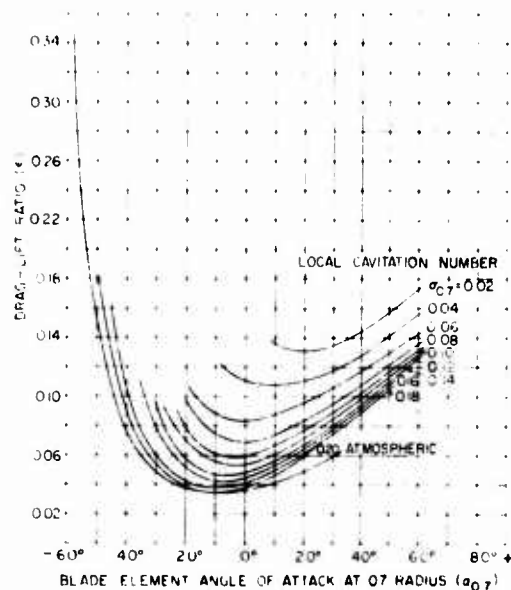


Fig. D2 - Drag-lift ratios of propeller blade sections at 0.7 radius as function of angle of attack ( $\alpha_{0.7}$ ) with local cavitation number ( $\sigma_{0.7}$ ) as parameter. (Typical values for good, high-speed propellers.)

Figure D2 shows the associated values of the drag-lift ratios. The curves for the different local cavitation numbers show more or less pronounced minima which increase with falling cavitation number and move to higher angles of attack. I have to add here that the drag-lift ratios shown in this and the following figures differ from the drag-lift ratios shown by Professor Lerbs. The drag coefficients in the drag-lift ratios shown here include the frictional losses and effects due to finite leading edge thickness, whereas the drag-lift ratios shown by Professor Lerbs allow for pressure drag only. This explains why in Professor Lerbs' graph the drag-lift ratios approach zero as the lift coefficients approach zero, whereas in my graphs the drag-lift ratios have a minimum at a certain angle of attack and approach infinity as the lift coefficients approach zero.

In Fig. D3, values of lift coefficients and drag-lift ratios of the equivalent blade sections at angle of attack  $\alpha_{0.7} = 2.5^\circ$ , for twelve geometrically similar, supercavitating

propellers, are plotted as a function of the local cavitation number. The face camber-chord ratios for blade sections at equal radii are the same, but the thickness-chord ratios of the blade sections at 0.7 radius, for instance, vary from  $t/c = 0.034$  for the small blade area ratio propellers to  $t/c = 0.016$  for the large blade area ratio propellers. The scatter of the lift coefficient values due to inaccuracies of model manufacture and experimental errors is such that one can draw a mean curve with reasonable fit. This proves the theoretical prediction that for supercavitating conditions the lift coefficient of a blade section depends only on cavitation number, angle of attack, and shape of the face, but not on the basic thickness form of the section. The values of the drag-lift ratios, however, show a definite trend with the thickness-chord ratio of the blade sections. This is due to the fact that it is physically impossible to use infinitely thin leading edges. It appears, however, that the drag-lift ratio for a given lift coefficient and cavitation number is not a function of a representative leading edge thickness but rather it is a function of the edge thickness-to-chord ratio which, of course, is directly proportional to the thickness-chord ratio of the blade section.

Remembering that for propellers of the same diameter which produce the same thrust at the same rate of advance the efficiency depends only on the drag-lift ratio, the possibilities of fully and supercavitating propellers can be assessed best by comparing their drag-lift ratios with those of noncavitating propellers at the same section lift coefficient. Such a comparison is shown graphically in Fig. D4. Values for the supercavitating DTMB propeller number 3509, at the design rate of advance,  $J = 1.125$ , and the ship cavitation numbers,  $\sigma = 0.30, 0.35$  and  $0.40$ , have been added. It appears that in the optimum incidence range the drag-lift ratios of fully cavitating



# Design and Performance of Supercavitating Propellers

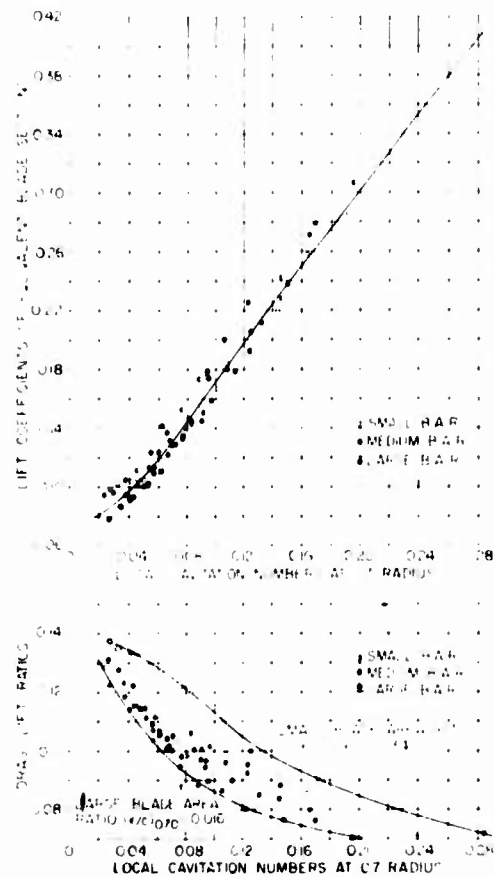


Fig. D3 - Lift coefficients and drag-lift ratios of equivalent blade sections ( $x = 0.7$ ) at  $\alpha_{0.7} = 2.5^\circ$  for twelve geometrically similar supercavitating propellers

propellers are about the same as for noncavitating propellers at the same lift coefficients. This implies, of course, that the lift coefficients for cavitating conditions are lower than for noncavitating conditions at the same angle of incidence or rate of advance. The drag-lift ratios for supercavitating conditions ( $\alpha_{0.7} = 2.5^\circ$  and DTMB propeller number 3509) are higher than the absolute minima achieved because the angles of incidence required to obtain sheet cavitation emanating from the leading edge are higher than is consistent with the requirements for minimum drag. This applies, in particular, to supercavitating propellers with narrow blades which require higher face camber ratios and, therefore, higher angles of incidence than supercavitating propellers with medium width or wide blades.

One last point. Mr. Tachmindji quoted as the lower limit for the application of supercavitating propellers a speed of 50 knots. In my opinion this limit is much lower. I would put it at about 35 knots or even lower provided of course the propeller

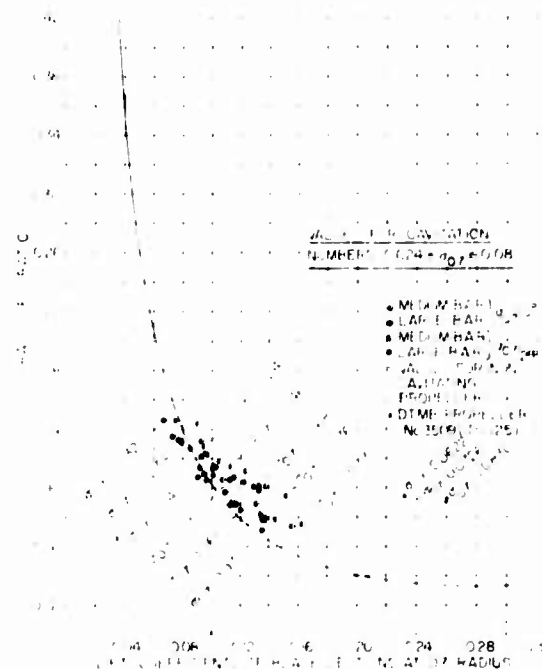


Fig. D4 - Drag-lift ratios of cavitating propellers as function of blade element lift coefficients for 0.7 radius

revolutions are high enough to obtain the low, local cavitation numbers required for supercavitating conditions. Recently we have fitted supercavitating propellers to an 80-ft. passenger launch with a cruising speed of about 35 knots. The performance is as good as it would be with good noncavitating propellers. There are no vibrations and so far the propellers have not shown any signs of cavitation erosion although the propeller shafts are at an angle of about 12 degrees relative to the direction of flow.

M. C. Eames (Naval Research Establishment, Halifax)

It is characteristic of the rapid and efficient manner in which both the theory and application of supercavitating flows have been progressed, that already we have the beginnings of a systematic series of supercavitating propellers. The authors are to be congratulated on this achievement.

I would like to add a word about some of the experimental results. The first open-water tests were conducted on the Canadian R-100 hydrofoil craft (Fig. D5) using DTMB propellers number 3509 and 3604.

This boat displaces 8.5 tons and has a length of 45 feet. The propellers were designed for a speed of advance of 50 knots and were required to develop 3500 pounds thrust at 3000 rpm.

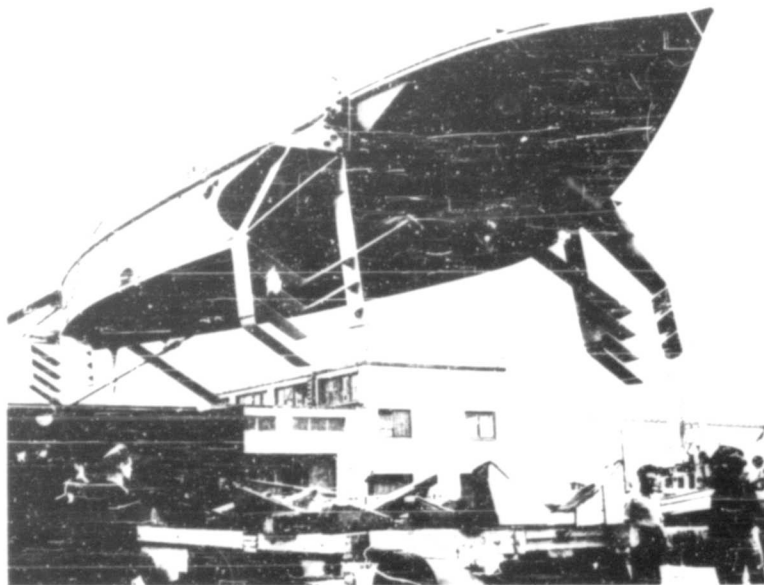


Fig. D5 - Canadian R-100 hydrofoil craft

The first propeller was designed to the theoretical cavity shape, that is to say, without the modified thickness distribution shown in Fig. D6 of the paper. This propeller failed from overstressing the first time a take off was attempted, and performance characteristics could not be obtained. The nature of the failure is shown in Fig. D6. It is believed that a high wake region generated by the stern hydrofoils of the craft was responsible for this failure.

It was anticipated that the strength of this propeller would be marginal, so a second propeller which incorporated the modified thickness distribution was provided. This second propeller is a member of the new DTMB series; Fig. D7 shows it mounted on the craft. The proximity of the lower stern hydrofoil is apparent.

Unfortunately the exact design conditions could not be realized, and it is interesting, in view of Dr. Lerbs' comments, to note that he might have anticipated this. The high-speed lifting foils of the boat use a Walchner section, and it has been found that cavitation occurs on these foils at a lower speed than predicted from Walchner's experimental results. In consequence of this early cavitation, the drag of the craft was significantly higher than predicted and the design thrust of 3500 pounds was demanded at about 40 knots instead of 50 knots.



Fig. D6 - Propeller of theoretical cavity shape, without modified thickness, showing wake failure

Despite the fact that the propeller was operating off its design condition, the results were most encouraging. Figure D8 shows the overall propulsive efficiency, defined as thrust horse power (t.h.p.)-to-shaft horse power (s.h.p.) at the engine, plotted on a base of speed in knots. The dotted curve is representative of results obtained with a conventional propeller of N.R.E. design, while the full curve shows the performance of DTMB propeller SC 3604.

Since a hydrofoil craft, with its inherently high speed of advance, is a natural application for the supercavitating propeller, these results are of interest apart from their verification of the propeller design itself. They point out the difficulty which must be faced under take-off conditions where a high drag exists in a speed range of low efficiency for the supercavitating propeller. During these particular trials, take-off was only just achieved.

# Design and Performance of Supercavitating Propellers

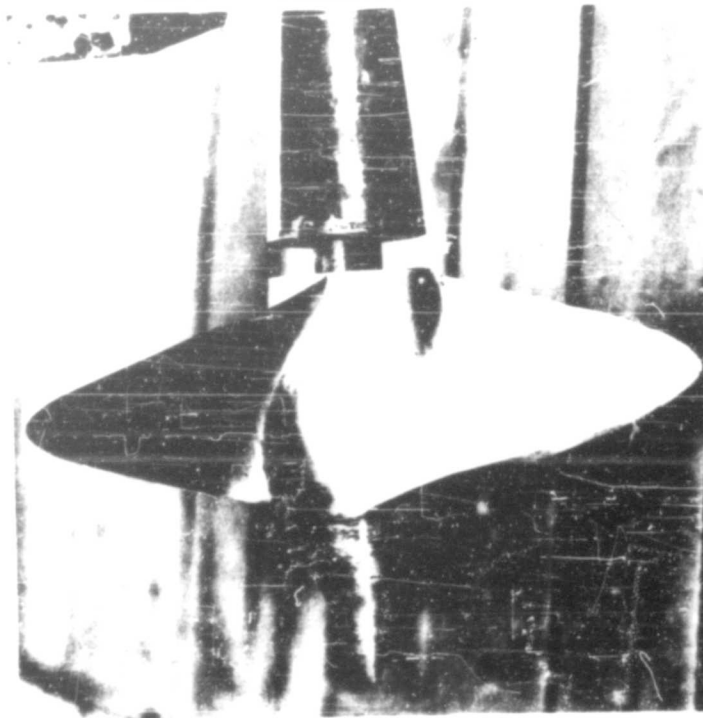


Fig. D7 - Propeller of new DTMB series, mounted on craft

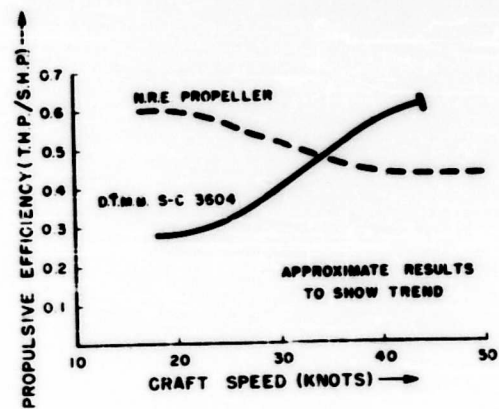


Fig. D8 - Plot of propulsive efficiency vs craft speed (knots)

D. C. O'Neill (British Admiralty)

Our thanks are due to the authors for their informative and interesting papers. The propeller designer has been concerned with the elimination of cavitation for many years. The effects of cavitation on propeller efficiency, vibration, erosion, and noise are well known. The present papers provide a solution to the problem when such high speeds are contemplated that the existence of severe cavitation becomes inevitable.

To the Naval Architect, perhaps the most directly informative feature of the Tachmindji-Morgan paper is Fig. 1 which indicates the region where the supercavitating design of propeller is likely to be applicable. Inspection of this diagram shows that very high speeds of advance are required. For example, at  $J = 0.6$  the corresponding speed for a practical SC propeller is of the order of 40-50 knots. At higher values of  $J$  this minimum speed rises to 70-80 knots. In each case, high shaft speeds and small propeller diameters are appropriate. To attain the high ship speeds in other than very small, fast craft, a significant increase in the power-to-weight ratio of existing machinery would be required. In this connection, the high shaft speed and the possibility of dispensing with reduction gearing is attractive.

To refer to points of detail, the authors have stressed their requirement for a blade section shape having a very thin leading edge in order to form the optimum cavity shape. In uniform flow this condition may well be obtained, but in the inclined and nonuniform flow behind the hull of a ship, it appears likely that fluctuations of the cavity shape will occur, leading to a reduction of efficiency and an increase in vibration and noise. The model test results shown in the paper are somewhat disappointing as the propeller, although designed for 50 knots speed of advance and running at 3000 rpm, falls within the marginal zone in Fig. 1. This serves, indeed, to emphasize the limitation of application of SC propellers referred to previously. In this marginal zone the propeller characteristics behave similar to those of more conventional propellers designed to reduce cavitation. This applies even at a cavitation number of 0.3 where one might expect the "marginal" SC design to show an advantage due to the decline of the conventional propeller's performance with increasing cavitation.

Further test results of model propellers designed and operated well within the supercavitating region will provide a more informative comparison with conventional "reduced cavitation" designs. It is hoped that the authors will extend their valuable researches to include tests of the propellers over a range of shaft inclinations and to investigate the effects of nonuniform flow.

J. P. Breslin (Stevens Institute of Technology)

The favorable prospects as outlined by Professor Lerbs should have a two-fold effect on naval engineers:

1. stimulate interest in the application of supercavitating propellers to high-speed ships,
2. provide them with the range of values of the controlling parameters to which any design must conform in order to obtain attractive efficiencies.

In this regard, it is to be noted that in order to achieve high efficiency it is necessary to design for moderate values of the thrust-loading coefficient as in the case of non-cavitating propellers.

It would also be most instructive to have a design chart which would indicate how the hydrodynamic efficiencies of both noncavitating and supercavitating propellers are confined or limited by the restraints imposed by structural requirements. Such a chart would clearly show the importance of structural limitations and might thereby increase research on this subject.

One favorable prospect for supercavitating propellers which has not been mentioned lies in the action of such propellers in producing vibration-exciting effects. In view of the fact that a supercavitating section has a lift-slope of one-quarter of that for a fully wetted section, one might expect that the vibratory thrust developed by an SC propeller operating in a circumferentially variable wake would be something of the order of one-quarter of that produced by the noncavitating propeller in the same wake. In addition, heuristically one may at first expect that the strength of the fluctuating pressure field would also be mitigated by the presence of the elongated cavity at constant pressure; however, recent work on the field about noncavitating propellers has indicated that the "thickness effect" of the blades is not at all negligible, so it may be that a blade with a cavity will produce a large pressure pulse by virtue of its enlarged "displacement." This field can and should be computed to check the truth of such a guess. It would certainly be an important asset of SC propellers if it could be demonstrated that in addition to providing high efficiencies they also provide a large reduction in excitation of ship vibration.

Another aspect in regard to vibration lies in the fact that the applied frequencies will be considerably higher than now obtained because of the higher rpm. This may well be of significance although it may turn out that components which are not at present excited may be found to be at a resonant condition at supercavitating propeller blade frequencies.

H. E. Saunders (Capt., U.S.N., Ret.)

I would like to point out that perhaps the low efficiency, which is found with even some of the modern supercavitating propellers, is not necessarily a drawback to their use or further development. With the old, racing motorboats which used supercavitating propellers, starting thirty years ago, speeds of 100 miles per hour were reached despite propulsive efficiencies of only about 0.25. The supercavitating propellers did the job despite this low efficiency, and perhaps in many present and future applications, efficiency may not be the prime consideration.

There is another point which I would like to emphasize. It was shown and explained to some extent by Mr. Eames, in connection with the Canadian hydrofoil boat, that a standard density of the water is assumed in the inflow jet to the supercavitating propellers. However, all of us, who have looked through windows of our naval vessels and have seen the so-called water in which the propeller works, realize that the inflow jet with its air bubbles looked like a howling blizzard of snow on the western plains; one can hardly see the propeller for the entrained air. Also in recent years, we have found with our large, fast ships, for some reason not adequately explained, that greater and greater quantities of air are encountered in the inflow jet. Mr. Eames pointed out that he had cavitation behind one of the hydrofoils. He also had separation behind that sloping shaft. The upper blades on his propeller were certainly not working in green water.

Some of the air in the inflow jet comes down under the bow of the ship. Some of it is pulled out of solution due to low pressures along the ship's length. But just where all of the air comes from, we do not know. There are indications that on some

of our latest and fastest ships we have pockets of air in the inflow jet which are longer than the pitch of the propellers. Thus, these are not bubbles any more but really big holes. My feeling is that while we should continue our work on the supercavitating propellers, we should also try to find out what to do about more air in the inflow jet as we get to higher speeds and perhaps even longer ships.

F. S. Burt (Admiralty Research Laboratory)

Mr. Tachmindji referred in his paper to the use of high speed computers for predicting propeller characteristics for a propeller series. We are very interested in this and would like to know if the DTMB has actually programmed a complete propeller design for computation on their computer. This is quite a formidable task as propeller design involves the use of correction factors such as Goldstein's  $k$ -factor and a correction for the lifting surface effect, which in themselves require some effort in programming. It may be of interest for you to know that at ARL we are at the moment having Ginzler camber correction factors, for the lifting surface effect, programmed for our Pegasus computer.

Incidentally, we would take slight issue with DTMB when they seem to use Lerb's angle-of-attack correction factor in addition to the Ginzler correction. We would argue that these conditions are equivalent and not complementary.

The possible disadvantage with supercavitating propellers may be in poor performance at off-design conditions. What information is there available on the performance at low speeds and at the incipient cavitation stage when the efficiency may be rather less than at the ultimate, fully cavitating state?

F. H. Todd (National Physical Laboratory, England)

My first contact with the problem of supercavitating propellers was in 1939 when an ordinary marine propeller was run up to supercavitating conditions in the propeller water tunnel at the National Physical Laboratory, Teddington. I presented the results of these experiments in a discussion on a paper given to the Institution of Naval Architects in 1944 by V. L. Posdunine, of the Moscow Academy, who developed a theoretical model of the flow picture and deduced expressions for the thrust and ideal efficiency.\* It is of interest to note that he spoke at this time of "wedge-shaped blades," and although he did not give any particulars of the shapes he had in mind it would seem likely that they resembled in general those used in the present propellers.

In these early NPL experiments the efficiency at the point where supercavitation was just fully developed was some 49 percent, as compared with 61 percent at the same slip in the noncavitating condition. At still higher slips the efficiency continued to fall. This work was not continued because of the outbreak of war, but the results indicated what could be achieved by running a normal marine propeller under such conditions.

The theoretical analysis carried out by Mr. Tulin, and first presented at a Symposium in England in 1955, has shown how, by using specially designed supercavitating

\*V. L. Posdunine, "On the Working of Supercavitating Propellers," paper presented to the Institution of Naval Architects, 1944.



sections, it is possible to regain a great deal of the loss in efficiency and so to produce propellers which, in supercavitating conditions, are not greatly inferior in efficiency to the corresponding ordinary marine propeller in the noncavitating condition.

In this paper Mr. Tschmindil and Mr. Morgan have applied the pioneer work of Tulin to the actual design problem for supercavitating propellers. By adapting the standard propeller design methods developed at the David Taylor Model Basin to this new problem, they have been able to calculate, on a high-speed computer, the performance of a large number of propellers and so produce the design charts given in their paper. The calculated performance characteristics have been checked by a limited number of experiments, which have shown that the charts can be relied upon for the design of supercavitating propellers within the region covered by the series. The authors are to be congratulated on making this approach to the problem, which has enabled them to produce design charts very much more quickly and cheaply than would have been possible if all the 30 propellers had had to be made and tested in the tank. Their work will be of great interest to all propeller designers who are involved in the particular field in which such supercavitating propellers may be of value.

In this respect the authors devote considerable attention to the question of when it is desirable and possible to use this type of propeller. It is interesting to study the charts which they give to see just what the practical speeds are in representative cases so that we may gain a clearer idea of the possible fields of usefulness. In order to do this, I have worked out three examples - for a fast liner (Table 1), a destroyer (Table 2), and a high-speed motorboat (Table 3).

For the liner a draft of 32 feet has been assumed, a maximum propeller diameter of 20 feet, with 7 feet of cover above the tips and an atmospheric pressure equivalent to 33 feet of water, giving a total head,  $H$ , of 50 feet. Taking the points marked A, B, C, D and E on Fig. D9, Table 1 can be constructed. The points A and B mark the limiting time for the use of such propellers, and we see that even in this case the speeds are high - ranging from 40 to 85 knots. Perhaps the most interesting case is that at point A, where the speed is not too far beyond those at present in use or contemplated for Atlantic liners.

Assuming a total shaft horsepower of 250,000, estimates can be made, from the charts given in the paper, of the efficiency and pitch ratio, and the optimum values are also given in Table 1.

For conventional propellers, the quadruple screw arrangement using propellers of 18.6 feet diameter and 1.23 pitch ratio, running at 200 rpm, might be expected to give an efficiency of the order of 0.68, assuming no cavitation. This latter qualification is, of course, the crux of the

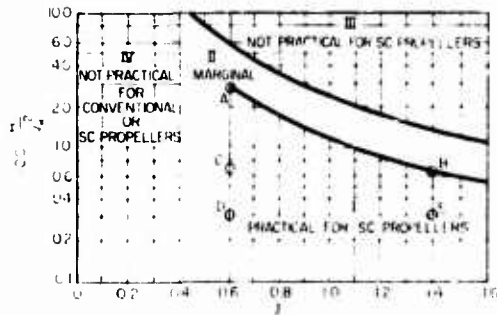
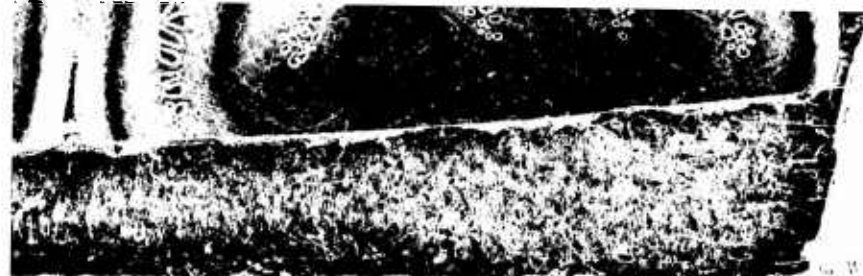


Fig. D9 - Chart of practical application of supercavitating propellers

\*M. P. Tulin, "Supercavitating Flow Past Fairs and Struts," Symposium on Cavitation in Hydrodynamics, NPI, 1955.



G. W. B. Morgan

Table 1

High Speed Liner  
Draft 32 feet, propeller diameter 20 feet, H = 50 feet

Point:	A			B			C			D			E		
$100 H/V_k^2$	2.0			0.7			0.7			0.5			0.3		
$V_k$ (knots)	40.8			84.5			84.5			129.0			129.0		
J	0.6			1.4			0.6			0.6			1.4		
Diam. (feet)	20	15	10	20	15	10	20	15	10	20	15	10	20	15	10
rpm	344	458	688	305	407	610	713	950	1426	1090	1450	2180	467	623	935
No. of screws*			4			2			4						
Propeller type			Supercavitating									Conventional (assuming no cavitation)			
Diam. (feet)			10			15			18.6						
rpm			688			407			200						
Pitch ratio			0.96			0.92			1.23						
Efficiency			0.61			0.625			0.68						

\* Shaft horsepower: 250,000

business. In present liners of this class, cavitation is already a problem and some already suffer from cavitation erosion. To design conventional propellers to run at 40 knots or above and absorb 60,000 to 70,000 horsepower each without suffering from cavitation would therefore be a real problem, and the supercavitating propeller may well be the answer to it. Under such conditions the conventional propeller would lose some of its margin of efficiency and any remaining difference in this respect would have to be set against the absence of erosion. If we consider still faster speeds, moving along the line from A to B, the problem of designing a conventional propeller becomes rapidly more difficult and the use of supercavitating propellers more attractive.

For the destroyer and high-speed motorboat, Tables 2 and 3 can be prepared. In these two types of ship, it will be seen that even at the present top speeds the supercavitating propeller may already be considered as a rival of the conventional propeller, and it is in the high-speed motorboats that it has already been adopted on numerous occasions, although without the benefit of the new type sections.

In the past, the supercavitating propellers used have in general had normal sections of the aerofoil or crescent (hollow-faced) type, and the relatively low efficiencies of these propellers under such conditions of operation have been accepted as part of the necessary price of working in this area. It has now been shown how, with the proper choice of sections, this loss of efficiency can be avoided to a large

Table 2

**Destroyer**  
 Draught 12 feet, propeller diameter 12 feet, cover 6 feet, H = 45 feet

Point:	A			B		C		D		E	
$100 H/V_k^2$	3.0			0.7		0.7		0.3		0.3	
$V_k$ (knots)	38.7			80.2		80.2		122.5		122.5	
J	0.6			1.4		0.6		0.6		1.4	
Diam. (feet)	12	6	10	12	6	12	6	12	6	12	6
rpm	545	1090	655	483	966	1127	2254	1728	3456	740	1480
No. of screws <sup>†</sup>	2						2				
Propeller type <sup>†</sup>	Supercavitating						Conventional (assuming no cavitation)				
Diam. (feet)	10						12.6				
rpm	655						350				
Pitch ratio	0.94						1.18				
Efficiency	0.62						0.66				

<sup>†</sup>Shaft horsepower: 100,000

<sup>†</sup>Comparison at 38.7 knots

extent, and supercavitating propellers can be designed to give reasonable efficiencies under very advanced design conditions, thus extending the range over which marine propellers may continue to be used for high-speed ship propulsion.

An inspection of the tables will also show the wide range of revolutions possible with such propellers, and this feature may well be of great interest to the marine engineer, enabling him to consider the adoption of lighter, faster-running engines and the elimination of gearing.

Of course, as in most new developments, the supercavitating propeller also brings its own problems, and one of the most important of these will undoubtedly be the need to obtain sufficient strength in the blades, particularly near the very fine leading edge. To avoid distortion and vibration in this vicinity will call for extremely hard and tough material.

Also, it is important to realize the limitations of this type of propeller. Many new ideas have been spoiled in the past because attempts were made to apply them indiscriminately in fields where their particular merits could not be realized. From the examples quoted above, it will be realized that the essential condition for the use of the supercavitating propeller is a relatively high speed. It will not assist the normal cargo ship to go faster, but in the field of high-speed motorboats and destroyers it may be considered as a practical propeller even with present-day speeds.

Table 3

High Speed Motorboat  
Immersion to centreline shaft assumed 7 feet,  $H = 40$  feet

Point:	A			B		C		D		E	
$100 H/V_k^2$	3.0			0.7		0.7		0.3		0.3	
$V_k$ (knots)	36.5			75.5		75.5		115.5		115.5	
$J$	0.6			1.4		0.6		0.6		1.4	
Diam. (feet)	4	3	2	4	2	4	2	4	2	4	2
rpm	1540	2055	3080	1363	2726	3185	6370	4875	9750	2090	4180
No. of screws*	4					4					
Propeller type†	Supercavitating					Conventional (assuming no cavitation)					
Diam. (feet)	2.40					2.38					
rpm	2570					1800					
Pitch ratio	0.90					1.16					
Efficiency	0.64					0.67					

\*Shaft horsepower: 8000

†Comparison at 36.5 knots

It is, indeed, interesting to note that its field of useful application begins just about at the point which we have now reached in such high-speed craft and even in Atlantic liners, and if the demand for still higher speeds in these classes of ships continues, then the supercavitating propeller has a promising field in front of it and the designer a useful new weapon in his armoury.

#### A. Silverleaf (National Physical Laboratory)

These papers summarize a very great amount of work, and the information which they give is an immense aid to those of us who do not yet have any personal experience with supercavitating propellers. My first reaction to the paper by Mr. Tachmindji and Mr. Morgan is surprise in that design methods developed for orthodox propellers (in the development of which Prof. Lerbs has played a major role) appear to work so well for supercavitating conditions. Do the physical conditions in the wake immediately downstream of a screw with long cavities over the back of its blades closely resemble those postulated for the conventional vortex-theory design method for propellers? Prof. Lerb's review of the flow models for supercavitating propellers suggests to me that a more complicated model may be necessary to understand fully the action of supercavitating propellers.

The pitch correction factors presented by Mr. Tachmindji and Mr. Morgan are clearly derived from a very extensive analysis, but I find them difficult to understand. Does the correction for finite cavitation number take account of the very marked radial variation in the local cavitation number, which in most propellers covers a range of about 8 to 1? Further, can Ludwig-Ginzler curvature correction factors, which depend closely on the blade width, apply to supercavitating propellers? What is the effective chord of a blade which has a long cavity extending far downstream of its trailing edge?

The principle of carrying out systematic design calculations before indulging in the costly, time-consuming, and often disappointing process of systematic model experiments is an excellent one, and undoubtedly Mr. Tachmindji and Mr. Morgan have applied it most thoroughly. However, I am not entirely clear how the curves of his Figs. 6 and 7 are computed; has the inverse of a design method been developed to calculate the performance characteristics of propellers with specified geometry, or has the design method itself been directly applied to determine the geometrical features of propellers satisfying a set of specified operating conditions? If the latter method has been followed, then presumably each of the thirty propellers for which calculations were made is an optimum design, and thus each curve of constant pitch ratio in Figs. 6 and 7 embraces a set of propellers which are otherwise not geometrically identical, unlike similar diagrams for conventional propeller series.

Mr. Tachmindji and Mr. Morgan claim satisfactory agreement between measured performance values for a number of supercavitating propellers and those derived from the calculated series. How were the experimental values determined? If they were based on water-tunnel test data, then what tunnel interference correction factors were used? It seems unlikely that simple corrections are adequate.

There is a brief reference to the possibility of using forced ventilation to operate supercavitating propellers at low ship and shaft rotation speeds. How much power would be needed to operate the necessary ancillary gear? Experiments with model supercavitating screws in a towing tank should help to answer such questions. What is the efficiency of supercavitating propellers when rotating in the astern direction? If it is low, then I should expect supercavitating propellers to be used for ships with shafts rotating unidirectionally; if so, then controllable pitch screws would be necessary. How do supercavitating sections behave over a wide range of pitch settings? Finally, it is important to remember that very large thrusts are needed to propel large ships; practical considerations of propeller blade strength may well be decisive factors in the ultimate adoption of supercavitating propellers for large, fast ships.

H. Lerbs

One question to which I would like to reply immediately was that by Mr. Burt. The question refers to the lifting surface effects of the propeller and the corrections which are necessary when you take the section property from two-dimensional flow.

Now, the lifting surface effect exhibits itself in the curvature of the streamlines, and if the lifting surface effect of the propeller were such that the curvature over the chord length would be constant, Ludwig's correction would suffice. Now, owing to the continuous change of the velocity the curvature of the flow is smaller at the leading edge and greater at the trailing edge, and in order to compensate for this change of curvature an angle of attack is necessary.

A. J. Tachmindji

I'd like to reply briefly to a few points. Regarding Mr. Rader's comments on the question of speed, I think he has misunderstood the 50 knot question. The important thing, of course, is cavitation number and not speed. The value of speed itself is immaterial.

Mr. O'Neill told us on the one hand that the supercavitating propeller was not quite comparable to the ones at AEW and then he showed us very nicely that this was in the marginal region. This was the basic reason that the diagram of Fig. 1. was given, i.e., to anticipate the comparison with arbitrary propellers. Of course, it has been shown that the efficiency of conventional propellers drops quite rapidly at low cavitation numbers.

On Mr. Burt's comments about computing machines, we do have at the Model Basin a complete program for computing machines. The method used there is induction factor method rather than the Goldstein method. It's a bit easier to program this particular method.

Dr. Todd has pointed out the ranges and speeds of supercavitating propellers.

Mr. Silverleaf has given a glimmer of some of the work necessary to produce this diagram and he is quite right in saying there is more to it than meets the eye.

Regarding the estimated performance of propellers in water tunnels, the one which was given was tested in full scale and also tested in the Basin and most of the work which has been carried on in the water tunnels is duplicated in the Basin.

\* \* \* \* \*

# AN EXPERIMENTAL STUDY OF CAVITATING INDUCERS

A. J. Acosta

*California Institute of Technology*

## INTRODUCTION

The user of a turbomachine is mainly interested only in the overall hydrodynamic performance of the device. However, the designer is almost always confronted with the problem of achieving the intended performance in the face of many conflicting hydrodynamic and system requirements. In certain areas it may happen that a formerly deleterious effect (such as the occurrence of cavitation) can be turned to good advantage as in the case of the supercavitating hydrofoil or propeller. Unfortunately, this happy circumstance is not the lot of the designer of a liquid pumping system when the effects of cavitation are predominant. That this is so, follows from the fact that the dissipation effects in production of lift by a hydrofoil are relatively unimportant whereas dissipation is important in the decrease of energy of a fluid stream as in the case of a pump.

The basic compromise in pump design that makes cavitation a problem is rotative speed. If the size and weight of a pumping unit were immaterial, then a suitable combination of rotative speed and pump(s) could always be found to eliminate virtually any problem of cavitation. Fortunately for the occupational outlook of hydraulic engineers, one rarely has such freedom. In fact, weight and overall size are of such importance in missile turbopump applications that the conventional limits of rotative speed and cavitation criteria have been far exceeded, so that the effect of cavitation on overall performance is critical. A substantial reduction in weight is obtained, of course, by operation at high speeds, since to a rough approximation the tip speed for a given pressure rise is fixed. As the rotative speed is increased, the diameter is reduced and the weight is reduced more or less as the cube of the diameter. Needless to say, the weight of auxiliary driving equipment will also be smaller at high rotative speeds since, as is invariably the case, a high-speed impulse drive turbine is used and fewer gears will be needed in the reduction train. The flow near the inlet portions of the pump is now quite susceptible to cavitation because of the large relative velocities that occur in this region. Thus there is every incentive to operate a liquid pump at the highest possible rotative speed, limited only by cavitation.

These flows as well as non-rotating flows are governed by a cavitation index  $k$  except that herein they are based upon the inlet relative velocity dynamic pressure, the upstream static pressure and the vapor pressure of the flowing fluid. Some appreciation of the fluid dynamic effects to be expected may be gained by a comparison of the cavitation numbers at which conventional pumps operate and those of modern

propellant pumps. A well-designed centrifugal (or axial) pump may be expected to operate with cavitation numbers as low as about 0.3 before serious deterioration in performance occurs. However, a missile propellant pump may be called upon to operate satisfactorily with values of  $k = 0.03$ , say, although at some loss of efficiency. (To make the comparison fair, the service life of the conventional unit as determined by cavitation damage will be many times that of the propellant pump.) It is clear that with such low values of  $k$ , a cavitation-free flow cannot be obtained and, in fact, considerations of cavitation dominate the design of inlet portions of such machines.

A characteristic feature of cavity flows in confined spaces is that for a given geometry there is a minimum cavitation number below which steady flow is not possible. This effect may be termed "choking" in analogy with the compressible phenomenon or cavitation "breakdown." Examples of such limiting flows in ducts are given in Ref. 1 and in cascades in Ref. 2. In the case of a pump operating at a given speed and flow rate, there also exists an inlet pressure below which maintenance of the flow rate is not possible. It is extremely important in design to be able to predict the minimum required inlet pressure, and to so design the machinery as to make this minimum as small as the circumstances allow.

From the foregoing remarks it will have been anticipated that the inlet configuration of a pump designed for cavitation will be quite different from a conventional machine. At small cavitation numbers (say less than 0.1) the cavity length becomes appreciable, and for the limiting cavitation number, the cavity length is infinite—at least in all planar flows. It is no surprise, then, that the blade length of the inlet portions of pumps for cavitating service must be long, or at least sufficiently long to insure finite cavity lengths over the desired operating range. The length of the blade is conveniently expressed in units of the circumferential blade spacing, and the ratio of these lengths is called the solidity. The inlet portions of such pumps will therefore be of high solidity (at least greater than unity) and to avoid high local velocities will be predominantly axial. For convenience of manufacture, this inlet region is often made separately and subsequently joined to the main stage. Following supercharger terminology, this separate piece is called an "inducer." The function of the inducer is to pressurize the flow sufficiently to enable the following pumping equipment to perform satisfactorily. If the primary rotor is of the centrifugal type, the pressure increase of the inducer portion usually needs to be only about ten percent of the pressure rise of the system. The power requirement of the inducer is then not an overriding consideration and the necessary cavitation performance of this component can then be obtained at the cost of efficiency if need be.

The inducer is thus only an extension of the main rotor. Its being separate, however, offers advantages in that it may be run at a different speed on a coaxial shaft and certain fabrication difficulties are alleviated. Figure 1 is a photograph of a typical pump-inducer combination.\* The inducer is hardly a new device. For example, one of the very first rocket engines, the Walter 109-509A engine for the Me-163 rocket plane, used an inducer-pump combination (3). In the intervening period there has been a rapid development of inducers and pumps for cavitating service by organizations interested in missile development. However, relatively little design information has appeared in the open literature. We find, for example, Zimmerman in 1950 discussing the effect of pump suction pressure requirements in terms of pumping machinery weight (4). Brumfield (5) and Ross (6) undertook an elementary analysis to show in effect that there is an optimum inlet diameter for a

\*For a novel scheme to eliminate the inducer, and for a good discussion of the problem, see Wislicenus, G.F., "Critical Considerations on Cavitation Limits of Centrifugal and Axial-Flow Pumps," Trans. ASME 78:1707 (1956).



given speed and flow rate. Ross was particularly interested in demonstrating the effect of inlet conditions on weight and Brumfield pointed out the advantages of pre-whirl in attaining low inlet pressures. The first paper dealing explicitly with the inducer was by Ross and Banerian (7) in which the function of the inducer is outlined and a general description of the flow is given. They report few details about the internal flow in the inducer but show that extremely low inlet pressures can be achieved.



Fig. 1 - A typical inducer installation on a centrifugal pump for liquid oxygen. (Courtesy of Mr. T. Carter, Turbocraft Corp., Pasadena.)

Both the photograph of Fig. 1 and those in Ref. 7 show the inducer to be generally helical in shape. It is usually machined, and in these examples consists of a helical surface, the lead of which may vary from inlet to discharge. The hub diameter as well as the tip diameter may also vary along the axis. Although there are many design variables, the general appearance of an inducer is a rotor of high solidity, small number of blades, and small blade angle. The purpose of this paper is to report the results of some experiments on typical inducer shapes. These experiments are intended to show in a qualitative way the general flow patterns in the inducer in various stages of cavitation from incipient to near breakdown. For this objective the simplest (but still useful) inducer shape is chosen; a rigid helix of constant lead. Three blade tip angles were studied, namely,  $6^\circ$ ,  $9^\circ$ , and  $12^\circ$ . The solidity was kept constant at 2.5 for each of these investigations. Additional tests were made with the  $9^\circ$  impeller by varying the solidity from 1.0 to 3.25 and by changing the tip clearance over a wide range.

Complete performance data (cavitating and noncavitating) was obtained for each of the foregoing arrangements. As will be seen, the flow through such a simple geometrical device is extremely complicated and not subject to exact analysis (although this may not be necessary for design). In the following sections the non-cavitating and cavitating performance of these inducers will be presented, together with some simple correlations based on two-dimensional free streamline theory. It will be shown that while we are not able to predict well the occurrence of breakdown the correlations found do offer "rules of thumb" for design that will serve until better information becomes available.

## EXPERIMENTAL PROGRAM

### The Test Rotors

The combination of flow coefficients and head coefficients required for inducer applications lies far outside conventional pump or fan practice. Accordingly, it was desired to cover a reasonably wide range of geometric variables in the test program. To simplify construction not only of the rotor but the rotor housing, the blade shapes (as noted before) were rigid, helical surfaces with tip blade angles of  $6^\circ$ ,  $9^\circ$ , and  $12^\circ$ . The tip diameter was 2 inches and the hub diameter was 1 inch. The solidity for the  $6^\circ$  and  $12^\circ$  rotors was maintained at 2.5 whereas it was systematically varied in the



Fig. 2 - The 6, 9, and 12 experimental inducers.  
The tip diameter is 2 inches.

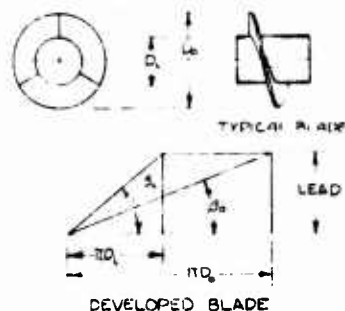


Fig. 3 - Definition sketch of impeller geometry

9° series from unity to 3.25. The tip clearance was also systematically varied in the 9° series for a given solidity (2.5) over a wide range.

Figure 2 is a photograph of several of the rotors tested. The various configurations tested are tabulated in Table 1, and Fig. 3 may be consulted for the definitions of the various geometrical terms.

All impellers were machined from 25 ST aluminum stock and anodized for corrosion and damage protection. The blade thickness was about 0.045 inch at the tip for most of the impellers. The leading edges in all cases were sharpened so that the resulting shape was a wedge with about a ten-degree included angle.

### Test Facility

At the start of this program no suitable test facility was available. The design of the arrangement shown in Fig. 4 was determined by the available funds and the desire for a simple, reliable, and compact system. The hydraulic circuit consists of a 60-gallon storage tank on which are mounted the cylindrical Lucite working section (Fig. 4) and the drive motor and associated controls. Considerations of the available motors and power supply dictated that the diameter of the working section be 2 inches. For maximum visual observation of the flow, the impellers were mounted on a 1-inch shaft that is supported by a water-lubricated bearing upstream and a grease-lubricated ball bearing in the downstream diffuser. A mechanical face-seal prevents water from getting into the bearing or prevents air from leaking into the circuit when operating at low pressures. A three-legged spider (with struts of 9-percent thickness) supports the upstream bearing. The support is 1-1/2 diameters upstream of the impeller so that no appreciable wake effects should remain in the flow.

The discharge from the diffuser then passes through a turbine-type flowmeter and an auxiliary circulating pump. The hydraulic circuit is completed by discharge back into the 60-gallon reservoir. The ambient pressure in the circuit is changed by applying vacuum or pressure to a separate container about 1 gallon in volume that is in turn connected to the storage tank. This tank is mounted approximately 1 foot above the working section, and purge lines from all high points in the circuit lead to it so that undissolved air obtained either by deaeration of the water or during the normal course of operation at low pressure can be removed.

# Experimental Study of Cavitating Inducers

Table 1

Constants of Impellers Tested  
Nominal Tip Diameter = 2.0 in.; Hub Diameter = 1.000 in.

Impeller No.	Blade Tip Angle (deg)	Solidity	No. of Blades	Radial Tip Clearance (in.)	Tip Clearance Ratio (gap/blade height)
1	12.05	2.5	4	0.002	0.004
2	12.05	2.5	4	0.005	0.010
3	9.1	2.5	3	0.0015	0.003
4	9.1	2.5	3	0.004	0.008
5	9.1	2.5	3	0.008	0.016
6	9.1	2.5	3	0.020	0.040
7	9.1	2.5	3	0.0055*	0.011
8	9.1	3.25	3	0.0055	0.011
9	9.1	2.0	3	0.0055	0.011
10	9.1	1.5	3	0.0055	0.011
11	9.1	1.0	3	0.0055	0.011
12	6.1	2.5	2	0.0045	0.009

\*This impeller appears to have systematic manufacturing differences between it and the preceding ones of the same blade angle.

The greatest compromise in the design of the test system was the impeller drive motor. With the small diameter (2 inches) of the rotor it is necessary to operate at high rotative speeds to obtain the low cavitation numbers sought. (Since hydraulic horsepower varies as the cube of the speed, and fifth power of the diameter, a small rotor operating at high speed is demanded if the power required is not to be excessive for a given tip speed.) The minimum useful rotative speed for cavitation studies was thought to be about 9000 rpm. A survey of the electric motor market quickly showed that no induction motor suitable for the laboratory variable frequency supply was readily available, and as a compromise choice a 1/2-hp universal motor was obtained that could operate at rotative speeds from 6000 to 12,000 rpm. The motor power output was calibrated at several speeds, and electrical input power measurements were subsequently used to establish the pump efficiency. This procedure was not completely satisfactory since the motor calibration depended upon the operating temperature as well as load.

## Instrumentation

All pressures were measured with mercury manometers. The flow rate was found from the rotative speed of a calibrated turbine-type flowmeter. Although the

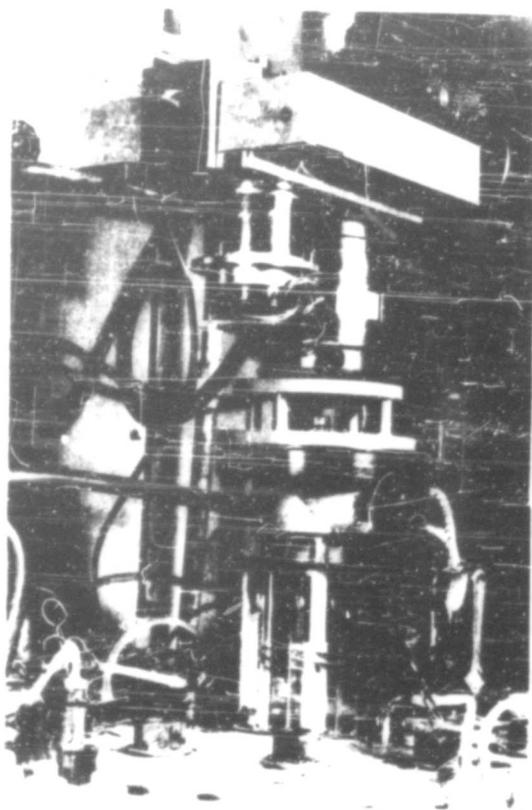


Fig. 4 - View of test facility showing the Lucite working section and the drive motor. The discharge piping and manometers are not visible.

motor speed was manually varied and controlled, it was measured by comparing it with the output of a known speed source. The comparison speed was capable of being varied in discrete units of 12 rpm. In practice, the armature current was varied until there was no difference between the motor speed and that of the source. The details of this system can be found in Ref. 8.

The impeller total head was measured with a small impact probe 0.05 inch in diameter at a station 1.5 inches downstream from the impeller. Surveys near the hub or case were made with a boundary layer probe 0.02 inch in height. Flow angles and static pressures were also measured in the midstream portion of the annulus. However, owing to the relatively large size of these instruments and the high curvature of the flow in the passage, accurate measurements of these quantities could not be obtained near the walls.

### Procedure

The limitation to the relatively low tip speeds of the present tests (about 90 ft/sec) required the inlet static pressures to the impeller be on the order of 5 feet absolute. The first step therefore in the tests was to deaerate the water to levels such that the fluid was not supersaturated with air at these inlet pressures. For all except the very lowest inlet pressures this was achieved by limiting the air content to 3 ppm (i.e., moles of air per mole of water). A Van Slyke blood gas analyzer was used to measure the air content. Needless to say, much time was expended in obtaining and maintaining the air-tightness of the system to get such relatively low values of dissolved air. Even so, an air content of say 1/2 ppm would have been preferable.

In these experiments the performance of the machine is separated into cavitating and noncavitating performance. The latter tests were made to get a general idea of the flow within the impeller and to see how the performance of such machines compared with that of more conventional designs. For this purpose, total head, flow rate, and input power measurements were made. Extraneous torques such as seal friction were measured by the electric power input to the motor and computations of the efficiency could then be made.

The cavitation tests were made by maintaining constant flow rate and speed and decreasing the system ambient pressure. The ambient pressure was lowered until the impeller could not maintain the given flow rate (termed cavitation breakdown) or the system minimum inlet pressure was reached. Operation near the breakdown point was quite unstable, since the power requirement of the impeller varied widely and constant speed could not be obtained with a universal motor. For this reason data at breakdown itself is of limited extent and most of the deductions made were based on information obtained near this point.

The quantity of principal interest in the cavitating tests was the total-pressure rise. It was measured at the downstream station in the middle of the annulus (at a radius ratio of 0.75). Although the total head at this position corresponds to a rough average of the total head over the annulus, the head so measured must be smaller than the properly weighted total head. The results thus obtained are conservative.

Both cavitating and noncavitating performance data were taken for each of the impeller combinations listed in Table 1. Studies on somewhat modified impeller forms were also made but will not be reported here. In fact, because of the large amount of experimental data gathered, only those salient features of impeller performance both cavitating and noncavitating will be mentioned.

### RESULTS

To facilitate the presentation, the noncavitating features of the flow through the inducers will be discussed first. As a further aid in visualizing the flow, the results of a tuft study made on a 12° inducer (No. 1, Table 1) will be given.

#### Tuft Photographs (Noncavitating)

Figure 5 shows a sequence of three photographs of a 12°-impeller operating various flow-rate coefficients. As seen in this picture, three rows of three tufts each are fastened to the case and in addition three tufts are mounted on the hub immediately upstream and downstream of the rotor. At the highest flow rate shown ( $C_f = 0.10$ , occurring at about the maximum efficiency), the unstream tufts show little

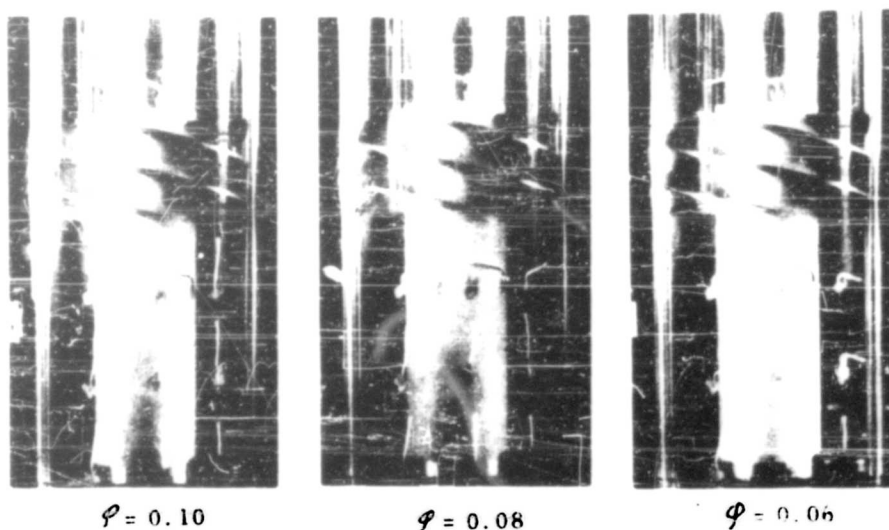


Fig. 5 - Sequence of tuft photographs on a 12° impeller at various flow rates. The rotation is from left to right and flow approaches the rotor from below.

or no disturbance and the hub tufts are in accordance with a smooth relative flow there. At the intermediate flow rate ( $\phi = 0.08$ ), however, the row of tufts nearest the impeller on the case show a strong influence from the impeller whereas the hub tufts are still relatively unaffected. At  $\phi = 0.06$  back flows on the case upstream of the impeller and on the hub immediately downstream of the trailing edge are quite noticeable.

Thus at the lowest flow rate shown any resemblance to straight axial flow is gone. The general circulation pattern in the meridian plane appears to be that of the strong ring vortices discussed by Spannhake (9). Additional visual tuft studies were made on a 9° impeller to confirm this point. From these it appears that at flow coefficients for which the strong upstream flow disturbance is observed, the suction surface of the blade near the leading edge is not separated. However, tufts on the pressure surface at the outside diameter indicate that a strong tip clearance flow at the leading edge may be the agent of the disturbance. The tip clearance in these observations was 1 percent of the blade height, but more observations with variable tip clearance are necessary before this question can be settled.

The course of the flow through the rest of the impeller is fairly complicated at these flow rates. Strong radial inflow on the pressure side of the blade just downstream of the leading edge was observed on the inner half of the blade height and secondary flows were observed on the hub. About halfway through the impeller, the flow on the hub appears to separate. The back flow at the trailing edge on the hub shown in Fig. 5 flows into this region. A compensating radial outflow is observed on the pressure side of the blade near the trailing edge.

Although the flow patterns just described ( $\phi = 0.08$  on the 12° inducer and 0.075 on the 9° impeller) are not yet fully understood, it seems certain that the upstream

disturbance is not a result of blade stall and centrifugal pumping action. It may be therefore that the resemblance between the present flow and that described by Spannhake is purely coincidental.

#### Overall Performance (Noncavitating)

Pump performance is usually expressed in terms of a dimensionless head coefficient and flow coefficient (see Notation). The noncavitating performance of impellers 2, 3, and 12 is given in Fig. 6. (Recall that the total head was measured at the midpassage position.) The efficiency even under noncavitating conditions is rather low (about 75 percent), by ordinary standards. The excessive passage length, poor flow conditions at the leading edge, and tip clearance leakage all contribute to this low figure.

Several elementary estimates of the pressure rise curve were made, none of which were wholly successful. One of these is shown in Fig. 6 for the 9° impeller. It was obtained by assuming that the root-mean-square radius was typical for the machine, by assuming that there is perfect guidance of the flow by the blades, by accounting for blockage due to vane thickness, and by subtracting off a "friction" loss based on an equivalent number of passage diameters and the relative velocity. At the best efficiency point this estimate is 22 percent high. It would be surprising if such a simple procedure were to work well, since it is known that a helical surface cannot impart a constant total head to all radii and since it is apparent that strong real fluid and tip clearance effects occur. Figure 7 shows a flow survey taken 1.5 diameters downstream of impeller 7 at a flow coefficient of  $\phi = 0.093$  (near the best efficiency point). The local flow coefficient and total head coefficient vary appreciably but smoothly across the channel. The velocity profile and output

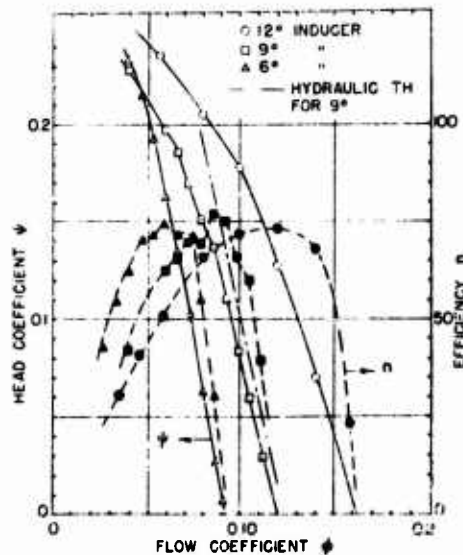


Fig. 6 - Noncavitating efficiency and head coefficient vs flow coefficient for a 6°, 9°, and 12° helical inducer (impellers 12, 3, and 2) and solidity of 2.5

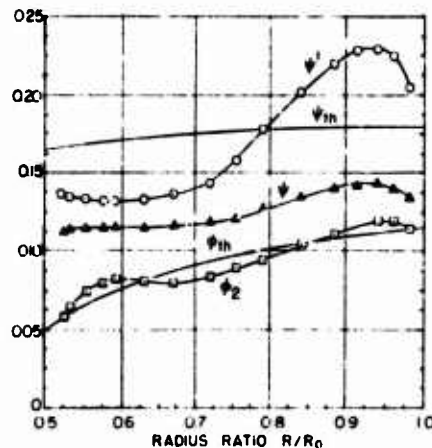


Fig. 7 - Measured axial velocity profile  $\psi$ , measured head coefficient  $\psi$ , measured input head coefficient  $\psi_i$ , theoretical axial velocity, and theoretical head coefficient distributions across the annulus of a 9° helical inducer at a mean flow coefficient of  $\phi = 0.093$

total head coefficient were computed on the basis of the simple radial equilibrium theory of Ref. 10 and are also shown on Fig. 7. (In these calculations, a constant 12-percent blockage of the annulus due to vane thickness was assumed.) The observed axial velocity profile follows the theoretical trend adequately but there is a great departure of the observed  $\psi'$  curve from the radial equilibrium value. We are not able to explain fully the reasons for the wide discrepancy except to remark that tip clearance leakage and the three-dimensional flows that undoubtedly take place violate the assumptions of perfect guidance and lossless relative flow used in the radial equilibrium computations. These effects are so pronounced at a flow coefficient only 7 percent lower (i.e.,  $\phi = 0.087$ ) that the axial velocity profile is nearly linear and is zero at the hub. At lower flow coefficients reverse flow is measured at the hub verifying the type of flow pattern shown in Fig. 5. For these conditions the simple radial equilibrium theory fails.

The flow-rate coefficient computed from the downstream velocity survey agreed satisfactorily with the measured value for a flow coefficient of 0.093 and higher. As a check on the electrical measurement of power input to the impeller, the torque was computed from the angular momentum measurements of Fig. 7. The agreement between these two methods was excellent (within 5 percent). In common with other investigations (11), an increase in tip clearance is found to decrease the maximum efficiency of the impellers, to reduce the head coefficient, and to increase the torque required. Over the range of tip clearances shown in Table 1, the maximum efficiency is reduced by 25 percentage points, and the head is reduced by 20 percent. Somewhat surprising is the finding that the head coefficient is nearly a linear function of the solidity at a given flow rate. For example (see Fig. 17), when the solidity is increased from unity to 3.25 the head coefficient at a flow coefficient of  $\phi = 0.093$  increases from 0.083 to 0.12 or an increase of about 45 percent. A detailed explanation of this phenomenon must await further experiment since according to two-dimensional unseparated cascade flow theory, substantially all of the guiding effect of a flat plate blade row is achieved when the solidity is about unity.

#### Performance During Cavitation

It is convenient when making cavitation tests to maintain the flow geometry and hence the flow coefficient constant and observe the change in head as a function of a cavitation parameter. In the pump and turbine literature the customary cavitation index is the "suction specific speed," a quantity closely related to the more familiar cavitation number, which may be converted into the suction specific speed ( $S$ ) by means of the formula in the Notation section. The total-head output of impellers 2, 3, 12 as a function of cavitation number was determined as discussed above and is shown in Fig. 8. A common feature of all of these curves is that the head is essentially unaffected until the cavitation number is 0.1 or less. Even then, the head drops off only slowly (except for the low flow rates) until a cavitation number is reached at which a further decrease causes the very rapid decrease in performance known as cavitation breakdown. As mentioned previously, limitations of the circuit prevented obtaining breakdown for all conditions. However, some definite breakdown points are shown in Fig. 8 and even for those flow rates when no sharp decrease occurs, at the minimum value of  $k$  shown, breakdown is imminent.

These diagrams show that extremely low cavitation numbers can be achieved (in the order of 0.03) for all impellers, so that suction specific speeds in the range 25,000 to 30,000 can be readily achieved (although at the risk of cavitation damage). However, these plots do not reveal the interesting and complicated flow patterns that develop as cavitation takes place. To illustrate these points, a number of photographs of the 12 impeller will be used. The first series (Fig. 9) shows the impeller



# Experimental Study of Cavitation Inducers

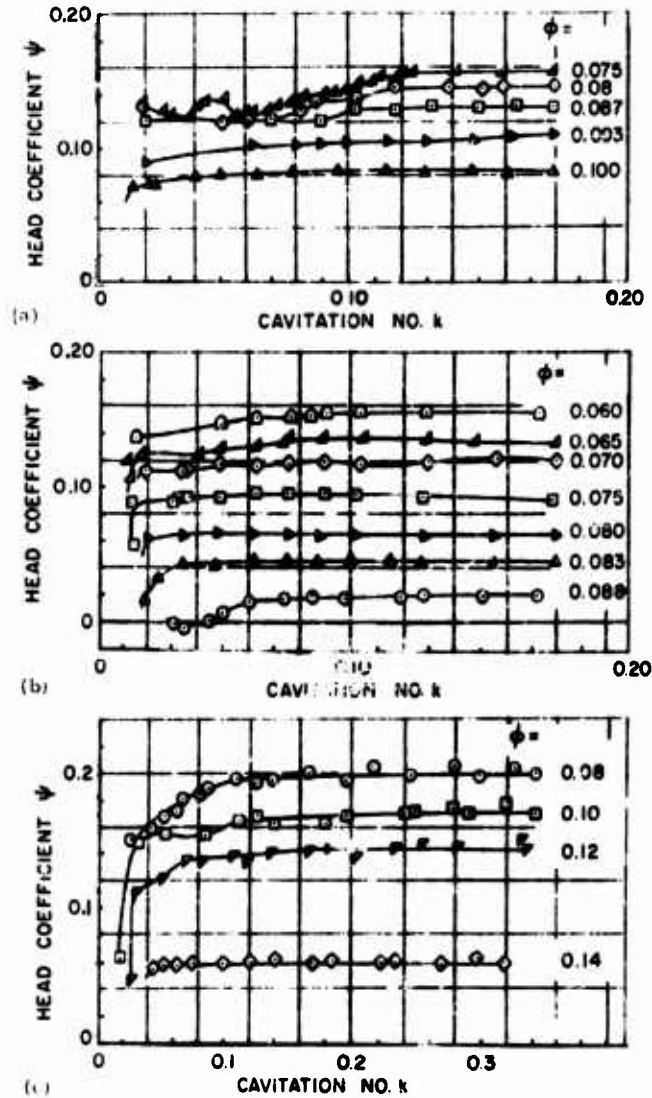


Fig. 8 - Cavitation performance of a series of helical inducers of 2.5 solidity and 0.5 hub ratio; (a) 12° inducer (impeller 2), (b) 9° inducer (impeller 3), (c) 6° inducer (impeller 12)

operating at a flow coefficient in the good efficiency range ( $\phi = 0.12$ ) as the inlet pressure or cavitation number is lowered. A patch of cavitation is seen at the blade tip in Fig. 9 that grows as the pressure is lowered until at  $k = 0.02$  it is about 3/4 as long as the blade. The cavitation bubble is never clear, as it is on a sharp-edge hydrofoil in a water tunnel, but always has a frothy appearance. Close inspection shows that the greatest part of the fuzzy cavitation patch arises from a tip clearance flow similar to that reported in Ref. 12. The cavitation is confined largely to the outer portions of the annulus, but at the lowest cavitation numbers it does occur from root to tip. The development shown in Fig. 9 satisfies one's intuitive idea of the growth of cavitation but at other flow coefficients the sequence is entirely different as for example those in Figs. 10, 11, and 12. In Fig. 10 ( $\phi = 0.14$ ) we see every other blade cavitating. This arrangement is stable and it does not always occur on the same blades. At lower flow rates, the alternate blade cavitation appears to propagate from blade to blade in much the same way as propagating stall in a cascade. The frequency of propagation depends upon the cavitation number, being high at high  $k$ 's

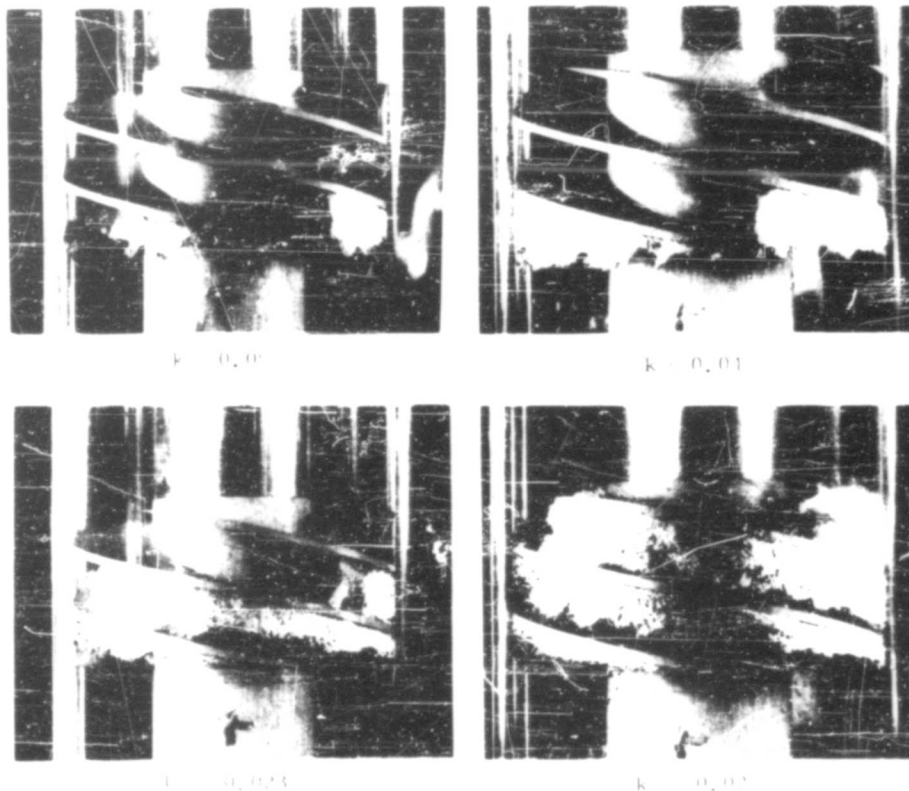


Fig. 9 - Development of cavitation in a 12° helical inducer for a flow rate coefficient  $\phi = 0.12$ . (These photographs are not strictly in a sequence since they were taken at different times and rotative speeds.)

# Experimental Study of Cavitating Inducers



Fig. 10 - Cavitation on the 12° inducer at a flow coefficient of  $\lambda = 0.14$ , showing the occurrence of alternate blade cavitation

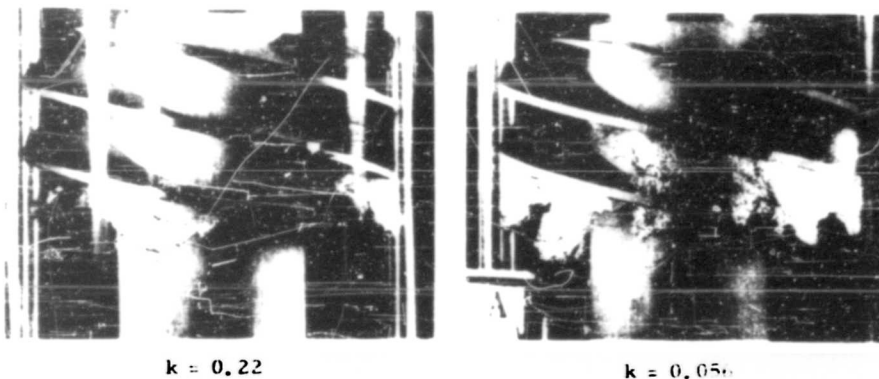


Fig. 11 - Cavitation on the 12° inducer at a flow coefficient of  $\lambda = 0.10$ . The confused flow pattern at the lower cavitation number is typical of nonsteady oscillating cavitation.

and decreasing to zero frequency just before cavitation breakdown.\* In this regime blade forces can be quite high and the various mechanical parts of the pump assembly can be easily excited to resonance. It is difficult to show the state of the flow in this "oscillating cavitation" condition but Fig. 11 gives some idea of the disturbed flow present. At even lower flow rates the back-flow phenomena illustrated in Fig. 5 gives rise to a spectacular vortical flow (Fig. 12). Even this peculiar flow pattern is able to achieve very low cavitation numbers (shown at breakdown in the last of this sequence).

\*The occurrence of these phenomena had been pointed out to the author by Dr. Toru Iwata in 1955.

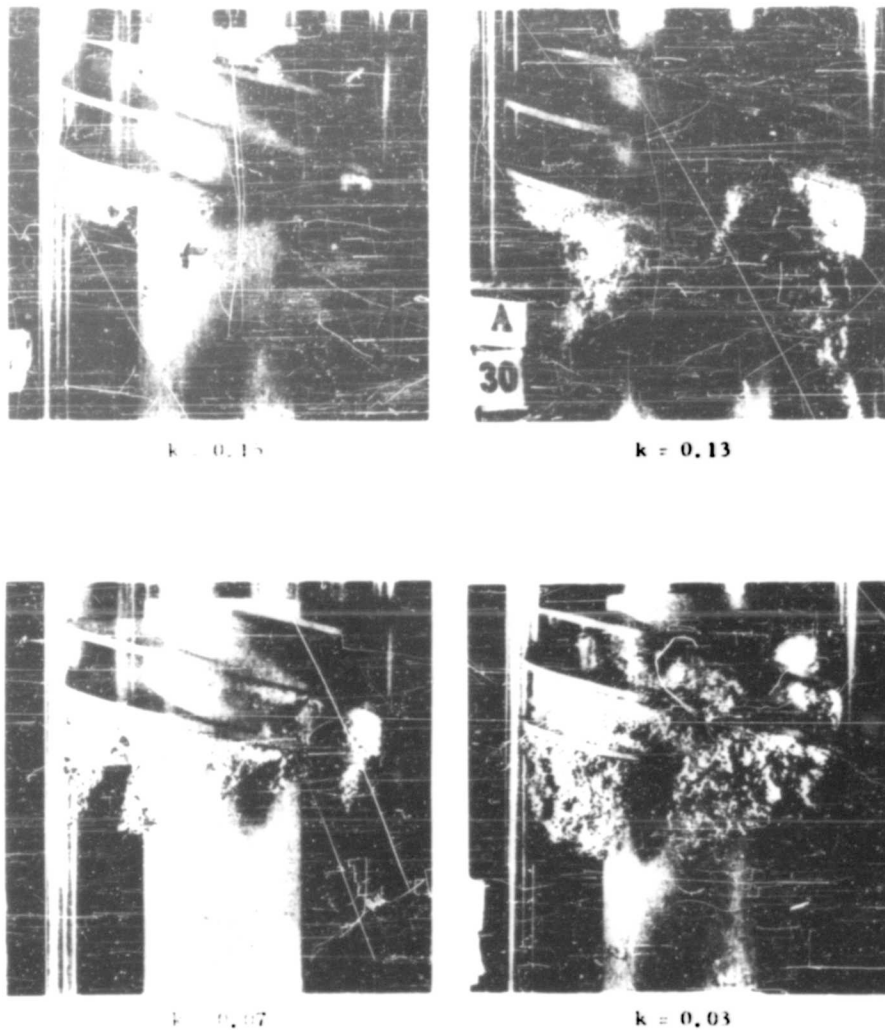


Fig. 12 - Cavitation development at a flow coefficient of  $k = 0.08$  on the  $12^\circ$  inducer

A diagram showing the location of these various regions is shown in Fig. 13. The boundaries of these regions are not sharply defined and depend to a considerable extent on the details of the leading edge design and somewhat on the tip clearance. However, it is typical of all of the helical inducers studied. The outlines of the oscillating cavitation region are also shown in Figs. 8b and 8c for the other blade angles.

# Experimental Study of Cavitating Inducers

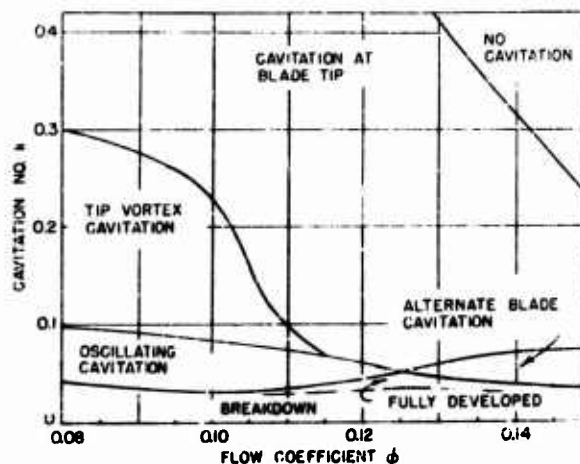


Fig. 13 - The various modes of cavitating flow in a 12° helical inducer as a function of cavitation number and flow coefficient

From these diagrams we see that most applications for highly cavitating inducers will be subject to this phenomenon, and accordingly some effort was made to find simple modifications of the impeller that would suppress it. Three were tried: (a) increasing the tip clearance, (b) changing the leading edge contour of the impeller and (c) varying the lead of the impeller blades from inlet to discharge. Increasing the tip clearance offered some help (in preventing oscillating cavitation) but at the expense of cavitating performance and overall efficiency. No extensive leading edge modifications were carried out, but the one tried which consisted of making the leading edge of the blade surface a spiral rather than a radial line, depressed the occurrence of oscillating cavitation to lower cavitation numbers and also improved the cavitation performance! In the last attempt an impeller was constructed with a blade angle of 6° at the inlet and 9° at the discharge and with a solidity of 2.5. The overall performance was similar to the 9° impeller and the cavitation performance was similar to the 6° impellers (although not quite as good), but the extent and severity of the oscillating mode was greatly reduced. The foregoing remarks imply that this zone is to be avoided at all cost. This is believed to be the case only for mechanical reasons, since there is no hydraulic reason to do so.

It has already been mentioned that increased tip clearance tends to reduce hydraulic performance. The same result is also found to be true when cavitation occurs, as Fig. 14 shows. According to the present results the smallest possible tip clearance gives the best cavitation performance. Even so, impressively low  $k$ 's are still achieved with the largest clearance used, although at greatly reduced output. (It should be mentioned here that there is probably no particular merit in making the tip clearance dimensionless with the blade thickness since for the ranges of Reynolds number used inertial forces prevail in the gap, and the rotor radius is then a better characteristic length (11).) Photographs taken of cavitation with the largest tip clearance suggest that the increased tip clearance flow that takes place gives rise to large disturbances in the outer portions of the passage that cavitate prematurely and thereby lower the output head.

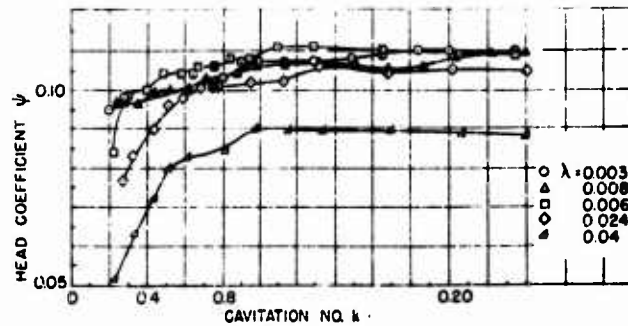


Fig. 14 - The effect of tip clearance on the cavitating performance of a 9° inducer with a solidity of 2.5 at a flow coefficient near the best efficiency point ( $\lambda = 0.093$ ). The solid symbols indicate inception of oscillating cavitation.

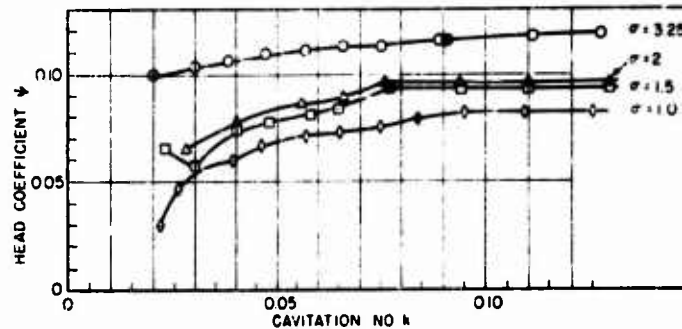


Fig. 15 - The effect of solidity on the cavitating performance of a 9° helical inducer at a flow coefficient of  $\lambda = 0.093$ . The solid symbols denote inception of oscillating cavitation.

The effect of solidity on cavitation performance is shown in Fig. 15. It is somewhat surprising that extremely low cavitation numbers can be achieved with a solidity as low as unity. However, the head had dropped off by a factor of three at the minimum  $k$  of 0.02 for  $\sigma = 1$ , whereas for  $\sigma = 3.25$ , the head had only decreased by 20 percent at the same  $k$ .

Some velocity profile measurements were also obtained during cavitating flow for a 9° impeller (No. 7) to see if significant changes occurred in the distributions of Fig. 7. Interestingly enough it was found that cavitation improved the axial velocity profile. The distribution of total head across the passage remained about the same although, of course, lower. At flow coefficients ranging over the efficiency peak of this impeller, and at all cavitation numbers, cavitation decreased the torque of the impeller as found from the velocity surveys. The efficiency, however, still decreased with decreasing  $k$ .

## DISCUSSION

## Cavitation Breakdown

One of the intentions of this work was to correlate the breakdown cavitation number with the impeller geometry. From the foregoing remarks it is seen that while there are examples of clearcut cavitation breakdown, both the limitation of the equipment and phenomenon itself do not always allow such a black-and-white distinction to be made. Nevertheless, many points at cavitation numbers below which operation was not practical were observed—both visually and with measurements. In all of the cases where breakdown had either occurred or was imminent, the length of the cavitation region was between 75 and 100 percent of the blade chord. In no case did the cavitation region extend beyond the chord before breakdown had occurred. The reason for this is quite clear since before breakdown the increase in the total head (and hence static pressure) is of the order of 10-15 percent of the tip velocity head. This pressure is much higher than the inlet pressure and is responsible for collapsing the cavity. But for this pressure rise and hence total pressure rise to exist, a peripheral velocity  $W_u$  of about 10-15 percent of the tip speed must be imparted to the flow. From Fig. 16 it is seen that a whirl velocity of this magnitude cannot be obtained with a high solidity cascade of flat plates if the leaving relative velocity is comparable to the velocity on a cavity boundary (i.e., greater than the inlet velocity).

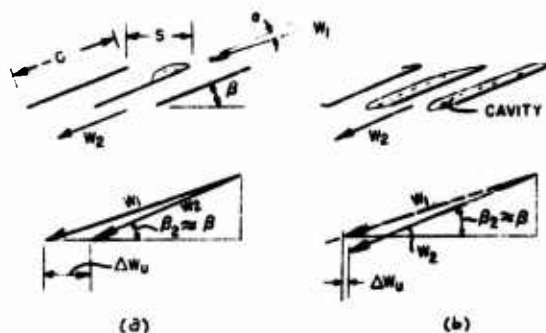


Fig. 16 - Velocity triangles in a flat plate cascade  
(a) without and (b) with extensive cavitation

The question then arises as to whether we can make a reasonable estimate of the cavitation number when the cavitating region is nearly as long as the chord. We will certainly have to exclude flow-rate coefficients less than the maximum efficiency point to rule out the strong three-dimensional effects seen in Fig. 12. For similar reasons impellers with large tip clearance will have to be excluded. Even then from the analysis of noncavitating results (Fig. 7), the main flow through the impeller is not frictionless nor wholly two-dimensional. Even so, correlations based on theory would be useful to have, even if they are ultimately empirical. For this purpose it was assumed that the flow through the helical impeller was equivalent to the flow through a two-dimensional cascade of flat plates with a streamline springing free at the leading edge and forming a partial cavity of length less than the chord. Now it is known that the linearized free streamline theory does not provide a solution to the problem of the partial cavity on an isolated plate when the cavity length is a reasonable fraction of the chord (12). Consequently, the view was taken that as far as the growth of the cavity in an inducer of high solidity is concerned, the most

significant length is the circumferential spacing between the blades. The length of the blades was then taken as infinite compared with the spacing and the growth of a partial cavity in such a cascade was carried out by exact and linearized free streamline methods.

The results of both methods agreed well except for large cavitation numbers where the limitations of the linearized theory were exceeded. Values of cavity length vs cavitation number were also calculated (by the linearized theory) for a cascade geometry equivalent to the mean radius of the  $9^\circ$  impeller at a flow coefficient of  $\psi = 0.093$ , and the results of this calculation are shown in Fig. 17. Also plotted in Fig. 17 are approximate lengths of the cavity as determined by visual measurements. The agreement is hardly overwhelming but several points are worth mentioning: (a) the general trend of both curves is the same although a systematic difference for small lengths and high  $k$ 's is found; (b) the minimum cavitation number is reached very soon after the ratio of cavity length to spacing is  $1-1/2$ , thereby indicating that excessively high solidities are unnecessary; and finally (c) our empirical observation is that for practically all the flow rates and impellers tested ( $6^\circ$ ,  $9^\circ$ , and  $12^\circ$ ) the minimum cavitation number reached before breakdown was less than two times the minimum cavitation number possible in a given cascade with a given angle of attack. In the present example the minimum is the asymptote of the curve shown in Fig. 17. The value of this asymptote can be obtained quite simply from elementary momentum considerations when it is recalled that there is no net force parallel to the plate and that the cascade is sufficiently long so that the flow is perfectly guided (see also Ref. 13). The result of this calculation is that the minimum cavitation number achievable in a cascade of infinitely long flat plates is  $k \approx \alpha(\beta - \alpha)$  where  $\alpha$  and  $\beta$  are the local angle of attack and blade angle respectively (both of these values to be small). This relation has a maximum of  $\beta^2/4$  and is zero at  $\alpha = 0$  and  $\alpha = \beta$ . The first

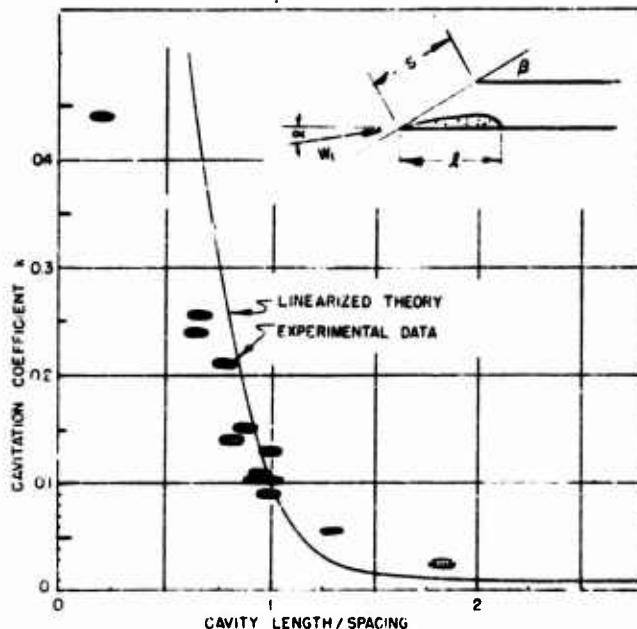


Fig. 17 - Growth of a partial cavity in a cascade as a function of cavitation number. The angle of attack and blade angle correspond to the mean radius of the  $9^\circ$  impeller at a flow coefficient of  $\psi = 0.093$ .



result follows from the assumed zero thickness of the blades, and the latter, although perhaps surprising, only occurs when there is zero flow through the blade row. This formula also shows that smaller blade angles are better for obtaining lower cavitation numbers and this conclusion is qualitatively borne out by the present experiments.

The present calculations, although crude, account for the trends in breakdown occurrence, at least for sufficiently high solidities and flow rates where the flow is predominantly two dimensional. Further work along these lines employing more elaborate models will be reported in the future.

#### Cavitation Similitude

In the absence of friction or body forces the cavitation number determines the location and extent of cavitation on a body. The only question is, What is the pressure in the cavity? In the present experiments the cavity pressure was assumed to be the vapor pressure of the bulk fluid, since it was not possible to measure it directly. This assumption cannot be right since in a fluid containing dissolved air, the cavity pressure can exceed the vapor pressure by the amount of the air diffused into the cavity. This possibility was investigated by removing the impeller and blocking the annulus of the test section to a sufficient extent to create a cavity behind a small lamina. The pressure in the cavity was found to be 20 to 25 percent higher than the vapor pressure of the fluid, (the air content in the water was the same as that in the inducer tests) confirming similar experiments of Parkin and Kermeen (13). We suspect therefore that the cavitation numbers listed in the present report are too high, but in lieu of direct measurement we have preferred to base them on the equilibrium vapor pressure of the liquid. Of course in pure liquids with no dissolved air (e.g., liquid oxygen) the pressure may be less than the vapor pressure of the bulk fluid due to thermal effects in evaporating the liquid to fill the cavity. It is known, for example, that cavitation performance in liquid oxygen is better than that in tap-water and it is almost certainly for this reason. At present several groups are working on this problem but no conclusive results are available yet.

#### Further Remarks

There are a number of difficult problems that remain to be solved before the understanding of cavitating flows in rotating machines is well in hand. They are, in fact, nearly too numerous to mention, for in addition to embracing the unknowns of the turbomachine field, the many effects of cavitation are included. Nevertheless, with the aid of a few rules of thumb and some empirical data such as that presented herein, an inducer can be designed for a specific application with a minimum of development. Thus even with our imperfect understanding of the cavitating flow through machines, the pumping of liquids at extremely low ambient pressures offers no insuperable problems.

#### ACKNOWLEDGMENT

A great part of the experimental work was done by Lt. H. J. Nawoj, U.S.N., and Capt. S. H. Carpenter, U.S.M.C. The author would like to acknowledge his debt to them and to the skillful talents of Mr. J. R. Kingan. This work was supported by the Office of Naval Research.

# NOTATION

$c$  = chord

$h$  = head (ft of water)

$k$  = cavitation number =  $(p_1 - p_k)/(\rho W_1^2/2)$

$N$  = rpm

$p$  = pressure

$r$  = radius

$s$  = spacing between blades

$S$  = suction specific speed =

$$\frac{N \sqrt{gpm}}{(h_{t1} - h_v)^{3/4}} = 8140 \sqrt{1 - \left(\frac{r_i}{r_o}\right)^2} \left/ \left[ (1 + \psi)^2 k + \psi^2 \right]^{3/4} \right.$$

where  $gpm$  is the flow rate in gallons per minute

$U$  = tip speed ( $r\omega$ )

$V$  = absolute velocity

$w$  = relative velocity

$\alpha$  = angle between blade chord and inlet relative velocity

$\beta$  = blade angle measured from plane of rotation

$\eta$  = efficiency

$\lambda$  = ratio of tip clearance to blade height

$\rho$  = density

$\sigma$  = solidity =  $c/s$

$\phi$  = flow coefficient = average axial velocity /  $U_o$  except as noted

$\psi$  = measured total head coefficient =  $gh_t / U_o^2$

$\psi'$  = input head coefficient =  $r(V_{u2} - V_{u1}) / r_o U_o$

$\omega$  = angular speed

# Experimental Study of Cavitation

## Subscripts

- 1. Free stream
- 2. Free stream
- 3. Free stream
- 4. Free stream
- 5. Free stream
- 6. Free stream
- 7. Free stream
- 8. Free stream
- 9. Free stream
- 10. Free stream
- 11. Free stream
- 12. Free stream
- 13. Free stream
- 14. Free stream
- 15. Free stream
- 16. Free stream
- 17. Free stream
- 18. Free stream
- 19. Free stream
- 20. Free stream
- 21. Free stream
- 22. Free stream
- 23. Free stream
- 24. Free stream
- 25. Free stream
- 26. Free stream
- 27. Free stream
- 28. Free stream
- 29. Free stream
- 30. Free stream
- 31. Free stream
- 32. Free stream
- 33. Free stream
- 34. Free stream
- 35. Free stream
- 36. Free stream
- 37. Free stream
- 38. Free stream
- 39. Free stream
- 40. Free stream
- 41. Free stream
- 42. Free stream
- 43. Free stream
- 44. Free stream
- 45. Free stream
- 46. Free stream
- 47. Free stream
- 48. Free stream
- 49. Free stream
- 50. Free stream
- 51. Free stream
- 52. Free stream
- 53. Free stream
- 54. Free stream
- 55. Free stream
- 56. Free stream
- 57. Free stream
- 58. Free stream
- 59. Free stream
- 60. Free stream
- 61. Free stream
- 62. Free stream
- 63. Free stream
- 64. Free stream
- 65. Free stream
- 66. Free stream
- 67. Free stream
- 68. Free stream
- 69. Free stream
- 70. Free stream
- 71. Free stream
- 72. Free stream
- 73. Free stream
- 74. Free stream
- 75. Free stream
- 76. Free stream
- 77. Free stream
- 78. Free stream
- 79. Free stream
- 80. Free stream
- 81. Free stream
- 82. Free stream
- 83. Free stream
- 84. Free stream
- 85. Free stream
- 86. Free stream
- 87. Free stream
- 88. Free stream
- 89. Free stream
- 90. Free stream
- 91. Free stream
- 92. Free stream
- 93. Free stream
- 94. Free stream
- 95. Free stream
- 96. Free stream
- 97. Free stream
- 98. Free stream
- 99. Free stream
- 100. Free stream

1. Birkhoff, G., Giesse, W., and ... "Flow-I," ...
2. Betz, ... "rahlen," ...
3. Sutton, G.P., "Rocket Propulsion Elements," 2nd ed., New York: Wiley, 1956, p. 252
4. Zimmerman, J.E., "Effect of ... Performance on Liquid Propellant Rocket ... report No. 79-52 (1952)
5. Drumfield, R.C., "A Study ... for Blade Cavitation Parameters," U.S. ... 61
6. Ross, C.T., "Pump ... Design," J. Rocket Soc., March 1951
7. ... "Aspects of High-Section-Specific-Speed ... 1713 (1956)
8. Knapp, P.T., ... J.F. and Brown, F.P., "The Hydrodynamics Laboratory, ... Institute of Technology," Trans. ASME 70:437 (1948)
9. Spanner, ... "Propellers," Cambridge: M.I.T. ... 193
10. Bowen, J., Sabersky, H., ... "Theoretical and Experimental Investigations of Axial Flow ... California Institute of Technology, ... Report, 1948
11. ... "The Clearance Flows ... and Pumps," ... California Institute of Technology, ... Report ... 1955
12. ... "Note on Partial Cavitation ... California Institute of Technology, Hydrodynamics Laboratory Report ... 19-9, 1955
13. ... and Kermeen, R.W., "Water ... Techniques for Force Measurements on Cavitating Hydrofoils," J. Ship Research (No. 1):36 (1957)

## DISCUSSION

T. Iura (Space Technology Laboratory)

I wish to supplement Dr. Acosta's results with some data obtained three years ago in the inducer test facility at Rocketdyne.

The cavitation patterns observed with helical inducers were similar to those described by Dr. Acosta. For inducers with four blades, at a given flow coefficient, a reduction in cavitation number produced the following sequence of cavitation behavior:

1. Initial cavitation - equal on all blades at the blade tips
2. Alternate blade cavitation - stable patterns on alternate blades
3. Oscillating or propagating cavitation
4. Fully developed cavitation - equal on all blades.

Figure D1, a cavitation performance curve of a 16.2-degree helical inducer, illustrates the cavitation regimes mentioned. The alternate blade and unstable cavitation patterns were most pronounced at the flow rates below the maximum-efficiency point while stable alternate blade cavitation pattern was not observed on inducers with an odd number of blades; asymmetric unstable patterns were in evidence between the initial and fully developed invitation regimes. The oscillating cavitation consisted

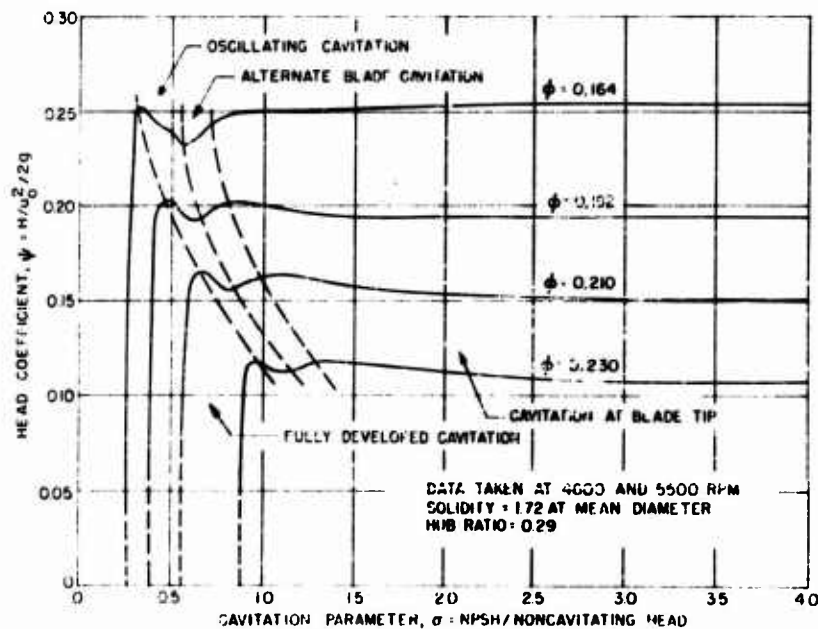


Fig. D1 - Cavitation performance of 16.2-degree (at tip) four-bladed helical inducer

of the cavitation pattern oscillating along the blade length in a highly erratic manner. In one case (for a 11.2-degree helical inducer) a definite propagation pattern was observed. The propagation speed, based on observations of high speed movies, was about one-tenth of the inducer rotative speed.

In regard to vibration accompanying inducer cavitation, Fig. D2 gives a qualitative picture of the vibration levels obtained with a 14.6-degree helical inducer. The measurements were made with a vibration pickup mounted on the test section. As the cavitation number (or net positive section head) is lowered, the vibration increases steadily through the first three zones of cavitation. The maximum vibration level occurs just prior to fully developed cavitation after which it decreases rapidly due to bubbles collapsing in midstream rather than against the blade surfaces.

In Fig. D3, the dimensionless breakdown NPSH (net positive suction head) is plotted as a function of the mean-diameter helix angle for various angles of attack. The breakdown NPSH is defined here as that value of NPSH at which the inducer head has completely dropped to zero. These data were obtained from tests of seven inducers ranging in tip solidity from 1.07 to 2.44. It was found that the breakdown NPSH was rather insensitive to solidity, although the rate of head drop-off was quite sensitive to solidity as pointed out by Dr. Acosta. Along with the breakdown NPSH data, the theoretical calculations based on Betz-Petersohn's two-dimensional analysis are plotted. The theoretical breakdown curve has the same slope as the experimental data, but falls considerable below the actual results. Although the trend of breakdown is indicated by the two-dimensional model, there certainly is a need for the more elaborate models mentioned by Dr. Acosta and for a three-dimensional model.

Figure D4 shows the maximum inducer efficiency as a function of solidity, and Fig. D5 shows the cavitation parameter corresponding to the maximum-efficiency points plotted as a function of solidity.

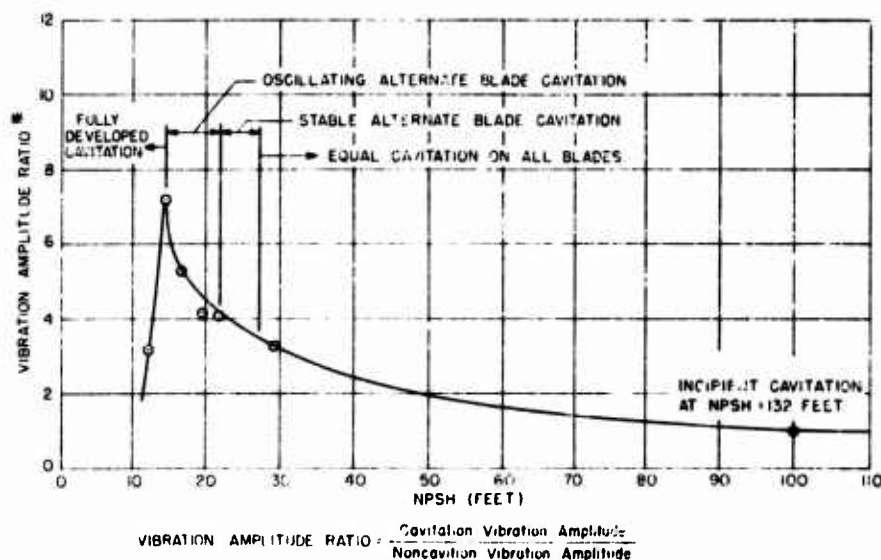


Fig. D2 - Cavitation vibration data of 14.6-degree helical inducer (amplitude measurements with vibration pickup on test section)

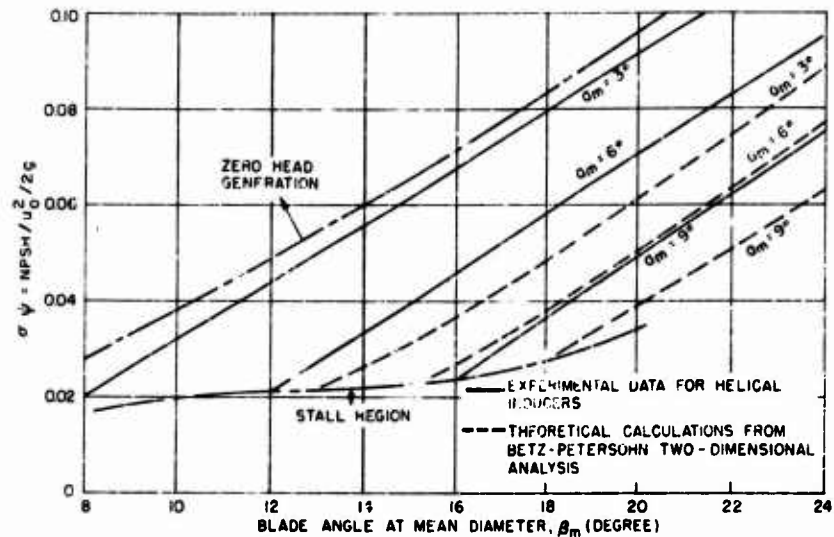


Fig. D3 - Cavitation head-breakdown characteristics of helical inducers: comparison of theory and experimental results

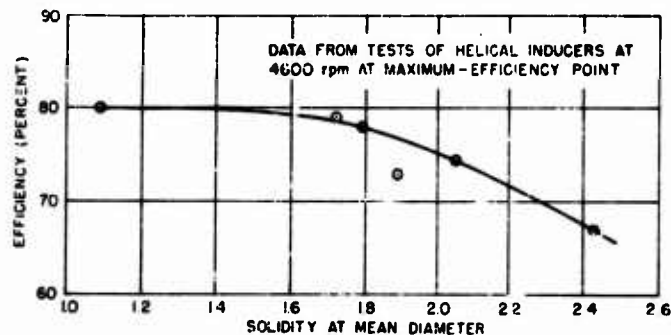


Fig. D4 - Effect of solidity on inducer efficiency

In regards to cavitation similitude, tests at Rocketdyne on centrifugal pumps with inducers show that cavitation performance in liquid oxygen is better than that in water, and in liquid nitrogen is better than that in liquid oxygen. For a given type of pump, the critical NPSH (one percent head drop-off point) in water was 1.3 times that in liquid oxygen and 1.9 times that in liquid nitrogen. However, these values are dependent on inlet conditions such as flow rate and design blade angle. With the inducer taken out of the same centrifugal pump, tests between water and liquid oxygen no longer showed a consistent difference in cavitation performance.

If one calculates the comparative vapor-bubble growth rates from Plesset and Zwick's theory (for superheated liquid), it is found that water has 10 times the growth

## Experimental Study of Cavitating Inducers

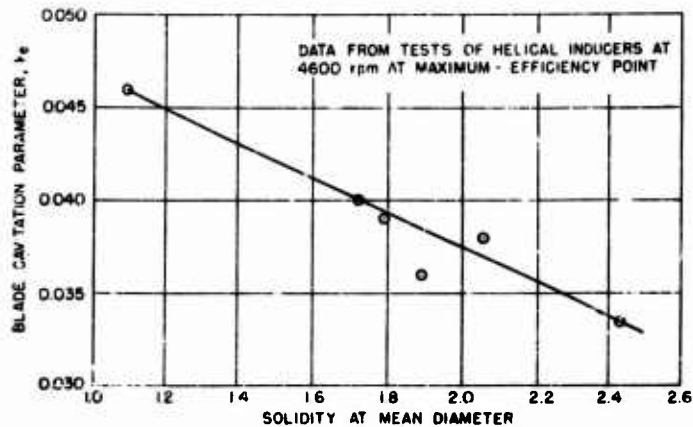


Fig D5 - Effect of solidity on blade cavitation parameter

rate of liquid oxygen or liquid nitrogen. However, Plesset's theory does not show much difference between the growth rate of liquid oxygen and liquid nitrogen. Clearly, some theory is needed to correlate the thermodynamic properties of the liquid with the dynamic features of the pump flow in order to explain the different behavior in various fluids.

### A. J. Acosta

It is clear that many organizations, such as Rocketdyne and Aerojet-General Corporation, have been actively working in this field for some time to good effect. I regret that they have not previously found opportunity to present their results. To some degree perhaps, the present paper may assist in bringing their work out.

It is gratifying that many of the observations made by Dr. Iura, evidently on larger experimental apparatus, verified in a general way our findings at the California Institute of Technology.

\* \* \* \* \*

# **A GENERAL LINEARIZED THEORY FOR CAVITATING HYDROFOILS IN NONSTEADY FLOW**

R. Timman

*Technische Hogeschool, Netherlands*

## **1. INTRODUCTION**

Since the exact theory of cavitating hydrofoils is rather complicated for fluid bodies, a linear theory will be developed which is assumed to be applicable to the bodies of small thickness ratio, such as propeller blades or thin hydrofoil, which prevail in most applications in naval architecture.

In particular the case of a nonuniform motion is considered here, which is important for vibrating motion as well as for the motion of a hydrofoil in a nonuniform field of flow.

The underlying assumptions can be stated as follows:

(a) The motion is two-dimensional, the hydrofoils move with velocity  $U$  in the direction of the negative  $x$ -axis.

(b) The fluid is considered incompressible and nonviscous as long as the pressure exceeds the vapor pressure  $p_v$ . If it reaches this value, the density abruptly falls off to zero, thus causing a cavity, on the surface of which the pressure has the value  $p_v$ , corresponding to vapor.

(c) The motion of the hydrofoil causes a small disturbance. Here both the thickness ratio of the hydrofoil as well as the amplitude of its nonsteady motion are of the same (small) order of magnitude.

(d) The motion of the fluid is irrotational outside the hydrofoil and its wake, which extends along the part of the  $x$ -axis which lies behind the hydrofoil.

It is further assumed that the disturbance created by the hydrofoil dies out at infinity, except eventually in the wake. This means that the pressure, which is continuous in the wake, must vanish at infinity.

Based on these assumptions the mathematical problem can now be formulated. The hydrofoil is assumed to extend along the segment  $-l \leq x \leq +l$  of the  $x$ -axis.



Its motion is given by

$$\begin{cases} y = h^+(x, t) & -l \leq x \leq +l & \text{upper side} \\ y = h^-(x, t) & & \text{lower side} \end{cases}$$

The cavity is assumed to extend only over a part of upper side of the hydrofoil, extending from  $x = -l$  to  $x = +c$ . Along this part the pressure has the constant value  $p_v$ . On the remaining part of the hydrofoil contour the fluid wets the surface. Since viscosity is neglected, the boundary condition is simply that the total normal velocity of the fluid must be equal to the normal velocity of the hydrofoil.

The moving hydrofoil creates a disturbance field with velocity components  $(u, v)$ . The linearized condition then gives on the wetted part of the hydrofoil

$$v = h_t + U h_x = w(x, t), \quad (1.1)$$

where  $w(x, t)$  is a known function of  $x$  and  $t$ . (Subscripts denote partial differentiation.)

In order to derive the boundary condition on the cavity in terms of the velocity, we remark that the flow is assumed to be irrotational outside the hydrofoil and the wake. Thence a velocity potential  $\phi$  exists which is related to the pressure by Bernoulli's law.

$$\phi_t + \frac{1}{2} \{(U + u)^2 + v^2\} + \frac{p}{\rho} = \frac{1}{2} U^2 + \frac{p_0}{\rho}, \quad (1.2)$$

which, in the linearized theory takes the form

$$\phi_t + U u = \frac{p_0 - p}{\rho}. \quad (1.3)$$

The velocity potential satisfies in an incompressible fluid Laplace's equation

$$\Delta \phi = 0 \quad (1.4)$$

and, since Eq. (1.3) is linear, we can introduce a pressure or acceleration potential  $\psi$ .

$$\psi = \frac{p_0 - p}{\rho}, \quad (1.5)$$

equally satisfying

$$\Delta \psi = 0. \quad (1.6)$$

Now the boundary value problem can be posed for the velocity potential  $\phi$  or for the acceleration potential  $\psi$ . Since the latter is regular in the complete plane outside the hydrofoil (the pressure is continuous in the wake), it is somewhat easier in the first stage of the problem to formulate the problem for the acceleration potential. It is, however, to be remarked here, that for an unsteady motion the length of the cavitation bubble depends on the time. The acceleration potential  $\psi$  is related to the velocity potential  $\phi$  by

$$\psi = \phi_t + U \phi_x. \quad (1.7)$$

From the condition for the velocity  $v = \phi_y$  we find on the wetted part of the hydrofoil:

$$\begin{aligned} c < x < l, \quad y = +0, \\ -l < x < l, \quad y = -0, \\ \phi_y = t_y + U \phi_{xy} = w_t + U w_x, \end{aligned} \quad (1.8)$$

On the cavity  $-l < x < c, y = +0$ , the pressure is the vapor pressure and hence

$$\phi = \frac{p_x - p_v}{\rho} = c, \quad (1.9)$$

where  $c$  has a constant positive value.

Since  $\phi$  must be a harmonic function, there are different methods available for the solution of this problem, e.g., Mushkelishvili's method of singular integral equations. In this paper a function of Green is introduced, which can be used to find a solution to this boundary value problem.

## 2. REGULAR SOLUTION TO THE BOUNDARY VALUE PROBLEM FOR THE PRESSURE POTENTIAL

Recapitulating the boundary value problem for the pressure potential:

$$\begin{aligned} \phi = c, \quad -l < x < c, \quad y = +0, \\ \phi_y = w(x, t) = c + x + t, \quad -l < x < l, \quad y = -0, \end{aligned} \quad (2.1)$$

and

$$\Delta \phi = 0.$$

We can solve this problem by the introduction of a Green's function

$$G_p(x, y; x_p, y_p).$$

This function is a solution of the nonhomogeneous equation

$$\Delta G_p = \delta(x_p, y_p) \quad (2.2)$$

(where  $\delta(x_p, y_p)$  is Dirac's  $\delta$ -function for the plane), which satisfies the boundary conditions

$$\begin{aligned} G_p = 0, \quad -l < x < c, \quad y = +0, \\ \frac{\partial G_p}{\partial y} = 0, \quad c < x < l, \quad y = +0, \\ -l < x < l, \quad y = -0. \end{aligned} \quad (2.3)$$

$G$  is regular at infinity.

Then, applying Green's theorem to the outer region of the hydrofoil, we obtain

$$\begin{aligned}\psi_p &= \frac{1}{2\pi} \int \left( \psi \frac{\partial G_p}{\partial n} - G_p \frac{\partial \psi}{\partial n} \right) ds \\ &= \frac{1}{2\pi} \left\{ \int_{-l}^c \left\{ \psi \frac{\partial G_p}{\partial y} \right\} dx + \int_c^l \left( \frac{\partial \psi}{\partial n} \right)^+ G_p dx + \int_l^c \left( \frac{\partial \psi}{\partial n} \right)^- G_p dx \right\}.\end{aligned}\quad (2.4)$$

If we assume that both  $G$ ,  $\partial G/\partial n$ ,  $\psi$  and  $\partial \psi/\partial n$  vanish at infinity of sufficient high order, the point at infinity gives no contribution. Hence, once the Green's function is known, the solution is obtained. This expression for the pressure potential, however, is not unique since, at the singular points  $-l$ ,  $+l$ , and  $+c$  the boundary conditions are not specified. If we put the point  $P$  of the Green's function in one of these points, we obtain a solution of the homogeneous equation, which is regular outside the hydrofoil and does not alter the boundary conditions. Thus we may assume for the total solution

$$\psi_p = \psi_{reg} + A_1 G_1 + A_2 G_2 + A_3 G_3, \quad (2.5)$$

where  $A_1$ ,  $A_2$ , and  $A_3$  are indeterminate constants which must be determined by additional conditions. Since the differential equation is Laplace's equation, Green's function can easily be found by conformal mapping (Fig. 1). At first the physical plane  $z = x+iy$  is mapped on a  $Z = X+iY$  plane.

$$Z = \sqrt{\frac{l-z}{l+z}}. \quad (2.6)$$

Then the hydrofoil  $-l < x < +l$  passes into the  $X$ -axis, and the outer region passes into the lower half plane. The outer region passes into the lower half plane  $Y < 0$  and point  $z = \infty$  into  $Z = i$ . On the hydrofoil we write  $z = x = -l \cos \theta$ , the interval  $0 < \theta < \pi$  corresponding to the upper side, and  $\pi < \theta < 2\pi$  to the lower side. If  $c = -l \cos \gamma$ , this point passes into  $c = \cot \gamma/2$ . For  $x > c$  the boundary condition is  $G = 0$ , for  $x < c$  it is  $\partial G/\partial n = 0$ . By a second mapping

$$\zeta = \xi + i\eta = \sqrt{Z - \cot \frac{1}{2} \gamma}. \quad (2.7)$$

The  $Z$ -plane is mapped into a  $\zeta$ -plane. Where the outer region now occupies the fourth quadrant,  $c$  passes into the origin and  $B$  into the point  $\eta = -\cot 1/2 \gamma$ . Green's function is constructed by a reflection of the pole  $P$  with respect to the axis  $\xi > 0$ ,  $\eta = 0$  and  $\eta < 0$ ,  $\xi = 0$ . Since on the first axis the boundary condition is  $G = 0$ , we must add a pole with negative sign in  $\bar{P} = \xi_p - i\eta_p$  and since on the second the condition is  $\partial G/\partial \xi = 0$  we add here a pole with positive sign. This gives the resulting complex potential

$$G_p + i H_p = \ln \frac{(\zeta - \zeta_p)(\zeta + \bar{\zeta}_p)}{(\zeta - \bar{\zeta}_p)(\zeta + \zeta_p)}. \quad (2.8)$$

# Cavitating Hydrofoils in Unsteady Flow

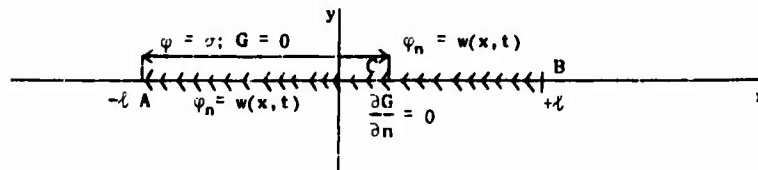


Figure 1

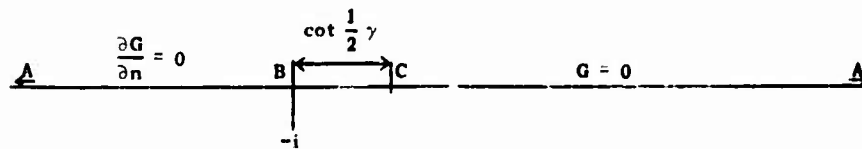


Figure 2

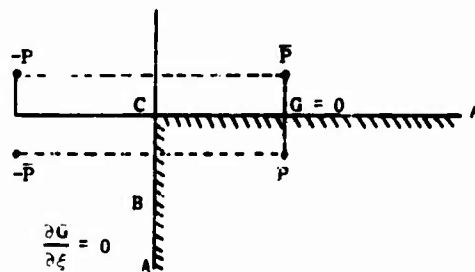


Figure 3

In the formula for the regular solution we need only the value for Green's function on the hydrofoil contour

$$x = -l \cos \mu, \quad x_p = -l \cos \mu_p,$$

$$Z = \cot \frac{1}{2} \mu, \quad Z_p = \cot \frac{1}{2} \mu_p,$$

$$Z = \sqrt{\cot^2 \frac{\mu}{2} - \cot^2 \frac{\gamma}{2}}, \quad Z_p = \sqrt{\cot^2 \frac{\mu_p}{2} - \cot^2 \frac{\gamma}{2}}.$$

The contribution of the first part in the integral in Eq. (2.4) can be evaluated easily by the use of the Cauchy-Riemann equations

$$\frac{\partial G_p}{\partial y} = -\frac{\partial H_p}{\partial x} \quad (2.9)$$

since  $G_p$  and  $H_p$  are conjugate harmonic functions. This gives

$$\frac{1}{2\pi} \int_{-\ell}^{\ell} \sigma \cdot \frac{\partial G_p}{\partial y} \cdot dx = -\frac{c}{2\pi} \int_{-\ell}^{\ell} \frac{\partial H_p}{\partial x} \cdot dx = \frac{\sigma}{2\pi} [H(-\ell) - H(\ell)] = \sigma. \quad (2.10)$$

Hence, we obtain the resulting regular solution

$$\psi_D \text{ reg} = \sigma + \ell \int_{\gamma}^{2\pi} (w_t + U w_x) \cdot G_p \cdot \sin \theta \cdot d\theta. \quad (2.11)$$

The additional singular solutions can be found from the expressions for  $G_p$  in the neighborhood of the singular points  $C: \zeta = 0$ ,  $A: \zeta = \pi$ ,  $B: \zeta = i \sqrt{\cot \gamma/2}$ . Near  $\zeta = 0$ , we put  $\zeta = i\varepsilon$ , i.e., we let  $\Gamma \rightarrow A$  along the upper side of the contour.

Then

$$\begin{aligned} G_p + iH_p &= \ln \frac{(i\varepsilon - \zeta_p)(i\varepsilon + \bar{\zeta}_p)}{(i\varepsilon - \bar{\zeta}_p)(i\varepsilon + \zeta_p)} = \ln \frac{(1 - i\varepsilon/\zeta_p)(1 + i\varepsilon/\bar{\zeta}_p)}{(1 - i\varepsilon/\bar{\zeta}_p)(1 + i\varepsilon/\zeta_p)} \\ &= 2i\varepsilon \left( \frac{1}{\zeta_p} - \frac{1}{\bar{\zeta}_p} \right) - \frac{2i\varepsilon^3}{3} \left( \frac{1}{\zeta_p^3} - \frac{1}{\bar{\zeta}_p^3} \right) + \dots \end{aligned} \quad (2.12)$$

This gives an infinite number of singular solutions of increasing order, each of which has a zero value on the cavity and a zero normal derivative on the wetted part of the hydrofoil. The higher singularities must be excluded by another physical condition, viz., the condition that the pressure must be integrable over the hydrofoil. On the segment CB we have  $\zeta_p = -i\tau_p$  and

$$\frac{dx}{d\tau} = i \frac{dz}{d\zeta} \cdot \frac{d\zeta}{d\tau} = -i \cdot \frac{\tau_p \left( \cot \frac{1}{2} \gamma - \tau_p^2 \right)}{\left\{ 1 + \left( \cot \frac{1}{2} \gamma - \tau_p^2 \right)^2 \right\}^2}.$$

Further, the first of the potentials is

$$\varphi_1 = \frac{2}{\tau_p},$$

and the integral

$$\int_{-\ell}^{\ell} \varphi_1 \cdot dx = \int_0^{\tau_p} \frac{\tau_p \left( \cot \frac{1}{2} \gamma - \tau_p^2 \right)}{\left\{ 1 + \left( \cot \frac{1}{2} \gamma - \tau_p^2 \right)^2 \right\}^2} d\tau_p$$

will exist, while for the higher solutions it becomes divergent. Therefore the singular solution corresponding to the point C is

$$\psi_1 = \frac{i}{2} \left( \frac{1}{\gamma_p} - \frac{1}{\bar{\gamma}_p} \right) = \frac{\eta_p}{\gamma_p^2 + \bar{\gamma}_p^2}. \quad (2.13)$$

In order to derive the second singular solution we put  $\eta_p = -1/\epsilon$ ,

$$G_p + iH_p = \kappa_n \frac{(-i/\epsilon - \gamma_p)(-i/\epsilon + \bar{\gamma}_p)}{(-i/\epsilon - \bar{\gamma}_p)(-i/\epsilon + \gamma_p)} \approx -2i\epsilon \left[ \gamma_p - \bar{\gamma}_p \right] - \frac{2i\epsilon^3}{3} \left[ \gamma_p^3 - \bar{\gamma}_p^3 \right] + \dots$$

Here the integrability condition does not give a unique singular solution, since both  $\gamma_p$  and  $\bar{\gamma}_p^3$  give an integrable expression. It is shown by Wu, however, that only the first term will give a pressure field, which is higher than the vapor pressure. Hence the second singular solution is

$$\psi_2 = \frac{(\gamma_p - \bar{\gamma}_p)i}{2} = \eta_p, \quad (2.14)$$

and the third is

$$\psi_3 = \frac{\gamma_p^3 - \bar{\gamma}_p^3}{2} = \gamma[3 - 2\gamma^2].$$

This singular solution, corresponding to the trailing edge B will give a pressure which is infinite at this point. This is excluded by the Kutta condition which requires the pressure to be finite at this point. Thus we are left with the following expression for the pressure potential:

$$\begin{aligned} \psi_p = & \kappa \int_{\gamma}^{2\pi} \{w_t + U w_x\} G_p \sin \theta \, d\theta \\ & + A_1 i \left( \frac{1}{\gamma_p} - \frac{1}{\bar{\gamma}_p} \right) + A_2 i (\gamma_p - \bar{\gamma}_p). \end{aligned} \quad (2.15)$$

We further remark that the disturbance pressure must vanish at infinity. Since in the  $z$ -plane the point at infinity corresponds to

$$\zeta_p = \sqrt{-i e^{-i\gamma/2} \cos \frac{\gamma}{2}} = \frac{e^{i(\gamma/4 - \pi/2)}}{\sqrt{\cos \frac{\gamma}{2}}} = -\frac{i e^{i\gamma/4}}{\sqrt{\cos \frac{\gamma}{2}}},$$

we obtain the condition

$$\kappa + \kappa \int_{\gamma}^{2\pi} (w_t + U w_x) G_p \sin \theta \, d\theta + A_1 2 \cos(\gamma/4) \sqrt{\cos \frac{\gamma}{2}} + A_2 \frac{\cos(\gamma/4)}{\sqrt{\cos(\gamma/2)}} = 0. \quad (2.16)$$

Near the trailing edge B we put  $\zeta = -i + \cot \gamma/2 \delta - i\delta$  which gives

$$\begin{aligned} G_p + iH_p &= \ln \frac{(-i \sqrt{\cot \gamma/2 - i\delta - \zeta_p})(-i \sqrt{\cot \gamma/2 - i\delta + \bar{\zeta}_p})}{(-i \sqrt{\cot \gamma/2 - i\delta - \bar{\zeta}_p})(-i \sqrt{\cot \gamma/2 - i\delta + \zeta_p})} = \\ &= \ln(\dots) + i\delta \left[ \frac{1}{-i \sqrt{\cot \gamma/2 - \zeta_p}} + \frac{1}{-i \sqrt{\cot \gamma/2 + \bar{\zeta}_p}} - \right. \\ &\quad \left. - \frac{1}{-i \sqrt{\cot \gamma/2 - \bar{\zeta}_p}} - \frac{1}{-i \sqrt{\cot \gamma/2 + \zeta_p}} \right] = \\ &= \ln(\dots) + i\delta \left[ \frac{-2\zeta_p}{\cot \gamma/2 + \zeta_p^2} + \frac{+2\bar{\zeta}_p}{\cot \gamma/2 + \bar{\zeta}_p^2} \right]. \end{aligned}$$

The first singular solution is

$$\begin{aligned} \psi_4 &= i \left\{ \frac{\zeta_p}{Z_p} - \frac{\bar{\zeta}_p}{\bar{Z}_p} \right\} = i \left[ \frac{\zeta_p + i\eta_p}{(C + \varepsilon^2 - \eta^2) + 2i\varepsilon\eta} - \frac{\bar{\zeta}_p - i\eta}{(C + \varepsilon^2 - \eta^2) - 2i\varepsilon\eta} \right] \\ &= i \frac{-4i\varepsilon^2\eta + 2i\eta(C + \varepsilon^2 - \eta^2)}{(C + \varepsilon^2 - \eta^2)^2 + 4\varepsilon^2\eta^2} - \frac{4\varepsilon^2\eta - 2\eta(C + \varepsilon^2 - \eta^2)}{C^2 + 2C(\varepsilon^2 - \eta^2) + (\varepsilon^2 + \eta^2)^2} \\ &= \frac{-2C\eta + 2\eta(\varepsilon^2 + \eta^2)}{C^2 + 2C(\varepsilon^2 - \eta^2) + (\varepsilon^2 + \eta^2)^2}. \end{aligned}$$

### 3. DETERMINATION OF THE COMPLETE SOLUTION

For the determination of the unknown functions of the time  $A_1(t)$ ,  $A_2(t)$ , and  $\gamma(t)$ , two additional conditions are necessary. These are found by first remarking that up to now the problem has only been solved for the acceleration potential, whereby only the differentiated form of the boundary condition (1.8) is used. In the original problem, however, not only the normal value of the acceleration, but also the velocity is given which contains more information. In fact, once more it can be seen that any solution, satisfying the velocity condition (1.1) satisfies also (1.8), but the singular solutions, which do not affect (1.8) must be added in such a way that (1.1) is satisfied. Another condition is that the cavitation bubble must be closed.

In order to express these two conditions in a mathematical formulation, it is necessary to derive an expression for the velocity potential  $\phi$  in terms of the acceleration potential  $\psi$ . This can be found by solution of the differential equation

$$\phi_t + U \phi_x = \psi. \quad (1.7)$$

Considering that the velocity potential must vanish at infinity upstream to the hydrofoil, this expression is

$$\Phi(x, y, t) = \frac{1}{U} \int_{-\infty}^x \varphi\left(x', y, t - \frac{x-x'}{U}\right) dx' = \int_{-\infty}^t \varphi(x-U(t-t'), y, t') dt'. \quad (3.1)$$

Substitution of (2.15) and (2.16) gives

$$\begin{aligned} \Phi(x, y, t) = & \frac{1}{U} \int_{-\infty}^x dx' \cdot \int_{\gamma}^{2\pi} w_t \left\{ -l \cos \theta, t - \frac{x-x'}{U} \right\} \sin \theta (G_p - G_\infty) d\theta \\ & + U w_t \left\{ -l \cos \theta, t - \frac{x-x'}{U} \right\} \cdot \\ & + \int_{-\infty}^x A_1 \left( t - \frac{x-x'}{U} \right) \cdot \left\{ i \left( \frac{1}{r_p} - \frac{1}{r} \right) - 2 \cos(\gamma/4) \sqrt{\cos \frac{1}{2} \gamma} \right\} dx' + \\ & + \int_{-\infty}^x A_2 \left( t - \frac{x-x'}{U} \right) \left\{ i (l_p - l_r) - \frac{\cos \gamma/4}{\sqrt{\cos(\gamma/4)}} \right\} dx'. \end{aligned} \quad (3.2)$$

After complicated calculations, which are given in the Appendix, the expression for the velocity on the hydrofoil takes the form given in Eq. (A10) of the Appendix. Applying this result to a point of the wetted surface, we derive

$$\begin{aligned} 0 = & \frac{1}{4} U \int_{-\infty}^x dx' \cdot \int_{\gamma}^{2\pi} w \left( t - \frac{x-x'}{U} \right) \left[ 3C\psi_1 \psi_1^p + (\psi_1 \psi_3^p + \psi_3 \psi_1^p) - \frac{(1-C^2)^2}{C} \psi_2 \psi_2^p \right. \\ & \left. + \frac{1}{C} \psi_4 \psi_4^p \right] \sin \theta dx' - \int_{-\infty}^x A_1 \left( t - \frac{x-x'}{U} \right) \cdot \frac{\psi_1}{\partial y} dx' - \int_{-\infty}^x A_2 \left( t - \frac{x-x'}{U} \right) \frac{\psi_2}{\partial y} dx' \\ & - U \int_{-\infty}^x dx' \cdot \int_{\gamma}^{2\pi} w \left( t - \frac{x-x'}{U} \right) \psi_2 \frac{\psi_2^p}{y} \cdot \frac{1}{\sin(\gamma/2)} \cdot \frac{\psi_2}{U} \sin \theta dx'. \end{aligned} \quad (3.3)$$

Since the first term gives the solution to the boundary value problem where the velocity on the wetted part has the given value  $w$ , this first term cancels against the left-hand member. Considering now the integrals with respect to  $x'$ , they again can be simplified, remarking that the singular potentials  $\psi_i$  are all imaginary parts of complex functions. Applying the Cauchy-Riemann equations,

$$\frac{\psi_i}{\partial y} = \frac{\psi_i^p}{\partial x}$$



where

$$\psi_1 = \operatorname{Re}(1/\zeta) = \frac{\xi}{\xi^2 + \eta^2},$$

$$\psi_2 = \operatorname{Re} \zeta = \xi,$$

$$\psi_3 = \operatorname{Re} \zeta^3 = \xi(\xi^2 - 3\eta^2),$$

$$\psi_4 = \operatorname{Re}(\zeta/Z) = \frac{\xi(C + \xi^2 + \eta^2)}{(C + \xi^2 - \eta^2)^2 + 4\xi^2\eta^2}.$$

We can reduce (3.3) by partial integration, remarking that the wetted surface corresponds to the line  $\xi = 0$  in the  $\zeta$  plane. Introducing

$$\int_{\gamma}^{2\pi} w_t \left( t, t - \frac{x-x'}{U} \right) \cdot \psi_i \cdot (t') \cdot \sin \theta' d\theta' = w_i(t, x'),$$

we obtain

$$0 = \frac{1}{4} \int_{-\infty}^{\ell} \left\{ 3C \psi_1 w_1 + \psi_3 w_1 + \psi_1 w_3 - \frac{(1+C^2)^2}{C} \psi_2 w_2 + \frac{1}{C} \psi_4 w_4 \right\} dx' \\ + \int_{-\infty}^{\ell} A_{1t} \cdot \psi_1 dx' + \int_{\ell}^{\infty} A_{2t} \cdot \psi_2 dx' - \int_{-\infty}^{\infty} dx' \cdot \dots$$

It should be noted that  $\psi_i = 0$  for  $\xi = 0$ . Therefore the only part of the integration which contributes to the result is the part of the  $x$ -axis extending from  $-\infty$  to  $\ell$ . The integration along the lower part of the hydrofoil, which corresponds to the  $\eta$ -axis in the  $\zeta$ -plane, gives a vanishing contribution. A point on the wetted upper surface between B and C is reached from the trailing edge. Taking the contour along the upper edge of the hydrofoil, i.e., along the real axis in the  $\zeta = \xi + i\eta$  plane, we get an additional contribution from the cavitation bubble. Hence, it is obvious that behind this bubble extends a line of discontinuity in  $\psi$ .

The last equation for  $A_1$  and  $A_2$  is furnished by the closure condition. If the contour of the hydrofoil and the cavitation bubble is represented by

$$y = h(x, t),$$

where  $h$  is only given on the wetted part. The normal velocity is

$$= \frac{h}{t} + U \frac{h}{x}.$$

In order to derive the contour of the bubble, we consider this as a partial differential equation

$$h_c - h_{-t} = \frac{1}{U} \int_{-t}^x v\left(x', t - \frac{x-x'}{U}\right) dx'.$$

Then the closure condition is

$$h_c - h_{-t} = \frac{1}{U} \int_{-t}^c v\left(x', t - \frac{c-x'}{U}\right) dx'.$$

The velocity  $v$  satisfies a similar partial differential equation

$$a = v_t + Uv_x,$$

where  $a$  is the normal acceleration. This gives in a similar way

$$v(x, t) - v(-t, t) = \frac{1}{U} \int_{-t}^x v\left(x', t - \frac{x-x'}{U}\right) dx'.$$

Here  $v(-t)$  is the given normal velocity, corresponding to the motion of the leading edge. Substitution gives

$$\begin{aligned} h_c - h_{-t} &= \frac{1}{U} \int_{-t}^c v\left(x', t - \frac{c-x'}{U}\right) dx' + \frac{1}{U^2} \int_{-t}^c dx \int_{-t}^x a\left(x', t - \frac{c-x}{U} - \frac{x-x'}{U}\right) dx' = \\ &= \frac{1}{U} \int_{-t}^c v\left(x', t - \frac{c-x}{U}\right) dx + \frac{1}{U^2} \int_{-t}^c dx \int_{-t}^x a\left(x', t - \frac{c-x}{U}\right) dx' = \\ &= \frac{1}{U} \int_{-t}^c v\left(x', t - \frac{c-x}{U}\right) dx + \frac{1}{U^2} \left[ x \int_{-t}^x a\left(x', t - \frac{c-x}{U}\right) dx' \right]_{-t}^c = \\ &= \frac{1}{U^2} \int_{-t}^c x \cdot dx \cdot a\left(x, t - \frac{c-x}{U}\right) dx = \\ &= \frac{1}{U} \int_{-t}^c v\left(x', t - \frac{c-x}{U}\right) dx + \frac{1}{U^2} \left[ c \int_{-t}^c a\left(x', t - \frac{c-x}{U}\right) dx' - \int_{-t}^c x \cdot a\left(x, t - \frac{c-x}{U}\right) dx \right] = \\ &= \frac{1}{U} \int_{-t}^c v\left(x', t - \frac{c-x}{U}\right) dx + \frac{1}{U^2} \int_{-t}^c (c-x) a\left(x, t - \frac{c-x}{U}\right) dx = h_c - h_{-t}. \end{aligned}$$

Substitution gives the third relation:

$$\begin{aligned} \frac{h}{U^2} \int_{-\ell}^c (\ell-x) \cdot \int_{\gamma}^{2\pi} \{w_t + U w_x\} \cdot \frac{\partial G}{\partial y_p} \cdot \sin \theta \cdot d\theta \cdot dx + \frac{1}{U^2} \int_{-\ell}^c (c-x) A_1 \left(t - \frac{c-x}{U}\right) \psi_1(x, t) \cdot dx + \\ + \frac{1}{U^2} \int_{-\ell}^c (c-x) A_2 \left(t - \frac{c-x}{U}\right) \psi_2 \left(x, t - \frac{c-x}{U}\right) \cdot dx = h_c - h_{-\ell} - \frac{1}{U} \int_{-\ell}^c v \left(-\ell, t - \frac{c-x}{U}\right) \cdot dx. \end{aligned}$$

#### 4. SOLUTIONS FOR SPECIAL CASES

Owing to the time-dependence of  $\gamma$  on  $t$ , the equations for  $A_1$ ,  $A_2$ , and  $\gamma$  are difficult to solve. For this reason only special cases can be considered.

##### The Steady Case

As a check on this theory we consider the steady case. The pressure potential is

$$\varphi_p = \dots + \int_{\gamma}^{2\pi} (U w_x) G_p \cdot \sin \theta \cdot d\theta + A_1 i \left( \frac{1}{\zeta_p} - \frac{1}{\bar{\zeta}_p} \right) + A_2 i (\zeta_p - \bar{\zeta}_p),$$

where  $A_1$  and  $A_2$  are constants. The first condition now reads:

$$c + \ell U \int_{\gamma}^{2\pi} w_x \cdot G_{\theta} \sin \theta \cdot d\theta + A_1 2 \cos(\gamma/4) \sqrt{\cos(\gamma/2)} + A_2 \cdot \frac{\cos(\gamma/4)}{\sqrt{\cos(\gamma/2)}} = 0.$$

In the second condition all the quantities  $w_i$  vanish and we obtain

$$0 = A_1 \cdot \int_{-\infty}^{-\ell} \psi_1 \cdot dx' + A_2 \cdot \int_{-\infty}^{-\ell} \psi_2 \cdot dx'.$$

The third condition gives:

$$\begin{aligned} \frac{1}{U} \int_{-\ell}^c (\ell-x) \int_{\gamma}^{2\pi} w_x \cdot \frac{\partial G}{\partial y_p} \cdot \sin \theta \cdot d\theta + \frac{A_1}{U^2} \int_{-\ell}^c (c-x) \cdot \psi_1(x) \cdot dx \\ + \frac{A_2}{U^2} \int_{-\ell}^c (c-x) \cdot \psi_2(x) \cdot dx = h_c - h_{-\ell} - \left( \frac{c+\ell}{U} \right) \cdot v(-\ell). \end{aligned}$$

### Cavitating Hydrofoils in Nonsteady Flow

For a flat plate the formulas simplify considerably. The pressure potential is

$$\varphi_p = \sigma + A_1 i \left( \frac{1}{\bar{z}_p} - \frac{1}{\bar{z}_p} \right) + A_2 i (\bar{z}_p - \bar{z}_p),$$

and the three conditions are

$$\sigma + A_1 2 \cos(\gamma/4) \cdot \sqrt{\cos(\gamma/2)} + A_2 \cdot \frac{\cos(\gamma/4)}{\sqrt{\cos(\gamma/4)}} = 0,$$

$$0 = A_1 \cdot \int_{-\infty}^{\infty} \psi_1 \cdot dx + A_2 \cdot \int_{-\infty}^{\infty} \psi_2 \cdot dx,$$

$$A_1 \int_{-\ell}^{\ell} (c-x) \varphi_1(x) dx + A_2 \int_{-\ell}^{\ell} (c-x) \varphi_2(x) dx = U^2 \left\{ h_c - h_{-\ell} - \frac{c-\ell}{U} v(-\ell) \right\}.$$

### Harmonic Oscillations About a Certain Steady Motion

We consider further the case that the hydrofoil performs harmonic oscillations about a certain steady motion. Owing to the dependence of the formula on the parameter  $\gamma$  we assume that the amplitude is so small, that the time dependence of  $\gamma$  is also small.

$$\gamma = \gamma_0 + \gamma_1^* \cdot e^{i\nu t}.$$

Then we introduce a "second linearization," expanding all quantities, containing  $\gamma$  into powers of  $\gamma_1$ . This gives rise to a set of equations for the determination of the amplitudes  $A_1, A_2$ , and  $\gamma_1$ . The pressure potential takes the form, (if  $w = \bar{w}^* e^{i\nu t} + w_0$ )

$$\begin{aligned} \varphi_p = & \sigma + i \ell \int_{\gamma_0}^{2\pi} w_x \cdot G_p \sin \theta d\theta + i \int_{\gamma_0}^{2\pi} (\nu \bar{w}^* + U w_x^*) G_p \sin \theta d\theta + \\ & + i \int_{\gamma_0}^{2\pi} w_x \cdot \frac{\partial G_p}{\partial \gamma} \cdot \sin \theta d\theta \gamma_0^* e^{i\nu t} + \\ & + A_1 \cdot \frac{\partial \varphi_2}{\partial \gamma} \cdot \gamma_0 e^{i\nu t} + A_2^* e^{i\nu t} \cdot \varphi_2 + A_1 \frac{\partial \varphi_2}{\partial \gamma} \cdot \gamma_0 e^{i\nu t}. \end{aligned}$$

The conditions for  $A_1, A_2$ , and  $\gamma_1$  are derived in a similar way. This gives three nonhomogeneous linear equations for the three amplitudes. It would be of interest to study the case, where the determinant of this system vanishes. This would mean that for the corresponding steady-state, spontaneous oscillations of the cavity can occur.

## 4. CONCLUSIONS

The general theory, laid down in this paper, is based on rather crude assumptions on the behavior of cavitating flow. Considering the underlying hypothesis, the assumption of potential flow is not sufficient to represent details of formation and decay of cavities. On the other hand, it is well known that for steady-flow, results from potential flow agree reasonably well with experiments. The further simplification, introduced by the linearization, seems, in the case of a free hydrofoil, sufficiently accurate for thin hydrofoils at small incidence. In a channel, however, this simplification might be the cause of considerable error, owing to blockage effects. This phenomenon is analogous to the behavior of linearized theory for transonic flow in wind tunnels, where the nonlinear approximation is necessary.

As regards the special additional assumptions, introduced to describe the nonsteady behavior, the condition is that in the cavitation bubble evaporation occurs instantly, as soon as the pressure has reached the cavitation pressure, which is constant. However, every other hypothesis which must be based on more detailed physical considerations will greatly involve the calculations. As regards the introduction of free sources and sinks, somewhat more explanation is necessary.\*

The concept is completely analogous to the concept of free vortices in nonsteady airfoil theory, which already goes back to Birnbaum (1923).

Calculation of forces, based on this assumption, yields reasonably good agreement with experiments. In linearized theory the circulation around the airfoil is defined by

$$\int \underline{v} \cdot d\mathbf{s} = \int \mathbf{U} \cdot d\mathbf{x},$$

where  $u$  is related to the pressure potential by

$$\psi = \phi_t + U \phi_x \quad \text{or} \quad \psi_x = u_t + U u_x,$$

which means that

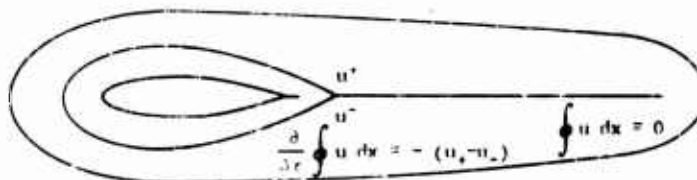
$$\oint \psi_x dx = \frac{\partial}{\partial t} \oint u dx + U \oint u_x dx + U \oint \phi_x dx.$$

If we suppose that  $\psi$  is a regular function outside the airfoil, including infinity,  $\oint \psi_x dx = 0$  for any contour enclosing the airfoil, and we find that

$$\frac{\partial}{\partial t} \oint u dx + \oint u_x dx = - (u_+ - u_-).$$

If in the wake the velocity  $u$  is discontinuous, we find that the time rate of the circulation around the airfoil is equal to the strength of the discontinuity at the trailing edge, which is the vorticity in the wake. For a motion started at a definite moment

\* This explanation was found in a discussion between the author and Mr. J. A. Geurst.



in the past, the wake is finite and the total circulation around a contour enclosing the airfoil and the wake vanishes. A similar consideration can be applied to the integral

$$V = \int h dx$$

if the contour is given by  $y = h(x)$ , which represents the total volume enclosed by the contour. Since

$$v = h_t + U h_x,$$

we have, for a closed contour,

$$\oint v dx = \frac{\partial}{\partial t} \int h dx,$$

which expresses that the time rate of change of the volume by the contour is equal to the contour integral of the function  $v$ .

For incompressible flow we have simply

$$\oint v dx = -\psi_+ + \psi_-.$$

where  $\psi$  is the stream function and  $v = -\psi_x$  for incompressible flow. If  $\psi$  is regular outside the hydrofoil, we have  $\psi_+ = \psi_-$  and the volume enclosed by the contour is a constant, as was posed by Wu.

We have seen previously that from our calculation it follows that a sheet of discontinuity in  $v$  extends behind the cavitation bubble. This gives rise to a sheet of discontinuity in the  $\psi$ . Hence, considering a contour which lies along the bubble and the wetted part of the hydrofoil, there is a discontinuity at the end of the bubble. The strength of the discontinuity is given by the change in volume of the bubble. Since, in linearized theory the pressure is a continuous function outside the hydrofoil, the discontinuity  $\Delta\psi$  in the wake satisfies

$$(\Delta\psi)_t + U(\Delta\psi)_x = 0,$$

which means that this discontinuity is propagated with the velocity  $U$ .

Since a discontinuity in  $v$  corresponds to a source distribution, the singularities are denoted as "free sources" in analogy to the free vortices considered before. The theory opens a possibility of an explanation of the oscillations, which are observed for a steady cavity of finite extent. The entrainment process at the end of the cavity during which small volumes of the gas phase are carried downstream with the fluid, as the cavity volume decreases, might correspond to the creation of the free sources.

Only quantitative calculations of the occurring frequencies and length of the steady state bubble would confirm whether or not even this potentially theoretical approach can account for this complicated phenomenon.

NOTE ADDED IN PROOF: From discussion of the author with Messrs. Geurst, Tulin, and Eisenberg (October 1959) a slightly different explanation of the "free sources" concept arose. In this concept they are localized in the reentrant jet. Hence, for a closed contour, including the stagnation point behind the reentrant jet, the volume is constant. The volume enclosed by the free surface varies and is compensated by "free sources" on the second blade of the Riemann surface. This theory gives consistent conditions and is worked out by Mr. Geurst. (To be published in Archiv for Rational Mechanics.)

\* \* \* \* \*

# APPENDIX

## REDUCTION OF THE FORMULA FOR THE VERTICAL VELOCITY ON THE HYDROFOIL

The formula for the velocity component  $v$  is:

$$v(x, 0, t) = \frac{1}{U} \int_{-\infty}^{\infty} dx' \int_0^{2\pi} \left( t - \frac{x-x'}{U} \right) w_t \left\{ -l \cos \theta, t - \frac{x-x'}{U} \right\} \frac{\partial G}{\partial y} \left\{ x', -l \cos \theta; t - \frac{x-x'}{U} \right\} \\ \sin \theta d\theta + l \int_{-\infty}^{\infty} dx' \cdot \int_0^{2\pi} \left( t - \frac{x-x'}{U} \right) w_\theta \left( -l \cos \theta, t - \frac{x-x'}{U} \right) \cdot \frac{\partial G}{\partial y} \left( x', -l \cos \theta; t - \frac{x-x'}{U} \right) d\theta \\ + \int_{-\infty}^{\infty} A_1 \left( t - \frac{x-x'}{U} \right) \frac{\partial \psi_1}{\partial y} \left( t - \frac{x-x'}{U} \right) dx' + \int_{-\infty}^{\infty} A_2 \left( t - \frac{x-x'}{U} \right) \cdot \frac{\partial \psi_2}{\partial y} \cdot dx'. \quad (A1)$$

We can reduce the first two terms by partial integration

$$\begin{aligned}
 & \int_{-\infty}^{\infty} dx' \int_{\gamma}^{2\pi} w_t \left( \theta, t - \frac{x-x'}{U} \right) \frac{\partial G}{\partial y} \sin \theta \, d\theta - U \int_{-\infty}^{\infty} dx' \int_{\gamma}^{2\pi} w_{x'} \left( \theta, t - \frac{x-x'}{U} \right) \cdot \frac{\partial G(\gamma)}{\partial y} \sin \theta \, d\theta \\
 &= U \int_{\gamma}^{2\pi} w(\theta, t) \frac{\partial G}{\partial y} \cdot \sin \theta \, d\theta - U \int_{-\infty}^{\infty} dx' \int_{\gamma}^{2\pi} w \left( \theta, t - \frac{x-x'}{U} \right) \cdot \frac{\partial^2 G}{\partial y \partial x'} \sin \theta \, d\theta \\
 &- \int_{-\infty}^{\infty} dx' \cdot \frac{\partial \gamma}{\partial t} \cdot w \left( \gamma, t - \frac{x-x'}{U} \right) \frac{\partial G}{\partial y} - U \int_{-\infty}^{\infty} dx' \int_{\gamma}^{2\pi} w \left( \theta, t - \frac{x-x'}{U} \right) \frac{\partial^2 G}{\partial y \partial \gamma} \frac{\partial \gamma}{\partial t} \sin \theta \, d\theta
 \end{aligned}$$

and

$$\begin{aligned}
 & \int_{-\infty}^{\infty} dx' \int_{\gamma}^{2\pi} w_{\theta} \left( \theta, t - \frac{x-x'}{U} \right) \frac{\partial G}{\partial y} \, d\theta = \int_{-\infty}^{\infty} dx' \left[ w \left( \theta, t - \frac{x-x'}{U} \right) \frac{\partial G}{\partial y} \right]_{\gamma}^{2\pi} \\
 &- \int_{-\infty}^{\infty} dx' \int_{\gamma}^{2\pi} w \left( \theta, t - \frac{x-x'}{U} \right) \frac{\partial^2 G}{\partial y \partial \theta} \cdot d\theta.
 \end{aligned}$$

Apparently we have to calculate the expression

$$\frac{\partial^2 G}{\partial y \partial x'} \sin \theta + \frac{\partial^2 G}{\partial y \partial \theta} = \sin \theta \frac{\partial}{\partial y} \left[ \frac{\partial^2 G}{\partial x} + \frac{\partial G}{\partial x'} \right]. \quad (A2)$$

From the definition

$$G + iH = i\pi \frac{(z'-z'')(z'+\bar{z}'')}{(z'-\bar{z}'')(z'+z'')} \quad (A3)$$



we see that

$$\begin{aligned}
 \frac{\partial G}{\partial x} + \frac{\partial G}{\partial x'} &= \operatorname{Re} \left\{ \frac{d}{dz} (G+iH) + \frac{\partial}{\partial z} (G+iH) + \frac{\partial}{\partial \bar{z}} (G+iH) \right\} \\
 &= \operatorname{Re} \left\{ \frac{\partial(G+iH)}{\partial \zeta} \cdot \frac{d\zeta}{dz} + \frac{\partial(G+iH)}{\partial \zeta'} \cdot \frac{d\zeta'}{dz} + \frac{\partial(G+iH)}{\partial \bar{\zeta}} \cdot \frac{d\bar{\zeta}}{dz} \right\} \\
 &= \operatorname{Re} \left\{ \left( \frac{1}{\zeta-\zeta'} - \frac{1}{\zeta+\zeta'} + \frac{1}{\zeta+\bar{\zeta}'} - \frac{1}{\zeta-\bar{\zeta}'} \right) \frac{d\zeta}{dz} + \left( \frac{-1}{\zeta-\zeta'} - \frac{1}{\zeta+\zeta'} \right) \frac{d\zeta'}{dz} \right. \\
 &\quad \left. + \left( \frac{1}{\zeta+\bar{\zeta}'} + \frac{1}{\zeta-\bar{\zeta}'} \right) \cdot \frac{d\bar{\zeta}}{dz} \right\}. \tag{A4}
 \end{aligned}$$

Since  $\zeta = \sqrt{Z-C}$ , where  $C = \cot(\gamma/2)$  and  $Z = \sqrt{l-z/l+z}$

we have

$$\frac{d\zeta}{dz} = \frac{d\zeta}{dZ} \cdot \frac{dZ}{dz} = \frac{1}{2\zeta} \cdot \frac{d}{dz} \sqrt{\frac{l-z}{l+z}} = -\frac{(l+z)^2}{\zeta 2l}.$$

Substitution gives

$$\begin{aligned}
 &= -\frac{1}{4l} \operatorname{Re} \left\{ \frac{1}{\zeta^2 - \bar{\zeta}_1^2} \left( \frac{\zeta'}{\zeta} \cdot \frac{(1+Z^2)^2}{Z} - \frac{\zeta}{\zeta'} \cdot \frac{(1+Z_1'^2)^2}{Z_1} \right) \right. \\
 &\quad \left. - \frac{1}{\zeta^2 - \bar{\zeta}_1^2} \left( \frac{\bar{\zeta}_1}{\zeta} \cdot \frac{(1+Z^2)^2}{Z} - \frac{\zeta}{\bar{\zeta}_1} \cdot \frac{(1+\bar{Z}_1'^2)^2}{\bar{Z}_1} \right) \right\} \\
 &= -\frac{1}{4l} \operatorname{Re} \left[ \frac{1}{\zeta \bar{\zeta}_1} \cdot \frac{Z_1(Z_1-C)(1+Z^2)^2 - (Z-C)(1+Z_1^2)Z^2}{(Z-Z_1)ZZ_1} \right. \\
 &\quad \left. - \frac{1}{\zeta \bar{\zeta}_1} \cdot \frac{\bar{Z}_1(\bar{Z}_1-C)(1+Z^2)^2 - (Z-C)(1+\bar{Z}_1^2)Z^2}{(Z-Z_1)Z\bar{Z}_1} \right] \\
 &= -\frac{1}{4l} \operatorname{Re} \left[ \frac{1}{\zeta \bar{\zeta}_1} \cdot \frac{+(Z+Z_1)(Z_1^2 Z^2 - 1) - C(-1+2Z\bar{Z}_1+Z_1 Z^3 + Z^2 Z_1^2 + Z\bar{Z}_1^3)}{ZZ_1} \right]
 \end{aligned}$$

$$\begin{aligned}
 & - \frac{1}{\zeta \bar{\zeta}_1} \cdot \frac{(Z + \bar{Z}_1)(Z^2 \bar{Z}_1^2 - 1) - C(-1 + 2Z\bar{Z}_1 + \bar{Z}_1 Z^3 + Z^2 \bar{Z}_1^2 + 7\bar{Z}_1^3)}{7\bar{Z}_1} \Big] \\
 & = - \frac{\text{Re}}{4l} - \frac{1}{\zeta} \left( \frac{1}{\bar{\zeta}_1 \bar{\zeta}_1} - \frac{1}{\bar{\zeta}_1 \bar{\zeta}_1} \right) - \frac{1}{\zeta \bar{\zeta}_1} \left( \frac{1}{\bar{\zeta}_1} - \frac{1}{\bar{\zeta}_1} \right) + \frac{Z^2}{\zeta} \left( \frac{\bar{Z}_1}{\bar{\zeta}_1} - \frac{\bar{Z}_1}{\bar{\zeta}_1} \right) + \frac{Z}{\zeta} \left( \frac{Z_1^2}{\bar{\zeta}_1} - \frac{Z_1^2}{\bar{\zeta}_1} \right) \\
 & \quad - C \frac{1}{\zeta \bar{\zeta}_1} \left( \frac{1}{\bar{\zeta}_1 \bar{\zeta}_1} - \frac{1}{\bar{\zeta}_1 \bar{\zeta}_1} \right) - 2C \frac{1}{\zeta} \left( \frac{1}{\bar{\zeta}_1} - \frac{1}{\bar{\zeta}_1} \right) \\
 & \quad - C \frac{Z^2}{\zeta} \left( \frac{1}{\bar{\zeta}_1} - \frac{1}{\bar{\zeta}_1} \right) - \frac{C}{\zeta} \left( \frac{Z_1^2}{\bar{\zeta}_1} - \frac{\bar{Z}_1^2}{\bar{\zeta}_1} \right) - C \frac{Z}{\zeta} \left( \frac{\bar{Z}_1}{\bar{\zeta}_1} - \frac{\bar{Z}_1}{\bar{\zeta}_1} \right). \tag{A5}
 \end{aligned}$$

We can express this into the four singular potentials

$$\begin{aligned}
 \psi_1 & = i(\zeta - \bar{\zeta}), \\
 \psi_2 & = \left( \frac{1}{\zeta} - \frac{1}{\bar{\zeta}} \right), \\
 \psi_3 & = (\zeta^3 - \bar{\zeta}^3), \\
 \psi_4 & = i \left( \frac{\zeta}{\bar{\zeta}} - \frac{\bar{\zeta}}{\zeta} \right). \tag{A6}
 \end{aligned}$$

and the corresponding quantities for  $\Gamma$ .

At first we remark that

$$\begin{aligned}
 -i \left( \frac{1}{\zeta \bar{\zeta}} - \frac{1}{\bar{\zeta} \bar{\zeta}} \right) & = \frac{\psi_2 - \bar{\psi}_2}{C}, \\
 -i \left( \frac{\zeta}{\bar{\zeta}} - \frac{\bar{\zeta}}{\zeta} \right) & = \psi_4 + C \psi_2, \\
 -i \left( \frac{\zeta^2}{\bar{\zeta}} - \frac{\bar{\zeta}^2}{\zeta} \right) & = \psi_3 + 2C\psi_1 + C^2\psi_2.
 \end{aligned}$$

This gives:

$$\begin{aligned}
 \frac{\partial G}{\partial x} + \frac{\partial G}{\partial x^*} & = \frac{1}{4l} \left[ -\psi_2 \cdot \frac{\psi_2^* - \bar{\psi}_2^*}{C} - \frac{\psi_2 - \bar{\psi}_2}{C} \cdot \psi_2^* + (\psi_3 + 2C\psi_1 + C^2\psi_2)(\psi_1^* + C\psi_2^*) \right. \\
 & \quad \left. + (\psi_1 + C\psi_2)(\psi_3^* + 2C\psi_1^* + C^2\psi_2^*) + \frac{(\psi_2 - \bar{\psi}_2)(\psi_2^* - \bar{\psi}_2^*)}{C} - 2C\psi_2\psi_2^* \right]
 \end{aligned}$$

$$\begin{aligned}
\frac{\partial G}{\partial x} &= C(\psi_3 + 2C\psi_1 + C^2\psi_2)\psi_2^2 - C(\psi_3^2 + 2C\psi_1^2 + C^2\psi_2^2)\psi_2 - C(\psi_1 + C\psi_3)(\psi_1^2 + C\psi_3^2) \\
&= \frac{1}{4\ell} \left[ \frac{\psi_4\psi_2^2 - \psi_2\psi_4^2}{C} + (\psi_3\psi_1^2 + \psi_1\psi_3^2) + C(3\psi_1\psi_1^2 - 2\psi_2\psi_2^2) - C^3\psi_2^2\psi_2^2 \right] \\
&= \frac{1}{4\ell} \left[ 3C\psi_1\psi_1^2 + (\psi_1\psi_3^2 + \psi_3\psi_1^2) - \left( \frac{1}{C} + 2C + C^3 \right) \psi_2\psi_2^2 + \frac{1}{C} \psi_4\psi_4^2 \right]. \quad (A7)
\end{aligned}$$

Further

$$\frac{\partial G}{\partial y} = \frac{\partial G}{\partial C} \cdot \frac{dC}{dy} = - \frac{1}{2 \sin^2 \gamma/2} \cdot \frac{\partial G}{\partial C}. \quad (A8)$$

$$\begin{aligned}
\frac{\partial(G+III)}{\partial C} &= \frac{\partial}{\partial C} \ln \frac{(\sqrt{2-C} - \sqrt{2_1-C})(\sqrt{2-C} + \sqrt{2_1-C})}{(\sqrt{2-C} - \sqrt{2_1-C})(\sqrt{2-C} + \sqrt{2_1-C})} \\
&= \frac{1}{2} \left[ \frac{1}{\sqrt{2-C} - \sqrt{2_1-C}} \left( \frac{1}{\sqrt{2-C}} - \frac{1}{\sqrt{2_1-C}} \right) + \frac{1}{\sqrt{2-C} + \sqrt{2_1-C}} \left( \frac{1}{\sqrt{2-C}} + \frac{1}{\sqrt{2_1-C}} \right) \right. \\
&\quad \left. - \frac{1}{\sqrt{2-C} - \sqrt{2_1-C}} \left( \frac{1}{\sqrt{2-C}} - \frac{1}{\sqrt{2_1-C}} \right) - \frac{1}{\sqrt{2-C} + \sqrt{2_1-C}} \left( \frac{1}{\sqrt{2-C}} + \frac{1}{\sqrt{2_1-C}} \right) \right] \\
&= - \frac{1}{2} \left[ \frac{1}{\ell - \ell_1} \left( \frac{1}{\ell} - \frac{1}{\ell_1} \right) + \frac{1}{\ell + \ell_1} \left( \frac{1}{\ell} + \frac{1}{\ell_1} \right) - \frac{1}{\ell - \ell_1} \left( \frac{1}{\ell} - \frac{1}{\ell_1} \right) - \frac{1}{\ell + \ell_1} \left( \frac{1}{\ell} + \frac{1}{\ell_1} \right) \right] \\
&= + \frac{1}{2} \left[ \frac{1}{\ell\ell_1} - \frac{1}{\ell^2\ell_1} - \frac{1}{\ell\ell_1^2} + \frac{1}{\ell\ell_1^3} \right] = \frac{1}{\ell} \left( \frac{1}{\ell_1} - \frac{1}{\ell_1^3} \right).
\end{aligned}$$

Hence

$$\frac{\partial G}{\partial C} = \frac{1}{2} \left( \frac{1}{\ell} - \frac{1}{\ell_1} \right) \left( \frac{1}{\ell_1} - \frac{1}{\ell_1^3} \right) = - 2 \psi_2 \psi_2^2. \quad (A9)$$

Substitution of these results into Eq. (A1) gives:

$$\begin{aligned}
v(x, 0, t) &= \ell \int_{\gamma}^{\pi} w(\theta, t) \cdot \frac{\partial G}{\partial y} \sin \theta \, d\theta - \frac{1}{U} \int_{-\infty}^x dx' \cdot \frac{\partial \gamma}{\partial t} \cdot w \left( \gamma, t - \frac{x-x'}{U} \right) \frac{\partial G}{\partial y} \sin \gamma \\
&\quad - \int_{-\infty}^x dx' \int_{\gamma}^{\pi} w \left( \theta, t - \frac{x-x'}{U} \right) \cdot \frac{\sin \theta}{4} \theta \frac{\partial}{\partial y} \left[ 3C\psi_1\psi_1^2 + (\psi_1\psi_3^2 + \psi_3\psi_1^2) \right. \\
&\quad \left. - \frac{(1+C^2)^2}{C} \psi_2\psi_2^2 + \frac{1}{C} \psi_4\psi_4^2 \right]
\end{aligned}$$

$$\begin{aligned}
& - U \int_{-\infty}^{\infty} dx' \int_{\gamma}^{2\pi} w \left( \theta, t - \frac{x-x'}{U} \right) \cdot \frac{\partial}{\partial y} (\psi_2 \psi_1^*) \cdot \frac{1}{\sin^2 \gamma/2} \cdot \frac{\partial \gamma}{\partial t} \sin \theta \, d\theta \\
& + \ell \int_{-\infty}^{\infty} dx' \left[ w \left( \theta, t - \frac{x-x'}{U} \right) \cdot \frac{\partial G}{\partial y} \right]_{\gamma}^{2\pi} \\
& + \int_{-\infty}^{\infty} A_1 \left( t - \frac{x-x'}{U} \right) \cdot \frac{\partial \psi_1}{\partial y} \cdot dx' + \int_{-\infty}^{\infty} A_2 \left( t - \frac{x-x'}{U} \right) \cdot \frac{\partial \psi_2}{\partial y} \cdot dx'.
\end{aligned}$$

\* \* \* \* \*

## DISCUSSION

L. Landweber

One usually thinks of Green's functions in connection with existence theorems or numerical methods in which the Green's function is obtained as the solution of an integral equation. In Professor Timman's paper, however, a Green's function which yields the solution of a time-dependent problem in potential theory is explicitly displayed. I believe that the subject of cavitating hydrofoils, which has yielded a remarkable succession of elegant papers, has attracted so many mathematicians as much for its aesthetic appeal as for its practical fruitfulness.

I would urge the author to assume less mathematical erudition on the part of the reader and to include more details of his mathematical developments. For example, I would have liked a demonstration that the expression for the acceleration potential in terms of the Green's function, Eq. (5), satisfies the boundary condition on the acceleration potential.

A condition not considered in the present paper is that the pressure should be a minimum within the cavitation bubble  $-l < x < c$ ,  $v = +0$ . It is known in the steady case, for example, that this latter condition is necessary in order to determine a unique solution. This raises the question concerning the uniqueness of the solution in the unsteady case.

M. Tulin (Office of Naval Research)

First I would like to comment on the question of the leading edge singularity which occurs in the linearized theory of lifting cavity flow. When I first did the linearized theory for zero cavitation number flows past lifting foils, I compared the

result for the flat plate with the expansion (in powers of the angle of attack) of Rayleigh's exact solution and I verified that the linearized theory solution, which had a  $-1/4$  singularity at the leading edge, was identical with the first term in that expansion. That was, of course, sufficient verification that the linearized solution was correct. Then, when I worked out the case of the finite cavity flow past the lifting flat plate I noticed that it was possible to select more than one solution to the boundary value problem; only one of these solutions had a  $-1/4$  singularity at the leading edge and I naturally assumed that that one was the proper solution. I never thought that it could be any other way—in view of the information provided by the infinite cavity case. In order, however, to "prove" the validity of the present linearized theory solution for finite cavities, may I suggest that some interested persons carry out an expansion (in powers of the angle of attack) of the Gilbarg-Serrin, re-entrant jet, exact theory solution of the flat plate problem. The result would also confirm the almost certain conjecture that the linearized theory for finite cavities, as I first formulated it, is in fact a linearized version of re-entrant jet theory.

Now may I comment on Professor Timman's model for the unsteady cavity flow—which includes some sources or sinks in the flow field trailing behind the cavity. First, I don't understand the physical basis for this model, I don't see how the flow field in the wake of the cavity can contain the postulated sources or sinks. Second, I don't see the mathematical necessity for the model. It is certainly true that a cavity of changing volume would imply, according to incompressible theory, that the pressures become unbounded at infinity, but it is also true that pressure waves are propagated with finite speed, even in water, and that as a result the effects of compressibility alter these pressure waves at large distances from a source (or cavity of changing volume) and cause the pressures at infinity to remain unchanged. I think that even acoustic theory applied to the problem of the flow field at some distance from a cavity of changing volume would reveal the true nature of the pressure field there and would dispel the need for both Professor Timman's model with distributed sources and sinks outside the cavity, and Professor Wu's model—which calls for a cavity of unchanging volume. I believe that the solution of the unsteady cavity problem which properly takes into account the boundary and dynamical conditions on the body and cavity will produce, in general, a cavity of changing volume without sources and sinks distributed in the wake.

W. G. Cornell (General Electric Company)

I certainly hope that some of the techniques that have been shown can be applied to the problems of unsteady, separated aerodynamic flows which, so far, have been treated by what one may call quasi-steady-state methods. I refer to problems such as rotating stall and propagating stall in cascades.

I would like to hear some comments about the use of the Kutta condition when one has an unsteady flow.

B. Parkin (California Institute of Technology)

I would appreciate it very much if Professor Wu would indicate the bearing of the pressure gradient at infinity on the values of the coefficients which he quoted from Karmouss work.

R. Timman

Professor Landweber asked whether I did verify that a constant pressure on the cavitation bubble was actually the minimum pressure in the field. I must again confess I was a bit careless and did not verify that.

With respect to the Kutta condition, if the cavity extends nearly the whole of the upper surface, I hardly believe that a Kutta condition could be valid. On the other hand, as long as the cavity is small I don't see why the Kutta condition should be dangerous. Also, there is a lot of experimental evidence in the use of the nonsteady flow theory. Of course, they all gave imperfect agreement with theory; they don't even agree completely in the steady case. In the steady case you know the Kutta condition, yet you predict 110 percent of the actual values, so why should you expect in a nonsteady theory the agreement to be better? So as far as I can see, as long as the cavity does not extend too close to the trailing edge, the Kutta condition is just as bad or as good as it is in all the hydrodynamical theories.

T. Wu (California Institute of Technology)

In reply to Dr. Parkin's question, it is true that the wake flow generated by a flat plate accelerating broadwise through the fluid which is otherwise at rest in an inertial frame is a problem different from that treated by Karman. In this case you may take a coordinate system fixed with respect to the fluid at infinity so that at infinity the velocity is zero and the pressure is equal to  $p_\infty$ , a constant. Then the plate will be moving with acceleration  $a$ .

If the shape of the free boundary is still a constant in time, then when the condition of constant pressure is applied on the moving boundary, you will have a different expression for the pressure equation.

Next, I wish to supply a uniqueness proof with respect to the leading edge singularity,  $z^{-3/4}$  or  $z^{-1/4}$ . The first time I looked at the  $3/4$  singularity I thought this singularity may be ruled out by the argument that the energy is not integrable at the leading edge. Though this statement is true, I wasn't too happy with this answer. Then I looked for other physical requirements and found a satisfactory one. I imposed another condition, namely that the pressure outside of the solid body and the cavity wake must not be less than the pressure in the cavity. That is,  $u = R \partial w = -1/2 C_p \leq 0$  in the flow field. Suppose the solution of  $w$  has in the neighborhood of the leading edge the expansion

$$w = iA z^{-3/4} + iB z^{-1/4} + O(z^{1/4}),$$

where  $A, B$  are two real coefficients so that  $u = 0$  on the cavity. Then, with  $z = r e^{i\theta}$ , we have near  $\gamma = 0$

$$u = A \gamma^{-3/4} \sin \frac{3\theta}{4} + B \gamma^{-1/4} \sin \frac{\theta}{4} + O(\gamma^{1/4}).$$

From this result, we notice that the term  $\sin(3\theta/4)$  will change sign, whereas the term  $\sin(\theta/4)$  will not, as  $\theta$  changes from 0 to  $2\pi$ . Since the first term violates this physical condition on the minimum pressure, we must therefore have  $A = 0$ .

My own viewpoint with respect to the existence of the flow source is as follows. Suppose we take a two-dimensional cylinder, and let it pulsate with its radius  $r$  as a function of  $t$  in a uniform stream of velocity  $U$ , then the velocity potential is

$$\varphi(r, \theta, t) = U \left( r + \frac{R^2}{r} \right) \cos \theta + R \dot{R} \log r,$$

so that we have a source of strength  $2\pi R \dot{R}$  which depends on the rate of change of the cross section or the radius. In the problem of unsteady cavity flows, however, it seems that the physical requirement must be imposed that the pressure be finite at infinity. Otherwise, we would require an infinite amount of energy, and hence an infinite time, to create such a flow.

Thus the question arises: why don't we let the cavity volume grow and have an infinite pressure at infinity? At the first sight it seems to me that the affirmative is not the case. One flow model which avoids the flow source at infinity is that, when the volume of the cavity near the body changes, there will be a wake which becomes thinner or fatter in the opposite sense.

In regard to the philosophical question about the physical background of these flow models and their agreement with experiments, I have the following point of view: We realize that all the wake flow is the end product of the real fluid effect. But in order to solve the problem in an easy way we want to keep the potential problem as a possible approximation by making some mathematical assumptions, which we call mathematical models. If any mathematical model gives a good approximation of the flow quantities near the solid body, so that we can predict very accurately the total hydrodynamic forces on the body, then, as far as I am concerned, the model should be quite acceptable. However, we should not expect that the simple model is also capable to provide a good description of the complicated wake flow downstream. The problem of the wake flow in the wake is entirely different from those considered here and I believe one cannot obtain a good result without considering the viscous effect, vortex shedding, the turbulent mixing, and so forth.

Several experimental results have been available for a few special cases of cavity flow past a flat plate inclined at a small angle. These results give substantial support to these mathematical models. With respect to the present linearized model, there are certain features which are different from the nonlinear cases. Here, again, the philosophical way to answer this question is to examine if it gives a fairly accurate description of the flow near the body, so as to determine if it is acceptable.

\* \* \* \* \*

## AUTHOR INDEX

Acosta, A. J. . . . .	533	Kraichnan, Robert A. . . . .	29
Benjamin, T. Brooke . . . . .	207	Lerbs, H. W. . . . .	203
Birkhoff, Garrett . . . . .	263	Liepmann, H. W. . . . .	65
Callaghan, Edmund E. . . . .	207	Meyer, Erwin . . . . .	179
Campbell, I. J. . . . .	401	Mollo-Christensen, E. . . . .	65
Cohen, Hirsh . . . . .	267	Morgan, W. B. . . . .	489
Cornell, William, G. . . . .	207	Muller, Ernst-August . . . . .	45
Dean, Lee W., III . . . . .	207	Powell, Alan . . . . .	1
DiPrima, R. C. . . . .	367	Saffman, P. G. . . . .	277
Dyer, Ira . . . . .	151	Skudrzyk, Eugen. . . . .	75
Fitzpatrick, Hugh M. . . . .	201	Tachmindji, A. J. . . . .	489
Haddle, Gillian . . . . .	75	Taylor, Sir Geoffrey . . . . .	277
Harrison, Mark . . . . .	107	Timman, R. . . . .	559
Hilborne, D. V. . . . .	467	Tulin, Marshall . . . . .	235
Ingard, Uno . . . . .	137	Wadlin, Kenneth, L. . . . .	425
Johnson, Virgil, E., Jr. . . . .	317	Wetzel, J. M. . . . .	447
		Wu, T. Y. . . . .	293

For sale by the Superintendent of Documents: U.S. Government Printing Office, Washington 25, D.C. Price \$1.00



**UNCLASSIFIED**

**UNCLASSIFIED**